MODELLING OF SIMPLE PRISMATIC CHANNELS WITH VARYING ROUGHNESS USING THE SKM AND A STUDY OF FLOWS IN SMOOTH NON-PRISMATIC CHANNELS WITH SKEWED FLOODPLAINS

by

JENNIFER CHLEBEK

A thesis submitted to

The University of Birmingham

for the degree of

DOCTOR OF PHILOSOPHY

Department of Civil Engineering

School of Engineering

The University of Birmingham

February 2009

Abstract

Accurate modelling, both numerical and physical, is vital to further our understanding of flow in rivers. This thesis examines both methods of flow applied to two distinct problems; numerical modelling of flow in simple channels with heterogeneous roughness and physical modelling of flow in compound channels with skewed floodplains.

In this thesis, the Shiono and Knight Method (SKM) is applied to homogeneously and heterogeneously roughened channels. The SKM is shown to be capable of accurately predicting the lateral distributions of depth-averaged velocity and boundary shear stress for both roughness types. Furthermore, the percentage shear force on the wall of a channel is accurately obtained for both roughness types and guidance is given as to the choice of the three calibration coefficients the model requires, namely f, λ and Γ representing friction, eddy viscosity and secondary flow respectively.

Finally, physical modelling has been undertaken on compound channels with skewed floodplains in addition to a full review of the work undertaken at a larger scale in the Flood Channel Facility. As a result appropriate expressions for shear force and apparent shear forces acting on the horizontal and vertical interfaces have been established.

TO MY FAMILY

Acknowledgements

Although a PhD constitutes a period of individual study, a number of people have impacted on it directly and indirectly and without them this piece of work would not have been possible.

Firstly, I would like to thank my supervisors Professor D.W. Knight and Doctor M. Sterling who have guided and supported me over the years in addition to providing technical knowledge and expertise.

I also have to thank Professor D.A. Ervine who encouraged and supported me through my undergraduate degree and in my application to undertake further studies. I am also grateful for the assistance he provided to me throughout my PhD.

A number of colleagues have provided assistance and include Dr. S. Atabay, Dr. C. McGahey, Dr. M.Omran, Dr. B. Rezaei and Mr. S. Shariffi. A special mention goes to Mr. M. Vanderstam for his assistance in the construction and use of the technical apparatus.

Family and friends have played the most important role. Special thanks goes to Mrs. D. Rambelli, Dr. S. Kharha and Ms. F. Brown for keeping me sane. Also, special recognition goes to Gavin Laight for his love and support, and to his family for being a family to me away from home.

The biggest thank-you goes to my family-my Dad, Mum and brother, Frank. They have loved and supported me in so many ways and for that I am eternally grateful.

TABLE OF CONTENTS

PART 2-COMPOUND CHANNELS

LIST OF TABLES

LIST OF FIGURES

NOMENCLATURE

Latin alphabet

a	Constant
a_i	Element (sub) area
A	Cross-sectional area
ASF_H	Apparent shear force on horizontal interfaces
ASF_i	Apparent shear force on vertical interfaces between the main channel and floodplain
b	Half-width of main channel
b	Constant
b_i	Element length
B	Total width of channel
B’	Half of total channel width
c	Constant
C	Chézy coefficient
C_{uv}	Coefficient for sinuosity (Ervine et al., 2000)
d	Constant
dx	Change in length
D	Pipe diameter
D_h	Hydraulic radius of a pipe
Dr	Relative depth
E_s	Specific energy
E_t	Total energy
f	Darcy-Weisbach friction factor

F	Hydrostatic force
Fr	Froude number
g	Acceleration due to gravity
h	Bankfull height
h	Depth of boundary layer
h_e	Energy loss
h_f	Head loss due to friction
h_i	Depth at which a measurement reading was taken
H	Depth of flow
H_e	Energy head
k	von Kármán coefficient
ks	Nikurade's equivalent sand grain
K	Conveyance
K_1	Head loss coefficients based on kinetic energy at beginning of the skewed transition
K_2	Head loss coefficients based on kinetic energy at the end of the skewed transition
K_{12}	Head loss coefficients based on the differences kinetic energy along the skewed transition
ℓ	Mixing length
ℓ_b	Normal distance from the division line to the bed (Yang & Lim, 2005)
ℓ_e	Development length
ℓ_w	Normal distance from the division line to the sidewall (Yang & Lim, 2005)
L	Length between measuring sections

L	Pipe length
M_x	Total momentum in the x-direction
n	Manning's roughness coefficient
n	Number of points
P	Perimeter
P_i	Perimeter of an element
q	Unit flow rate
q	Discharge intensity in k-method (Ervine et al., 2000)
Q	Discharge
q_{cf}	Cross (transverse) flow
Q_i	Experimental (integrated) discharge
Q_m	Actual (measured) discharge
Q_z	Proportion of flow in a given area
R	Hydraulic radius
Re	Reynolds number
R_f	Reaction force
s	Side slope
SF	Shear force
$\%SF_w$	Percentage shear force on the wall
$\%SF_i$	Percentage shear force on each element
S_e	Energy slope
S_f	Friction slope
S_o	Bed slope
S_w	Water surface slope

t	Time
T	Temperature
u	Instantaneous velocity
u’	Velocity fluctuation with respect to time
u_i	Local (adjusted) velocity reading
u_r	Local (un-adjusted) velocity reading
U	Section mean velocity
U_{cf}	Cross-flow (transverse) velocity
U_d	Depth-averaged velocity
$U_{(Hz)}$	Frequency in Hertz at a specific point
u_*	Shear velocity
v	Turbulent fluctuation in y-direction
V	Mean velocity in the lateral direction
V	Volume
w	Turbulent fluctuation in z-direction
W	Mean velocity in the direction normal to the bed
W	Weight
x	Chainage, longitudinal distance
x	Streamwise direction
X*	Non-dimensional variable in Patel’s (1965) calibration of the Preston tube
y	Transverse (lateral) distance
y	Transverse (lateral) direction
y	Distance along sidewall from channel corner (Yang & Lim, 2005)
Y*	Non-dimensional variable in Patel’s (1965) calibration of the Preston tube

z	Direction normal to bed
z	Transverse spanwise distance from channel sidewall (Yang & Lim, 2005)
z_b	Bed elevation
Z	Distance to the centroid

Greek alphabet

α	Angle of division line from Yang & Lim (2005)
α	Energy correction factor
α	Coefficient used in the analytical solution of the SKM
β	Angle of sloping wall from Yang & Lim (2005)
β	Momentum correction factor
β	Parameter in k-method (Ervine et al., 2000)
β	Coefficient used in the analytical solution of the SKM
γ	Specific weight of water (=ρg)
γ	Coefficient used in the analytical solution of the SKM
Γ	Secondary flow parameter
δ	Angle of division line from Yang & Lim (2005)
Δ	Change/difference
Δ_b	Bed roughness (Yang & Lim, 2005)
Δh	Pressure head
ΔP	Pressure difference
Δ_w	Sidewall roughness (Yang & Lim, 2005)
Δx	Change in length

ε Rate of dispersion of κ

ε_{yx} Depth averaged eddy viscosity

η Coefficient used in the analytical solution of the SKM

θ Angle of skew (relative to centreline of main channel)

θ Angle of manometers

κ Turbulent kinetic energy

λ Dimensionless eddy viscosity

μ Coefficient used in the boundary conditions of the SKM

μ Dynamic viscosity

μ_t Turbulent viscosity

ν Kinematic viscosity

ξ Local depth

ρ Density of water (1000kg/m^3)

σ Degree of sinuosity

Σ Sum

τ_b Boundary shear stress

τ_b Boundary shear stress on the bed

τ_{exp} Measured boundary shear stress

τ_o Theoretical boundary shear stress

τ_w Boundary shear stress on the wall

τ_{yx} Reynolds shear stress in the x-direction on the plane perpendicular to the y-direction

τ_{2D} Two-dimensional value of the average boundary shear stress

ψ	Coefficient used in alternative method for dealing with secondary flows and planform vorticity in SKM
ψ	Factor for adjusting measured discharge to the actual discharge
ω	Coefficient used in the analytical solution of the SKM

Subscripts

b	bed
cf	cross-flow
d/s	Downstream section
e	Error
FCF	Flood channel facility
FP	Floodplain
g	Global (friction factor)
H	Horizontal
i	Adjusted point measurements
IB	Inbank
l	Local (friction factor)
l	Cross-flow interface
L	Left
LDA	Laser doppler anemometer
LFP	Left floodplain
MC	Main channel
R	Right
RFP	Right floodplain

r	Raw, non-adjusted measured values
u/s	Upstream section
V	Vertical
w	Wall
z	Zonal

Acronyms

ASF	Apparent shear force
CAES	Conveyance and Afflux Estimation System
COHM	Coherence method of Ackers
DCM	Divided Channel method
EDM	Exchange discharge method
EMF	Electro magnetic flow meter
LDM	Lateral distribution method
Mom	Momentum
MPM	Mini propeller meter
RANS	Reynolds averaged Navier-Stokes equation
SKM	Shiono and Knight Method

CHAPTER 1-INTRODUCTION

When you put your hand in a flowing stream, you touch the last that has gone before and the first of what is still to come. Leonardo da Vinci

1.1 Introduction

From source to sea, rivers play an integral part in the day to day functioning of our planet. Existence would not have been possible, at least not in the forms we know, unless there was a plentiful supply of fresh water. Water is necessary for the most basic of needs and for this reason, people have always flourished where there has been a ready supply of water. Rivers can mean a variety of different things to different people. They can bring prosperity and hardship. They give life, but in the worst of cases can take it in a second. Hence, the flow in natural rivers and man made channels and conduits has been of great interest throughout the ages. Historically, settlements have developed and prospered when in close proximity to a fluvial system; examples include the Egyptians and Mesopotamians which prospered due to the "fertile crescent". The Rivers Tigres, Euphrates and Nile were within the "fertile crescent" which was a crescent shaped area within the Middle East which flourished culturally and economically which gave it its nickname of "the cradle of civilisation".

The River Nile was the lifeblood of ancient Egypt, and is still today. It provides food, water, transportation and leisure. For this reason, the Nile was formally used to determine the strength of the Egyptian economy. The Egyptians took detailed measurements of the depth in the river using nileometers and linked the level to taxation; as the Nile rose, taxes rose because it was assumed farmers would produce

more, there would be more river traffic and overall the country was healthier, examples of the Nileometers are shown in **Figures 1.1a** and **1.1b.** The Nile today is used mainly for tourism and transportation, but upstream from Cairo (**Figure 1.1c**) it is still used for irrigation.

Figure 1.1 (a, b and c)-Nilometer at Cairo, Nilometer at Aswan and a view of the Nile from Cairo

Similarly, the Rivers Tigress and Euphrates were paramount in Mesopotamia, named from the Greek for "the land between two rivers". The Mesopotamians became highly adept at irrigation of land in addition to water control devices such as dams and aqueducts.

It is no different today; great cities such as London, Paris and Prague have all centred on a river. In other parts of the world, many tribes still follow the patterns of rivers; when the river floods the people move to safer ground, when it is at a lower level the people return.

In the developed world, we tend to see watercourses as amenities, but there is increasing development on floodplains resulting in the loss of attenuation, realignment of the channel, the creation of flood alleviation channels and geomorphological changes. Therefore, there is increasing reliance on fluvial modelling within industry, especially with the increased incidence of flood events. The summer 2007 floods saw rainfall of 4-6 times the average for previous years (Pitt, 2007). Flooding accounts for almost a third of all natural disasters in the world (Berz, 2000) but over half the fatalities, as can be seen in **Figure 1.2**.

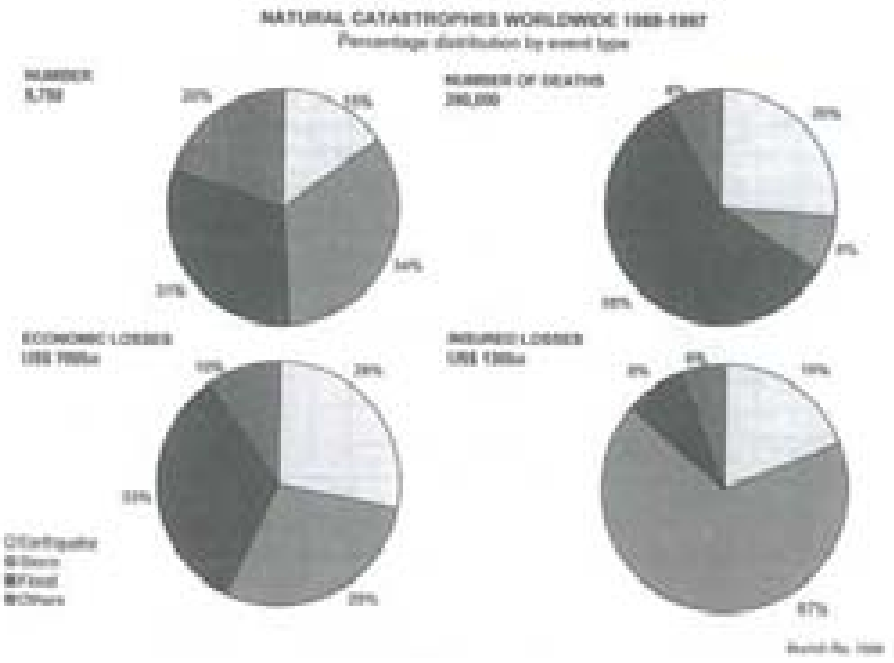

Figure 1.2-Natural catastrophes worldwide, 1988-1997 (from Berz, 2000)

This results in growing costs to the insurance industry (there were 180,000 claims directly arising from the summer 2007 floods (Pitt, 2008)). In 2007, the cost of the summer floods in the United Kingdom was estimated at £3bn (Tibbetts, 2007). In the 2007 Interim Review into the flood events of 2007, Sir Michael Pitt suggested that the

flooding in the UK was of such importance that it should be treated as seriously as terrorism. Within Europe, flooding accounted for 10% of worldwide flooding, but resulted in 35% of the overall cost (**Figure 1.3**).

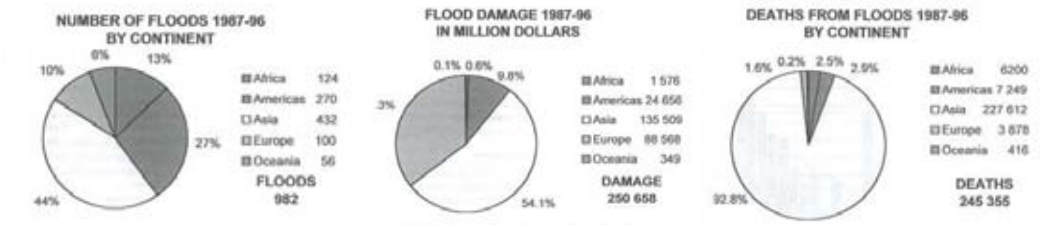

Figure 1.3-Number of floods by continent, 1987-1996 (Berz, 2000)

For the reasons identified above, every development in the United Kingdom has to undertake a flood risk assessment (FRA) and it is important that this is carried out accurately. In order to do this, it is important that the behaviour of flow, both inbank and overbank is understood physically and accurately modelled.

The Environment Agency for England and Wales (EA) have begun to move away from traditional hard engineering solutions such as culverting watercourses which are within development land to softer engineering. A greater importance has been given to the improvement of habitat and the river as a whole. This can involve the realignment of a channel or the creation of a flood alleviation channel. Both of which require an accurate model to compute the velocity and boundary shear stress. This information is required by ecologists to assess the impact on fish and other wildlife, and by geomorphologists who investigate the risk of erosion and effects on vegetation or possible paths of flow. Often, distant flood banks are used to allow parks to be

built which allows the floodplain to be multifunctional, without compromising the housing areas.

There are a number of modelling tools available (see Chapter 2) to aid our understanding with respect to flooding. However, each tool is built on a number of assumptions which in some cases are questionable. Traditionally, modelling has been divided into two categories; numerical modelling and physical modelling.

1.2 Numerical modelling tools

Traditionally, the modelling of flow in rivers has been undertaken using a simple one-dimensional model. Popular models used within industry include ISIS, MIKE 11, HEC-RAS and Infoworks RS. These 1D models are unable to give accurate predictions of velocity across the cross-section. Although these simple modelling packages are still commonplace, there is now a move to use a one-dimensional model when inbank flow occurs and two-dimensional when out of bank or a fully 2D model, for example ISIS/TuFlow or Mike 21. These models add to the complexity of the task, require more data and take longer to process.

Quasi 2D models, such as the Shiono and Knight Method, offers a middle ground in terms of modelling capabilities. This method incorporates some 3D elements, such as secondary flow, which enable the user to obtain accurate discharge data as well as lateral distributions of depth-averaged velocity and boundary shear stress without the complexity of a fully 2D or 3D program. This method can be applied to any river

section using a spreadsheet application, but has also been incorporated into the Conveyance and Afflux Estimation System.

The Conveyance and Afflux Estimation System, CAES, (further details available from www.river-conveyance.net) offers a quasi-2D solution to the depth-averaged form of the Reynolds Averaged Navier-Stokes (RANS) equations. This model is stand alone (and imbedded into ISIS) to allow the modeller to interrogate specific cross-sections of interest within a river reach. The conveyance generator offers a quick method of computing depth-averaged velocity profile and boundary shear stress distribution for any cross-section and can also be used to compute the stage-discharge relationship. CAES is based on the Shiono and Knight Method (SKM) when the sinuosity is equal to 1.0, but has some simplifications made to allow modelling of meandering channels. These simplifications include empirical relationships between velocity and sinuosity by the introduction of k-factors and depth to eddy viscosity and secondary currents (DEFRA/EA, 2004). CAES has been based on overbank flow regimes.

However, as rivers are inbank for the majority of the time, it is important that they are modelled accurately. This thesis considers the application of a quasi-2D model to inbank flow with both homogeneous and heterogeneous roughness.

1.3 Physical modelling

There are a number of studies into inbank and overbank flows, but these tend to examine flow in prismatic channels i.e. where the geometry of the cross-section does

not change along the length of the channel. In the case of two-stage channels (where there is a clearly defined main channel which carries a low discharge all of the time and floodplain(s)) which are designed to carry increased flow during flood events (Rameshwaran & Willetts, 1999), the modelling undertaken has largely been concerned with straight or fully meandering geometries with the floodplains being of constant width.

However, in today's development driven world, there are more floodbanks being constructed which impose a form onto the floodplain which results in floodplains which are at an angle to the main channel (herein termed skewed). There are only a limited number of experiments on these skewed channel forms. This thesis extends the limited body of evidence available with respect to skewed channels through a series of physical experiments. These experiments also offer a cross-over between prismatic channels and fully meandering experiments.

In order to extend and develop the current understanding with respect to the hydrodynamic behaviour of flow in simple and skewed channels, both inbank and overbank flows will be addressed. To aid this understanding, this thesis is divided into two parts which deal with each problem individually. This division is purely for presentation purposes since it is acknowledged that in reality a holistic perspective is required for river modelling.

1.4 Aims, objectives and outline of Part 1

Part 1 of this thesis investigates the application of the SKM to inbank flows and also examines the model's ability to accurately model the channel when there is heterogeneous roughness. The objectives of this section are to:

- Apply the SKM to inbank flow in rectangular and trapezoidal channels with homogeneous roughness;
- Investigate the variation in model coefficients and develop a set of rules for modelling inbank flows with homogeneous roughness with a limited number of panels;
- Compute the lateral variation of depth-averaged velocity and boundary shear stress;
- Compute the total discharge and percentage shear force on the walls, and how they vary with stage;
- Apply the SKM to inbank flows with heterogeneous roughness and investigate the variation of lateral distributions of depth-averaged velocity, boundary shear stress, discharge and percentage shear force on the wall, followed by a comparison with the homogeneous roughness cases.

To this end, the following chapter structure has been adopted:

Chapter 2 gives a review of literature on river hydraulics and identifies the knowledge gaps. It also reviews modelling techniques and more specifically, the Shiono and Knight Method.

Chapter 3 applies the SKM to simple channels with homogeneous, smooth, roughness. The method has been applied to both rectangular and trapezoidal channels. Relationships between depth and the coefficients used within the model have been proposed.

Chapter 4 also applies the SKM to simple trapezoidal channels, but considers the case of heterogeneous roughness in the form of rough walls and a smooth bed.

1.5 Aims, objectives and outline of Part 2

Part 2 investigates non-prismatic flow conditions; more specifically skewed floodplain flows and the effect of an imposed geometry on the flow in both the floodplains and the main channel. The objectives are:

- Undertake a critical analysis of available skewed channel data;
- Carry out a thorough re-assessment of the Flood Channel Facility (FCF) data;
- Undertake a series of skewed channel experiments, measuring water surface profiles, point velocity, depth-averaged velocity and boundary shear stress within the transition;
- Perform force-momentum balances for both the FCF and Birmingham data;
- Understand the flow mechanisms in skewed channel flow.

In order to fulfil the above objectives the following structure has been adopted:

In **Chapter 5**, a literature review has been completed and this focuses on overbank flow mechanisms and skewed channel data.

Chapter 6 gives details on the apparatus used and the procedures followed during the skewed channel experiments undertaken at The University of Birmingham. Much of the information contained herein is also applicable to the FCF experiments.

In **Chapter 7** a thorough review of the FCF skewed channel data carried out by Elliot and Sellin (1990). The patterns of isovels and depth-averaged velocity have been analysed in addition to the boundary shear stress profiles. Force-momentum balances have also been carried out and an analysis of the resistance data.

Chapter 8 details the skewed channel experiments undertaken by the author at The University of Birmingham. These experiments measured the velocity and boundary shear stress within the channel. This chapter also describes the analysis of this data (such as the force-momentum balances) and compares the results to that of Elliot and Sellin (1990) in addition to Atabay's (2001) and Rezaei's (2006) studies (also undertaken at The University of Birmingham) on asymmetric flow and converging flow respectively.

1.6 Details and outline of summary chapters

Chapter 9 consolidates the work undertaken in Parts 1 and 2. It gives guidance on modelling inbank flows in smooth and heterogeneously roughened channels, together

with a summary of the key findings of the experimental studies on overbank flows in compound channels with skewed floodplains.

Chapter 10 summaries the key findings of this research, the practical applications of the studies undertaken and recommendations for future work.

PART 1-SIMPLE CHANNELS

CHAPTER 2-LITERATURE REVIEW ON FLOW IN SIMPLE CHANNELS

It takes a great deal of history to produce a little literature. Henry James (1843 - 1916)

2.1 Introduction

This chapter provides an overview of previous research undertaken in the field of open channel hydraulics. A review of flow features and energy transfer mechanisms is given in addition to an assessment of modelling methods. Although this literature review is aimed at flow in simple channels, much of what is contained herein is also applicable to flow in compound channels. A more specific review of compound channel research (with emphasis on skewed channels) has been given in Chapter 5.

It is important that inbank flow (i.e. flow within the main channel) is modelled accurately, since flow is present in the main channel all of the time and it is only during flood events that flow is prevalent on the floodplain(s). Many of the flow mechanisms that occur in simple channels also occur in compound channel flow, although in some cases these flow features can be dominated or drowned out by stronger mechanisms due to the overtopping of the flow from the main channel onto the floodplains. Simple rectangular channels in particular have interesting, albeit complex, secondary flow cells. This chapter intends to detail flow mechanisms common to both simple and compound channels, but does not intend to give an exhaustive explanation, as this can be found in a variety of textbooks (Chang, 1988; Chow, 1959).

2.2 Flow mechanisms

It is vital to understand flow behaviour before physical or numerical modelling is undertaken as the structure of flow affects the energy dissipation, boundary shear stress, resistance to flow and therefore the overall conveyance (Knight, 2001).

The flow features are classed here as energy transfer mechanisms as they convert energy from one form to another via the development of vortex structures over various scales. Vortices can be created in open channel flow due to boundary shear, vertical and horizontal interface shear, transverse currents and coherent structures, but can also be created from the geometry of the channel, the depth of flow and the nature of flow (i.e. laminar or turbulent).

2.2.1 Boundary shear and turbulence

Flow may be considered as being laminar, transitional or turbulent, and open channel flow is no exception. In laminar flow there are no turbulent fluctuations with respect to time, within the transition zone there are turbulent 'bursts' and within the turbulent zone there are frequent, random turbulent fluctuations. Vortices can be induced either by boundary shear, bursting phenomena or a combination of both.

Boundary shear due to surface roughness may cause the formation of vortices (Nezu & Nakagawa, 1993) as can be seen in **Figure 2.1a** and **2.1b**. In **Figure 2.1a**, the radius of the apparent roughness elements tend towards zero. The streamlines adjacent to the bed run parallel to it and therefore, separation is unlikely to occur, this is termed smooth turbulent flow. Where roughness elements penetrate outwards from

the viscous sub layer, as in **Figure 2.1b**, the boundary vortices adjacent to the bed tend to accelerate over the irregularities and come to a standstill between roughness elements which results in flow separation as the velocity is reduced to zero (McGahey, 2006). This flow condition is termed "hydraulically rough" turbulent flow and is present in most rivers.

A second type of boundary turbulence is due to "bursting phenomena", which is where the boundary is dominated by a sequence of events such as ejections and sweeps (Nezu & Nakagawa, 1984). This can occur on both smooth and rough bed and occurs randomly due to local uplift of fluid in the area of low velocity parallel to the channel bed, sudden oscillations, bursting and ejection (Kline et al., 1967). This can be seen in **Figure 2.1**, where high velocities move close to the boundary which intensifies near wall vortices by lateral spanwise stretching and generating new vortices which is subsequently transported away by the ejections (McGahey, 2006).

Turbulence has no one definition, although many have tried. Therefore, herein an overview will be given of possible definitions of turbulence and some background to behaviour induced by turbulence. If the reader wishes to expand on these concepts they should consult one of the many works on turbulence.

Chow (1959) describes it as "*…flow is turbulent if the viscous forces are weak relative to the inertial forces. In turbulent flow, the water particles move in irregular paths which are neither smooth nor fixed but which in the aggregate still represent the forward motion of the entire stream.*" Whereas others, such as Johansson &

Alfredsson, 1986, prefer not to define it and simply state "*Existing theories are unable to give detailed and quantitative explanations of the mechanism of turbulence generation…*" Similarly Munson et al. (2002) state "*…turbulent flow is a very complex process. Numerous persons have devoted considerable effort in attempting to understand the variety of baffling aspects of turbulence. Although a considerable amount of knowledge about the topic has been developed, the field of turbulent flow still remains the least understood area of fluid mechanics*." They go on to say that "*A simplistic way of thinking about turbulent flow is to consider it as consisting of a series of random, three-dimensional eddy type motions….These eddies range in size from very small diameter (on the order of size of a fluid particle) to fairly large diameter (on the order of the size of the object or flow geometry considered). They move randomly, conveying mass…promotes mixing and increases the transport of momentum*".

It is known that turbulent flows exhibit unsteady, irregular and random behaviour and contain eddies of unpredictable motion. When defining the approximate location when a fluid changes from laminar flow to turbulent the Reynolds number (*Re*) is used. In pipe flow for example, a fluid with a *Re* value of less than 2000 is considered laminar whereas when it is in excess of 4000 it is considered to be fully turbulent. Similarly on plate flows, the transition between laminar and turbulence begins when *Re* is approximately 500,000. The Reynolds number is the effect of viscosity relative to inertia and is defined as Equation 2.1 for pipe flow.

$$\mathrm{Re} = \frac{UD}{\upsilon} \qquad \textbf{2.1}$$

Where, U is the mean velocity, D is the pipe diameter and υ the kinematic viscosity. However, in open channel flows, it is taken that D=4R $\left[R = \frac{A}{P} = \frac{\pi D^2}{4\pi D} \right]$, where R is the hydraulic radius, A is the cross-sectional area and P the wetted perimeter, hence Equation 2.2 is applicable.

$$\mathrm{Re} = \frac{4UR}{\upsilon} \qquad \textbf{2.2}$$

In open channel flow, laminar flow generally exists if Re<500 and turbulent flow if Re>12,500. It should be noted that these are approximate guidelines, although the transition is usually taken as 2000. Generally in open channel flow the viscosity is low resulting in a larger Reynolds number, hence, most open channel flows are not within the laminar region.

In turbulent flows, the chaotic behaviour is prevalent in velocity, pressure and shear stress and is characterised by random three-dimensional eddies. In turbulent flow the instantaneous velocity (u) is the sum of the mean velocity (U) and the fluctuating portion of the velocity, u', the time varying part of the velocity which differs from the average value (Equation 2.3).

$$u = U \pm u' \qquad \textbf{2.3}$$

The velocity fluctuations cause a transfer of momentum generated by shear stresses. These turbulent shear stresses are referred to as Reynolds stresses and as they only occur in turbulent flow they result in increased shear stresses from those found in laminar flow.

2.2.2 Vertical and horizontal interfacial shear

Vertical and horizontal vortices may be induced in straight channels due to the steep velocity gradients at the main channel and floodplain interface as shown in **Figure 2.2** for overbank flow. Vortices induced by vertical interfacial shear tend to be small scale, with the eddy structures being smallest at the floodplain bed and gradually expanding through the water surface.

Horizontal interfacial shear is induced by two flows which are acting in different directions, such as the case in meandering or skewed channel flows, as shown in **Figure 2.3** and **2.4**. Shiono & Muto (1998) found that at low relative depths, Dr=(H-h)/h where *H* is the total flow depth and *h* the bankfull depth, (e.g. Dr=0.15), the out of bank flow in the main channel tended to follow the main channel flow direction, whereas at high relative depths (e.g. Dr=0.25), the out of bank flow was parallel to the floodplains. This phenomenon is further discussed in Section 5.3.2.

2.2.3 Transverse (secondary) currents

The anisotropy of turbulence causes secondary currents to be generated and modified. This anisotropy is caused by the boundary conditions of the bed, sidewall, the free surface as well as the aspect ratio and channel geometry (Tominaga et al., 1989). These secondary currents are approximately only 2-3% of the mean streamwise velocity which makes them extremely difficult to measure.

The pattern of secondary currents is affected by the free surface and in rectangular prismatic channels, the free surface causes the secondary currents to flow toward the side wall along the horizontal plane at about y/H=0.6 (Tominaga et al., 1989). A pair of vortices separated by the horizontal plane is generated near the sidewall, hence, the upper vortex is termed the "free surface vortex" and the lower side vortex is called the "bottom vortex". At large aspect ratios, the spanwise scale of the free surface vortex increases and reaches about 2*H*. The bottom vortex is confined to less than about *H* in open channel flows. The pattern of vortices differs in open channels to closed conduit flows as can be seen in **Figure 2.5**.

In trapezoidal channels, the pattern of secondary flow cells is quite different from that of rectangular channel flows. Tominaga et al. (1989) found that the patterns of longitudinal vortices depend on the angle of the sidewall. They investigated the pattern of these vortices in three trapezoidal channels with varying side slopes of 60^o, 44^o and 32^o, the results of which are shown in **Figure 2.6**. Here they named the vortices A, B and C which correspond to the bottom vortex, the longitudinal vortex and the free surface vortex respectively. As the side slope angle reduces from 90^o,

vortex B is generated, vortex C is weaker and vortex A develops into the depth-scale vortex. In trapezoidal channels, the maximum value of the secondary currents is of the same magnitude as that in rectangular channels, but the pattern differs.

2.2.4 Coherent structures

Coherent structures, also known as large planform eddies, are caused by shear instability in regions where there is high velocity gradient, for example, at the interface of the main channel and floodplain (Ikeda & Kuga, 1997). Ikeda et al. (2001) carried out a series of laboratory experiments for compound channels of varying relative depth. At low relative depths (Dr=0.180), the presence of planform eddies can be clearly observed (**Figure 2.7**), however, at higher relative depths (**Figure 2.8**, Dr=0.344), the vortices have been replaced by intermittent boils.

Elliott & Sellin (1990), observed in skewed compound channels the slower moving flow on the narrowing floodplain moves over the main channel flow in a different flow direction which resulted in helical secondary currents developing along the centreline of the main channel. The enlarging floodplain experienced increased velocity due to the faster moving main channel flow entering this region. The overall effect was a reduction in the conveyance when it was compared to the equivalent straight channel case.

Richardson (1922) summarises the pattern of the breaking up of eddies as "…*big whorls have little whorls, which feed on their velocity; and little whorls have lesser whorls, and so on to viscosity*".

2.2.5 Other causes of vortices in channels

Vortices can also be induced due to the natural form of the channel or by man-made obstructions. These include:

- Asymmetrical channels have different channel circulations as the floodplain only affects one side of the main channel.
- Berms affect the structure of secondary flows and their orientation with depth.
- Braided channels often have a common floodplain; this may result in the floodplain flow structures interacting causing further instability and flow separation.
- Natural channels tend to have large width to depth ratios which results in non-homogeneous turbulence, hence the flow is affected by small-scale wall turbulence (scaled by depth) and free turbulence from the large-scale eddy structures which have lateral freedom (Ikeda, 1999).
- Vegetation may reduce or remove the vertical interfacial turbulent exchanges as it acts as a streamwise barrier between the main channel and floodplain.
- Structures such as bridges and weirs may generate a "vortex street" which may affects the downstream reach.

2.2.6 Boundary shear stress

Boundary shear stress has been researched for many years as it is an important factor in flow structure in open channels. Factors including the channels geometry (both cross-sectional and longitudinal), the variation of roughness and sediment concentration all influence the boundary shear stress distribution.

A simple technique was developed by Preston (1954) for measurement of boundary shear stress which involves the placement of a Pitot tube against a boundary and a second static tube located in the centre of the channel. This was originally developed for smooth boundaries in a turbulent boundary layer using a Pitot tube in contact with the surface. This method assumes the boundary shear stress is related to the velocity distribution near to the wall (law of the wall). Assessment of the velocity distribution near the wall is empirically inferred from the differential pressure between the Pitot tube and the static pressure.

The Preston tube technique does have some limitations though. Patel (1965) found that the Preston tube overestimated the skin friction in severe favourable and adverse pressure gradients. It has also been found that in order to take an accurate reading of static pressure none of the fluid's kinetic energy can be converted to a pressure rise at the point of measurement. Therefore a smooth hole with no imperfections must be used and no additional pressure should be applied to either tube. Great care must be taken in the lateral positioning both the static and dynamic tubes as any misalignment will produce a non-symmetrical flow field which can induce errors. It is unlikely in practice that the tube positioning will be directly into the flow, however yaw angles of between 12° to 20° (depending on the particular probe design) give typical errors of less than 1% from the perfectly aligned values. In order to assist the user, direction finding static Pitot tubes are available which have 3 small holes drilled into a small circular cylinder, one in the centre and one either side which are connected to three pressure transducers. The cylinder is rotated until the pressures in the two side holes are equal with the central tap measuring the pressure (Munson et al., 2002). In the

skewed channel, the Pitot tube was aligned parallel to the centreline of the main channel and near the walls of the floodplain it was aligned in the direction of the floodplain wall, as discussed in Section 6.2.7.

Following Patel's calibration many investigators have studied boundary shear stress distributions in different channel geometries using the Preston tube. Myers and Elsawy (1975) studied boundary shear stress distributions in compound channels with a single floodplain and observed distorted boundary shear stress distributions. Myers (1978) studied momentum transfer mechanisms and found the apparent shear stresses were significantly greater than those exerted on a solid boundary or floodplain wall at the interface. McKee et al. (1985) confirmed Myers momentum balance approach using the Laser Doppler Anemometry (LDA) method.

Rajaratnam & Ahmadi (1981) demonstrated that the boundary shear stress reduces from the centre of the main channel towards the interface of the main channel and floodplain where it increases sharply. They also found that the boundary shear stress distribution levels off along the main channel before reducing at the walls. They also concluded that the effect of the floodplain reduces the boundary shear stress in the main channel which is a direct effect of the reduction of velocity in the main channel due to the slower moving floodplain flow.

Nikuradse in 1926 observed distortions in isotach (lines of equal velocity) patterns in turbulent flow but it was Prandtl (1926) who suggested that turbulent velocity fluctuations in regions of isotach curvature causes secondary flow (Gessner, 1973).

This can be seen in **Figure 2.9** and typical secondary flow streamline patterns are shown in **Figure 2.10**. However, it was work carried out by Knight and Patel in the 1980's which suggested a link between the perturbations in shear stress and the location of secondary cells and also that the number of cells (**Figure 2.11**) increased with aspect ratio.

Tominaga et al. (1989) and Knight & Demetriou (1983) stated that the shear stress distribution is significantly affected by secondary currents; the boundary shear stress increases where the secondary currents flow towards the wall and decrease when they flow away from the wall. In addition, Rhodes & Knight (1994) suggest that the bank slope has a significant effect on boundary shear distributions at the interface of the main channel and floodplains.

The calculation of boundary shear stress from experimental results using Preston's (1954) method in conjunction with Patel's (1965) calibration is detailed in Section 6.2.7.

Hence, by using a model which is able to replicate the boundary shear stress distributions across the channel, river engineers will be able to more accurately determine sediment transport, bank erosion and river morphology.

Flow resistance was classified into four components by Rouse (1965);

i. Surface or skin friction

ii. Form resistance or drag

iii. Wave resistance from free surface distortion

iv. Resistance associated with local acceleration or flow unsteadiness

Here, the first two will be concentrated on as these are considered to be the most significant for the work presented herein.

2.3 Boundary layer theory

Flow resistance is closely related to boundary layer theory, therefore a brief review has been provided.

In uniform open channel flow, the boundary layer is fully developed and extends from the channel boundary throughout the flow depth, including a viscous laminar sub-layer adjacent to the boundary, a transitional zone characterised by both viscous and inertia effects and a turbulent zone where the inertia forces dominate (McGahey, 2006). The boundary layer formation stages can be seen in **Figure 2.12**. The differences between laminar and turbulent flow was demonstrated by Reynolds (1883), which can be seen in **Figure 2.13**.

The general expression for turbulent flow, which relates the mean rate of deformation to the turbulent stresses was proposed by Saint-Venant (1843) and Boussinesq (1877) and takes the form (McGahey, 2006; Rutherford1994):

$$\tau_{yx} = -\rho\overline{v'u'} = (\mu + \mu_t)\left(\frac{\partial v}{\partial x} + \frac{\partial u}{\partial y}\right) \qquad \textbf{2.4}$$

where, τ_{yx} is the Reynolds stress, μ and μ_t are the dynamic and turbulent viscosities (Ns/m^2) respectively, *u'* and *v'* are the fluctuations from mean velocity in the *x* and *y* directions respectively and ρ the density of fluid.

Prandtl (1925) developed the "mixing length" theory and related shear stress, τ_o, in terms of the velocity gradient, $\frac{du}{dz}$ and mixing length, ℓ:

$$\tau_o = \rho \ell^2 \left(\frac{du}{dz} \right)^2 \qquad \textbf{2.5}$$

The mixing length can be related to the distance from the boundary by $\ell = \kappa H$, where *H* is the depth of the boundary layer and κ is the von Kármán coefficient, which has been experimentally determined as 0.41 for clear water. Prandtl further assumed that for near-wall conditions the shearing is constant giving:

$$\frac{du}{dy} = \frac{1}{\kappa} \sqrt{\frac{\tau_o}{\rho}} \frac{1}{H} \qquad \textbf{2.6}$$

where $\sqrt{\frac{\tau_o}{\rho}}$ is the shear velocity, u_*.

Integrating Equation 2.6 and setting the constant of integration for smooth surfaces as ν/9u* (as based on Nikuradse's 1923 data) and for rough surfaces as k/30 gives the universal laws for smooth and rough turbulent flow (Chow, 1959), then:

$$\frac{U}{u_*} = 5.75 \log\left(\frac{9u_* H}{v}\right) \quad \text{(smooth)} \qquad \textbf{2.7}$$

$$\frac{U}{u_*} = 5.75 \log\left(\frac{30H}{k}\right) \quad \text{(rough)} \qquad \textbf{2.8}$$

where, ν is the kinematic viscosity and k is similar to Nikurades's equivalent sand size, k_s.

Rouse (1959) demonstrated that these two universal laws can be approximated by a single logarithmic function of the form:

$$\frac{U}{u_*} = c_1 \log y^* + c_2 \qquad \textbf{2.9}$$

Where c_1 and c_2 are constants for a given channel and y^* (=u*y/ν) is similar to a Reynolds "shear" number. These equations can be simplified further by a power law function:

$$\frac{U}{u_*} = c_3 \left(y^*\right)^m \qquad \textbf{2.10}$$

Where c_3 is a constant and the exponent m is of the order $\frac{1}{12}$ to $\frac{3}{12}$ (Chen, 1991).

2.4 Resistance in open channel flow

Resistance has been investigated from as early as 1768 when Antoine Chézy first postulated the, now, well known Chézy equation which states that:

$$U = C\sqrt{RS_f} \qquad \textbf{2.11}$$

Where, U is the average velocity in a given cross-section, R the hydraulic radius, C is the Chézy coefficient and S_f the friction slope.

Darcy (1857) and Weisbach (1845) undertook studies into incompressible flow in pipes and found that:

$$h_f = \frac{fLU^2}{2gD} \qquad \textbf{2.12}$$

where, h_f is the head loss due to friction, L the pipe length, g the force due to gravity, f the Darcy-Weisbach friction factor and D the pipe diameter.

This can be applied to open channel flow by noting that $\frac{h_f}{L}$ is equal to the friction slope, S_f, which is approximately equal to the bed slope S_o. In order to apply Equation 2.12 to non circular sections, it is convenient to replace D with the hydraulic radius,

and since for circular pipes, R=$\frac{D}{4}$, for non-circular sections, the Darcy-Weisbach equation becomes:

$$f = \frac{8gRS_o}{U^2} \quad \textbf{2.13}$$

For Equation 2.12, when laminar flow occurs

$$f = \frac{64}{\mathrm{Re}} \quad \textbf{2.14}$$

and when turbulent flow occurs;

$$f = \frac{0.3164}{\mathrm{Re}^{\frac{1}{4}}} \quad \textbf{2.15}$$

(from the work by Blasius (1913) on smooth pipes).

Prandtl and Nikurase later carried out work on smooth and artificially roughened pipes and found three zones of turbulent flow as discussed below (Nalluri & Featherstone, 2001).

i. Smooth turbulent zone in which *f* is a function of the Reynolds number only

$$\frac{1}{\sqrt{f}} = 2\log\frac{\mathrm{Re}\sqrt{f}}{2.51} \quad \textbf{2.16}$$

ii. Transitional zone where *f* is a function of *k/D* (relative roughness) and Re

iii. A rough turbulent zone where *f* is a function of *k/D* only

$$\frac{1}{\sqrt{f}} = 2\log\frac{3.7D}{k} \qquad \textbf{2.17}$$

Combining Equations 2.16 and 2.17 (known as the Kármán-Prandtl equations), results in the Colebrook-White equation (1939), as given by Equation 2.18.

$$\frac{1}{\sqrt{f}} = -2\log\left(\frac{k}{3.7D} + \frac{2.51}{\mathrm{Re}\sqrt{f}}\right) \qquad \textbf{2.18}$$

The Manning equation (1889) is probably one of the best known resistance equations and is widely used in practice. This was derived from the Chézy equation by taking $C = \frac{R^{1/6}}{n}$, resulting in:

$$U = \frac{R^{2/3}}{n}\sqrt{S_o} \qquad \textbf{2.19}$$

where, n is the Manning coefficient of resistance.

A comprehensive list of Manning 'n' values for a number of channel types is available in Chow (1959). Guidance on individual values of Manning's n and also composite values based on vegetation, channel material and bed forms/irregularities has been incorporated in the Conveyance and Afflux Estimation System, CAES, (www.river-conveyance.net). This helps the user to identify their channel type via a

series of photographs and gives upper and lower bounds to help identify the uncertainties in roughness values.

The Chézy and Manning's equations are still widely used in Europe and the UK, particularly in flow calculations. They have been incorporated into many one-dimensional flow modelling software including, HEC-RAS, ISIS and MIKE 11.

2.5 Conveyance

Conveyance is a quantitative measure of the discharge capacity of a watercourse or channel (Evans et al., 2001). It relates the overall discharge to the slope or gradient of the channel.

A simple definition of conveyance (K) is given by Equation 2.20, and relates the discharge (Q) to the slope (S) and it is assumed that the bed slope, friction (or energy) and water surface slopes coincide.

$$Q = K\sqrt{S} \qquad \textbf{2.20}$$

This is clearly not applicable to non-uniform flow (where the flow characteristics change with distance), and therefore it is beneficial to consider the specific energy (E_s) which is the balance between the potential and kinetic energy.

$$E_s = H + \frac{U^2}{2g} \qquad \textbf{2.21}$$

In order to obtain the conveyance, Equation 2.20 is used, but the slope used is the friction slope, here defined as:

$$S_f = -\frac{d(E_t)}{dx} = -\frac{d(E_s + z_b)}{dx} \qquad \textbf{2.22}$$

Where, E_t is the total energy above datum, dx the change of length and z_b the bed level above datum.

2.6 Modelling techniques

With advancing technology there are increasing complex methods of flow, velocity and shear stress calculation tools. This section examines a number of common techniques ranging from simple one-dimensional equations to complex two- and three-dimensional models. The models and methods reviewed herein is not a complete list, but gives an indication to the variety of methods available. Section 2.7 gives a review of advances in boundary shear stress modelling with an emphasis on inbank flow conditions.

2.6.1 Single channel method (SCM)

This method treats the channel as a single cross-section, regardless of geometry or flow resistance parameters. These simple hand calculations are often based on the Chézy or Manning's equations (the latter is in common use in the UK and is given below in Equation 2.23).

$$Q = \frac{AR^{2/3}}{n}\sqrt{S_o} \qquad \textbf{2.23}$$

However, in natural channels, boundary roughness changes across the channel boundary due to changes in bed material, vegetation or flow obstructions as well as depth. In addition, in heavily vegetated channels the roughness may also vary with velocity as vegetation may bend which reduces the overall roughness (McGahey, 2006). Therefore, a number of approaches have been developed to account for this including Pavlovskii (1931), Horton & Einstein (1933/4) and Lotter (1933).

A single channel method can give a crude approximation to discharge in a channel, but implies that the boundary shear stress is constant over the wetted perimeter which is not true. The total conveyance in the channel may also be overestimated as the model cannot account for secondary flow cells, coherent structures or lateral shearing. This method has been shown by Myers and Brennan (1990) to have significant errors at low overbank flow due to the sudden decrease in hydraulic radius just above bankfull level. To overcome some of these limitations, the divided channel methods were developed.

2.6.2 Divided channel method (DCM)

Divided channel methods try to overcome some of the limitations of the single channel method, but are often based on the Manning's formula and can be quickly calculated by hand.

DCMs divide the channel into a number of zones which have similar flow characteristics, as shown by **Figure 2.14**. These division lines usually coincide with physical boundaries and can be horizontal, vertical or inclined. The flow in each of these zones is calculated by either the Manning's or Chézy equations and summed. This method usually overestimates the total flow within the channel as the momentum exchange between the divisions is not accounted for.

Where there are vertical division lines (which correspond to the bank edge), the vertical interfaces are counted as part of the wetted perimeter of the main channel but excluded from the floodplain wetted perimeter. This is to try to simulate the retardation of the main channel flow due to the slower moving floodplain flows and lateral interfacial shearing, as observed in overbank flows. This approach is not ideal at low overbank flow as the vertical interface is small and has a small overall effect on the calculation, yet in reality, this region exhibits high interaction and energy transfers.

Inclined divisions are based on lines of zero shear stress (Yen & Overton, 1973), i.e. where the velocity gradients and hence momentum exchange is minimum. Typically, these division lines start at the top of the bank and extend out towards the surface at 45°.

The weighted divided channel method (Lambert & Myers, 1998) uses both horizontal and vertical division lines and applies a weighting factor to each division and the

contributions summed. This method is based on empirical factors and has been shown to be able to model compound channels and varying roughness, but is only applicable to prismatic channels.

The coherence method (COHM) by Ackers is a hand calculation which deals with compound channel flow and heterogeneous roughness. This method calculates the flow based on both SCM and DCM methods and the coherence is determined as a ratio of them (i.e. Q_{SCM}/Q_{DCM}), as shown in Equation 2.24.

$$COH = \frac{\sum_i^n A_i \sqrt{\left[\frac{\sum_i^n A_i}{\sum_i^n fP_i}\right]}}{\sum_i^n \left[A_i \sqrt{\frac{A_i}{f_i P_i}}\right]} \qquad \textbf{2.24}$$

It is assumed that the shear stresses between the artificial interfaces in the DCM will be small when compared by the boundary stresses and are neglected in the model. The coherence is always less than unity and a discharge adjustment factor is applied to each zonal flow. The method identifies four distinct regions as follows:

Region 1-Low relative flow depths, interaction increasing with depth

Region 2-Moderate relative flow depths, interaction decreases

Region 3-At high relative flow depths a further interaction occurs

Region 4-Compound channel behaves like a single channel

A total of 22 equations for different scenarios has prevented this method being widely adopted.

DCMs require highly idealised and simplified geometries to compute flow within the channel. These methods are generally only applicable to prismatic channels or mildly skewed channels, but cannot be applied to meandering channels. It is taken that the flow is homogeneous and most methods cannot compute discharge in heterogeneously roughened channels.

2.6.3 Exchange discharge model (EDM)

The exchange discharge model (EDM), was proposed by Bousmar & Zech (1999) and is a one-dimensional model which quantifies momentum transfer between the main channel and prismatic or non-prismatic floodplains. This model is based on two physical concepts:

- Turbulence exchange due to shear layer development
- Geometrical transfer due to cross-sectional changes

This method requires calibration of both turbulent and geometric exchange parameters. This method also requires idealised cross-sectional geometry and is not applicable to meandering channels.

2.6.4 Lateral distribution methods (LDMs)

There are a number of lateral distribution models which are based on the depth-averaged Reynolds Averaged Navier-Stokes equations (RANS), Equation 2.25.

$$\frac{\partial u}{\partial t} + U\frac{\partial u}{\partial x} + V\frac{\partial u}{\partial y} + W\frac{\partial u}{\partial z} = -\frac{1}{\rho}\frac{\partial p}{\partial x} + \mu\left(\frac{\partial^2 u}{\partial x^2} + \frac{\partial^2 u}{\partial y^2} + \frac{\partial^2 u}{\partial z^2}\right) - \left(\frac{\partial u'^2}{\partial x} + \frac{\partial u'v'}{\partial y} + \frac{\partial u'w'}{\partial z}\right) \quad \textbf{2.25}$$

As these methods are derived from fundamental fluid flow equations, they are physically based and theoretically sound. The channel is divided into a number of "panels" and the unit flow rate (or depth-averaged velocity) is calculated at these locations and summed to give the overall discharge in the channel as shown in equation 2.26.

$$Q = \int_0^B q\,dy = \int_0^B U_d\,dA \quad \textbf{2.26}$$

These models are not strictly 1-D or 2-D and are perhaps best described as *a 1-D models with 2-D terms describing 3-D effects*. There are a number of methods which fall into this classification but includes the flood discharge assessment by Wark et al. (1990), Cunge (1980), Vreugdenhill and Wijbenga (1982), Samuels (1985) Wormleaton (1988), Wark et al. (1991), the k-method by Ervine at al. (2000) and the Shiono-Knight method (Shiono & Knight, 1988 & 1990).

Each of these methods has differing assumptions, emphasise the importance of different terms, but all somehow model the processes as opposed to directly evaluating them. The calibration coefficients and turbulence closure model is specific to a given method. A comprehensive review of the above methods can be found in McGahey (2006). A full review of the Shiono and Knight Method (SKM) is given in the following section.

2.6.5 Shiono and Knight Method (SKM)

The Shiono and Knight Method (1988 & 1990), or SKM, is a lateral distribution method based on the RANS equations which calculates the depth-averaged velocity and boundary shear stress laterally across the channel.

At point 'J' (**Figure 2.15**), for steady flow in a prismatic open channel, the equation for the streamwise momentum may be combined with the continuity equation to give:

$$\rho\left[\frac{\partial UV}{\partial y}+\frac{\partial UW}{\partial z}\right]=\rho g S_o+\frac{\partial}{\partial y}(-\rho\overline{u'v'})+\frac{\partial}{\partial z}(-\rho\overline{u'w'}) \qquad \textbf{2.27}$$

where U, V, W are the mean velocity components in the x (streamwise), y (lateral) and z (normal to bed) directions respectively, u', v', w' are turbulent fluctuations of velocity with respect to the mean, ρ is the density of water, and S_o is the bed slope gradient ($S_o = \sin\theta$). See **Figures 2.16** and **2.17** for notation.

The depth-mean-averaged momentum equation can be obtained by integrating Equation 2.27 over the water depth, H, provided $W(H)=W(0)=0$, and is given by Shiono & Knight (1988) in the form:

$$\frac{\partial\left[H(\rho UV)_{\mathrm{d}}\right]}{\partial y}=\rho gHS_o+\frac{\partial H\bar{\tau}_{yz}}{\partial y}-\tau_b\sqrt{1+\frac{1}{s^2}} \qquad \textbf{2.28}$$

in which τ_b is the bed shear stress, s is the side slope (1:s = vertical: horizontal), and

$$(\rho UV)_{\mathrm{d}}=\frac{1}{H}\int_0^H(\rho UV)dz \qquad \textbf{2.29}$$

$$\bar{\tau}_{yx}=\frac{1}{H}\int_0^H(-\rho uv)dz \qquad \textbf{2.30}$$

$$U_d=\frac{1}{H}\int_0^H Udz \qquad \textbf{2.31}$$

The solution of the SKM or other depth-integrated RANS equation, requires a method for approximating the shear stresses for closure. Models which relate the shear stresses to mean flow rate are typically used and termed turbulence closure models. For incompressible flow, the turbulence has been found to decay unless there are shear stresses present. Turbulent stresses have also been found to increase as the mean rate of deformation increased. Boussinesq (1877) proposed that with the onset of turbulence, the Reynolds stresses could be related to the mean rate of deformation by a turbulent or eddy viscosity, as shown by Equation 2.4. Other turbulence closure models are available such as Wormleaton (1988), Cunge et al. (1980), Jones &

Launder (1973) who proposed the k-ε model and there is also the Reynolds stress model which solve for the rate of viscous dissipation.

Using the eddy viscosity approach, shown herein by Shiono and Knight (1990), first proposed by Boussinesq (1877) for dealing with the Reynolds stress term, $\overline{\tau}_{yx}$, then:

$$\overline{\tau}_{yx} = \rho \overline{\varepsilon}_{yx} \frac{\partial U_{\mathrm{d}}}{\partial y} \qquad \textbf{2.32}$$

$$\overline{\varepsilon}_{yx} = \lambda U_{*} H \qquad \textbf{2.33}$$

where λ is the dimensionless eddy viscosity coefficient and $U_*(=\tau_b/\rho^{1/2})$ is the local shear velocity. The local boundary shear stress, τ_b, may be related to the depth-mean velocity, U_d, by use of the Darcy-Weisbach friction coefficient, f, giving

$$\tau_b = \rho \frac{f}{8} U_d{}^2 \qquad \textbf{2.34}$$

$$U_* = \sqrt{\frac{f}{8}} U_d \qquad \textbf{2.35}$$

Then, substituting Equations 2.33 and 2.35 into Equation 2.28 yields:

$$\rho g H S_o - \rho \frac{f}{8} U_b{}^2 \sqrt{1+\frac{1}{s^2}} + \frac{\partial}{\partial y}\left[\rho \lambda H^2 \sqrt{\frac{f}{8}} U_d \frac{\partial U_d}{\partial y} \right] = \frac{\partial}{\partial y}\left[H(\rho UV)_{\mathrm{d}} \right] \qquad \textbf{2.36}$$

Experimental results by Shiono & Knight (1991) show that in overbank flow the shear stress due to secondary flow, $(\rho UV)_d$, varies approximately linearly in certain regions of a channel. Using this concept, the lateral gradient of the secondary flow force per unit length of the channel may then be written as:

$$\frac{\partial}{\partial y}\left[H(\rho UV)_{\mathrm{d}}\right]=\Gamma \qquad \textbf{2.37}$$

where Γ is a dimensionless secondary flow parameter, which is different for different flow regions, as illustrated in **Figure 2.17** for a rectangular channel. Thus Equation 2.28 may be expressed in a simpler form as

$$\tau_b\sqrt{1+\frac{1}{s^2}}=\rho gHS_o+\frac{\partial H\overline{\tau}_{yz}}{\partial y}-\Gamma \qquad \textbf{2.38}$$

This method can be applied to both overbank and inbank flows but is, as yet, limited to prismatic channels. The model is calibrated through the three coefficients; f (friction factor), λ (dimensionless eddy viscosity) and Γ (secondary flow cells). The friction factor can be calculated directly from measured velocity and shear stress data (using equation 2.32) and λ is often taken as 0.07 (Ikeda, 1981) for experimental channels as $\lambda=\dfrac{\overline{\varepsilon}_{yx}}{u_* H}\approx\dfrac{\kappa}{6}=0.068\approx 0.07$ (see **Figure 2.18**); 0.13 which is based on wind tunnel data (Rhodes & Knight, 1995) or 0.24 for natural channels (Cunge et al., 1980). Of the three calibration coefficients, Γ is the most difficult parameter to quantify. Abril & Knight (2004) proposed:

$\Gamma = 0.05\, H\ \rho\ g\ S_o$ for inbank flow **2.39**

$\Gamma = 0.15\, H_{mc}\ \rho\ g\ S_o$ for the main channel during overbank flow **2.40**

$\Gamma = -0.25\, H_{fp}\ \rho\ g\ S_o$ for the floodplain during overbank flow **2.41**

where, H_{mc} and H_{fp} indicate main channel and floodplain depths.

From Shiono & Knight (1988 & 1991), the analytical solution of Equation 2.36 distinguishes between a constant depth domain and a side slope domain as follows:

$U_d = \left[A_1 e^{\gamma y} + A_2 e^{-\gamma y} + k\right]^{1/2}$ for a constant depth domain **2.42**

where, **2.43**

$$\gamma = \sqrt{\frac{2}{\lambda}}\left(\frac{f}{8}\right)^{1/4}\frac{1}{H}\ ;\ \kappa = \frac{8gH\,S_o}{f}(1-\beta)\ ;\ \beta = \frac{\Gamma}{\rho g H S_o}$$ **A,B,C**

$U_d = \left[A_3\xi^{\alpha} + A_4\xi^{-\alpha-1} + \omega\xi + \eta\right]^{1/2}$ for a sloping bed,1:s (vertical: horizontal) **2.44**

where,

$$\alpha = -\frac{1}{2} + \frac{1}{2}\sqrt{1 + \frac{s(1+s)^{1/2}}{\lambda}(8f)^{1/2}}\ ;\ \omega = \frac{gs}{\left[\frac{\left(1+s^2\right)^{1/2}}{s}\left(\frac{f}{8}\right) - \left(\frac{\lambda}{s^2}\right)\left(\frac{f}{8}\right)^{1/2}\right]}\ ;$$ **2.45 A,B,C,D**

$$\eta = -\frac{\Gamma}{\left[\frac{\left(1+s^2\right)^{1/2}}{s}\rho\left(\frac{f}{8}\right)\right]}\ \text{and}\ \xi = H \mp \frac{y \mp b}{s}$$

Negative if right of the lowest point in the channel bed and positive if on the left hand side

The "*A*" coefficients in Equations 2.42 and 2.44 can be solved either analytically or numerically.

2.6.5.1 Boundary conditions

Analytical solutions to Equation 2.36 were provided by Shiono & Knight (1988) and Knight & Shiono (1996) distinguishing between constant and variable depth domains using Equations 2.42 and 2.44.

Originally, Shiono & Knight (1988 & 1990) proposed three boundary conditions at the interface between two adjacent panels as follows:

- Continuity of the depth-averaged velocity

$$\left(U_d\right)_i = \left(U_d\right)_{i+1} \qquad \textbf{2.46}$$

- Continuity of the lateral gradient of the depth-averaged velocity

$$\left(\frac{\partial U_d}{\partial y}\right)_i = \left(\frac{\partial U_d}{\partial y}\right)_{i+1} \qquad \textbf{2.47}$$

- Continuity of the unit force at each domain junction

$$\left(H\bar{\tau}_{yx}\right)_i = \left(H\bar{\tau}_{yx}\right)_{i+1} \qquad \textbf{2.48}$$

In addition, at the terminal panels where the no-slip condition holds, the velocity should be equal to zero, hence:

$$(U_d)_i = 0 \qquad \textbf{2.49}$$

Omran (2005) provides a detailed review of boundary conditions within the model. Omran (2005) went on to include a μ factor into the boundary conditions to account for continuity of unit force where *f* and λ are different between panels. For a constant depth domain, Equation 2.50 holds;

$$\left(\mu \frac{\partial U_d}{\partial y}\right)_i = \left(\mu \frac{\partial U_d}{\partial y}\right)_{i+1} \qquad \textbf{2.50}$$

where,

$$\mu = \lambda \sqrt{\frac{f}{8}} \qquad \textbf{2.51}$$

When the channel is symmetrical, the flow can be modelled for half of the channel and doubled to give the overall discharge. In this case, an extra "boundary" condition is stipulated at the centerline which states:

$$\left(\frac{\partial U_d}{\partial y}\right)_i = 0 \qquad \textbf{2.52}$$

Boundary conditions for a half of a rectangular channel divided into four equally spaced panels can be seen in **Figure 2.19**.

2.6.5.2 Solution of Shiono and Knight Method

The SKM can be solved analytically (Shiono & Knight, 1988 & 1991; Liao & Knight, 2007) or numerically (Knight & Abril, 1996; Abril & Knight, 2004). The channel is divided into a number of panels (**Figures 2.19** and **2.20** divide rectangular and trapezoidal channels into 4 panels per half channel). These panels are further sub-divided (for example, 10 sub-panels) and Equations 2.42 and/or 2.44 applied. The "A" coefficients can either be obtained directly (see Section 3.3.1) for analytical solution to a 1 panel rectangular channel, or numerically using a matrix solution.

To solve the SKM numerically, Equations 2.42 and/or 2.44 are applied at nodes (see **Figures 2.19** and **2.20** for notation) using the boundary conditions from Section 2.6.5.1. This gives a system of equations and in the case of a 4 panel solution (for half a symmetrical channel) there are 8 equations in total as follows for a trapezoidal channel with 2 panels on the flat bed region and 2 panels on the sloping wall region:

At node 1 (channel centreline), $\left(\frac{\partial U_d}{\partial y}\right)_i = 0$ holds, hence;

$$A_1 - A_2 = 0 \qquad \textbf{2.53}$$

At nodes 2, 3, 4 (middle panels), $(U_d)_i = (U_d)_{i+1}$ and $\left(\mu\frac{\partial U_d}{\partial y}\right)_i = \left(\mu\frac{\partial U_d}{\partial y}\right)_{i+1}$ applies giving:

$$-\mu_1\gamma_1 A_{\ 1}e^{\gamma_1 b/2}+\mu_1\gamma_1 A_{\ 2}e^{-\gamma_1 b/2}+\mu_2\gamma_2 A_{\ 3}e^{\gamma_2 b/2}-\mu_2\gamma_2 A_{\ 4}e^{-\gamma_2 b/2}=0 \quad \textbf{2.54}$$

$$A_{\ 1}e^{\gamma_1 b/2}+A_{\ 2}e^{-\gamma_1 b/2}-A_{\ 3}e^{\gamma_2 b/2}-A_{\ 4}e^{-\gamma_2 b/2}=k_{\ 2}-k_{\ 1} \quad \textbf{2.55}$$

$$-\mu_2 s\,\gamma_2 A_{\ 3}e^{\gamma_2 b}+\mu_2 s\,\gamma_2 A_{\ 4}e^{-\gamma_2 b}-\mu_3\alpha_3 A_{\ 5}H^{\ \alpha_3-1}+\mu_3(\alpha_3+1)A_{\ 6}H^{\ -\alpha_3-2}=\mu_3\omega_3 \quad \textbf{2.56}$$

$$-A_{\ 3}e^{\gamma_2 b}-A_{\ 4}e^{-\gamma_2 b}+A_{\ 5}(H)^{\alpha_3}+A_{\ 6}(H)^{-\alpha_3-1}=k_2-\omega_3 H-\eta_3 \quad \textbf{2.57}$$

$$-\mu_3 s\alpha_3 A_{\ 5}\left(\frac{H}{2}\right)^{\alpha_3-1}+\mu_3 s(\alpha_3+1)A_{\ 6}\left(\frac{H}{2}\right)^{-\alpha_3-1}+\mu_4 s\alpha_4 A_{\ 7}\left(\frac{H}{2}\right)^{\alpha_4-1}=\mu_3\omega_3-\mu_4\omega_4 \quad \textbf{2.58}$$

$$A_{\ 5}\left(\frac{H}{2}\right)^{\alpha_3}+A_{\ 6}\left(\frac{H}{2}\right)^{-\alpha_3-1}-A_{\ 7}\left(\frac{H}{2}\right)^{\alpha_4}=\omega_4\left(\frac{H}{2}\right)+\eta_4-\omega_3\left(\frac{H}{2}\right)-\eta_3 \quad \textbf{2.59}$$

At the terminal boundary (node 5), $(U_d)_i = 0$, here $\xi \to 0$, hence $A_8 \to 0$ therefore:

$$A_{\ 8}=0 \quad \textbf{2.60}$$

A matrix can then be employed to solve for the "A" coefficients using:

$$[x]\begin{bmatrix}A_1\\A_2\\A_3\\A_4\\A_5\\A_6\\A_7\\A_8\end{bmatrix}=[C] \quad \textbf{2.61}$$

Due to the simplicity of the method, it can be solved easily using any spreadsheet based application.

2.6.6 Commercial software programs

There are a number of "industry standard" software programs which can be one-, two- or fully three-dimensional. One-dimensional models have been touched on in Chapter 1, but include Mike 11, ISIS and HEC-RAS. These models are widely used to predict discharge and water levels within a river reach, but are unable to accurately compute the lateral variations of velocity or boundary shear stress which are important for a number of engineering applications previously highlighted.

2-D models are being used more often, particularly for modelling flow on floodplains, and are often based on the finite element method (FEM) where the error is minimised based on the global problem or the finite volume method (FVM) where the error is minimised at a local level. This means that a FVM conserves mass at each time-step where as FEM will only have true mass conservation once the grid is refined to a level that further refinement does not alter the solution. Examples of FEM packages are TELEMAC-2D, SMS and CCHE2D and FEV packages include DIVAST and MIKE21C. 2-D models do not predict or calculate secondary flow but some take account of it by calculating a measure of secondary (helical) flow from an analysis of the velocity and acceleration vector at a point.

2D models may never replace 1D models but should be used in specific reaches where more detailed information may be required; the ISIS-Tuflow package uses a 1D solution when the flow is contained within the banks, after which the ISIS results are integrated into the Tuflow model which is used to determine the flow on the floodplain. 2D models are required when there are significant variations in cross-

section and area which includes floodplain flow and meandering channels. 2D models are time consuming to set up and the codes used are generally more difficult than 1D and 3D ones according to Wright (2001).

3-D models are again more complex than 1D or 2D but can once again complement them. A 3D model may be used to study composite roughness for example, with the results of which being used in 1D and 2D models. They can also be used for small scale modelling of, for example, fish passes, weirs and sluice gates. Most 3D computational fluid dynamics, CFD, models are based on the FVM although some work on the FEM. 3D models calculate the free surface using conservation of mass and momentum whereas 1D and 2D models do it solely on conservation of mass and momentum purely in the streamwise direction and takes no account of that in the transverse direction. In 1D and 2D models turbulence is accounted for through the Chézy or Manning coefficients whereas in 3D modelling results can be much more detailed and local changes can also be modelled. 3D models divide the channel into a number of vertical strips and calculate the velocity in each layer; this is a layered model. This takes into account variations such as velocity, temperature and salinity. Turbulence modelling in 3D CFD models is usually based on Reynolds-Averaged turbulence models (κ-ε model used for turbulence closure; where κ is the turbulent kinetic energy and ε is the rate of dissipation of κ (Wright, 2001). The downfall of the κ-ε model is that it is unable to reproduce boundary driven turbulence as it cannot accurately predict the transition and viscous boundary layers near to the wall. It can be used in flow modelling where the boundary driven turbulence is secondary to bend driven turbulence such as in meandering channels.

Although 3D models can mimic the effects of turbulence and secondary flows much better than 1D and 2D counterparts it has largely remained a research tool. This is mainly due to the complexity of the model, the run time and associated costs.

2.7 Previous modelling studies using the SKM and other techniques for computation of distributions of depth-averaged velocity and boundary shear stress

A number of studies have been carried out showing that the SKM and other models can accurately predict the depth-averaged velocity profile and the boundary shear stress distribution in a number of channel configurations. This section provides a review of a variety of different models used to predict distributions of depth-averaged velocity and boundary shear stress for a number of channel geometries, but with an emphasis on inbank flow and methods capable of predicting the percentage of shear force acting on the walls ($\%SF_w$).

Much work has been undertaken by researchers Knight and Shiono to demonstrate that their approach, the Shiono & Knight Method (SKM), can accurately determine the boundary shear stress, and depth-averaged velocity for compound channels. Studies include Shiono & Knight (1988; 1991) and Knight & Shiono (1990; 1996). These studies have been undertaken largely for overbank flow, therefore, the review herein will concentrate on the approaches which have been applied to inbank flow.

Tang & Knight (2008a) have shown that the SKM can be applied to inbank symmetrical channels (including trapezoidal, V-shaped and V-shaped with a vertical wall channels) in addition to compound trapezoidal channels. This generic version of the 'traditional' SKM redefines Γ as a linear distribution as follows:

$$\Gamma = \frac{\partial}{\partial y}\left[H\left(\rho\overline{UV}\right)_d\right] = \frac{\partial}{\partial y}[\xi\psi] = \xi\frac{\partial\psi}{\partial y} + \psi\frac{\partial\xi}{\partial y} = \Gamma^*\xi + \psi\frac{\partial\xi}{\partial y} \qquad \textbf{2.62}$$

where $\psi = (\rho UV)_d$ .and $\Gamma^* = \dfrac{\partial[(\rho UV)_d]}{\partial y} = \dfrac{\partial\psi}{\partial y}_d$

Therefore, for a constant depth where s→∞, ξ=H, therefore $\Gamma = \Gamma^* H$ and for a linearly varying depth, $\Gamma = \Gamma^*\xi + \psi\dfrac{\partial\xi}{\partial y}$. Equation 2.45 gives the expression for ξ in terms of *H* and *s*. The depth-averaged velocity and boundary shear stress is calculated as per Equations 2.42, 2.44 and 2.34.

Omran (2005) and Knight et al. (2007) have applied the SKM to a number of channels, with both inbank and overbank flows. It was demonstrated that the depth-averaged velocity and boundary shear stress could be accurately computed for simple trapezoidal channels and compound channels by calculating *f* based on measured data, keeping λ constant at 0.07, and calibrating Γ. Omran, however did not explore the relationship of Γ to channel geometry but did apply the SKM to natural channels including the River Severn at Montford. Omran also thoroughly explored the boundary conditions of the model, particularly for simple trapezoidal channels.

Chlebek & Knight (2006) have shown that for inbank flow in a rectangular channel, a simple 1 panel (per half channel, assuming symmetry along the centreline) solution can accurately predict the percentage of shear force acting on the wall and total discharge (typically maximum error was less than 5% for each parameter). This method was unable to accurately predict the lateral distribution of depth-averaged velocity and boundary shear stress, but demonstrated that if overall channel values of discharge or $\%SF_w$ are required, this approach can determine these parameters both quickly and accurately. See Appendix A-Author's Publications, for further details.

Khodashenas and Paquier (1999) suggested a method of calculating boundary shear stress based on the Merged Perpendicular Method (M.P.M.). This method bisects the channel into a flat bed region and sloping wall region and further divides the wetted perimeter into small segments (as shown in **Figure 2.21**). Although, there are variations on this method due to bisectors intersecting one another, generally, the boundary shear stress, τ, is calculated using Equation 2.63.

$$\tau = \gamma R_h S_e \qquad \textbf{2.63}$$

where, γ is the specific weight of water ($=\rho g$), R_h is the hydraulic radius as the ratio of areas between two lines to the length of the corresponding segment (**Figure 2.22**) and S_e the average energy slope. Although the errors given by Khodashenas & Paquier are well within the bounds of acceptability, the distribution of boundary shear stress tended to overestimate the boundary shear stress along the flat bed region and

underestimate in the sloping bed region for inbank flow, and similarly underestimated boundary shear stress across the channel in overbank flow, but significantly overestimate (approximately double the measured) it at the interface of the main channel and floodplain, as seen in **Figure 2.23**. This method is also not applicable in channels with near to vertical side slopes. Khodashenas & Paquier give a comparison of $\%SF_w$ calculated by the M.P.M method and Knight et al. (1984) and Knight and Patel (1985) experimental data (in addition to others) reproduced here in **Figure 2.24**. This clearly shows that the M.P.M. overestimates $\%SF_w$ for aspect ratios (b/h) less than 2.5 and underestimates it for aspect ratios greater than 2.5 by approximately 5%, although at large aspect ratios (b/h>10), the differences are smaller (2-3%). This method clearly shows errors in the distribution of boundary shear stress, and there is no direct calculation for depth-averaged velocity. This method clearly is simpler in computational effort of a RANS based approach, but is more limited in its application and accuracy.

Yang & Lim (2005) detailed an approach for calculation of boundary shear stress in trapezoidal channels based on division lines which are determined based on Equation 2.64 and shown pictorially in **Figures 2.25** and **2.26**.

$$\frac{l_w}{\Delta_w} = \frac{l_b}{\Delta_b} \qquad \textbf{2.64}$$

where, l_w and l_b are the normal distances from the division line to the side wall and bed respectively and Δ_w and Δ_b the side wall roughness and bed roughness respectively.

This method determines the boundary shear stress, dependent on whether the division lines are above or below the surface and whether there is a constant depth domain or a variable side slope.

For a channel with division lines out with the water surface:

$$\tau_{b(z)} = \begin{cases} \rho\, g\, S_o (z \tan\alpha) & for\ 0 \le z \le H\ \cot\alpha \\ \rho\, g\, HS_o & for\ H\ \cot\alpha \le z \le (B - H\ \cot\alpha) \\ \rho\, g\, S_o [(B - z)\tan\alpha] & for\ (B - H\ \cot\alpha) \le z \le B \end{cases} \quad \textbf{2.65}$$

$$\tau_{w(y)} = \begin{cases} \rho\, g\, S_o (y \tan\alpha) & for\ 0 \le y \le H\ \cot\alpha \\ \rho\, g\, S_o \left(\dfrac{H}{\sin\beta} - y \right) \tan\beta & for\ H\ \cot\alpha \le y \le \dfrac{H}{\sin\beta} \end{cases} \quad \textbf{2.66}$$

For a channel with division lines within the water surface:

$$\tau_{b(z)} = \begin{cases} \rho\, g\, S_o (z \tan\alpha) & for\ 0 \le z \le \dfrac{B}{2} \\ \rho\, g\, S_o [(B - z)\tan\alpha] & for\ \dfrac{b}{2} \le z \le B \end{cases} \quad \textbf{2.67}$$

$$\tau_{w(y)} = \begin{cases} \rho\, g\, S_o (y \tan\alpha) & for\ 0 \le y \le \dfrac{B}{2} \\ \rho\, g\, S_o \left[\dfrac{B}{2}\tan\alpha + \left(y - \dfrac{B}{2} \right) \Big/ \tan\beta \right] & for\ \dfrac{B}{2} \le y \le y1 \\ \rho\, g\, S_o \left(\dfrac{H}{\sin\beta} - y \right) \tan\beta & for\ y1 \le y \le \dfrac{H}{\sin\beta} \end{cases} \quad \textbf{2.68}$$

where, τ_b and τ_w are the boundary shear stresses acting on the bed and walls respectively, α is the angle of division line, β the angle of the sloping wall, z the transverse spanwise distance measured from the channel side wall, y the distance along the side wall measured from the channel corner, $y1 = H/\sin\beta - B/2 - \left(H - B/2 \tan\alpha\right) \sin\beta$ and H the water depth. For notation see **Figures 2.25** and **2.26**. This method showed good comparison when compared to measured data as can be seen in **Figures 2.27** and **2.28**. This method built upon work by Yang & McCorquodale (2004) on determination of boundary shear stress in trapezoidal channels based also based on division lines. In this instance, the boundary shear stress on the bed and walls is calculated using:

$$\frac{\bar{\tau}_b}{\rho\, g\, H\, S_o} = 1 - \frac{\bar{u}_{*b}}{\bar{u}_{*w}} \frac{H}{B} \quad for\ \frac{B}{H} > 2 \quad \textbf{2.69}$$

$$\frac{\bar{\tau}_b}{\rho\, g\, H\, S_o} = 1 - \frac{\bar{u}_{*w}}{\bar{u}_{*b}} \frac{B}{4H} \quad for\ \frac{B}{H} \le 2 \quad \textbf{2.70}$$

$$\frac{\bar{\tau}_w}{\rho\, g\, H\, S_o} = 1 - \frac{\bar{u}_{*b}}{\bar{2u}_{*w}} \quad for\ \frac{B}{H} > 2 \quad \textbf{2.71}$$

$$\frac{\bar{\tau}_w}{\rho g H S_o} = \left(1 - \frac{\bar{u}_{*w}}{\bar{u}_{*b}} \frac{B}{4H}\right) \frac{B}{2H} \quad for \frac{B}{H} \leq 2 \qquad \textbf{2.72}$$

Both of these approaches yield good approximations of $\%SF_w$, but neither is able to compute the depth-averaged velocity or discharge within the channel.

Guo & Julien (2005) determined averaged wall and bed boundary shear stress based on:

$$\frac{\bar{\tau}_b}{\rho g H S_o} = \frac{4}{\pi} \tan^{-1} \exp\left(-\frac{\pi H}{B}\right) + \frac{\pi}{4} \frac{H}{B} \exp\left(-\frac{H}{B}\right) \qquad \textbf{2.73}$$

$$\frac{\bar{\tau}_w}{\rho g H S_o} = \frac{B}{2H}\left[1 - \frac{4}{\pi} \tan^{-1} \exp\left(-\frac{\pi H}{B}\right) + \frac{\pi}{4} \frac{H}{B} \exp\left(-\frac{H}{B}\right)\right] \qquad \textbf{2.74}$$

This approach compared well to various experimental data, which can be seen in **Figures 2.29** and **2.30** for approximation 2. In this case the model could predict the average bed and side wall boundary shear stress with an average error of 5.6%. However, this method is unable to give the distribution of boundary shear stress laterally across the channel.

McGahey (2006) showed the application of the SKM and Ervine k-method (for meandering channels) to natural rivers, and these methods have been integrated into the Conveyance and Afflux Estimation System, CAES, (www.river-conveyance.net).

The channel is not modelled as a whole or a series of reaches but rather as individual cross-sections and each of these sections is assigned a reach sinuosity, σ. If σ=1 then the SKM is used (Equation 2.75), if σ≥1.015 then the k-method is used (Equation 2.76) but if 1<σ<1.015 then a combination of the two is used (Equation 2.77).

$$gHS_o - \frac{f\beta q^2}{8H^2} + \frac{\partial}{\partial y}\left[\lambda H\left(\frac{f}{8}\right)^{1/2} q\frac{\partial}{\partial y}\left(\frac{q}{H}\right)\right] = \Gamma \qquad \text{When } \sigma=1 \qquad \textbf{2.75}$$

$$gHS_o - \frac{f\beta q^2}{8H^2} + \frac{\partial}{\partial y}\left[\lambda H\left(\frac{f}{8}\right)^{1/2} q\frac{\partial}{\partial y}\left(\frac{q}{H}\right)\right] = C_{uv}\frac{\partial}{\partial y}\left[\frac{q^2}{H}\right] \qquad \text{When } \sigma\geq 1.015 \qquad \textbf{2.76}$$

$$gHS_o - \frac{f\beta q^2}{8H^2} + \frac{\partial}{\partial y}\left[\lambda H\left(\frac{f}{8}\right)^{1/2} q\frac{\partial}{\partial y}\left(\frac{q}{H}\right)\right] = \frac{(1.015-\sigma)}{0.015}\Gamma + \frac{(\sigma-1.0)}{0.015}C_{uv}\frac{\partial}{\partial y}\left[\frac{q^2}{H}\right] \qquad \text{When } 1<\sigma>1.015 \qquad \textbf{2.77}$$

Where, β is the Boussinesq (momentum) coefficient, σ is the measure of sinuosity, Γ is calculated from Abril & Knight (2004) using Equations 2.39 to 2.41, q is the discharge intensity and the "C" coefficients are given by:

$$C_{uv} = 4.3274\sigma^2 - 7.8669\sigma + 3.5395 \qquad \text{For inbank flow, } 1.0<\sigma\leq 2.5 \qquad \textbf{2.78}$$

$$C_{uv} = 7.1659\sigma - 6.6257 \qquad \text{For overbank flow, } 1.015<\sigma\leq 2.5 \qquad \textbf{2.79}$$

These equations are solved for a set number of lateral divisions and at a set number of depth intervals. By default the channel is divided into 100 lateral divisions and 25 depth increments as shown in **Figure 2.31** (Defra/EA, 2004). This approach accurately calculates the total discharge for a given cross-section (and includes uncertainty bands (**Figure 2.32**), but can also determined the lateral distribution of

depth-averaged velocity (**Figure 2.33** and **2.34**) for both natural and artificial channels. This method however, applies general equations for Γ, and the user specifies the friction through Manning's *n*. The only parameter which the user can calibrate is λ (default setting 0.24 for natural channels).

2.8 Sidewall correction procedures

Sidewall correction procedures are used to process experimental flume or channel data where the influence of the sidewalls is to be excluded from the analysis of bed related phenomena. They typically reduce an essentially three-dimensional flow problem down to a quasi two-dimensional flow problem (Chlebek & Knight, 2006).

Einstein (1942) used the Manning's roughness coefficient, n, to separate the flow resistance portions related to the bed and wall, this yielded (Cheng & Chua, 2005):

$$\frac{\tau_b}{\rho g H S_o} = 1 - \frac{2n_w^{1.5} U^{1.5}}{B S_o^{0.75}} \qquad \textbf{2.80}$$

$$2Hn_w^{1.5} + Bn_b^{1.5} = (2H + B)n^{1.5} \qquad \textbf{2.81}$$

where, n is the overall Manning's roughness coefficient, n_w and n_b refer to the Manning's roughness coefficients acting on the wall and bed respectively, U is the average cross-sectional velocity, H the depth of flow and B the channel width.

If Equation 2.80 is adapted to view roughness in terms of the Darcy-Weisbach friction factor, and assuming that wall-related friction can be estimated using the Blasius

expression $f_w = 0.316\left(4UR_w/\nu\right)^{-0.25}$, where ν is the viscosity of the fluid (≈10^{-6}), and noting that $f_w = 8\,g\,R_w\,S_o/U^2$, then $R_w = 0.057\left[U^7\nu/S_o^4\,g^4\right]^{0.2}$ and knowing that g is approximately equal to 9.81m/s^2 (Cheng & Chua, 2005), then:

$$\frac{\tau_b}{\rho\,g\,H\,S_o} = 1 - 0.0012\frac{U^{1.4}}{B\,S_o^{0.8}} \qquad \textbf{2.82}$$

Vanoni & Brooks (1957) first proposed that for flow in a flume with smooth side walls and for a given Reynolds number, *Re*, a correction can be made so that the friction factor on the bed, f_b, can be determined from:

$$f_b = f + \frac{2H\left(f - f_w\right)}{B} \qquad \textbf{2.83}$$

Where, f is the overall friction factor, f_w the friction factor on the walls, H the depth of flow and B the channel width.

Giving the bed boundary shear stress;

$$\frac{\tau_b}{\rho\,g\,H\,S_o} = \frac{B}{B+2H}\frac{f_b}{f} \qquad \textbf{2.84}$$

Brownlie (1981) expanded on this and divided the channel into two zones (**Figure 2.35**) and for a given Reynolds number:

$$\mathrm{Re} = \frac{4RU}{\nu}\ ;\ \mathrm{Re}_w = \frac{4R_wU}{\nu}\ ;\ \mathrm{Re}_b = \frac{4R_bU}{\nu} \qquad \textbf{2.85}$$

The friction factor is related to the Reynolds number and hydraulic radius by:

$$\frac{\mathrm{Re}_w}{f_w} = \frac{\mathrm{Re}}{f}\ ;\ \frac{R_w}{f_w} = \frac{R_b}{f_b} = \frac{R}{f} \qquad \textbf{2.86}$$

R_w is computed using Equation 2.86 and the boundary shear stress computed using $\tau_b = \tau R_b S_o$ with the full methodology outlined by Brownlie (1981) or Chang (1988).

Cheng & Chua (2005) found that the above methods and utilising the experimental data of Knight and MacDonald. (1979a&b), there is general agreement of τ_b in the approaches. However, none of the approaches can be extended beyond calculation of the average shear stress acting on the bed and walls.

The SKM is a novel approach which has demonstrated success in the prediction of the lateral distribution of boundary shear stress. Part 1 of this thesis examines the application of the SKM to calculate the percentage shear force on the wall directly for both homogeneous and heterogeneous roughened channels with inbank flow. The key objective is to see whether the SKM can simulate the relationship proposed by Knight et al. (1994), illustrated in **Figures 2.36** to **2.39**. In particular, the $\%SF_w$ versus the wetted perimeter ratio, P_b/P_w, is of prime importance.

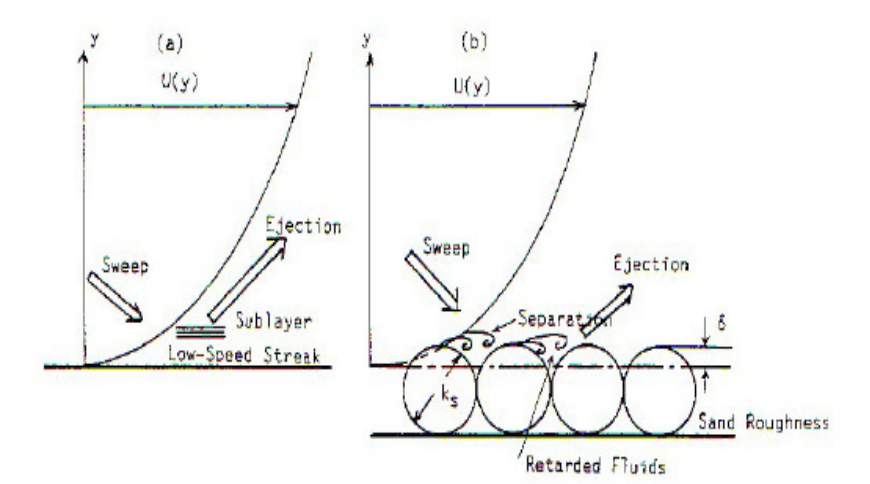

Figure 2.1-Turbulent flow over (a) smooth and (b) rough beds (Nezu & Nakagawa, 1993)

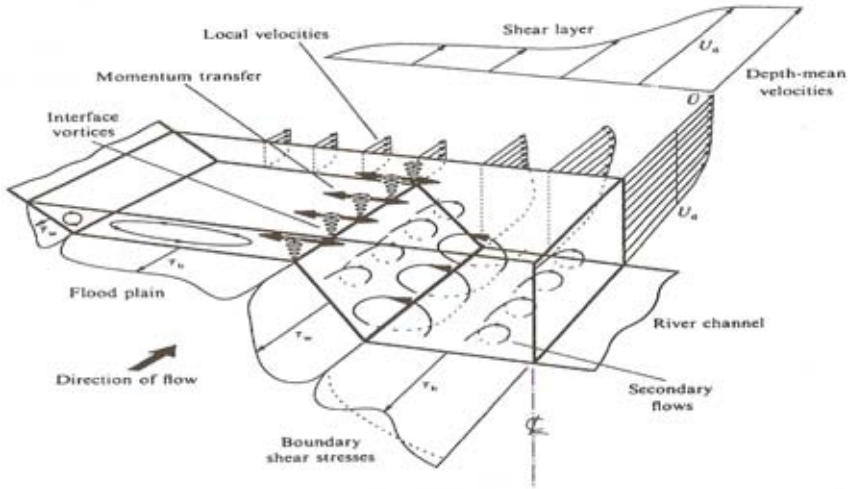

Figure 2.2-Flow mechanisms associated with straight overbank flow in a two-stage channel (Shiono & Knight, 1990)

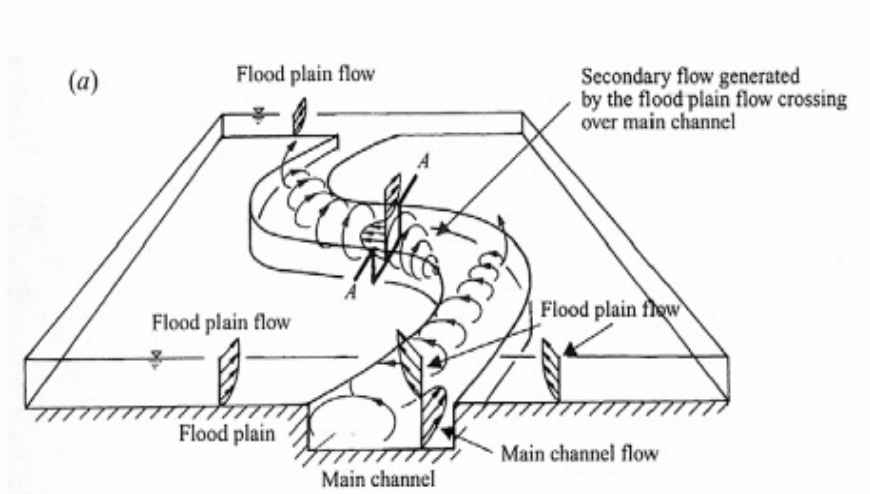

Figure 2.3-Flow mechanisms in a compound meandering channel (Shiono & Muto, 1998)

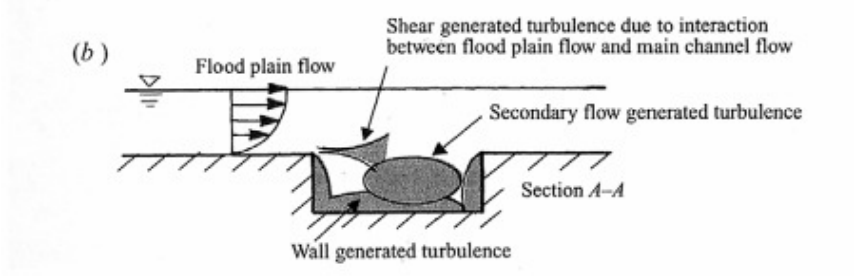

Figure 2.4- Flow mechanisms in a compound meandering channel (Shiono & Muto, 1998)

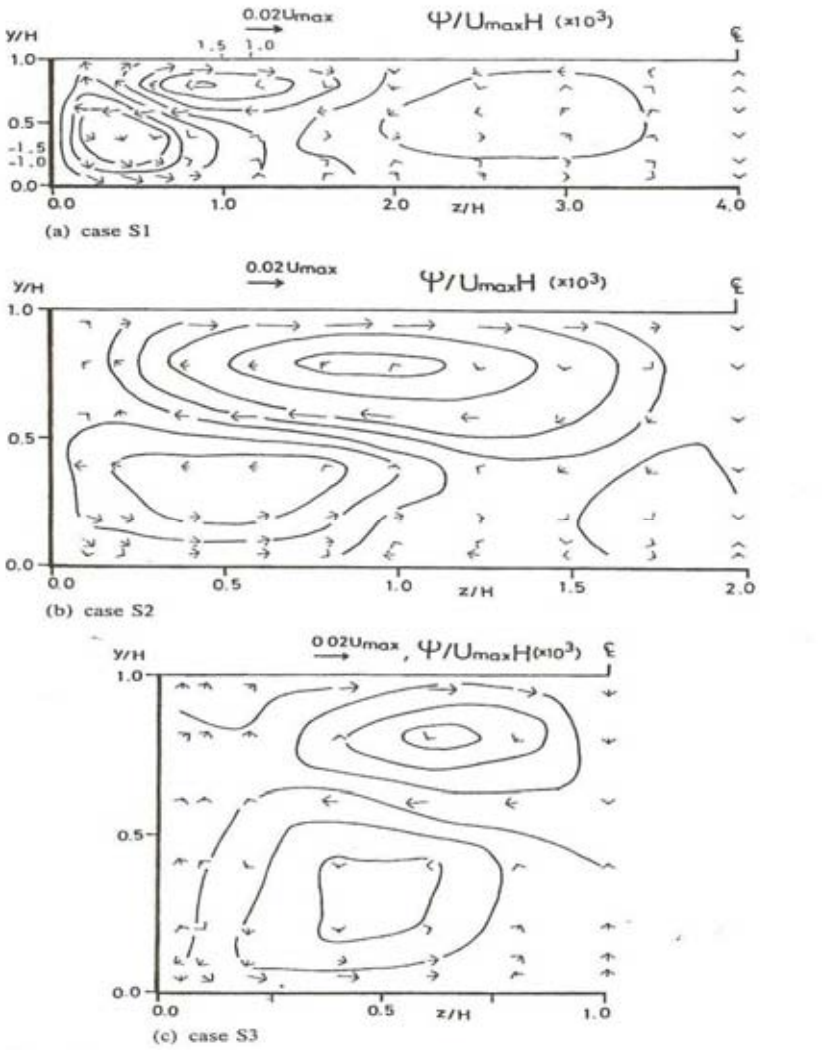

Figure 2.5- Secondary current vectors in rectangular smooth channels (Tominaga et al., 1989)

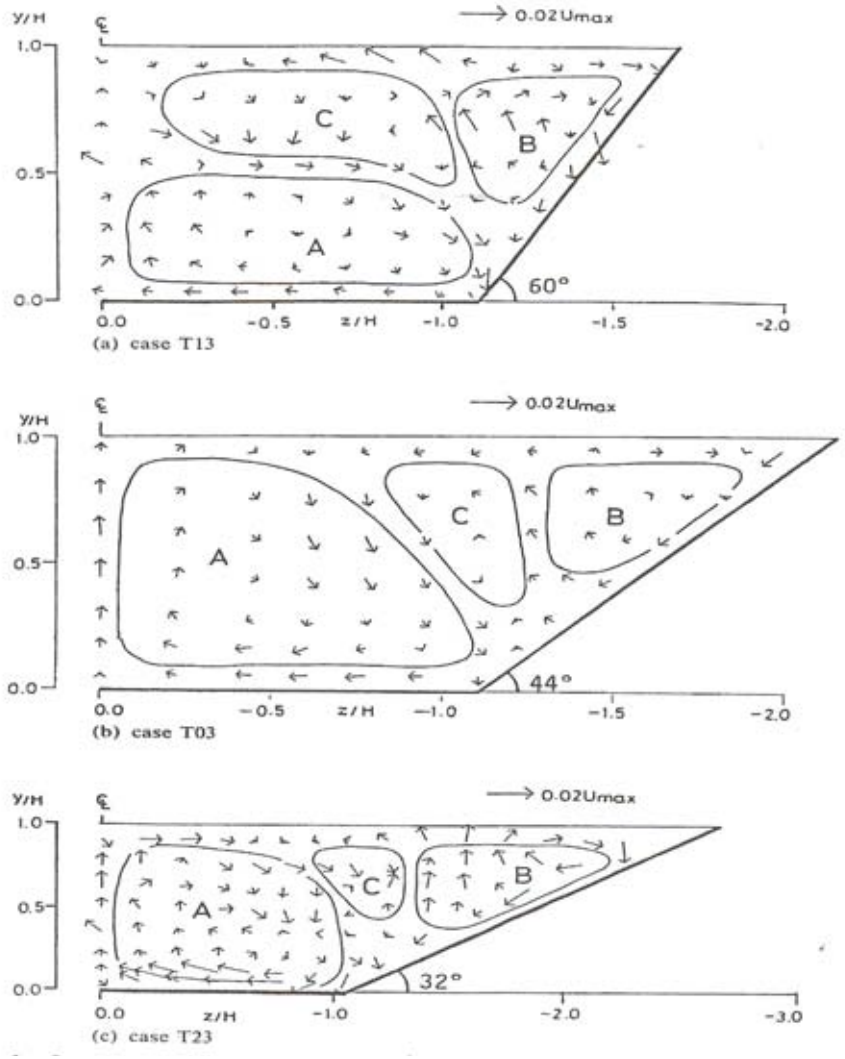

Figure 2.6- Secondary current vectors in trapezoidal smooth channels (Tominaga et al., 1989)

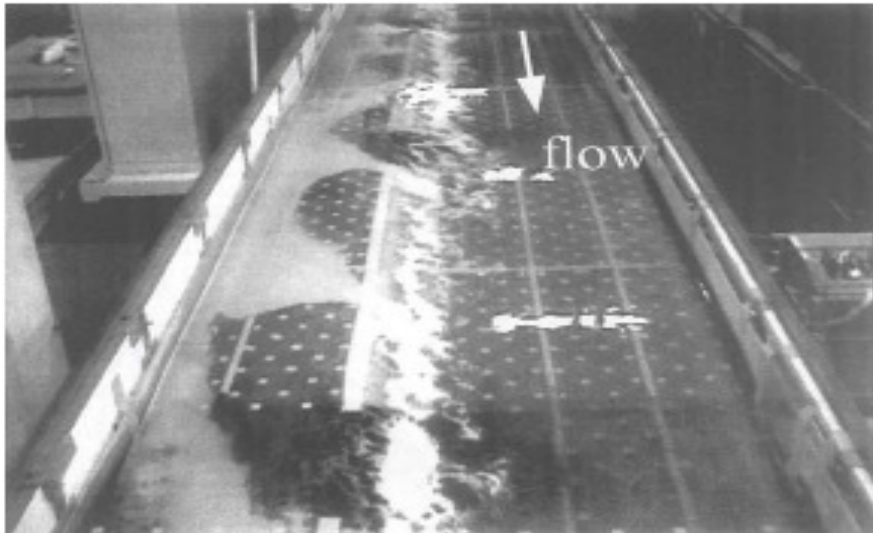

Figure 2.7-Visualisation of the free surface in a straight compound channel at relative depth 0.180 (Ikeda et al., 2001)

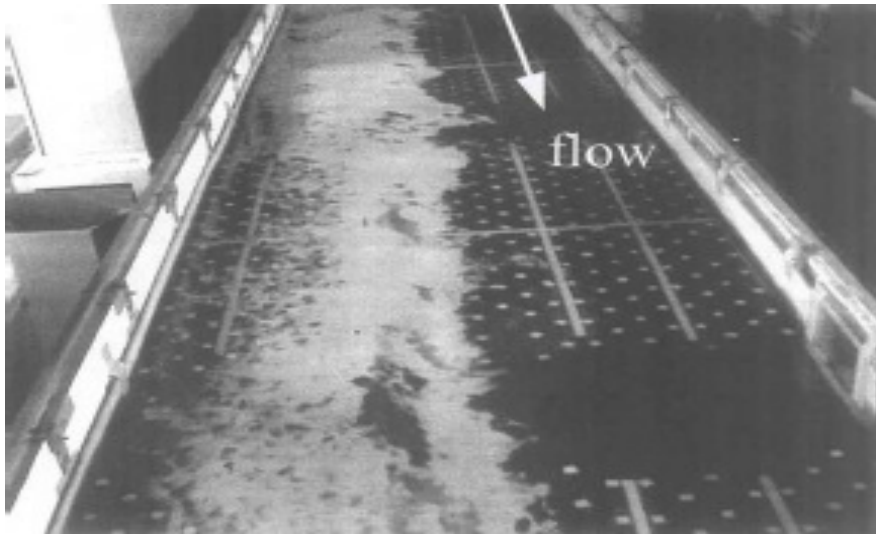

Figure 2.8-Visualisation of the free surface in a straight compound channel at relative depth 0.344 (Ikeda et al., 2001)

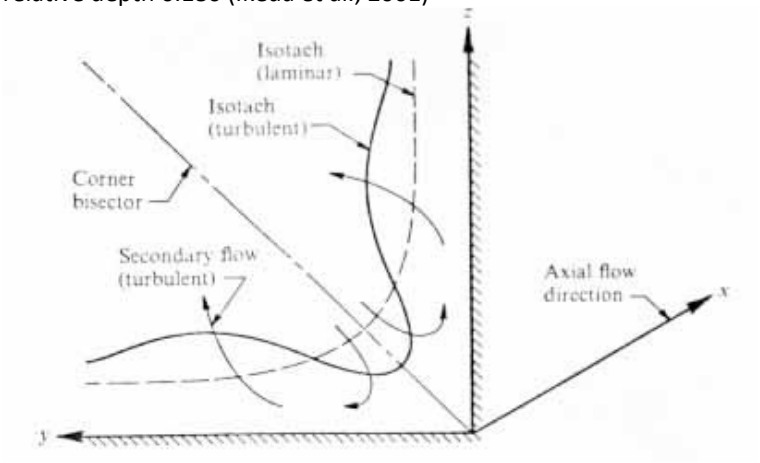

Figure 2.9-Typical isotach patters for flow along a corner (Gessner, 1973)

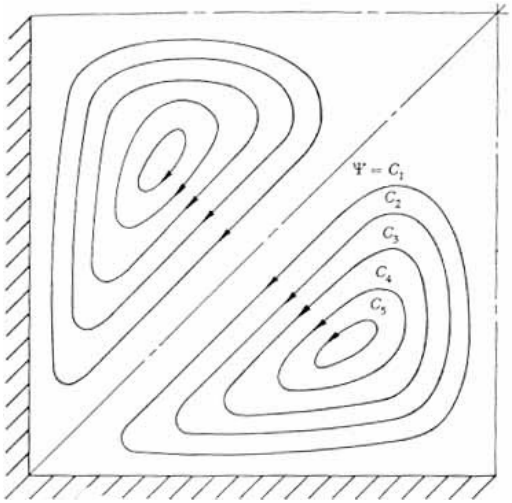

Figure 2.10-Typical secondary flow streamline patterns in a square channel (Gessner and Jones, 1965)

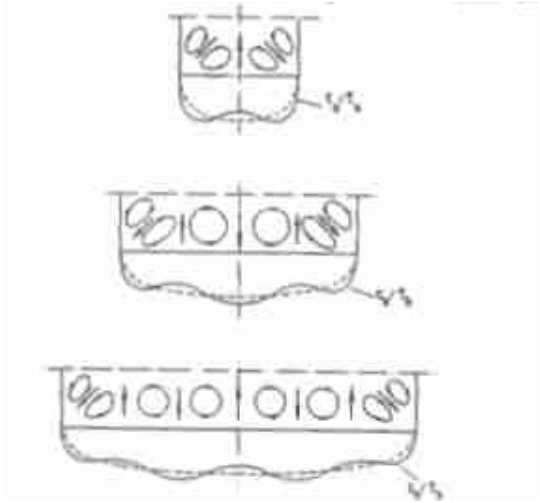

Figure 2.11-Possible interaction between secondary flow cells and boundary shear stress (Knight & Patel, 1985)

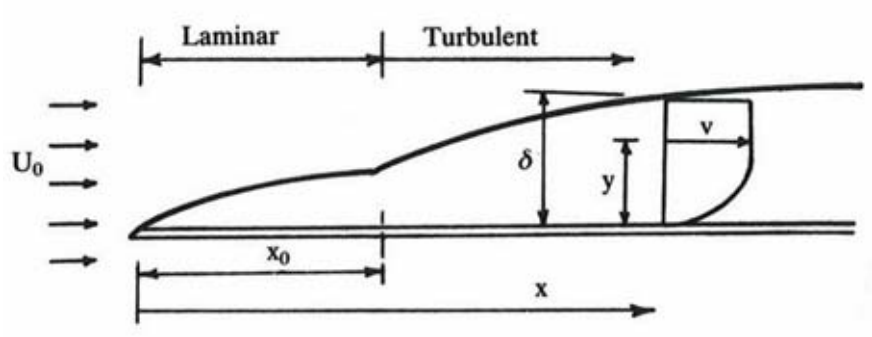

Figure 2.12-Boundary layer formation on flat plate (from Nalluri & Featherstone, 2001)

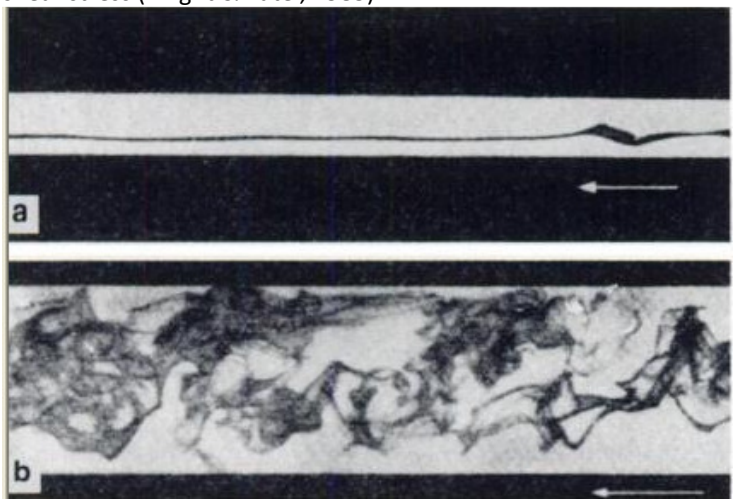

Figure 2.13-Coloured filament experiment by Reynolds (1883); Flow in water made visible by a coloured filament by Dules (1939); (a) laminar flow Re-1150, (b) turbulent flow Re=2520 (Reproduced from Schlichting & Gersten, 2000

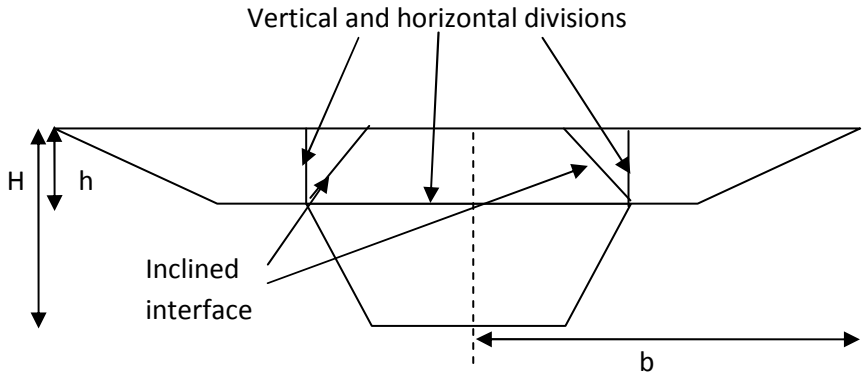

Figure 2.14-Possible division lines (both horizontal, vertical and inclined) for divided channel methods

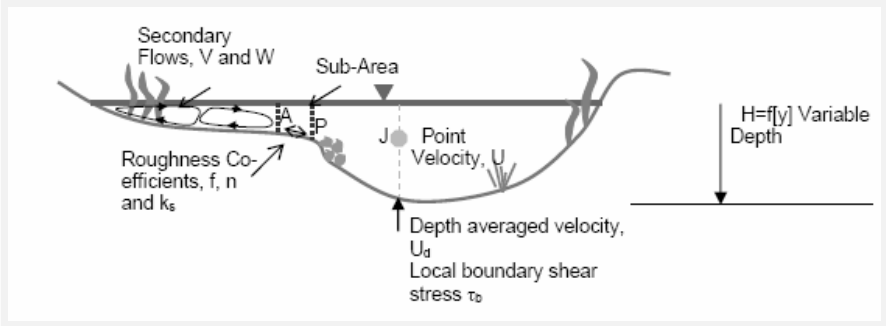

Figure 2.15- Schematic of natural river cross-section, after Ervine et al. (2000)

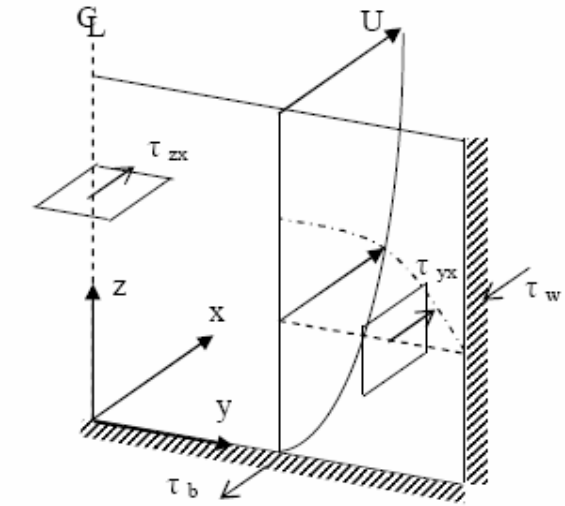

Figure 2.16- Bed and wall shear (after Chlebek & Knight, 2006)

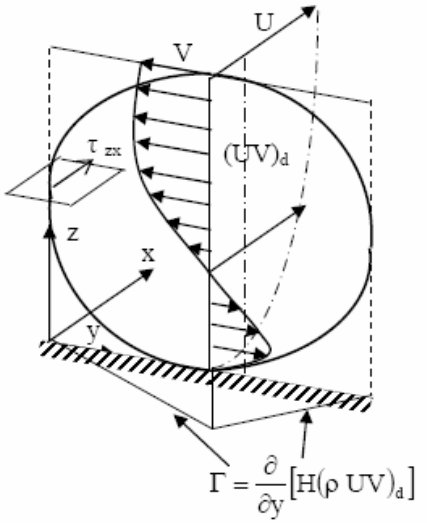

Figure 2.17-Depth-averaged secondary flow term (after Chlebek & Knight, 2006)

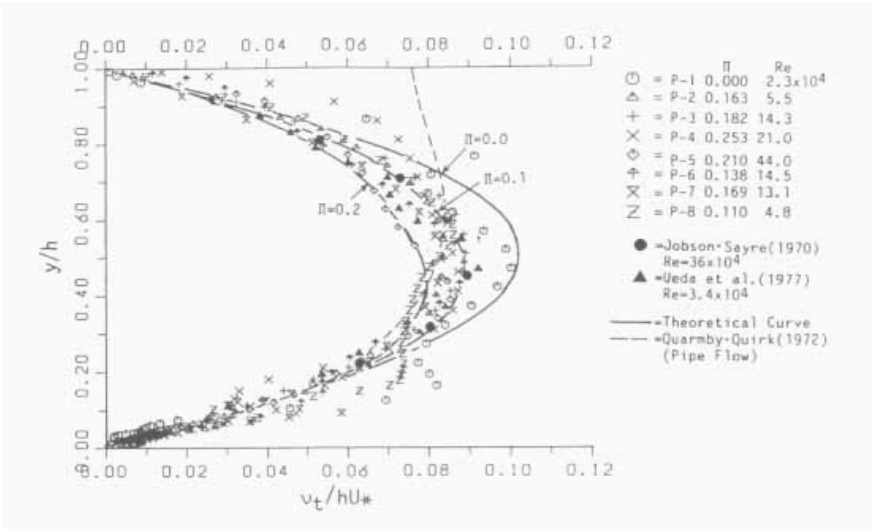

Figure 2.18-Distributions of eddy viscosity for open and closed channel data (Nezu & Nakagawa, 1993)

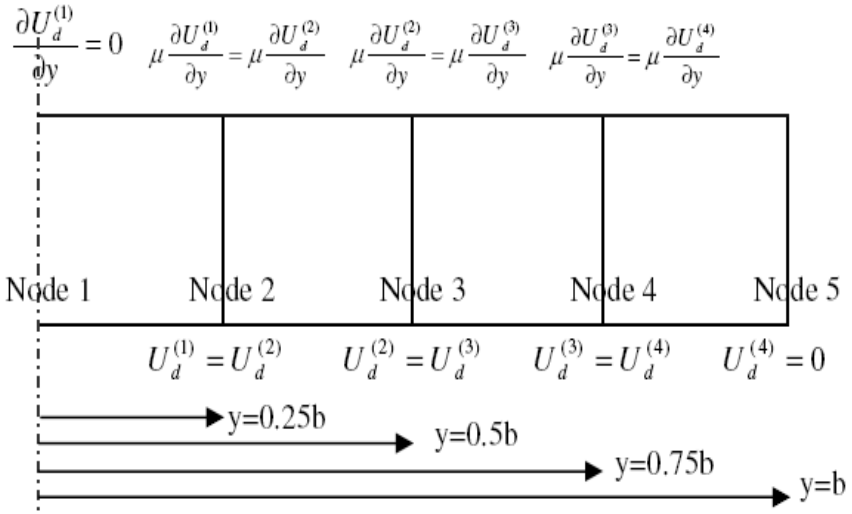

Figure 2.19-Boundary conditions for half a rectangular channel

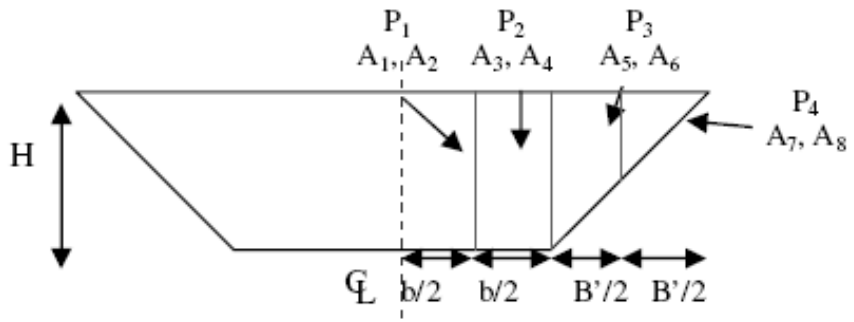

Figure 2.20-Panels and "A" coefficients for half a trapezoidal channel

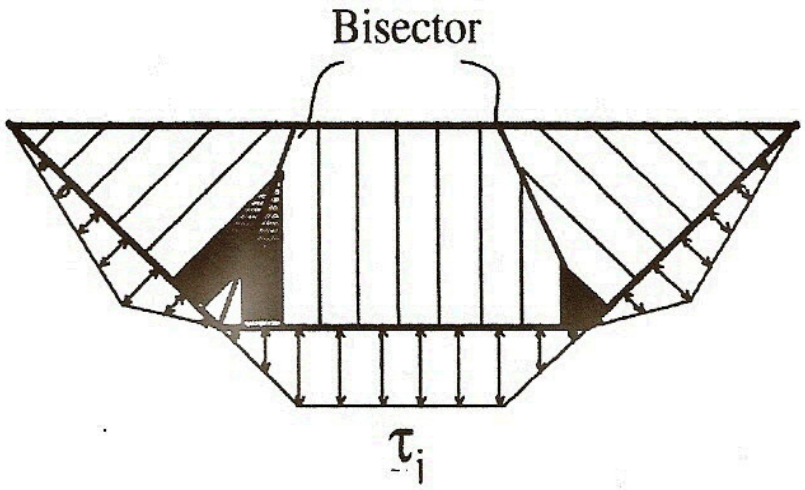

Figure 2.21-Boundary shear stress variations computed by M.P.M. (after Khodashenas & Paquier, 1999)

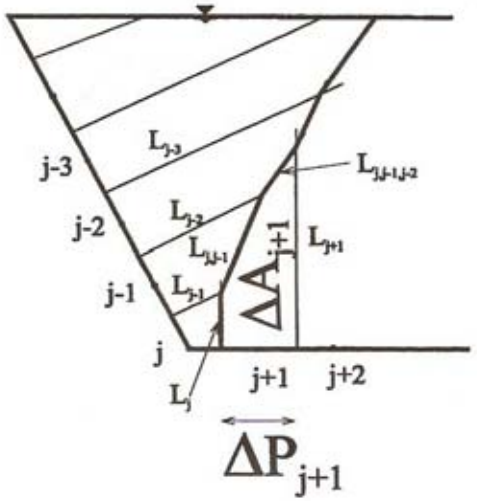

Figure 2.22-Areas determined by M.P.M. (after Khodashenas & Paquier, 1999)

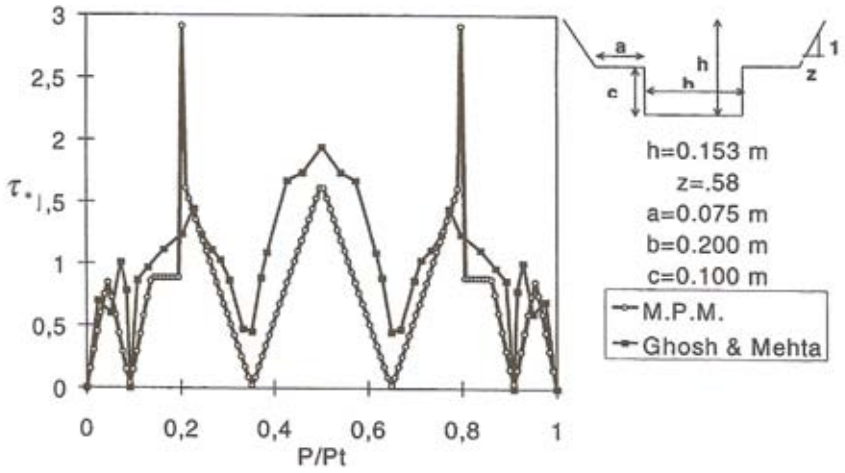

Figure 2.23-Comparison of dimensionless shear stress from the M.P.M. with experimental data from Ghosh & Mehta (1974) (after Khodashenas & Paquier, 1999)

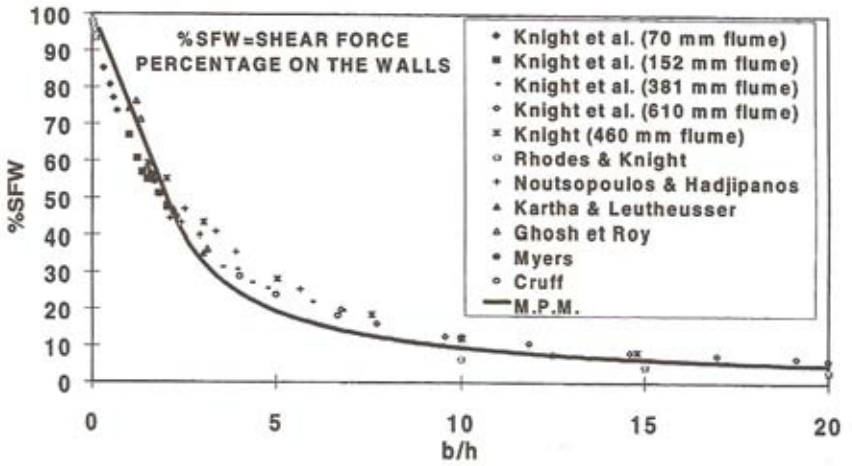

Figure 2.24-Percentage of total shear force carried by the walls versus width to depth ratio (after Khodashenas & Paquier, 1999)

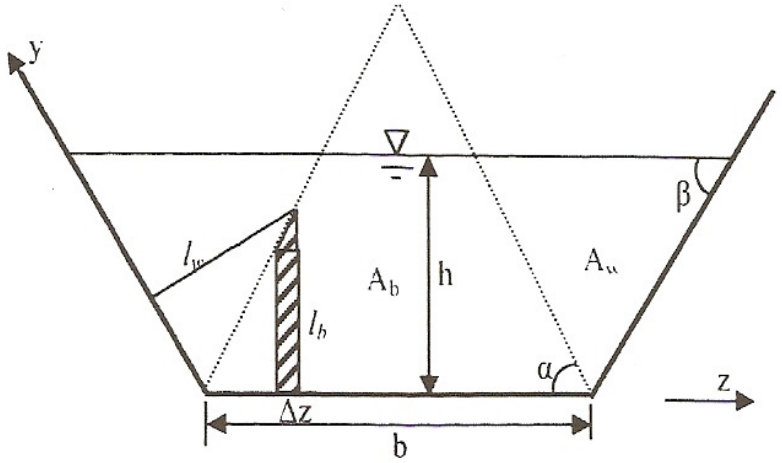

Figure 2.25-Intersection of division lines above the water surface (after Yang & Lim, 2005)

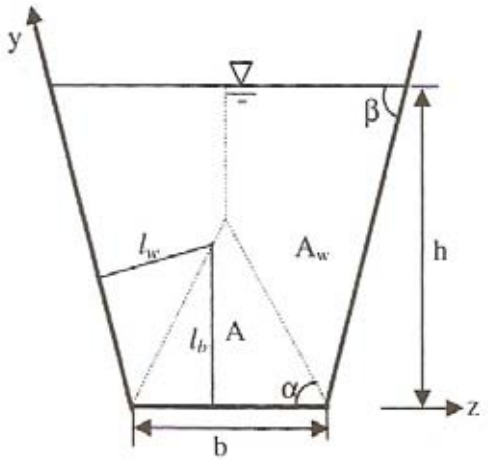

Figure 2.26-Intersection of division lines below the water surface (after Yang & Lim, 2005)

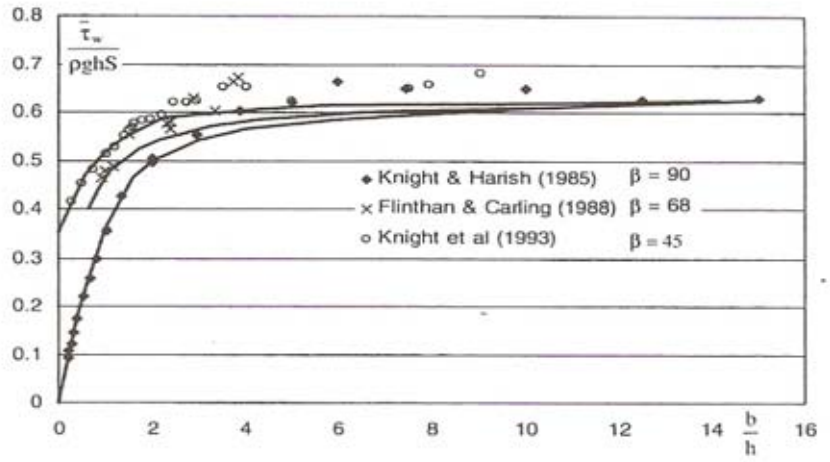

Figure 2.27-Mean side wall shear stresses versus aspect ratio in smooth trapezoidal channels (after Yang & Lim, 2005)

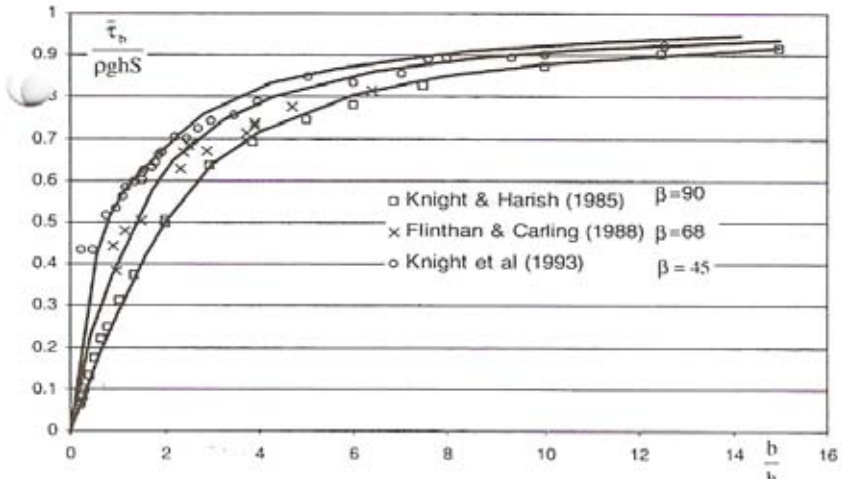

Figure 2.28-Mean bed shear stresses versus aspect ratio in smooth trapezoidal channels (after Yang & Lim, 2005)

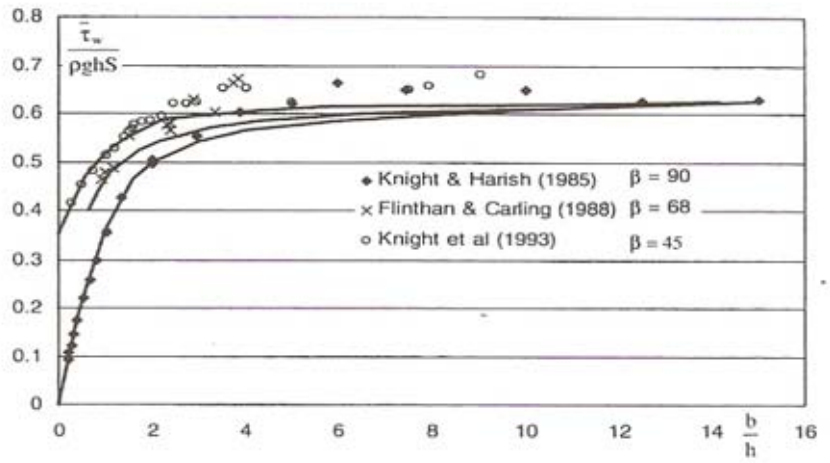

Figure 2.29-Comparison of experimental data and model for average bed shear stress (after Guo & Julien, 2005)

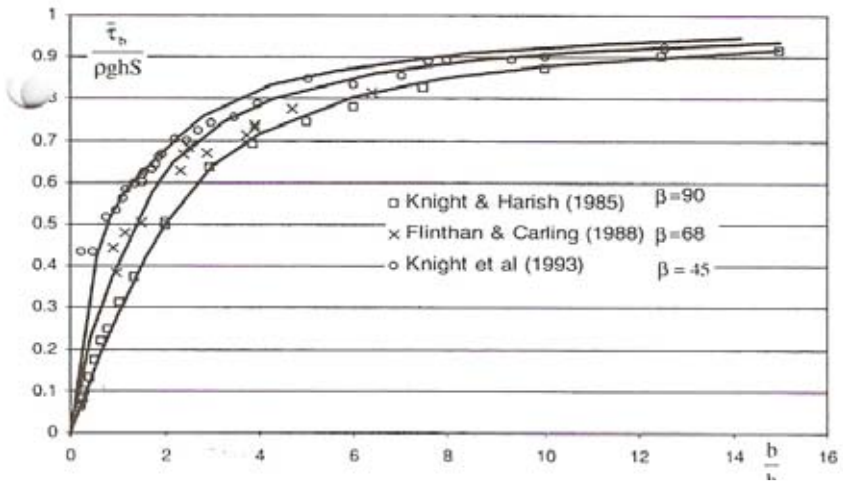

Figure 2.30-Comparison of experimental data and model for average side wall shear stress (after Guo & Julien, 2005)

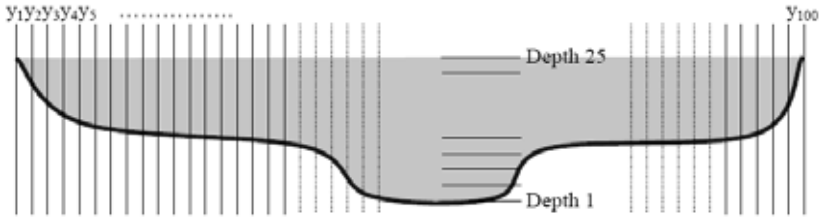

Figure 2.31-Discretised cross-section as used in CAES (Defra/EA, 2004)

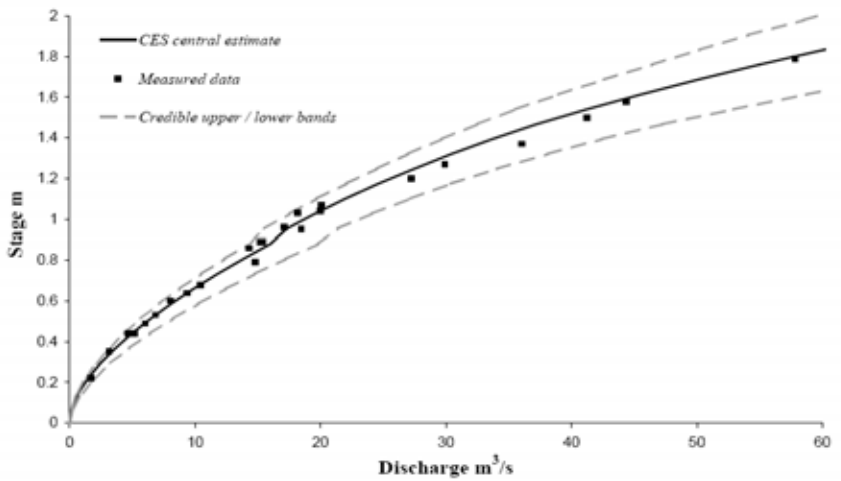

Figure 2.32- Upper and lower uncertainty bands for the conveyance calculation for the River Main from CAES program (Defra/EA, 2004)

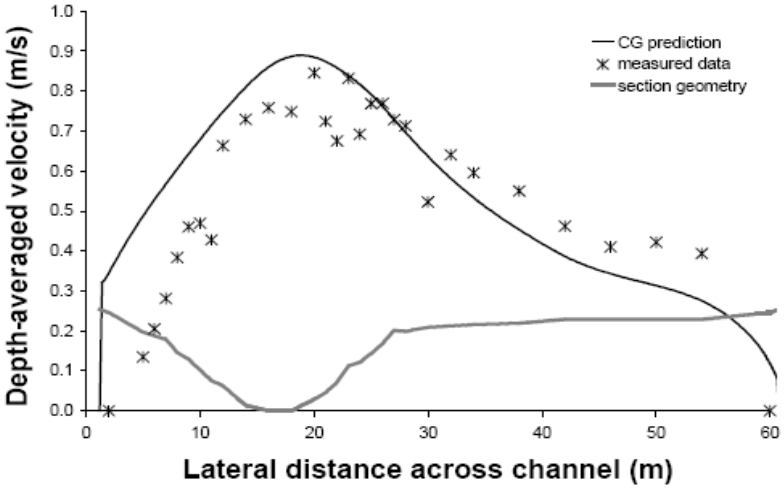

Figure 2.33- Lateral distribution of depth-averaged velocity calculated by the CAES program for the River Severn at Shrewsbury (McGahey & Samuels, 2003)

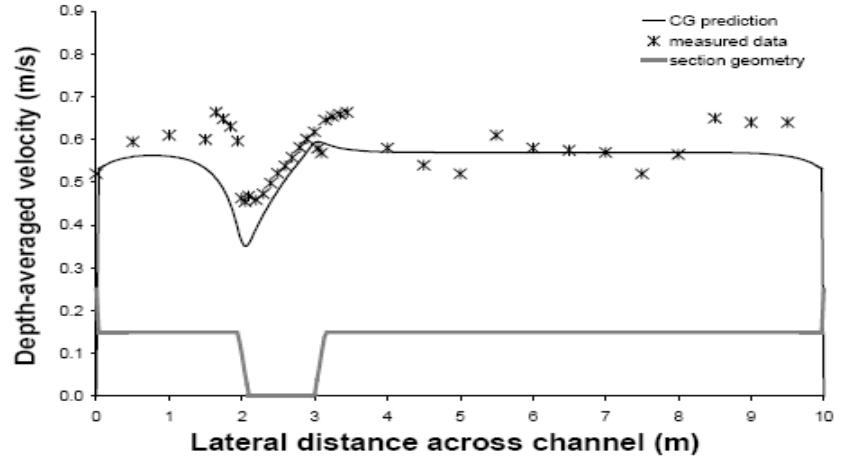

Figure 2.34- Lateral distribution of depth-averaged velocity calculated by the CAES program for the experiment B24, FCF data (McGahey & Samuels, 2003)

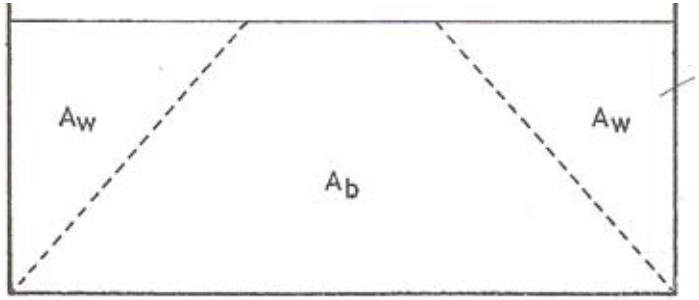

Figure 2.35-Division lines for rectangular channel for Brownlee side wall correction procedure (Brownlee, 1981)

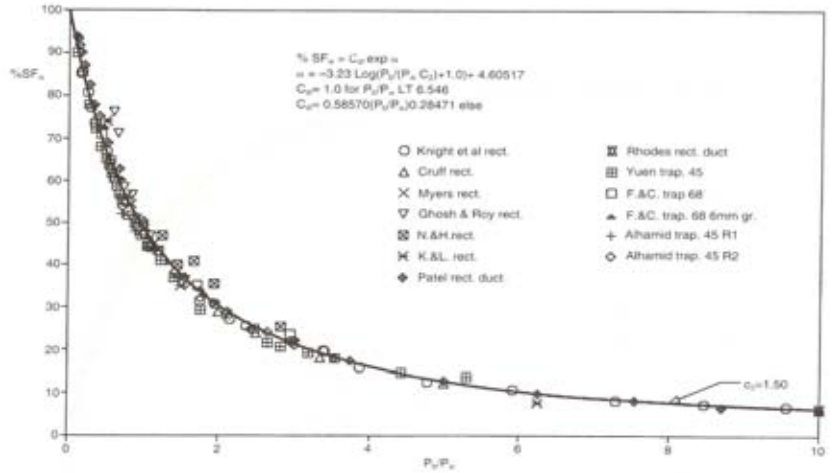

Figure 2.36-%SF_w versus wetted perimeter ratio (0 -10) (Knight et al., 1994)

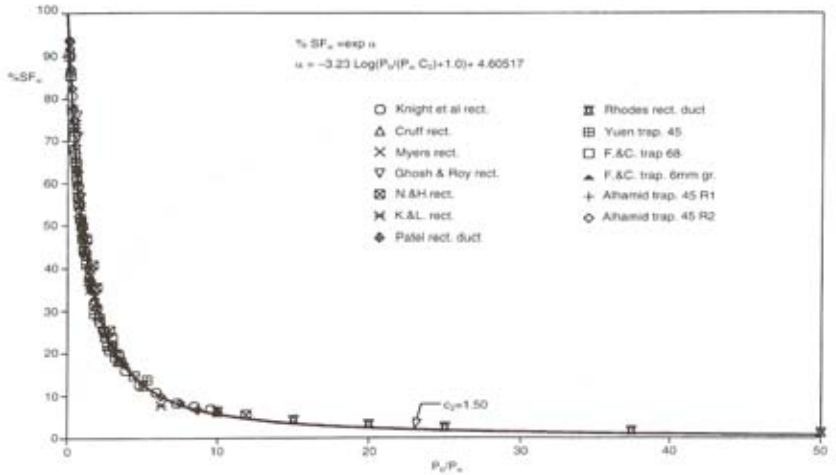

Figure 2.37-%SF_w versus wetted perimeter ratio (0-50) (Knight et al., 1994)

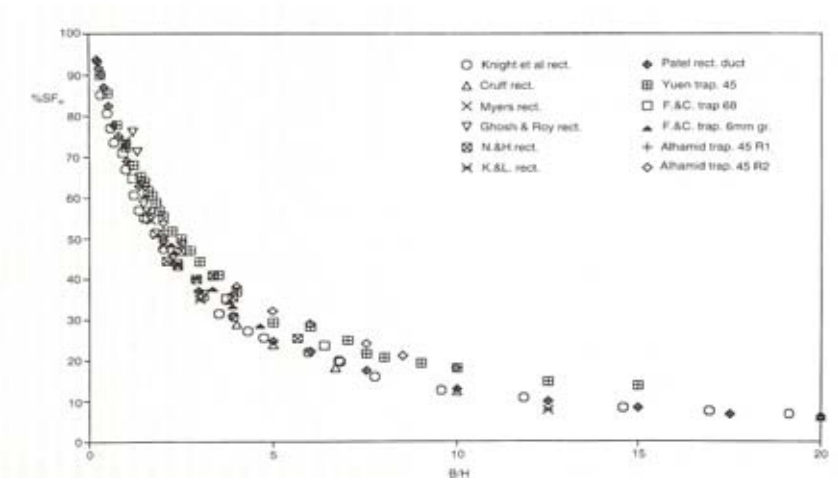

Figure 2.38-%SF_w versus wetted aspect ratio (Knight et al., 1994)

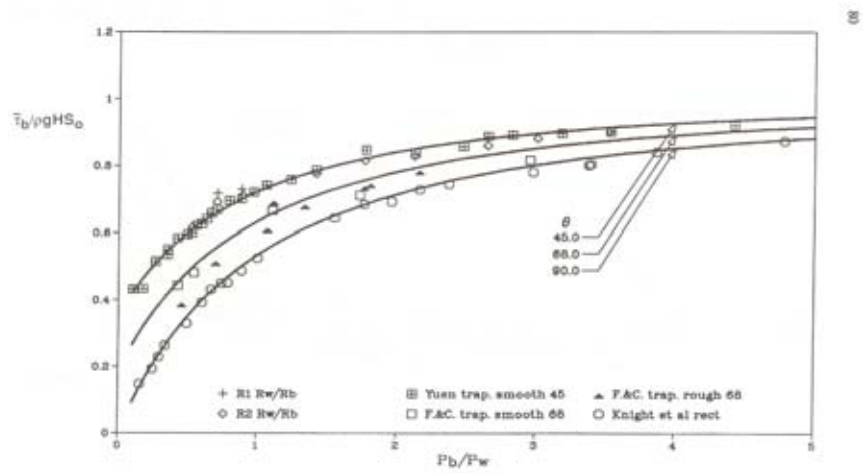

Figure 2.39-Mean bed shear stress for different side slope angles (smooth boundaries) (Knight et al., 1994)

CHAPTER 3-MODELLING FLOW IN SIMPLE CHANNELS WITH HOMOGENEOUS ROUGHNESS USING THE SHIONO AND KNIGHT METHOD

Yes, we have to divide up our time like that, between our politics and our equations. But to me our equations are far more important, for politics are only a matter of present concern. A mathematical equation stands forever. Albert Einstein (1879 - 1955)

3.1 Introduction

Simple channels are often more difficult to model than compound channels, as shown by Nezu & Nakagawa (1993) and Chiu & Chiou (1986). This is partly due to the nature of the anisotropic turbulence, governed by the channel geometry and roughness distribution, together with the consequence of secondary flow cells. Nevertheless, it is important to model the flow accurately. Various studies (Tang & Knight (2008b), Liao & Knight (2007), Knight et al. (2007) and Omran, (2005) have shown that the Shiono and Knight Method can accurately model the distributions of depth-averaged velocity and boundary shear stress in simple channels. This has largely been applied to trapezoidal channels and, in comparison, little work has been carried out on rectangular channels. The accurate modelling of parameters such as depth-averaged velocity and boundary shear stress plays an important role in engineering applications such as flood modelling, bank stability/erosion and sediment transport. In addition, many studies require the percentage shear force on the wall, particularly for sediment transport problems as the effect of the sidewall often has to be removed from the overall shear stress to determine the effective bed shear stress (Cheng & Chua, 2005). Methods of sidewall correction have been described in Section 2.8. In order to

remove the effect of the sidewall, a model which can accurately predict the boundary shear stress is required, one such model being the SKM.

This chapter uses the Shiono and Knight Method, SKM, (detailed in section 2.6.5) to predict the distributions of depth-averaged velocity and boundary shear stress on the bed. From this, the discharge and percentage shear force acting on the wall can be computed, and this can then be applied in sidewall correction procedures.

The SKM has been used in conjunction with a visual basic application within a spreadsheet program to calculate the depth-averaged velocity and boundary shear stress, which when integrated gives the respective discharge and shear force for non-vertical elements of the channel.

The aim of this modelling section on flows in channels with simple geometries is to show that the SKM can be used to accurately predict both discharge and the percentage shear force acting on the wall of a channel. This is particularly aimed at finding a rational approach to sidewall correction procedures. For rectangular and trapezoidal channels, guidance is given on the selection of the number of panels to be used and the values to be assigned to the calibration parameters, f, λ and Γ in each panel. Explanations as to the function of each of the coefficients within the model has been given in Section 2.6.5.

3.2 Experimental data

This study utilises readily available data from rectangular and trapezoidal channels to validate the modelling approach (data available from www.flowdata.bham.ac.uk). It should be noted that since both types of geometry are to be analysed together, the aspect ratio, often defined as the base width to depth ratio, 2b/h, will be used in conjunction with the wetted perimeter ratio, as defined by P_b/P_w, where P_b is the wetted perimeter of the bed, $2b$ and P_w the wetted perimeter of the walls ($=2H\sqrt{1+s^2}$). Where, b is the half-width of the bed, s is the side slope (1:s, vertical:horizontal) and H the depth of flow.

3.2.1 Smooth rectangular channel data

The rectangular data used herein was from experimental work by Knight et al. (1984), where experiments were performed in a 15m long, tilting flume set at various bed slopes. For sub-critical flows the flume was set at a bed slope of S_o=9.66 x 10^{-4}. The flume had a total width of 610mm, with three smaller channels (of widths 70mm, 152mm and 381mm) constructed within it. This made it possible to conduct four series of experiments in channels at the same slope, but with various depths giving approximate wetted perimeter ratios (P_b/P_w) varying from 0.15 to 10. For all configurations depth-averaged velocity data were measured and in the case of the 152mm wide channel, boundary shear stress measurements were also taken. Summary data for these experiments are given in **Table 3.1**, and full details are available in Knight et al. (1984).

At the same time, ancillary experiments were carried out in rectangular ducts using air as a medium to investigate a wider range of aspect ratios than would be possible in standard open channel flow experiments, details of which are given by Patel (1984) and Lai (1986). Other data were measured using duct flow which gave aspect ratios (2b/H) up to 100, **Figure 3.1** (Rhodes & Knight, 1994). Although this data is not examined herein, it was used in the derivation of the empirical equation for percentage shear force on the wall used later in Sections 3.3 and 3.6.

3.2.2 Smooth trapezoidal channel data

Yuen (1989) undertook a separate series of experiments in a smooth trapezoidal channel. These experiments were carried out in a 22m tilting flume set at different bed slopes and investigated wetted perimeter ratios (P_b/P_w) over the range 0.15 to 7.5 in both sub-critical and super-critical flow conditions.

The experiments were carried out using five bed slopes; 1.000, 3.969, 8.706, 14.52 and 23.37 ($x10^{-3}$) and three channel widths; 0.044m, 0.15m and 0.45m. The side slope of the walls was a constant 1:1 (horizontal: vertical). Of all these experiments carried out by Yuen, a selection of eight was made for use in this work. These eight experiments were selected on the grounds that they have both depth-averaged velocity and boundary shear stress data, a range of sub- and super-critical flow, a range of aspect ratios and bed slopes. Details of the experiments are given in **Table 3.2**. Details of all experiments are given in Yuen (1989) or at The University of Birmingham's Flow Data website (www.flowdata.bham.ac.uk).

3.3 Modelling simple rectangular channels

Modelling of inbank rectangular channels differs in many ways from other channels. Firstly, the depth-averaged modelling of secondary current cells is made difficult by the formation of two counter rotating cells which form on top of one another, as clearly shown in **Figure 2.5**. Secondly, the boundary shear force acting on the wall of a rectangular channel must be back calculated as a depth-averaged model can only model boundary shear on horizontal and sloping beds and not on vertical interfaces.

In this section, a number of modelling approaches will be investigated to ascertain the optimum panel number and spacing as outlined below:

- One panel solution
- Multiple panel solution
    - Spacing of panels
    - Effect of calibration coefficients on modelling outcomes

3.3.1 One panel solution

In order to assess whether the SKM was going to be suitable for predicting the percentage shear force on the wall of a channel ($\%SF_W$), a one panel solution to the SKM was carried out in which only one panel was used to model an entire region. A full explanation of the findings are given in Chlebek & Knight (2006), but for the purposes of completeness, a synopsis of the methodology and findings are given below.

In this case, only half of the channel was analysed as the velocity and boundary shear stress are symmetric and thus half of the channel may be regarded as a single region or panel. Hence, the panel spacing is *b*, where *b* is the half the channel width, as shown in **Figure 2.19**, but with no intermediate division lines. The analytical solution for a single panel with constant depth has been produced below in Equations 3.1-3.15 (see Shiono & Knight 1988) for full details.

$$\rho g H S_0 - \rho \frac{f}{8} U_d{}^2 \sqrt{1+\frac{1}{s^2}} + \frac{\partial}{\partial y}\left[\rho \lambda H^2 \sqrt{\frac{f}{8}} U_d \frac{\partial U_d}{\partial y}\right] = \frac{\partial}{\partial y}\left[H(\rho UV)_{\mathrm{d}}\right] \qquad \textbf{3.1}$$

where, ρ is the density of water, g the gravitational force, H is water depth, S_0 bed slope, f the friction factor, U_d depth-averaged velocity, s side slope (1:s, vertical to horizontal) and λ dimensionless eddy viscosity.

In the case of rectangular channels, the $\sqrt{1+\frac{1}{s^2}}$ term is excluded as s tends towards ∞, therefore $1/s^2 \rightarrow 0$, hence $\sqrt{1+\frac{1}{s^2}} \rightarrow 1$. Tang & Knight (2008b) have undertaken research into trapezoidal channels with very steep slopes to assess whether the solution degenerates into a rectangular solution. In this, they found that for trapezoidal channels with very steep side slopes (i.e. s=0.001), the result is almost identical to the rectangular solution.

For a sub-area with constant water depth, H, the analytic U_d distribution takes the form:

$$U_d = \left[A_1 e^{\gamma y} + A_2 e^{-\gamma y} + k\right]^{1/2} \quad \textbf{3.2}$$

where,

$$k = \frac{8gS_0H}{f}(1-\beta) \quad \textbf{3.3}$$

$$\gamma = \sqrt{\frac{2}{\lambda}}\left(\frac{f}{8}\right)^{\frac{1}{4}}\frac{1}{H} \quad \textbf{3.4}$$

$$\beta = \frac{\Gamma}{\rho g H S_0} \quad \textbf{3.5}$$

where, Γ accounts for secondary currents.

The coefficients A_1 and A_2 can be determined by considering the relevant boundary conditions of flow continuity and the no-slip condition at the wall, as shown by Knight et al. (2004). A full explanation of boundary conditions has been given in Section 2.6.5.1. For a simple rectangular channel of half-width, *b*, (assuming symmetric flow parameters), using just a single panel to represent half the cross-section, the two '*A*' coefficients are:

$$A_1 = A_2 = -\frac{k\sinh(\gamma b)}{\sinh(2\gamma b)} = -\frac{k}{2\cosh(\gamma b)} \quad \textbf{3.6}$$

$$U_d = \left[C_1\cosh(\gamma y) + C_2\right]^{1/2} \quad \textbf{3.7}$$

$$C_1 = -\frac{k}{\cosh(\gamma b)} \qquad \textbf{3.8}$$

$$C_2 = \frac{8gS_0H}{f}(1-\beta) \qquad \textbf{3.9}$$

Similarly, for boundary shear stress, the analytic solution is:

$$\tau_b = \rho\frac{f}{8}\left[C_1\cosh(\gamma y) + C_2\right] \qquad \textbf{3.10}$$

The mean shear stress, $\bar{\tau}_b$, is then obtained by integration

$$\bar{\tau}_b = \frac{\rho f}{8}\left[\frac{C_1}{\gamma b}\sinh(\gamma b) + C_2\right] \qquad \textbf{3.11}$$

and the shear force on the bed, SF_b (= $\bar{\tau}_b$ x 2b) is

$$SF_b = 2b\rho gHS_0(1-\beta)\left[1 - \frac{\sinh(\gamma b)}{\gamma b\cosh(\gamma b)}\right] \qquad \textbf{3.12}$$

The mean wall shear force, SF_w, (both walls) may then be calculated from a total force balance:

$$\tau_o P = SF_b + SF_w \qquad \textbf{3.13}$$

where P is the total wetted perimeter and τ_o is the mean boundary shear stress ($=\rho gRS_o$) where R is the hydraulic radius, and A is the cross-sectional area. Thus;

$$SF_w = \rho gAS_0 - SF_b \qquad \textbf{3.14}$$

The percentage of the total shear force that acts on the walls is then given by:

$$\%SF_w = \frac{SF_W}{\rho\, g\, A\, S_o} \times 100 \qquad \textbf{3.15}$$

Within this single panel, there are a total of 20 sub-panels. To each of these sub-panels, the above equations are applied, but only one value of f, λ and Γ is assigned. This allows sufficient number of calculations to be carried out to generate smooth distributions, but a limited number of user defined coefficients.

The three calibration coefficients were altered in a number of ways to analyse the effect on the distributions of depth-averaged velocity and boundary shear stress, It was found that when λ was increased the velocity at across the section decreased. For example, when λ was altered from 0.005 to 0.011, the peak depth-averaged velocity (which occurs at the channel centreline) decreased by approximately 0.14m/s.

In general terms, each parameter was varied in turn with the effects on $\%SF_W$ and discharge noted below in **Insert 1**. This was based on keeping two of the calibration

coefficients and altering one in isolation. The effects of varying these parameters for a 1 panel solution has been further examined in Chlebek & Knight (2006).

Vary	Fixed	+/-	$\%SF_w$	Q
f	λ & Γ	increase f	-	-
		decrease f	+	+
λ	f & Γ	increase λ	+	-
		decrease λ	-	+
Γ	f & λ	increase Γ	+	-
		decrease Γ	-	+

Insert 1: Effect of varying calibration coefficients on discharge and $\%SF_w$ results

Secondly, preliminary optimisation and error analysis was undertaken. In this case, each factor was varied across a range of values by a set increment, for example, the friction factor, f, was varied between 0.01 and 0.046 in increments of 0.002 with λ and Γ being held constant. The $\%SF_w$ and Q were determined for each *f* value and the errors plotted. If the zero errors for both $\%SF_w$ and Q occurred at the same *f* value, this was taken as being the optimal value (see Figures 3 and 4 from Chlebek & Knight, 2006). Where they did not coincide, the average *f* value was taken. λ and Γ were subsequently altered in the same manner until the discharge and $\%SF_W$ were within ±5% i.e. within the limits of the physical experiments.

Figure 3.2 shows the results of the SKM modelling in comparison with the experimental data of Knight et al. (1984). This shows good agreement between the two methods. However, despite the similarity between mean values, the distributions of boundary shear stress and depth-averaged velocity data across the channel were significantly different from those measured, as seen in **Figures 3.3-3.4**. The model has been unable to accurately reproduce the distributions of depth-averaged velocity

and boundary shear stress as the perturbations in shear stress caused by secondary current flows have not been accounted for. The use of a single panel obviously eliminates the possibility of calibrating the model well at different lateral positions. However, given that good results for discharge and $\%SF_W$ were achieved, it was possible to produce tentative distributions and expressions for the calibration coefficients.

For the friction factor, the best fit data from all experiments compares well to that produced by the Colebrook-White equation (Equation 3.16). Using this equation, f can be calculated based on k_s (Nikuradse roughness factor), the velocity (U), the viscosity (ν) and D is the pipe diameter.

$$\frac{1}{\sqrt{f}} = -2.0\log\left[\frac{k_s}{3.71D} + \frac{2.51}{(UD/\nu)\sqrt{f}}\right] \qquad \textbf{3.16}$$

In open channel flow, D is taken as $4R$ (i.e. a pipe running full), then for rectangular channels D=4R=4[H/(1+2/asp)], where asp=2b/H, Equation 3.16 becomes:

$$\frac{1}{\sqrt{f}} = -2.0\log\left[\frac{k_s}{14.84\{H/(1+2/Asp)\}} + \frac{2.51\nu}{4\sqrt{8gS_f}\{H/(1+2/Asp)\}^{3/2}}\right] \qquad \textbf{3.17}$$

The comparison between the calculated friction factor and the best-fit data used in the model is shown in **Figures 3.5-3.6**. Although there are slight differences in the values, the overall trend compares well.

Similarly, the best-fit values used in the model for λ and Γ have also been plotted in **Figures 3.7** and **3.8** respectively. The best fit equations through all data were:

$$\lambda = 6.25x10^{-5} Asp^3 - 0.001625 Asp^2 + 0.01145 Asp + 0.0032 \quad \textbf{3.18}$$

$$\Gamma = -0.0002 Asp^2 + 0.00105 Asp + 0.0464 \quad \textbf{3.19}$$

These Figures and equations show that λ tends to increase to a maximum at P_b/P_w=2.0 before reducing again, whereas Γ tends to be more of less constant at 0.04 for all channel configurations.

Although much of this work was at an elementary level it has highlighted some interesting points. Firstly, it has been shown that this method is able to accurately predict the $\%SF_W$ (which is used in sidewall correction procedures), although not accurate distributions of boundary shear stress or velocity. It has also been shown that it is possible to obtain equations to express the calibration coefficients.

In order to improve on the accuracy of the distributions of boundary shear stress and depth-averaged velocity, a four panel solution was investigated, building on the previous work by Chlebek & Knight (2006) and Omran (2005).

3.3.2 Four panel solution

A four panel solution was undertaken for the rectangular data of Knight et al. (1984). Again, assuming symmetrical flow, only half the channel was modelled and this half

channel was divided into four panels. Initially the four panels were equally spaced (spacing =b/4) and each of the calibration coefficients was altered in turn and later the panel spacing was altered to better account for the secondary current cells. These four panels were divided into 10 sub-panels and the SKM equation applied to each to give a computationally reasonable number of calculations with the minimum number of inputs. The friction coefficient, *f*, was kept constant across the channel and was taken from the experimental data (see **Table 3.1**). These methods have been compared to Knight et al.'s (1994) equation for $\%SF_W$ for subcritical flow, which is of the form:

$$\%SF_W = C_{sf} e^{\alpha} \quad \textbf{3.20}$$

$$\alpha = -3.230 \log_{10}\left(\frac{P_b}{P_w C_2} + 1.0\right) + 4.6052 \quad \textbf{3.21}$$

where,

$C_2 = 1.50$, and $C_{sf} = 1.0$ for $P_b/P_w < 6.546$ **3.22**

otherwise,

$$C_{sf} = 0.5857(P_b/P_w)^{0.28471} \quad \textbf{3.23}$$

3.3.2.1 Four panel solution with constant panel spacing-variation of Γ

It has been shown by Omran (2005) that it is possible to obtain good distributions of depth-averaged velocity by keeping λ constant at 0.07, which will also be assumed in this example. The friction factor, *f*, was calculated from Equation 3.24.

$$f = \frac{8\,\overline{\tau_b}}{1000\,U^2} \qquad \textbf{3.24}$$

where, $\overline{\tau_b}$ is the average boundary shear stress and *U* is the average channel velocity. Γ will be varied using an alternating sign from the centreline (+ - + -), which takes account of the gradient of the lateral gradient of the secondary flow cells (see Chapter 2). This method showed that the Γ values in panels 2 and 3 (the centre panels) were close to zero (± 0.001). This method returned good predictions for $\%SF_W$ and discharge (see **Figure 3.9** and **Table 3.3**).

From this it was found that more accurate distributions of depth-averaged velocity and boundary shear stress could be produced when comparing the measured and modelled data, using the data in **Table 3.3**, rather than the one panel data previously presented. These distributions are shown in **Figures 3.10-3.11**. Comparing **Figures 3.10** and **3.3** (one panel), it is clear that the distribution of depth-averaged velocity is improved and it is only near to the wall the model is unable to predict the velocity profile. Similarly, comparing **Figures 3.4** and **3.11** (distributions of boundary shear stress), the model more accurately represents the shape of the data, but it over predicts the boundary shear stress through panels 1-3 and underestimates it in panel 4. As stated above, the

model fails to predict the distributions near to the wall and the boundary shear distribution is being over predicted in the first three quarters of the channel, and is then significantly under predicted in the last quarter (near to the channel wall). This is due to boundary shear stress being the more sensitive of the two parameters. Overall, the errors in discharge and $\%SF_W$ are low, on average less than 1%. The value of Γ_1 (i.e. Γ in panel 1) tends to decrease with increasing aspect ratio (**Figure 3.12**), which is to be expected as the strength of the secondary current cells diminishes in the centre of wide channels. However, this method results in a high values for Γ_4, (panel 4 is near to the wall) for low aspect ratios ($P_b/P_w \leq 1.0$), as shown in **Figure 3.13**. Equations have been determined for these Γ relationships with the aspect ratio as follows:

$$\Gamma_1 = 0.3408\left(P_b/P_w\right)^{-1.4495} \qquad (R^2=0.7751) \qquad \textbf{3.25}$$

$$\Gamma_4 = -\left[7.3812\left(P_b/P_w\right)^{-2.0378}\right] \qquad (R^2=0.7751) \qquad \textbf{3.26}$$

Physically, this implies that the near wall effects of increased secondary current strength and increased roughness is being lumped into this one parameter (Γ). By increasing λ to 0.14 (chosen to show the effect of doubling the contribution and similar to 0.13 as used in practice), the average error in percentage shear force on the wall increased from 0.38% to 46%, with some runs increasing the error by up to 60%. In order to regain acceptable errors, the value of Γ_4 had to be increased by up to 150% with Γ_1 remaining unchanged. This demonstrates the sensitivity of the model to λ.

By altering λ, it has shown that this has a marked effect on the reduction of depth-averaged velocity and ultimately on the discharge in the channel (see **Insert 1**). In order to rectify this, Γ_4 has to be increased to force the model to increase the calculated depth-averaged velocity values. As the model (in this case) is more sensitive to Γ_4 due to the near wall effects of the secondary current motion, it is this parameter which has the greatest impact on rectifying the effect of λ.

3.3.2.2 Four panel solution with constant panel spacing-variation of λ

In the SKM model, λ is a dimensionless factor which represents the eddy viscosity in the channel. The SKM has been shown by Omran (2005) to produce reasonably accurate distributions of velocity and boundary shear stress in trapezoidal channels using a constant λ value of 0.07. As discussed in Chapter 2, a value of 0.07 is often selected as a constant representing the dimensionless eddy viscosity as this is the depth-averaged value for a logarithmic velocity profile, as shown by Rutherford (1994). Some investigation of this parameter for use in the SKM for rectangular channels has been undertaken in Section 3.3.1 (one-panel solution), but this section will examine its importance in a four-panel solution by keeping Γ and f constant. It has already been shown that the sign for the Γ should alternate +-+- from the centreline of the channel, and therefore this sign convention will also be adopted herein. It was decided to keep Γ as ±0.05 to assess the models reaction to λ. This value was initially chosen on the grounds of simplicity as being not unreasonable, except near to the wall. The friction factor f was also kept constant as before.

It was found that panels 1-3 were not particularly sensitive to λ, and therefore a constant value of 0.07 was found to give the best results overall. By increasing or decreasing the value of λ by up to 50% only had minor effect on the percentage discharge and had a small effect on $\%SF_w$ (up to approximately 3% increase/decrease but the overall error band was within ±5%). λ in panel 4 dominated the model and its value was found to be significantly lower than in panels 1-3. In rectangular channels, the local velocity remains quite constant across the channel until very near to the wall where it diminishes quickly. The SKM assumes that the velocity in the end panel decreases from the interface of panels 3 and 4 to the wall, hence for 4 panels of constant spacing, the model has to be forced to keep the velocity high until near to the wall. This can be done either by increasing Γ or decreasing λ in this end panel. Therefore, in this case λ decreases in panel 4 to take account of the velocity profile in this region. The distribution of λ_4, as shown in **Figure 3.14**, is similar to that of the one panel case. The values of λ_4 increases with aspect ratio and reaches a peak at approximately P_b/P_w=3.5, then the values of λ decrease steadily.

This approach was able to accurately predict the $\%SF_w$ and discharge within the flume with errors of 0.11% and 0.28% respectively. The calculated $\%SF_w$ are shown in comparison to Knight et al. (1994) equation and to the experimental data in **Figure 3.15**. From this it is clear that the SKM accurately predicts the $\%SF_w$, but Knight et al. (1994) equation is slightly over-predicting the percentage shear force acting on the wall.

Although the overall values for $\%SF_w$ and discharge were predicted well by the model, the distributions of boundary shear stress and depth-averaged velocity were not as good at those presented in Section 3.3.2.1. The distribution of depth-averaged velocity (shown in **Figure 3.16**) is reasonable in the most part, although velocity is being slightly over-predicted in panels 1-3. The distribution of bed shear stress (**Figure 3.17**) is however significantly over-predicted in panels 1-3. At the centreline, the model over-estimates the boundary shear stress by almost 25%. However, as the model is unable to predict the boundary shear stress in panel 4 (near to the wall), the errors even out and good overall values of $\%SF_w$ can be achieved. Similar distributions were found for the other channels investigated, although not presented here. A table presenting the coefficients used and the results for discharge and $\%SF_w$ is given in **Table 3.4**.

From this and from the previous trial with a constant λ, it is clear that neither one factor can solely calibrate the model. In both cases the model is unable to compute the distributions of boundary shear stress and velocity near to the channel wall. In this region the flow is often slightly rougher and, hence, the friction factor f increases. In all the cases examined to date, f has been held constant. However, using a constant f does give good overall values of discharge and $\%SF_w$, and in the case of calibrating Γ, reasonable distributions for velocity.

3.3.2.3 Four panel solution with constant panel spacing-variation of f and Γ

Omran (2005) has previously shown that it is possible to use the SKM to model the distributions of boundary shear stress and depth-averaged velocity in simple

trapezoidal channels by varying *f* in each panel, based on experimental data, using a constant λ (0.07) in panels 1-3, varying it in panel 4 and calibrating the model using Γ. The intention of this thesis is not to re-create his results, but to show that it is also possible to model rectangular channels accurately using the SKM and to improve on the distributions shown in Sections 3.3.2.1 and 3.3.2.2.

In this section, data from the 152mm channel will be used as these experiments measured both depth-averaged velocity and also boundary shear stress, thus allowing the calculation of the friction factor across the channel for each panel. The friction factor was calculated in a similar way to that described in Section 3.3.2.1, but here is calculated for each measuring point using Equation 3.27, and then averaged for each panel. Furthermore, the average panel values have been linearly varied across the panel (equation 3.28) to produce smooth boundary shear stress distributions as described elsewhere by Omran (2005).

$$f = \frac{8\,\tau_b}{1000\,U_d^2} \qquad \textbf{3.27}$$

$$f_{linear} = \frac{f_n + f_{n+1}}{2} + \frac{\frac{f_{n+1} + f_{n+2}}{2} - \frac{f_n + f_{n+1}}{2}}{panel\ width} \times y_p \qquad \textbf{3.28}$$

where, τ_b is the point measurement of boundary shear stress and U_d is the depth-averaged velocity at the location of the boundary shear stress measurement and y_p the distance between the panel edge and the location at which friction is to be determined.

The values of panel friction, along with the values used for λ and Γ are given in **Table 3.5**.

From **Table 3.5**, it can be seen that the friction factor increases substantially towards the wall, particularly towards the lower end of the aspect ratios considered. λ was kept at 0.07 for panels 1-3, but decreased slightly to between 0.06-0.065 in panel 4, particularly again at lower aspect ratios. Γ remained largely unchanged from the values found in Section 3.3.2.1, but did decrease slightly in panel 4 in low aspect ratios. This method also calculated $\%SF_w$ and discharge well, with average errors of 0.57% and 1.26% respectively. **Figure 3.18** shows a comparison of the calculated values of $\%SF_w$ to the measured data and to Knight et al. (1994) equation. The results show a good comparison between the three data sets, indicating that the SKM can accurately predict the $\%SF_w$ for a rectangular channel by varying all three coefficients. The distributions of boundary shear stress and depth-averaged velocity improved on those of Section 3.3.2.1, as can be seen in **Figure 3.19** and **3.20**. The data shown are for the 152m wide channel with a depth of 102.6mm. The distribution of depth-averaged velocity compare well to the measured values, but the distribution of boundary shear stress is still being over predicted in the first three panels and under predicted in panel 4. The distributions of the method proposed in Section 3.3.2.1 are also shown. The distributions for both velocity and boundary shear stress are improved when the friction factor is varied, particularly in panel 4 in the case of depth-averaged velocity. However, it is clear that near the boundary with the wall, the model is unable to accurately reproduce the distributions. Therefore, the final

modelling philosophy which is being proposed is to vary the panel spacing and to specify a much smaller panel adjacent to the wall.

3.3.2.4 Four panel solution with variable panel spacing

In the four iterations tried previously, the panel spacing was always kept constant at 0.25b (where *b* is the half width). This resulted in poor prediction of the distributions of depth-averaged velocity and boundary shear stress in panel 4 which was near the wall. In this trial, the panel spacing will be varied. The spacing was changed to 0.25b, 0.325b, 0.325b and 0.1b for panels 1 to 4 respectively. The two middle panels were considered to be less significant from the results above (i.e. it was found that constant values of Γ and λ resulted in good distributions of depth-averaged velocity and boundary shear stress) and were therefore increased in size. Whereas, panel 1 was kept as before as it was considered somewhat influential on the model and panel 4 deemed the most significant and hence the smallest. The location of panel 4 is in keeping with the work of Omran (2005) who studied 'equivalent' secondary flow cells. These cells are identified by comparing the mean boundary shear stress profile to the actual boundary shear stress profile, where the two lines interest this identifies an 'equivalent' cell. Once again the 152mm channel data will be considered here as the friction factor can be calculated from the depth-averaged velocity and boundary shear stress data using Equation 3.27. The friction factor will also be linearly varied across the panel, with λ and Γ being kept constant per panel, but varied between panels.

With this modelling philosophy, much better distributions of boundary shear stress and depth-averaged velocity were produced, particularly in the corner region due to the much smaller panel adjacent to the wall. **Figures 3.21-3.22** show the distributions of boundary shear stress and depth-averaged velocity for the 152mm wide, 102.6mm deep channel. These Figures compare the results from this approach, varying *f* but keeping the panel spacing constant and keeping both the panel spacing and *f* constant. From these Figures it is clear that this approach is better able to replicate the distributions, particularly near to the wall, especially for depth-averaged velocity. Boundary shear stress measurements are taken closer to the wall than velocity data and therefore in order to model this distribution more accurately, at least one additional panel near to the wall is required. This has not been undertaken as for most uses the model is able to accurately predict the boundary shear stress distribution and hence the percentage shear force on the wall, which is shown in **Figure 3.23**. In this case the average error for calculated percentage shear force on the wall was 1.79%, with zero average error in discharge (**Table 3.6**).

The modelling philosophy of this approach mirrored that of the previous approaches. The value of λ was constant in panels 1-3, λ_1 and λ_2 was kept constant at 0.07, whilst λ_3 was decreased to 0.045 in all but one case (P_b/P_w=0.89). λ_4 was found to reduce with decreasing aspect ratio, which is consistent with what was found in Section 3.3.2.2. Γ was found to stay constant in panels 2 and 3 (±0.001), whilst in panel 1 it increased with decreasing aspect ratio and Γ_4 increased negatively with decreasing aspect ratio. Unlike previous methods where Γ_4 was very negative (**Table 3.3,** 70mm channel Γ_4=-254), this method resulted in more realistic values of Γ (of -5 to -16) as

the friction factor was also varied across the channel. These values are still higher than those proposed by Abril & Knight (2004), Equation 2.39 herein, but it needs to be borne in mind that this equation was not developed for flow in rectangular channels, nor does it account for changing of sign between panels in simple channels, but assumes it is constant.

3.4 Relative contribution of terms in the SKM for smooth rectangular channels

In order to give guidance on using the SKM and the values of the coefficients (f, λ and Γ) for rectangular channels, it is important to know the relative contribution of each factor in the model and how they vary with position within the channel.

The SKM equation for a rectangular channel where the side slope, s, is zero is given below in Equation 3.29, and has four main terms:

$$\rho g H S_0 - \rho \frac{f}{8} U_d{}^2 + \frac{\partial}{\partial y}\left[\rho \lambda H^2 \sqrt{\frac{f}{8}} U_d \frac{\partial U_d}{\partial y} \right] = \frac{\partial}{\partial y}\left[H(\rho UV)_{\mathrm{d}} \right] \qquad \textbf{3.29}$$

Term 1 Term 2 Term 3 Term 4

Where terms 1-4 represent,

Term 1- the weight of the fluid component in the longitudinal direction

Term 2- for the bed friction

Term 3- the lateral shear

Term 4- the secondary flow currents

Terms 1 and 2 can be easily calculated based on the geometry of the channel and velocity data, and term 4 is simply equal to Γ in the particular panel which is being examined. Therefore, term 3 can be calculated by Equation 3.30. The percentage contribution is calculated by taking the magnitude of the term in question and dividing it by the sum of the magnitude of all terms as in Equation 3.31.

$$\frac{\partial}{\partial y}\left[\rho\lambda H^2\sqrt{\frac{f}{8}}U_d\frac{\partial U_d}{\partial y}\right]=\rho\frac{f}{8}U_d{}^2-\rho gHS_0+\frac{\partial}{\partial y}\left[H(\rho UV)_{\mathrm{d}}\right] \qquad \textbf{3.30}$$

$$\%\ contribution=\frac{|Term|}{|sum\ of\ terms|}\times 100\% \qquad \textbf{3.31}$$

Table 3.7 gives the percentage contributions per panel, and this is also shown graphically in **Figures 3.24-3.27**. From these Tables and Figures, it is clear that in panels 1-3, the contribution of weight (Term 1) and friction (Term 2) are similar and are on average 50% and 20% respectively. Term 3 (lateral shear) is low in panel 1 (5%), but higher in panels 2 and 3 (approximately 30%). In panels 2 and 3, the secondary current term has only negligible contribution (less than 1%), whereas panel 1 has a higher contribution of 23%. This is due to the position and size of the secondary current cells. Panel 4 has quite different contributions of terms. The weight term is unsurprisingly much smaller given the panel size and only accounts for approximately 6% of the total. Similarly, the friction term also contributes significantly less in this panel due to the notably increased contribution of lateral shear and secondary currents. The lateral shear term and secondary current term in

panel 4 increases to 48% and 44% respectively. This substantial increase is due to the position of the secondary current cells in this location.

3.5 Recommendations for modelling rectangular channels

It has been shown that the SKM is able to accurately model the lateral distributions of depth-averaged velocity and boundary shear stress. Further, it is capable of predicting the discharge and $\%SF_w$ to within ±2%, well within the bands of accuracy of the measured data.

The panel spacing has a significant effect on the accuracy of the model; 4 panels of equal spacing give reasonably good approximations of discharge and $\%SF_w$, but is unable to predict the distributions of depth-averaged velocity and boundary shear stress in the region close to the wall. Using a smaller panel adjacent to the wall results in better distributions, but slightly less good overall values of discharge and $\%SF_w$. More panels will increase the accuracy of the model, but it is not believed that it will be significant for most applications. Thus, four panels, with spacings of 0.25b, 0.325b, 0.325b and 0.1b for panels 1-4 respectively, are recommended for SKM modelling of flow in simple rectangular channels.

It is recommended that f be calculated from available data, or if it is a natural channel f should be estimated based on field observations. The Conveyance and Afflux Estimation System (CAES) which is available within ISIS, can be used to estimate Manning's roughness coefficient based on vegetation, bed material and irregularities. This will help the inexperienced modeller to estimate the roughness in the channel.

Manning's roughness coefficient can be used to estimate the friction coefficient. Where data are unavailable, it is suggested that a constant value of *f* be used initially, and then increased in panels 2-4 if the results are unacceptable.

Γ should be varied in panels 1 and 4, with panels 2 and 3 being kept constant and close to zero. Γ is most significant in panel 4, but panel 1 is still influential, particularly on boundary shear stress. Γ_4 becomes increasingly negative with decreasing aspect ratio, while Γ_1 becomes increasingly positive.

In most cases, λ=0.07 should be adopted, at least in panels 1 and 2. Depending on the aspect ratio of the channel, λ_3 should be reduced from 0.07 and in all cases λ_4 is smaller than $\lambda_{1\text{-}3}$.

3.6 Modelling simple trapezoidal channels

In order to complement the work on rectangular channels and to give foundation to Chapter 4 (modelling of trapezoidal channels with heterogeneous roughness), the SKM modelling of simple trapezoidal channels was also undertaken, using the data from Yuen (1989). Yuen carried out a total of 56 experiments using a number of channel dimensions, slopes and discharges, but of these 56 experiments only eight will be examined here. The experiments which have been selected have measured both boundary shear stress and depth-averaged velocity and have a number of different channel geometries and discharges. The aspect ratios (P_b/P_w) range from 0.35-3.54 with a mixture of sub and supercritical flow. **Table 3.2** details the

experiments used in this Section. The approach adopted has reflected the lessons learned from Section 3.3, but also draws on the work of Omran (2005).

The half channel will again be split into four panels, two equally spaced panels on the bed at spacing b/2, and two equally spaced panels on the sloping wall at spacing H/2 (as s=1). No small wall panel will be required in this instance as the secondary currents in trapezoidal channels are not formed on top of one another as in rectangular channels (see **Figures 2.5** and **2.6** for secondary current formations in rectangular and trapezoidal channels).

It was found that this model was able to accurately predict the overall values of discharge and $\%SF_w$ (see **Table 3.8** for modelling coefficients in addition to discharge and $\%SF_w$ results). The boundary shear stress and depth-averaged velocity distribution were predicted well when there were little perturbations in the shear stress, but in cases where there were perturbations it resulted in an "averaging out". Plots of the distributions are given in **Figures 3.28-3.31**, with the comparison of $\%SF_w$ to Knight et al. (1994) method given in **Figure 3.32**.

From these models it is clear that the coefficients are influenced by a number of factors such as bed slope and aspect ratio. It is also clear that the Γ term in panel 4 is less influential than in rectangular channels as the secondary flow cells do not form on top of one another.

The friction factor plays an important role in the prediction of the distributions of boundary shear stress and depth-averaged velocity, and as in the rectangular channels, increases in magnitude close to the wall. Ideally, measured data would be used to calibrate the model.

In the rectangular channel it was found that λ reduced near to the walls, this is not the case in the trapezoidal channel, and generally the λ values were quite constant throughout the channel, especially in panels 2-4 where λ increased from that in panel 1.

It was found that as the longitudinal bed slope increased, S_o, the values of Γ became more constant throughout the channel, possibly due to the smoother boundary shear stress distributions (see **Figure 3.31**). Generally Γ_4 was lower than that of $\Gamma_{1\text{-}3}$ and Γ_2 and Γ_3 play a more significant role than in the rectangular channels. This is due to the changing angle of the wall at the interface between panels 2 and 3. From **Figure 3.32**, it is clear that the SKM approach presented here in can accurately compute the $\%SF_w$ for both rectangular and trapezoidal data.

3.7 Relative contribution of terms in the SKM for smooth trapezoidal channels

As in Section 3.5, the relative contributions of each term in the SKM were analysed for smooth trapezoidal channels to show where each term has most effect on the model as a whole. This was based on the method outlined in Section 3.5, but the full SKM equation (equation 3.32) will be used, i.e. with side slope included.

$$\rho g H S_0 - \rho \frac{f}{8} U_d{}^2 \sqrt{1+\frac{1}{s^2}} + \frac{\partial}{\partial y}\left[\rho \lambda H^2 \sqrt{\frac{f}{8}} U_d \frac{\partial U_d}{\partial y}\right] = \frac{\partial}{\partial y}\left[H(\rho UV)_d\right] \qquad \textbf{3.32}$$

Term 1 Term 2 Term 3 Term 4

The weighting of each term is calculated as per Section 3.5.

Table 3.9 gives the percentage contributions per panel, and this is also shown graphically in **Figures 3.33-3.36**. From these Tables and Figures, it can be seen that the results are quite different from the rectangular channel data. In panels 1 and 2 the contributions of each term are similar between panels; the weight term is approximately 38%, friction is on average 35%, lateral shear 22% and secondary currents term is on average 5%. These values are similar to natural river data presented by McGahey (2006) which is not surprising considering most of the channels studied by McGahey can be idealised to a trapezoidal section. In panels 3 and 4 the contribution of weight diminishes to 28% in panel 3 and to 15% in panel 4, whereas the friction term becomes more significant and raises to 41% in panel 3 and to 50% in panel 4. This was to be expected as the friction increased towards the wall. The lateral shear term increases slightly in panels 3 and 4, to approximately 27% indicating that there are increased shear in the sloping region in comparison to the flat bed. The secondary current term is similar to those in panels 1 and 2 and is, on average, 5%. The contribution of secondary flow cells do not increase as in rectangular channels as trapezoidal channels do not have as complex a cell arrangement near to the wall as rectangular channels do.

3.8 Recommendations for modelling trapezoidal channels

It has been found that the method used to model trapezoidal and rectangular channels is similar. The friction factor plays an important role in the accurate prediction of the boundary shear stress and depth-averaged velocity profiles. Γ also plays an important role in the profile predictions, but particularly in the computation of the overall values of discharge and $\%SF_w$. λ plays a less significant role in the prediction of discharge and $\%SF_w$ in rectangular channels (with the exception of λ_4), but is significant in trapezoidal channels, particularly in panels 2-4.

The panel spacing in trapezoidal channels is dictated by the shape of the channel; two panels on the horizontal portion and two panels on the sloping wall. As with rectangular channels, if the channel is symmetrical (in all respects including geometry and roughness), only half of the channel needs to be analysed.

3.9 Concluding remarks

Although the Shiono and Knight Method was developed for overbank flow, it has been shown that it is possible to accurately model the distributions of depth-averaged velocity and boundary shear stress. Further, it can accurately predict the overall discharge and $\%SF_w$ within the channel for both rectangular and trapezoidal geometries.

The following conclusions have been drawn with regards to modelling methodology:

- Rectangular channels should have variable panel spacing with a small panel near to the wall to take account of the secondary current cells which form on top of one another in this region.
- It is proposed that the panel spacing should be set at 0.25b, 0.325b, 0.325b and 0.1b; assuming the channel is symmetrical with smooth bed and walls.
- Four panels gives good distributions of depth-averaged velocity and boundary shear stress (**Figures 3.21** and **3.22**) in addition to overall discharge and $\%SF_w$ (**Figure 3.23**). Using only one panel can give a good approximation of discharge and $\%SF_w$ (**Figure 3.2**) with little effort.
- Trapezoidal channels can also be modelled using four panels, but with two equally spaced panels on the flat bed and two equally spaced panels in the sloping region.
- Less than four panels give good overall values for discharge and %SFw, and although increasing the number of panels will lead to more accurate distributions, it is not believed that it will significantly improve the results. A comparison has been made to Omran's 6 panel method and the proposed four panel approach for Yuen's Experiment 8 in **Figures 3.37-3.38**. From these it is clear that the six panel method predicts the depth-averaged velocity no better than the four panel approach. It does predict the boundary shear stress slightly better, but results with a larger error in $\%SF_w$ in this particular case.
- The friction factor is very influential on the model, and ideally friction factor data would be used to calibrate the model. When the friction factor is kept constant across the channel it results in a high value of Γ_4.
- Γ should increase towards the wall, and in the case of the rectangular channel, the Γ values in panels 2 and 3 are close to zero. In trapezoidal channels, Γ_2 and Γ_3 are

more important and where there is a steep bed slope ($S_0 \geq 8.7 \times 10^{-3}$) Γ is more constant across the channel.

- λ tends to reduce towards the wall in the rectangular channel. It is recommended that $\lambda_{1\text{-}3}$ be kept at a constant value of 0.07.
- In trapezoidal channels, the λ value increases towards the wall. The λ values in panels 2 and 3 are also more influential due to the change in side slope of the bed.
- The relative contribution of the SKM terms for trapezoidal and rectangular channels have been calculated. This showed that in rectangular channels the contribution of secondary current cells increases significantly near the wall, but in trapezoidal channels the contribution of secondary currents is more constant across the channel width (at approximately 5%). This is due to the position and strength of the cells in rectangular channels.

This work gave a good indication of the methodology of modelling simple trapezoidal and rectangular channels. However, most "real-life" modelling applications involve roughened beds and/or walls. The following Chapter will draw on the lessons learned from the smooth cases and use the Shiono and Knight method to model the boundary shear stress and velocities in heterogeneously roughened channels.

Exp	B, mm	b, mm	H, mm	P_b/P_w	$S_o \times 10^{-3}$	Q, l/s	Q, m^3/s	U=Q/A, m/s	τ_e, N/m^2	$\%SF_w$	f
1	610	305	31.9	9.56	9.66	6.19	0.00619	0.3181	0.2736	6.89	0.0216
2	610	305	36.0	8.47	9.66	7.47	0.00747	0.3402	0.3050	7.45	0.0211
3	610	305	41.8	7.30	9.66	9.27	0.00927	0.3636	0.3482	8.28	0.0211
4	610	305	51.5	5.92	9.66	11.96	0.01196	0.3807	0.4174	10.79	0.0230
5	610	305	63.8	4.78	9.66	16.35	0.01635	0.4201	0.4998	12.56	0.0227
6	610	305	78.9	3.87	9.66	22.34	0.02234	0.4642	0.5937	16.01	0.0220
7	610	305	90.2	3.38	9.66	28.66	0.02866	0.5209	0.6594	19.93	0.0194
8	381	190.5	56.1	3.40	9.66	8.17	0.00817	0.3822	0.4105	19.56	0.0225
9	381	190.5	64.1	2.97	9.66	10.21	0.01021	0.4181	0.4543	22.01	0.0208
10	381	190.5	80.4	2.37	9.66	13.30	0.01330	0.4342	0.5356	25.60	0.0227
11	381	190.5	88.5	2.15	9.66	15.50	0.01550	0.4597	0.5724	27.24	0.0217
12	381	190.5	97.5	1.95	9.66	18.38	0.01838	0.4948	0.6109	30.75	0.0200
13	381	190.5	108.6	1.75	9.66	22.31	0.02231	0.5392	0.6552	31.50	0.0180
14	381	190.5	123.3	1.55	9.66	26.60	0.02660	0.5662	0.7090	35.64	0.0177
15	152	76	76.0	1.00	9.66	3.90	0.02231	0.3380	0.3600	47.50	0.0252
16	152	76	85.8	0.89	9.66	4.80	0.02660	0.3680	0.3820	51.34	0.0226
17	152	76	97.0	0.78	9.66	5.60	0.00560	0.3800	0.4040	54.87	0.0224
18	152	76	102.6	0.74	9.66	6.07	0.00607	0.3890	0.4140	54.98	0.0219
19	152	76	113.6	0.67	9.66	7.00	0.00700	0.4050	0.4310	56.85	0.0210
20	152	76	125.9	0.60	9.66	8.00	0.00800	0.4180	0.4490	60.67	0.0206
21	152	76	153.0	0.50	9.66	9.85	0.00985	0.4240	0.4810	67.00	0.0214
22	70	35	103.8	0.34	9.66	1.98	0.00198	0.2725	0.2479	73.60	0.0267
23	70	35	120.9	0.29	9.66	2.39	0.00239	0.2824	0.2571	77.10	0.0258
24	70	35	144.3	0.24	9.66	2.99	0.00299	0.2960	0.2668	80.70	0.0244
25	70	35	223.7	0.16	9.66	4.65	0.00465	0.2970	0.2866	85.20	0.0260

Table 3.1-Knight et al. (1984) rectangular channel data

Exp	B, mm	b, mm	H, mm	P_b/P_w	$S_o \times 10^{-3}$	Q, l/s	Q, m^3/s	U=Q/A, m/s	τ_e, N/m^2	$\%SF_w$	Fr	f
8	150	75	75	0.71	1.00	7	0.007	0.207	0.45698	28.712	0.5585	2.13E-02
13	150	75	100	0.53	1.00	12	0.012	0.686	0.56641	31.981	0.5735	1.97E-02
16	150	75	150	0.35	1.00	26.3	0.0263	0.779	0.76846	36.2315	0.5902	1.80E-02
23	450	225	45	3.54	1.00	8.2	0.0082	0.480	0.378401	9.0155	0.5788	2.23E-02
26	450	225	60	2.65	1.00	13.42	0.01342	0.785	0.484236	10.822	0.6044	2.01E-02
206	150	75	73	0.73	8.7050	23.9	0.0239	2.212	3.898789	26.7085	1.9991	1.45E-02
406	150	75	73	0.73	23.3702	39	0.039	3.610	10.466015	26.7	3.2621	1.46E-02
407	150	75	99	0.54	23.7019	66.3	0.0663	3.849	13.138161	31.148	3.2269	1.45E-02

Table 3.2-Yuen (1989) trapezoidal channel data

B, mm	H, mm	B/H	f	λ_1	λ_2	λ_3	λ_4	Γ_1	Γ_2	Γ_3	Γ_4	$\%SF_w$	$\%SF_w$ % error	Q, m^3/s	Q, %error	Q, l/s	P_b/P_w
610	31.9	19.12	0.022	0.07	0.07	0.07	0.07	0.02	-0.001	0.001	-0.06	6.95	0.93	0.01	0.36	6.21	9.56
610	36	16.94	0.021	0.07	0.07	0.07	0.07	0.001	-0.001	0.001	-0.051	7.49	0.48	0.01	0.58	7.51	8.47
610	41.8	14.59	0.021	0.07	0.07	0.07	0.07	0.002	-0.001	0.001	-0.085	8.29	0.16	0.01	0.91	9.35	7.30
610	51.5	11.84	0.023	0.07	0.07	0.07	0.07	0.05	-0.001	0.001	-0.2	10.69	-0.93	0.01	0.94	12.07	5.92
610	63.8	9.56	0.023	0.07	0.07	0.07	0.07	0.05	-0.001	0.001	-0.33	12.55	-0.09	0.02	1.46	16.59	4.78
610	78.9	7.73	0.022	0.07	0.07	0.07	0.07	0.07	-0.001	0.001	-0.53	16.11	0.63	0.02	1.24	22.62	3.87
610	90.2	6.76	0.019	0.07	0.07	0.07	0.07	0.15	-0.001	0.001	-0.85	19.97	0.23	0.03	0.29	28.74	3.38
381	56.1	6.79	0.022	0.07	0.07	0.07	0.07	0.1	-0.001	0.001	-0.5	19.56	-0.01	0.01	0.52	8.21	3.40
381	64.1	5.94	0.021	0.07	0.07	0.07	0.07	0.1	-0.001	0.001	-0.7	21.95	-0.26	0.01	0.51	10.26	2.97
381	80.4	4.74	0.023	0.07	0.07	0.07	0.07	0.1	-0.001	0.001	-1.18	25.76	0.61	0.01	0.95	13.43	2.37
381	88.5	4.31	0.022	0.07	0.07	0.07	0.07	0.1	-0.001	0.001	-1.63	27.45	0.78	0.02	1.24	15.69	2.15
381	97.5	3.91	0.020	0.07	0.07	0.07	0.07	0.34	-0.001	0.001	-2.9	30.82	0.22	0.02	0.72	18.51	1.95
381	108.6	3.51	0.018	0.07	0.07	0.07	0.07	0.34	-0.001	0.001	-4.24	31.96	1.47	0.02	1.76	22.70	1.75
381	123.3	3.09	0.018	0.07	0.07	0.07	0.07	0.34	-0.001	0.001	-5.58	35.99	0.99	0.03	1.01	26.87	1.55
152	76	2.00	0.025	0.07	0.07	0.07	0.07	0.49	-0.001	0.001	-6.7	47.58	0.17	0.00	0.99	3.94	1.00
152	85.8	1.77	0.023	0.07	0.07	0.07	0.07	0.5	-0.001	0.001	-9.3	51.34	0.00	0.00	0.20	4.81	0.89
152	97	1.57	0.022	0.07	0.07	0.07	0.07	0.7	-0.001	0.001	-13	55.75	1.61	0.01	-1.10	5.54	0.78
152	102.6	1.48	0.022	0.07	0.07	0.07	0.07	0.8	-0.001	0.001	-16	55.46	0.89	0.01	0.72	6.11	0.74
152	113.6	1.34	0.021	0.07	0.07	0.07	0.07	0.8	-0.001	0.001	-20.9	57.70	1.51	0.02	1.17	18.51	0.67
152	125.9	1.21	0.021	0.07	0.07	0.07	0.07	1	-0.001	0.001	-27	61.05	0.62	0.01	0.24	8.02	0.60
152	153	0.99	0.021	0.07	0.07	0.07	0.07	1	-0.001	0.001	-40	66.54	-0.68	0.01	-0.97	9.75	0.50
70	103.8	0.67	0.027	0.07	0.07	0.07	0.07	0.9	-0.001	0.001	-43.5	73.85	0.34	0.00	0.39	1.99	0.34
70	120.9	0.58	0.026	0.07	0.07	0.07	0.07	0.9	-0.001	0.001	-62	76.85	-0.33	0.00	0.10	2.39	0.29
70	144.3	0.49	0.024	0.07	0.07	0.07	0.07	0.9	-0.001	0.001	-93	80.26	-0.55	0.00	-0.86	2.96	0.24
70	223.7	0.31	0.026	0.07	0.07	0.07	0.07	3	-0.001	0.001	-254	85.89	0.81	0.00	0.76	4.69	0.16
												Ave error	0.38 %		0.57 %		

Table 3.3-Modelling data used (constant *f* per experiment, λ and vary Γ in panels 1 and 4), panel spacing=0.25b

B, mm	H, mm	B/H	f	λ_1	λ_2	λ_3	λ_4	Γ_1	Γ_2	Γ_3	Γ_4	$\%SF_w$	$\%SF_w$ % error	Q, m^3/s	Q, %error	Q, l/s
610	31.9	19.12	0.022	0.07	0.07	0.07	0.0320	0.05	-0.05	0.05	-0.05	6.84	-0.66	0.0062	0.54%	9.56
610	36	16.94	0.021	0.07	0.07	0.07	0.0310	0.05	-0.05	0.05	-0.05	7.49	0.54	0.0075	0.80%	8.47
610	41.8	14.59	0.021	0.07	0.07	0.07	0.0300	0.05	-0.05	0.05	-0.05	8.36	0.98	0.0094	1.11%	7.30
610	51.5	11.84	0.023	0.07	0.07	0.07	0.0370	0.05	-0.05	0.05	-0.05	10.85	0.51	0.0121	0.89%	5.92
610	63.8	9.56	0.023	0.07	0.07	0.07	0.0340	0.05	-0.05	0.05	-0.05	12.68	0.99	0.0166	1.39%	4.78
610	78.9	7.73	0.022	0.07	0.07	0.07	0.0365	0.05	-0.05	0.05	-0.05	16.14	0.83	0.0226	1.11%	3.87
610	90.2	6.76	0.019	0.07	0.07	0.07	0.0400	0.05	-0.05	0.05	-0.05	19.84	-0.43	0.0287	0.03%	3.38
381	56.1	6.79	0.022	0.07	0.07	0.07	0.0400	0.05	-0.05	0.05	-0.05	19.42	-0.73	0.0082	0.33%	3.40
381	64.1	5.94	0.021	0.07	0.07	0.07	0.0380	0.05	-0.05	0.05	-0.05	21.98	-0.16	0.0102	0.18%	2.97
381	80.4	4.74	0.023	0.07	0.07	0.07	0.0340	0.05	-0.05	0.05	-0.05	25.54	-0.23	0.0134	0.78%	2.37
381	88.5	4.31	0.022	0.07	0.07	0.07	0.0314	0.05	-0.05	0.05	-0.05	27.47	0.85	0.0156	0.89%	2.15
381	97.5	3.91	0.020	0.07	0.07	0.07	0.0310	0.05	-0.05	0.05	-0.05	30.82	0.23	0.0184	0.01%	1.95
381	108.6	3.51	0.018	0.07	0.07	0.07	0.0246	0.05	-0.05	0.05	-0.05	31.79	0.92	0.0226	1.26%	1.75
381	123.3	3.09	0.018	0.07	0.07	0.07	0.0230	0.05	-0.05	0.05	-0.05	35.33	-0.88	0.0268	0.94%	1.55
152	76	2.00	0.025	0.07	0.07	0.07	0.0200	0.05	-0.05	0.05	-0.05	47.14	-0.76	0.0039	0.60%	1.00
152	85.8	1.77	0.023	0.07	0.07	0.07	0.0180	0.05	-0.05	0.05	-0.05	51.64	0.59	0.0048	-0.88%	0.89
152	97	1.57	0.022	0.07	0.07	0.07	0.0160	0.05	-0.05	0.05	-0.05	54.87	0.01	0.0055	-0.92%	0.78
152	102.6	1.48	0.022	0.07	0.07	0.07	0.0140	0.05	-0.05	0.05	-0.05	54.97	-0.02	0.0061	0.49%	0.74
152	113.6	1.34	0.021	0.07	0.07	0.07	0.0123	0.05	-0.05	0.05	-0.05	57.37	0.92	0.0071	0.82%	0.67
152	125.9	1.21	0.021	0.07	0.07	0.07	0.0115	0.05	-0.05	0.05	-0.05	60.85	0.29	0.0080	-0.25%	0.60
152	153	0.99	0.021	0.07	0.07	0.07	0.0100	0.05	-0.05	0.05	-0.05	66.10	-1.34	0.0097	-1.02%	0.50
70	103.8	0.67	0.027	0.07	0.07	0.07	0.0075	0.05	-0.05	0.05	-0.05	74.14	0.73	0.0020	-0.86%	0.34
70	120.9	0.58	0.026	0.07	0.07	0.07	0.0063	0.05	-0.05	0.05	-0.05	76.96	-0.19	0.0024	-0.81%	0.29
70	144.3	0.49	0.024	0.07	0.07	0.07	0.0051	0.05	-0.05	0.05	-0.05	79.94	-0.95	0.0030	-0.72%	0.24
70	223.7	0.31	0.026	0.07	0.07	0.07	0.0033	0.05	-0.05	0.05	-0.05	85.80	0.70	0.0047	0.39%	0.16
												Ave error	0.11	%	0.28%	

Table 3.4-Modelling data used (constant *f* per experiment, Γ and vary λ in panel 4), panel spacing=0.25b

B, mm	H, mm	B/H	f_1	f_2	f_3	f_4	λ_1	λ_2	λ_3	λ_4	Γ_1	Γ_2	Γ_3	Γ_4	$\%SF_w$	$\%SF_w$ % error	Q, m^3/s	Q, %error	P_b/P_w
152	85.8	1.77	0.0197	0.0203	0.0216	0.0309	0.07	0.07	0.07	0.065	0.07	-0.001	0.001	-8.1	51.58	0.47	0.0048	-0.11	0.89
152	97	1.57	0.0195	0.0197	0.0212	0.0305	0.07	0.07	0.07	0.06	0.07	-0.001	0.001	-10	55.83	1.74	0.0056	0.76	0.78
152	102.6	1.48	0.0207	0.0201	0.0220	0.0296	0.07	0.07	0.07	0.065	0.07	-0.001	0.001	-13	56.09	2.03	0.0060	1.97	0.74
152	113.6	1.34	0.0210	0.0201	0.0211	0.0269	0.07	0.07	0.07	0.065	0.8	-0.05	0.05	-20.9	57.15	0.53	0.0069	0.77	0.67
152	125.9	1.21	0.0195	0.0194	0.0209	0.0280	0.07	0.07	0.07	0.065	0.05	-0.001	0.05	-24	60.77	0.16	0.0079	1.81	0.60
152	153	0.99	0.0205	0.0212	0.0220	0.0271	0.07	0.07	0.07	0.07	0.05	-0.001	0.05	-40	65.97	-1.53	0.0096	2.37	0.50
															Ave error	0.57	%	1.26	%

Table 3.5-Modelling data used, (vary *f* per panel, per experiment, Γ panels 1 and 4 and λ in panel 4), panel spacing=0.25b

B, mm	H, mm	B/H	f_1	f_2	f_3	f_4	λ_1	λ_2	λ_3	λ_4	Γ_1	Γ_2	Γ_3	Γ_4	$\%SF_w$	$\%SF_w$ % error	Q, m^3/s	Q %error	P_b/P_w
152	85.8	1.77	0.020	0.020	0.022	0.030	0.07	0.07	0.07	0.0125	0.300	-0.001	0.001	-5.0	52.45	2.16	0.0049	-2.03%	0.89
152	97	1.57	0.020	0.020	0.021	0.030	0.07	0.07	0.045	0.011	0.450	-0.001	0.001	-5.5	56.16	2.36	0.0057	-1.70%	0.78
152	102.6	1.48	0.021	0.020	0.022	0.029	0.07	0.07	0.045	0.009	0.600	-0.001	0.001	-5.5	56.13	2.10	0.0061	-0.70%	0.74
152	113.6	1.34	0.021	0.020	0.021	0.026	0.07	0.07	0.045	0.009	0.600	-0.001	0.001	-7.5	58.26	2.49	0.0070	-0.04%	0.67
152	125.9	1.21	0.019	0.019	0.021	0.028	0.07	0.07	0.045	0.009	0.600	-0.001	0.001	-10.5	61.70	1.69	0.0080	0.52%	0.60
152	153	0.99	0.021	0.021	0.022	0.027	0.07	0.07	0.045	0.009	0.600	-0.001	0.001	-16.0	66.97	-0.05	0.0097	1.89%	0.50
															Ave error	1.79	%	0.00	%

Table 3.6-Modelling data used, (vary *f*, Γ and λ), panel 1=0.25b; panel 2=0.325b; panel 3=0.325b; panel 4=0.1b

	Panel 1-percentage weightings of terms				Panel 2-percentage weightings of terms				Panel 3-percentage weightings of terms				Panel 4-percentage weightings of terms			
H, m	**Term 1**	**Term 2**	**Term 3**	**Term 4**	**Term 1**	**Term 2**	**Term 3**	**Term 4**	**Term 1**	**Term 2**	**Term 3**	**Term 4**	**Term 1**	**Term 2**	**Term 3**	**Term 4**
0.0858	50.00	24.67	7.06	18.26	49.94	24.39	25.61	0.06	50.00	22.23	27.71	0.06	7.05	2.21	47.79	42.95
0.097	50.00	22.92	2.85	24.23	49.95	22.52	27.48	0.05	50.00	20.38	29.56	0.05	7.22	1.98	48.02	42.78
0.1026	46.70	21.47	3.30	28.53	49.95	22.10	27.90	0.05	50.00	21.13	28.81	0.05	7.58	2.06	47.94	42.42
0.1136	49.86	22.49	0.14	27.51	49.95	21.37	28.63	0.05	50.00	19.59	30.36	0.05	6.33	1.57	48.43	43.67
0.1259	50.00	19.97	5.13	24.89	49.96	19.49	30.51	0.04	50.00	18.26	31.70	0.04	5.15	1.26	48.74	44.85
0.153	50.00	17.32	12.20	20.48	49.97	17.34	32.66	0.03	50.00	15.95	34.01	0.03	4.19	0.82	49.18	45.81

Table 3.7-Relative percentage contribution of each term in the SKM, rectangular channel data with variable panel spacing (panel 1=0.25b; panel 2=0.325b; panel 3=0.325b; panel 4=0.1b), see Equations 3.29-31

Experiment	b, m	h, m	P_b/P_w	Q, l/s	Fr	S_o	f_1	f_2	f_3	f_4	λ_1	λ_2	λ_3	λ_4	Γ_1	Γ_2	Γ_3	Γ_4
8	0.075	0.075	0.707107	7	0.5585	1	0.0214	0.0223	0.0233	0.0296	0.05	0.07	0.3	0.3	0.300	-0.23	0.03	-0.1
13	0.075	0.1	0.53033	12	0.5735	1	0.0191	0.0192	0.0220	0.0285	0.03	0.07	0.2	0.2	0.300	-0.2	0.03	-0.03
16	0.075	0.15	0.353553	26.3	0.5902	1	0.0178	0.0181	0.0193	0.0220	0.07	0.07	0.3	0.4	0.060	-0.06	0.04	-0.04
23	0.225	0.045	3.535534	8.2	0.5788	1	0.0230	0.0228	0.0268	0.0314	0.07	1	0.5	0.07	0.030	-0.001	0.05	-0.03
26	0.225	0.06	2.65165	13.42	0.6044	1	0.0215	0.0205	0.0229	0.0235	0.07	0.7	0.7	0.07	0.030	-0.001	0.05	-0.03
206	0.075	0.073	0.72648	23.9	1.9991	8.706	0.0141	0.0152	0.0178	0.0237	0.09	0.09	0.08	0.1	1.2	-1	1.2	-1.2
406	0.075	0.073	0.72648	39	3.2621	23.37	0.0143	0.0156	0.0178	0.0230	0.13	0.1	0.1	0.13	2.1	-2.1	2.1	-2.1
407	0.075	0.099	0.535687	66.3	3.2269	23.37	0.0143	0.0149	0.0164	0.0260	0.1	0.1	0.1	0.1	2	-1	0.9	-0.9

Experiment	b, m	h, m	P_b/P_w	$\%SF_w$	$\%SF_w$ % error	Q, m^3/s	Q, %error	Q, l/s
8	0.075	0.075	0.707	55.36	-0.11	0.0069	0.73	6.95
13	0.075	0.1	0.530	61.70	-3.54	0.0119	0.43	11.95
16	0.075	0.15	0.354	71.09	-1.90	0.0265	-0.68	26.48
23	0.225	0.045	3.536	18.33	1.63	0.0080	1.90	8.04
26	0.225	0.06	2.652	21.72	0.37	0.0132	1.29	13.25
206	0.075	0.073	0.726	52.85	-1.07	0.0237	0.95	23.67
406	0.075	0.073	0.726	52.93	-0.88	0.0388	0.58	38.77
407	0.075	0.099	0.536	61.26	-1.66	0.0664	-0.22	66.45
				Ave error	-0.90	%	0.62	%

Table 3.8-Modelling data used and results for Yuen (1989) data, (vary *f*, Γ and λ), panel 1=panel 2=0.5b; panel 3=4=0.5H

	Panel 1-percentage weightings of terms				Panel 2-percentage weightings of terms				Panel 3-percentage weightings of terms				Panel 4-percentage weightings of terms			
Exp	**Term 1**	**Term 2**	**Term 3**	**Term 4**	**Term 1**	**Term 2**	**Term 3**	**Term 4**	**Term 1**	**Term 2**	**Term 3**	**Term 4**	**Term 1**	**Term 2**	**Term 3**	**Term 4**
16	50.00	46.99	0.98	2.04	48.04	44.74	5.26	1.96	27.66	49.00	22.34	1.00	10.24	50.00	38.65	1.11
13	32.42	40.09	17.58	9.91	41.24	50.00	5.40	3.36	20.39	49.17	29.61	0.83	7.26	50.00	37.40	5.33
206	50.00	21.98	18.40	9.62	43.09	19.87	30.13	6.91	43.23	38.91	6.77	11.09	19.84	50.00	14.88	15.28
8	25.47	39.61	24.53	10.39	31.19	50.00	9.06	9.75	16.79	49.09	33.21	0.91	5.70	50.00	41.20	3.10
23	20.05	48.64	29.95	1.36	21.76	50.00	28.19	0.05	10.01	48.49	39.99	1.51	4.40	50.00	44.41	1.19
26	23.90	48.78	26.10	1.22	26.74	50.00	23.22	0.05	12.84	48.55	37.16	1.45	6.19	50.00	42.54	1.26
407	50.00	11.38	34.22	4.41	47.89	11.08	38.92	2.11	50.00	21.93	25.43	2.64	36.61	50.00	7.58	5.81
406	50.00	13.57	30.16	6.27	44.43	12.76	37.24	5.57	50.00	27.70	13.93	8.37	32.92	50.00	0.56	16.52

Table 3.9-Relative percentage contribution of each term in the SKM, for Yuen (1989) trapezoidal channel data

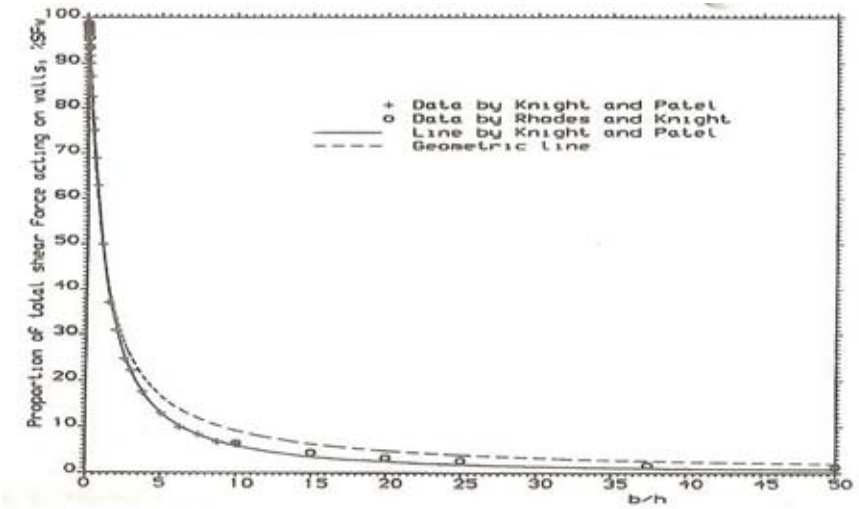

Figure 3.1-%SFw against b/h (Rhodes & Knight, 1994)

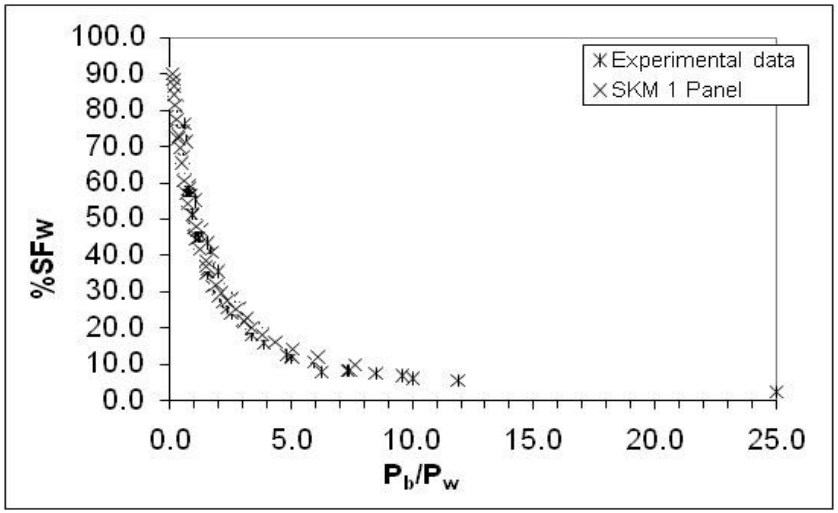

Figure 3.2-Comparison of one panel SKM solution to experimental data

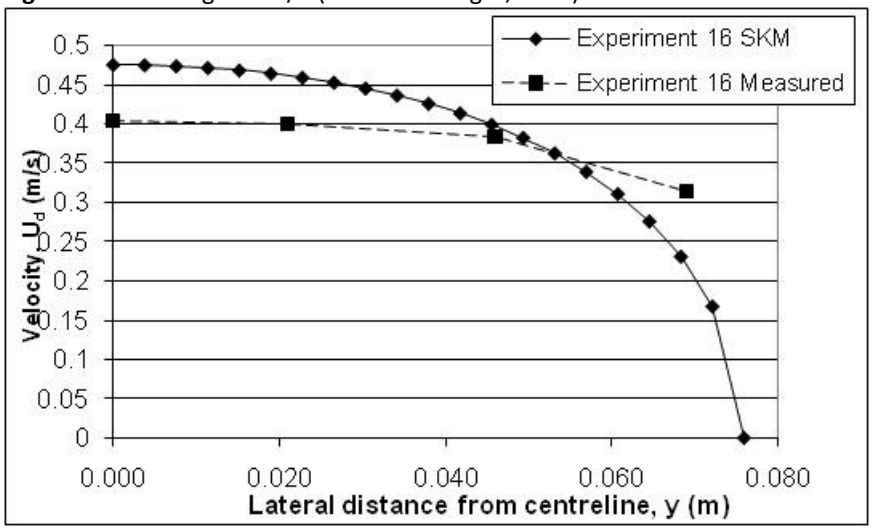

Figure 3.3-Comparison of SKM and measured depth-averaged velocity profile, H=85.8mm, Q=4.80ℓ/s

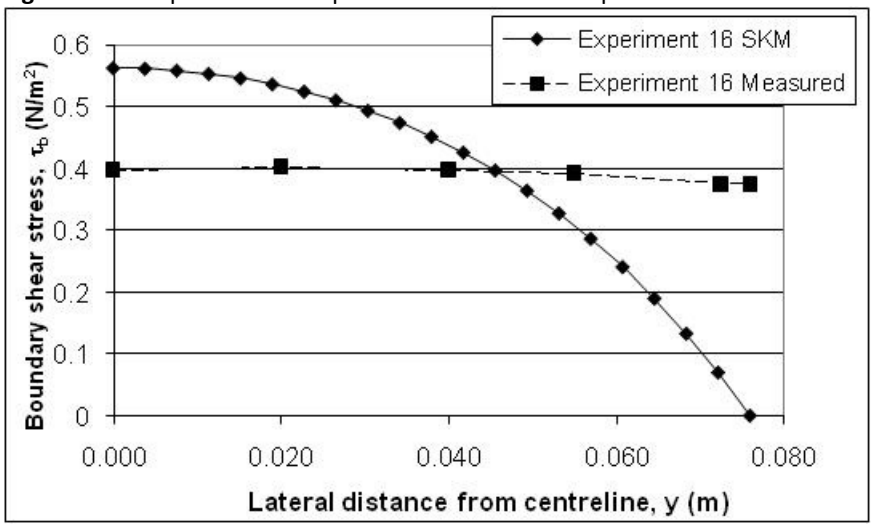

Figure 3.4-Comparison of SKM and measured boundary shear stress profile, H=85.8mm, Q=4.80ℓ/s

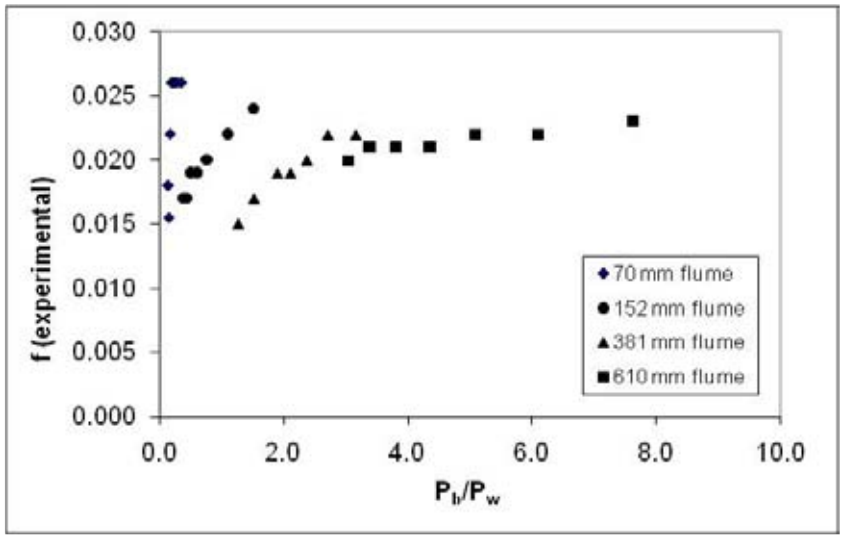

Figure 3.5-Best fit *f* values used in modelling all data

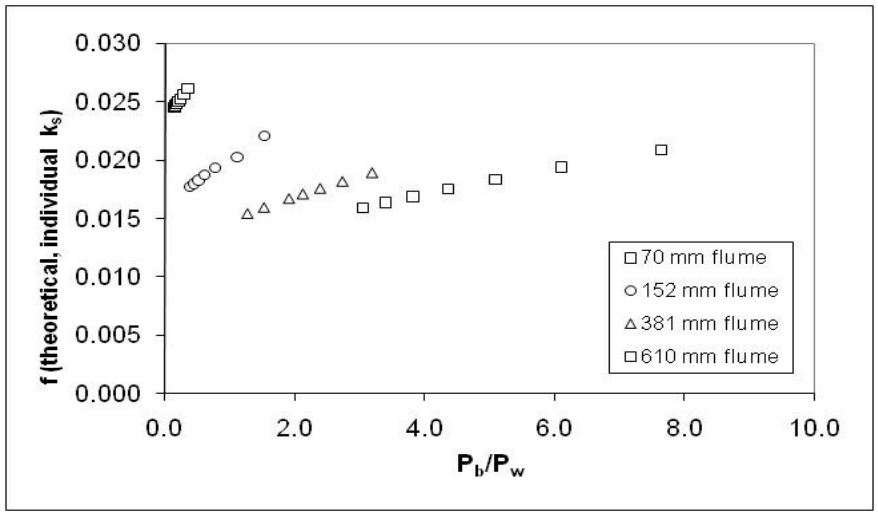

Figure 3.6- *f* values based on Equation 3.16 assuming a rough channel

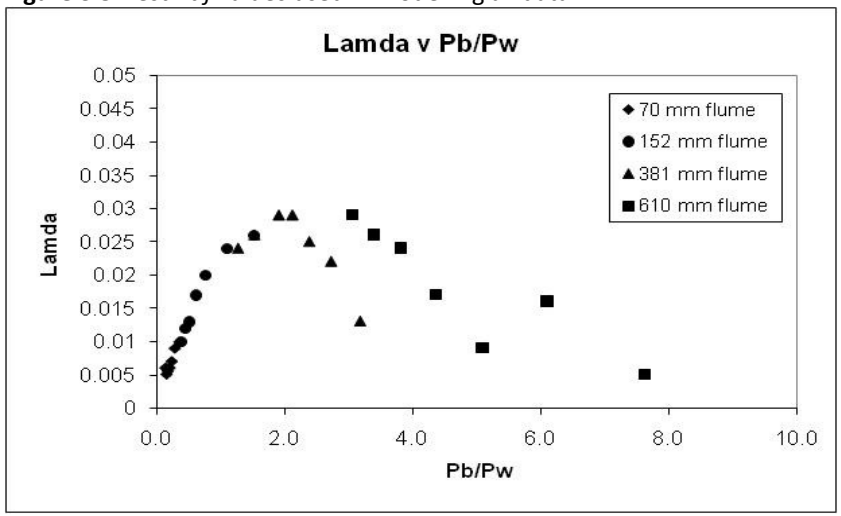

Figure 3.7-Best-fit values of λ used in modelling all data

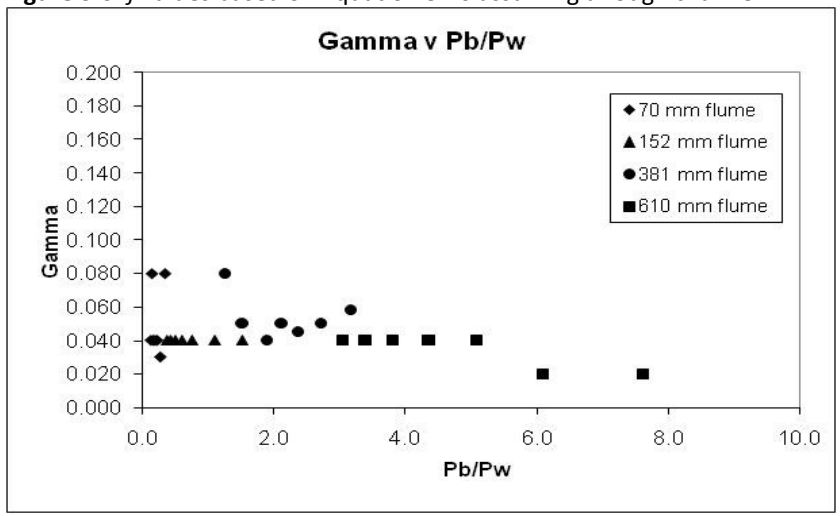

Figure 3.8-Best-fit values of Γ used in modelling all data

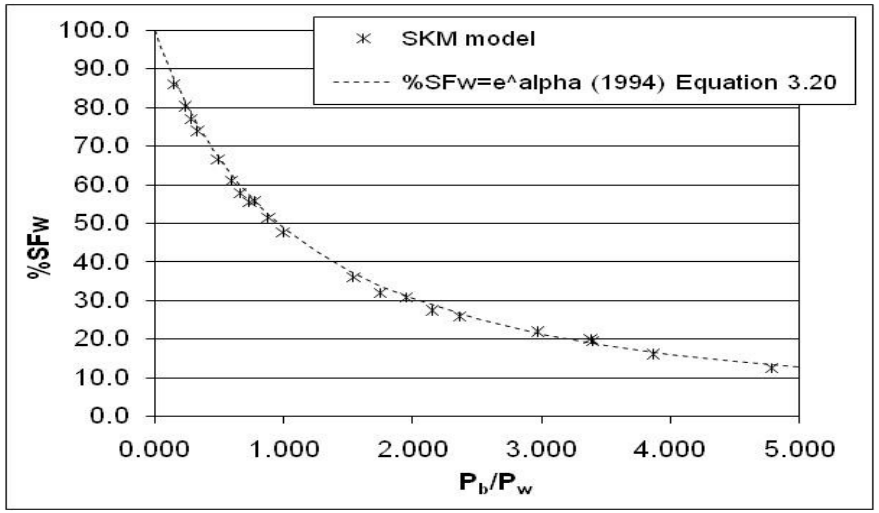

Figure 3.9-Comparison of model (constant *f*, λ and vary Γ), panel spacing=0.25b and Equation 3.20

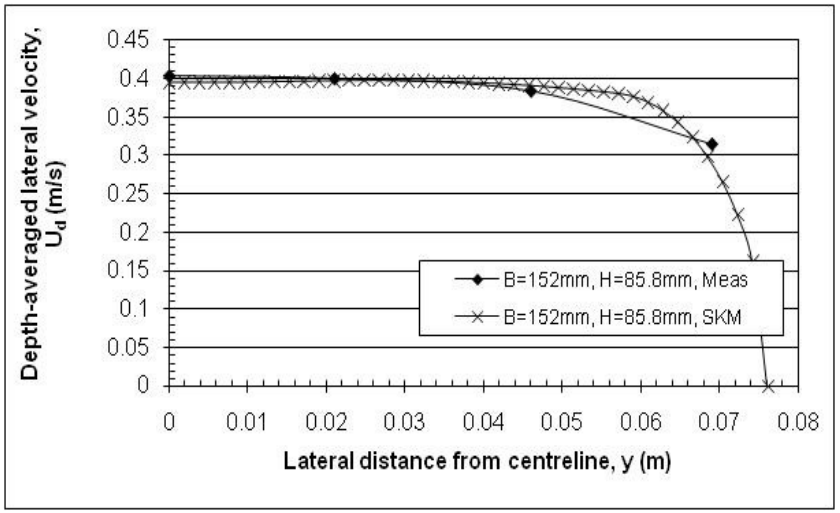

Figure 3.10-Depth-averaged velocity, comparison of SKM model and experimental data (constant *f*, λ and vary Γ), panel spacing=0.25b

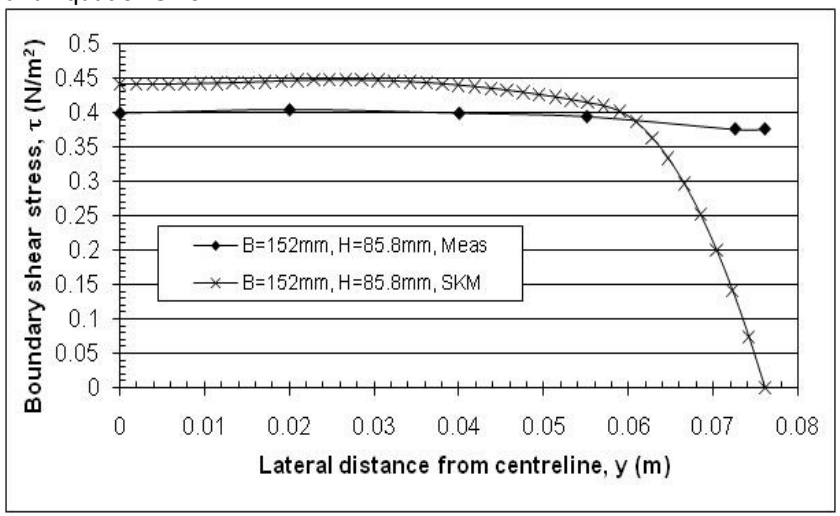

Figure 3.11-Boundary shear stress, comparison of SKM model and experimental data (constant *f*, λ and vary Γ), panel spacing=0.25b

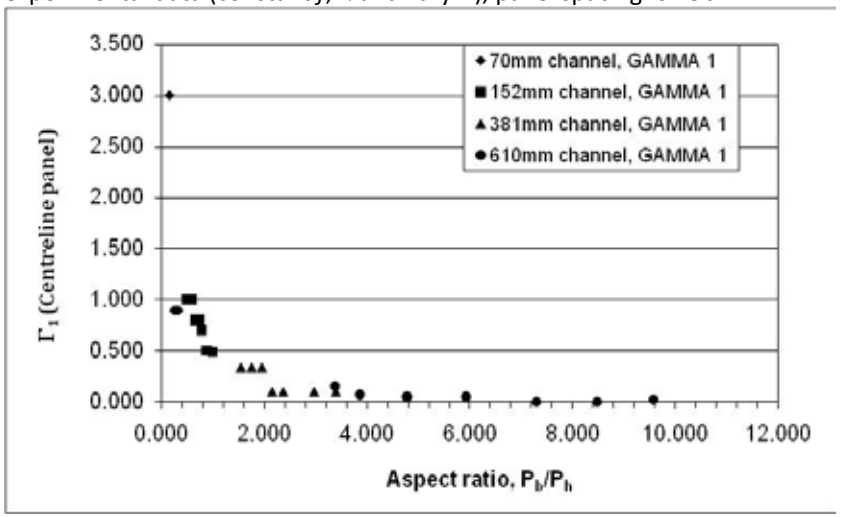

Figure 3.12-Distribution of Γ_1 (centreline panel), constant *f*, λ and vary Γ, panel spacing=0.25b

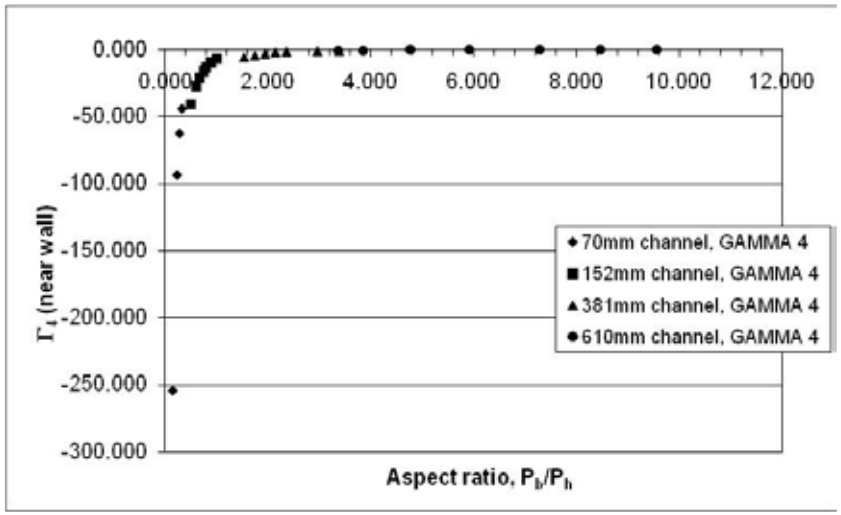

Figure 3.13-Distribution of Γ_4 (near wall panel), constant *f*, λ and vary Γ, panel spacing=0.25b

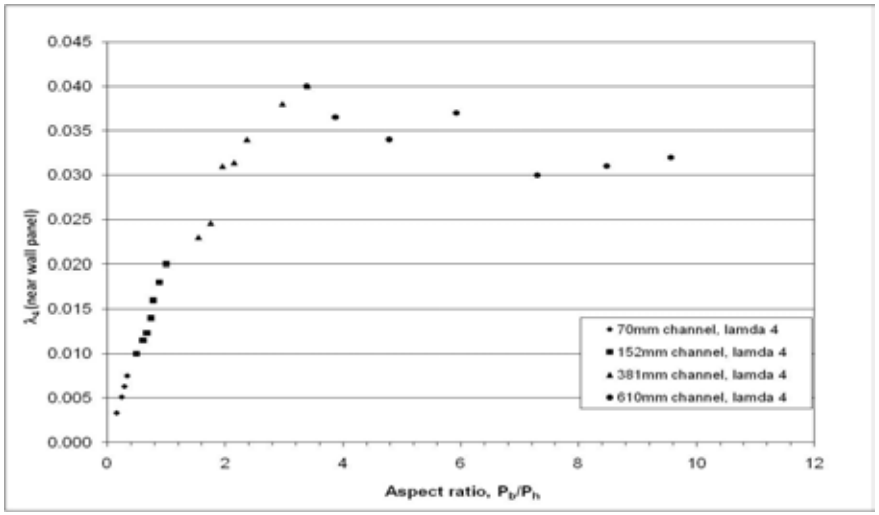

Figure 3.14-Distribution of λ_4 (near wall panel), constant *f*, Γ and vary λ, panel spacing=0.25b

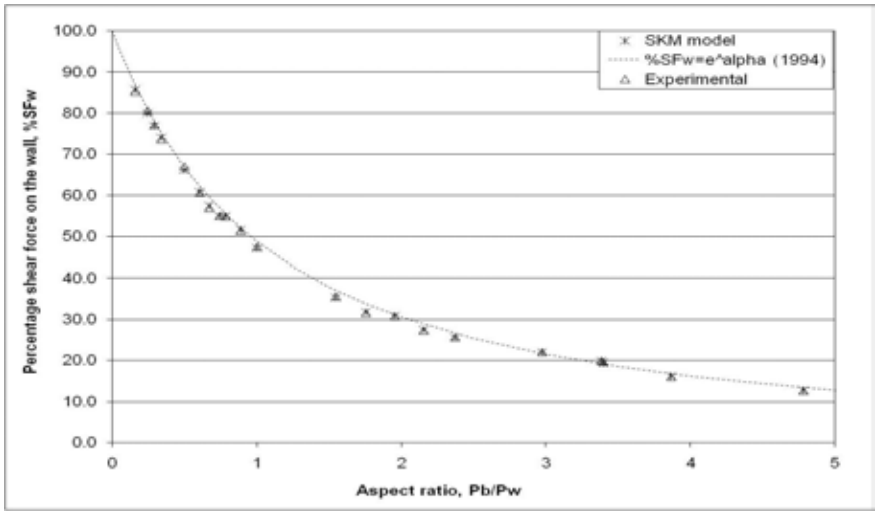

Figure 3.15-Comparison of model, experiments and Knight et al. (1994) equation (constant *f*, Γ and vary λ), panel spacing=0.25b

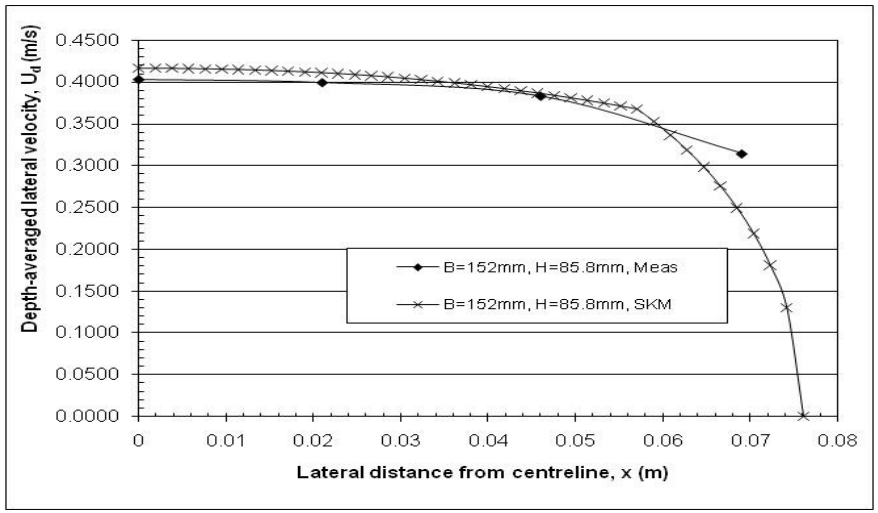

Figure 3.16-Depth-averaged velocity, comparison of SKM model and experimental data (constant *f*, Γ and vary λ), panel spacing=0.25b

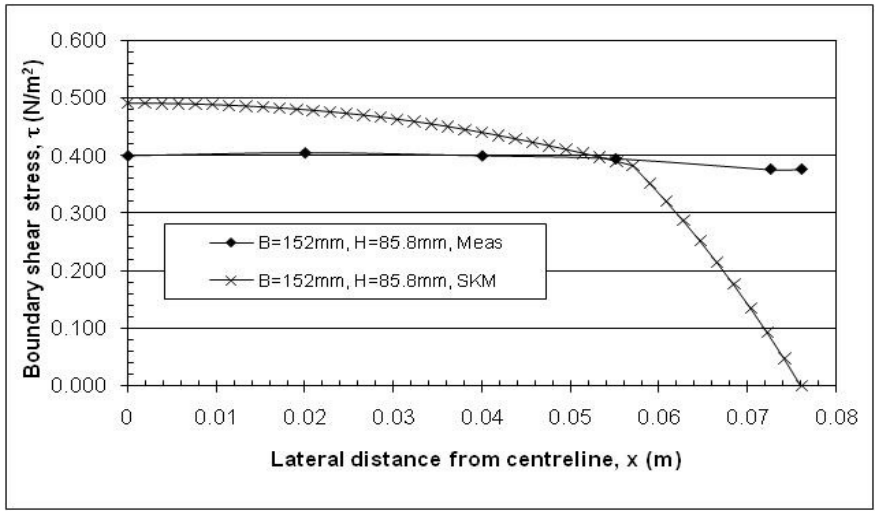

Figure 3.17-Boundary shear stress, comparison of SKM model and experimental data (constant *f*, Γ and vary λ), panel spacing=0.25b

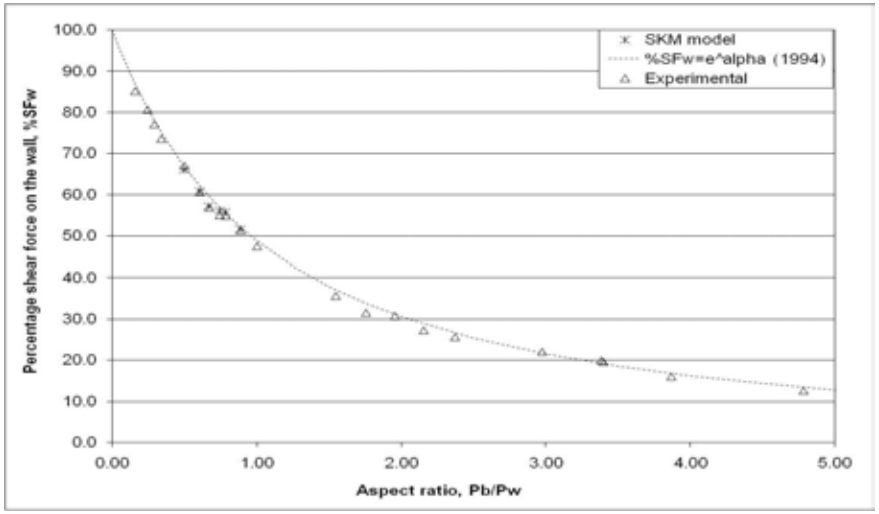

Figure 3.18-Comparison of model, experiments and Knight et al. (1994) equation (variable *f*, Γ and λ), panel spacing=0.25b

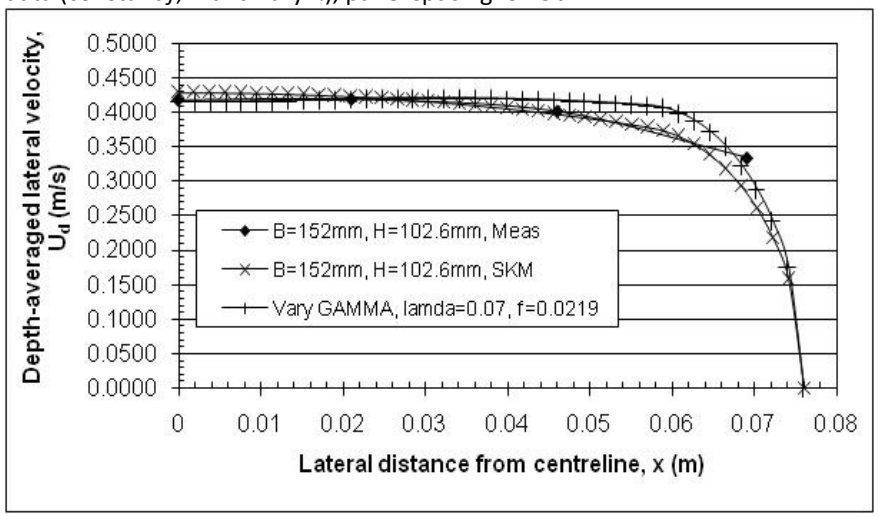

Figure 3.19-Depth-averaged velocity, comparison of SKM model and experimental data (variable *f*, Γ and λ), panel spacing=0.25b

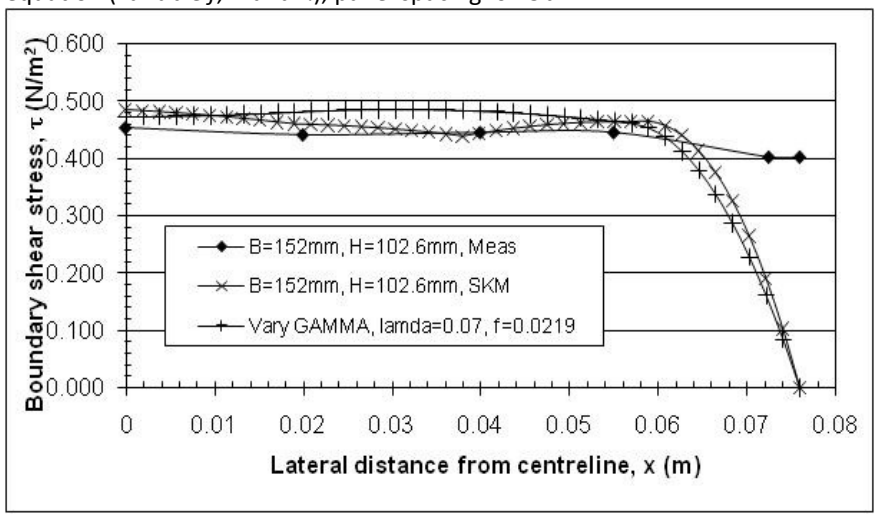

Figure 3.20- Boundary shear stress, comparison of SKM model and experimental data (variable *f*, Γ and λ), panel spacing=0.25b

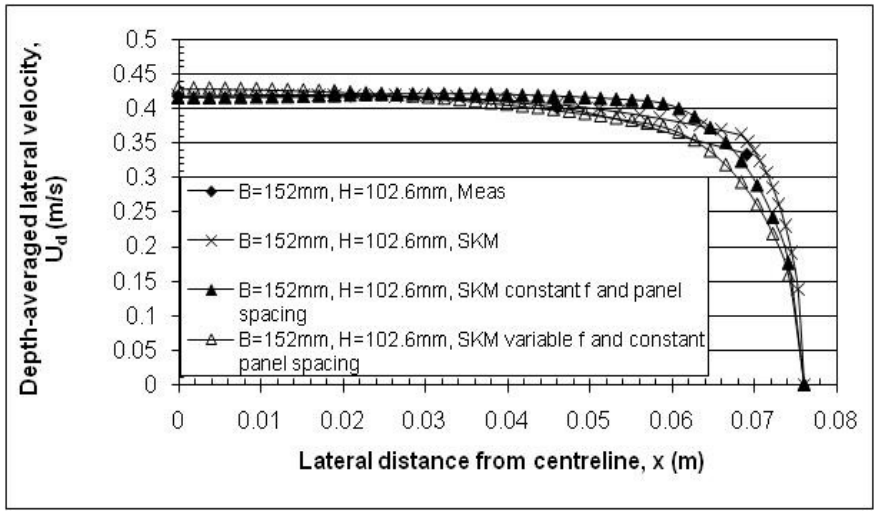

Figure 3.21- Depth-averaged velocity, comparison of SKM model and experimental data (variable *f*, Γ and λ), variable panel spacing

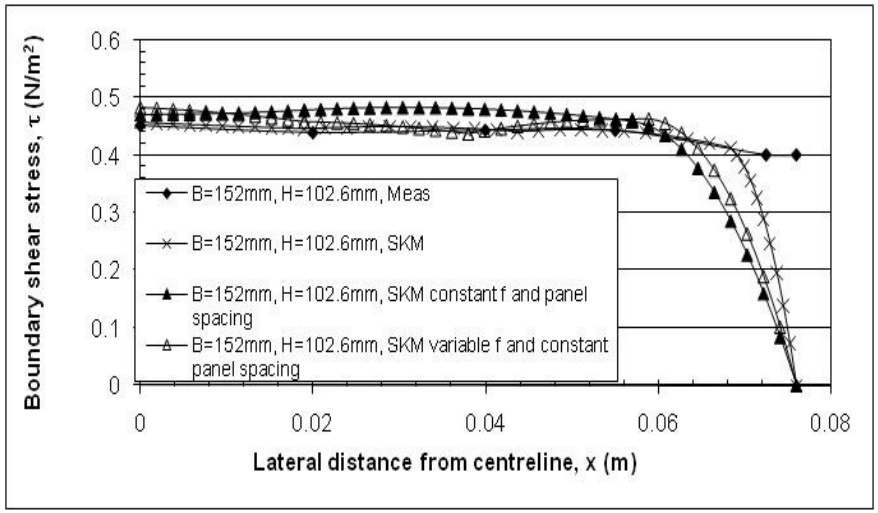

Figure 3.22- Boundary shear stress, comparison of SKM model and experimental data (variable *f*, Γ and λ), variable panel spacing

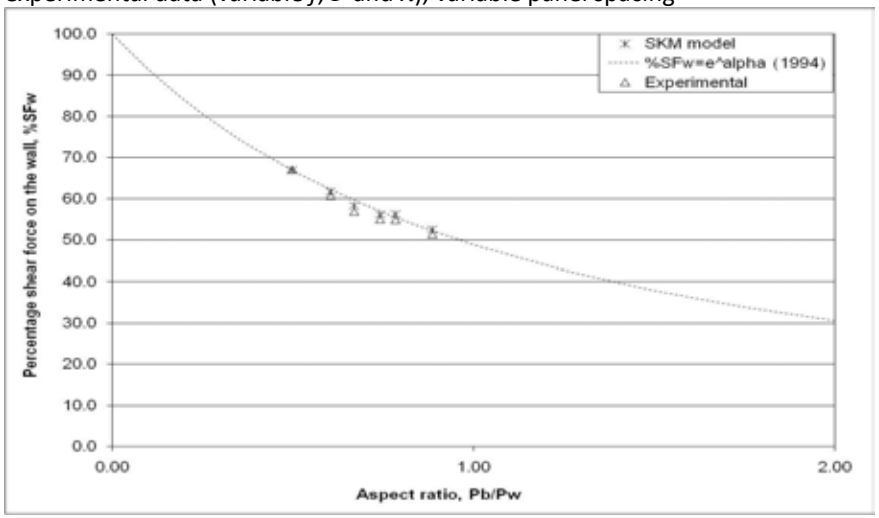

Figure 3.23-Comparison of model, experiments and Knight et al. (1994) equation (variable *f*, Γ and λ), variable panel spacing

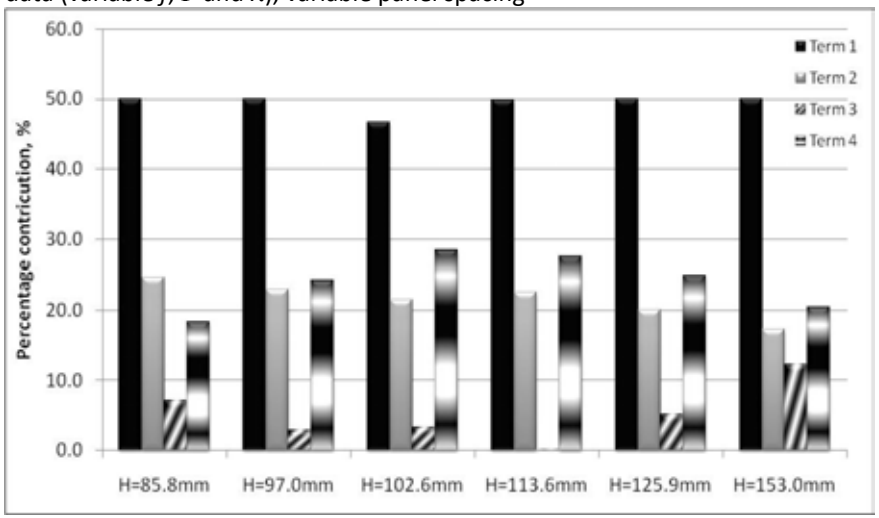

Figure 3.24-Relative contribution of each term in the SKM for Panel 1, variable panel spacing

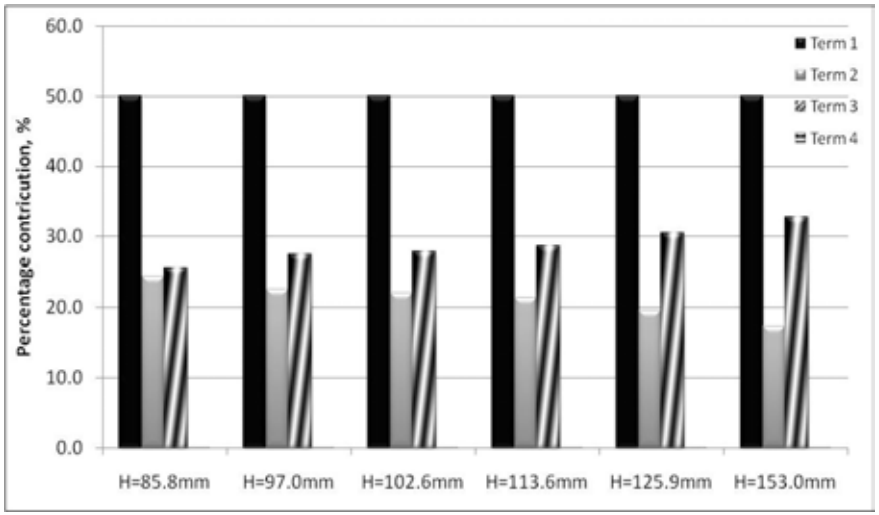

Figure 3.25-Relative contribution of each term in the SKM for Panel 2, variable panel spacing

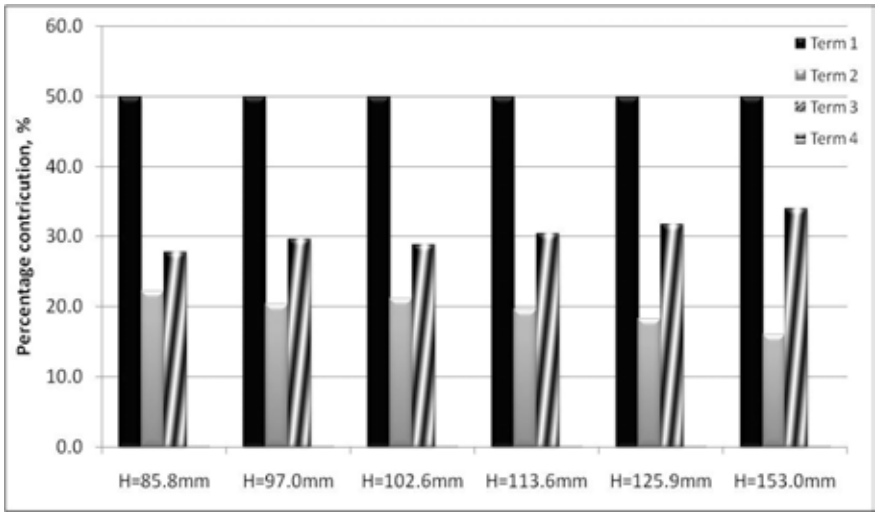

Figure 3.26-Relative contribution of each term in the SKM for Panel 3, variable panel spacing

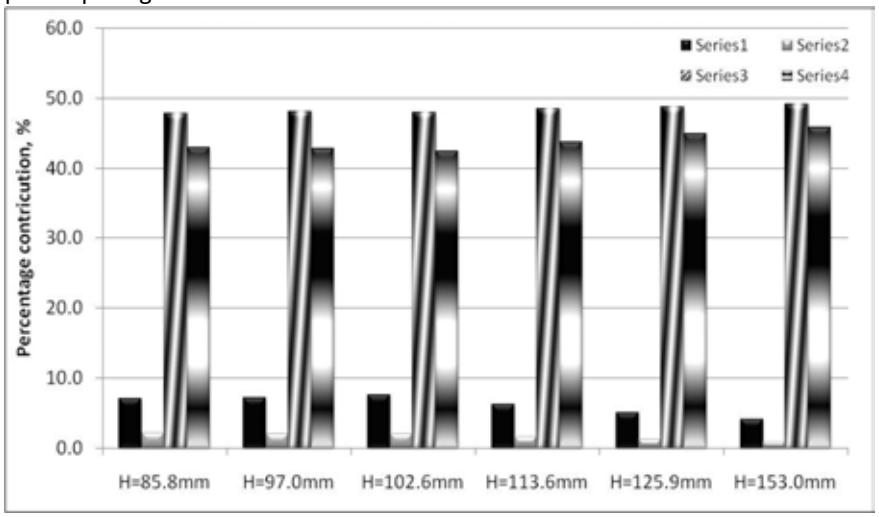

Figure 3.27-Relative contribution of each term in the SKM for Panel 4, variable panel spacing

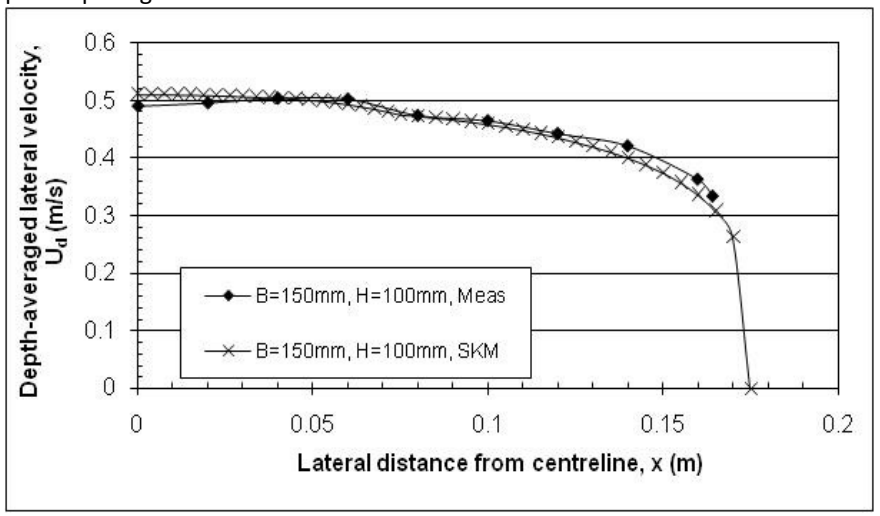

Figure 3.28- Depth-averaged velocity, comparison of SKM model and experimental data (variable *f*, Γ and λ), Yuen Experiment 13

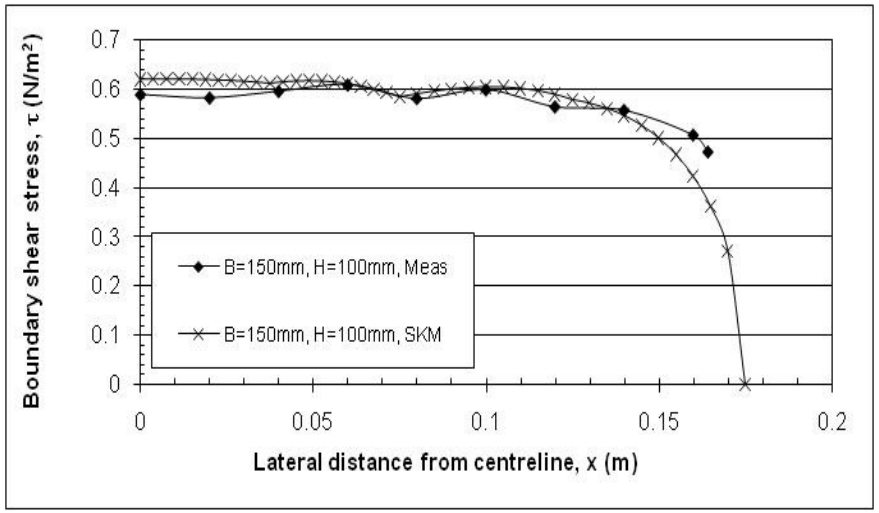

Figure 3.29- Boundary shear stress, comparison of SKM model and experimental data (variable *f*, Γ and λ), Yuen Experiment 13

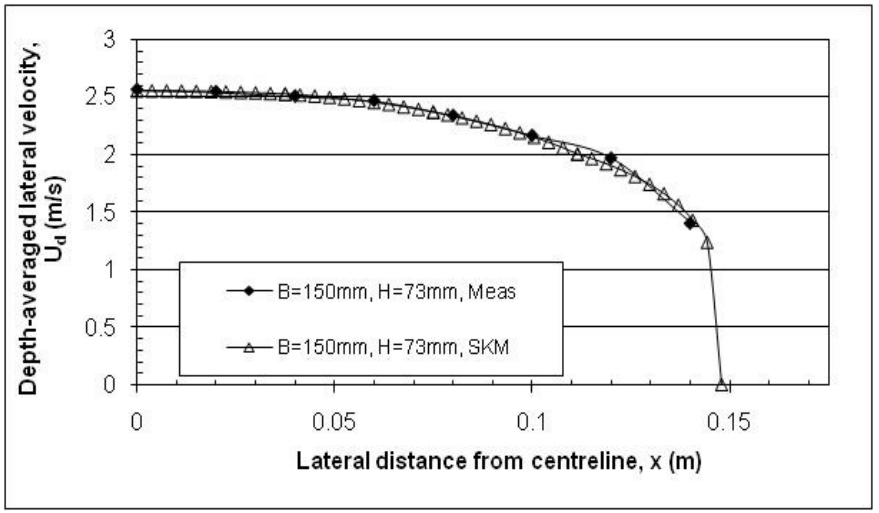

Figure 3.30- Depth-averaged velocity, comparison of SKM model and experimental data (variable *f*, Γ and λ), Yuen Experiment 406

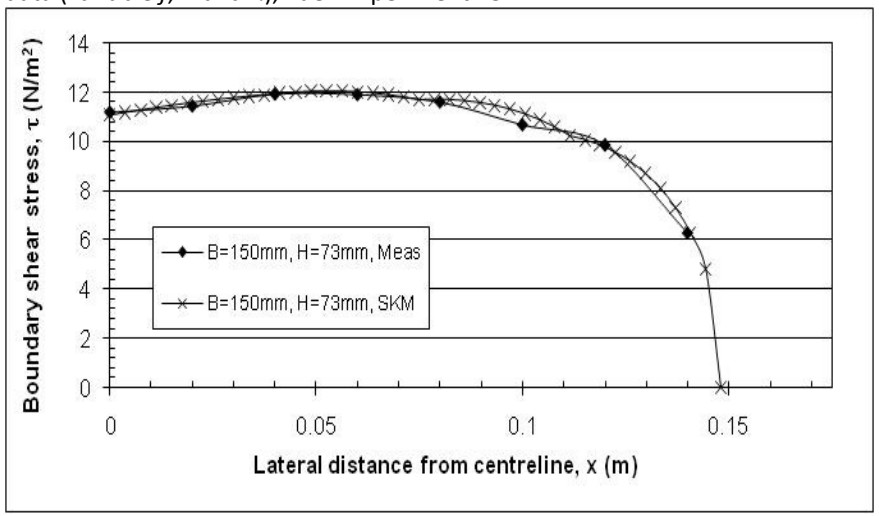

Figure 3.31- Boundary shear stress, comparison of SKM model and experimental data (variable *f*, Γ and λ), Yuen Experiment 406

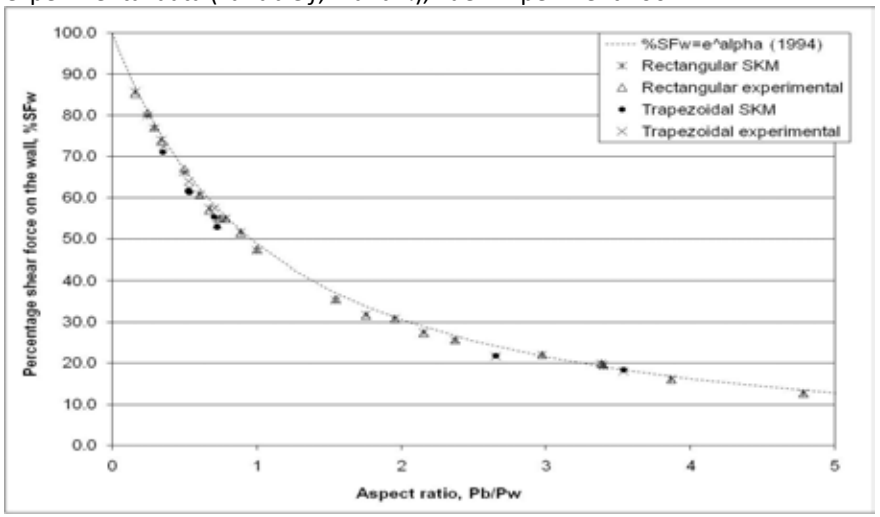

Figure 3.32-Comparison of model, experiments and Knight et al. (1994) equation rectangular (method 3.3.2.1) and trapezoidal data

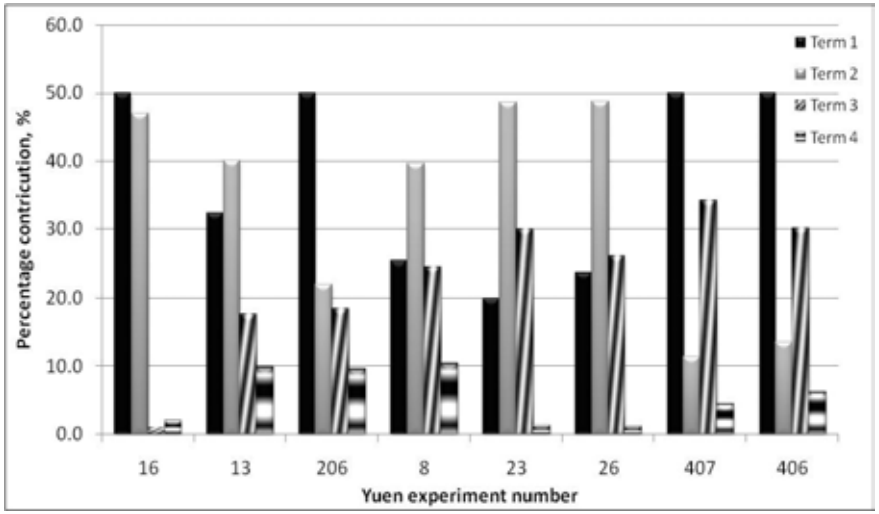

Figure 3.33-Relative contribution of each term in the SKM for Panel 1, Yuen trapezoidal channel data

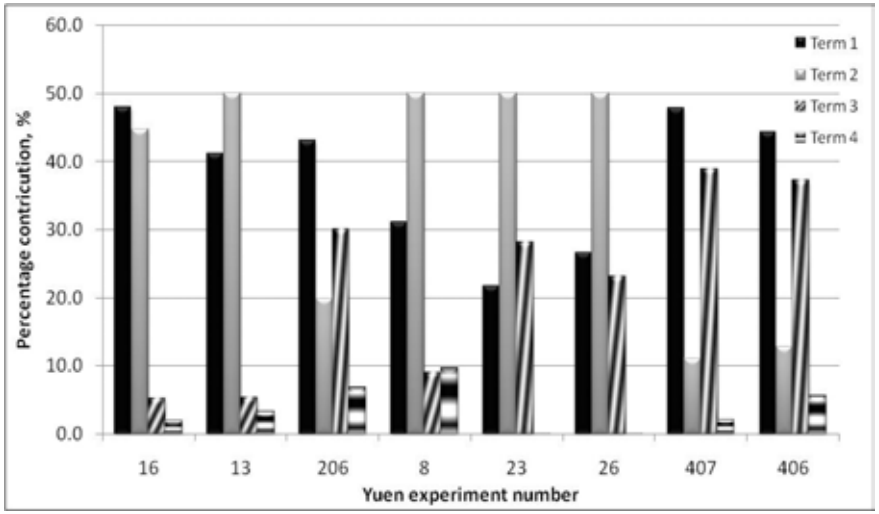

Figure 3.34-Relative contribution of each term in the SKM for Panel 2, Yuen trapezoidal channel data

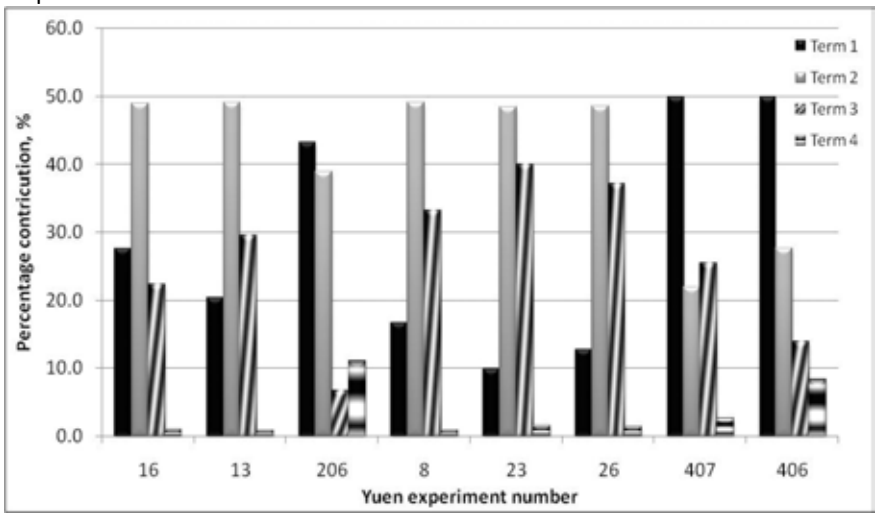

Figure 3.35-Relative contribution of each term in the SKM for Panel 3, Yuen trapezoidal channel data

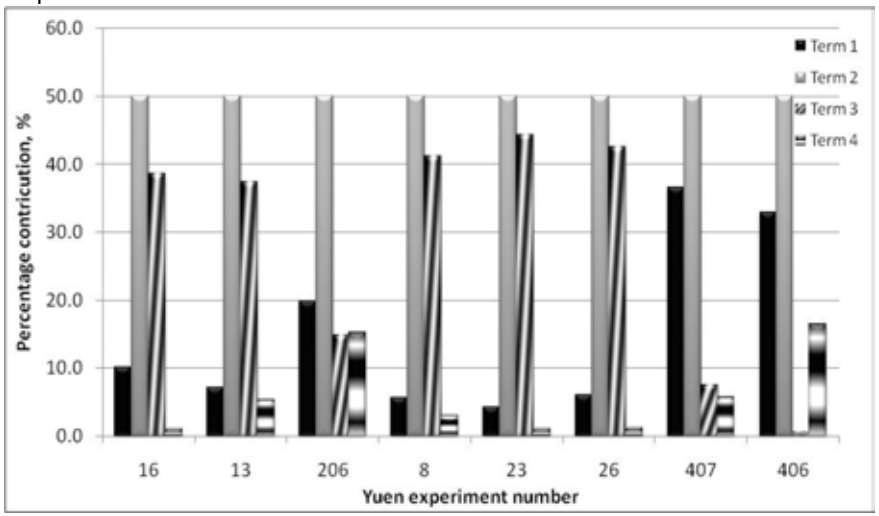

Figure 3.36-Relative contribution of each term in the SKM for Panel 4, Yuen trapezoidal channel data

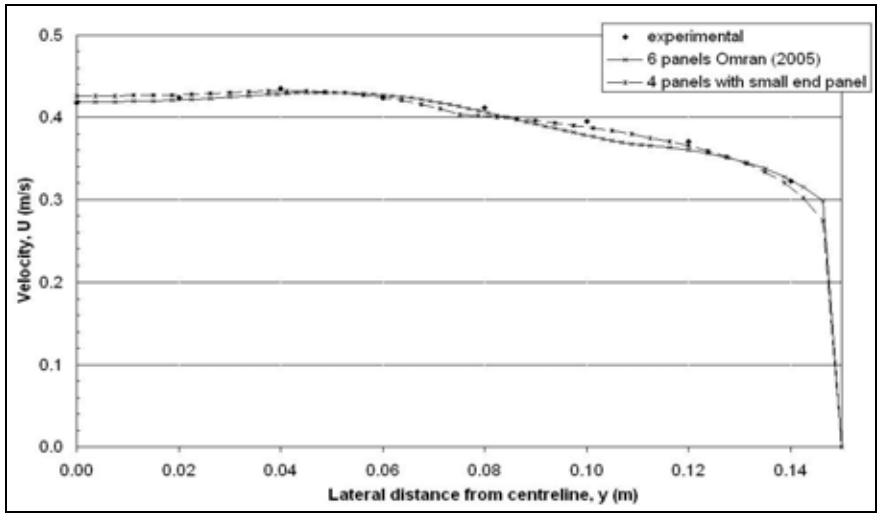

Figure 3.37-Comparison of experimental data to Omran's (2005) 6 panel method and the proposed 4 panel method; depth-averaged velocity

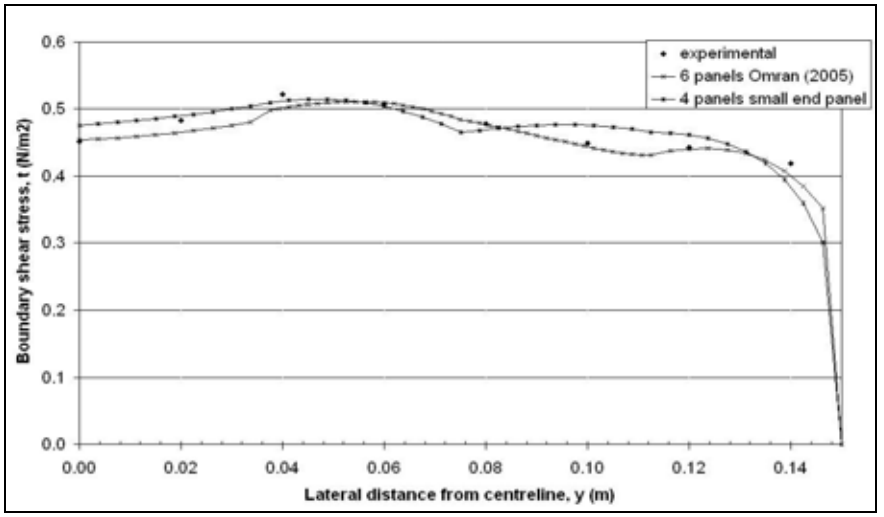

Figure 3.38-Comparison of experimental data to Omran's (2005) 6 panel method and the proposed 4 panel method; boundary shear stress

CHAPTER 4- MODELLING FLOW IN SIMPLE CHANNELS WITH HETEROGENEOUS ROUGHNESS USING THE SHIONO AND KNIGHT METHOD

Equations are just the boring part of mathematics. I attempt to see things in terms of geometry.

Stephen Hawking (1942 -)

4.1 Introduction

It has been shown in many studies (Omran, 2005; Knight et al., 2007; Abril & Knight, 2004) and in the previous chapter, that the Shiono and Knight Method can be applied to straight channels with homogeneous roughness. However, it is important to be able to accurately model flow in channels with heterogeneous roughness as this type of roughness occurs in many practical engineering problems (e.g. river rehabilitation, vegetation control, bank stability and erosion). In this chapter, the SKM will be applied to channels of heterogeneous roughness to investigate the applicability of this method to this problem. This makes the method much more applicable, as the roughness on the banks of natural rivers can be quite different from the bed. This chapter sheds light on the modelling techniques required to undertake accurate modelling of discharge, distributions of depth-averaged velocity and boundary shear stress where there is differential roughness on the channel and builds on the work of Chapter 3.

4.2 Experimental data

Alhamid (1991) carried out several series of experiments at The University of Birmingham, examining two types of roughness in a simple trapezoidal channel. The

roughness (gravel) was generally attached to the walls of the channel only, as shown in **Figure 4.1**. Alhamid measured the discharge in the channel, point velocity measurements and boundary shear stress on smooth surfaces. A summary of the data is presented in **Table 4.1** and plots showing the normal depth-discharge data given in **Figure 4.2** with the full data available at The University of Birmingham's Flow Data website (www.flowdata.bham.ac.uk). The plots of distributions of depth-averaged velocity and boundary shear stress presented by Alhamid (1991) in his thesis have been digitised, as the raw data were only available from Figures within his thesis. This introduces an extra uncertainty, but, the overall values of discharge and percentage shear force on the wall have been compared to the data recorded by Alhamid, and therefore the errors within the individual distributions are likely to be small.

Roughness 1 had a d_{84} of 18.0mm and roughness 2 a d_{84} of 9.3mm. A total of 26 experiments were conducted with rough walls and a smooth bed with aspect ratios (=b/H) ranging from 0.85-10 and used two bed slopes; 3.92×10^{-3} and 1.935×10^{-3}. The discharges measured were between 2-22*l*/s and percentage shear force on the wall between 46-94%. One series was calculated with all the same size roughness on both bed and walls, making it a homogeneous case.

4.3 Modelling philosophy

Following from the success of the work carried out in Chapter 3, the approach of using four panels (two of which were equally spaced on the flat bed, and two equally spaced on the sloping wall) was adopted, since this approach was found to accurately

model both the depth-averaged velocity and boundary shear stress distributions in trapezoidal channels. This same approach will also be used in this Chapter.

The calibration of this model, the friction factor, *f*, was calculated based on the measured depth-averaged velocity and boundary shear stress. The values of friction were averaged over each panel and linearly varied within each panel. **Figure 4.3** shows a schematic of a trapezoidal channel and Equations 4.1 to 4.4 were used to calculate the linear friction distribution.

$$f_{P1} = \frac{f_1 + f_2}{2} - \left[\frac{\frac{f_1 + f_2}{2} - f_1}{\frac{b}{4}} \times \left(\frac{b}{2} - y \right) \right] \quad \textbf{4.1}$$

$$f_{P2} = \frac{f_1 + f_2}{2} + \left[\frac{f_{2-} \frac{f_1 + f_2}{2}}{\frac{b}{4}} \times \left(y - \frac{b}{2} \right) \right] \quad \textbf{4.2}$$

$$f_{P3} = \frac{f_3 + f_4}{2} - \left[\frac{\frac{f_3 + f_4}{2} - f_3}{\frac{H}{4}} \times \left(b + \frac{H}{2} - y \right) \right] \quad \textbf{4.3}$$

$$f_{P4} = \frac{f_3 + f_4}{2} + \left[\frac{f_{4-} \frac{f_3 + f_4}{2}}{\frac{H}{4}} \times \left(y - b + \frac{H}{2} \right) \right] \quad \textbf{4.4}$$

By linearly varying *f* in this manner, it ensures a smooth boundary shear profile over the flat bed region and allows the model to have a differential roughness between panels 2 and 3 (at the interface of change of roughness). **Figure 4.4** shows the effect

of averaging the friction data per panel, and then subsequently linearly varying it within.

Previously, Γ was the "main" factor of calibration due to the location and strength of the secondary current cells. In this case it is hypothesised that λ will be more important due to the differential roughness. λ will increase from that in the smooth cases, especially in panels 3-4 due to the high lateral shear near to the channel boundary.

4.4 Modelling trapezoidal channels with heterogeneous roughness

The method used herein has been described above, and also in Section 3.3.2. Again, only half of the channel was modelled as it was symmetrical about the centreline and the results presented by Alhamid (1991) also illustrate that the flow was symmetrical about the centreline.

Although the Shiono and Knight method was not designed to model differential roughness, this method was able to accurately model the distributions of both depth-averaged velocity and boundary shear stress, as shown in **Figures 4.5-4.8**. The calibration parameters used have been dealt with in the following section. From **Figures 4.5-4.8**, it is clear that the model can accurately replicate the depth-averaged velocity (overall discharge errors of 0.35% and 1.08% for experiments 29 and 35 respectively), although in the corner region there is a slight discrepancy between the measured and modelled data. This is due to the high roughness in this region and corresponding steep velocity gradient. This can be also seen from the boundary shear

stress curves. It is clear that for boundary shear stress the model can replicate the measured data over panels 1 and 2 (flat bed, smooth channel), whereas in panels 3 and 4 (sloping wall, rough channel) the model is unable to replicate the measured data as accurately as one might wish. For example, in **Figure 4.7** for experiment 35, the model can mimic the peak boundary shear stress, with error in $\%SF_w$ only -1.35%, but the point of peak measured boundary shear stress is approximately 0.015m from the modelled. This is due to the model assuming the peak boundary shear stress is at the point of change of the friction value. In experiment 29 (**Figure 4.8**), the measured data has many peaks and troughs in the data, which the model is unable to predict using 4 panels, however, overall the error in $\%SF_w$ is only -1.39%.

The modelled values of discharge and percentage shear stress on the wall are well within acceptable tolerances, with the average errors for discharge and $\%SF_w$ being 0.16% and -1.08% for roughness 1 and 0.38% and -0.25% for roughness 2 respectively. Plots of the measured $\%SF_w$ versus wetted perimeter ratio, P_b/P_w, and modelled data are shown in **Figures 4.9-4.10**. From these it can be seen that the model is able to accurately predict the percentage shear force on the wall over a range of measured data. **Tables 4.3** and **4.5** give the results of model for all of the cases investigated. From these Tables and Figures, it has been shown that the model can accurately predict both the discharge and $\%SF_w$ in addition to providing accurate distributions of depth-averaged velocity. However, the model is unable to reproduce every undulation in boundary shear stress in the sloping bed region (high roughness), but does give the overall shape of the distribution in addition to giving accurate values of $\%SF_w$.

4.5 Guidance on calibration coefficients used within the model

Plots of the coefficients used in this modelling approach (values of *f*, λ and Γ) are given in **Figures 4.11** to **4.16** with the numerical values given in **Tables 4.2** and **4.4**. These values are different from those used in the smooth cases investigated in Chapter 3, as might be expected (see **Table 3.8** for corresponding smooth channel modelling coefficients).

The values of friction factor have been determined from experimental data, and from the plots provided, it is clear that the roughness depends on the experimental configuration; i.e. shape of the channel, slope and the characteristics of the artificial roughness attached to the channel. Where possible, it is beneficial to obtain measured roughness from the actual data, typically based on the velocity and boundary shear stress within the channel. Where this is not possible, or will be exceptionally problematic e.g. in the field, the roughness should be based on that observed, and values chosen using tried and tested methods, for example, Chow (1959) and the recently produced Conveyance and Afflux Estimation System (CAES, www.river-conveyance.net) gives guidance on roughness characteristics. This is usually given in terms of Manning's roughness coefficient, n, but can be related back to the friction factor, f, using Equation 4.5.

$$f = \frac{8gn^2}{R^{1/3}} \qquad \textbf{4.5}$$

In the case of rough channels, the dimensionless eddy viscosity coefficient, λ, appears to be more significant than in smooth channels. The values of λ can be found in **Tables 4.2** and **4.4**, and in **Figures 4.12** and **4.15**. From **Tables 4.2** and **4.4**, it is clear that the values of f in panels 3 and 4 are higher in **Table 4.2** than in **Table 4.4**. This is physically true as the artificial roughness is larger in experiments quoted in **Table 4.2**.

Generally, λ in panels 1 and 2 were higher than those in panels 3 and 4. In order to examine the sensitivity of the mode to the factors l and G, these were altered by (by ±10%). When the values of λ used in **Tables 4.2** and **4.4**, were increased/decreased the overall values of discharge and $\%SF_w$ changed between ±0.5-2% with similar differences being noted when Γ was increased or decreased by the same amount. Where values of roughness were similar, the values of λ between roughness 1 and 2 were virtually identical for similar aspect ratios, indicating that in these cases, λ was less significant and channel shape and values of f were more important. When comparing the results to **Table 3.8** (Yuen data, smooth trapezoidal), the values of λ in panels 1 and 2 were lower for the smooth cases and panels 3 and 4 were similar between the rough and smooth experiments, indicating that in the rough channels, the friction term is more significant. When λ was set as 0.07 in panels 1 and 2 for the rough case, the overall values of discharge increase by up to 30% and similarly $\%SF_w$ decreased by up to 30%. In order to regain acceptable values of discharge and $\%SF_w$, Γ in panel 1 had to be increased (often doubled) and Γ_2 decreased. In some cases, acceptable errors could not be achieved, and often the distributions of depth-averaged velocity and boundary shear stress bore little resemblance to the measured, particularly at the corner region where discharge was often overestimated and

boundary shear stress was significantly lower. It can also be seen from the **Figures 4.12** and **4.15**, that λ plateaus between wetted perimeter ratios of 1.0-3.0, with the exception of experiment 32 (roughness 2), see **Figure 4.15** at P_b/P_w=2.48, where there is a dip in panels 3 and 4 and a subsequent increase in panel 2.

When comparing the values of Γ between the smooth and rough cases, using **Tables 3.8** (smooth trapezoidal) and **Tables 4.2** and **4.4** (heterogeneously roughened trapezoidal) in addition to **Figures 4.13** and **4.16**, it is clear that Γ in all panels is more significant in the rough cases than in the smooth cases. This is required to "force" the model to have a rapid increase in depth-averaged velocity/boundary shear stress at the interface between the smooth and rough elements. Generally, Γ in panels 1 and 2 is higher than in panels 3 and 4, this is because in panels 3 and 4, the values of friction dominate. From **Figures 4.13** and **4.16**, Γ is of higher magnitude at low aspect ratios (less than 1.0), and tends towards zero with increasing wetted perimeter ratio. This is due to the values of friction generally increasing with aspect ratio and therefore Γ being less significant overall.

4.6 Relative contribution of terms in the SKM equation for differentially rough trapezoidal channels

The method used to determine the relative contribution of each term has previously been described in sections 3.4 and 3.7.

Using the above and the calibrated values of f, λ and Γ, in addition to the modelled velocity data, it is possible to calculate the weightings of each of the terms of the

SKM. The results of this are presented in **Tables 4.6** and **4.7** for roughness 1 and 2 respectively and these can be compared to the smooth data in **Tables 3.7** and **3.9**. **Figures 4.17** to **4.24** shows the contribution of each term, per panel for each experiment and roughness.

The contribution of terms in the SKM for roughness 1 and 2 are similar to one another and there are only minor differences between the two data sets.

In panel 1, the results of the rough channels are similar to that of the smooth. The weight term accounts for 40% and lateral shear approximately 10%. The friction term in the rough channels actually accounts for slightly less overall when compared to the smooth case. In the rough channels, the friction term makes up approximately 27% of the model, whereas in the smooth case it is 38%. In the rough channels, the secondary flow term in panel 1 is higher than that in the smooth channels, indicating that the secondary current cells are stronger in the rough channel, although to date there is no experimental data to support this hypothesis.

The relative contributions of the SKM for rough channels in panel 2 are very similar to the smooth channels for weight and secondary current cells (approximately 37% and 11% respectively). The rough channel has significantly higher lateral shear in this region (which should be expected as this is the location of laterally changing bed slope). The friction term in the rough cases are lower than the smooth cases, this is due to the increased importance of lateral shear through the λ term.

In panels 3 and 4, the rough channel data shows differences between that and the smooth channel data, although the differences between roughness 1 and 2 are less evident. In panels 3 and 4, the weight term is much reduced from the smooth channels. The contribution of friction (term 2) in panels 3 and 4 are similar to those in the smooth channel and contribute to almost half of all of the SKM. The lateral shear (term 3) in this region (panels 3 and 4) is significantly higher in the rough channels than in the smooth channels. In the smooth channels, the contribution of lateral shear is approximately 27%, where as in the rough channels it is in the region of 44%. This is as anticipated. In this region, there is complex boundary shear stress acting on the sloping wall region resulting from the increased roughness on the walls. In panels 3 and 4, the secondary current cell term (term 4), has a slightly reduced influence from that of the smooth channel cases. This is due to the increased effect of the lateral shear stress term.

4.7 Recommendations for modelling differential roughness in trapezoidal channels

From the work undertaken on modelling trapezoidal channels with artificially roughened walls, a number of recommendations can be made.

It is important to obtain good friction data, as from **Figures 4.19**, **4.20**, **4.23** and **4.24**, it is clear that friction is a dominant term throughout. This can be done through experimental data (where available), knowledge of the site/experience, literature such as Chow (1959) or through the Roughness Advisor (RA) embedded in the Conveyance and Afflux Estimation System (CAES). See www.river-conveyance.net

for further details. In the SKM the friction term, *f*, takes account of many factors such as the material in the channel, roughness due to flow mechanisms and is also averaged over the depth of flow and it is therefore important this is fully recognised and appreciated.

λ is also more significant in rough channels than in smooth channels, this can be seen when comparing the relative contribution of λ in panels 3 and 4, see **Figures 3.35** and **3.35** for the smooth data and **Figures 4.19**, **4.20**, **4.23** and **4.24** for the roughened channel data. It has been found that λ in panels 1 and 2 is higher than in panels 3 and 4. This factor has been used to retard the flow in the flat bed region as the SKM does not take into consideration that the roughened walls will retard the flow in the smooth bed. Γ is also higher in the rough channel as this term takes account of the secondary flow cells generated by the roughened walls of the channel. However, this value of Γ generally decreases with aspect ratio as the friction is generally increasing and this becomes a more dominant term. In addition, in a wide channel the secondary current cells become weaker, therefore it would be expected that Γ reduces.

4.8 Comparison to homogeneously roughened channels

Alhamid undertook a series of homogeneously roughened channels in addition to the heterogeneous roughened ones. The homogeneous rough data gives similar percentage shear force on the wall to the smooth channel data as can be seen in **Figure 4.25**, which shows a comparison to Knight et al.'s (1994) equation for $\%SF_w$ previously presented in Section 3.3.2 (Equation 3.20). **Table 4.8** gives the channel data for a selected number of flow data. These were chosen as they had similar aspect

ratios as Yuen (1989) data and offers a direct comparison. The friction in the homogeneously roughened channels were calculated based on the depth-averaged velocity and boundary shear stress data. The values of λ and Γ were chosen based on the smooth channel data from those used in the SKM modelling of Yuen's data for comparable aspect ratios, see **Tables 4.8** (rough) and **3.8** (smooth). The values of λ and Γ were not altered from the smooth data.

The distributions of depth-averaged velocity and boundary shear stress for experiment 15 are shown in **Figures 4.26** and **4.27** respectively. From these, it is clear that the model predicts the depth-averaged velocity distribution well across the channel, but overestimates the depth-averaged velocity near to the wall. The boundary shear stress is less well modelled, but is capable of simulating the overall shape. Furthermore, the discharge and percentage shear force on the wall is computed well for this case (errors of -1.87% and -3.26% respectively) and overall for the five cases modelled using these assumptions, the average error in discharge is -0.30% and -5.76% in $\%SF_w$.

This shows that a homogeneously roughened channel is similar to a equivalent smooth channel and can be modelled well using the same λ and Γ coefficients regardless of f being significantly higher.

4.9 Concluding remarks

The SKM was originally developed for overbank flow in smooth channels and later extended to cases with roughened floodplains. Chapter 3 showed that it is able to be applied to inbank flows in smooth channels. This chapter has built on the work of

Chapter 3 and has shown that it is also applicable to inbank flows with heterogeneous roughness and roughened walls. This is an important step in the ability of the SKM, as it makes it more applicable to natural fluvial systems.

The following conclusions have been drawn with regards to modelling flows in trapezoidal channels with roughened walls:

- The SKM has been shown to be able to accurately determine the discharge (**Tables 4.3** and **4.5)** in the channel as well as the percentage shear force on the wall (**Figures 4.9** and **4.10, Tables 4.3** and **4.5**).
- The model has also been able to accurately predict the lateral distributions of depth-averaged velocity, and boundary shear stress profile reasonably well (**Figures 4.5-4.8**).
- The model is not capable of predicting the undulations in boundary shear stress in the roughened wall region using a four panel approach. However, as the peaks and troughs are unique for each experiment, individual models would have to be created knowing where these peaks are. Despite this, the method using four panels gives a good overall interpretation of the data and can be applied to all channels and stages.
- The friction factor, term 2, is the dominant term in all panels but especially in panels 3 and 4 where it accounts for approximately 50% of the SKM terms. It is therefore important to model this accurately either by measured data or through tried and tested means (e.g. CAES).

- λ is more significant in modelling flows in rough channels than in smooth channel models, especially on the smooth, flat bed region (panels 1 and 2). This factor is used to retard the flow in this area. In terms of weighting (**Figures 4.17** and **4.18** for roughness 1), the smooth data has higher values of contribution of term 3 in the SKM than the rough data, but this is due to the higher velocities in the smooth channel data.
- The Γ term is still highly significant, especially in panels 1 and 2. It becomes less significant in panels 3 and 4 as the friction becomes the dominant term (**Figures 4.17-4.24**).
- λ tends to plateau for P_b/P_w ratios of 1.0-3.0 for trapezoidal channels with roughened walls.
- Modelling channels with homogeneous roughened boundaries is modelled in the same manner as smooth channels as shown by section 4.8.

It has now been shown that the SKM can accurately model discharge, percentage shear force on the wall, and distributions of depth-averaged velocity and boundary shear stress, when there is roughened walls. This greatly extends its use in fluvial engineering where heterogeneous roughness occurs in most natural rivers and watercourses. This then concludes Part 1 of this thesis, but certain issues will be returned to in Chapter 9 after Part 2.

Part Two of this thesis now goes on to investigate an equally important practical problem, namely that of overbank flow with skewed floodplains, a topic that has received relatively little attention in the past. As a result, there is very little data on

flows with non-prismatic floodplains. Unlike Part 1, where there was a wealth of data upon which to base the modelling using the SKM, the work in Part 2 had to include a more focused literature review (Chapter 5), a re-assessment of what data were available (Chapter 7), as well as to design some experiments to fill the 'knowledge gap'. These are fully described in Chapters 6 and 8. The aim of Part 2 was to concentrate on data acquisition for the case where flows switch from one floodplain to another, here referred to as "skewed" floodplains, to distinguish it from the case where floodplains either converge or diverge as in studies by Rezaei (2006) and Bousmar (2002). Although no detailed SKM modelling was undertaken, reference is made to the simulations by Rezaei, and it is hoped that data provided herein will eventually provide a useful benchmark for all types of models.

Roughness Type	Experiment Number	b, mm	H, mm	b/H	P_b/P_w	S_o	Q, l/s	$\%SF_w$
1	1	107.1	126.0	0.85	0.30	0.0039	13.7	94.7
1	2	107.1	107.0	1.00	0.35	0.0039	10.0	93.3
1	3	107.1	75.0	1.43	0.50	0.0039	5.2	91.0
1	4	107.1	54.0	1.98	0.70	0.0039	2.9	87.4
1	5	107.1	43.0	2.49	0.88	0.0039	2.0	84.7
1	23	255.6	84.9	3.01	1.06	0.0039	15.5	81.1
1	24	255.6	63.8	4.01	1.42	0.0039	9.7	76.6
1	25	255.6	51.1	5.00	1.77	0.0039	6.7	73.6
1	26	399.5	66.7	5.99	2.12	0.0039	20.1	67.8
1	27	399.5	56.8	7.03	2.49	0.0039	15.8	64.0
1	28	399.5	50.0	8.00	2.83	0.0039	13.0	61.5
1	29	399.5	44.3	9.03	3.19	0.0039	10.8	57.9
1	30	399.5	40.0	9.99	3.53	0.0039	9.3	56.3
2	09	120.6	142.0	0.85	0.30	0.0039	21.95	92.87
2	10	120.6	121.0	1.00	0.35	0.0039	15.91	91.16
2	11	120.6	80.5	1.50	0.53	0.0039	7.38	87.36
2	12	120.6	60.3	2.00	0.71	0.0039	4.48	82.73
2	13	120.6	48.0	2.51	0.89	0.0039	3.11	79.59
2	17	272.0	90.8	2.99	1.06	0.0039	22.25	74.68
2	18	272.0	67.9	4.01	1.42	0.0039	14.09	68.32
2	19	272.0	54.5	4.99	1.76	0.0039	10.00	64.36
2	31	416.2	69.5	5.99	2.12	0.0019	18.47	59.66
2	32	416.2	59.4	7.01	2.48	0.0019	14.30	55.56
2	33	416.2	52.0	8.00	2.83	0.0019	11.53	52.22
2	34	416.2	46.5	8.96	3.17	0.0019	9.61	49.99
2	35	416.2	41.6	10.00	3.54	0.0019	8.03	46.91

Table 4.1-Summary of Alhamid's (1991) data for heterogeneous roughness experiments

Roughness Type	Experiment Number	b, mm	H, mm	b/H	P_b/P_w	f_1	f_2	f_3	f_4	λ_1	λ_2	λ_3	λ_4	Γ_1	Γ_2	Γ_3	Γ_4
1	1	107.10	126.00	0.85	0.30	0.0161	0.0146	0.1388	0.2401	0.05	0.07	0.30	0.05	3.500	-0.230	0.030	-1.000
1	2	107.10	107.00	1.00	0.35	0.0192	0.0179	0.1392	0.1841	0.10	0.07	0.30	0.05	3.500	-0.230	0.200	-1.000
1	3	107.10	75.00	1.43	0.50	0.0200	0.0191	0.3159	0.3146	0.10	0.30	0.70	0.03	2.600	-5.000	0.010	-0.001
1	4	107.10	54.00	1.98	0.70	0.0227	0.0212	0.2948	0.2903	0.10	0.30	0.30	0.03	2.000	-2.700	1.000	-0.001
1	5	107.10	43.00	2.49	0.88	0.0234	0.0224	0.4536	0.4535	0.10	0.30	0.30	0.03	1.300	-2.200	1.000	-0.001
1	23	255.60	84.89	3.01	1.06	0.0200	0.0148	0.2681	0.1904	0.50	0.50	0.20	0.20	0.010	-0.001	1.000	-0.001
1	24	255.60	63.76	4.01	1.42	0.0230	0.0183	0.3650	0.3156	0.50	0.50	0.20	0.20	1.000	-1.000	1.000	-0.500
1	25	255.60	51.08	5.00	1.77	0.0238	0.0211	0.6872	0.5777	0.50	0.50	0.20	0.20	1.000	-1.000	1.000	-0.500
1	26	399.46	66.70	5.99	2.12	0.0160	0.0136	0.5271	0.8073	0.50	0.50	0.20	0.20	1.000	-1.000	0.500	-0.500
1	27	399.46	56.81	7.03	2.49	0.0168	0.0160	0.4991	1.1823	0.50	0.50	0.20	0.20	0.800	-0.800	0.500	-1.100
1	28	399.46	49.95	8.00	2.83	0.0176	0.0136	0.4375	0.5855	0.50	0.50	0.20	0.20	0.700	-0.050	0.001	-1.500
1	29	399.46	44.26	9.03	3.19	0.0186	0.0184	0.3428	0.2815	0.20	0.50	0.70	0.70	0.600	-0.001	0.001	-2.500
1	30	399.46	40.00	9.99	3.53	0.0189	0.0163	0.3883	0.3701	0.20	0.70	0.70	0.70	0.500	-0.001	0.001	-1.500

Table 4.2-Coefficients used within SKM for roughness 1 (Alhamid data) modelling

Roughness Type	Experiment Number	b, mm	H, mm	b/H	P_b/P_w	Q_{meas} (l/s)	$\%SF_{w\ meas}$	Q_{SKM} (m^3/s)	$\%Q_{error}$	$\%SF_{w\ SKM}$	$\%SF_{W\ error}$
1	1	107.10	126.00	0.85	0.30	13.69	94.70	0.0137	0.33	94.23	-0.49
1	2	107.10	107.00	1.00	0.35	9.99	93.33	0.0101	0.89	92.21	-1.21
1	3	107.10	75.00	1.43	0.50	5.15	90.99	0.0051	-1.55	93.00	2.21
1	4	107.10	54.00	1.98	0.70	2.91	87.38	0.0029	0.01	87.02	-0.41
1	5	107.10	43.00	2.49	0.88	2.01	84.69	0.0020	1.41	84.05	-0.75
1	23	255.60	84.89	3.01	1.06	15.53	81.14	0.0158	1.58	79.90	-1.53
1	24	255.60	63.76	4.01	1.42	9.68	76.65	0.0098	1.16	75.02	-2.12
1	25	255.60	51.08	5.00	1.77	6.71	73.65	0.0066	-0.97	72.32	-1.80
1	26	399.46	66.70	5.99	2.12	20.05	67.81	0.0195	-2.52	68.65	1.24
1	27	399.46	56.81	7.03	2.49	15.76	64.04	0.0159	0.60	61.50	-3.96
1	28	399.46	49.95	8.00	2.83	12.99	61.50	0.0131	1.09	59.82	-2.73
1	29	399.46	44.26	9.03	3.19	10.83	57.90	0.0109	0.35	57.10	-1.39
1	30	399.46	40.00	9.99	3.53	9.30	56.34	0.0093	-0.35	55.72	-1.10

Table 4.3-Results of SKM modelling for discharge and $\%SF_w$ for roughness 1 (Alhamid data)

Roughness Type	Experiment Number	b, mm	H, mm	b/H	P_b/P_w	f_1	f_2	f_3	f_4	λ_1	λ_2	λ_3	λ_4	Γ_1	Γ_2	Γ_3	Γ_4
2	9	120.60	142.00	0.85	0.30	0.0151	0.0145	0.0936	0.2067	0.05	0.07	0.25	0.10	3.000	-0.400	0.030	-1.000
2	10	120.60	121.00	1.00	0.35	0.0188	0.0159	0.0978	0.1846	0.10	0.07	0.30	0.05	3.500	-0.230	0.010	-1.000
2	11	120.60	80.50	1.50	0.53	0.0217	0.0201	0.1421	0.2278	0.10	0.30	0.70	0.03	3.500	-4.000	0.010	-0.001
2	12	120.60	60.30	2.00	0.71	0.0242	0.0226	0.1665	0.3105	0.10	0.30	0.30	0.03	2.000	-2.800	1.000	-0.001
2	13	120.60	48.00	2.51	0.89	0.0234	0.0232	0.1789	0.3590	0.10	0.30	0.30	0.03	1.400	-2.200	2.000	-1.000
2	17	272.00	90.84	2.99	1.06	0.0174	0.0148	0.1370	0.1697	0.50	0.50	0.20	0.20	0.010	-0.300	1.000	-0.001
2	18	272.00	67.91	4.01	1.42	0.0202	0.0178	0.1828	0.1973	0.50	0.50	0.20	0.20	1.000	-2.000	1.000	-0.500
2	19	272.00	54.51	4.99	1.76	0.0198	0.0195	0.2683	0.3323	0.50	0.50	0.20	0.20	0.500	-1.000	1.000	-0.500
2	31	416.20	69.53	5.99	2.12	0.0148	0.0134	0.1452	0.2000	0.50	0.50	0.20	0.20	0.500	-0.700	0.500	-0.500
2	32	416.20	59.37	7.01	2.48	0.0170	0.0146	0.1700	0.1649	0.50	0.70	0.07	0.10	0.500	-0.500	1.000	-1.100
2	33	416.20	52.00	8.00	2.83	0.0164	0.0168	0.2229	0.2455	0.50	0.50	0.20	0.20	0.200	-0.050	0.001	-0.500
2	34	416.20	46.47	8.96	3.17	0.0176	0.0177	0.3289	0.4590	0.50	0.50	0.10	0.20	0.200	-0.050	0.001	-0.500
2	35	416.20	41.60	10.0	3.54	0.0188	0.0186	0.2930	0.4468	0.70	0.80	0.10	0.10	0.040	-0.010	0.010	-0.500

Table 4.4-Coefficients used within SKM for roughness 2 (Alhamid data) modelling

Roughness Type	Experiment Number	b, mm	H, mm	b/H	P_b/P_w	Q_{meas} (l/s)	$\%SF_{w\ meas}$	Q_{SKM} (m^3/s)	$\%Q_{error}$	$\%SF_{w\ SKM}$	$\%SF_{W\ error}$
2	9	120.60	142.00	0.85	0.30	21.947	92.87	0.0215	-2.03	92.65	-0.24
2	10	120.60	121.00	1.00	0.35	15.908	91.16	0.0156	-1.88	90.62	-0.58
2	11	120.60	80.50	1.50	0.53	7.381	87.36	0.0074	-0.39	88.13	0.88
2	12	120.60	60.30	2.00	0.71	4.482	82.73	0.0045	0.13	81.28	-1.75
2	13	120.60	48.00	2.51	0.89	3.113	79.59	0.0031	0.87	78.15	-1.81
2	17	272.00	90.84	2.99	1.06	22.246	74.68	0.0220	-0.96	75.58	1.20
2	18	272.00	67.91	4.01	1.42	14.093	68.32	0.0144	2.02	70.34	2.97
2	19	272.00	54.51	4.99	1.76	9.996	64.36	0.0099	-1.14	66.00	2.55
2	31	416.20	69.53	5.99	2.12	18.470	59.66	0.0189	2.08	61.28	2.71
2	32	416.20	59.37	7.01	2.48	14.300	55.56	0.0114	-1.20	53.09	1.65
2	33	416.20	52.00	8.00	2.83	11.530	52.22	0.0115	-0.33	57.29	9.70
2	34	416.20	46.47	8.96	3.17	9.610	49.99	0.0094	-2.20	49.05	-1.88
2	35	416.20	41.60	10.00	3.54	8.030	46.91	0.0081	1.08	46.27	-1.35

Table 4.5-Results of SKM modelling for discharge and $\%SF_w$ for roughness 2 (Alhamid data)

	Panel 1-percentage weightings of terms				Panel 2-percentage weightings of terms				Panel 3-percentage weightings of terms				Panel 4-percentage weightings of terms			
	Term 1	Term 2	Term 3	Term 4	Term 1	Term 2	Term 3	Term 4	Term 1	Term 2	Term 3	Term 4	Term 1	Term 2	Term 3	Term 4
9	50.00	11.55	2.33	36.12	47.73	9.29	40.71	2.27	16.88	49.86	33.12	0.14	5.51	50.00	39.94	4.55
10	43.69	12.84	6.31	37.16	47.35	12.32	37.68	2.65	15.01	49.03	34.99	0.97	5.95	50.00	38.26	5.79
11	39.31	14.57	10.69	35.43	18.29	6.14	43.86	31.71	5.71	49.97	44.29	0.03	4.21	50.00	45.78	0.01
12	33.73	17.51	16.27	32.49	21.74	10.17	39.83	28.26	4.99	46.79	45.01	3.21	4.00	50.00	45.99	0.01
13	34.34	23.01	15.66	26.99	21.46	12.41	37.59	28.54	3.26	47.37	46.74	2.63	2.78	50.00	47.22	0.01
17	50.00	24.88	24.96	0.15	49.98	15.66	34.34	0.02	6.19	47.47	43.81	2.53	5.23	50.00	44.76	0.01
18	46.75	30.93	3.25	19.07	35.52	16.19	33.81	14.48	4.27	47.68	45.73	2.32	2.99	50.00	44.57	2.44
19	39.21	30.04	10.79	19.96	33.13	18.93	31.07	16.87	2.58	48.25	47.42	1.75	1.97	50.00	46.02	2.01
31	50.00	29.36	1.15	19.49	35.97	14.61	35.39	14.03	3.28	49.15	46.72	0.85	1.59	50.00	47.17	1.24
32	47.04	32.77	2.96	17.23	36.60	19.84	30.16	13.40	3.14	49.04	46.86	0.96	1.03	50.00	46.91	2.07
33	43.59	34.11	6.41	15.89	48.73	24.11	25.89	1.27	3.23	50.00	46.77	0.00	1.41	50.00	44.20	4.39
34	40.72	35.65	9.28	14.35	49.97	34.75	15.25	0.03	3.39	50.00	46.61	0.00	1.68	50.00	38.44	9.88
35	39.32	37.22	10.68	12.78	49.97	31.98	18.02	0.03	2.99	50.00	47.01	0.00	1.38	50.00	43.24	5.38

Table 4.6-Percentage weighting of each term in the SKM for roughness 1 (Alhamid data)

	Panel 1-percentage weightings of terms				Panel 2-percentage weightings of terms				Panel 3-percentage weightings of terms				Panel 4-percentage weightings of terms			
	Term 1	Term 2	Term 3	Term 4	Term 1	Term 2	Term 3	Term 4	Term 1	Term 2	Term 3	Term 4	Term 1	Term 2	Term 3	Term 4
1	50.00	11.88	10.65	27.47	46.59	9.79	40.21	3.41	22.94	49.83	27.06	0.17	5.82	50.00	39.92	4.26
2	47.11	14.56	2.89	35.44	47.64	11.84	38.16	2.36	19.98	49.94	30.02	0.06	5.95	50.00	38.93	5.12
3	32.15	13.65	17.85	36.35	21.81	8.70	41.30	28.19	10.34	49.96	39.66	0.04	4.74	50.00	45.26	0.01
4	34.20	20.50	15.80	29.50	22.65	12.34	37.66	27.35	7.40	45.74	42.60	4.26	3.52	50.00	46.47	0.01
5	34.32	23.97	15.68	26.03	22.81	14.84	35.16	27.19	5.85	41.55	44.15	8.45	2.18	50.00	43.10	4.72
23	50.00	23.86	26.00	0.14	46.05	16.68	33.32	3.95	9.45	46.39	40.55	3.61	4.80	50.00	45.20	0.01
24	47.33	31.87	2.67	18.13	28.32	15.38	34.62	21.68	6.06	46.91	43.94	3.09	3.41	50.00	43.98	2.61
25	50.00	38.05	0.02	11.93	33.85	21.69	28.31	16.15	4.36	47.23	45.64	2.77	2.29	50.00	45.53	2.18
26	40.01	34.84	9.99	15.16	32.67	23.18	26.82	17.33	4.72	47.62	45.28	2.38	2.04	50.00	44.86	3.10
27	33.65	35.07	16.35	14.93	34.63	29.08	20.92	15.37	3.75	45.56	46.25	4.44	2.29	50.00	38.78	8.93
28	37.84	42.33	12.16	7.67	47.59	45.16	4.84	2.41	3.32	50.00	46.68	0.00	1.65	50.00	45.00	3.35
29	33.67	42.37	16.33	7.63	47.32	49.57	0.43	2.68	2.51	50.00	47.49	0.00	1.20	50.00	46.09	2.71
30	33.37	48.31	16.63	1.69	42.16	50.00	7.31	0.53	2.36	49.96	47.64	0.04	1.10	50.00	46.10	2.79

Table 4.7- Percentage weighting of each term in the SKM for roughness 2 (Alhamid data)

Roughness Type	Experiment Number	b, mm	h, mm	b/h	Pb/Pw	So	Q, l/s	%SFw	Q_{SKM} (m^3 /s)	$\%Q_{error}$	$\%SF_{w\ SKM}$	$\%SF_{W\ error}$
All type 1	**6**	140.22	94.00	1.49	0.53	0.00392	8.02	64.09	0.0082	1.66%	60.66	-5.35
All type 1	**7**	140.22	70.00	2.00	0.71	0.00392	4.43	52.13	0.0046	2.75%	50.50	-3.14
All type 2	**14**	143.40	95.30	1.50	0.53	0.00392	9.50	62.93	0.0099	3.80%	58.07	-7.71
All type 2	**15**	143.40	71.70	2.00	0.71	0.00392	5.33	53.88	0.0052	-1.87%	52.13	-3.26
All type 2	**36**	441.00	58.87	7.49	2.65	0.00403	11.43	24.12	0.0115	0.55%	25.37	5.18

Experiment Number	f_1	f_2	f_3	f_4	λ_1	λ_2	λ_3	λ_4	Γ_1	Γ_2	Γ_3	Γ_4
6	0.0151	0.0145	0.0936	0.2067	0.05	0.07	0.25	0.10	3.000	-0.400	0.030	-1.000
7	0.0188	0.0159	0.0978	0.1846	0.10	0.07	0.30	0.05	3.500	-0.230	0.010	-1.000
14	0.0217	0.0201	0.1421	0.2278	0.10	0.30	0.70	0.03	3.500	-4.000	0.010	-0.001
15	0.0242	0.0226	0.1665	0.3105	0.10	0.30	0.30	0.03	2.000	-2.800	1.000	-0.001
36	0.0234	0.0232	0.1789	0.3590	0.10	0.30	0.30	0.03	1.400	-2.200	2.000	-1.000

Table 4.8-Alhamid (1991) homogenously roughened channel flow data, results of discharge and $\%SF_w$ SKM modelling and modelling coefficients

Figure 4.1-Alhamid (1991) flume with heterogeneous roughness

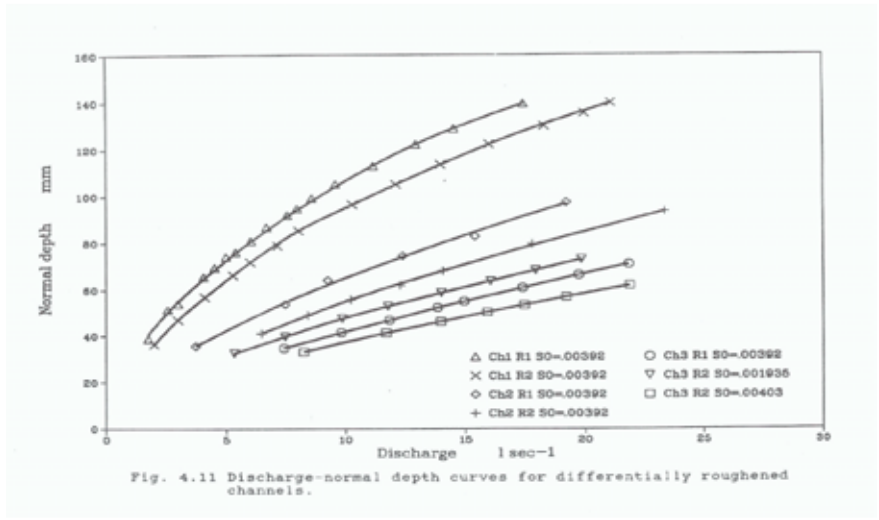

Fig. 4.11 Discharge-normal depth curves for differentially roughened channels.

Figure 4.2-Normal depth-discharge data for differentially roughened channel data (from Alhamid, 1991)

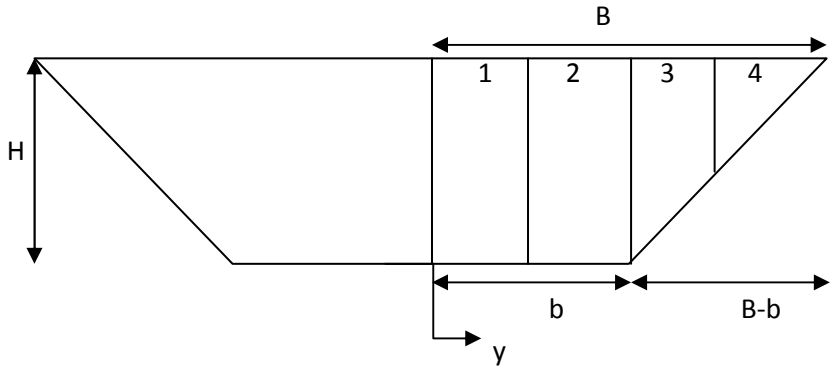

Figure 4.3-Schematic representation of trapezoidal channel

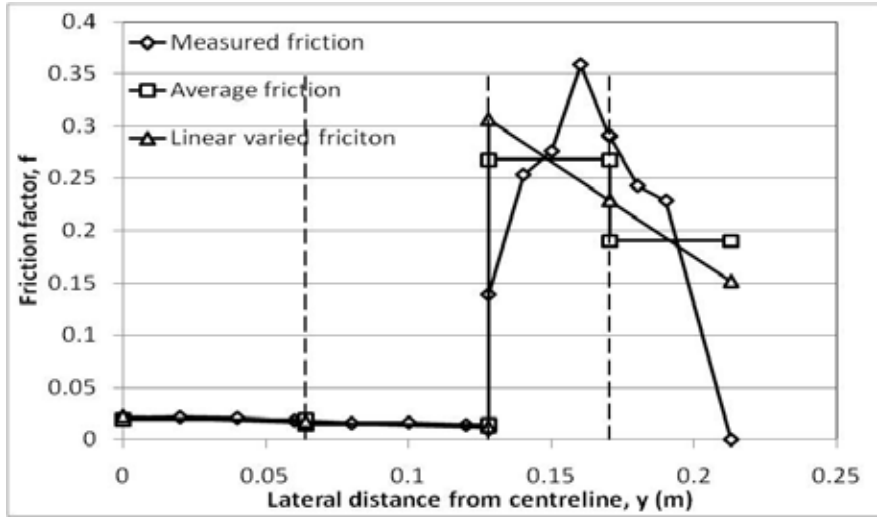

Figure 4.4-Friction factor variations

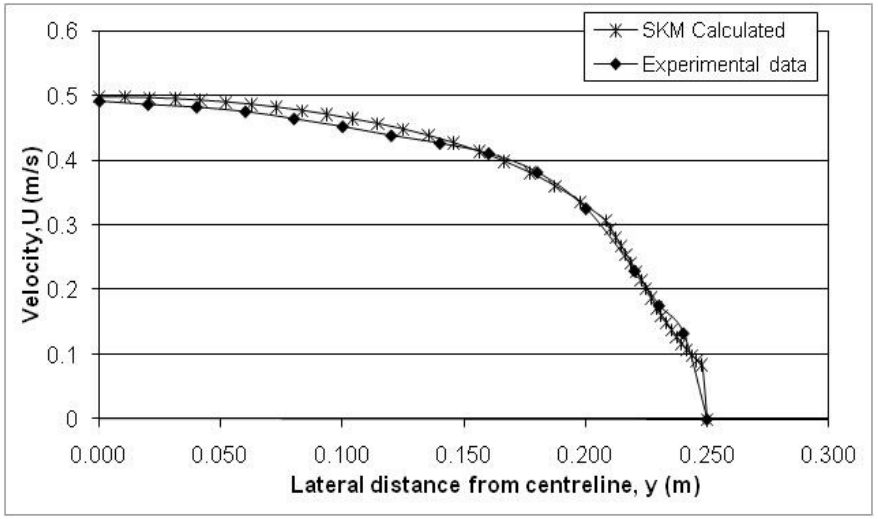

Figure 4.5- Depth-averaged velocity, comparison of SKM model and experimental data (roughness 2 exp. 35, H=41.6mm, b=208.1mm)

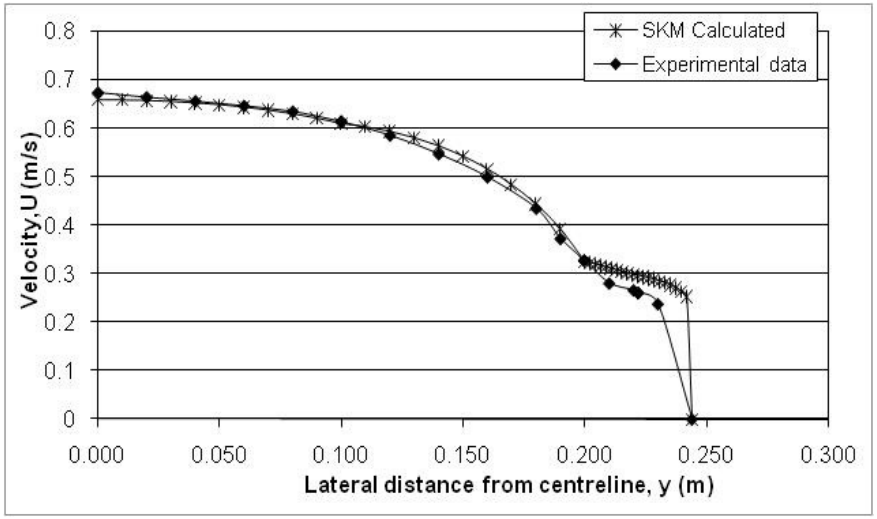

Figure 4.6- Depth-averaged velocity, comparison of SKM model and experimental data (roughness 1 exp. 29, H=44.36mm, b=199.7mm)

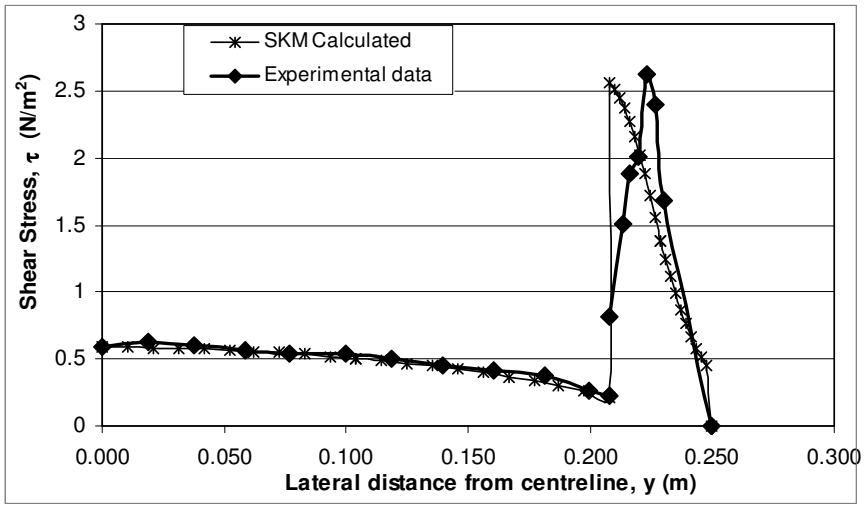

Figure 4.7- Boundary shear stress, comparison of SKM model and experimental data (roughness 2 exp. 35, H=41.6mm, b=208.1mm)

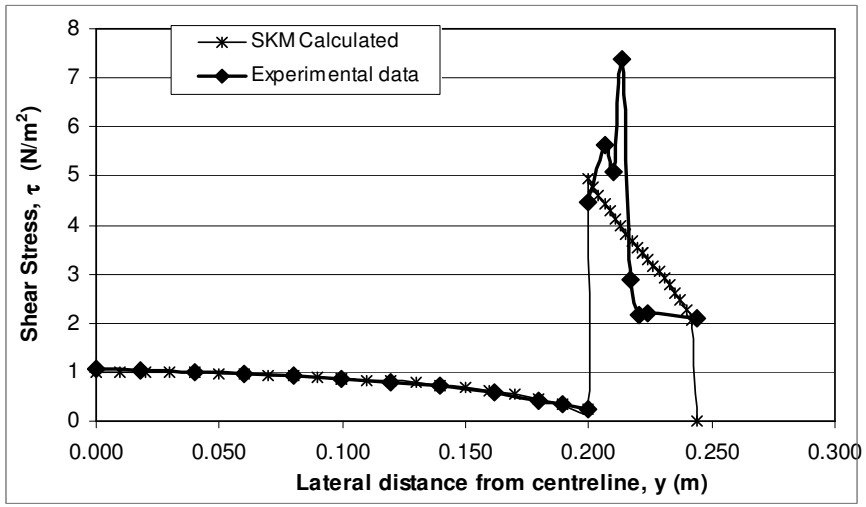

Figure 4.8- Boundary shear stress, comparison of SKM model and experimental data (roughness 1 exp. 29, H=44.36mm, b=199.7mm)

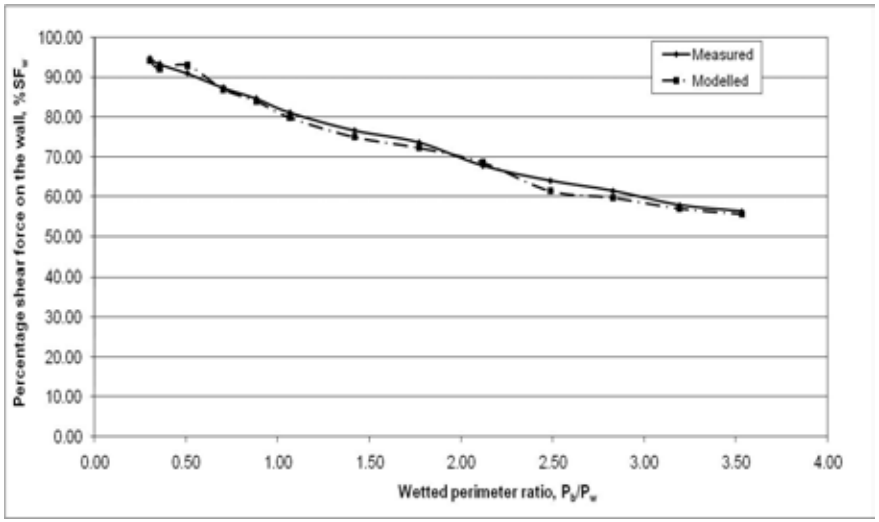

Figure 4.9-Measured and modelled variation of %SF_w with wetted perimeter ratio, P_b/P_w for roughness 1

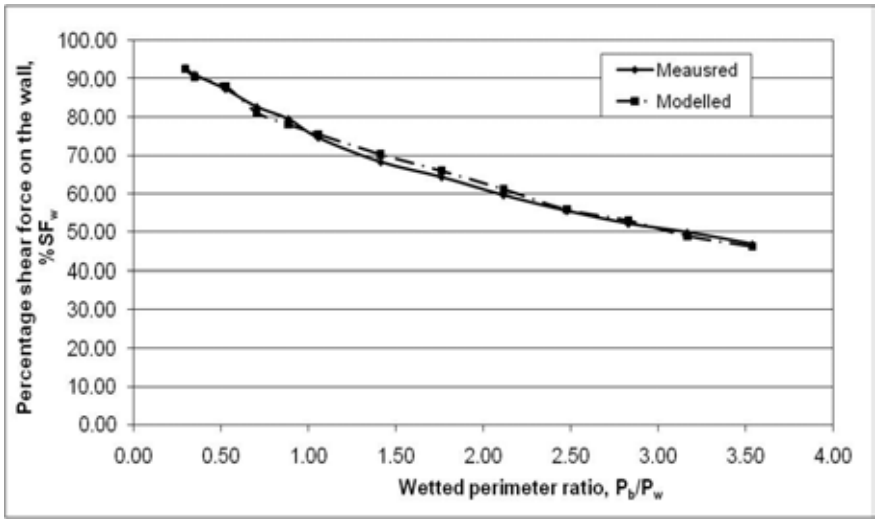

Figure 4.10-Measured and modelled variation of %SF_w with wetted perimeter ratio, P_b/P_w for roughness 2

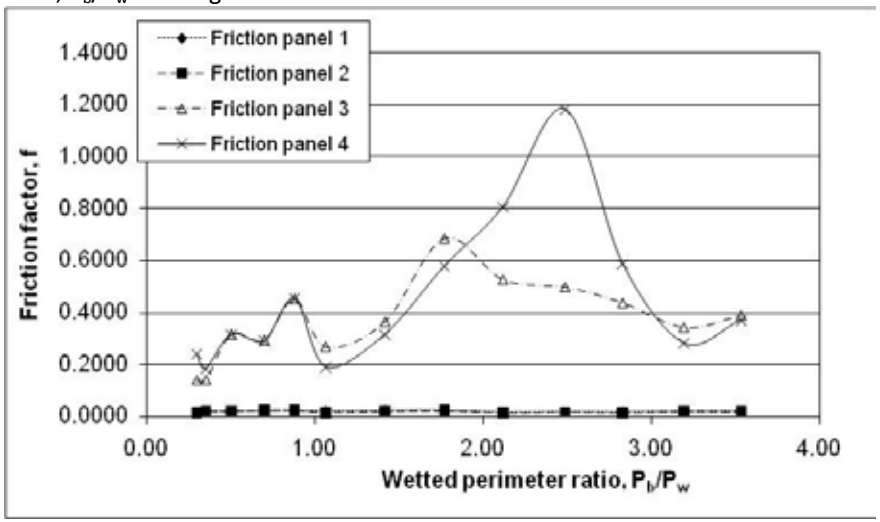

Figure 4.11-Distribution of friction factor, *f*, in panels 1-4 for roughness 1

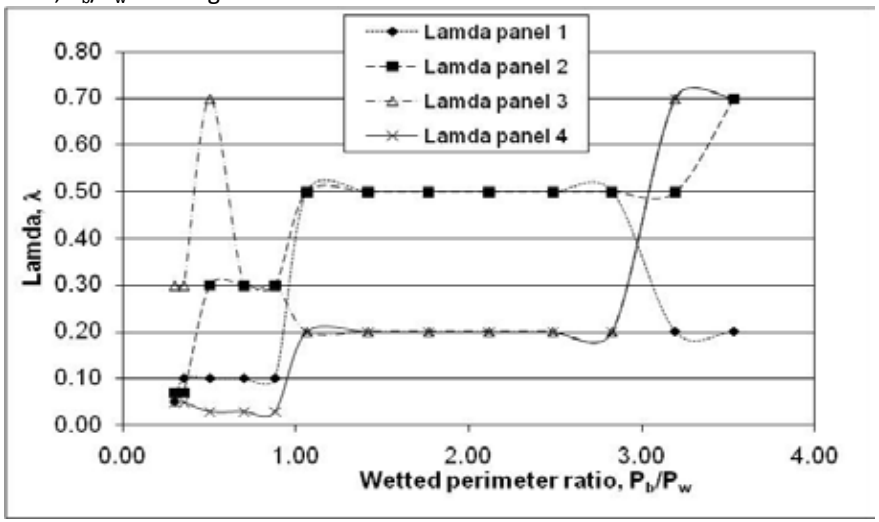

Figure 4.12-Distribution of lamda, λ, in panels 1-4 for roughness 1

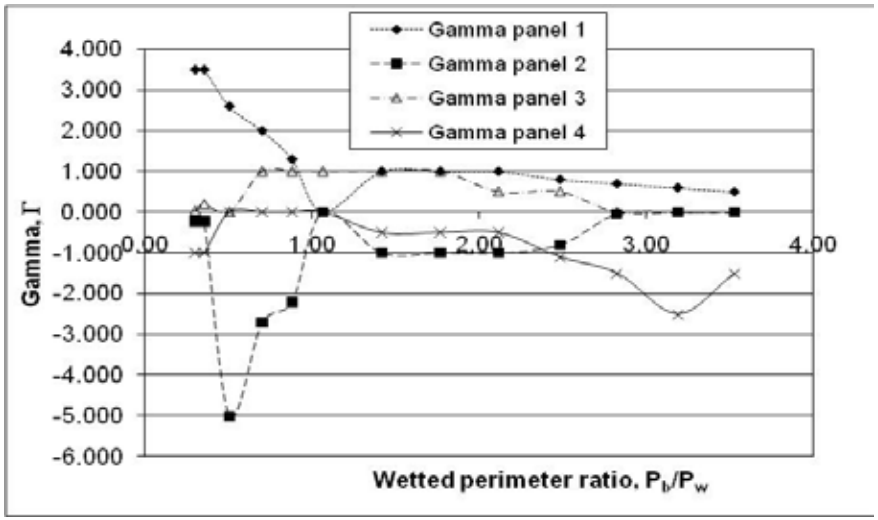

Figure 4.13-Distribution of gamma, Γ, in panels 1-4 for roughness 1

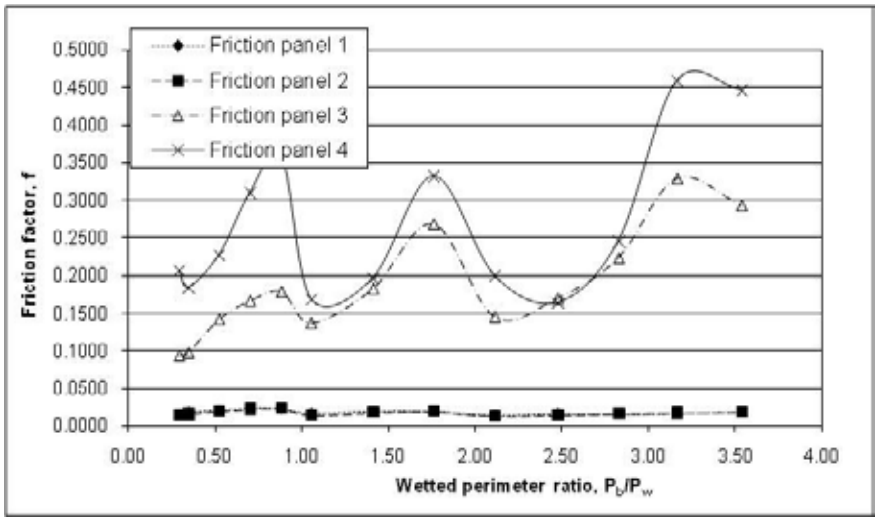

Figure 4.14-Distribution of friction factor, *f*, in panels 1-4 for roughness 2

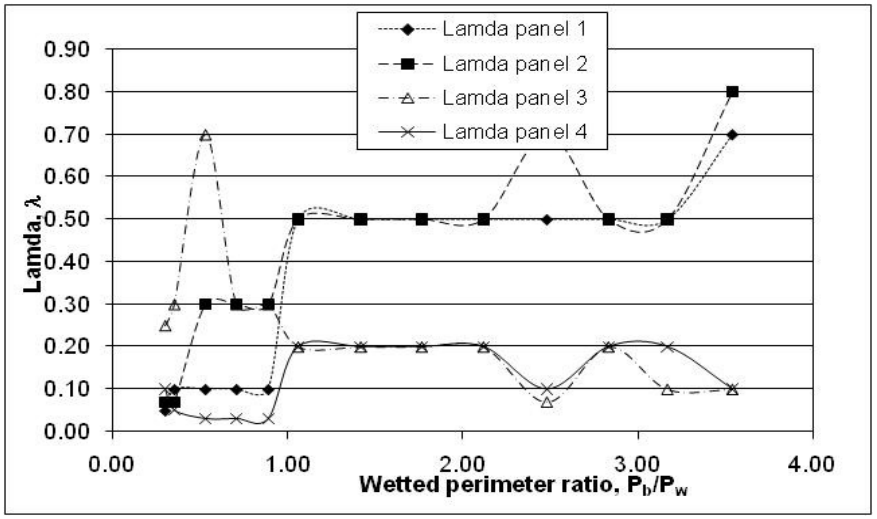

Figure 4.15-Distribution of lamda, λ, in panels 1-4 for roughness 2

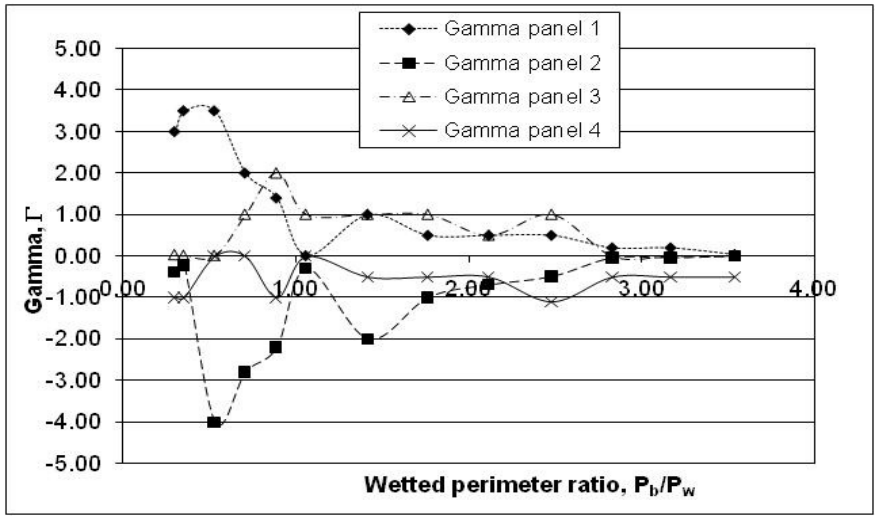

Figure 4.16-Distribution of gamma, Γ, in panels 1-4 for roughness 2

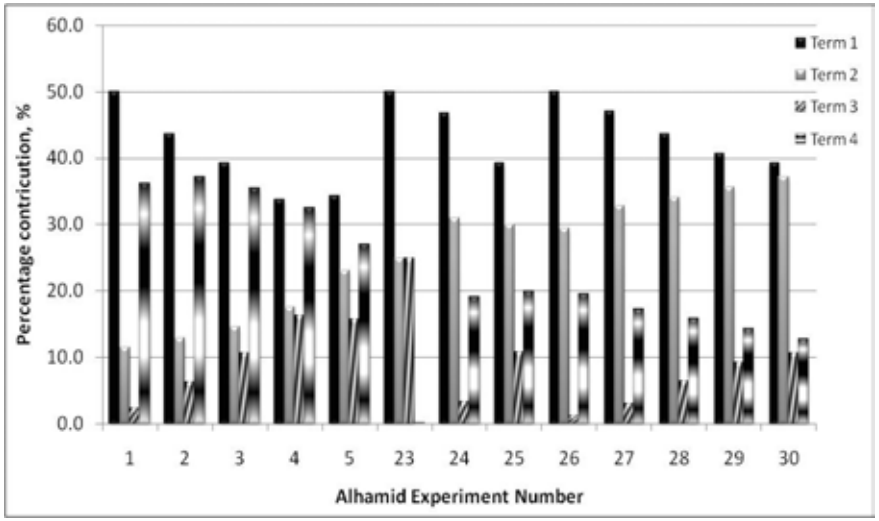

Figure 4.17-Percentage weightings given to each term in the SKM for Roughness 1, panel 1 for Alhamid channel data

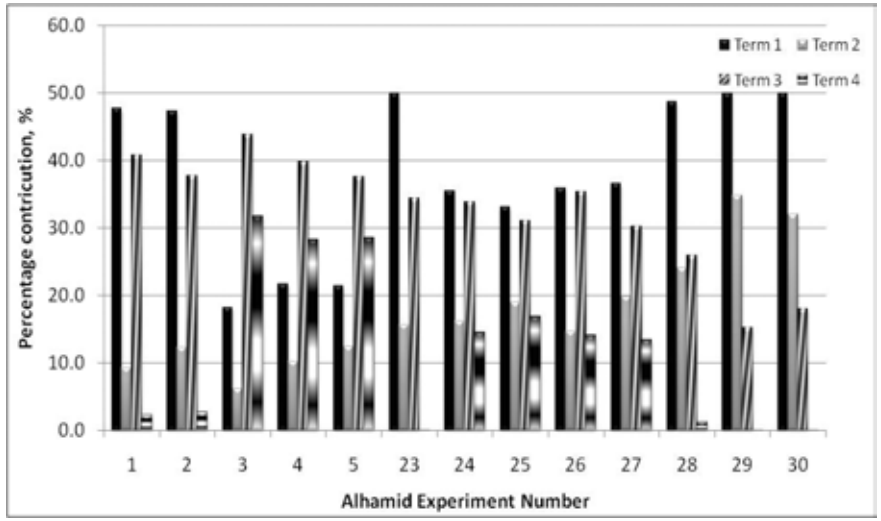

Figure 4.18-Percentage weightings given to each term in the SKM for Roughness 1, panel 2 for Alhamid channel data

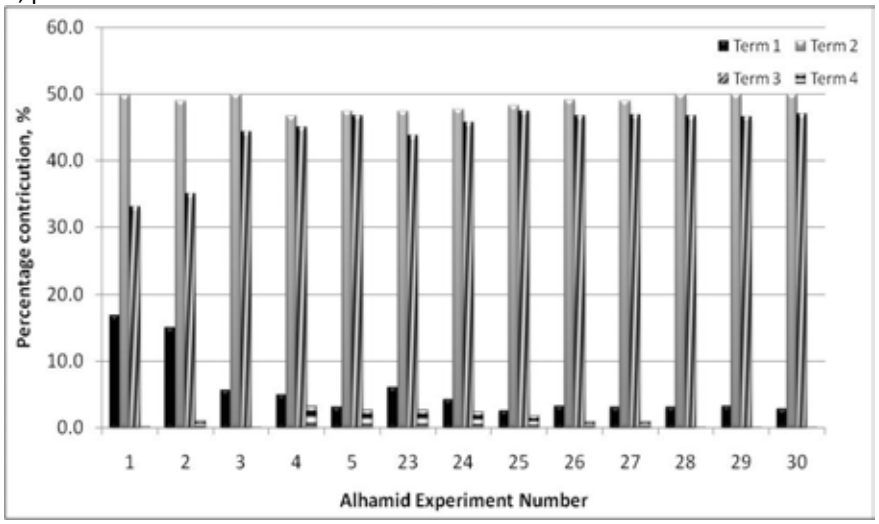

Figure 4.19-Percentage weightings given to each term in the SKM for Roughness 1, panel 3 for Alhamid channel data

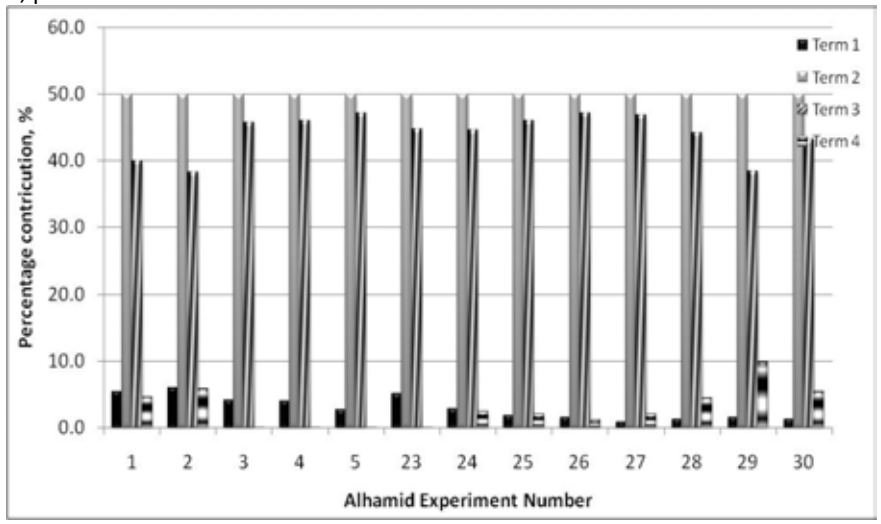

Figure 4.20-Percentage weightings given to each term in the SKM for Roughness 1, panel 4 for Alhamid channel data

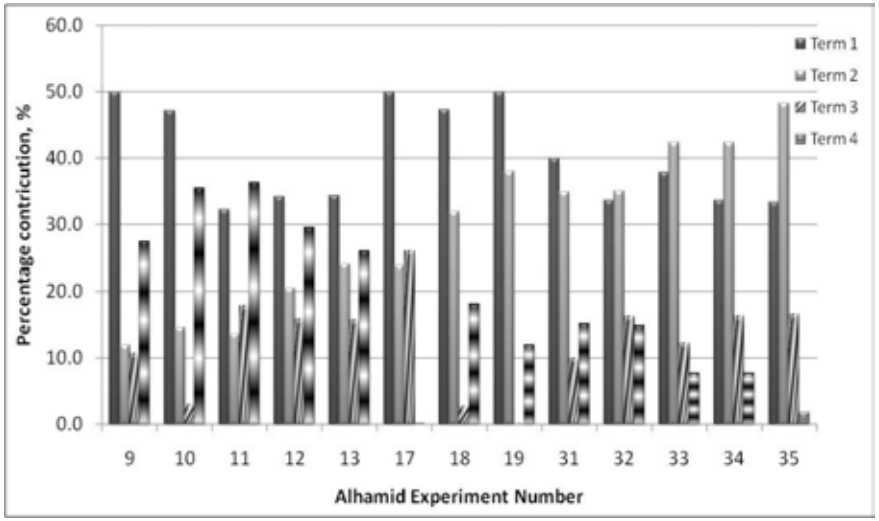

Figure 4.21-Percentage weightings given to each term in the SKM for Roughness 2, panel 1 for Alhamid channel data

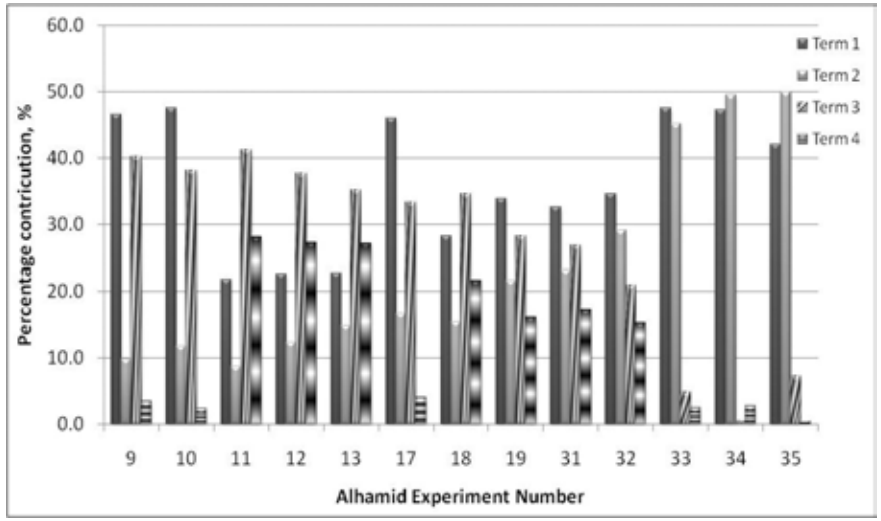

Figure 4.22-Percentage weightings given to each term in the SKM for Roughness 2, panel 2 for Alhamid channel data

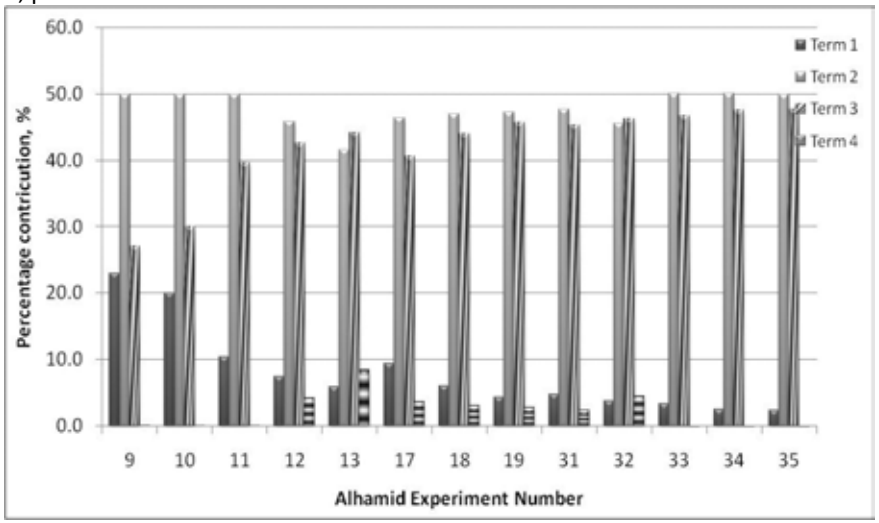

Figure 4.23-Percentage weightings given to each term in the SKM for Roughness 2, panel 3 for Alhamid channel data

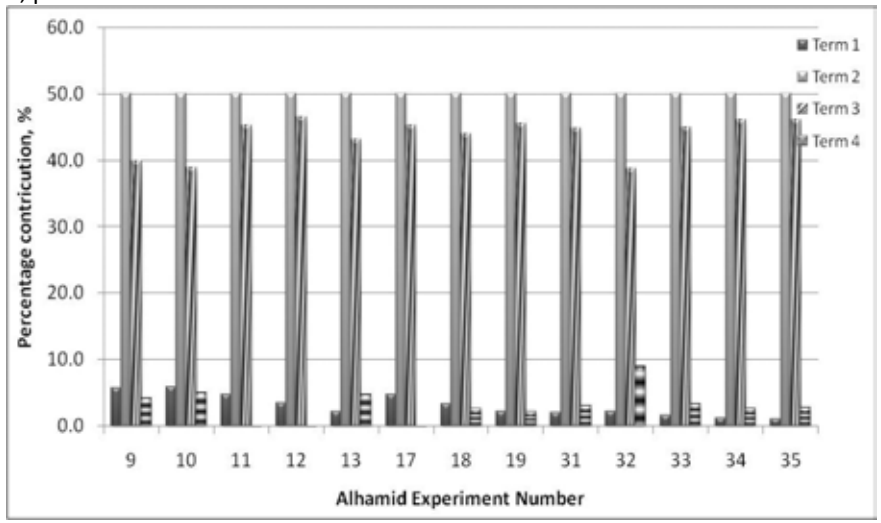

Figure 4.24-Percentage weightings given to each term in the SKM for Roughness 2, panel 4 for Alhamid channel data

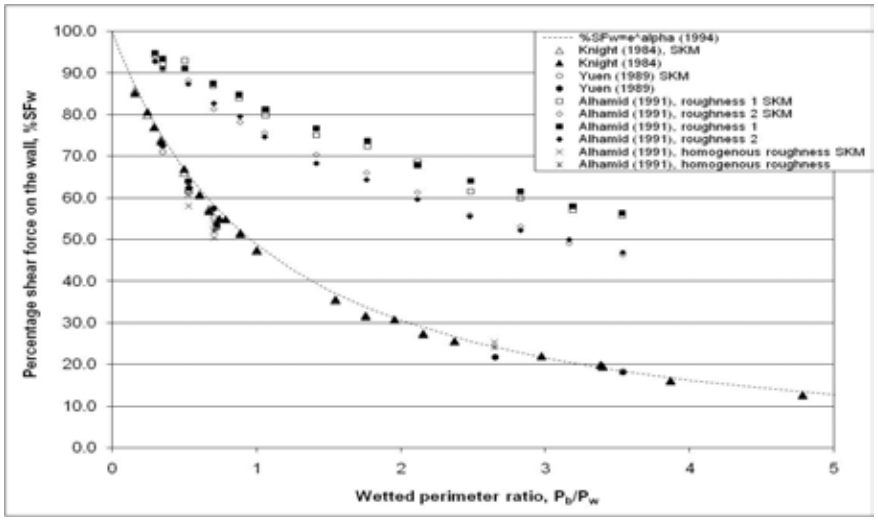

Figure 4.25-Comparison of SKM model with experimental data for trapezoidal and rectangular channels, both with rough and smooth boundaries

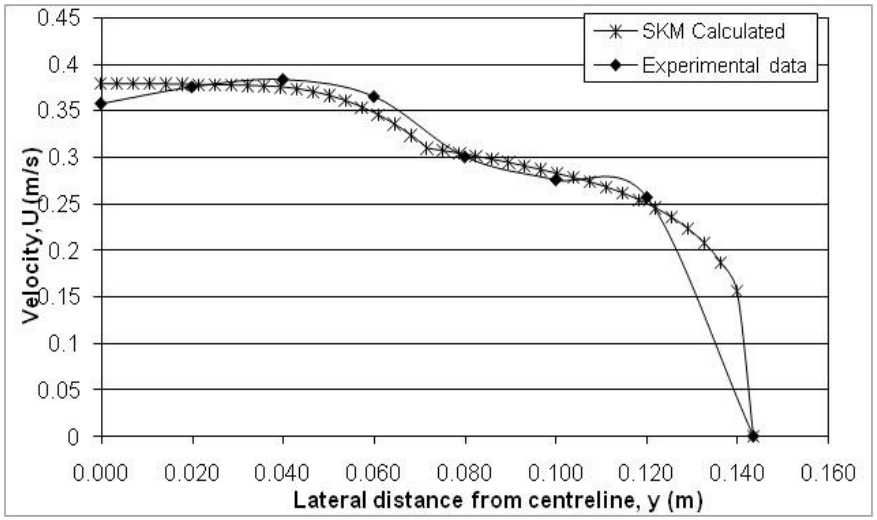

Figure 4.26- Depth-averaged velocity, comparison of SKM model and experimental data (roughness 2 exp. 15, H=71.7mm, b=71.7mm)

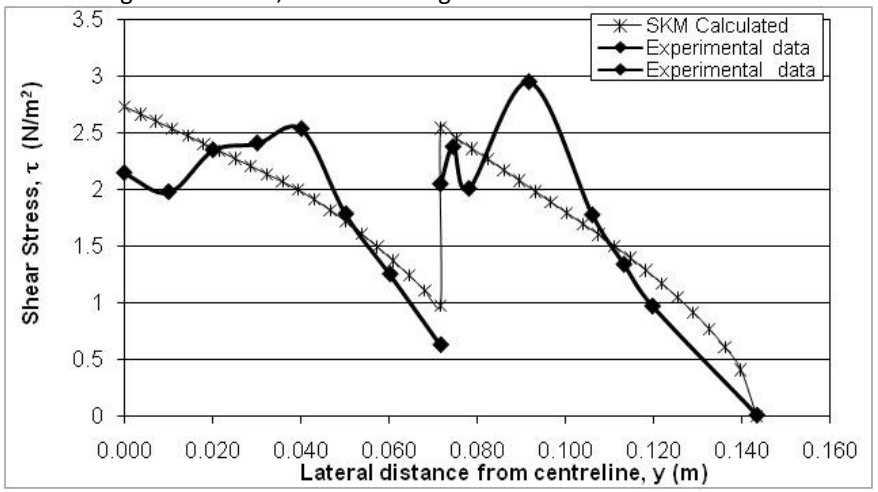

Figure 4.27- Boundary shear stress, comparison of SKM model and experimental data (roughness 2 exp. 15, H=71.7mm, b=71.7mm)

PART 2-COMPOUND CHANNELS

CHAPTER 5-LITERATURE REVIEW ON FLOW IN SKEWED COMPOUND CHANNELS

Sometimes, if you stand on the bottom rail of a bridge and lean over to watch the river slipping slowly away beneath you, you will suddenly know everything there is to be known. (Pooh's Little Instruction Book, inspired by A. A. Milne)

5.1 Introduction

Each river in the natural world is unique. Some gently curve, others meander, some become braided and others are relatively straight. However, one thing can be said for the vast majority, is that they are usually compound i.e. have at least one floodplain with a deeper main channel. Much work has been carried out on prismatic compound channels with one of the most complete data sets being that of the Flood Channel Facility (FCF) in the 1980's and early 1990's (Knight & Shiono, 1990). There has also been significant progress in meandering channels with notable work again being carried out at the FCF and Loughborough University (Spooner & Shiono, 2002). However, an area which has been somewhat neglected is that of skewed channels. By carrying out research into skewed channels a transition between the prismatic and meandering channels may be made and comparisons drawn. Skewed channels can generally have two configurations; either the main channel will skew relative to the floodplain or the floodplain will skew relative to the main channel.

This chapter gives an overview of the importance of compound channels, a review of compound channel behaviour and a summary of some previous work that has been carried out on skewed channels. Many of the modelling approaches reviewed in

Chapter 2 are applicable to that of compound channels and therefore no further details are presented here. Nevertheless, a brief critique is presented on the advantages/failings of current modelling methods with regards to compound channels.

5.2 Brief review of the importance of compound channels

Historically, people built their homes near to rivers as the floodplain land was highly fertile due to the deposition of nutrients during times of flood and offered a ready supply of water and food. London, York and Oxford, to name but a few, are all ancient UK cities that built up around their rivers (Fleming et al., 2001 & 2002). However, in the 19th and 20th centuries many rivers were straightened and deepened, especially where the river flowed through built-up and industrialised areas. Such examples include the River Thames and the River Clyde. This was done for a number of reasons but largely to allow for industrial development and for the floodplains to be built upon. Therefore, many rivers in industrial areas tend to be wide, deep and trained to be straight by the use of concrete barriers (which are also used for flood protection). This results in a simple channel with isolated floodplains. Purseglove (1988) stated that as a consequence of straightening, dredging and widening rivers it results in the river becoming a 'drain', resulting in the disruption of the natural environment due to trees and vegetation being removed with fish life and other riverside species endangered. This is reflected in Knight & Samuels (2007) appraisal of recent major European flood events where it is stated "*Once the larger waterways had been corrected, almost all other streams and brooks were forced into 'straitjackets' as well.*"

This manipulation of rivers has resulted in many having a large straight channel with alternating floodplains, i.e. a skewed channel. In addition, many natural channels, simply due to their geometry, have portions of the channel where the floodplain switches from one side to the other.

By the end of the 20th century, and now into the 21st century, perceptions and attitudes towards rivers and flooding have changed. No longer are the hard engineering solutions (straightening, deepening, fixed barriers) top of the agenda but a softer engineering approach favoured (two-stage channels, relief channels, temporary barriers) which helps to attenuate the downstream peak flows, encourages flora and fauna and allow the river to once again become a useful amenity. With climate change increasing the frequency of flood events, and our increased awareness of flooding across the UK and the world, it is more important than ever that we understand the flow characteristics of compound channels better and improve our modelling methods.

Due to the interference of mankind, many channels are now of skewed configuration, especially in built up, industrial areas. With the increasing risks of flooding it is vital that we understand the complexities involved in two stage channels by carrying out experimental research in conjunction with computer simulations.

5.3 Flow mechanisms in compound channels

Many characteristics of simple channels can also be found in compound channels, as shown in Section 2.2, but compound channels have additional features not found in

simple channels. In compound channels, the floodplain flow is typically much shallower than the main channel flow, the floodplain may be much rougher than the main channel, the slope of the floodplain may differ to that of the main channel, the floodplain flow may run parallel to the main channel or it may cross-over the main channel as in meandering or skewed flows. As a result of all these influences, the floodplain flow may retard the main channel flow with substantial mixing and turbulent interaction between the two. Due to the complexities of the main channel/floodplain interactions in compound channels they have to be treated differently from simple channels which are often simplified to one-dimensional problems (Knight & Shiono, 1996). A representation of these effects is shown in **Figure 5.1** with the mechanisms described below in Section 5.3.1.

5.3.1 Shear layer

Generally the velocity in the main channel is greater than that of the floodplain. This discontinuity causes a shear layer to form at the interface between the main channel and the floodplain. This shear layer causes a reduction in conveyance of the main channel and an associated increase in the floodplain conveyance, but overall it causes a decrease in total channel conveyance (Knight and Mohammed, 1984). These strong lateral shear layers typically lead to the formation of organised plan form vortices induced by inflectional point instability, Knight (2006). **Figure 5.1** sketches the hydraulic behaviour of compound (overbank) flow. The secondary flow cells are shown to have developed on both the main channel and floodplains and are of varying size and magnitude. Within the shear layer, lateral momentum exchange arises due to the differing velocities of the flows on the floodplain and main channel. Also at this

main channel/floodplain interface, interface vortices form due to the differing flows on the floodplain and main channel.

Wormleaton (1996) stated that the effects of the shear layer extend across the width of the floodplain but decreases to zero towards the outer edges of the floodplain. Myers (1978) found that the effects of the shear layer were greater at lower depths and decrease as the flow increases.

5.3.2 Vortices and secondary currents

Prandtl (1964) differentiated two types of secondary flow; the first related to changes in planform curvature and cross-sectional area and the second type arising from the turbulent velocity fluctuations.

At the interface of the main channel and floodplain(s) where the two co-flowing streams travel at differing velocities, vortices with vertical axes develop in this highly sheared zone. Helical secondary flow forms alongside these vortices in the longitudinal streamwise direction (**Figure 5.1**), these are caused by irregularities in the channel but also occur spontaneously in turbulent, prismatic flows (Einstein & Li, 1958) due to the anisotropy of turbulence and are generally termed secondary currents. These vortices and secondary flow produce momentum transfer between the main channel and floodplain(s) causing a decrease in conveyance capacity in the main channel and an increase in the floodplain. This lateral momentum transfer produces an apparent shear stress at the vertical interface between the main channel and floodplain(s). This apparent shear stress can be calculated from the balance of terms

in a depth-averaged momentum equation. The physical development of these vortices is described by Bousmar (2002). The vortices develop in a time-space domain and where there are no perturbations visible, the velocity field remains uniform. As the vortices develop in the velocity field, the instability appears and extends laterally while increasing the shear layer width. When the initial vortices are completely developed, they start to combine to form larger ones. As the merging process stops, the size of vortices remains constant, indicating that they have reached maximum size, limited by the channel walls.

Tominaga et al. (1989) postulated that secondary currents have a fundamental function in open channel flow as they influence the velocity distribution, boundary shear stress, and consequently the three-dimensional bed configuration.

Many researchers including Shiono & Knight (1988; 1991), Tominaga et al. (1989) and Tominaga & Nezu (1991) have investigated the secondary flows in prismatic, compound channels. Tominaga & Nezu (1991) found two secondary current cells located at the interface of the main channel and floodplain with an additional large cell extending across the width of the floodplain. The free surface vortices (longitudinal vortices) form due to the turbulence caused by the free surface. The third vortex forms on the side of the floodplain and is hence termed the “floodplain vortex, whereas the vortex in the main channel is termed the “main channel vortex”. These can be seen in **Figure 5.2**. Kiely & McKeogh (1993) stated that these cells move the water at surface level away from the main channel/floodplain interface. The

pattern and location of these cells is found to be affected by the geometry of the channel with their strength being dependent on the depth of flow in the floodplain.

5.3.3 Boundary shear stress

The background has been discussed in detail in Section 2.2.6 with full calculation details given in Section 6.2.7.

5.4 Experimental research into skewed channels

Although skewed channels are common, an example being when there are distant flood banks imposing on the natural floodplain, little research has been carried out in this area. However, by studying the effects of skewing a knowledge gap will be filled between straight and fully meandering channels. Herein, three studies have been reviewed which have been carried out by a number of researchers over the past 30 years. Later in this thesis, results from some additional experiments are described to add to this limited data set.

James & Brown (1977) are believed to be the first to carry out research into skewed channels. They tested the effect of skewing the main channel relative to the floodplain (**Figure 5.3**). Three angles were tested; 7.2°, 11.0° and 24.05°. Flow on the receiving (expanding) floodplain was found to accelerate whereas on the converging floodplain the flow decelerated. They also found that the resistance factor, determined by the Colebrook-White formula, increased as the angle of skew increased. In some cases the resistance doubled between the 7.2° and 24.05° channels, but in general, there was not a significant increase.

Elliott (1990) carried out further work at the Flood Channel Facility in the UK as part of the Series A experiments on straight channels. This work is perhaps the most complete of all the skewed channel work carried out to date as detailed measurements of velocity, boundary shear stress and direction of flow were taken for each of the configurations. This work will be examined in detail in Chapter 7. In essence, Elliott skewed the floodplain relative to the main channels at angles of 2.1°, 5.1° and 9.2° and incorporated varying main channel side slopes (s=1, s=1:1 and s=1:2) and changing roughness. The flume had a usable channel length of 55m and a maximum width of 10m, the bed slope was kept constant at 1.027×10^{-3}. The main channel bed was 1.5m wide and 0.5m deep.

It was found that skewing floodplains at an angle relative to the main channel reduces the capacity of the compound channels. Overbank resistance also increases slightly (approximately 7%) by skewing, especially at the lowest depth, H≈0.176m. Elliott also observed that the narrowing floodplain had reducing section mean velocity as the flow progresses downstream and even at small skews the distributions of velocity and boundary shear stress are significantly different from non-skew channels of similar geometry. It was also found that the peak value of boundary shear stress can be up to 15% larger than in the straight channel equivalent and the peak value of boundary shear stress in the skew found at the interface receiving floodplain and main channel can be up to 100% greater than that of the straight channel. Elliott also observed that the principal direction of flow on the narrowing floodplain was parallel to the floodplain walls with the surface flow of the main channel changing from being

parallel to the main channel at low depths to being parallel to the floodplain walls at increasing relative depths. The secondary flow cells of a straight channel were significantly altered by an imposed cross-flow. Elliott and Sellin (1990) stated that ancillary experiments were carried out at the University of Bristol, but at the time of writing no specific details could be found.

The final study reported here is that of Jasem (1990). This was aimed at complementing the work carried out by Elliott (1990) at the FCF. This work was carried out on 8.2m long flume, 0.764m wide and 0.3m deep with the main channel skewing at 5.84° to the floodplain (**Figure 5.4)** with a fixed bed slope of $1x10^{-3}$. The skewed main channel was 0.15m wide and 0.061m deep. Jasem conducted a number of experiments including infilling the main channel to assess the floodplain behaviour in isolation, sectioning off the main channel from the floodplain to consider the main channel's behaviour and roughening the floodplains. The experiments concentrated on the velocity field, stage-discharge data, roughness and secondary flow with no boundary shear stress data being presented.

Ervine and Jasem (1995) stated that while injecting dye at or near to the floodplain bed it enters a large secondary swirl within the main channel and is transported off within the main channel with the remainder of the floodplain flow passing over the top of the main channel. They also found that the velocity in the main channel is approximately constant or decreases slightly downstream, implying that a process of substitution is occurring whereby the flow entering the main channel from the right floodplain (by entrainment into the large secondary current) must produce a

comparable removal of fluid from the main channel onto the left floodplain. They go on to state that secondary flow is driven in this case by the floodplain flow. They proved this by isolating the floodplains from the main channel and found that the percentage of recirculating velocity relative to longitudinal velocity was 0.5%-1%, whereas when the floodplains were no longer in isolation this increased to approximately 3%. It was also found that the value of recirculating velocity along the length of the channel decreases between the upstream and downstream sections.

In order to add to and complement the work to date, a series of experiments was carried out at the University of Birmingham. The experiments were carried out in a smooth non-tilting 18m long flume with a bed slope of 2.003×10^{-3} (further details in Chapters 6 and 8). In these experiments the floodplains were skewed at an angle of 3.81° to the main channel over 6m. Although only one skew angle was investigated, 4 depths were examined with 6 measuring sections per depth allowing the progression and development of the flow, velocity and boundary shear stress to be seen throughout the skewed transition. Where appropriate, this work is compared to other available data but in particular to the FCF work of Elliott (1990) and to additional experiments carried out by Atabay (2001) and Rezaei (2006) at the University of Birmingham in the same flume as used for the skewed research. Atabay carried out asymmetric compound channel experiments with floodplains parallel to the main channel whereas Rezeai investigated the effects of converging floodplains.

5.5 Modelling methods for compound channels

A detailed review of modelling methods has been presented in Chapter 2 and it is not intended to describe the methods further here, apart from offering a brief critique of the difficulties of modelling compound channels.

As found in Chapter 2 it is always difficult to model the behaviour of river flow accurately. Some models have been found to give tolerable results for one, two or more parameters, but the river engineer is still waiting for the perfect modelling package.

When selecting a model it is important that the user is clear on what the model is required to do. If only discharge is of interest then there are many commercial packages which can model this fairly well, such as ISIS, HEC-RAS and Mike 11, not to mention two-dimensional programs which are becoming more frequently utilised (such as Tuflow and Mike 21). However, if distributions of velocity or boundary shear stress are of interest then the model requires more complexity and is therefore inherently more time consuming to construct and has much longer processing times.

Compound channel behaviour varies from that seen in simple channels, with some aspects of compound channel behaviour being described earlier. The velocity on the floodplains differs from that of the main channel and the boundary shear stress varies significantly between the floodplains and main channel, and also peaks in a number of locations (at the main channel/floodplain interface and also within the main channel,

generally close to the centreline of the main channel) and this makes modelling compound channels problematic.

The single channel method, SCM, and the divided channel method, DCM, are both still in use today with many one-dimensional software packages being based upon them. However, due to their inability to take account of the increase of wetted perimeter when a river goes into an overbank state (in the case of the SCM), or neglecting the complexity of the interaction at the main channel/floodplain interface in the DCM, results in under- and over-estimation of the discharge respectively. Both of these methods are therefore incapable of accurately predicting velocity or boundary shear stress.

With advancements in computing technology it is now possible to incorporate some two-dimensional aspects into computer models which should allow for more accurate computations. Recently the Environment Agency for England and Wales in conjunction with HR Wallingford released the Conveyance and Afflux Estimation System (CAES) which is based on the Shiono and Knight Method (SKM). This package has many uses as it allows the user to 'guesstimate' the roughness of the channel by allowing the user to specify the bed material, bank material and floodplain bed material, resulting in a global friction factor. This information can then be fed into the conveyance generator allowing for a more accurate assessment of the channel's capacity. This package also has the ability to allow it to be fully integrated into ISIS or to export the results into other river modelling software.

Fully two- (e.g. Mike 21, Tuflow) and three-dimensional packages (e.g. CXF, PHOENICS, FLOW3D, TELEMAC 3D etc) usage is increasing but the time taken to set up the model and the computation time limits their use to portions of the channel which are of particular interest.

5.6 Concluding remarks

In their natural state rivers tend to be compound channels and therefore it is important to study their behaviour. It is important that channels of a various geometries, roughness and scales be examined. Much work has been carried out on both prismatic and meandering channels at both small and large scale with a limited amount being conducted in the field. One of the most neglected areas of work appears to be that of the flow in skewed channels, of which only three studies have been reviewed herein. One of which will be studied further in Chapter 7.

From the studies examined, many commonalities are to be found such as increasing resistance with increasing skew angle and a peak in boundary shear stress at the main channel/floodplain boundary. However, there are still some gaps in knowledge that needs to be filled. None of the examined work has taken regular velocity and boundary shear stress measurements along the length of the skewed transition, this was therefore carried out by the author, as detailed in Chapter 8. This allowed for resistance to be determined at a number of locations, in addition to permitting a force-momentum balance to be undertaken. The author's work was carried out in the same channel at Birmingham as previous work, including studies into asymmetric prismatic

and converging channel configurations allowing for direct comparisons to be made, as well as comparisons with the skewed channel work carried out by Elliott (1990).

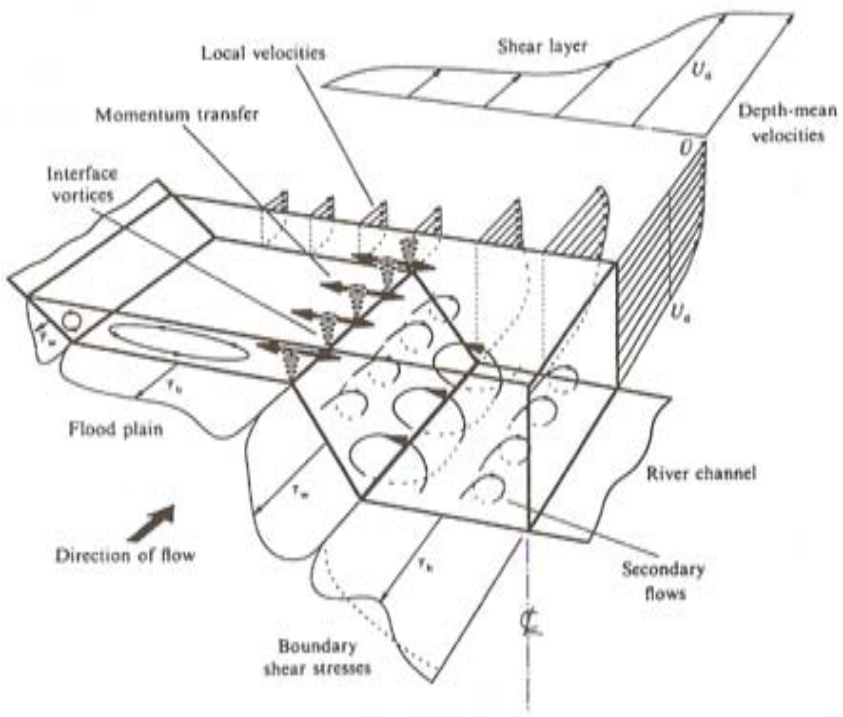

Figure 5.1-Flow structures in a straight compound channel (after Shiono & Knight, 1991)

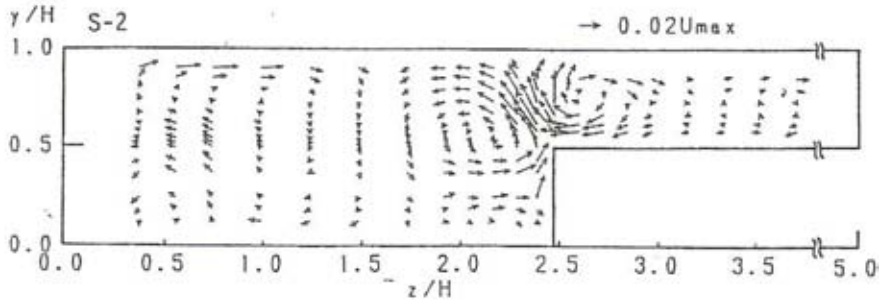

Figure 5.2-Secondary current cell formation in compound channel flow (Tominaga & Nezu, 1991) Secondary current vectors (h/H=0.5)

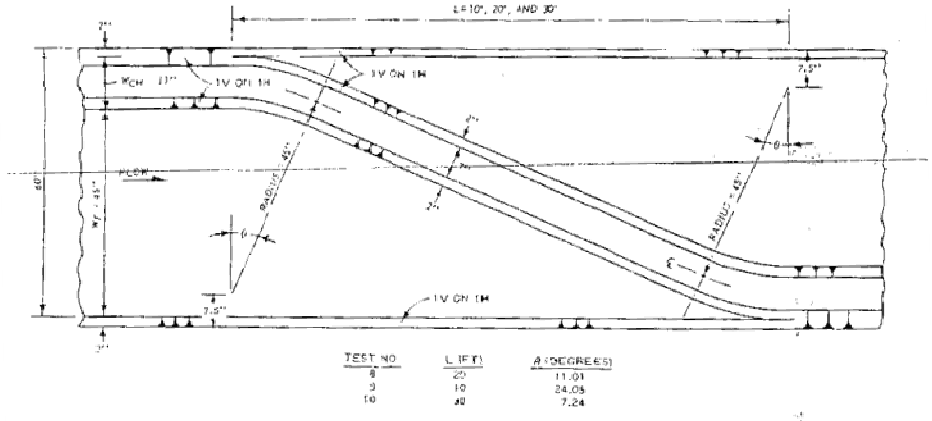

Figure 3. Plan view of single crossover configurations

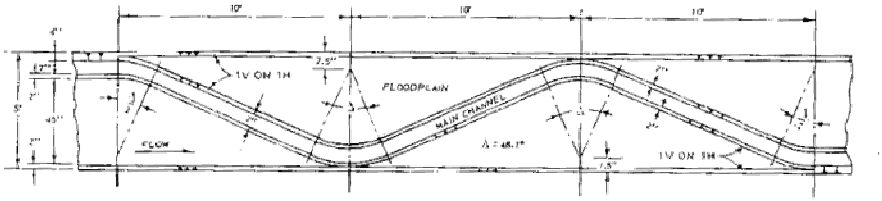

Figure 4. Plan view of three consecutive crossovers, Test 11

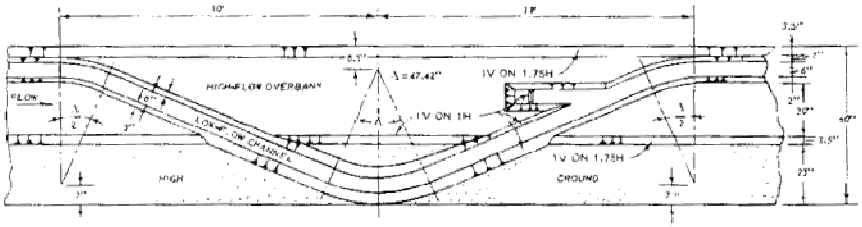

Figure 5. Plan view of two consecutive crossovers with channel separating from floodplain, Test 14

Figure 5.3-James and Brown (1977) test flume

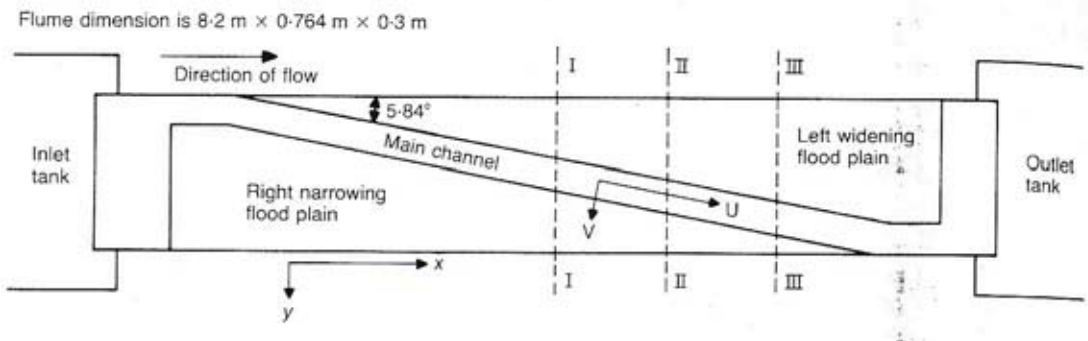

Figure 5.4-Jasem (1990) flume

CHAPTER 6-EXPERIMENTAL APPARATUS AND PROCEDURE

1. If reproducibility may be a problem, conduct the test only once.

2. If a straight line fit is required, obtain only two data points

(Velilind's Rules of Experimentation)

6.1 Introduction

As stated in Chapter 5, skewed channels are found due to artificial straightening of the natural meandering geometry of the river to increase conveyance in the channel and when distant flood banks have been constructed. Flume studies are important to understand the complex behaviour of flow and allow for detailed measurements to be made with relative accuracy, something that is difficult (bordering on impossible) in the field. Although much of this chapter is specific to the skewed channel experiments carried out at the University of Birmingham (Chapter 8), many of the general techniques discussed are common to the Flood Channel Facility (FCF) skewed work (discussed in the following chapter). Details on the FCF set up and specific apparatus are discussed in Chapter 7 with more detailed explanations given by Knight & Sellin (1987).

The main aim of this study was to add to the limited amount of skewed channel data by carrying out additional experiments and to draw comparisons with what has preceded this work. Boundary shear stress and velocities will be measured in order to evaluate the evolution of these parameters along the channel and to analyse the apparent shear forces acting along the interface between the main channel and the floodplain(s).

In order to fulfil the objectives as outlined in Chapter 1, a number of experiments were conducted using an 18m flume at the Department of Civil Engineering, The University of Birmingham. The general and schematic views of the flume are shown in **Figures 6.1a-c** (after Atabay, 2001 and Rezaei, 2006). The flume was straight with a depth of 400mm and a total usable width of 1198mm comprising of two 400mm wide floodplains and a 398mm wide channel. The average bed slope was 2.003×10^{-3}. The boundaries were both rigid and smooth and were constructed using a P.V.C. material.

In these experiments the floodplains skewed to the main channel over a 6m length, a skew angle of 3.81° starting 9m downstream of the entrance. The skew was positioned at this location to allow the flow to fully develop before entering the skew whilst leaving sufficient length at the end of the transition to see the development of the flow back to the asymmetric case.

These boundaries were constructed from smooth L-shaped aluminium sections. **Figure 6.2** gives a plan view of the channel with **Figures 6.3a-f** giving cross-section views for each of the measuring sections. **Figure 6.4** shows an overall view of the channel.

In order to improve the inflow conditions and remove any wave phenomena induced at the opening a smooth transition section was made in both the vertical and horizontal directions from P.V.C. A honeycomb screen was used to separate the inlet

tanks from the transition, **Figures 6.1a** and **6.5**. A floating polystyrene dampener was attached to a beam at the entrance (**Figure 6.6**) in order to reduce the water surface fluctuations at the flume entrance.

Water is supplied from 3 separate pipelines, 150mm, 100mm and 50mm in diameter with their respective discharges being measured by a Dall tube, a Venturi meter and an Electro Magnetic Flow (EMF) meter, **Figures 6.7a** and **6.7b**. Both the Dall tube and Venturi meter had two manometers, a mercury one and water manometer measuring the static and dynamic pressure heads.

The downstream end of the flume has a series of 3 adjustable tailgates (**Figure 6.8**), which were used to achieve a specific depth of flow and slope in the flume. The water surface profiles were measured directly using a pointer gauge accurate to $1/10^{th}$ of a millimetre, which was located on an instrument carriage (**Figure 6.9**). The depths were initially taken every 1m along the centreline of the main channel and every 0.5m through the skewed transition. The rail levelling was checked by raising the tailgates to 150mm and filling the flume, this would ensure that the water level data was accurate along the channel. The water level was allowed to settle overnight and the static levels recorded every 1m along the centreline of the main channel and every 0.5m from the start of the transition to the end of the channel, **Figure 6.10**.

Depth-averaged velocity and velocity distributions were measured using a 13mm diameter Novar Nixon miniature propeller current meter, **Figure 6.11a** and **6.11b**. Boundary shear stresses were measured using static and dynamic Pitot tubes of

4.77mm outer diameter with the related pressure heads measured using inclined manometers (**Figures 6.12** and **6.13**).

Four relative depths were examined and 6 cross-sections making for repeatable experiments consisting of a number of examinable sections. However, unless there were high errors, the experiments were only conducted once for each flow at each section. The transition was divided into 5 equally spaced measuring sections, 1.5m apart, with an additional measuring section 1m downstream of the transition. For each depth, the water level, depth-averaged velocity and boundary shear stress was taken at all 6 measuring sections. Velocity distributions were taken at 4 sections, the upstream section (1), in the middle of the transition, section (3), at the end of the transition, section (5) and 1m downstream of the skew, section (6) (**Figures 6.3a-f**). **Table 6.1** gives a matrix of all of the experiments carried out and the respective measurements.

The analysis of the data was carried out using a number of Microsoft Excel programs which were written to determine the water surface slope, the depth-averaged velocity, the discharge at any position along a section and the boundary shear stress.

6.2 Experimental techniques and procedures

6.2.1 Development length of flow

Flow becomes fully developed over a length termed the development length, which is dependent on the cross-sectional geometry of the duct. It is important that the development length is determined and that the flow is fully developed before any

readings are taken. There are many formulae for determining the possible development length in pipe and duct flow which can give an approximate indication to the development length for an open channel. Klein (1981) states that

$$l_e = 60D_h \qquad \textbf{6.1}$$

Where l_e is the development length and D_h the hydraulic radius which is defined as:

$$D_h = 4\frac{A}{P} = 4R \qquad \textbf{6.2}$$

where A is the cross-sectional area and P the wetted perimeter. Re-arranging Equation 6.1 and taking l_e as 9m, in order that the flow is fully developed by 9m the hydraulic radius, R, must be less than 0.0375m. This implies that only the lowest flow is fully developed. However, in Klein's (1981) experiments the ducts used were very smooth whereas in the Birmingham flume the entry had been roughened in order that the boundary layer is almost fully developed on entry. **Figure 6.14** shows the velocity against depth for each experiment at the centreline of the main channel against depth. From this, the distributions are mainly smooth with a few minor perturbations indicating that the flow is indeed fully developed and suitable for experimental readings to be taken.

6.2.2 Discharge measurements

As mentioned in Section 6.1, the flume had three different supply pipelines, 150mm, 100mm and 50mm in diameter with the discharges measured by a Dall tube, a Venturi meter and an Electro-Magnetic Flow (EMF) meter respectively (**Figures 6.7a** and **6.7b**). The maximum capacity of the Dall tube was 70ℓ/s and was only used for flows in the region of 30ℓ/s. The EMF supplied a maximum discharge of 7ℓ/s at an accuracy of 1%, but was set at a constant level of 3ℓ/s. The Venturi meter had a capacity of 30ℓ/s. To determine the flows in each pipeline, Equations 6.3 to 6.5 were used (Rezaei, 2006).

For the Dall tube with 150mm diameter pipeline:

$$Q = 0.8369(\Delta h)^{0.4961} \qquad \textbf{6.3}$$

For the Venturi meter of 100mm diameter pipe:

$$Q = a(\Delta h)^{b} \qquad \textbf{6.4}$$

For Δh<236mm water $Q = 0.2263(\Delta h)^{0.582547}$ **6.5a**

For Δh>236mm water $Q = 0.31395(\Delta h)^{0.5138229}$ **6.5b**

Where Q is the discharge in any given pipeline in ℓ/s and Δh is the pressure head measured by the manometer in mm of water or mercury for flows above 10ℓ/s. When

using the Dall tube and Venturi meter, the head difference, Δh for each experiment was determined in advance using Equations 6.3 and 6.4 (as the required flow was known, further details on flows and the reasons for choosing them is given in Section 6.2.1) and on the day of the experiment Δh was set to the required value.

The head difference, Δh, in the Dall tube and Venturi meter was checked periodically throughout each experiment, the discharge calculated using the appropriate formulae and averaged to give a more accurate discharge. In the case of the Venturi meter the mercury manometer was always used, therefore the level of mercury was recorded three times during the experiment and averaged. This average reading was used in conjunction with Equation 6.4 to determine the measured discharge. The Dall tube was linked to a static and dynamic manometer filled with water. Again, the known pressure difference was set at the start of the beginning of the experiment and the static and dynamic levels recorded. The static and dynamic levels were recorded two additional times and the pressure head found. These three readings were averaged and used with Equation 6.3 to determine the measured flow.

As the Venturi meter and Dall tube had two isolated methods of determining the discharge passing through both (the mercury and water manometers), a flow was set and the pressure head was read from both the mercury meter and the water manometers in order to check the accuracy of each. This was an important check, especially on the Venturi meter, as the water manometer is on a scale 12 times that of the mercury meter. No further checks were made on the accuracy of any of the discharge measuring equipment as it was taken that if the integrated velocities were

within approximately 3% of the measured then there should be no inaccuracy in the measuring apparatus.

The EMF measures the discharge in ℓ/s directly, however when the experiment is running for long periods of time it is better to calculate the discharge from the volume passing through the meter and the time over which the experiments were conducted as follows:

$$Q = \frac{V_2 - V_1}{t_2 - t_1} \qquad \textbf{6.6}$$

Where Q is the discharge in ℓ/s, V_1 and V_2 are the volumes in litres passing though the pipeline at the beginning and end of the experiment respectively; similarly t_1 and t_2 are the times at which V_1 and V_2 were recorded.

The discharges though each system was summed to give the total discharge entering the flume, Q_m.

6.2.3 Choice of flows

Atabay (2001) carried out a number of asymmetric compound channel experiments in The University of Birmingham flume, but with slightly wider floodplains (407.3mm) and a slightly steeper slope of 2.024×10^{-3}. Atabay found that in this flume the stage-discharge relationship took the form:

$$H = 0.4476Q^{0.4777} \quad \textbf{6.7}$$

Where H is the total depth of flow in m and Q the discharge in m^3/s.

Four relative depths were decided upon (Dr=0.2, 0.3, 0.4 and 0.5) and given that the main channel depth is 50mm the depth of flow was determined from:

$$Dr = (H - h)/H \quad \textbf{6.8}$$

where h is the bankfull depth.

This gave depths of 62.5mm, 71.4mm, 83.3mm and 100mm for Dr=0.2, 0.3, 0.4 and 0.5 respectively. Using Atabay's stage-discharge relationship (Equation 6.7) the corresponding flows (Q=16.2ℓ/s, 21.4ℓ/s, 29.6ℓ/s and 43.4ℓ/s) were chosen. By using conditions similar to Atabay's allowed for comparisons between the prismatic asymmetric case and the conditions at the start and end of the skew.

6.2.4 Tailgate setting

In the skewed channel experiments, the water surface slope was crucial. In this channel configuration it was not possible to set uniform flow throughout the length of the flume, but it was possible to establish it through the first 9m before the transition. When the flow entered the skewed portion of the channel there was an abrupt change in geometry and a slight decrease in cross-sectional area, resulting in significant mixing of the flow and thereby causing a rise in water surface.

In order to set the tailgates, 4 relative depths were pre-determined (Section 6.2.3), and four flows determined using Equation 6.7. Uniform flow was set in upstream portion of the flume (i.e. S_e=S_w=S_o; the energy slope equals the water surface slope which equals the bed slope). For a given discharge, the tailgates were adjusted slightly to give a number of *M1* and *M2* profiles, the mean water surface slope and average depths were then plotted versus the tailgate level. The tailgate level could then be interpolated in order that the water slope equalled that of the bed. Measurements were taken every 1m, with it being measured every 0.5m through the transition, this is in accordance with the same method as used by Knight & Demetriou (1983). **Figures 6.15-6.18** show the plots of tailgate adjustments for each experiment. As can be seen from these figures, the normal depth for each experiment is approximately 62.9mm, 72.7mm, 85.4mm and 102.8mm. These vary from those calculated in Section 6.2.3 by 0.4mm to 2.8mm, this is simply due to the narrowing of the floodplains and the shallower bed slope.

As will be demonstrated in Section 8.3, the water surface through the transition rose significantly, resulting in the average flow depth in the channel varying slightly from those predicted above using the tailgate setting procedure. However, at the start of the transition the depth was very close to normal depth (within 1-2mm), which was regarded as reasonable given the non-uniform nature of the flow as it entered the transitional zone.

6.2.5 Water temperature measurements

Water temperature measurements were necessary in order to determine the viscosity of the water. The measurements were taken 3 times throughout each experiment at the same position, next to the tailgates. The following relationship between the kinematic viscosity and water temperature was assumed (Bettess, 1994):

$$\nu = \frac{a}{1 + bT + cT^2} \qquad \textbf{6.9}$$

Where ν is the viscosity in m^2/s, T is the water temperature in $°C$ and a, b and c are constants with the values 0.00000174, 0.03368 and 0.00022099 respectively.

6.2.6 Velocity measurements

6.2.6.1 Depth-averaged velocity

In all of the measuring sections, point velocity measurements were taken at one vertical position, $0.4H$ from the bed in the main channel and $0.4(H\text{-}h)$ on the floodplain(s) using a Novar Nixon miniature propeller meter (MPM) with a diameter of 13mm, **Figure 6.11**. The readings were taken every 25mm from the centreline, due to the diameter of the MPM the closest reading was taken 6.5mm from any boundary.

The velocity was taken over a 10 second interval and repeated 5 times at each location, giving a total integration time of 50 seconds. The MPM measures the frequency in Hertz and therefore a conversion to velocity in m/s was carried out using a linear equation provided by HR Wallingford, Equation 6.10 (Rezeai, 2006).

$$u_r = \frac{\left(0.4987U_{(Hz)} + 4.3289\right)}{100} \quad \textbf{6.10}$$

Where $U_{(Hz)}$ is the frequency in Hertz at a given point and u_r the corresponding velocity in m/s. The Pitot static tube was used to assess the accuracy of this method by independently determining the velocity at certain sections and compared to the results from the MPM.

These were then averaged to obtain the local depth-averaged velocity at any point. These readings were integrated over the area to give the discharge, Q_i. This was compared to the measured discharge, Q_m, through the Dall tube, Venturi meter and the EMF, an acceptable tolerance in the order of ±3% was adhered to. The error was determined using Equation 6.11.

$$\%error = \frac{\left(Q_i - Q_m\right)}{Q_m} \times 100 \quad \textbf{6.11}$$

Each depth-averaged velocity was adjusted over the whole cross-section by the ratio of the integrated discharge and the measured, Equation 6.12.

$$u_i = u_r \times \frac{Q_m}{Q_i} \quad \textbf{6.12}$$

where, u_i is the adjusted point velocity reading.

The mini-propeller should, theoretically only be used for flow depths in excess of 16.25mm to allow sufficient coverage of the MPM. In a four cases the flow depth was less, but all cases the MPM was fully submerged. It was decided that it should still be used in place of alternative techniques. This was decided due to the flow on the floodplains having only a small impact on the overall flow in the channel, only one section was the MPM not fully submerged and at most the 0.4(H-h) reading was only 0.8mm from the theoretical location. It was therefore concluded that it would be used and the data compared to the other sets. In this case the results were not significantly different from the other sections and although the velocity was higher on the floodplain than Atabay (2001) found in his asymmetric experiments, this trend was also found in the Dr=0.3 experiment. It was therefore concluded that the MPM gave an acceptable indication of the flow behaviour in the floodplains. If the flow depth was below 16.25mm over a larger area other techniques should be evaluated, such as surface velocity readings used in conjunction with a 7^{th} power law. In all cases, care was taken and independent checks were made to assess the suitability of using a MPM.

6.2.6.2 Full velocity profiles

In 4 of the cross-sections (x=19m, x=22m, x=25m and x=26m) the velocity distribution though the whole cross-section was evaluated. The velocity readings were taken using the procedure outlined above, but the channel was divided into a grid with the velocity being measured every 25mm laterally and every 10mm vertically, again with boundary measurements being 6.5mm from the wall/bed. The readings were converted to velocity using Equation 6.10, integrated laterally and

vertically by multiplying each point velocity by its corresponding area and summing (see Section 7.4), compared to the measured and the error calculated using Equation 6.11 and adjusted using Equation 6.12.

6.2.7 Boundary shear stress measurements

Boundary shear stress measurements along the boundary (including the walls) were taken using a Preston tube of outer diameter 4.77mm. The Preston tube consists of two isolated pipes; the static and the dynamic tube. The static tube was fixed in the centre of the main channel in the middle of the flow depth and measured the static head of the flow on the manometer (**Figure 6.13**). The dynamic tube was placed within the boundary shear layer facing into the direction of flow in the streamwise direction and measured the dynamic pressure on the manometer. Due to the skewing of flow, the flow was not necessarily parallel to the streamwise direction, however the skew angle was small and will have a small effect (cosine of 3.81° is 0.998). Where measurements were taken close to the floodplain wall or on the wall, the Pitot tube was aligned with the floodplain wall.

Preston presented a non-dimensional relationship between the pressure difference, ΔP, and the boundary shear stress τ_b:

$$\left(\frac{\tau_b d^2}{4\rho\nu^2}\right) = F\left(\frac{\Delta P d^2}{4\rho\nu^2}\right) \qquad \textbf{6.13}$$

Where d is the outer diameter of the Pitot tube, ρ the density of fluid, ν the kinematic viscosity and F is an empirical function,. Bradshaw & Gregory (1961) and Head and Rechenberg (1962) cited reservations about the applicability and accuracy of Preston's method. Following these remarks, Patel (1965) calibrated an alternative technique given in terms of two non-dimensional parameters X^* and Y^*, where:

$$X^* = \log_{10}\left(\frac{\Delta P\, d^2}{4\rho\nu^2}\right) \qquad \textbf{6.14}$$

$$Y^* = \log_{10}\left(\frac{\tau_b\, d^2}{4\rho\nu^2}\right) \qquad \textbf{6.15}$$

$$\Delta P = \rho\, g\, \Delta h \sin\theta \qquad \textbf{6.16}$$

Where Δh the difference in pressure head between the static and dynamic tubes as read on inclined manometers and θ the angle of inclination of the manometers.

Knowing X^*, Y^* is determined using Equations 6.17 to 6.19 depending on the limits and τ_b calculated from Equation 6.16. A comparison between Patel's (1965) method and others is given in **Figure 6.19**. Here it can be seen that Patel divides the experimental data into three distinct regions, unlike Preston (1954) who simply fitted one line.

In the range of $Y^*<1.5$, Patel found that the experimental results lay on a straight line fitted by Equation 6.17.

$$Y^* = 0.037 + 0.5X^* \quad \textbf{6.17}$$

Within the second region, 1.5<Y*<3.5, a cubic function was fitted through the data and predicted the boundary shear stress within ±1½%

$$Y^* = 0.8287 - 0.1318X^* + 0.1437X^{*2} - 0.006X^{*3} \quad \textbf{6.18}$$

In the range of 3.5<Y*<5.3, Equation 6.19 can predict the boundary shear stress data (as used by Patel) to with ±1%

$$X^* = Y^* + 2\log_{10}(1.95Y^* + 4.10) \quad \textbf{6.19}$$

Boundary shear measurements were taken at each section on the same day as the velocity measurements using the same lateral and vertical spacing as the velocity readings (i.e. every 25mm laterally and 10mm vertically). The closest reading to any boundary was at 2.385mm i.e. the radius of the Preston tube.

Before any readings were taken, checks were made to ensure that there was no air trapped in either tube or within the manometers with the tubing being cleaned weekly. The inclined manometers were set at an angle of 14.27°.

Using the inclined manometer, the pressure difference (Δp) between the static and dynamic head could be converted to boundary shear stress using Patel's calibration for smooth boundaries as outlined above.

To check the static and dynamic readings, the static and dynamic pressures were taken using a static water level at each section for a number of depths. The tailgates were initially raised and the flume filled and allowed to settle. The dynamic and static readings were taken (as there is no flow they should be equal), the tailgates were lowered, the water surface allowed to settle and new readings taken; this was repeated a number of times. A plot was subsequently made to ensure that the static readings were the same as they dynamic ones and would serve as a check on the static readings recorded during each experiment. From **Figure 6.20**, it is clear that there is some small differences between the static and dynamic tubes, the differences are generally negligible and are likely to be due to movement in the flow if not enough time lapsed between lowering the water and taking the readings. At the end of each experiment a similar check was carried out, the pumps were switched off and the static and dynamic readings compared to ensure they were equal.

6.3 Concluding remarks

There has been much research carried out on The University of Birmingham's flume examining a number of geometries and configurations. Contributions have been made by Tang (1999), Ayyoubzadeh (1997), Atabay (2001), Rezeai (2006) on asymmetric prismatic channels, converging channels, sediment transport and channels of varying roughness. This programme has now been added too by the work contained within

Chapter 8 on skewed flumes, and no doubt further work is yet to be carried out. Much of this work is available at www.flowdata.bham.ac.uk, and in the future, further data will be included. These experiments make a modest contribution to work on overbank, non-prismatic channels, and add to the skewed channel work discussed in Chapter 5.

Relative Depth, Dr	Section	Water profile	Depth averaged velocity at 0.4H and 0.4(H-h)	Full velocity distribution	Boundary shear stress
0.234	x=19m *	Every 1m from entrance, every 0.5m from x=19m	Y	Y	Y
	x=20.5m		Y	N	Y
	x=22m		Y	Y	Y
	x=23.5m		Y	N	Y
	x=25m #		Y	Y	Y
	x=26m		Y	Y	Y
0.314	x=19m *	Every 1m from entrance, every 0.5m from x=19m	Y	Y	Y
	x=20.5m		Y	N	Y
	x=22m		Y	Y	Y
	x=23.5m		Y	N	Y
	x=25m #		Y	Y	Y
	x=26m		Y	Y	Y
0.414	x=19m *	Every 1m from entrance, every 0.5m from x=19m	Y	Y	Y
	x=20.5m		Y	N	Y
	x=22m		Y	Y	Y
	x=23.5m		Y	N	Y
	x=25m #		Y	Y	Y
	x=26m		Y	Y	Y
0.518	x=19m *	Every 1m from entrance, every 0.5m from x=19m	Y	Y	Y
	x=20.5m		Y	N	Y
	x=22m		Y	Y	Y
	x=23.5m		Y	N	Y
	x=25m #		Y	Y	Y
	x=26m		Y	Y	Y

Symbols: *-start of skew; #-end of skew; Y-data measured; N-no measurements taken

Table 6.1-Matrix of skewed channel experimental programme with a skew angle of 3.81^{o} over 6m

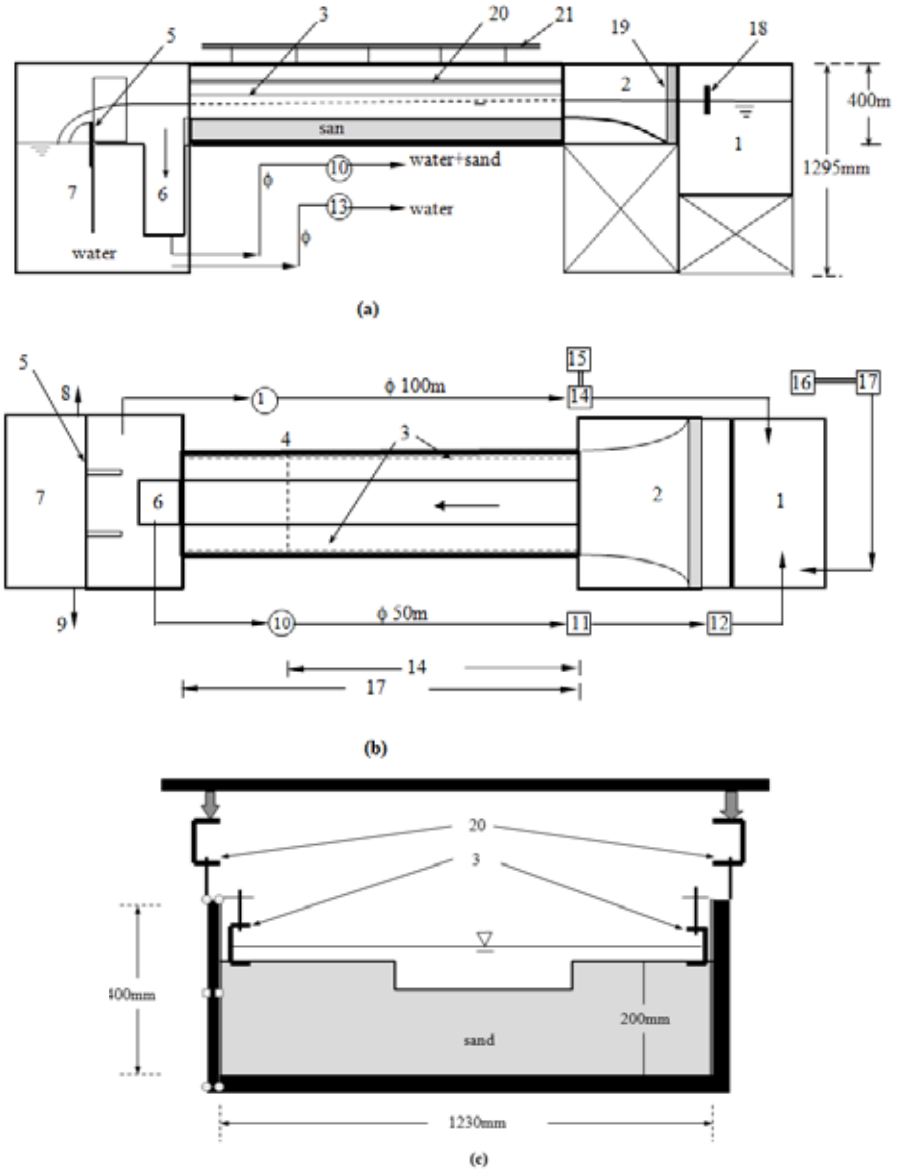

Figure 6.1- Schematic (a) profile, (b) plan and (c) typical cross-section views of the 18m Birmingham University Flume (after Atabay, 2001 and Rezaei, 2006)

Description

(1) Inlet tank
(2) Entrance box
(3) Scraper rails/bed slope control rails
(4) Measuring section
(5) Adjustable tail gate
(6) Sediment trap
(7) Water trap
(8) 150mm f , to volumetric measuring tanks
(9) 50mm f , waste
(10) Pump No. 1
(11) Electro-magnetic flow meter (EMF)
(12) Valve
(13) Pump No. 2
(14) Venturi meter
(15) & (16) Manometer
(17) From main laboratory supply/pump No. 1
(18) Surface turbulent trap
(19) Honeycomb screen
(20) Carriage rails
(21) Carriage

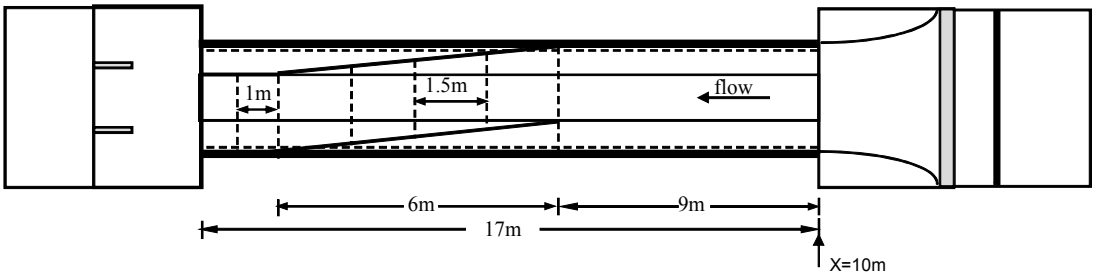

Figure 6.2-Plan view of skewed channel over 6m length

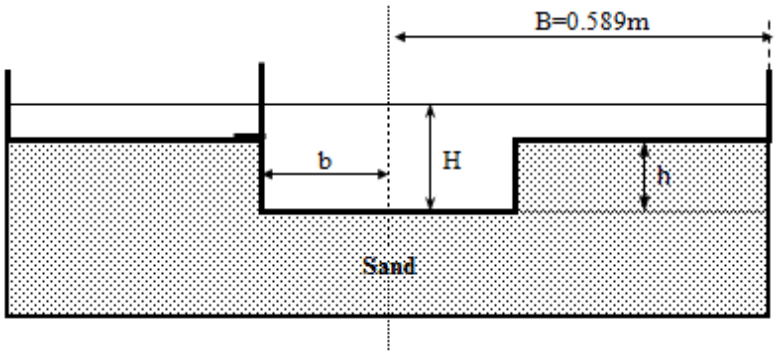

Figure 6.3a-Cross-section view of section 1 (upstream, x=19m)

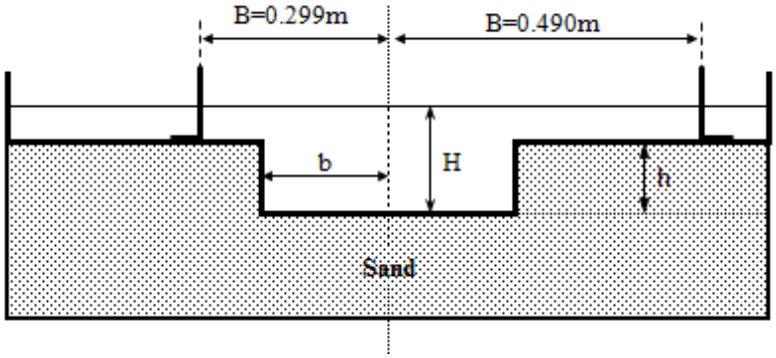

Figure 6.3b-Cross-section view of section 2, x=20.5m

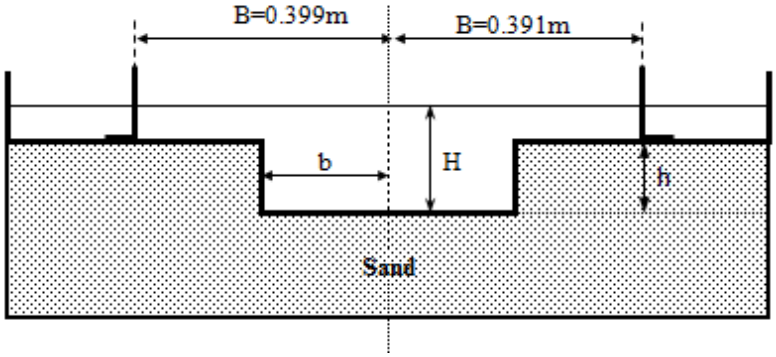

Figure 6.3c-Cross-section view of section 3 (centre of transition, x=22m)

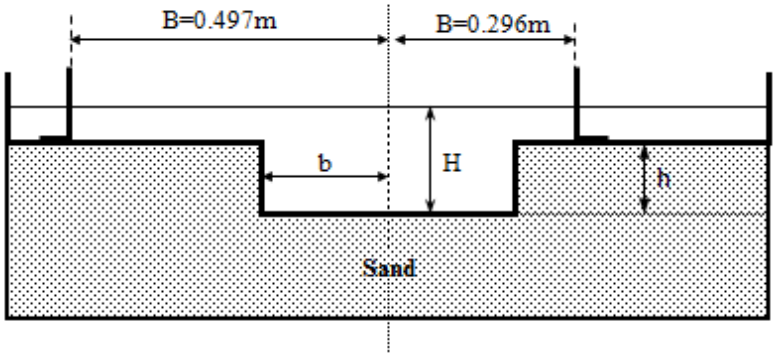

Figure 6.3d-Cross-section view of section 4, x=23.5m

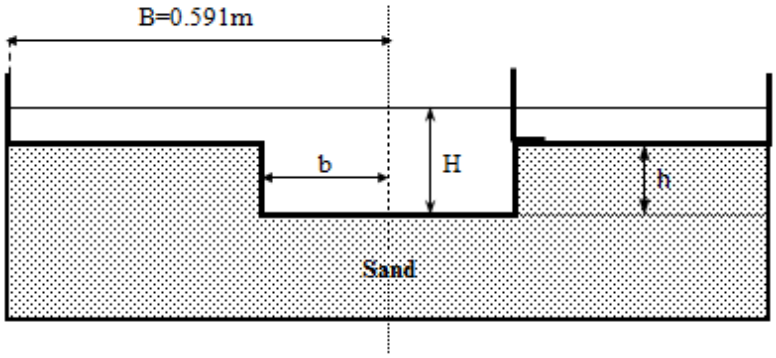

Figure 6.3e-Cross-section view of section 5 (end of transition, x=25m)

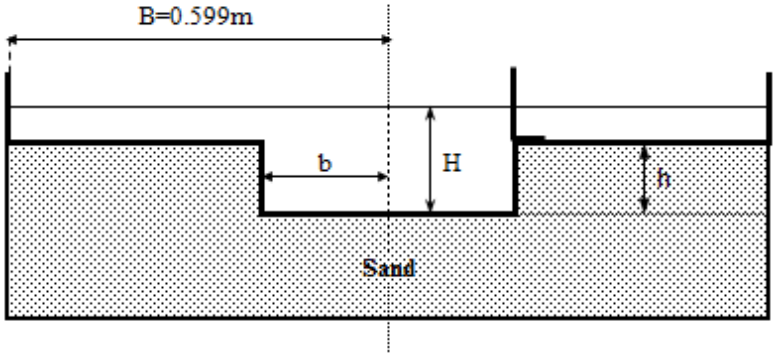

Figure 6.3f-Cross-section view of section 6 (1m from end of transition, x=26m)

Figure 6.4-General view of Birmingham flume with skewed floodplains looking downstream

Figure 6.5-View of the inlet tank and transition zone with honeycomb separation

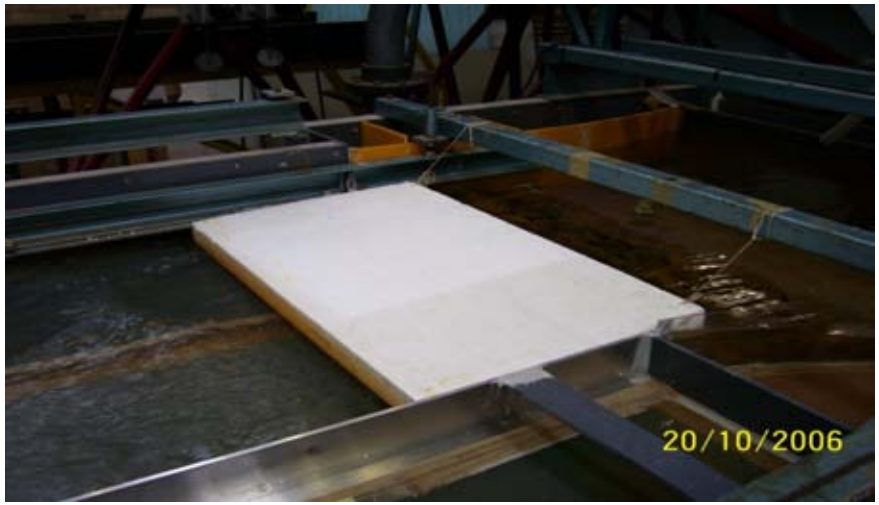

Figure 6.6-View of the polystyrene dampener

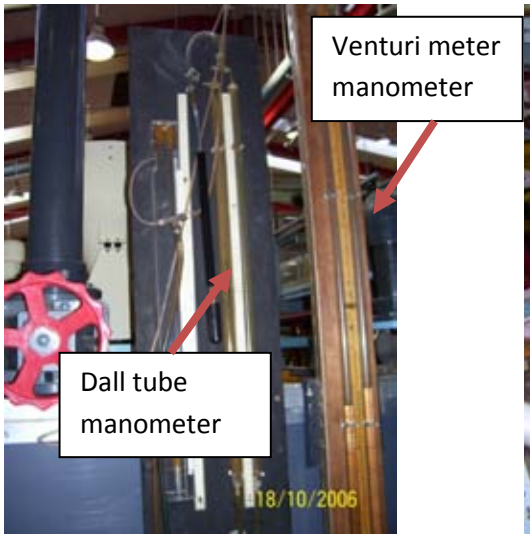

Figure 6.7 a & b-View of the electro-magnetic flow meter, Dall tube and Venturi meter

Figure 6.8-Adjustable tailgates at the downstream end of the flume

Figure 6.9-Instrument carriage with pointer gauge(s)

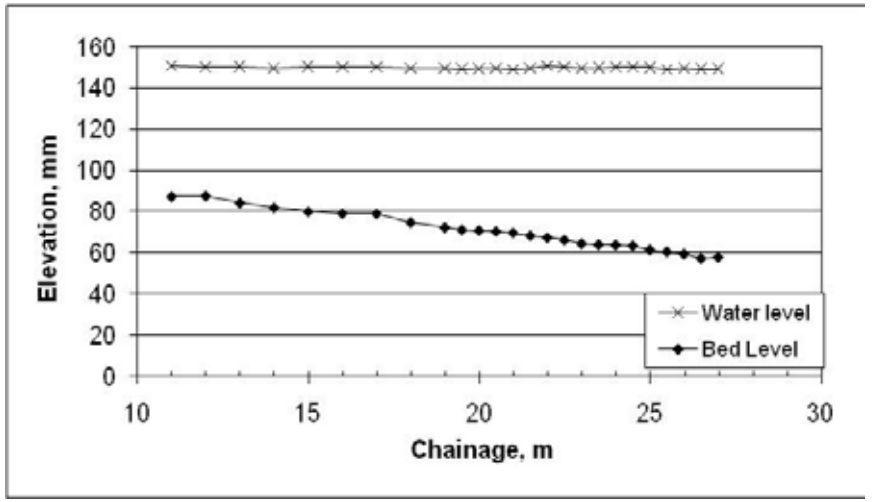

Figure 6.10-Check on levelling of instrument carriage using a static water level

Figure 6.11a & b-Novar Nixon miniature propeller current meter for velocity measurements

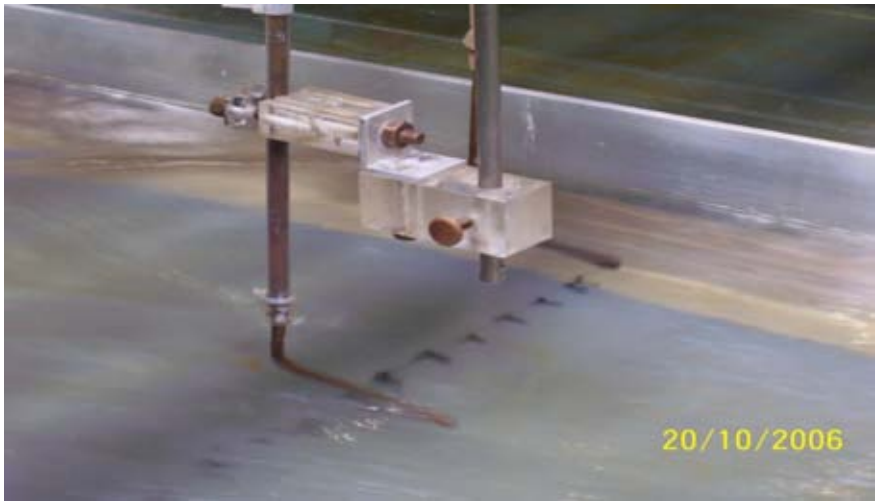

Figure 6.12-Dynamic Preston tube for measuring boundary shear stress

Figure 6.13-Inclined manometers for boundary shear stress measurements

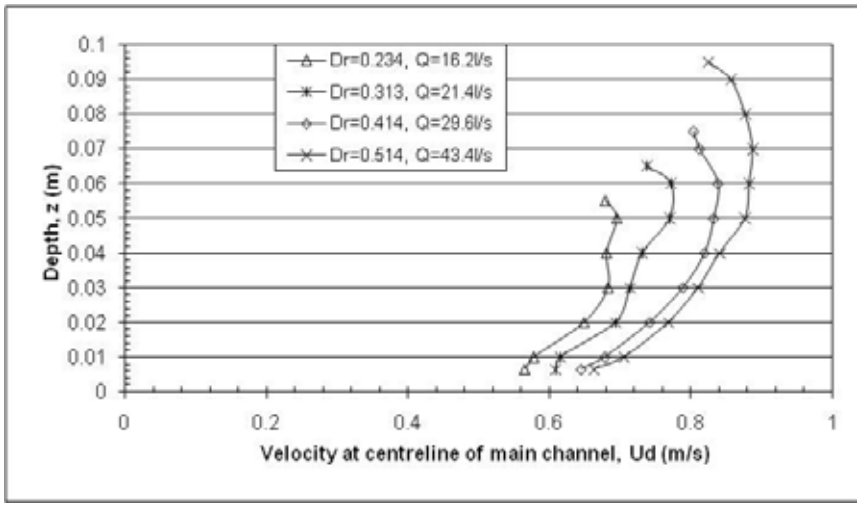

Figure 6.14-Velocity at centre point of main channel, X=19m

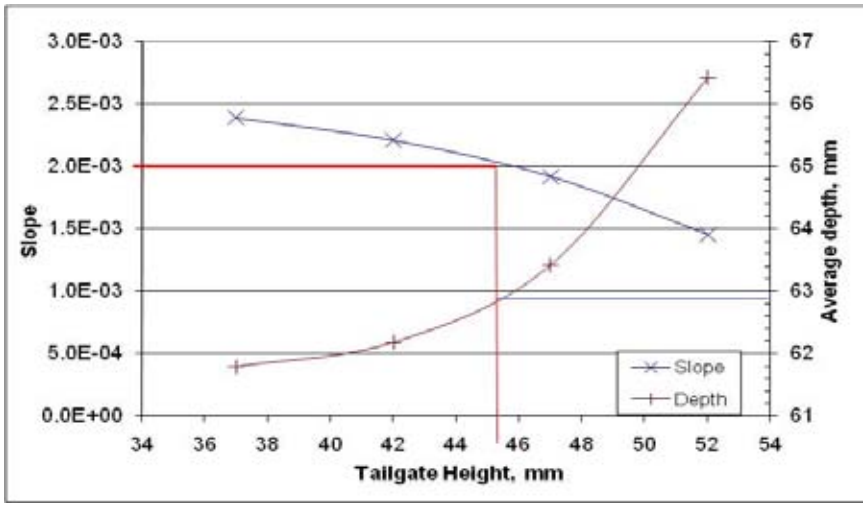

Figure 6.15-Tailgate setting procedure for skewed channel, Q=16.2ℓ/s Dr=0.2

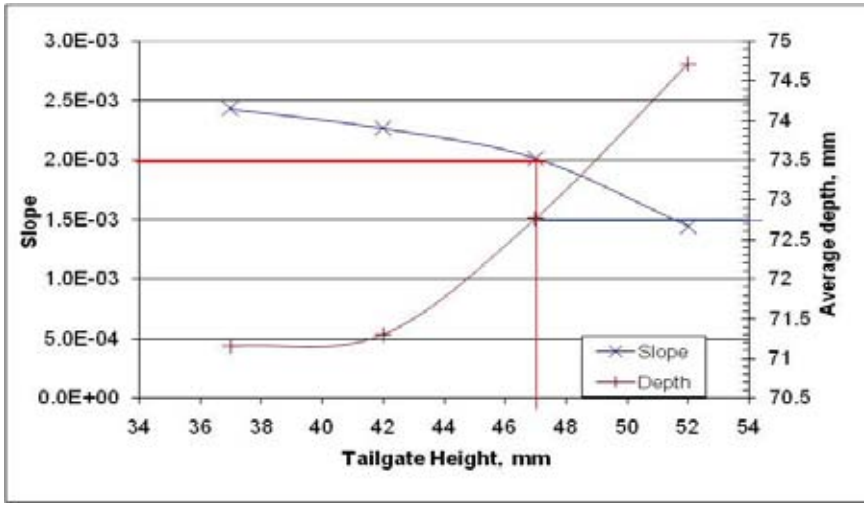

Figure 6.16-Tailgate setting procedure for skewed channel, Q=21.4ℓ/s Dr=0.3

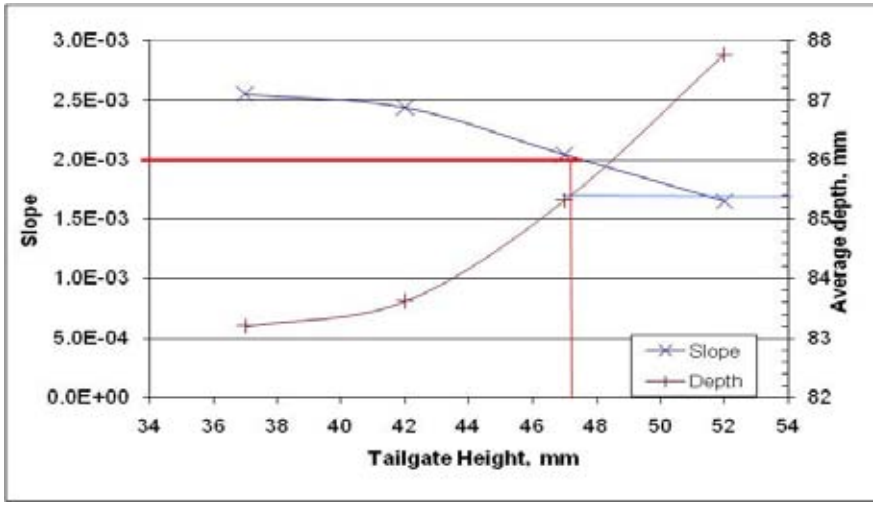

Figure 6.17-Tailgate setting procedure for skewed channel, Q=29.6ℓ/s Dr=0.4

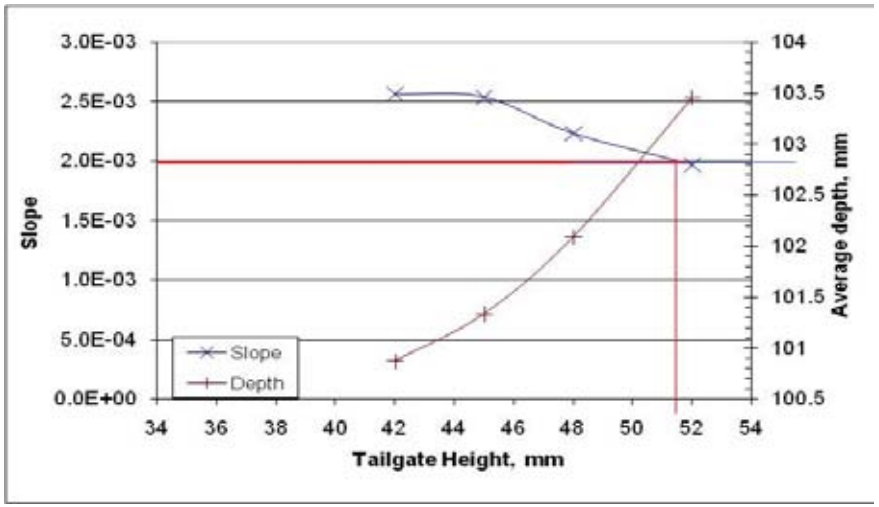

Figure 6.18-Tailgate setting procedure for skewed channel, Q=43.4ℓ/s Dr=0.5

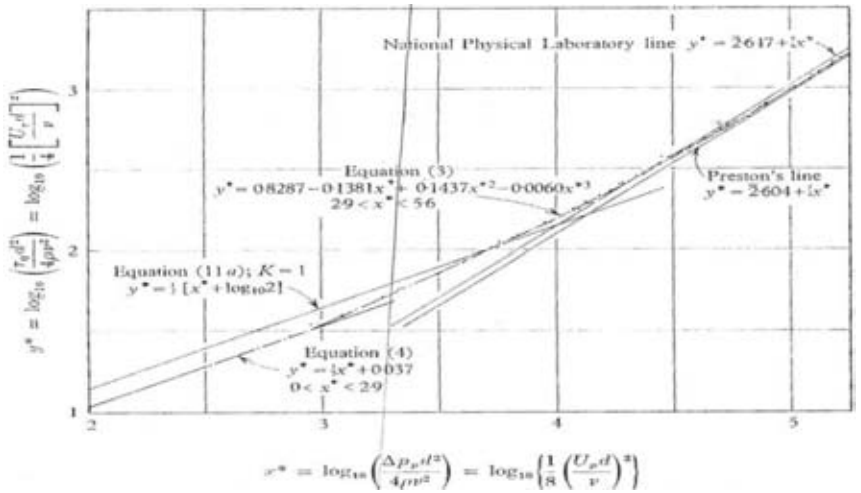

Figure 6.19-Comparison of Preston's (1954) method and others from Patel (1965)

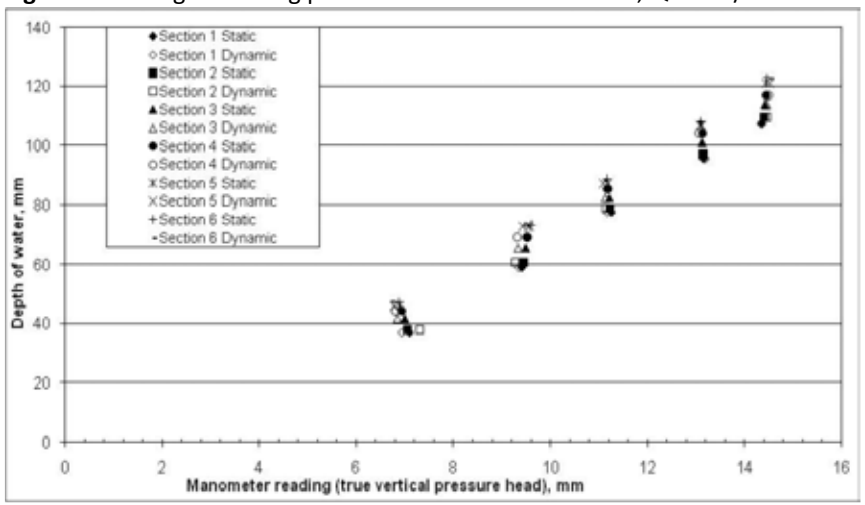

Figure 6.20-Plot of differences between the static and dynamic pressure heads (true vertical depth) against flow depth

CHAPTER 7-REANALYSIS OF EXPERIMENTAL RESULTS FOR FLOOD CHANNEL FACILITY SKEWED CHANNEL

No amount of experimentation can ever prove me right; a single experiment can prove me wrong.

(Albert Einstein, 1879-1955)

7.1 Introduction

The UK Flood Channel Facility (FCF) was originally set up by the Science and Engineering Research Council (SERC), now known as the Engineering and Physical Sciences Research Council (EPSRC), at Hydraulics Research, Wallingford and completed in 1986. The FCF was overseen by a working group of academics and HR Wallingford staff. The main aim of the studies in the FCF was to examine fundamental flow phenomena in rigid boundary straight and skewed channels (Series A), rigid boundary meandering channels (Series B) and loose boundary straight and meandering channels (Series C). This work would allow academics to study the conveyance of river channels, two-stage channels and floodplain behaviour, river flooding issues and sediment transport and morphology (Ervine et al., 2000; Knight et al., 1999). Details on the facility can be found in Knight & Sellin (1987) and the overall experimental programme in Knight & Shiono (1990) and Shiono & Knight (1991), with pictures and data at www.flowdata.bham.ac.uk.

A series of experiments in skewed channels was undertaken by Elliot (1990), Elliott & Sellin (1990) and Sellin (1993a; 1993b), which formed part of the Series A experiments, with the aim of examining the cross-flow which occurs between the main channel and floodplains and to prepare the way for meandering work (Elliott and

Sellin, 1990). A view of the channel can be seen in **Figure 7.1** and the various configurations tested in **Figure 7.2**. The data from Elliott (1990) and Sellin (1993a;1993b) was checked, re-analysed and compared with the Birmingham data from the 18m flume experiments (details contained within Chapter 8).

The flume configurations of the FCF channel (**Figure 7.2**) and the Birmingham channel (**Figures 8.1-8.3**) are in some ways quite different. The Birmingham flume had a long lead in to allow the flow to become fully developed within a compound section before the skewed transition, whereas the FCF channel was generally designed to allow the flow to enter the channel directly at the entrance to a skewed transition. Furthermore, the Birmingham flume had the skewed transition ending before the end of the flume to allow uniform flow to be established there and for additional measurements to be taken downstream of the transition. The FCF flume ended the transition at the end of the flume, and therefore few comparisons could be made between the entry and exit velocity and boundary shear stress measurements.

Initially Elliot's work was digitised onto a CD using Microsoft Excel (which is enclosed at the back of this thesis) to allow for a review of the data (Sections 7.4-7.13) and a re-analysis of the momentum balance as carried out by Elliott (1990) and Elliott and Sellin (1990). Subsequently, a force-momentum analysis was carried out and comparisons made with the Birmingham data (Section 8.11) and the straight FCF data. By comparing the very limited amount of skewed data, similarities were found, understanding increased and a method of analysing this complex flow found.

7.2 Channel configuration

The FCF was 56m long and 10m wide, with a usable length of 45m. The longitudinal bed slope was 1.027×10^{-3}. The entry flow was carefully controlled by an inlet weir and a stilling boom, and downstream water levels controlled by 5 tailgates. See Elliott (1990) for a more detailed description of the channel. The flow was through six re-circulating pumps with a maximum discharge of $1.1 m^3/s$. The main channel water surface slope was the same as the slope of the bed. However, due to the skewing effect the water slope in the floodplain was between 0.3-1.2% less than the bed slope. The University of Bristol carried out complementary experiments whereby the floodplain water slope followed that of the bed (Elliott and Sellin, 1990) but these have not been included in this study due to insufficient data being available.

The main channel ran down the centreline of the flume with a bottom width of 1.5m and a constant depth of 0.15m. A total of 3 skew angles were investigated: 2.1º, 5.1º and 9.2º (see **Figure 7.2**), with relative depths ranging from 0.05 to 0.5. The floodplains were constructed from movable plywood boards with side slopes of 45º, but the main channel side slopes were altered to give s=0, 1 and 2 (1:s; vertical:horizontal).

The discharge was measured using orifice plates in each delivery pipe, flow depth via tapping points along the centreline of the main channel (21 in total), water surface elevation via stilling pots using digital pointer gauges (0.01mm accuracy), flow velocity using 15 miniature current meters (MCMs) in a protective wire casing of 14mm diameter with an integration time of 45 seconds and boundary shear stress with

a Preston tube of diameter 4.02mm with pressure differences being measured using a 5 millibar pressure transducer.

In the FCF experiments, Elliott measured the transverse distributions of streamwise velocity at an upstream and downstream location 10m apart, with no velocity measurements between these locations. However, the longitudinal velocity (i.e. the velocity at the interface between the main channel and floodplain) was measured for the purpose of momentum transfer. **Table 7.1** gives an overview of the experiments with the locations of the velocity and boundary shear stress measurements which correspond to the sections on **Figure 7.2**.

7.3 Overview of experiments

The aforementioned skewed data made up a proportion of the FCF work on prismatic channels, Series A. In total six skewed experiments were conducted, as indicated in **Table 7.1**. Most of the experiments were conducted using smooth main channel and floodplains, but one experiment was carried out using floodplains roughened by wooden dowels. Velocity and boundary shear stresses were both measured, but were, in general, measured at different locations. Transverse distributions of streamwise velocity were only measured generally, at two locations, whereas boundary shear stresses were measured at two or three sections. Laser Doppler Anemometry (LDA) was used for experiment A18 in the main channel only.

For A14, A15, A16 and A18, measurements were carried out at four relative depths (Dr=0.15, 0.25, 0.4 and 0.5), whereas for A17 only 3 relative depths were examined

(Dr=0.15, Dr=0.25 and Dr=0.4). There are no data available on A19 which had roughened floodplains. **Table 7.2** gives an overview of the experimental results. When referring to experiments the series number will be given in conjunction to the main channel side slope, s, the depth of flow, H and the angle of skew, θ.

7.4 Data review

The FCF skewed data has been presented in 2 volumes. Volume 1 (Sellin, 1993a) presents the stage-discharge, general hydraulic data, depth-averaged velocities and discharge and boundary shear stress measurements whereas volume 2 (Sellin, 1993b) details the full velocity measurements in the transverse and longitudinal directions. In addition, small vanes were used to measure the local angle of the principal flow direction.

As a first step, the FCF data was digitised into Microsoft Excel, in order to check that the depth averaging values agreed with the tabulated velocity data (i.e volume 1 data is in keeping with volume 2). One experiment (A16, H=0.1755m, s=0, θ=5.1°) was independently depth averaged in order to check that the digitised velocity data corresponded to the proportional discharge data presented. A simple approach was taken whereby the point velocity corresponded to the area surrounding it, i.e. single point averaging. Each velocity point, u_r was given a corresponding surrounding area, a_i, and discharge, Q_i, calculated using Equation 7.1.

$$Q_i = \sum_{i=1}^{n} u_r a_i \qquad \textbf{7.1}$$

The corresponding area was calculated by assuming that the area over which the velocity was applicable was equidistant from the adjacent readings. If the reading in question was taken at (y_i, z_i), where y is the horizontal, lateral direction and z the vertical, then the area was determined using Equation 7.2.

$$a_i = \left[\left(\frac{y_i + y_{i+1}}{2}\right) - \left(\frac{y_i + y_{i-1}}{2}\right)\right] \times \left[\left(\frac{z_i + z_{i+1}}{2}\right) - \left(\frac{z_i + z_{i-1}}{2}\right)\right] \quad \textbf{7.2}$$

If the reading was taken at the bed, then Equation 7.3 applied:

$$a_i = \left[\left(\frac{y_i + y_{i+1}}{2}\right) - \left(\frac{y_i + y_{i-1}}{2}\right)\right] \times \left[\left(\frac{z_i + z_{i+1}}{2}\right) - (0)\right] \quad \textbf{7.3}$$

And similarly, for example, against the right hand wall the area was found using Equation 7.4.

$$a_i = \left[\left(\frac{y_i + y_{i+1}}{2}\right) - (0)\right] \times \left[\left(\frac{z_i + z_{i+1}}{2}\right) - \left(\frac{z_i + z_{i-1}}{2}\right)\right] \quad \textbf{7.4}$$

These equations can be similarly manipulated to give the corresponding area when a reading was taken near to the water surface and against the left hand wall.

In the completely straight experiments of the FCF Series A work, the Preston tube was used to find the velocity 2mm from any boundary which was included in the

velocity analyses and proportional flow. In the skewed work the Preston tube readings could not be used to compute the velocity 2mm from the bed as the location of shear and velocity measurements did not correspond. Elliott analysed the data in a similar manner to that described above, and using equations similar to Equations 7.1 to 7.4, but extrapolated the velocities to the bed assuming a linear transition over 5mm from the boundary and the velocity at the point closest to the boundary (where the velocity would be equal to zero).

Depth-averaging of the velocity data was undertaken for the same aforementioned series (A16, H=0.1755m, θ=5.1°), using Equation 7.5, and the comparison between Elliot's depth-averaged velocity and this method can be seen in **Figure 7.3**.

$$U_d = \frac{\sum_{1}^{n} u_r h_i}{H} \qquad \textbf{7.5}$$

Where U_d is the depth-averaged velocity, u_r the measured point velocity, h_i the depth associated with the point velocity and H the total depth of flow.

There are some differences between the Elliot's depth-averaging and the more simplistic form undertaken as a check (i.e. no interpolation to 5mm from the boundary), which is also apparent when the discharge is determined using Equation 7.1. The discharge as measured by Elliott was 0.2318m^3/s, the newly determined discharge was slightly less at 0.2297m^3/s, a difference of approximately -0.91% to the measured value. Elliott calculated the discharge through integration of the velocity to

be 0.22937m^3/s, an error of -1.05% to the measured value but only 0.14% to the integrated check value. It is believed that the differences are simply due to slightly different methods of analysis; Elliott extrapolated the velocity to the bed, the current analysis did not. Slight differences are therefore inevitable as Elliott would have used raw not rounded data, and the check was carried out mainly to ensure that the depth-averaging and proportional discharges were correct. It was not aimed at re-computing all the previously determined data. The difference between the two depth-averaging methods was a mere 0.14% and therefore judged to be quite acceptable. Further, it is unlikely that the discharge in the flume could have been measured to such a degree of accuracy and therefore errors between the measured and integrated values are inevitable. In general it has been accepted that errors below ±3% are within tolerable limits for velocity measurements. From here on therefore, Elliot's velocity and discharge data will be used and not re-calculated.

The velocity data presented by Sellin (1993a; 1993b), is 'as-measured' and has not been adjusted to match the measured total orifice discharge. It was also found that the section mean velocity, U, was taken as the orifice discharge divided by the total area. This implies that the energy (α) and momentum (β) correction factors would have to be re-calculated. As Elliott has determined α and β using two different data types; the point velocities, u_r, uses the raw, uncorrected velocity measurements whereas U, the section mean velocity, uses the corrected, true mean, therefore these too were adjusted. These factors are explored in greater detail in Section 7.12.

7.5 Stage-discharge data

The stage-discharge relationship has been determined for the inbank (no skewing) and overbank (skewed) cases separately. For inbank flows there are three stage discharge curves, due to having three different side slopes in the main channel, skew angles are not relevant as it is the floodplains which are skewed. The three plots are shown in **Figure 7.4**. For each experiment a simple polynomial function was fitted, Equations 7.6 to 7.8. All of the expressions had R^2 values of 0.997 or above.

s=0 $H = 0.4144Q^{0.6044}$ R^2=0.9986 **7.6**

s=1 $H = 0.3814Q^{0.5868}$ R^2=0.9992 **7.7**

s=2 $H = 0.3638Q^{0.5888}$ R^2=0.9994 **7.8**

For overbank flows the relationships tended not to vary with skew angle but vary with the main channel side slope, s, as shown in **Figure 7.5**. The depth of flow for a given discharge is seen to be the greatest when s=0 and the lowest when s=2. Equations were therefore fitted for each main channel side slope data as shown in **Figure 7.6** (A16, s=0, θ=5.1° and A17, s=0, θ=2.1°), **Figure 7.7** (A14, s=1, θ=5.1°, A15, s=1, θ=9.2° and A19, s=1, θ=5.1° (roughened floodplains)) and **Figure 7.8** (A18, s=2, θ=5.1°).

Simple exponential expressions for the overbank flow cases are given below. The R^2 values are at least equal to 0.9777.

Main channel side slope, s=0

A17, θ=2.1° $H = 0.2965Q^{0.3896}$ R^2=0.9777 **7.9**

A16, θ=5.1° $H = 0.2905Q^{0.3446}$ R^2=0.9973 **7.10**

Main channel side slope, s=1

A14, θ=5.1° $H = 0.2867Q^{0.3631}$ R^2=0.9966 **7.11**

A15, θ=9.2° $H = 0.2887Q^{0.3660}$ R^2=0.9959 **7.12**

A19, θ=5.1° (roughened floodplains) $H = 0.4806Q^{0.7231}$ R^2=0.9992 **7.13**

Main channel side slope, s=2

A18, θ=5.1° $H = 0.2813Q^{0.3780}$ R^2=0.9985 **7.14**

The differences in flow depth were relatively small (1mm) when compared with the effect of skew for series A14 (s=1, θ=5.1°) & A15 (s=1, θ=9.2°). The effect of skewing was more pronounced when comparing A16 (s=0, θ=5.1°) & A17 (s=0, θ=2.1°) with the differences in flow depth being quite large just above bankfull (approximately ±8mm). However, overall, the average difference was again small, and generally less than 1mm. The major differences were between the side slope angles where the difference between s=0 and s=2 (greatest and lowest flow depth)

was on average 11mm with the difference between s=0 and s=1 being approximately 5mm.

All the skewed channel data was carried out at a width ratio (*B'/b*) of 3.73, different from all of the other FCF work, and so a direct comparison of the skewed and straight prismatic stage-discharge curves is not straightforward. However, Atabay and Knight (2002) developed a stage-discharge relationship (Equation 7.15) based entirely on the floodplain width ratio (*B'/b*), where *B'* is half the total width and *b* the half main channel width, as:

$$H = 0.4039\left(B'/b\right)^{-0.2577} Q^{0.6927(B/b)^{-0.4686}} \qquad \textbf{7.15}$$

This polynomial was based on six full sets of straight, rigid, series A data (1, 2, 3, 6, 8 and 10), details of which are available at www.flowadata.bham.ac.uk. Series A1-8, s=1, Series 10 s=2.

This relationship has been added to the skewed stage-discharge data in **Figure 7.5** and clearly shows a good correlation between the Atabay and Knight model. The best correlation is with series A14 and A15 where s=1, the same side slope as the majority of the data used in the development of the Atabay and Knight model. When s=0 the model underestimates the flow depth, and when s=2 it overestimates it. This is due to the model being largely based on s=1. The model tends to underestimate the stage in all cases at discharges less than 0.55m^3/s (with the exception of A18, s=2, θ=5.1°). Above 0.55m^3/s the agreement between the model and the actual data appears to

depend on the main channel side slope. There appears little correlation between the model and the angle of skew. Hence, the angle of skew has little effect on the stage-discharge relationship when compared to the straight case, but the side slopes do. When s=0 there is a loss in area (9.1%) within the main channel causing slightly elevated flow depths, and when s=2 there is an increase in area of 9% causing a reduction in depth.

7.6 Water surface profile data

Water surface levels did not vary significantly between each section, and therefore the flow was as close to uniform as possible. Although the water surface elevation was measured, no complete data have been presented by Elliot (1990), Elliott and Sellin (1990) or Sellin (1993a; 1993b). Elliott (1990) does present data for Dr=0.25, s=1, (**Figure 7.9**), and compares them with θ=0° (B'/b=4.2), θ =5.1° (B'/b=3.73) and θ =9.2° (B'/b=3.73). The assumption made is that the water depth is constant along the length of the channel (for depths see **Table 7.2**). The standard deviations of depth fluctuations from the best fit line were less than 1mm and the water surface slope was generally within 1% of the bed slope (Elliott, 1990).

7.7 Velocity data

Velocities were measured in two directions using 8 MCMs with an outer diameter of 14mm. The 8 MCMs were mounted on a horizontal rotary carousel and connected to a computer which was capable of sampling all 8 propellers simultaneously over a period of 45 seconds and calibrated regularly (approximately every five months) allowing for measurements to be taken both quickly and accurately. Velocity was

measured across the section perpendicular to the centreline of the main channel also along the boundary of the floodplain and main channel interface, with the propeller orientated in the main direction of flow (**Figure 7.39**). These longitudinal velocities were measured at both the right and left hand interface boundaries. **Table 7.2** gives details of the section mean velocities.

7.7.1 Lateral distribution of transverse velocities

All of the measurements were taken with the axis of the propeller parallel to the centreline of the main channel. The velocity was measured in increments of 5mm horizontally on the main channel and 10mm on the floodplain with readings being taken every 10mm vertically in both regions.

The depth-averaged velocities that Sellin (1993a; 1993b) presented are non-adjusted values, therefore the velocities have been now subsequently altered by a constant, ψ in the present thesis. Adjustment of velocity values is necessary in order that when integrated, Q_i, they sum to the measured, Q_M, (the discharge recorded through the orifice plates). If the velocities are not adjusted to the measured it implies that the flume is gaining or losing flow along the length, a physical impossibility. This is a necessary and important step especially when force-momentum balances are analysed. This constant (ψ) will vary between experiments and also between cross-sections it defined as the ratio between the measured and integrated values of discharge (Equation 7.16).

$$\psi = \frac{Q_M}{Q_i} \qquad \textbf{7.16}$$

The adjusted velocity therefore becomes:

$$u_i = u_r \times \psi \qquad \textbf{7.17}$$

Where u_r is an non-adjusted point velocity.

Tables 7.3a and **7.3b** show the unadjusted zonal mean velocities and **Table 7.3c** and **7.3d** show the ψ factors applied. **Table 7.3e** and **7.3f** give the adjusted mean zonal velocities.

Figures 7.10a-d show the differences between upstream and downstream velocity distributions for series A14(s=1, θ=5.1°). In general the upstream and downstream velocities did not vary significantly between sections, the main exception being A14 (s=1, θ=5.1°, H=0.1760m), shown in **Figure 7.10a**, where the velocity on the left hand floodplain upstream is seen to be significantly greater than that of the downstream cross-section. Other depths are shown in **Figures 7.10b-d**. It is clear from these Figures that as the discharge in the channel increases the velocity profile becomes much more uniform across the section, especially when $Q \geq 0.700 m^3/s$, for example in **Figure 7.10d** where H=0.2977m. When the discharge is above this threshold the difference between the mean and peak velocity for series A14 is only approximately 20%, compared to almost 60% for $Q=0.261 m^3/s$ and 30% for

$Q=0.361m^3/s$. In **Figures 7.10a-d** there is a minor shift to the left in maximum velocity but not enough of a shift to quantify conclusively. Additional velocity measurements when the channel was asymmetrical would have shown the maximum velocity move from near the main channel centreline towards the left floodplain.

Figures 7.11a-e and **Figures 7.12a-d** show the variation of velocity distributions for all series, plotted for each configuration (A14-A18) over the measured depth range (H≈0.176m to H≈0.299m), separating upstream (**Figures 7.11a-e**) from downstream (**Figures 7.12a-d**) results. From these Figures it can also be seen that as the depth increases, so does the velocity and that the peak velocity, is in general, not always at the centreline of the main channel. The maximum velocity usually occurs to the left of the main channel centreline (i.e. in the direction of the skew). **Figures 7.11a-e** and **7.12a-d** also show that as the depth or discharge increases, the velocity in the main channel does not increase by the amount as in the floodplains. As might be expected, the floodplain velocities increase substantially more than those in the main channel. On average (for both upstream and downstream sections), the main channel velocity increases by approximately 0.29m/s between the lowest and highest relative depths, whereas the right hand floodplain increases by approximately 0.56m/s. The upstream left hand floodplain increases by approximately 0.43m/s whereas the downstream increases by 0.64m/s, i.e. double that of the main channel and a third more than the upstream value. This indicates that there is substantial mixing and transfer of flow onto the left, or receiving, floodplain. The increments of increase for the main channel and floodplains are roughly equal between each flow depth.

In all cases the velocity was not measured at the terminal ends of the skew (i.e. with one floodplain in complete isolation) and was always measured part way into the skew. This makes direct comparison with the author's results impossible. It would have been interesting to see the development of the velocity and boundary shear stress distributions along the length of the transition with eventual regression back to the asymmetric case. This would have allowed one to see the mutation of maximum velocity/shear from the centreline of the main channel and its migration back again.

Figures 7.13a-d and **Figures 7.14a-d** give a comparison between data tests at comparable depths (Dr=0.15, 0.25, 0.4 and 0.5). These show that the angle of skew has little effect on the depth-averaged velocity at the upstream or downstream measurement sections. It can be seen that for series A17 (s=0, θ=2.1º) and A16 (s=0, θ=5.1º), the depth-averaged velocity is slightly lower than the other side slopes investigated. The main channel side slope does seem to have a discernible effect on the depth-averaged velocity across the section, albeit a small one. Generally, the velocity is lower for s=0 than when s=1 or s=2 (greatest velocity). This is in keeping with the stage discharge results discussed in Section 7.5, whereby s=2 showed the greatest depth of flow for a given discharge and s=0 the least. The differences in velocity between s=0 and s=2 are in the region of 0.1-0.2m/s, regardless of position in the channel (i.e. floodplain or main channel). This is once again due to the additional cross-sectional area s=1 or s=2 has. That is to say that when s=0 the cross-sectional area is smaller than comparable experiments with s=1 or s=2, resulting in higher flow depths and therefore lower velocities. The reduction of cross-sectional area in the main channel was due to an infill block placed in the main channel to alter the

geometry from a sloping side wall to a vertical side wall. Hence, comparing A16 (s=0, θ=5.1º) and A18 (s=2, θ=5.1º), both of which have a depth, H=0.1755m, the cross-sectional area for A16 is 8.4% less than that of A18. When comparing the section mean velocities (**Table 7.2**) for the above experiments there is a 10% decrease in mean velocity between A18 and A16. Due to the changing cross-sectional areas, the flow depth was kept (relatively) constant and the discharge was altered accordingly.

The adjusted mean velocity in each zone (main channel and left/right floodplains) of the channel is shown in **Tables 7.3e** and **7.3f**. From these Tables it can be seen that the average velocity in the main channel remains relatively constant between upstream and downstream sections, it is believed that any fluctuations are purely down to experimental variance. The velocity in the right hand floodplain reduces slightly (by on average 0.07m/s) between the two measuring sections whereas the left hand floodplain increases slightly (typically in the region of 0.01m/s).

7.7.2 Interface velocities

The interface velocity data could not be adjusted as there is no way of knowing the adjustment factor, ψ. The transverse distributions measured upstream and downstream were corrected by differing ψ values, and there is no way of knowing which factor is appropriate to the interface data. Hence they will remain un-adjusted in the subsequent analysis.

The interface velocity was measured along both the right and left hand interfaces between the main channel and floodplain in order to estimate the momentum transfer taking place in these locations. The measurement section was 10m long with the first and last measurement being taken at 1m downstream of the upstream section and 1m upstream of the downstream section, in other words the interface velocity was measured over 8m of the transition. The interface velocity was not measured for Series A17 (s=0, θ=2.1°). **Table 7.4** details the average interface velocity for every experiment and also the corresponding cross-flow discharges as determined by Elliott (1990).

Depth-averaged interface velocity values were not given in the original FCF skewed channel data volumes, so these were computed in accordance with the method presented in Section 7.4 and Equation 7.5 and are shown in **Figures 7.15a-d** and **Figures 7.16a-h**. It can be seen that the depth-averaged longitudinal velocity on the left hand (receiving) floodplain was always greater than that of the right hand floodplain due to it giving flow. See for example **Figure 7.15a** it is clear that as the depth increases the difference between the velocities along each interface decreases.

Figures 7.15a-d show the variation of these interface velocities along the flume over the 8m measuring section. The data are presented for each configuration and depth for left and right interfaces separately so that the differences are seen. The interface mean velocity values are given in **Table 7.4** along with the corresponding cross-flows. There is a weak correlation between velocity and location along the flume; at the right hand interface, the velocity decreases slightly (0.02-0.03m/s) along the

channel and on the left hand floodplain it increases by a somewhat similar amount. This indicates that as the right floodplain is narrowing more discharge is being forced onto the left floodplain increasing the interface velocity.

Figures 7.16a-h show that the depth-averaged interface velocity varied between experiments for a given depth by between 0.05-0.3m/s. Along the left hand interface, for A15 (s=1, θ=9.2º), the velocity is slightly higher than the 5.1º cases investigated (A14, s=1, A16, s=0 and A17, s=2) by up to 0.3m/s. This is due to the angle of skew being larger, causing the flow to be forced onto the left hand floodplain at a greater velocity than the shallower angles. It was also noted that at low relative depths (0.15 and 0.25, **Figures 7.16 a-d**), that experiment series A14 (s=1, θ=5.1º), was less than A16 (s=0, θ=5.1º), when intuitively it would be expected that A18 (s=2, θ=5.1º), would give the highest values of interfacial velocity, A14 the second highest and A16 the least. This appears to be less evident in the higher relative depths (0.4 and 0.5), and may be associated with the difficulties of taking measurements at lower depths of flow than at higher depths.

When comparing the depth-averaged velocity for upstream and downstream cross-sections (**Figures 7.10a-d**, **7.11a-e** and **7.12a-d**), a similar trend is apparent. The downstream velocity on the left hand floodplain is predominately higher than the upstream velocity at the same location; conversely, on the right hand side the velocity upstream tends to be greater than that of the left hand side. The differences in velocity are typically small and in the order of 0.05m/s.

These interface velocities are examined further in Section 7.8.

Elliott (1990) either directly measured the interfacial velocities by using an LDA or inferred them by using directional vanes and the velocity measurements. **Figures 7.17a-d** show the velocity vector VW (velocity in the y- and z-directions) with corresponding isovels, boundary shear stress and secondary circulations. Elliott (1990) stated that when these secondary flow cells were compared to work carried out by Shiono & Knight (1989) in an equivalent straight channel, a skew angle of 5.1 increased the averaged secondary flow velocity by 4 times at a relative depth of 0.25. In addition, as the depth increases to Dr=0.5, there is little secondary circulation above bankfull level (**Figures 7.17c-d**).

7.8 Distribution of discharge

Using the velocity profiles, it was possible for Elliott (1990) and Sellin (1993a) to calculate the proportion and percentage of flow in the main channel and on the floodplain(s). These proportional discharges presented by Sellin (1993a), and shown in **Table 7.5**, were based on the non-adjusted velocity data so they also had to be adjusted to the mean by a factor ψ (Equation 7.16), using Equation 7.18.

$$Q_z = Q_{z(r)} \times \psi \qquad \textbf{7.18}$$

Where, $Q_{z(r)}$ is the non-adjusted values of proportional flow as determined by Sellin (1993a).

Table 7.6 gives adjusted flow percentages in the main channel and floodplains for both the upstream and downstream locations. **Table 7.7a** gives the adjusted proportions (Q_z) on the main channel and floodplains for each experiment at both upstream and downstream locations, the percentage of flow in each zone remaining unchanged. In general it can be seen that the proportion of flow in the main channel for each experiment varies little between downstream and upstream locations, indicating that the proportion of discharge flowing into the main channel from the right hand floodplain simply spills onto the left hand floodplain. **Figures 7.18** to **7.22** show graphically the distribution of discharge in each zone. It is clear that as the depth of flow increases the proportion of flow in the floodplain increases. The proportion of flow in the main channel tends to reduce by approximately 30%-40% between the lowest and highest flow, and contains a similar proportion of regardless of skew angle. Initially at H≈0.1760m (lowest depth) the main channel carries between 83% and 90% of the flow, whereas at H≈0.2990m (highest depth) this decreases to between 45-56%. As the depth increases, the proportion of flow on both floodplains increases, similarly the proportion of flow carried by the floodplains was dependent on the skew of the channel, A15 (s=1, θ=9.2°) the proportion of flow on the left hand floodplain at the upstream location was significantly less than that of A14 (s=1, θ=5.1°), A16 (s=0, θ=5.1°) or A18 (s=2, θ=5.1°), and the proportion carried by the right hand floodplain when θ=9.2° is significantly more than the 5.1° skewed channel (up to 45% more).

As the flow moved downstream, the proportion of flow carried by the left floodplain increases significantly, particularly with the three higher discharges (Q≥0.32m^3/s),

where the percentage of discharge doubled, and in the case of A15 (s=0, θ=9.2°) tripled. The converse was apparent in the right hand floodplain where the flow generally halved between the upstream and downstream cross-sections.

Using this information it is possible to determine simple formulae to describe the flow distributions in the main channel and floodplains. **Figures 7.23** to **7.25** show the variation of discharge from the upstream to the downstream end for the floodplains and main channel as well as the percentage of cross-sectional area in each zone. As there were only 2 measuring positions, linear expressions were used. There are no distributions for Series A17, (s=0, θ=2.1°) as there was only one measuring section. **Figures 7.23a-d** show the longitudinal distributions of discharge for the left floodplain, **Figures 7.24a-d** show the proportions of discharge in the main channel and **Figures 7.25a-d** show the distributions in the right floodplain.

Series A14 valid for 23.2≤x≤33.2

H=0.1760m

$$\%Q_{LFP} = -0.0015x + 0.1386 \quad \textbf{7.19}$$

$$\%Q_{MC} = 0.0045x + 0.7251 \quad \textbf{7.20}$$

$$\%Q_{RFP} = -0.003x + 0.1362 \quad \textbf{7.21}$$

H=0.1981m

$$\%Q_{LFP} = 0.0066x - 0.0258 \quad \textbf{7.22}$$

$$\%Q_{MC} = -0.0006x + 0.7548 \quad \textbf{7.23}$$

$$\%Q_{RFP} = -0.006x + 0.271 \quad \textbf{7.24}$$

H=0.2532m

$$\%Q_{LFP} = 0.0112x - 0.0573 \quad \textbf{7.25}$$

$$\%Q_{MC} = -0.0004x + 0.581 \quad \textbf{7.26}$$

$$\%Q_{RFP} = -0.0108x + 0.4762 \quad \textbf{7.27}$$

H=0.2977m

$$\%Q_{LFP} = 0.0141x - 0.1081 \quad \textbf{7.28}$$

$$\%Q_{MC} = -0.0018x + 0.5627 \quad \textbf{7.29}$$

$$\%Q_{RFP} = -0.0123x + 0.5454 \quad \textbf{7.30}$$

where x is the longitudinal distance along the channel, $\%Q_{LFP/MC/RFP}$ is the percentage of the discharge in the left hand floodplain/main channel/right hand floodplain. The expressions all take the general form of Equation 7.31, where $\%Q_z$ is the percentage flow in any zone (main channel or floodplains) and m and c are constants (**Table 7.7b**).

$$\%Q_z = mx + c \quad \textbf{7.31}$$

Obviously since it was a linear variation, the R^2 value in all cases is 1. These equations are only valid over the measuring sections (see **Table 7.7b** for the limits) and no inference can be made of behaviour out with the measuring section.

Figures 7.23a, b and **d** all show data for a skew angle of 5.1° with side slopes, s=1 (A14), s=0 (A16) and s=2 (A18) respectively. From these Figures it can be seen that the gradients of increasing flow are all similar for each depth increment, indicating that the discharge on the floodplain increases by proportionally similar amounts and it is merely the starting proportions of discharges which alter. **Figure 7.23c** shows that when the skew angle increases to 9.2° the gradients are much steeper indicating that the flow is coming onto the floodplain at a faster rate, as would be expected as the transition length is much shorter. The patterns are mirrored in **Figures 7.25a-d** which show the distributions of discharge in the right hand floodplain. Here the proportion of flow carried by the floodplain decreases along the channel, with the 9.2° channel decreasing much more quickly than the 5.1° channels. **Figures 7.24a-d** show the main channel distributions of flow, which are relatively uniform along the length and therefore have very shallow gradients. In around half of the experiments the flow slightly decreases, with the remainder increasing. These fluctuations are very small and it is unlikely it is due to any features of the flow.

Figures 7.23-7.25 show a comparison of percentage area to percentage discharge in each zone of the channel. When comparing the percentage of discharge to the percentage of cross-sectional area, there is little commonality especially at low depths. When $Dr \leq 0.25$, the percentage discharge tends to be lower than the corresponding percentage area in the floodplains with the opposite being found in the main channel. As the flow depth increases, there are smaller differences between the percentage discharge and area, for example in **Figures 7.23c**, **7.24c** and **7.25c** (A16, s=0, θ=5.1°) when H=0.1755m the percentage area is approximately 5% greater than the

percentage discharge in the left floodplain, 15% lower than %Q in the main channel and approximately 7% greater in the right floodplain. When the flow depth increases to 0.2528m, the differences between the discharge and area are much smaller, 0%, -3% and 3% in the left floodplain, main channel and right floodplain respectively. **Figures 7.26a-b** show the percentage of discharge and area for Series A14, θ=5.1°, s=1 for both the upstream and downstream values. From these Figures is it clear that at low depths the percentage of area is less than the corresponding discharge, however, as the depth increases (Dr>0.4) the difference decreases. This is similar to the results by Knight & Demetriou (1983) who concluded that the differences were due to the influence of the floodplains.

7.9 Boundary shear stress data

Boundary shear stresses were measured around the wetted perimeter of each cross-section, set perpendicular to the main channel, using a Preston tube (4.02mm outer diameter) with an internal spacing of between 50mm and 200mm. Closer spacing was used in the main channel corner regions (Elliott, 1990).

Error estimation was carried out using the assumption that the boundary shear stress equal the weight of fluid when resolved in the direction of flow (Equation 7.32), which is consistent with the normal depth assumption outlined previously.

$$\%\tau_{error} = \frac{\tau_r - \rho g R S_o}{\rho g R S_o} \qquad \textbf{7.32}$$

where, τ_r is the unadjusted (measured) values of boundary shear stress.

In a skewed channel this assumption is incorrect in some cases where the water depths may be non-uniform or the skew angle greater than those angles considered here. However, in the case of the FCF skewed work, the change in momentum between the upstream and downstream transverse velocity measurement sections differed by only 1% in all cases except one (A14, s=1, θ=5.1°). A correction factor (the percentage difference between the experimental and theoretical total shear stress) was applied to the measured shear stress results. The errors ranges between ±5% with the exception of the work involving a main channel side slope of zero, where the errors were in the region of –8 % to –14%. Elliott believed this to be due to an incorrect calibration constant applied to the pressure transducer voltages.

Tables 7.2, 7.8 and **7.9** detail the mean boundary shear stress and force, the boundary shear stress and the boundary shear force in each zone respectively. **Figures 7.27a-k** show the transverse distributions of boundary shear stress at upstream, downstream and intermediate sections wherever measured. In general, as the flow depth increases, there tends to be less difference between the bed shear stress in the main channel and the floodplains, as is also seen in equivalent straight compound channel data. As with velocity, the shear stress profiles show that the shear stresses in the right floodplain are less than those in the main channel, and tend to decrease in the downstream direction. The shear stresses in the main channel fluctuate slightly between upstream and downstream cross-sections but no trend is apparent.

It is clear that on the receiving floodplain (left side) there is a peak in the boundary shear stress at the interface between the main channel and floodplain of up to 250% of the mean boundary shear stress in the channel, see for example **Figure 7.27c** (A15, s=1, θ=9.2°) at y=-0.9m. This is similar to Elliott's interpretation of the experimental results. **Figures 7.28a-c** show a comparison of Elliott's original data to straight channel data also taken at the FCF. From these Figures it is clear that there is a peak on the left floodplain and the boundary shear stress for the skewed channels on the right floodplain is less than the straight flume comparison. This is due to the transfer of flow from the main channel onto the floodplain. The interface position is obviously dependent on the slope of the main channel walls. The peak was approximately at the location where the top of the wall meets the floodplain bed. Hence, the peaks are located at y=-0.75m, y=-0.9m and y=-1.05m for s=0, s=1 and s=2 respectively.

The peak values of shear stress tend to increase in the downstream direction, but the profiles are quite similar (i.e. the location of the peak). However, there are no measurements taken with one completely isolated floodplain and all readings are taking mid-skew, unlike the author's measurements. The peak in shear stress is significantly larger than the section mean boundary shear stress, with the most significant increases at Dr=0.15 where the peak shear stress is between two and three times larger than the average. Even at the highest flow depth (H≈0.2990m), the peak shear stress is still up to 50% larger than the section mean.

7.10 Shear force data

The average shear force in the flume was determined by Elliot and is presented here in **Table 7.2**. The average shear forces in each zone are given in **Table 7.9** and are shown plotted against depth in **Figures 7.29a-c** using Elliott's (1990) data. In order to assess the percentage shear force on each boundary element, the shear forces per unit length were calculated using Elliott's boundary shear stress measurements assuming:

$$SF_i = \tau_i \times b_i \times 1 \qquad \textbf{7.33}$$

where SF_i is the shear force acting at a point per unit length (N), τ_i is the shear stress at the point (N/m^2) and b_i is the corresponding length of wetted perimeter (m).

In the case of Series A14, the boundary shear stress was measured at the same location as the velocity measurements, but in the other series no shear data coincided with the location of the velocity data.

When integrating the calculated zonal shear forces acting on the main channel and floodplain(s) there is some discrepancy (approximately 6% on average) between the values calculated herein and those calculated by Elliott (1990). Elliot only presents the zonal shear forces for the main channel and floodplains and does not break it into the individual components i.e. wall and bed values. It is thought that Elliott (1990) simply took the average shear stress on, for example, the main channel boundary and multiplied it by the appropriate wetted perimeter. When this re-analysis was carried

out, each individual point was given an associated length which was then subsequently summed (as outlined above in Equation 7.32), and this possibly accounts for some of the differences. It is assumed that any discrepancy is spread over the whole length of the channel and as hereon only the percentage contributions are being investigated, it has a negligible effect.

Tables 7.10a-c and 7.11a-c give the results from these calculations, in terms of the shear forces and percentage shear forces acting on the walls and bed for the main channel and floodplains for each series **Figures 7.30a-e** show plots of the percentage shear force on any element against the relative depth using Equation 7.33.

In general, regardless of where the measurements were taken (i.e. upstream, intermediate or downstream locations), the shear forces within any zone increase with depth. As the flow in the channel is uniform with little depth changes between sections the shear forces vary little between sections in the main channel. On average the shear force in this location increases by only 0.1-0.4N. More significant changes are apparent in the floodplains where the shear force acting on the left hand floodplain increases by up to 1.0N from the upstream section, whereas on the right hand floodplain it decreases by a similar amount. This effect supports the view that with this channel configuration, an equal amount of flow from the right hand floodplain enters the left hand one and therefore it is to be expected that if the shear force drops by 1.0N on the right hand side that there should be a similar increase on the left hand side.

7.11 Resistance data

The Darcy-Weisbach friction factor, *f*, and Manning's roughness coefficient, *n*, were determined for the main channel and floodplains for each experiment using Equations 7.34 and 7.35.

$$n = \frac{R_i^{2/3}\sqrt{S_o}}{U_i} \quad \textbf{7.34}$$

$$f = \frac{8\,g\,R_i\,S_o}{U_i^2} \quad \textbf{7.35}$$

$$R = \frac{A_i}{P_i} \quad \textbf{7.36}$$

Where R_i is the appropriate hydraulic radius , A_i the appropriate cross-sectional area , P_i the appropriate wetted perimeter; where appropriate indicates the area/perimeter/hydraulic radius excluding interfacial division lines, S_o the bed slope, U_i the appropriate mean velocity and g the gravitational acceleration. Three types of resistance coefficient, global, zonal and local (Knight, 2006) were calculated as follows:

7.11.1 Global resistance

The global resistance was calculated using Equations 7.34 and 7.35 for Manning's *n* and Darcy-Weisbach friction factor, *f*. The global resistance of the channel will not alter between upstream and downstream locations if it is assumed that the depths do not change along the channel, i.e. uniform flow conditions apply. In this case the mean velocity between sections is constant and all other parameters do not change

between sections. The results of this can be seen in **Table 7.12**. The mean value of Manning n and Darcy-Weisbach f, are 0.0093 and 0.0142 respectively. These compare with values of 0.0082 and 0.0122 in the equivalent straight channel Phase A cases.

Figures 7.31 and **7.32** show the global Manning n and Darcy-Weisbach f values plotted against depth for all experiments. Generally, as the depth increases the friction factors also increases, but in the deepest flow (Dr=0.5, H≈0.299m) the friction factor begins to reduce. This may be due to less mixing of flow occurring as a result of the skewing. Elliott (1990) compared the skewed channel results to the straight cases from the FCF on a Moody type diagram (**Figure 7.33**). From this it can be seen that the skewed channel is much rougher than the straight equivalent channel and then tends towards the overbank trapezoidal case at high Reynolds numbers.

7.11.2 Zonal resistance

Zonal resistance values have been calculated using Equations 7.34 and 7.35. When computing the wetted perimeter the interfaces of the main channel and floodplains have been excluded, as is normal practice. Hence in the main channel, the wetted perimeter is equal to the sum of the width and walls only. Similarly, for the floodplain the wetted perimeter is the sum of the floodplain bed width and the wall height. The area is the actual cross-sectional area, so in the case of the main channel the area is the product of the main channel bed width and the depth of flow (with s=0).

The zonal (left floodplain, main channel and right floodplain) values of friction factor, *f*, and Manning's coefficient, *n*, are given in **Tables 7.13a** and **7.13b**. **Figures 7.34a-c** and **Figures 7.35a-c** show Manning *n* against depth for the upstream and downstream locations respectively, similarly **Figures 7.36a-c** and **7.37a-c** show Darcy-Weisbach *f* against depth for upstream and downstream locations.

The main channel resistance coefficient remains relatively constant, whereas the resistance coefficient on the right floodplain increases between the upstream and downstream values by approximately 0.004 in Manning *n*. This phenomenon is due to the discharge being forced off the floodplain as it narrows which is causing increased mixing. The left floodplain generally becomes less rough downstream due to the transfer of momentum into it.

7.11.3 Local resistance

Local resistance has been calculated for two of the five series, namely series A14 and A15. These data were the only two sets which had boundary shear stress and depth-averaged velocity measurements at the same longitudinal sections. The local resistance was calculated using Equation 7.37.

$$f = \frac{8\tau_b}{\rho u^2} \qquad \textbf{7.37}$$

From these data (contained within **Figures 7.38a-d**), it is clear that the channel becomes much rougher at the downstream location. This is especially true of the left

hand floodplain, but an increase of roughness parameter is also observed in the main channel.

7.12 Energy and momentum correction coefficients

The Coriolis (or kinetic energy) and Boussinesq (momentum) coefficients, α and β, are important factors, especially with regards to the force momentum balance and in determining the energy slope. Due to the non-uniformity of velocity distribution, the velocity head of an open channel flow is generally greater than the value computed by $U^2/2g$, (where the mean velocity U=Q/A). Hence, the true energy head is expressed by $\alpha U^2/2g$, where α is the energy correction coefficient. Similarly, the non-uniform distribution of velocity also affects the momentum of open channel flow and must be corrected by a factor, β.

$$\alpha = \sum \frac{u_i^3 a_i}{U^3 A} \qquad \textbf{7.38}$$

$$\beta = \sum \frac{u_i^2 a_i}{U^2 A} \qquad \textbf{7.39}$$

Where u_i is a point velocity, a_i the corresponding area, U the mean velocity and A the total cross-section area.

Elliot (1990) determined these coefficients using Equations 7.38 and 7.39, but used a mixture of both non-adjusted and adjusted velocity data. When correcting the proportional discharges and velocities, these were adjusted by a factor, ψ (Equation

7.16), and therefore this factor was also used when determining α and β. In Elliot's work, the u_i component of Equations 7.38 and 7.39 is the unadjusted velocity data whereas U is the true mean velocity, Q_m/A, where Q_m is the measured discharge through the orifice meters.

In order to adjust the raw α values (α_r) the following corrections were applied.

$$\alpha = \sum \frac{(u_r \Psi)^3 a_i}{U^3 A} \qquad \textbf{7.40}$$

Hence,

$$\alpha = \psi^3 \alpha_r \qquad \textbf{7.41}$$

The β_r was adjusted to give the true β value in a similar manner.

$$\beta = \psi^2 \beta_r \qquad \textbf{7.42}$$

Clearly, as ψ is now a power function, the resulting changes may be large, especially in compound channel cases. **Table 7.2** give the adjusted, global values of α and β. **Tables 7.3a-b** give the unadjusted values of α and β, **Tables 7.3c-d** give the correction factors, ψ, applied and **Tables 7.3e-f** give the adjusted values for α and β.

7.13 Force-momentum balance and apparent shear forces

A force-momentum balance was carried on the FCF data, for the whole channel and also for each zone, i.e. the main channel and floodplains and compared to the results given by Elliott and Sellin (1990). This was carried out for only four of the five skewed series as series A17 had only one measuring section and so no force-momentum balance was possible. The control volume used is the volume between the two velocity measuring sections, located 10m apart. **Figure 7.39** shows a perspective view of the FCF flume, taken from Elliot (1990), and shows the directions of the forces involved within the control volume. By dividing the channels into a number of sections, the apparent shear forces acting at the interfaces of the main channel and floodplains can be approximated.

Elliott and Sellin (1990) state that:

$$W - SF_b - SF_w + ASF = (Mom)_2 - (Mom)_1 - (Mom)_{cf} \qquad \textbf{7.43}$$

where W is the weight component of the fluid element in the streamwise bed slope direction, SF is the shear force on the bed (subscript b) or wall (subscript w), ASF the vertical apparent shear force, (Mom) is the momentum with subscripts 1, 2 and cf indicate the momentum at section 1 (upstream), section 2 (downstream) and across any boundary in the lateral direction respectively.

Looking at the momentum only portion of Equation 7.43, Elliott (1990), states that the total momentum in the x-direction, M_x, (streamwise) is equal to:

$$M_x = \rho \left(\int_{u/s} u_i^2 a_i \, dz.dy - \int_{d/s} u_i^2 a_i \, dz.dy - \int_{l} u_i \, \mathrm{v}_i a_i \, dx.dz \right) \quad \textbf{7.44}$$

where u_i and v_i are point velocities, a_i the corresponding surrounding area and *u/s*, *d/s* and *l* are the upstream, downstream sections and cross-flow interface respectively.

This method therefore does not require β correction coefficients as every point measurement is being used. β factors are only required when the mean is being used as this correction factor accounts from variance from the mean due to velocity fluctuations.

In the reanalysis, the section mean values will be used (although the channel will be divided into left & right floodplains and main channel), and therefore (from Tables 7.2 and 7.3), β values will be included in this. The hydrostatic pressure forces have also been neglected since the water depth did not appear to fluctuate much and were assumed equal. Re-writing Equation 7.43 fully and including the hydrostatic pressure forces, gives:

$$F_1 - F_2 - \Sigma SF + W = \rho Q(U_2\beta_2 - U_1\beta_1) + (Mom)_{cf} \quad \textbf{7.45}$$

$$(Mom)_{cf} = \rho \, gLu_{cf}^2 \frac{\sin 2\theta}{2} \quad \textbf{7.46}$$

Where F_1 and F_2 are the hydrostatic forces at section 1 and 2, U is the mean velocity and ΣSF is the total shear force on the walls and bed over the control volume, u_{cf} is the interface velocity and θ is the angle of skew. Equation 7.46 is the generic equation for the whole channel, but can be broken down into the zonal components (i.e. main channel and floodplains), as per Equations 7.47-7.52. When analysing the whole channel, there would be no cross-flow momentum $(Mom)_{cf}$ as there can be no momentum transfer out with the channel. This term appears when the channel is divided into main channel, left floodplain and right floodplain to account for momentum transfer between regions.

Equation 7.45 can be adapted further for the main channel and floodplains control volumes shown in **Figure 7.39**.

For the main channel

$$F_{MC1} - F_{MC2} - \Sigma SF_{MC} + W_{MC} - ASF_{cfR} - ASF_{cfL} - R_{LF} - R_{RF} = \rho\left(Q_{MC2}U_{MC2}\beta_{MC2} - Q_{MC1}U_{MC1}\beta_{MC1} + q_{cfL}U_{cfL} - q_{cfR}U_{cfR}\right) \quad \textbf{7.47}$$

But for uniform flow $F_{MC1} - F_{MC2} = 0$ **7.48**

For the left hand floodplain

$$F_{L1} - F_{L2} - \Sigma SF_L + W_L + R_{LF} + ASF_{cfL} = \rho\left(Q_{L2}U_{L2}\beta_{L2} - Q_{L1}U_{L1}\beta_{L1} - q_{cfL}U_{cfL}\right) \quad \textbf{7.49}$$

But for uniform flow $F_{L1} - F_{L2} + R_{LF} = 0$ **7.50**

And for the right floodplain

$$F_{R1} - F_{R2} - \Sigma SF_R + W_R + R_{RF} + ASF_{cfR} = \rho\left(Q_{R2}U_{R2}\beta_{R2} - Q_{R1}U_{R1}\beta_{R1} - q_{cfR}U_{cfR}\right) \quad \textbf{7.51}$$

But for uniform flow $F_{R1} - F_{R2} + R_{RF} = 0$ **7.52**

Where R_F is the hydrostatic wall reaction in the x-direction, ASF_{cf} and ASF_{cf} are the vertical apparent shear forces on the left and right hand floodplain/main channel interfaces, q_{cf} is the lateral flow off the right and onto left hand floodplains, and U_{cf} is the interface velocity along the boundary of the floodplain and main channel. Subscripts *MC*, *L* and *R* refer to the main channel, left and right floodplains respectively.

All data required (discharges, velocities, shear stresses and forces) have been pre-determined by Elliott (1990), but the proportional discharges and velocities have now been adjusted to the measured discharge, as described in Sections 7.7 and 7.8. It therefore follows that there will be some variance between the original results by Elliott & Sellin (1990) and this re-analysis. Additional discrepancies will come from Elliott & Sellin ignoring the momentum correction coefficient, β. A number of different approaches, involving different assumptions, will now be tried and the results then compared to the work by Elliott & Sellin (1990).

7.13.1 Direct comparison to Elliott & Sellin (1990)

Elliott & Sellin (1990) presented the results of their calculations for the apparent shear forces acting on a vertical interface between the main channel and floodplains in

graphical and tabulated form, as shown in **Figure 7.40** and **Tables 7.14b** and **7.15b**. These results are based on control volumes for the left and right floodplains only (**Figure 7.39**), and for Series A14 (s=1, θ=5.1°) and A15 (s=1, θ=9.2°). A re-analysis was carried out, for these particular control volumes and series, with a view to checking and reproducing the same results. The same method was then also applied to two more series, A16 (s=0, θ=5.1°) and A18 (s=2, θ=5.1°). In order to facilitate this, the shear force over the control volume was calculated from Elliott's (1990) data and the momentum data based on the un-adjusted velocities from Sellin (1993a). It should also be noted that β values were assumed to be 1.0, in absence of any other information. In addition, an analysis of the main channel and the floodplains separately, and the channel as a whole, were also carried out. A sample calculation is given for **Table 7.14a**, A14 (s=1, θ=5.1°, H=0.1981m) for the left floodplain, with the values in Newtons (N) over a 10m length.

Calculation	Table cross-reference
$\Sigma SF = \frac{SF_{L(U/S)} + SF_{L(D/S)}}{2} \times 10 = \frac{1.5327 + 2.1338}{2} \times 10 = 18.33$	**Table 7.9**
$W = \rho g L S_o A$ $= 1000 \times 9.807 \times 10 \times 1.027 \times 10^{-3} \frac{0.085091 + 0.126217}{2} = 10.64$	**Table 7.2**
$\rho Q_{L2} U_{L2} = 1000 \times 0.06712 \times 0.5318 = 35.69$	**U_2 data Table 7.3b** **Q_2 data Table 7.5**
$\rho Q_{L1} U_{L1} = 1000 \times 0.04473 \times 0.5257 = 23.51$	**U_1 data Table 7.3a** **Q_1 data Table 7.5**

$\rho q_{cfL} U_{cfL} L = 1000 \times \left[\frac{0.06712 - 0.04473}{10} \right] \times 0.698 \times 10 = 15.63$	**U_{cf} data Table 7.4** **Q data Table 7.5**
$ASF_{cfL} = \rho Q_{2L} U_{2L} - \rho Q_{1L} U_{1L} - \rho q_{cfL} U_{cf} L + \Sigma SF - W$ $ASF_{cfL} = 35.69 - 23.51 - 15.63 + 18.33 - 10.64 = 4.24$	

Tables 7.14 to **7.17** and **Figures 7.41a-c** show the force-momentum balances for the FCF skewed data, using the "raw" data (Sellin, 1993a& 1993b) and compared to that published by Elliott & Sellin, 1990. There are a number of discrepancies between the vertical ASF calculated by Elliott & Sellin and the re-calculated values. Firstly, the weight forces terms are similar in both cases, and in the majority so are the shear forces. The differences are therefore likely to be due to the different summation methods, particularly with regards to the momentum. The differences are probably due to the different methods adopted. Elliott and Sellin calculated momentum based on Equation 7.44, where every point velocity was considered. During the re-calculation, Equations 7.45 to 7.51 were used (assuming β=1 as Elliott & Sellin presumed) which is based on the total flow and the average velocity. The variance becomes greater as the depth increases. When the main channel analysis was carried out it was clear that there are out of balance forces. Similarly, when the whole channel was analysed there were, in some cases, very large out of balance forces. This is due to the non-adjusted values of velocity and discharge being used resulting in the discharge upstream being larger or smaller than that downstream. This would indicate the system was losing or gaining flow, which was physically not possible, so must be accounted for by adjusting the velocities.

7.13.2 Comparison to Elliott & Sellin (1990) using adjusted velocities

A second analysis was carried out using the same method as in Section 7.12.1 but using the adjusted velocities and still taking β=1. The adjusted velocity apparent shear forces are detailed in **Tables 7.18** to **7.21** and plotted in **Figures 7.42a-c**. Generally, using the adjusted velocities the apparent shear forces have similar trends to those plotted in **Figure 7.41**, but tend to be larger in magnitude. Again, the main channel had an out of balance force, but in all cases (with the exception of A15, s=1:1, θ=9.2°) this force was less. This was due to using the adjusted velocities as the discharge downstream is now equal to the upstream value and hence no discharge is being "lost" or "gained". When the whole channel analysis was carried out, there was only a little out of balance force, a resultant of using the adjusted values. A sample calculation is given for **Table 7.18a**, A14 (s=1, θ=5.1°, H=0.1981m) for the left floodplain.

Calculation	Table cross-reference
$\Sigma SF = \frac{SF_{L(U/S)} + SF_{L(D/S)}}{2} \times 10 = \frac{1.5327 + 2.1338}{2} \times 10 = 18.33$	**Table 7.9**
$W = \rho g L S_o A$ $= 1000 \times 9.807 \times 10 \times 1.027 \times 10^{-3} \frac{0.085091 + 0.126217}{2} = 10.64$	**Table 7.2**
$\rho Q_{L2} U_{L2} = 1000 \times 0.07001 \times 0.5547 = 38.83$	**U_2 data Table 7.3f** **Q_2 data Table 7.7a**
$\rho Q_{L1} U_{L1} = 1000 \times 0.04612 \times 0.5420 = 25.00$	**U_1 data Table 7.3e** **Q_1 data Table 7.7a**

$\rho q_{cfL} U_{cfL} L = 1000 \times \left[\frac{0.07001 - 0.04612}{10} \right] \times 0.698 \times 10 = 16.67$	**U_{cf} data Table 7.4** **q_{cf} data Table 7.7a**
$ASF_{cfL} = \rho Q_{2L} U_{2L} - \rho Q_{1L} U_{1L} - \rho q_{cfL} U_{cf} L + \Sigma SF - W$ $ASF_{cfL} = 38.83 - 25.00 - 16.67 + 18.33 - 10.64 = 4.85$	

When Elliott & Sellin carried out their study they appeared to neglect the momentum correction coefficients, even although it is important to use them in open channel flow analysis in order to take into account the non-uniformity of the flow. A third and final analysis was therefore carried out using the momentum correction coefficients and adjusted velocities.

7.13.3 Comparison to Elliott & Sellin (1990) using adjusted velocities and β coefficients

Tables 7.22 to **7.25** give the results of the third force-momentum analysis for the main channel, floodplains and for the channel as a whole. Overall it is clear that the momentum coefficients make a marked difference on the force-momentum balance for all zones and for the overall balance too. **Figures 7.43a-c** show the apparent shear force against depth for all of the experiments examined. A sample calculation is given for **Table 7.22a**, A14 (s=1, θ=5.1°, H=0.1981m) for the left floodplain.

Calculation	Table cross-reference
$\Sigma SF = \frac{SF_{L(U/S)} + SF_{L(D/S)}}{2} \times 10 = \frac{1.5327 + 2.1338}{2} \times 10 = 18.33$	**Table 7.9**

$W = \rho g L S_o A$ $= 1000 \times 9.807 \times 10 \times 1.027 \times 10^{-3} \frac{0.085091 + 0.126217}{2} = 10.64$	**Table 7.2**
$\rho \beta_{2L} Q_{L2} U_{L2} = 1000 \times 1.1489 \times 0.07001 \times 0.5547 = 44.61$	**β_2 & U_2 data Table 7.3f** **Q_2 data Table 7.7a**
$\rho \beta_{1L} Q_{L1} U_{L1} = 1000 \times 1.1374 \times 0.04612 \times 0.5420 = 28.43$	**β_1 & U_1 data Table 7.3e** **Q_1 data Table 7.7a**
$\rho q_{cfL} U_{cfL} L = 1000 \times \left[\frac{0.07001 - 0.04612}{10} \right] \times 0.698 \times 10 = 16.67$	**U_{cf} data Table 7.4** **q_{cf} data Table 7.7a**
$ASF_{cfL} = \rho Q_{2L} U_{2L} - \rho Q_{1L} U_{1L} - \rho q_{cfL} U_{cf} L + \Sigma SF - W$ $ASF_{cfL} = 44.61 - 28.43 - 16.67 + 18.33 - 10.64 = 7.20$	

Generally the whole channel, regardless of experiment, has a discrepancy of approximately ±20N, but Series A14, s=1, θ=5.1°, has much larger "error" of up to ±180N, this is accounted for by the much lower β value downstream, indicating the importance of including them in this balance.

Three approaches to calculating the force-momentum balance have been presented, none of which are able to replicate entirely satisfactory all of Elliott & Sellin's (1990) results. Using Sellin's (1993a) data, **Tables 7.26a-e**, β values were applied to the momentum at sections 1 and 2 and assuming that the hydrostatic forces, shear forces and weight force all sum to zero, it was possible to carry out a check on the whole

channel momentum balance. From these results and comparing with **Tables 7.22-7.25** it is clear that there are processes which are not being taken account of in the momentum balance. Both sets of data indicate imbalances in the channel. These may be caused by the complex mixing processes and could be a result of the measuring devices not fully measuring the boundary shear stress or velocities (such as when they are acting at an angle to the direction of measuring apparatus).

7.14 Concluding remarks

The FCF skewed data make a considerable contribution to the limited data on skewed channels. The flume allowed for large scale experiments to be undertaken, some at low flow depths where the lateral mixing is likely to be most intense, with high discharges and many geometry configurations. A re-analysis of the original data published by Elliott & Sellin (1990) has been carried out and compared to the straight FCF data.

The following observations are made:

- The water levels between upstream and downstream locations were constant resulting in near to uniform flow conditions.
- The velocity data presented herein is adjusted data i.e. the velocity data was adjusted by a factor ψ to give, when integrated, the measured discharge through the orifice plates. This has resulted in discrepancies from the original data (Sellin, 1993a & 1993b). This correction factor has been applied appropriately to velocity, discharge, momentum and α and β values. The

importance of using adjusted data was clearly recognised when the force-momentum balance was carried out.

- The lateral variations in depth-averaged velocities (**Figures 7.10-7.14**) show that there is a peak near the interface of the main channel and the receiving floodplain, and may be as large as 100-160% of the mean channel velocity. In addition the maximum velocity is biased toward the left (receiving) floodplain. Both of these phenomena are more pronounced at the lower flow depths ($Dr \leq 0.25$). At higher flows ($Dr \geq 0.4$) the velocity profile becomes flatter, an indication that the channel may be behaving more like a prismatic single channel.
- The interface velocity plots shown in **Figures 7.15a-d** and **Figures 7.16a-h** indicate that it is quite constant along the length of the channel. At the largest skew angle, (A15, s=1, θ=9.2°), there is a difference of up to 0.3m/s between the left and right floodplain velocities. This is likely due to the discharge being forced onto the receiving floodplain at a higher rate. Unfortunately no interface velocities were taken at the lowest skew angle, θ=2.1°.
- Using the velocity distributions the proportional discharges have been calculated and presented in **Figures 7.18-7.22**. Simple relationships have been determined for the floodplains and main channel for each experiment (with the exception of A17), **Figures 7.23-7.25**. Although only 2 locations were measured and linear expressions fitted, the author's skewed data show similar trends (Section 8.5). **Figures 7.23-7.25** also show a comparison between the percentage of discharge and area in any zone, with **Figures 7.26a-b** showing it on a larger scale. From these it is clear that the percentage discharge in the

main channel is usually greater than the percentage area, however as the depth increases the difference lessens.

- The boundary shear stress results presented in **Figures 7.27a-k** and **Figures 8.28a-c**, indicates that there is a peak in shear stress at the interface of the main channel and the left (receiving) floodplain (up to 250% of the average channel boundary shear stress value). The boundary shear stress on the right hand floodplain remains quite constant. This mirrors the lateral distributions of velocity shown earlier.
- The shear force on each boundary element and the percentage of the total shear force acting on each element have been determined and given in **Tables 7.10** and **7.11** respectively, **Figures 7.29-7.30**. The shear forces acting in the main channel tend not to vary substantially between measuring sections, whereas the left floodplain increases between 0.25N when Dr=0.15 to 1.0N when Dr=0.5, the opposite is true on the right floodplain. When looking at individual elements (**Figures 7.30a-e**), The main changes in total boundary shear force comes from the increase in the shear force carried by the left floodplain bed and the decrease in the right floodplain bed.
- The force-momentum balance was carried out using three methods; (a) unadjusted velocity with β=1, (b) adjusted velocity with β=1 and (c) adjusted velocity and inclusion of β factors. It was found that the inclusion of the momentum correction factors made a marked difference to those presented by Elliott & Sellin (1990) and resulted in large out of balance forces of up to almost 200N. When Elliott & Sellin's data was re-examined with the inclusion of β factors similarly large unaccounted forces were apparent. The

force-momentum balance with adjusted velocities and inclusion of β factors, **Tables 7.22-7.24** are believed to be the most reliable.

- The vertical apparent shear forces acting at the interface of the main channel and floodplains have also been determined and compared to Elliott & Sellin for all three variations as listed above. The results from **Tables 7.22-7.24** are thought to give the best indication of the apparent shear forces. From these Tables and shown graphically in **Figures 7.43a-c**, as the skew angle increases the apparent shear force also decreases from approximately 1.0N to –80N in the case of Series A15, s=1, θ=9.2°.
- The global, zonal and local resistance in the channel was calculated using the Darcy-Wiesbach friction factor, *f*, and the Manning's roughness co-efficient, *n*. These were both in keeping with Elliott's values. Generally the resistance in the main channel was relatively constant whereas the right floodplain increased in roughness between the upstream and downstream sections; the left floodplains roughness decreases between sections.

Although the work at the FCF gave significant insights into the behaviour of skewed channels, there are still knowledge gaps to be filled. The FCF experiments only examined 2 velocity measuring sections with boundary shear stress data not always being taken at the same locations. A more comprehensive series of experiments were therefore devised at The University of Birmingham, aimed at adding to the FCF programme by measuring velocity and boundary shear stress at more regular intervals throughout a skewed floodplain transition. The experimental results and a comparison with the FCF data are given in the following chapter.

Series A No.	Skew angle	Main channel side slope, s	Tapping points locations used for water surface, m	Velocity, u			Boundary shear stress, τ_o			LDA Main channel
	θ			Upstream	Downstream	Interfaces	Section 1	Section 2	Section 3	
14	5.1^o	1	4-20 (inc.)	A-A	E-E	A-E	A-A	E-E	-	-
15	9.2^o	1	9-20 (inc.)	F-F	I-I	F-I	G-G	H-H	-	-
16	5.1^o	0	4-20 (inc.)	A-A	E-E	A-E	B-B	C-C	D-D	-
17	2.1^o	0	4-20 (inc.)	-	J-J	-	-	-	J-J	-
18	5.1^o	2	4-20 (inc.)	A-A	E-E	A-E	B-B	C-C	D-D	E-E
19*	5.1^o	1	4-20 (inc.)	-	-	-	-	-	-	-

* Roughened floodplains using 12 dowels/m^2

Table 7.1-Details of Flood Channel Facility skewed channel experimental parametric study (Elliott, 1990). Use in conjunction with Figure 7.2

Series A No.	s	θ	Depth, H	Relative depth, Dr	Discharge, Q	Mean velocity, U	Mean boundary shear stress, τ	Mean boundary shear force	Energy correction coefficients*, α		Momentum correction coefficients*, β	
		o	*m*		*m^3/s*	*m/s*	*N/m^2*	*N*	*Upstream*	*Downstream*	*Upstream*	*Downstream*
A14 H=0.1760m	1	5.1	0.1760	0.148	0.261	0.662	0.6846	3.969	1.2338	1.4869	1.0815	1.1960
A14 H=0.1981m	1	5.1	0.1981	0.243	0.361	0.695	0.8922	5.229	1.3278	1.3973	1.1431	1.1759
A14 H=0.2532m	1	5.1	0.2532	0.408	0.710	0.849	1.3995	8.419	1.2712	1.1274	1.1365	1.0496
A14 H=0.2977m	1	5.1	0.2977	0.496	1.109	1.012	1.7973	11.039	1.4953	1.1999	1.2624	1.0986
A15 H=0.1756m	1	9.2	0.1756	0.146	0.257	0.656	0.6803	3.943	1.3822	1.4478	1.1500	1.1793
A15 H=0.1978m	1	9.2	0.1978	0.242	0.356	0.688	0.8892	5.210	1.2454	1.2677	1.0907	1.1064
A15 H=0.2534m	1	9.2	0.2534	0.408	0.700	0.834	1.4012	8.430	1.2195	1.2125	1.1051	1.1008
A15 H=0.2990m	1	9.2	0.2990	0.498	1.100	0.997	1.8090	11.117	1.3172	1.3394	1.1667	1.1799
A16 H=0.1755m	0	5.1	0.1755	0.145	0.232	0.629	0.6213	3.711	1.3761	1.3966	1.1411	1.1407
A16 H=0.1984m	0	5.1	0.1984	0.244	0.331	0.663	0.8310	5.017	1.2508	1.2905	1.1007	1.1149
A16 H=0.2528m	0	5.1	0.2528	0.407	0.668	0.824	1.3196	8.169	1.1003	1.1195	1.0409	1.0501
A16 H=0.2968m	0	5.1	0.2968	0.495	1.065	0.996	1.7042	10.762	1.3896	1.2796	1.2119	1.1504
A17 H=0.1746m	0	2.1	0.1746	0.141	0.233	0.641	0.6130	3.659	1.4179	-	1.1522	-
A17 H=0.1981m	0	2.1	0.1981	0.243	0.332	0.669	0.8285	5.001	1.2869	-	1.1044	-
A17 H=0.2540m	0	2.1	0.2540	0.409	0.668	0.817	1.3303	8.240	1.0991	-	1.0360	-
A18 H=0.1755m	2	5.1	0.1755	0.145	0.298	0.699	0.7250	4.164	1.5522	1.5904	1.2491	1.2540
A18 H=0.1980m	2	5.1	0.1980	0.242	0.400	0.734	0.9385	5.449	1.3426	1.3352	1.1524	1.1388
A18 H=0.2513m	2	5.1	0.2513	0.403	0.740	0.873	1.4330	8.535	1.1652	1.1699	1.0776	1.0714
A18 H=0.2920m	2	5.1	0.2920	0.486	1.089	1.004	1.8000	10.930	1.1188	1.1654	1.0542	1.0789

* adjusted

Table 7.2-Summary of FCF skewed experimental data

			Unadjusted velocity			Unadjusted energy correction coefficients, α			Unadjusted momentum correction coefficients, β		
Series A No.	**s**	**θ**	**Left floodplain**	**Main channel**	**Right floodplain**	**Left floodplain**	**Main channel**	**Right floodplain**	**Left floodplain**	**Main channel**	**Right floodplain**
		°	***m/s***	***m/s***	***m/s***						
A14 H=0.1760m	1	5.1	0.5912	0.7389	0.3230	1.4670	1.0830	1.1163	1.1610	1.0288	1.0499
A14 H=0.1981m	1	5.1	0.5257	0.7772	0.4576	1.1742	1.0679	1.1140	1.0699	1.0236	1.0599
A14 H=0.2532m	1	5.1	0.7497	0.9139	0.7336	1.3240	1.0451	1.2139	1.1422	1.0158	1.0960
A14 H=0.2977m	1	5.1	0.8334	1.0371	0.8510	1.3635	1.0380	1.3037	1.1588	1.0133	1.1357
A15 H=0.1756m	1	9.2	0.4859	0.7480	0.3004	1.1665	1.0917	1.1216	1.0618	1.0326	1.0531
A15 H=0.1978m	1	9.2	0.6102	0.7844	0.4671	1.1465	1.0850	1.0530	1.0586	1.0298	1.0211
A15 H=0.2534m	1	9.2	0.7125	0.9127	0.7209	1.5534	1.0420	1.1487	1.2379	1.0146	1.0662
A15 H=0.2990m	1	9.2	0.7900	1.0363	0.8983	1.6248	1.0315	1.1830	1.2674	1.0111	1.0804
A16 H=0.1755m	0	5.1	0.3591	0.7357	0.3200	1.1690	1.0842	1.1052	1.0641	1.0291	1.0453
A16 H=0.1984m	0	5.1	0.5336	0.7572	0.4717	1.1629	1.0683	1.1050	1.0650	1.0235	1.0471
A16 H=0.2528m	0	5.1	0.7884	0.8861	0.7543	1.1577	1.0436	1.1349	1.0689	1.0151	1.0608
A16 H=0.2968m	0	5.1	0.8495	1.0092	0.9094	1.3117	1.0353	1.1560	1.1393	1.0126	1.0708
A17 H=0.1746m	0	2.1	0.3236	0.7609	0.2999	1.1502	1.0923	1.0760	1.0486	1.0315	1.0281
A17 H=0.1981m	0	2.1	0.4810	0.7947	0.4456	1.1001	1.0682	1.0699	1.0366	1.0234	1.0284
A17 H=0.2540m	0	2.1	0.7500	0.9101	0.7179	1.1039	1.0456	1.1018	1.0421	1.0159	1.0439
A18 H=0.1755m	2	5.1	0.3667	0.7734	0.3138	1.2118	1.0904	1.1261	1.0787	1.0323	1.0539
A18 H=0.1980m	2	5.1	0.5405	0.8110	0.4803	1.1906	1.0732	1.1221	1.0761	1.0732	1.0546
A18 H=0.2513m	2	5.1	0.7642	0.9413	0.7440	1.1879	1.0419	1.1499	1.0814	1.0146	1.0680
A18 H=0.2920m	2	5.1	0.9082	1.0714	0.9317	1.1969	1.0314	1.1734	1.0884	1.0111	1.0789

Table 7.3a-Upstream (A14, A16, A18 x=23.2m, A15 x=28.2m, A17 x=32.4m) unadjusted proportional velocities and velocity correction coefficients (Sellin, 1993a)

			Unadjusted velocity			Unadjusted energy correction coefficients, α			Unadjusted momentum correction coefficients, β		
Series A No.	**s**	**θ**	**Left floodplain**	**Main channel**	**Right floodplain**	**Left floodplain**	**Main channel**	**Right floodplain**	**Left floodplain**	**Main channel**	**Right floodplain**
		°	***m/s***	***m/s***	***m/s***						
A14 H=0.1760m	1	5.1	0.3284	0.7537	0.2916	1.2513	1.1027	1.0657	1.0758	1.0359	1.0260
A14 H=0.1981m	1	5.1	0.5318	0.7624	0.4130	1.1661	1.0945	1.2778	1.0561	1.0324	1.1254
A14 H=0.2532m	1	5.1	0.8157	0.9310	0.6532	1.1130	1.0522	1.3441	1.0443	1.0180	1.1533
A14 H=0.2977m	1	5.1	0.9865	1.0657	0.7956	1.1057	1.0445	1.4129	1.0446	1.0156	1.1806
A15 H=0.1756m	1	9.2	0.3993	0.7421	0.2505	1.2800	1.1151	1.3322	1.0944	1.0405	1.1473
A15 H=0.1978m	1	9.2	0.6119	0.7587	0.4202	1.1640	1.1069	1.1698	1.0622	1.0369	1.0762
A15 H=0.2534m	1	9.2	0.8489	0.8771	0.6361	1.1276	1.0545	1.3987	1.0550	1.0186	1.1756
A15 H=0.2990m	1	9.2	0.9542	1.0139	0.7959	1.1418	1.0400	1.4382	1.0625	1.0139	1.1918
A16 H=0.1755m	0	5.1	0.3391	0.7518	0.2766	1.2360	1.0980	1.2369	1.0704	1.0340	1.1060
A16 H=0.1984m	0	5.1	0.5363	0.7578	0.4182	1.1737	1.0851	1.1125	1.0578	1.0291	1.1125
A16 H=0.2528m	0	5.1	0.8167	0.8821	0.6738	1.0938	1.0480	1.2978	1.0375	1.0165	1.1341
A16 H=0.2968m	0	5.1	0.9481	1.0092	0.8358	1.1005	1.0397	1.3368	1.0424	1.0139	1.1513
A17 H=0.1746m	0	2.1	-	-	-	-	-	-	-	-	-
A17 H=0.1981m	0	2.1	-	-	-	-	-	-	-	-	-
A17 H=0.2540m	0	2.1	-	-	-	-	-	-	-	-	-
A18 H=0.1755m	2	5.1	0.2956	0.7946	0.2861	1.3308	1.1036	1.0683	1.1148	1.0368	1.0273
A18 H=0.1980m	2	5.1	0.5349	0.8246	0.4146	1.1409	1.0950	1.3201	1.0491	1.0334	1.1438
A18 H=0.2513m	2	5.1	0.8033	0.9427	0.6523	1.1116	1.0533	1.3812	1.0440	1.0185	1.1705
A18 H=0.2920m	2	5.1	0.9485	1.0663	0.8182	1.1095	1.0475	1.4337	1.0495	1.0177	1.1924

Table 7.3b-Downstream (A14, A16, A18 x=33.2m, A15 x=38.2m) unadjusted proportional velocities and velocity correction coefficients (Sellin, 1993a)

			Velocity correction factor, ψ			Energy correction factor, ψ^3			Momentum correction factor, ψ^2		
Series A No.	**s**	**θ**	**Left floodplain**	**Main channel**	**Right floodplain**	**Left floodplain**	**Main channel**	**Right floodplain**	**Left floodplain**	**Main channel**	**Right floodplain**
		°	*m/s*	*m/s*	*m/s*						
A14 H=0.1760m	1	5.1	0.9962	0.9962	0.9962	0.9887	0.9887	0.9887	0.9925	0.9925	0.9925
A14 H=0.1981m	1	5.1	1.0310	1.0310	1.0310	1.0961	1.0961	1.0961	1.0631	1.0631	1.0631
A14 H=0.2532m	1	5.1	1.0327	1.0327	1.0327	1.1012	1.1012	1.1012	1.0664	1.0664	1.0664
A14 H=0.2977m	1	5.1	1.0802	1.0802	1.0802	1.2606	1.2606	1.2606	1.1669	1.1669	1.1669
A15 H=0.1756m	1	9.2	1.0154	1.0154	1.0154	1.0470	1.0470	1.0470	1.0311	1.0311	1.0311
A15 H=0.1978m	1	9.2	1.0074	1.0074	1.0074	1.0223	1.0223	1.0223	1.0148	1.0148	1.0148
A15 H=0.2534m	1	9.2	1.0203	1.0203	1.0203	1.0620	1.0620	1.0620	1.0409	1.0409	1.0409
A15 H=0.2990m	1	9.2	1.0461	1.0461	1.0461	1.1447	1.1447	1.1447	1.0943	1.0943	1.0943
A16 H=0.1755m	0	5.1	1.0106	1.0106	1.0106	1.0321	1.0321	1.0321	1.0213	1.0213	1.0213
A16 H=0.1984m	0	5.1	1.0141	1.0141	1.0141	1.0430	1.0430	1.0430	1.0285	1.0285	1.0285
A16 H=0.2528m	0	5.1	0.9988	0.9988	0.9988	0.9964	0.9964	0.9964	0.9976	0.9976	0.9976
A16 H=0.2968m	0	5.1	1.0676	1.0676	1.0676	1.2168	1.2168	1.2168	1.1398	1.1398	1.1398
A17 H=0.1746m	0	2.1	1.0077	1.0077	1.0077	1.0231	1.0231	1.0231	1.0154	1.0154	1.0154
A17 H=0.1981m	0	2.1	1.0084	1.0084	1.0084	1.0253	1.0253	1.0253	1.0168	1.0168	1.0168
A17 H=0.2540m	0	2.1	0.9985	0.9985	0.9985	0.9954	0.9954	0.9954	0.9970	0.9970	0.9970
A18 H=0.1755m	2	5.1	1.0623	1.0623	1.0623	1.1989	1.1989	1.1989	1.1285	1.1285	1.1285
A18 H=0.1980m	2	5.1	1.0331	1.0331	1.0331	1.1026	1.1026	1.1026	1.0673	1.0673	1.0673
A18 H=0.2513m	2	5.1	1.0149	1.0149	1.0149	1.0453	1.0453	1.0453	1.0300	1.0300	1.0300
A18 H=0.2920m	2	5.1	1.0039	1.0039	1.0039	1.0117	1.0117	1.0117	1.0078	1.0078	1.0078

Table 7.3c-Upstream (A14, A16, A18 x=23.2m, A15 x=28.2m, A17 x=32.4m) proportional velocities, energy and momentum correction coefficients, ψ

			Velocity correction factor, ψ			Energy correction factor, ψ^3			Momentum correction factor, ψ^2		
Series A No.	**s**	**θ**	**Left floodplain**	**Main channel**	**Right floodplain**	**Left floodplain**	**Main channel**	**Right floodplain**	**Left floodplain**	**Main channel**	**Right floodplain**
		o	*m/s*	*m/s*	*m/s*						
A14 H=0.1760m	1	5.1	1.0297	1.0297	1.0297	1.0918	1.0918	1.0918	1.0603	1.0603	1.0603
A14 H=0.1981m	1	5.1	1.0430	1.0430	1.0430	1.1346	1.1346	1.1346	1.0878	1.0878	1.0878
A14 H=0.2532m	1	5.1	0.9988	0.9988	0.9988	0.9965	0.9965	0.9965	0.9977	0.9977	0.9977
A14 H=0.2977m	1	5.1	1.0211	1.0211	1.0211	1.0646	1.0646	1.0646	1.0426	1.0426	1.0426
A15 H=0.1756m	1	9.2	1.0232	1.0232	1.0232	1.0713	1.0713	1.0713	1.0470	1.0470	1.0470
A15 H=0.1978m	1	9.2	1.0136	1.0136	1.0136	1.0414	1.0414	1.0414	1.0274	1.0274	1.0274
A15 H=0.2534m	1	9.2	1.0184	1.0184	1.0184	1.0563	1.0563	1.0563	1.0372	1.0372	1.0372
A15 H=0.2990m	1	9.2	1.0524	1.0524	1.0524	1.1656	1.1656	1.1656	1.1076	1.1076	1.1076
A16 H=0.1755m	0	5.1	1.0010	1.0010	1.0010	1.0031	1.0031	1.0031	1.0021	1.0021	1.0021
A16 H=0.1984m	0	5.1	1.0154	1.0154	1.0154	1.0470	1.0470	1.0470	1.0311	1.0311	1.0311
A16 H=0.2528m	0	5.1	1.0018	1.0018	1.0018	1.0054	1.0054	1.0054	1.0036	1.0036	1.0036
A16 H=0.2968m	0	5.1	1.0467	1.0467	1.0467	1.1468	1.1468	1.1468	1.0956	1.0956	1.0956
A17 H=0.1746m	0	2.1	-	-	-	-	-	-	-	-	-
A17 H=0.1981m	0	2.1	-	-	-	-	-	-	-	-	-
A17 H=0.2540m	0	2.1	-	-	-	-	-	-	-	-	-
A18 H=0.1755m	2	5.1	1.0519	1.0519	1.0519	1.1638	1.1638	1.1638	1.1064	1.1064	1.1064
A18 H=0.1980m	2	5.1	1.0239	1.0239	1.0239	1.0735	1.0735	1.0735	1.0484	1.0484	1.0484
A18 H=0.2513m	2	5.1	1.0119	1.0119	1.0119	1.0362	1.0362	1.0362	1.0240	1.0240	1.0240
A18 H=0.2920m	2	5.1	1.0127	1.0127	1.0127	1.0386	1.0386	1.0386	1.0255	1.0255	1.0255

Table 7.3d-Downstream (A14, A16, A18 x=33.2m, A15 x=38.2m) proportional velocities, energy and momentum correction coefficients, ψ

			Adjusted velocity			Adjusted energy correction coefficients, α			Adjusted momentum correction coefficients, β		
Series A No.	**s**	**θ**	**Left floodplain**	**Main channel**	**Right floodplain**	**Left floodplain**	**Main channel**	**Right floodplain**	**Left floodplain**	**Main channel**	**Right floodplain**
		°	***m/s***	***m/s***	***m/s***						
A14 H=0.1760m	1	5.1	0.5890	0.7361	0.3218	1.4504	1.0708	1.1037	1.1522	1.0210	1.0420
A14 H=0.1981m	1	5.1	0.5420	0.8013	0.4718	1.2870	1.1705	1.2210	1.1374	1.0881	1.1267
A14 H=0.2532m	1	5.1	0.7742	0.9438	0.7576	1.4580	1.1509	1.3368	1.2180	1.0833	1.1688
A14 H=0.2977m	1	5.1	0.9003	1.1203	0.9193	1.7188	1.3085	1.6434	1.3522	1.1824	1.3253
A15 H=0.1756m	1	9.2	0.4934	0.7595	0.3050	1.2213	1.1430	1.1743	1.0948	1.0647	1.0858
A15 H=0.1978m	1	9.2	0.6147	0.7902	0.4705	1.1720	1.1091	1.0764	1.0742	1.0450	1.0362
A15 H=0.2534m	1	9.2	0.7269	0.9312	0.7355	1.6498	1.1066	1.2200	1.2886	1.0561	1.1099
A15 H=0.2990m	1	9.2	0.8264	1.0840	0.9397	1.8598	1.1807	1.3541	1.3869	1.1064	1.1822
A16 H=0.1755m	0	5.1	0.3629	0.7435	0.3234	1.2065	1.1190	1.1407	1.0868	1.0510	1.0676
A16 H=0.1984m	0	5.1	0.5411	0.7679	0.4784	1.2130	1.1143	1.1526	1.0953	1.0527	1.0769
A16 H=0.2528m	0	5.1	0.7875	0.8850	0.7534	1.1536	1.0399	1.1308	1.0663	1.0127	1.0583
A16 H=0.2968m	0	5.1	0.9069	1.0774	0.9709	1.5961	1.2598	1.4066	1.2985	1.1541	1.2205
A17 H=0.1746m	0	2.1	0.3261	0.7667	0.3022	1.1768	1.1176	1.1009	1.0647	1.0474	1.0439
A17 H=0.1981m	0	2.1	0.4850	0.8013	0.4493	1.1279	1.0952	1.0969	1.0540	1.0406	1.0457
A17 H=0.2540m	0	2.1	0.7489	0.9087	0.7168	1.0989	1.0408	1.0968	1.0389	1.0128	1.0407
A18 H=0.1755m	2	5.1	0.3896	0.8216	0.3334	1.4528	1.3073	1.3501	1.2174	1.1650	1.1894
A18 H=0.1980m	2	5.1	0.5584	0.8378	0.4962	1.3127	1.1833	1.2372	1.1485	1.1454	1.1255
A18 H=0.2513m	2	5.1	0.7756	0.9553	0.7551	1.2417	1.0891	1.2020	1.1138	1.0450	1.1000
A18 H=0.2920m	2	5.1	0.9117	1.0756	0.9353	1.2109	1.0435	1.1871	1.0969	1.0190	1.0873

Table 7.3e-Upstream (A14, A16, A18 x=23.2m, A15 x=28.2m, A17 x=32.4m) adjusted proportional velocities and velocity correction coefficients

			Adjusted velocity			Adjusted energy correction coefficients, α			Adjusted momentum correction coefficients, β		
Series A No.	**s**	**θ**	**Left floodplain**	**Main channel**	**Right floodplain**	**Left floodplain**	**Main channel**	**Right floodplain**	**Left floodplain**	**Main channel**	**Right floodplain**
		°	***m/s***	***m/s***	***m/s***						
A14 H=0.1760m	1	5.1	0.3382	0.7761	0.3003	1.3662	1.2039	1.1635	1.1407	1.0984	1.0879
A14 H=0.1981m	1	5.1	0.5547	0.7952	0.4308	1.3231	1.2418	1.4498	1.1489	1.1231	1.2242
A14 H=0.2532m	1	5.1	0.8147	0.9299	0.6524	1.1091	1.0485	1.3394	1.0419	1.0156	1.1506
A14 H=0.2977m	1	5.1	1.0073	1.0882	0.8124	1.1771	1.1119	1.5041	1.0891	1.0589	1.2309
A15 H=0.1756m	1	9.2	0.4086	0.7593	0.2563	1.3713	1.1946	1.4272	1.1458	1.0894	1.2012
A15 H=0.1978m	1	9.2	0.6202	0.7690	0.4259	1.2122	1.1528	1.2183	1.0913	1.0653	1.1057
A15 H=0.2534m	1	9.2	0.8645	0.8932	0.6478	1.1910	1.1138	1.4774	1.0942	1.0564	1.2193
A15 H=0.2990m	1	9.2	1.0042	1.0670	0.8376	1.3309	1.2123	1.6764	1.1768	1.1230	1.3200
A16 H=0.1755m	0	5.1	0.3395	0.7526	0.2769	1.2398	1.1014	1.2407	1.0726	1.0361	1.1083
A16 H=0.1984m	0	5.1	0.5446	0.7695	0.4247	1.2288	1.1361	1.1648	1.0907	1.0611	1.1471
A16 H=0.2528m	0	5.1	0.8182	0.8837	0.6750	1.0997	1.0537	1.3048	1.0412	1.0202	1.1382
A16 H=0.2968m	0	5.1	0.9924	1.0563	0.8748	1.2620	1.1923	1.5330	1.1420	1.1108	1.2614
A17 H=0.1746m	0	2.1	-	-	-	-	-	-	-	-	-
A17 H=0.1981m	0	2.1	-	-	-	-	-	-	-	-	-
A17 H=0.2540m	0	2.1	-	-	-	-	-	-	-	-	-
A18 H=0.1755m	2	5.1	0.3109	0.8358	0.3009	1.5488	1.2844	1.2433	1.2334	1.1471	1.1366
A18 H=0.1980m	2	5.1	0.5477	0.8443	0.4245	1.2248	1.1755	1.4172	1.0999	1.0835	1.1992
A18 H=0.2513m	2	5.1	0.8129	0.9539	0.6601	1.1518	1.0914	1.4312	1.0690	1.0429	1.1986
A18 H=0.2920m	2	5.1	0.9605	1.0798	0.8286	1.1523	1.0879	1.4890	1.0763	1.0437	1.2229

Table 7.3f-Downstream (A14, A16, A18 x=33.2m, A15 x=38.2m) adjusted proportional velocities and velocity correction coefficients

			Interface velocity, U_{cf}		Cross-flow discharge, Q_{cf}	
Series A No.	**s**	**θ**	**Left hand interface**	**Right hand interface**	**Left hand interface**	**Right hand interface**
		o	***m/s***	***m/s***	***m^3/s***	***m^3/s***
A14 H=0.1760m	1	5.1	0.574	0.329	-0.0047	0.0075
A14 H=0.1981m	1	5.1	0.698	0.459	0.0224	0.0215
A14 H=0.2532m	1	5.1	0.992	0.813	0.0842	0.0713
A14 H=0.2977m	1	5.1	1.068	0.986	0.1656	0.1179
A15 H=0.1756m	1	9.2	0.749	0.313	0.0128	0.0130
A15 H=0.1978m	1	9.2	0.843	0.487	0.0417	0.0365
A15 H=0.2534m	1	9.2	1.027	0.812	0.1375	0.1208
A15 H=0.2990m	1	9.2	1.124	0.996	0.2247	0.2195
A16 H=0.1755m	0	5.1	0.620	0.325	0.0064	0.0085
A16 H=0.1984m	0	5.1	0.772	0.472	0.0225	0.0231
A16 H=0.2528m	0	5.1	0.926	0.766	0.0774	0.0779
A16 H=0.2968m	0	5.1	1.056	0.973	0.1494	0.1295
A18 H=0.1755m	2	5.1	0.632	0.324	0.0035	0.0076
A18 H=0.1980m	2	5.1	0.819	0.515	0.0215	0.0231
A18 H=0.2513m	2	5.1	1.006	0.817	0.0761	0.0747
A18 H=0.2920m	2	5.1	1.101	1.009	0.1247	0.1404

Table 7.4-Interface average velocity and corresponding cross-flow discharge on each interface between the main channel and floodplain(s)

			Unadjusted upstream discharge (A14, A16, A18 x=23.2m, A15 x=28.2m, A17 x=32.4m)					Unadjusted downstream discharge (A14, A16, A18 x=33.2m, A15 x=38.2m)				
Series A No.	**s**	**θ**	**Left floodplain**	**Main channel**	**Right floodplain**	**Total**	**%Q error to measured**	**Left floodplain**	**Main channel**	**Right floodplain**	**Total**	**%Q error to measured**
		o	m^3/s	m^3/s	m^3/s	m^3/s	*%*	m^3/s	m^3/s	m^3/s	m^3/s	*%*
A14 H=0.1760m	1	5.1	0.02709	0.21749	0.01741	0.26199	0.379	0.02236	0.22189	0.00922	0.25347	-2.885
A14 H=0.1981m	1	5.1	0.04473	0.25964	0.04576	0.35013	-3.011	0.06712	0.25469	0.02431	0.34612	-4.122
A14 H=0.2532m	1	5.1	0.13900	0.39297	0.15557	0.68754	-3.163	0.22320	0.40338	0.08425	0.71083	0.117
A14 H=0.2977m	1	5.1	0.22382	0.53531	0.26749	1.02662	-7.428	0.38945	0.54702	0.14964	1.08611	-2.064
A15 H=0.1756m	1	9.2	0.01011	0.21961	0.02318	0.25290	-1.519	0.02293	0.21789	0.01015	0.25097	-2.270
A15 H=0.1978m	1	9.2	0.02402	0.26160	0.06748	0.35310	-0.731	0.06589	0.25303	0.03200	0.35092	-1.344
A15 H=0.2534m	1	9.2	0.06273	0.39573	0.22744	0.68590	-1.986	0.20023	0.38028	0.10664	0.68715	-1.808
A15 H=0.2990m	1	9.2	0.10291	0.53438	0.41446	1.05175	-4.404	0.32757	0.52284	0.19499	1.04540	-4.981
A16 H=0.1755m	0	5.1	0.01746	0.19382	0.01809	0.22937	-1.048	0.02388	0.19807	0.00961	0.23156	-0.104
A16 H=0.1984m	0	5.1	0.04954	0.22551	0.05084	0.32589	-1.395	0.07199	0.22570	0.02779	0.32548	-1.519
A16 H=0.2528m	0	5.1	0.15770	0.33630	0.17490	0.66890	0.120	0.23510	0.33480	0.09700	0.66690	-0.180
A16 H=0.2968m	0	5.1	0.24340	0.44970	0.30400	0.99710	-6.332	0.39280	0.44970	0.17450	1.01700	-4.462
A17 H=0.1746m	0	2.1	0.01880	0.19944	0.01299	0.23123	-0.760	-	-	-	-	
A17 H=0.1981m	0	2.1	0.05490	0.23635	0.03800	0.32925	-0.828	-	-	-	-	
A17 H=0.2540m	0	2.1	0.18728	0.34708	0.13466	0.66902	0.153	-	-	-	-	
A18 H=0.1755m	2	5.1	0.01504	0.25022	0.01535	0.28061	-5.867	0.01857	0.25708	0.00775	0.28340	-4.931
A18 H=0.1980m	2	5.1	0.04200	0.30072	0.04447	0.38719	-3.203	0.06353	0.30575	0.02137	0.39065	-2.337
A18 H=0.2513m	2	5.1	0.12740	0.45438	0.14738	0.72916	-1.465	0.20349	0.45506	0.07273	0.73128	-1.178
A18 H=0.2920m	2	5.1	0.21486	0.60880	0.26142	1.08508	-0.387	0.33955	0.60586	0.13024	1.07565	-1.253

Table 7.5-Unadjusted proportional discharge for FCF skewed channel

			Percentage upstream discharge			Percentage downstream discharge		
Series A No.	**s**	**θ**	**Left floodplain**	**Main channel**	**Right floodplain**	**Left floodplain**	**Main channel**	**Right floodplain**
		°	*%*	*%*	*%*	*%*	*%*	*%*
A14 H=0.1760m	1	5.1	10.34	83.01	6.65	8.82	87.54	3.64
A14 H=0.1981m	1	5.1	12.78	74.16	13.07	19.39	73.58	7.02
A14 H=0.2532m	1	5.1	20.22	57.16	22.63	31.40	56.75	11.85
A14 H=0.2977m	1	5.1	21.80	52.14	26.06	35.86	50.37	13.78
A15 H=0.1756m	1	9.2	4.00	86.84	9.17	9.14	86.82	4.04
A15 H=0.1978m	1	9.2	6.80	74.09	19.11	18.78	72.10	9.12
A15 H=0.2534m	1	9.2	9.15	57.69	33.16	29.14	55.34	15.52
A15 H=0.2990m	1	9.2	9.78	50.81	39.41	31.33	50.01	18.65
A16 H=0.1755m	0	5.1	7.61	84.50	7.89	10.31	85.54	4.15
A16 H=0.1984m	0	5.1	15.20	69.20	15.60	22.12	69.34	8.54
A16 H=0.2528m	0	5.1	23.58	50.28	26.15	35.25	50.20	14.54
A16 H=0.2968m	0	5.1	24.41	45.10	30.49	38.62	44.22	17.16
A17 H=0.1746m	0	2.1	8.13	86.25	5.62	-	-	-
A17 H=0.1981m	0	2.1	16.67	71.78	11.54	-	-	-
A17 H=0.2540m	0	2.1	27.99	51.88	20.13	-	-	-
A18 H=0.1755m	2	5.1	5.36	89.17	5.47	6.55	90.71	2.73
A18 H=0.1980m	2	5.1	10.85	77.67	11.49	16.26	78.27	5.47
A18 H=0.2513m	2	5.1	17.47	62.32	20.21	27.83	62.23	9.95
A18 H=0.2920m	2	5.1	19.80	56.11	24.09	31.57	56.33	12.11

Table 7.6-Adjusted percentage proportional discharge for FCF skewed channel

			Adjusted upstream discharge (A14, A16, A18 x=23.2m, A15 x=28.2m, A17 x=32.4m)				Adjusted downstream discharge (A14, A16, A18 x=33.2m, A15 x=38.2m)			
Series A No.	**s**	**θ**	**Left floodplain**	**Main channel**	**Right floodplain**	**Total**	**Left floodplain**	**Main channel**	**Right floodplain**	**Total**
		o	m^3/s	m^3/s	m^3/s	m^3/s	m^3/s	m^3/s	m^3/s	m^3/s
A14 H=0.1760m	1	5.1	0.02699	0.21667	0.01734	0.26100	0.02302	0.22848	0.00949	0.26100
A14 H=0.1981m	1	5.1	0.04612	0.26770	0.04718	0.36100	0.07001	0.26564	0.02536	0.36100
A14 H=0.2532m	1	5.1	0.14354	0.40581	0.16065	0.71000	0.22294	0.40291	0.08415	0.71000
A14 H=0.2977m	1	5.1	0.24178	0.57827	0.28895	1.10900	0.39766	0.55855	0.15279	1.10900
A15 H=0.1756m	1	9.2	0.01027	0.22300	0.02354	0.25680	0.02346	0.22295	0.01039	0.25680
A15 H=0.1978m	1	9.2	0.02420	0.26353	0.06798	0.35570	0.06679	0.25648	0.03244	0.35570
A15 H=0.2534m	1	9.2	0.06400	0.40375	0.23205	0.69980	0.20392	0.38728	0.10860	0.69980
A15 H=0.2990m	1	9.2	0.10765	0.55900	0.43355	1.10020	0.34474	0.55025	0.20521	1.10020
A16 H=0.1755m	0	5.1	0.01764	0.19587	0.01828	0.23180	0.02390	0.19828	0.00962	0.23180
A16 H=0.1984m	0	5.1	0.05024	0.22870	0.05156	0.33050	0.07310	0.22918	0.02822	0.33050
A16 H=0.2528m	0	5.1	0.15751	0.33590	0.17469	0.66810	0.23552	0.33540	0.09717	0.66810
A16 H=0.2968m	0	5.1	0.25985	0.48010	0.32455	1.06450	0.41115	0.47070	0.18265	1.06450
A17 H=0.1746m	0	2.1	0.01894	0.20097	0.01309	0.23300	-	-	-	-
A17 H=0.1981m	0	2.1	0.05536	0.23832	0.03832	0.33200	-	-	-	-
A17 H=0.2540m	0	2.1	0.18699	0.34655	0.13445	0.66800	-	-	-	-
A18 H=0.1755m	2	5.1	0.01598	0.26582	0.01631	0.29810	0.01953	0.27041	0.00815	0.29810
A18 H=0.1980m	2	5.1	0.04339	0.31067	0.04594	0.40000	0.06505	0.31307	0.02188	0.40000
A18 H=0.2513m	2	5.1	0.12929	0.46114	0.14957	0.74000	0.20592	0.46049	0.07360	0.74000
A18 H=0.2920m	2	5.1	0.21570	0.61117	0.26244	1.08930	0.34386	0.61355	0.13189	1.08930

Table 7.7a-Adjusted proportional discharge for FCF skewed channel

	s	θ	Depth, H	"m" constants			"c" constants			Valid over
Series A No.		°	*m*	Left floodplain	Main channel	Right floodplain	Left floodplain	Main channel	Right floodplain	
A14 H=0.1760m	1	5.1	0.1760	-0.0015	0.0045	-0.0030	0.1386	0.7251	0.1362	23.2≤x≤33.2
A14 H=0.1981m	1	5.1	0.1981	0.0066	-0.0006	-0.0060	-0.0258	0.7548	0.2710	23.2≤x≤33.2
A14 H=0.2532m	1	5.1	0.2532	0.0112	-0.0004	-0.0108	0.0573	0.5810	0.4762	23.2≤x≤33.2
A14 H=0.2977m	1	5.1	0.2977	0.0141	-0.0018	-0.0123	0.1081	0.5627	0.5454	23.2≤x≤33.2
A15 H=0.1756m	1	9.2	0.1756	0.0051	-0.00002	-0.0051	-0.1049	0.8689	0.2361	28.2≤x≤38.2
A15 H=0.1978m	1	9.2	0.1978	0.0120	-0.0020	-0.0100	-0.2696	0.7968	0.4729	28.2≤x≤38.2
A15 H=0.2534m	1	9.2	0.2534	0.0200	-0.0024	-0.0176	0.4724	0.6433	0.8290	28.2≤x≤38.2
A15 H=0.2990m	1	9.2	0.2990	0.0215	-0.0008	-0.0208	-0.5099	0.5305	0.9793	28.2≤x≤38.2
A16 H=0.1755m	0	5.1	0.1755	0.0027	-0.0010	-0.0037	0.0135	0.8210	0.1656	23.2≤x≤33.2
A16 H=0.1984m	0	5.1	0.1984	0.00696	-0.0001	-0.0071	-0.0085	0.6886	0.3198	23.2≤x≤33.2
A16 H=0.2528m	0	5.1	0.2528	0.0117	-0.00007	-0.0116	0.0351	0.5045	0.5307	23.2≤x≤33.2
A16 H=0.2968m	0	5.1	0.2968	0.0142	-0.0009	-0.0133	-0.0856	0.4715	0.6141	23.2≤x≤33.2
A17 H=0.1746m	0	2.1	0.1746	-	-	-	-	-	-	
A17 H=0.1981m	0	2.1	0.1981	-	-	-	-	-	-	
A17 H=0.2540m	0	2.1	0.2540	-	-	-	-	-	-	
A18 H=0.1755m	2	5.1	0.1755	0.0012	0.0015	-0.0027	0.0259	0.8559	0.1182	23.2≤x≤33.2
A18 H=0.1980m	2	5.1	0.1980	0.0054	0.0006	-0.0060	-0.0172	0.7628	0.2544	23.2≤x≤33.2
A18 H=0.2513m	2	5.1	0.2513	0.0104	-0.00009	-0.0103	-0.0655	0.6252	0.4403	23.2≤x≤33.2
A18 H=0.2920m	2	5.1	0.2920	0.0118	0.0002	-0.0120	-0.0750	0.5560	0.5190	23.2≤x≤33.2

Table 7.7b-Constants for proportional flow formulae (Equation 7.31)

			Upstream shear stress (A14 x=23.2m, A15 x=28.2m, A16, A18 x=24.9m and A17 x=23.7m)				Intermediate shear stress (A16 and A18 x=28.2m)				Downstream shear stress (A14 x=33.2m, A15 x=38.2m and A16, A18 x=31.5m)			
Series A No.	**s**	**θ**	**Left floodplain**	**Main channel**	**Right floodplain**	**Peak**	**Left floodplain**	**Main channel**	**Right floodplain**	**Peak**	**Left floodplain**	**Main channel**	**Right floodplain**	**Peak**
		o	N/m^2	N/m^2	N/m^2	N/m^2	N/m^2	N/m^2	N/m^2	N/m^2	N/m^2	N/m^2	N/m^2	N/m^2
A14 H=0.1760m	1	5.1	0.521	1.147	0.399	1.593	-	-	-		0.461	1.201	0.360	1.623
A14 H=0.1981m	1	5.1	0.845	1.191	0.661	1.634	-	-	-		0.800	1.234	0.568	1.956
A14 H=0.2532m	1	5.1	1.434	1.545	1.244	2.397	-	-	-		1.466	1.523	1.088	2.282
A14 H=0.2977m	1	5.1	1.779	1.883	1.809	2.725	-	-	-		1.809	1.929	1.596	2.913
A15 H=0.1756m	1	9.2	0.828	1.402	0.335	1.859	-	-	-		0.657	1.091	0.321	1.838
A15 H=0.1978m	1	9.2	1.117	1.117	0.604	1.855	-	-	-		1.005	1.120	0.581	1.665
A15 H=0.2534m	1	9.2	1.621	1.491	1.225	2.314	-	-	-		1.534	1.551	1.157	2.314
A15 H=0.2990m	1	9.2	1.939	1.849	1.712	2.731	-	-	-		1.848	1.986	1.627	2.566
A16 H=0.1755m	0	5.1	0.496	0.996	0.427	1.430	0.500	0.994	0.412	1.525	0.460	1.040	0.411	1.579
A16 H=0.1984m	0	5.1	0.901	1.079	0.713	1.547	0.922	1.077	0.657	1.951	0.862	1.112	0.672	1.696
A16 H=0.2528m	0	5.1	1.457	1.191	1.292	1.847	1.416	1.396	1.158	1.969	1.368	1.310	1.250	2.006
A16 H=0.2968m	0	5.1	1.871	1.538	1.675	2.428	1.837	1.480	1.740	2.022	1.796	1.500	1.771	2.290
A17 H=0.1746m	0	2.1	0.440	1.805	0.369	1.077	-	-	-		-	-	-	
A17 H=0.1981m	0	2.1	0.702	1.180	0.649	1.415	-	-	-		-	-	-	
A17 H=0.2540m	0	2.1	1.338	1.395	1.259	1.909	-	-	-		-	-	-	
A18 H=0.1755m	2	5.1	0.508	1.173	0.401	1.467	0.481	1.191	0.389	1.520	0.449	1.230	0.361	1.581
A18 H=0.1980m	2	5.1	0.858	1.220	0.687	1.513	0.850	1.242	0.633	1.740	0.799	1.293	0.593	1.834
A18 H=0.2513m	2	5.1	1.446	1.590	1.244	1.810	1.498	1.553	1.186	2.239	1.438	1.547	1.242	2.080
A18 H=0.2920m	2	5.1	1.801	1.815	1.785	2.131	1.806	1.824	1.764	2.273	1.839	2.020	1.392	2.584

Table 7.8a-Average boundary shear stresses in each zone

	Upstream shear stress				Intermediate shear stress				Downstream shear stress			
Series A No.	Left floodplain	Main channel	Right floodplain	%Peak	Left floodplain	Main channel	Right floodplain	%Peak	Left floodplain	Main channel	Right floodplain	%Peak
	N/m^2	N/m^2	N/m^2	N/m^2	N/m^2	N/m^2	N/m^2	N/m^2	N/m^2	N/m^2	N/m^2	N/m^2
A14 H=0.1760m	0.521	1.147	0.399	232.73%	-	-	-	0.00%	0.461	1.201	0.360	237.06%
A14 H=0.1981m	0.845	1.191	0.661	183.17%	-	-	-	0.00%	0.800	1.234	0.568	219.21%
A14 H=0.2532m	1.434	1.545	1.244	171.28%	-	-	-	0.00%	1.466	1.523	1.088	163.05%
A14 H=0.2977m	1.779	1.883	1.809	151.59%	-	-	-	0.00%	1.809	1.929	1.596	162.05%
A15 H=0.1756m	0.828	1.402	0.335	273.28%	-	-	-	0.00%	0.657	1.091	0.321	270.15%
A15 H=0.1978m	1.117	1.117	0.604	208.59%	-	-	-	0.00%	1.005	1.120	0.581	187.20%
A15 H=0.2534m	1.621	1.491	1.225	165.12%	-	-	-	0.00%	1.534	1.551	1.157	165.12%
A15 H=0.2990m	1.939	1.849	1.712	150.96%	-	-	-	0.00%	1.848	1.986	1.627	141.86%
A16 H=0.1755m	0.496	0.996	0.427	230.16%	0.500	0.994	0.412	245.50%	0.460	1.040	0.411	254.13%
A16 H=0.1984m	0.901	1.079	0.713	186.10%	0.922	1.077	0.657	234.83%	0.862	1.112	0.672	204.06%
A16 H=0.2528m	1.457	1.191	1.292	139.93%	1.416	1.396	1.158	149.24%	1.368	1.310	1.250	152.02%
A16 H=0.2968m	1.871	1.538	1.675	142.50%	1.837	1.480	1.740	118.63%	1.796	1.500	1.771	134.36%
A17 H=0.1746m	0.440	1.805	0.369	175.63%	-	-	-	0.00%	-	-	-	0.00%
A17 H=0.1981m	0.702	1.180	0.649	170.80%	-	-	-	0.00%	-	-	-	0.00%
A17 H=0.2540m	1.338	1.395	1.259	143.49%	-	-	-	0.00%	-	-	-	0.00%
A18 H=0.1755m	0.508	1.173	0.401	202.39%	0.481	1.191	0.389	209.68%	0.449	1.230	0.361	218.06%
A18 H=0.1980m	0.858	1.220	0.687	161.24%	0.850	1.242	0.633	185.38%	0.799	1.293	0.593	195.46%
A18 H=0.2513m	1.446	1.590	1.244	126.29%	1.498	1.553	1.186	156.26%	1.438	1.547	1.242	145.16%
A18 H=0.2920m	1.801	1.815	1.785	118.40%	1.806	1.824	1.764	126.29%	1.839	2.020	1.392	143.57%

Table 7.8b-Average boundary shear stresses in each zone and percentage of peak boundary shear stress

			Upstream shear force			Intermediate shear force			Downstream shear force		
Series A No.	**s**	**θ**	**Left floodplain**	**Main channel**	**Right floodplain**	**Left floodplain**	**Main channel**	**Right floodplain**	**Left floodplain**	**Main channel**	**Right floodplain**
		°	***N***	***N***	***N***	***N***	***N***	***N***	***N***	***N***	***N***
A14 H=0.1760m	1	5.1	0.9284	2.2072	0.8351	-	-	-	1.2144	2.3115	0.4448
A14 H=0.1981m	1	5.1	1.5327	2.2915	1.1404	-	-	-	2.1338	2.3784	0.7198
A14 H=0.2532m	1	5.1	2.7113	2.9722	2.7381	-	-	-	4.0254	2.9315	1.4646
A14 H=0.2977m	1	5.1	3.4758	3.6239	3.9438	-	-	-	5.0815	3.7123	2.2497
A15 H=0.1756m	1	9.2	1.0871	2.0046	0.8588	-	-	-	1.1733	2.1011	0.6706
A15 H=0.1978m	1	9.2	1.4941	2.1486	1.5696	-	-	-	1.8270	2.1554	1.2298
A15 H=0.2534m	1	9.2	2.2958	2.8692	3.2689	-	-	-	2.9090	2.9845	2.5404
A15 H=0.2990m	1	9.2	2.8715	3.5582	4.6922	-	-	-	3.6231	3.8218	3.6770
A16 H=0.1755m	0	5.1	1.0189	1.7927	0.9028	1.1822	1.7886	0.7436	1.2163	1.8714	0.6267
A16 H=0.1984m	0	5.1	1.8901	1.9422	1.5388	2.2190	1.9390	1.2130	2.3165	2.0011	1.0535
A16 H=0.2528m	0	5.1	3.1549	2.1434	2.8743	3.5058	2.4490	2.2178	3.7704	2.3578	2.0445
A16 H=0.2968m	0	5.1	4.1668	2.7679	3.8321	4.6619	2.6638	3.4412	5.0592	2.7006	3.0071
A17 H=0.1746m	0	2.1	1.0494	1.9534	0.6580	-	-	-	-	-	-
A17 H=0.1981m	0	2.1	1.6970	2.1230	1.1820	-	-	-	-	-	-
A17 H=0.2540m	0	2.1	3.3410	2.5120	2.3890	-	-	-	-	-	-
A18 H=0.1755m	2	5.1	0.8925	2.5455	0.7275	0.9945	2.5851	0.5859	1.0505	2.6700	0.4447
A18 H=0.1980m	2	5.1	1.5246	2.6473	1.2696	1.7823	2.6962	0.9730	1.8954	2.8070	0.7487
A18 H=0.2513m	2	5.1	2.6938	3.4519	2.3932	3.2547	3.3717	1.9125	3.5197	3.3583	1.6617
A18 H=0.2920m	2	5.1	3.4595	3.9404	3.5350	4.0283	3.9595	2.9471	4.6065	4.3839	1.9431

Table 7.9-Average boundary shear forces in each zone

	Upstream (A14 x=23.2m, A15 x=28.2m, A16, A18 x=24.9m, A17 x=23.7m)							
	Left floodplain		Main channel			Right floodplain		
	Wall	Bed	Left Wall	Bed	Right Wall	Bed	Wall	Total
Series No.	*N*	*N*	*N*	*N*	*N*	*N*	*N*	*N*
A14 H=0.1760m	0.0124	0.9477	0.3538	1.8638	0.1741	0.8499	0.0092	4.2109
A15 H=0.1756m	0.0122	1.2047	0.3988	1.8171	0.1501	0.9508	0.0098	4.5435
A16 H=0.1755m	0.0153	0.8950	0.2703	1.5832	0.1327	0.7952	0.0114	3.7032
A17 H=0.1746m	0.0161	0.8684	0.2087	1.6885	0.1687	0.5604	0.0115	3.5223
A18 H=0.1755m	0.0179	0.8998	0.7791	2.0456	0.3623	0.7414	0.0131	4.8593

	Upstream (A14 x=23.2m, A15 x=28.2m, A16, A18 x=24.9m, A17 x=23.7m)							
	Left floodplain		Main channel			Right floodplain		
	Wall	Bed	Left Wall	Bed	Right Wall	Bed	Wall	Total
Series No.	*N*	*N*	*N*	*N*	*N*	*N*	*N*	*N*
A14 H=0.1981m	0.0232	1.5970	0.3529	1.9801	0.2095	1.4709	0.0106	5.6441
A15 H=0.1978m	0.0407	1.5862	0.3855	1.8907	0.1807	1.6545	0.0480	5.7864
A16 H=0.1984m	0.0329	1.6546	0.2416	1.7109	0.1544	1.3412	0.0308	5.1663
A17 H=0.1981m	0.0234	1.4493	0.2237	1.8301	0.1905	1.0020	0.0287	4.7477
A18 H=0.1980m	0.0445	1.5557	0.8156	2.1848	0.4151	1.2996	0.0432	6.3585

	Upstream (A14 x=23.2m, A15 x=28.2m, A16, A18 x=24.9m, A17 x=23.7m)							
	Left floodplain		Main channel			Right floodplain		
	Wall	Bed	Left Wall	Bed	Right Wall	Bed	Wall	Total
Series No.	*N*	*N*	*N*	*N*	*N*	*N*	*N*	*N*
A14 H=0.2532m	0.1131	2.6991	0.4913	2.4425	0.3204	2.7499	0.0467	8.8632
A15 H=0.2534m	0.1152	2.2384	0.4915	2.3345	0.2899	3.2030	0.1475	8.8201
A16 H=0.2528m	0.1363	2.7900	0.2975	1.9597	0.1796	2.5275	0.1386	8.0292
A17 H=0.2540m	0.1151	2.7381	0.3995	2.1644	0.2046	1.9348	0.1199	7.6764
A18 H=0.2513m	0.1610	2.5649	1.0579	2.5134	0.8417	2.2970	0.1397	9.5755

	Upstream (A14 x=23.2m, A15 x=28.2m, A16, A18 x=24.9m, A17 x=23.7m)							
	Left floodplain		Main channel			Right floodplain		
	Wall	Bed	Left Wall	Bed	Right Wall	Bed	Wall	Total
Series No.	*N*	*N*	*N*	*N*	*N*	*N*	*N*	*N*
A14 H=0.2977m	0.2412	3.3396	0.6139	3.0000	0.3576	3.7227	0.3312	11.6061
A15 H=0.2990m	0.2580	2.6995	0.6094	2.9046	0.3984	4.5511	0.2863	11.7074
A16 H=0.2968m	0.2395	3.6305	0.3489	2.5495	0.2696	3.3848	0.2657	10.6885
A18 H=0.2920m	0.2771	3.1573	1.2393	2.8390	0.9531	3.2759	0.3095	12.0512

Table 7.10a-Shear forces on each element for upstream FCF skewed data

	Intermediate (A16, A18 x=28.2m)							
	Left floodplain		Main channel			Right floodplain		
	Wall	Bed	Left Wall	Bed	Right Wall	Bed	Wall	Total
Series No.	***N***	***N***	***N***	***N***	***N***	***N***	***N***	***N***
A16 H=0.1755m	0.0141	1.0546	0.2787	1.5967	0.1344	0.6601	0.0086	3.7471
A18 H=0.1755m	0.0159	1.0293	0.8585	2.0388	0.3703	0.5949	0.0109	4.9186

	Intermediate (A16, A18 x=28.2m)							
	Left floodplain		Main channel			Right floodplain		
	Wall	Bed	Left Wall	Bed	Right Wall	Bed	Wall	Total
Series No.	***N***	***N***	***N***	***N***	***N***	***N***	***N***	***N***
A16 H=0.1984m	0.0295	1.9093	0.3149	1.6622	0.1636	1.0339	0.0228	5.1362
A18 H=0.1980m	0.0406	1.8813	1.0007	2.1424	0.3925	1.0022	0.0323	6.4920

	Intermediate (A16, A18 x=28.2m)							
	Left floodplain		Main channel			Right floodplain		
	Wall	Bed	Left Wall	Bed	Right Wall	Bed	Wall	Total
Series No.	***N***	***N***	***N***	***N***	***N***	***N***	***N***	***N***
A16 H=0.2528m	0.1311	3.3184	0.3212	2.0706	0.1939	2.0538	0.1132	8.2022
A18 H=0.2513m	0.1501	3.2206	1.1925	2.4966	0.7144	1.8580	0.1220	9.7541

	Intermediate (A16, A18 x=28.2m)							
	Left floodplain		Main channel			Right floodplain		
	Wall	Bed	Left Wall	Bed	Right Wall	Bed	Wall	Total
Series No.	***N***	***N***	***N***	***N***	***N***	***N***	***N***	***N***
A16 H=0.2968m	0.2151	4.0316	0.3298	2.4009	0.2533	2.7673	0.2391	10.2371
A18 H=0.2920m	0.2658	3.9029	1.3427	2.8947	0.9816	2.7596	0.2886	12.4358

Table 7.10b-Shear forces on each element for intermediate FCF skewed data

	Downstream (A14 x=33.2m, A15 x=38.2m, A16, A18 x=31.5m)							
	Left floodplain		Main channel			Right floodplain		
	Wall	Bed	Left Wall	Bed	Right Wall	Bed	Wall	Total
Series No.	***N***	***N***	***N***	***N***	***N***	***N***	***N***	***N***
A14 H=0.1760m	0.0131	1.1849	0.3696	1.8686	0.1500	0.4255	0.0122	4.0239
A15 H=0.1756m	0.0140	1.2166	0.3592	1.8078	0.1341	0.6880	0.0118	4.2314
A16 H=0.1755m	0.0123	1.0661	0.3070	1.6395	0.1359	0.5404	0.0124	3.7135
A18 H=0.1755m	0.0126	1.0480	0.8118	2.0602	0.3400	0.4291	0.0128	4.7146

	Downstream (A14 x=33.2m, A15 x=38.2m, A16, A18 x=31.5m)							
	Left floodplain		Main channel			Right floodplain		
	Wall	Bed	Left Wall	Bed	Right Wall	Bed	Wall	Total
Series No.	***N***	***N***	***N***	***N***	***N***	***N***	***N***	***N***
A14 H=0.1981m	0.0303	2.2077	0.4204	2.0100	0.2027	0.7216	0.0293	5.6220
A15 H=0.1978m	0.0349	1.6793	0.3665	1.8909	0.1624	1.2209	0.0264	5.3813
A16 H=0.1984m	0.0264	1.9561	0.2712	1.6872	0.1741	0.8702	0.0234	5.0087
A18 H=0.1980m	0.0354	2.0459	1.0030	2.1700	0.3892	0.7734	0.0384	6.4553

	Downstream (A14 x=33.2m, A15 x=38.2m, A16, A18 x=31.5m)							
	Left floodplain		Main channel			Right floodplain		
	Wall	Bed	Left Wall	Bed	Right Wall	Bed	Wall	Total
Series No.	***N***	***N***	***N***	***N***	***N***	***N***	***N***	***N***
A14 H=0.2532m	0.1201	3.9650	0.4593	2.4118	0.2572	1.3816	0.1068	8.7017
A15 H=0.2534m	0.1087	2.7925	0.5080	2.3576	0.2881	2.4318	0.1137	8.6006
A16 H=0.2528m	0.0847	3.7370	0.3169	2.0860	0.2029	1.9443	0.1315	8.5033
A18 H=0.2513m	0.1302	3.4375	1.1633	2.4419	0.6735	1.5469	0.1441	9.5375

	Downstream (A14 x=33.2m, A15 x=38.2m, A16, A18 x=31.5m)							
	Left floodplain		Main channel			Right floodplain		
	Wall	Bed	Left Wall	Bed	Right Wall	Bed	Wall	Total
Series No.	***N***	***N***	***N***	***N***	***N***	***N***	***N***	***N***
A14 H=0.2977m	0.2316	5.0615	0.6468	3.0921	0.3677	2.0628	0.2689	11.7313
A15 H=0.2990m	0.2550	3.4751	0.5727	3.2340	0.3613	3.5409	0.2455	11.6845
A16 H=0.2968m	0.2001	4.3823	0.3485	2.4248	0.2627	2.3997	0.2499	10.2680
A18 H=0.2920m	0.2543	4.5445	1.4036	3.3364	0.9257	2.0236	0.2705	12.7584

Table 7.10c-Shear forces on each element for downstream FCF skewed data

	Upstream (A14 x=23.2m, A15 x=28.2m, A16, A18 x=24.9m, A17 x=23.7m)						
	Left floodplain		Main channel			Right floodplain	
	Wall	Bed	Left Wall	Bed	Right Wall	Bed	Wall
Series No.	%	%	%	%	%	%	%
A14 H=0.1760m	0.30	22.51	8.40	44.26	4.13	20.18	0.22
A15 H=0.1756m	0.27	26.51	8.78	39.99	3.30	20.93	0.22
A16 H=0.1755m	0.41	24.17	7.30	42.75	3.58	21.47	0.31
A17 H=0.1746m	0.46	24.65	5.93	47.94	4.79	15.91	0.33
A18 H=0.1755m	0.37	18.52	16.03	42.10	7.46	15.26	0.27

	Upstream (A14 x=23.2m, A15 x=28.2m, A16, A18 x=24.9m, A17 x=23.7m)						
	Left floodplain		Main channel			Right floodplain	
	Wall	Bed	Left Wall	Bed	Right Wall	Bed	Wall
Series No.	%	%	%	%	%	%	%
A14 H=0.1981m	0.41	28.29	6.25	35.08	3.71	26.06	0.19
A15 H=0.1978m	0.70	27.41	6.66	32.68	3.12	28.59	0.83
A16 H=0.1984m	0.64	32.03	4.68	33.12	2.99	25.96	0.60
A17 H=0.1981m	0.49	30.53	4.71	38.55	4.01	21.11	0.60
A18 H=0.1980m	0.70	24.47	12.83	34.36	6.53	20.44	0.68

	Upstream (A14 x=23.2m, A15 x=28.2m, A16, A18 x=24.9m, A17 x=23.7m)						
	Left floodplain		Main channel			Right floodplain	
	Wall	Bed	Left Wall	Bed	Right Wall	Bed	Wall
Series No.	%	%	%	%	%	%	%
A14 H=0.2532m	1.28	30.45	5.54	27.56	3.62	31.03	0.53
A15 H=0.2534m	1.31	25.38	5.57	26.47	3.29	36.31	1.67
A16 H=0.2528m	1.70	34.75	3.70	24.41	2.24	31.48	1.73
A17 H=0.2540m	1.50	35.67	5.20	28.20	2.66	25.20	1.56
A18 H=0.2513m	1.68	26.79	11.05	26.25	8.79	23.99	1.46

	Upstream (A14 x=23.2m, A15 x=28.2m, A16, A18 x=24.9m, A17 x=23.7m)						
	Left floodplain		Main channel			Right floodplain	
	Wall	Bed	Left Wall	Bed	Right Wall	Bed	Wall
Series No.	%	%	%	%	%	%	%
A14 H=0.2977m	2.08	28.77	5.29	25.85	3.08	32.08	2.85
A15 H=0.2990m	2.20	23.06	5.21	24.81	3.40	38.87	2.45
A16 H=0.2968m	2.24	33.97	3.26	23.85	2.52	31.67	2.49
A18 H=0.2920m	2.30	26.20	10.28	23.56	7.91	27.18	2.57

Table 7.11a-Percentage shear forces on each element for upstream FCF skewed data

	Intermediate (A16, A18 x=28.2m)						
	Left floodplain		Main channel			Right floodplain	
	Wall	Bed	Left Wall	Bed	Right Wall	Bed	Wall
Series No.	*%*	*%*	*%*	*%*	*%*	*%*	*%*
A16 H=0.1755m	0.38	28.14	7.44	42.61	3.59	17.62	0.23
A18 H=0.1755m	0.32	20.93	17.45	41.45	7.53	12.10	0.22

	Intermediate (A16, A18 x=28.2m)						
	Left floodplain		Main channel			Right floodplain	
	Wall	Bed	Left Wall	Bed	Right Wall	Bed	Wall
Series No.	*%*	*%*	*%*	*%*	*%*	*%*	*%*
A16 H=0.1984m	0.57	37.17	6.13	32.36	3.19	20.13	0.44
A18 H=0.1980m	0.62	28.98	15.41	33.00	6.05	15.44	0.50

	Intermediate (A16, A18 x=28.2m)						
	Left floodplain		Main channel			Right floodplain	
	Wall	Bed	Left Wall	Bed	Right Wall	Bed	Wall
Series No.	*%*	*%*	*%*	*%*	*%*	*%*	*%*
A16 H=0.2528m	1.60	40.46	3.92	25.24	2.36	25.04	1.38
A18 H=0.2513m	1.54	33.02	12.23	25.59	7.32	19.05	1.25

	Intermediate (A16, A18 x=28.2m)						
	Left floodplain		Main channel			Right floodplain	
	Wall	Bed	Left Wall	Bed	Right Wall	Bed	Wall
Series No.	*%*	*%*	*%*	*%*	*%*	*%*	*%*
A16 H=0.2968m	2.10	39.38	3.22	23.45	2.47	27.03	2.34
A18 H=0.2920m	2.14	31.38	10.80	23.28	7.89	22.19	2.32

Table 7.11b-Percentage shear forces on each element for intermediate FCF skewed data

	Downstream (A14 x=33.2m, A15 x=38.2m, A16, A18 x=31.5m)						
	Left floodplain		Main channel			Right floodplain	
	Wall	Bed	Left Wall	Bed	Right Wall	Bed	Wall
Series No.	*%*	*%*	*%*	*%*	*%*	*%*	*%*
A14 H=0.1760m	0.33	29.45	9.19	46.44	3.73	10.57	0.30
A15 H=0.1756m	0.33	28.75	8.49	42.72	3.17	16.26	0.28
A16 H=0.1755m	0.33	28.71	8.27	44.15	3.66	14.55	0.33
A18 H=0.1755m	0.27	22.23	17.22	43.70	7.21	9.10	0.27

	Downstream (A14 x=33.2m, A15 x=38.2m, A16, A18 x=31.5m)						
	Left floodplain		Main channel			Right floodplain	
	Wall	Bed	Left Wall	Bed	Right Wall	Bed	Wall
Series No.	*%*	*%*	*%*	*%*	*%*	*%*	*%*
A14 H=0.1981m	0.54	39.27	7.48	35.75	3.61	12.83	0.52
A15 A=0.1978m	0.65	31.21	6.81	35.14	3.02	22.69	0.49
A16 H=0.1984m	0.53	39.05	5.41	33.69	3.48	17.37	0.47
A18 H=0.1980m	0.55	31.69	15.54	33.62	6.03	11.98	0.59

	Downstream (A14 x=33.2m, A15 x=38.2m, A16, A18 x=31.5m)						
	Left floodplain		Main channel			Right floodplain	
	Wall	Bed	Left Wall	Bed	Right Wall	Bed	Wall
Series No.	*%*	*%*	*%*	*%*	*%*	*%*	*%*
A14 H=0.2532m	1.38	45.57	5.28	27.72	2.96	15.88	1.23
A15 H=0.2534m	1.26	32.47	5.91	27.41	3.35	28.28	1.32
A16 H=0.2528m	1.00	43.95	3.73	24.53	2.39	22.87	1.55
A18 H=0.2513m	1.37	36.04	12.20	25.60	7.06	16.22	1.51

	Downstream (A14 x=33.2m, A15 x=38.2m, A16, A18 x=31.5m)						
	Left floodplain		Main channel			Right floodplain	
	Wall	Bed	Left Wall	Bed	Right Wall	Bed	Wall
Series No.	*%*	*%*	*%*	*%*	*%*	*%*	*%*
A14 H=0.2977m	1.97	43.14	5.51	26.36	3.13	17.58	2.29
A15 H=0.2990m	2.18	29.74	4.90	27.68	3.09	30.30	2.10
A16 H=0.2968m	1.95	42.68	3.39	23.62	2.56	23.37	2.43
A18 H=0.2920m	1.99	35.62	11.00	26.15	7.26	15.86	2.12

Table 7.11c-Percentage shear forces on each element for downstream FCF skewed data

			Global Manning's *n* roughness coefficient		Global friction factor *f*	
Series A No.	**s**	**θ**	***Upstream***	***Downstream***	***Upstream***	***Downstream***
		°				
A14 H=0.1760m	1	5.1	0.0081	0.0081	0.0125	0.0125
A14 H=0.1981m	1	5.1	0.0092	0.0092	0.0148	0.0148
A14 H=0.2532m	1	5.1	0.0101	0.0101	0.0155	0.0155
A14 H=0.2977m	1	5.1	0.0100	0.0100	0.0140	0.0140
A15 H=0.1756m	1	9.2	0.0081	0.0080	0.0127	0.0125
A15 H=0.1978m	1	9.2	0.0092	0.0092	0.0150	0.0149
A15 H=0.2534m	1	9.2	0.0103	0.0102	0.0161	0.0159
A15 H=0.2990m	1	9.2	0.0102	0.0102	0.0146	0.0144
A16 H=0.1755m	0	5.1	0.0080	0.0080	0.0126	0.0126
A16 H=0.1984m	0	5.1	0.0092	0.0092	0.0151	0.0151
A16 H=0.2528m	0	5.1	0.0100	0.0100	0.0156	0.0156
A16 H=0.2968m	0	5.1	0.0098	0.0098	0.0137	0.0137
A17 H=0.1746m	0	2.1	0.0077	-	0.0119	-
A17 H=0.1981m	0	2.1	0.0091	-	0.0148	-
A17 H=0.2540m	0	2.1	0.0102	-	0.0160	-
A18 H=0.1755m	2	5.1	0.0078	0.0078	0.0116	0.0116
A18 H=0.1980m	2	5.1	0.0088	0.0088	0.0137	0.0137
A18 H=0.2513m	2	5.1	0.0099	0.0099	0.0148	0.0148
A18 H=0.2920m	2	5.1	0.0101	0.0101	0.0141	0.0141
Average			**0.0093**	**0.0093**	**0.0142**	**0.0141**

Table 7.12-Global Manning's *n* and Darcy-Weisbach roughness coefficients

			Upstream					
			Zonal Manning's *n* roughness coefficient			Zonal friction factor, *f*		
Series A No.	**s**	**θ**	***Left floodplain***	***Main channel***	***Right floodplain***	***Left floodplain***	***Main channel***	***Right floodplain***
		°						
A14 H=0.1760m	1	5.1	0.0047	0.0125	0.0087	0.0060	0.0227	0.0200
A14 H=0.1981m	1	5.1	0.0077	0.0124	0.0089	0.0129	0.0218	0.0171
A14 H=0.2532m	1	5.1	0.0088	0.0126	0.0090	0.0132	0.0204	0.0139
A14 H=0.2977m	1	5.1	0.0095	0.0119	0.0093	0.0137	0.0171	0.0132
A15 H=0.1756m	1	9.2	0.0055	0.0120	0.0091	0.0082	0.0213	0.0220
A15 H=0.1978m	1	9.2	0.0066	0.0126	0.0089	0.0097	0.0224	0.0172
A15 H=0.2534m	1	9.2	0.0091	0.0127	0.0094	0.0142	0.0209	0.0149
A15 H=0.2990m	1	9.2	0.0099	0.0123	0.0093	0.0152	0.0184	0.0130
A16 H=0.1755m	0	5.1	0.0076	0.0120	0.0085	0.0154	0.0213	0.0194
A16 H=0.1984m	0	5.1	0.0077	0.0126	0.0088	0.0130	0.0226	0.0167
A16 H=0.2528m	0	5.1	0.0087	0.0128	0.0091	0.0127	0.0217	0.0140
A16 H=0.2968m	0	5.1	0.0094	0.0117	0.0088	0.0135	0.0172	0.0119
A17 H=0.1746m	0	2.1	0.0083	0.0116	0.0089	0.0185	0.0199	0.0214
A17 H=0.1981m	0	2.1	0.0086	0.0120	0.0093	0.0162	0.0207	0.0187
A17 H=0.2540m	0	2.1	0.0092	0.0125	0.0096	0.0144	0.0207	0.0155
A18 H=0.1755m	2	5.1	0.0075	0.0105	0.0087	0.0146	0.0168	0.0197
A18 H=0.1980m	2	5.1	0.0079	0.0112	0.0088	0.0132	0.0183	0.0166
A18 H=0.2513m	2	5.1	0.0092	0.0116	0.0094	0.0140	0.0179	0.0147
A18 H=0.2920m	2	5.1	0.0096	0.0114	0.0094	0.0139	0.0165	0.0132
Average			**0.0082**	**0.0121**	**0.0090**	**0.0133**	**0.0199**	**0.0165**

Table 7.13a-Upstream (A14, A16, A18 x=23.2m, A15 x=28.2m, A17 x=32.4m) zonal Manning's *n* roughness coefficients

			Downstream					
			Zonal Manning's *n* roughness coefficient			Zonal friction factor, *f*		
Series A No.	**s**	**θ**	***Left floodplain***	***Main channel***	***Right floodplain***	***Left floodplain***	***Main channel***	***Right floodplain***
		°						
A14 H=0.1760m	1	5.1	0.0063	0.0118	0.0132	0.0122	0.0205	0.0389
A14 H=0.1981m	1	5.1	0.0058	0.0125	0.0137	0.0084	0.0221	0.0343
A14 H=0.2532m	1	5.1	0.0065	0.0128	0.0146	0.0082	0.0210	0.0306
A14 H=0.2977m	1	5.1	0.0067	0.0122	0.0145	0.0076	0.0182	0.0273
A15 H=0.1756m	1	9.2	0.0034	0.0121	0.0165	0.0043	0.0213	0.0589
A15 H=0.1978m	1	9.2	0.0034	0.0130	0.0149	0.0035	0.0236	0.0392
A15 H=0.2534m	1	9.2	0.0040	0.0133	0.0160	0.0039	0.0228	0.0353
A15 H=0.2990m	1	9.2	0.0044	0.0125	0.0155	0.0041	0.0190	0.0296
A16 H=0.1755m	0	5.1	0.0064	0.0118	0.0137	0.0122	0.0208	0.0429
A16 H=0.1984m	0	5.1	0.0060	0.0125	0.0135	0.0090	0.0225	0.0340
A16 H=0.2528m	0	5.1	0.0066	0.0128	0.0137	0.0083	0.0217	0.0274
A16 H=0.2968m	0	5.1	0.0069	0.0120	0.0131	0.0080	0.0179	0.0226
A17 H=0.1746m	0	2.1	-	-	-	-	-	-
A17 H=0.1981m	0	2.1	-	-	-	-	-	-
A17 H=0.2540m	0	2.1	-	-	-	-	-	-
A18 H=0.1755m	2	5.1	0.0071	0.0104	0.0142	0.0150	0.0162	0.0432
A18 H=0.1980m	2	5.1	0.0061	0.0111	0.0151	0.0091	0.0180	0.0399
A18 H=0.2513m	2	5.1	0.0067	0.0116	0.0154	0.0086	0.0180	0.0331
A18 H=0.2920m	2	5.1	0.0071	0.0114	0.0150	0.0085	0.0164	0.0283
Average			**0.0058**	**0.0121**	**0.0145**	**0.0082**	**0.0200**	**0.0353**

Table 7.13b-Downstream (A14, A16, A18 x=33.2m, A15 x=38.2m) zonal Darcy-Weisbach roughness coefficients

	Depth	ΣSF	W	-ΣSF+W	$\rho Q_{2L}U_{2L}$	$\rho Q_{1L}U_{1L}$	$\rho q_{cfL}U_{cfL}\cos\theta$	$\rho Q_{2L}U_{2L}-\rho Q_{1L}U_{1L}-\rho q_{cfL}U_{cfL}\cos\theta$	ASF_{cfL}	ASF_{cfL} per metre
Left floodplain	***m***	***N***	***N***	***N***	***N***	***N***	***N***	***N***	***N***	***N/m***
	0.176	10.71	5.72	-4.99	7.34	16.02	-2.72	-5.96	-0.97	-0.10
	0.1981	18.33	10.64	-7.69	35.69	23.51	15.63	-3.45	4.24	0.42
	0.2532	33.68	23.12	-10.57	182.06	104.21	83.53	-5.67	4.90	0.49
	0.2977	42.79	33.42	-9.37	384.19	186.53	176.89	20.77	30.14	3.01

	Depth	ΣSF	W	-ΣSF+W	$\rho Q_{2R}U_{2R}$	$\rho Q_{1R}U_{1R}$	$\rho q_{cfR}U_{cfR}\cos\theta$	$\rho Q_{2R}U_{2R}-\rho Q_{1R}U_{1R}-\rho q_{cfR}U_{cfR}\cos\theta$	ASF_{cfR}	ASF_{cfR} per metre
Right floodplain	***m***	***N***	***N***	***N***	***N***	***N***	***N***	***N***	***N***	***N/m***
	0.176	6.40	4.30	-2.10	2.69	5.62	-2.69	-0.24	1.86	0.19
	0.1981	9.30	8.00	-1.30	10.04	20.94	-9.85	-1.05	0.25	0.02
	0.2532	21.01	17.45	-3.56	55.03	114.13	-57.98	-1.11	2.45	0.24
	0.2977	30.97	25.31	-5.66	119.05	227.63	-116.20	7.62	13.28	1.33

	Depth	ΣSF	W	$-\Sigma SF+W-ASF_L-ASF_R$	$\rho Q_{2MC}U_{2MC}$	$\rho Q_{1MC}U_{1MC}$	$\rho q_{cfL}U_{cfL}\cos\theta+\rho q_{cfR}U_{cfR}\cos\theta$	$\rho Q_{2MC}U_{2MC}-Q_{1MC}U_{1MC}+\rho q_{cfL}U_{cfL}\cos\theta+\rho q_{cfR}U_{cfR}\cos\theta$	Error	Error per metre
Main channel	***m***	***N***	***N***	***N***	***N***	***N***	***N***	***N***	***N***	***N/m***
	0.176	22.59	29.64	9.88	167.24	160.70	-5.41	1.13	-8.75	-0.88
	0.1981	23.35	33.65	6.30	194.18	201.79	5.78	-1.83	-8.14	-0.81
	0.2532	29.52	43.64	11.67	375.55	359.14	25.54	41.95	30.28	3.03
	0.2977	36.68	51.70	-1.84	582.96	555.17	60.69	88.48	90.32	9.03

	Depth	F_1	F_2	ΣSF	W	$F_1-F_2-\Sigma SF+W$	ρQ_2U_2	ρQ_1U_1	$\rho Q_2U_2-\rho Q_1U_1$	Error	Error per metre
Overall	***m***	***N***	***N***	***N***	***N***	***N***	***N***	***N***	***N***	***N***	***N/m***
	0.176	296.71	296.71	39.69	39.66	-0.03	163.16	174.31	-11.15	-11.12	-1.11
	0.1981	391.05	391.05	52.29	52.29	0.00	230.75	236.13	-5.38	-5.38	-0.54
	0.2532	748.01	748.01	84.19	84.21	0.02	604.35	565.40	38.95	38.94	3.89
	0.2977	1166.67	1166.67	110.39	110.43	0.04	1075.88	961.25	114.63	114.59	11.46

Table 7.14a-Force-momentum balance for FCF skew data series A14, s=1:1, θ=5.1° ignoring all hydrostatic forces in the zonal analysis. Unadjusted velocity and β=1

	Depth	ΣSF	W	-ΣSF+W	$\rho Q_{2L}U_{2L}$	$\rho Q_{1L}U_{1L}$	$\rho q_{cfL}U_{cfL}\cos\theta$	$\rho Q_{2L}U_{2L}-\rho Q_{1L}U_{1L}-\rho q_{cfL}U_{cfL}\cos\theta$	ASF_{cfL}	ASF_{cfL} per metre
Left floodplain	***m***	***N***	***N***	***N***	***N***	***N***	***N***	***N***	***N***	***N/m***
	0.176	8.70	5.88	-2.82	8.20	15.40	-1.50	-5.70	-2.88	-0.29
	0.1981	18.32	11.07	-7.25	40.30	26.80	16.00	-2.50	4.75	0.48
	0.2532	31.23	22.39	-8.84	185.70	125.70	69.40	-9.40	-0.56	-0.06
	0.2977	43.31	33.96	-9.35	398.10	240.80	154.00	3.30	12.65	1.27

	Depth	ΣSF	W	-ΣSF+W	$\rho Q_{2R}U_{2R}$	$\rho Q_{1R}U_{1R}$	$\rho q_{cfR}U_{cfR}\cos\theta$	$\rho Q_{2R}U_{2R}-\rho Q_{1R}U_{1R}-\rho q_{cfR}U_{cfR}\cos\theta$	ASF_{cfR}	ASF_{cfR} per metre
Right Floodplain	***m***	***N***	***N***	***N***	***N***	***N***	***N***	***N***	***N***	***N/m***
	0.176	5.24	4.41	-0.83	2.90	5.90	-2.70	-0.30	0.53	0.05
	0.1981	10.63	8.32	-2.31	13.90	23.70	-9.60	-0.20	2.11	0.21
	0.2532	17.54	16.90	-0.64	67.60	132.90	-60.30	-5.00	-4.36	-0.44
	0.2977	31.30	25.73	-5.57	153.00	300.30	-135.70	-11.60	-6.03	-0.60

Table 7.14b-Force-momentum balance for FCF skew data series A14, s=1:1, $\theta=5.1^{o}$ Elliott & Sellin's (1990) results

	Depth	ΣSF	W	-ΣSF+W	$\rho Q_{2L}U_{2L}$	$\rho Q_{1L}U_{1L}$	$\rho q_{cfL}U_{cfL}\cos\theta$	$\rho Q_{2L}U_{2L}-\rho Q_{1L}U_{1L}-\rho q_{cfL}U_{cfL}\cos\theta$	ASF_{cfL}	ASF_{cfL} per metre
	m	*N*	*N*	*N*	*N*	*N*	*N*	*N*	*N*	*N/m*
Left floodplain	0.1756	11.30	3.94	-7.36	9.16	4.91	9.60	-5.36	2.00	0.20
	0.1978	16.61	7.41	-9.20	40.32	14.66	35.30	-9.64	-0.44	-0.04
	0.2534	26.02	16.32	-9.71	169.98	44.70	141.21	-15.93	-6.22	-0.62
	0.299	32.47	23.85	-8.62	312.57	81.30	252.52	-21.25	-12.63	-1.26

	Depth	ΣSF	W	-ΣSF+W	$\rho Q_{2R}U_{2R}$	$\rho Q_{1R}U_{1R}$	$\rho q_{cfR}U_{cfR}\cos\theta$	$\rho Q_{2R}U_{2R}-\rho Q_{1R}U_{1R}-\rho q_{cfR}U_{cfR}\cos\theta$	ASF_{cfR}	ASF_{cfR} per metre
	m	*N*	*N*	*N*	*N*	*N*	*N*	*N*	*N*	*N/m*
Right floodplain	0.1756	7.65	5.92	-1.72	2.31	6.96	-4.08	-0.58	1.15	0.11
	0.1978	14.00	11.12	-2.88	10.22	31.52	-17.28	-4.03	-1.14	-0.11
	0.2534	29.05	24.33	-4.71	53.59	163.96	-98.09	-12.28	-7.57	-0.76
	0.299	41.85	35.41	-6.44	119.10	372.31	-218.59	-34.62	-28.18	-2.82

	Depth	ΣSF	W	$-\Sigma SF+W-ASF_L-ASF_R$	$\rho Q_{2MC}U_{2MC}$	$\rho Q_{1MC}U_{1MC}$	$\rho q_{cfL}U_{cfL}\cos\theta+\rho q_{cfR}U_{cfR}\cos\theta$	$\rho Q_{2MC}U_{2MC}-\rho Q_{1MC}U_{1MC}+\rho q_{cfL}U_{cfL}\cos\theta+\rho q_{cfR}U_{cfR}\cos\theta$	Error	Error per metre
	m	*N*	*N*	*N*	*N*	*N*	*N*	*N*	*N*	*N/m*
Main channel	0.1756	20.53	29.57	8.18	161.70	164.27	5.52	2.95	-5.23	-0.52
	0.1978	21.52	33.59	11.37	191.97	205.20	18.02	4.79	-6.57	-0.66
	0.2534	29.27	43.67	13.06	333.54	361.18	43.12	15.48	2.42	0.24
	0.299	36.90	51.94	-0.51	530.11	553.78	33.93	10.26	10.77	1.08

	Depth	F_1	F_2	ΣSF	W	$F_1-F_2-\Sigma SF+W$	ρQ_2U_2	ρQ_1U_1	$\rho Q_2U_2-\rho Q_1U_1$	Error	Error per metre
	m	*N*	*N*	*N*	*N*	*N*	*N*	*N*	*N*	*N*	*N/m*
Overall	0.1756	295.25	295.25	39.43	39.43	0.00	160.88	163.36	-2.48	-2.49	-0.25
	0.1978	389.59	389.59	52.10	52.12	0.02	237.98	240.94	-2.97	-2.98	-0.30
	0.2534	749.63	749.63	84.30	84.32	0.02	563.97	561.92	2.05	2.03	0.20
	0.299	1180.70	1180.70	111.17	111.20	0.03	989.82	1001.88	-12.06	-12.09	-1.21

Table 7.15a-Force-momentum balance for FCF skew data series A15, s=1:1, $\theta=9.2^{o}$ ignoring all hydrostatic forces in the zonal analysis. unadjusted velocity and $\beta=1$

	Depth	ΣSF	W	-ΣSF+W	$\rho Q_{2L}U_{2L}$	$\rho Q_{1L}U_{1L}$	$\rho q_{cfL}U_{cfL}\cos\theta$	$\rho Q_{2L}U_{2L}-\rho Q_{1L}U_{1L}-\rho q_{cfL}U_{cfL}\cos\theta$	ASF_{cfL}	ASF_{cfL} per metre
	m	*N*	*N*	*N*	*N*	*N*	*N*	*N*	*N*	*N/m*
Left floodplain	0.1756	10.00	3.70	-6.30	10.30	5.30	9.90	-4.90	1.40	0.14
	0.1978	16.82	6.98	-9.84	43.70	16.00	36.40	-8.70	1.14	0.11
	0.2534	22.63	14.19	-8.44	180.50	62.40	131.60	-13.50	-5.06	-0.51
	0.299	29.51	21.63	-7.88	348.10	122.90	244.00	-18.80	-10.92	-1.09

	Depth	ΣSF	W	-ΣSF+W	$\rho Q_{2R}U_{2R}$	$\rho Q_{1R}U_{1R}$	$\rho q_{cfR}U_{cfR}\cos\theta$	$\rho Q_{2R}U_{2R}-\rho Q_{1R}U_{1R}-\rho q_{cfR}U_{cfR}\cos\theta$	ASF_{cfR}	ASF_{cfR} per metre
	m	*N*	*N*	*N*	*N*	*N*	*N*	*N*	*N*	*N/m*
Right floodplain	0.1756	6.82	5.56	-1.26	3.30	7.70	-4.00	-0.40	0.86	0.09
	0.1978	14.28	10.47	-3.81	15.20	31.80	-15.90	-0.70	3.11	0.31
	0.2534	25.34	21.17	-4.17	87.80	179.20	-91.90	0.50	4.67	0.47
	0.299	38.02	32.10	-5.92	210.40	419.00	-207.60	-1.00	4.92	0.49

Table 7.15b-Force-momentum balance for FCF skew data series A15, s=1:1, θ=9.2° Elliott & Sellin's (1990) results

	Depth	ΣSF	W	-ΣSF+W	$\rho Q_{2L} U_{2L}$	$\rho Q_{1L} U_{1L}$	$\rho Q_{cfL} U_{cfL} \cos\theta$	$\rho Q_{2L} U_{2L} - \rho Q_{1L} U_{1L} - \rho q_{cfL} U_{cfL} \cos\theta$	ASF_{cfL}	ASF_{cfL} per metre
	m	*N*	*N*	*N*	*N*	*N*	*N*	*N*	*N*	*N/m*
Left floodplain	0.1755	11.39	6.00	-5.39	8.10	6.27	3.98	-2.15	3.24	0.32
	0.1984	21.42	11.44	-9.98	38.61	26.43	17.33	-5.16	4.82	0.48
	0.2528	34.77	24.58	-10.19	192.01	124.33	71.67	-4.00	6.19	0.62
	0.2968	46.29	35.42	-10.87	372.41	206.77	157.77	7.88	18.75	1.87

	Depth	ΣSF	W	-ΣSF+W	$\rho Q_{2R} U_{2R}$	$\rho Q_{1R} U_{1R}$	$\rho Q_{cfR} U_{cfR} \cos\theta$	$\rho Q_{2R} U_{2R} - \rho Q_{1R} U_{1R} - \rho q_{cfR} U_{cfR} \cos\theta$	ASF_{cfR}	ASF_{cfR} per metre
	m	*N*	*N*	*N*	*N*	*N*	*N*	*N*	*N*	*N/m*
Right floodplain	0.1755	7.58	4.60	-2.98	2.66	5.79	-2.76	-0.37	2.60	0.26
	0.1984	12.68	8.78	-3.90	11.62	23.98	-10.88	-1.48	2.42	0.24
	0.2528	23.79	18.94	-4.85	65.36	131.93	-59.67	-6.90	-2.04	-0.20
	0.2968	34.27	27.37	-6.90	145.85	276.46	-126.00	-4.61	2.29	0.23

	Depth	ΣSF	W	$-\Sigma SF+W-ASF_L-ASF_R$	$\rho Q_{2MC} U_{2MC}$	$\rho Q_{1MC} U_{1MC}$	$\rho q_{cfL} U_{cfL} \cos\theta + \rho q_{cfR} U_{cfR} \cos\theta$	$\rho Q_{2MC} U_{2MC} - \rho Q_{1MC} U_{1MC} + \rho q_{cfL} U_{cfL} \cos\theta + \rho q_{cfR} U_{cfR} \cos\theta$	Error	Error per metre
	m	*N*	*N*	*N*	*N*	*N*	*N*	*N*	*N*	*N/m*
Main channel	0.1755	18.18	26.51	7.70	148.91	142.59	1.22	7.54	-0.16	-0.02
	0.1984	19.61	29.97	7.97	171.04	170.76	6.45	6.73	-1.24	-0.12
	0.2528	23.17	38.19	6.79	295.33	298.00	12.00	9.33	2.55	0.25
	0.2968	27.11	44.84	1.28	453.84	453.84	31.76	31.76	30.48	3.05

	Depth	F_1	F_2	ΣSF	W	$F_1-F_2-\Sigma SF+W$	$\rho Q_2 U_2$	$\rho Q_1 U_1$	$\rho Q_2 U_2 - \rho Q_1 U_1$	Error	Error per metre
	m	*N*	*N*	*N*	*N*	*N*	*N*	*N*	*N*	*N*	*N/m*
Overall	0.1755	239.72	239.72	37.11	37.11	0.00	145.53	142.79	2.74	2.74	0.27
	0.1984	337.36	337.36	50.17	50.20	0.03	212.56	213.10	-0.54	-0.56	-0.06
	0.2528	689.62	689.62	81.69	81.71	0.02	548.24	551.53	-3.29	-3.31	-0.33
	0.2968	1101.86	1101.86	107.62	107.63	0.01	967.86	930.36	37.51	37.50	3.75

Table 7.16-Force-momentum balance for FCF skew data series A16, s=0, θ=5.1^{o} ignoring all hydrostatic forces in the zonal analysis. Unadjusted velocity and β=1

	Depth	ΣSF	W	-ΣSF+W	$\rho Q_{2L} U_{2L}$	$\rho Q_{1L} U_{1L}$	$\rho q_{cfL} U_{cfL} \cos\theta$	$\rho Q_{2L} U_{2L} - \rho Q_{1L} U_{1L} - \rho q_{cfL} U_{cfL} \cos\theta$	ASF_{cfL}	ASF_{cfL} per metre
	m	*N*	*N*	*N*	*N*	*N*	*N*	*N*	*N*	*N/m*
Left floodplain	0.1755	9.79	5.61	-4.18	5.49	5.52	2.23	-2.26	1.92	0.19
	0.198	17.34	10.62	-6.72	33.98	22.70	17.63	-6.35	0.37	0.04
	0.2513	31.56	22.68	-8.88	163.46	97.36	76.55	-10.44	-1.56	-0.16
	0.292	40.31	32.09	-8.23	322.06	195.14	137.28	-10.36	-2.13	-0.21

	Depth	ΣSF	W	-ΣSF+W	$\rho Q_{2R} U_{2R}$	$\rho Q_{1R} U_{1R}$	$\rho q_{cfR} U_{cfR} \cos\theta$	$\rho Q_{2R} U_{2R} - \rho Q_{1R} U_{1R} - \rho q_{cfR} U_{cfR} \cos\theta$	ASF_{cfR}	ASF_{cfR} per metre
	m	*N*	*N*	*N*	*N*	*N*	*N*	*N*	*N*	*N/m*
Right floodplain	0.1755	5.86	4.21	-1.65	2.22	4.82	-2.46	-0.14	1.51	0.15
	0.198	9.97	7.98	-1.99	8.86	21.36	-11.90	-0.60	1.38	0.14
	0.2513	19.89	17.12	-2.77	47.44	109.65	-60.99	-1.22	1.55	0.15
	0.292	28.08	24.29	-3.79	106.56	243.57	-132.36	-4.64	-0.85	-0.08

	Depth	ΣSF	W	$-\Sigma SF+W-ASF_L-ASF_R$	$\rho Q_{2MC} U_{2MC}$	$\rho Q_{1MC} U_{1MC}$	$\rho q_{cfL} U_{cfL} \cos\theta + \rho q_{cfR} U_{cfR} \cos\theta$	$\rho Q_{2MC} U_{2MC} - \rho Q_{1MC} U_{1MC} + \rho q_{cfL} U_{cfL} \cos\theta + \rho q_{cfR} U_{cfR} \cos\theta$	Error	Error per metre
	m	*N*	*N*	*N*	*N*	*N*	*N*	*N*	*N*	*N/m*
Main channel	0.1755	26.00	30.68	4.27	204.28	193.52	-0.23	10.52	6.25	0.63
	0.198	27.17	34.76	8.61	252.12	243.88	5.74	13.97	5.37	0.54
	0.2513	33.94	44.43	13.60	428.99	427.71	15.56	16.83	3.24	0.32
	0.292	40.95	51.80	12.14	646.03	652.27	4.92	-1.32	-13.45	-1.35

	Depth	F_1	F_2	ΣSF	W	$F_1-F_2-\Sigma SF+W$	$\rho Q_2 U_2$	$\rho Q_1 U_1$	$\rho Q_2 U_2 - \rho Q_1 U_1$	Error	Error per metre
	m	*N*	*N*	*N*	*N*	*N*	*N*	*N*	*N*	*N*	*N/m*
Overall	0.1755	322.47	322.47	41.64	40.51	-1.13	199.69	195.78	3.91	5.04	0.50
	0.198	418.15	418.15	54.49	53.37	-1.13	288.02	282.94	5.08	6.21	0.62
	0.2513	760.34	760.34	85.35	84.23	-1.12	639.45	635.75	3.70	4.83	0.48
	0.292	1133.99	1133.99	109.30	108.18	-1.12	1077.19	1096.16	-18.97	-17.85	-1.78

Table 7.17-Force-momentum balance for FCF skew data series A18, s=0, $\theta=2.1^{o}$ ignoring all hydrostatic forces in the zonal analysis. unadjusted velocity and $\beta=1$

	Depth	ΣSF	W	-ΣSF+W	$\rho Q_{2L} U_{2L}$	$\rho Q_{1L} U_{1L}$	$\rho q_{cfL} U_{cfL} \cos\theta$	$\rho Q_{2L} U_{2L} - \rho Q_{1L} U_{1L} - \rho q_{cfL} U_{cfL} \cos\theta$	ASF_{cfL}	ASF_{cfL} per metre
	m	*N*	*N*	*N*	*N*	*N*	*N*	*N*	*N*	*N/m*
Left floodplain	0.176	10.71	5.72	-4.99	7.79	15.89	-2.27	-5.83	-0.84	-0.08
	0.1981	18.33	10.64	-7.69	38.83	25.00	16.67	-2.84	4.85	0.49
	0.2532	33.68	23.12	-10.57	181.64	111.13	78.76	-8.25	2.31	0.23
	0.2977	42.79	33.42	-9.37	400.56	217.67	166.48	16.41	25.78	2.58

	Depth	ΣSF	W	-ΣSF+W	$\rho Q_{2R} U_{2R}$	$\rho Q_{1R} U_{1R}$	$\rho q_{cfR} U_{cfR} \cos\theta$	$\rho Q_{2R} U_{2R} - \rho Q_{1R} U_{1R} - \rho q_{cfR} U_{cfR} \cos\theta$	ASF_{cfR}	ASF_{cfR} per metre
	m	*N*	*N*	*N*	*N*	*N*	*N*	*N*	*N*	*N/m*
Right floodplain	0.176	6.40	4.30	-2.10	2.85	5.58	-2.58	-0.15	1.96	0.20
	0.1981	9.30	8.00	-1.30	10.92	22.26	-10.02	-1.32	-0.02	0.00
	0.2532	21.01	17.45	-3.56	54.90	121.70	-62.19	-4.61	-1.05	-0.10
	0.2977	30.97	25.31	-5.66	124.12	265.63	-134.25	-7.25	-1.59	-0.16

	Depth	ΣSF	W	$-\Sigma SF+W-ASF_L-ASF_R$	$\rho Q_{2MC} U_{2MC}$	$\rho Q_{1MC} U_{1MC}$	$\rho\theta Q_{cfL} U_{cfL} \cos\theta + \rho q_{cfR} U_{cfR} \cos\theta$	$\rho Q_{2MC} U_{2MC} - \rho Q_{1MC} U_{1MC} + \rho q_{cfL} U_{cfL} \cos\theta + \rho q_{cfR} U_{cfR} \cos\theta$	Error	Error per metre
	m	*N*	*N*	*N*	*N*	*N*	*N*	*N*	*N*	*N/m*
Main channel	0.176	22.59	29.64	9.85	177.32	159.49	-4.86	12.97	3.13	0.31
	0.1981	23.35	33.65	5.43	211.23	214.52	6.66	3.37	-2.06	-0.21
	0.2532	29.52	43.64	10.76	374.67	382.98	16.57	8.26	-2.50	-0.25
	0.2977	36.68	51.70	-12.35	607.79	647.84	32.22	-7.83	4.52	0.45

	Depth	F_1	F_2	ΣSF	W	$F_1-F_2-\Sigma SF+W$	$\rho Q_2 U_2$	$\rho Q_1 U_1$	$\rho Q_2 U_2 - \rho Q_1 U_1$	Error	Error per metre
	m	*N*	*N*	*N*	*N*	*N*	*N*	*N*	*N*	*N*	*N/m*
Overall	0.176	296.71	296.71	39.69	39.66	-0.03	172.78	172.78	0.00	0.03	0.00
	0.1981	391.05	391.05	52.29	52.29	0.00	250.90	250.90	0.00	0.00	0.00
	0.2532	748.01	748.01	84.19	84.21	0.02	602.79	602.79	0.00	-0.02	0.00
	0.2977	1166.67	1166.67	110.39	110.43	0.04	1122.31	1122.31	0.00	-0.04	0.00

Table 7.18a-Force-momentum balance for FCF skew data series A14, s=1:1, θ=5.1^o ignoring all hydrostatic forces in the zonal analysis. adjusted velocity and β=1

	Depth	ΣSF	W	-ΣSF+W	$\rho Q_{2L}U_{2L}$	$\rho Q_{1L}U_{1L}$	$\rho q_{cfL}U_{cfL}\cos\theta$	$\rho Q_{2L}U_{2L}-\rho Q_{1L}U_{1L}-\rho q_{cfL}U_{cfL}\cos\theta$	ASF_{cfL}	ASF_{cfL} per metre
	m	*N*	*N*	*N*	*N*	*N*	*N*	*N*	*N*	*N/m*
Left floodplain	0.176	8.70	5.88	-2.82	8.20	15.40	-1.50	-5.70	-2.88	-0.29
	0.1981	18.32	11.07	-7.25	40.30	26.80	16.00	-2.50	4.75	0.48
	0.2532	31.23	22.39	-8.84	185.70	125.70	69.40	-9.40	-0.56	-0.06
	0.2977	43.31	33.96	-9.35	398.10	240.80	154.00	3.30	12.65	1.27

	Depth	ΣSF	W	-ΣSF+W	$\rho Q_{2R}U_{2R}$	$\rho Q_{1R}U_{1R}$	$\rho q_{cfR}U_{cfR}\cos\theta$	$\rho Q_{2R}U_{2R}-\rho Q_{1R}U_{1R}-\rho q_{cfR}U_{cfR}\cos\theta$	ASF_{cfR}	ASF_{cfR} per metre
	m	*N*	*N*	*N*	*N*	*N*	*N*	*N*	*N*	*N/m*
Right floodplain	0.176	5.24	4.41	-0.83	2.90	5.90	-2.70	-0.30	0.53	0.05
	0.1981	10.63	8.32	-2.31	13.90	23.70	-9.60	-0.20	2.11	0.21
	0.2532	17.54	16.90	-0.64	67.60	132.90	-60.30	-5.00	-4.36	-0.44
	0.2977	31.30	25.73	-5.57	153.00	300.30	-135.70	-11.60	-6.03	-0.60

Table 7.18b-Force-momentum balance for FCF skew data series A14, s=1:1, θ=5.1° Elliott & Sellin's (1990) results

	Depth	ΣSF	W	- ΣSF +W	$\rho Q_{2L}U_{2L}$	$\rho Q_{1L}U_{1L}$	$\rho Q_{cfL}U_{cfL}\cos\theta$	$\rho Q_{2L}U_{2L}-\rho Q_{1L}U_{1L}-\rho q_{cfL}U_{cfL}\cos\theta$	ASF_{cfL}	ASF_{cfL} per metre
	m	*N*	*N*	*N*	*N*	*N*	*N*	*N*	*N*	*N/m*
Left floodplain	0.1756	11.30	3.94	-7.36	9.59	5.07	9.88	-5.36	2.00	0.20
	0.1978	16.61	7.41	-9.20	41.42	14.87	35.90	-9.35	-0.16	-0.02
	0.2534	26.02	16.32	-9.71	176.29	46.53	143.69	-13.93	-4.22	-0.42
	0.299	32.47	23.85	-8.62	346.20	88.96	266.49	-9.26	-0.64	-0.06

	Depth	ΣSF	W	- ΣSF +W	$\rho Q_{2R}U_{2R}$	$\rho Q_{1R}U_{1R}$	$\rho Q_{cfR}U_{cfR}\cos\theta$	$\rho Q_{2R}U_{2R}-\rho Q_{1R}U_{1R}-\rho q_{cfR}U_{cfR}\cos\theta$	ASF_{cfR}	ASF_{cfR} per metre
	m	*N*	*N*	*N*	*N*	*N*	*N*	*N*	*N*	*N/m*
Right floodplain	0.1756	7.65	5.92	-1.72	2.43	7.18	-4.12	-0.63	1.09	0.11
	0.1978	14.00	11.12	-2.88	10.80	31.99	-17.31	-3.88	-1.00	-0.10
	0.2534	29.05	24.33	-4.71	54.51	170.67	-100.24	-15.92	-11.21	-1.12
	0.299	41.85	35.41	-6.44	127.98	407.40	-227.43	-51.99	-45.55	-4.56

	Depth	ΣSF	W	- ΣSF +W-ASF_L-ASF_R	$\rho Q_{2MC}U_{2MC}$	$\rho Q_{1MC}U_{1MC}$	$\rho Q_{cfL}U_{cfL}\cos\theta+\rho Q_{cfR}U_{cfR}\cos\theta$	$\rho Q_{2MC}U_{2MC}-\rho Q_{1MC}U_{1MC}+\rho q_{cfL}U_{cfL}\cos\theta+\rho q_{cfR}U_{cfR}\cos\theta$	Error	Error per metre
	m	*N*	*N*	*N*	*N*	*N*	*N*	*N*	*N*	*N/m*
Main channel	0.1756	20.53	29.57	8.13	169.30	169.37	5.77	5.69	-2.44	-0.24
	0.1978	21.52	33.59	11.23	197.24	208.23	18.60	7.60	-3.63	-0.36
	0.2534	29.27	43.67	7.41	345.94	375.97	43.45	13.42	6.01	0.60
	0.299	36.90	51.94	-29.88	587.14	605.97	39.06	20.23	50.11	5.01

	Depth	F_1	F_2	ΣSF	W	$F_1-F_2-\Sigma SF+W$	ρQ_2U_2	ρQ_1U_1	$\rho Q_2U_2-\rho Q_1U_1$	Error	Error per metre
	m	*N*	*N*	*N*	*N*	*N*	*N*	*N*	*N*	*N*	*N/m*
Overall	0.1756	295.25	295.25	39.43	39.43	0.00	168.46	168.46	0.00	0.00	0.00
	0.1978	389.59	389.59	52.10	52.12	0.02	244.72	244.72	0.00	-0.02	0.00
	0.2534	749.63	749.63	84.30	84.32	0.02	583.63	583.63	0.00	-0.02	0.00
	0.299	1180.70	1180.70	111.17	111.20	0.03	1096.90	1096.90	0.00	-0.03	0.00

Table 7.19a-Force-momentum balance for FCF skew data series A15, s=1:1, $\theta=9.2^{o}$ ignoring all hydrostatic forces in the zonal analysis. Adjusted velocity and $\beta=1$

	Depth	ΣSF	W	-ΣSF+W	$\rho Q_{2L}U_{2L}$	$\rho Q_{1L}U_{1L}$	$\rho q_{cfL}U_{cfL}\cos\theta$	$\rho Q_{2L}U_{2L}-\rho Q_{1L}U_{1L}-\rho q_{cfL}U_{cfL}\cos\theta$	ASF_{cfL}	ASF_{cfL} per metre
	m	*N*	*N*	*N*	*N*	*N*	*N*	*N*	*N*	*N/m*
Left floodplain	0.1756	10.00	3.70	-6.30	10.30	5.30	9.90	-4.90	1.40	0.14
	0.1978	16.82	6.98	-9.84	43.70	16.00	36.40	-8.70	1.14	0.11
	0.2534	22.63	14.19	-8.44	180.50	62.40	131.60	-13.50	-5.06	-0.51
	0.299	29.51	21.63	-7.88	348.10	122.90	244.00	-18.80	-10.92	-1.09

	Depth	ΣSF	W	-ΣSF+W	$\rho Q_{2R}U_{2R}$	$\rho Q_{1R}U_{1R}$	$\rho q_{cfR}U_{cfR}\cos\theta$	$\rho Q_{2R}U_{2R}-\rho Q_{1R}U_{1R}-\rho q_{cfR}U_{cfR}\cos\theta$	ASF_{cfR}	ASF_{cfR} per metre
	m	*N*	*N*	*N*	*N*	*N*	*N*	*N*	*N*	*N/m*
Right floodplain	0.1756	6.82	5.56	-1.26	3.30	7.70	-4.00	-0.40	0.86	0.09
	0.1978	14.28	10.47	-3.81	15.20	31.80	-15.90	-0.70	3.11	0.31
	0.2534	25.34	21.17	-4.17	87.80	179.20	-91.90	0.50	4.67	0.47
	0.299	38.02	32.10	-5.92	210.40	419.00	-207.60	-1.00	4.92	0.49

Table 7.19b-Force-momentum balance for FCF skew data series A15, s=1:1, θ=9.2° Elliott & Sellin's (1990) results

	Depth	ΣSF	W	-ΣSF+W	$\rho Q_{2L}U_{2L}$	$\rho Q_{1L}U_{1L}$	$\rho Q_{cfL}U_{cfL}\cos\theta$	$\rho Q_{2L}U_{2L}-\rho Q_{1L}U_{1L}-\rho q_{cfL}U_{cfL}\cos\theta$	ASF_{cfL}	ASF_{cfL} per metre
	m	*N*	*N*	*N*	*N*	*N*	*N*	*N*	*N*	*N/m*
Left floodplain	0.1755	11.39	6.00	-5.39	8.11	6.40	3.88	-2.17	3.22	0.32
	0.1984	21.42	11.44	-9.98	39.81	27.19	17.65	-5.03	4.95	0.50
	0.2528	34.77	24.58	-10.19	192.70	124.03	72.24	-3.57	6.62	0.66
	0.2968	46.29	35.42	-10.87	408.01	235.67	159.77	12.58	23.45	2.35

	Depth	ΣSF	W	-ΣSF+W	$\rho Q_{2R}U_{2R}$	$\rho Q_{1R}U_{1R}$	$\rho Q_{cfR}U_{cfR}\cos\theta$	$\rho Q_{2R}U_{2R}-\rho Q_{1R}U_{1R}-\rho q_{cfR}U_{cfR}\cos\theta$	ASF_{cfR}	ASF_{cfR} per metre
	m	*N*	*N*	*N*	*N*	*N*	*N*	*N*	*N*	*N/m*
Right floodplain	0.1755	7.58	4.60	-2.98	2.66	5.91	-2.82	-0.43	2.55	0.25
	0.1984	12.68	8.78	-3.90	11.98	24.66	-11.02	-1.66	2.24	0.22
	0.2528	23.79	18.94	-4.85	65.59	131.61	-59.38	-6.64	-1.79	-0.18
	0.2968	34.27	27.37	-6.90	159.79	315.10	-138.07	-17.24	-10.34	-1.03

	Depth	ΣSF	W	$-\Sigma SF+W-ASF_L-ASF_R$	$\rho Q_{2MC}U_{2MC}$	$\rho Q_{1MC}U_{1MC}$	$\rho Q_{cfL}U_{cfL}\cos\theta+\rho Q_{cfR}U_{cfR}\cos\theta$	$\rho Q_{2MC}U_{2MC}-\rho Q_{1MC}U_{1MC}+\rho q_{cfL}U_{cfL}\cos\theta+\rho q_{cfR}U_{cfR}\cos\theta$	Error	Error per metre
	m	*N*	*N*	*N*	*N*	*N*	*N*	*N*	*N*	*N/m*
Main channel	0.1755	18.18	26.51	7.66	149.22	145.63	1.07	4.65	-3.01	-0.30
	0.1984	19.61	29.97	7.65	176.35	175.62	6.63	7.36	-0.29	-0.03
	0.2528	23.17	38.19	6.62	296.39	297.28	12.86	11.97	5.35	0.53
	0.2968	27.11	44.84	-16.06	497.22	517.27	21.70	1.65	17.71	1.77

	Depth	F_1	F_2	ΣSF	W	$F_1-F_2-\Sigma SF+W$	ρQ_2U_2	ρQ_1U_1	$\rho Q_2U_2-\rho Q_1U_1$	Error	Error per metre
	m	*N*	*N*	*N*	*N*		*N*	*N*	*N*	*N*	*N/m*
Overall	0.1755	239.72	239.72	37.11	37.11	0.00	145.80	145.80	0.00	0.00	0.00
	0.1984	337.36	337.36	50.17	50.20	0.03	219.12	219.12	0.00	-0.03	0.00
	0.2528	689.62	689.62	81.69	81.71	0.02	550.51	550.51	0.00	-0.02	0.00
	0.2968	1101.86	1101.86	107.62	107.63	0.01	1060.24	1060.24	0.00	-0.01	0.00

Table 7.20-Force-momentum balance for FCF skew data series A16, s=0, $\theta=5.1^{o}$ ignoring all hydrostatic forces in the zonal analysis. Adjusted velocity and $\beta=1$

	Depth	ΣSF	W	-ΣSF+W	$\rho Q_{2L}U_{2L}$	$\rho Q_{1L}U_{1L}$	$\rho Q_{cfL}U_{cfL}\cos\theta$	$\rho Q_{2L}U_{2L}-\rho Q_{1L}U_{1L}-\rho q_{cfL}U_{cfL}\cos\theta$	ASF_{cfL}	ASF_{cfL} per metre
	m	*N*	*N*	*N*	*N*	*N*	*N*	*N*	*N*	*N/m*
Left floodplain	0.1755	9.79	5.61	-4.18	6.07	6.22	2.25	-2.40	1.78	0.18
	0.198	17.34	10.62	-6.72	35.63	24.23	17.74	-6.34	0.38	0.04
	0.2513	31.56	22.68	-8.88	167.39	100.28	77.08	-9.97	-1.09	-0.11
	0.292	40.31	32.09	-8.23	330.29	196.66	141.11	-7.48	0.75	0.08

	Depth	ΣSF	W	-ΣSF+W	$\rho Q_{2R}U_{2R}$	$\rho Q_{1R}U_{1R}$	$\rho Q_{cfR}U_{cfR}\cos\theta$	$\rho Q_{2R}U_{2R}-\rho Q_{1R}U_{1R}-\rho q_{cfR}U_{cfR}\cos\theta$	ASF_{cfR}	ASF_{cfR} per metre
	m	*N*	*N*	*N*	*N*	*N*	*N*	*N*	*N*	*N/m*
Right floodplain	0.1755	5.86	4.21	-1.65	2.45	5.44	-2.64	-0.34	1.31	0.13
	0.198	9.97	7.98	-1.99	9.29	22.80	-12.39	-1.12	0.87	0.09
	0.2513	19.89	17.12	-2.77	48.58	112.94	-62.07	-2.28	0.48	0.05
	0.292	28.08	24.29	-3.79	109.28	245.46	-131.72	-4.46	-0.67	-0.07

	Depth	ΣSF	W	$-\Sigma SF+W-ASF_L-ASF_R$	$\rho Q_{2MC}U_{2MC}$	$\rho Q_{1MC}U_{1MC}$	$\rho Q_{cfL}U_{cfL}\cos\theta+\rho Q_{cfR}U_{cfR}\cos\theta$	$\rho Q_{2MC}U_{2MC}-\rho Q_{1MC}U_{1MC}+\rho q_{cfL}U_{cfL}\cos\theta+\rho q_{cfR}U_{cfR}\cos\theta$	Error	Error per metre
	m	*N*	*N*	*N*	*N*	*N*	*N*	*N*	*N*	*N/m*
Main channel	0.1755	26.00	30.68	4.21	226.02	218.40	-0.39	7.23	3.02	0.30
	0.198	27.17	34.76	8.08	264.33	260.29	5.35	9.40	1.31	0.13
	0.2513	33.94	44.43	12.06	439.28	440.52	15.01	13.77	1.70	0.17
	0.292	40.95	51.80	9.44	662.53	657.35	9.39	14.57	5.13	0.51

	Depth	F_1	F_2	ΣSF	W	$F_1-F_2-\Sigma SF+W$	ρQ_2U_2	ρQ_1U_1	$\rho Q_2U_2-\rho Q_1U_1$	Error	Error per metre
	m	*N*	*N*	*N*	*N*	*N*	*N*	*N*	*N*	*N*	*N/m*
Overall	0.1755	322.47	322.47	41.64	40.51	-1.13	208.37	208.37	0.00	1.13	0.11
	0.198	418.15	418.15	54.49	53.37	-1.13	293.60	293.60	0.00	1.13	0.11
	0.2513	760.34	760.34	85.35	84.23	-1.12	646.02	646.02	0.00	1.12	0.11
	0.292	1133.99	1133.99	109.30	108.18	-1.12	1093.66	1093.66	0.00	1.12	0.11

Table 7.21-Force-momentum balance for FCF skew data series A18, s=0, $\theta=2.1^{o}$ ignoring all hydrostatic forces in the zonal analysis. Unadjusted velocity and $\beta=1$

	Depth	ΣSF	W	-ΣSF+W	$\rho\beta_{2L}Q_{2L}U_{2L}$	$\rho\beta_{1L}Q_{1L}U_{1L}$	$\rho q_{cfL}U_{cfL}\cos\theta$	$\rho\beta_{2R}Q_{2L}U_{2L}-\rho\beta_{1L}Q_{1L}U_{1L}-\rho q_{cfL}U_{cfL}\cos\theta$	ASF_{cfL}	ASF_{cfL} per metre
	m	*N*	*N*	*N*	*N*	*N*	*N*	*N*	*N*	*N/m*
Left floodplain	0.176	10.71	5.72	-4.99	8.88	18.31	-2.27	-7.16	-2.17	-0.22
	0.1981	18.33	10.64	-7.69	44.61	28.43	16.67	-0.49	7.20	0.72
	0.2532	33.68	23.12	-10.57	189.24	135.36	78.76	-24.88	-14.31	-1.43
	0.2977	42.79	33.42	-9.37	436.24	294.34	166.48	-24.57	-15.20	-1.52

	Depth	ΣSF	W	-ΣSF+W	$\rho\beta_{2R}Q_{2R}U_{2R}$	$\rho\beta_{1R}Q_{1R}U_{1R}$	$\rho q_{cfR}U_{cfR}\cos\theta$	$\rho\beta_{2R}Q_{2R}U_{2R}-\rho\beta_{1R}Q_{1R}U_{1R}-\rho q_{cfR}U_{cfR}\cos\theta$	ASF_{cfR}	ASF_{cfR} per metre
	m	*N*	*N*	*N*	*N*	*N*	*N*	*N*	*N*	*N/m*
Right floodplain	0.176	6.40	4.30	-2.10	3.10	5.82	-2.58	-0.13	1.97	0.20
	0.1981	9.30	8.00	-1.30	13.37	25.08	-10.02	-1.69	-0.39	-0.04
	0.2532	21.01	17.45	-3.56	63.17	142.25	-62.19	-16.88	-13.32	-1.33
	0.2977	30.97	25.31	-5.66	152.78	352.04	-134.25	-65.00	-59.34	-5.93

	Depth	ΣSF	W	$-\Sigma SF+W-ASF_L-ASF_R$	$\rho\beta_{2MC}Q_{2MC}U_{2MC}$	$\rho\beta_{1MC}Q_{1MC}U_{1MC}$	$\rho q_{cfL}U_{cfL}\cos\theta+\rho q_{cfR}U_{cfR}\cos\theta$	$\rho\beta_{2MC}Q_{2MC}U_{2MC}-\rho\beta_{1MC}Q_{1MC}U_{1MC}+\rho q_{cfL}U_{cfL}\cos\theta+\rho q_{cfR}U_{cfR}\cos\theta$	Error	Error per metre
	m	*N*	*N*	*N*	*N*	*N*	*N*	*N*	*N*	*N/m*
Main channel	0.176	22.59	29.64	11.19	194.76	162.85	-4.86	27.06	15.87	1.59
	0.1981	23.35	33.65	2.71	237.23	233.42	6.66	10.46	7.75	0.77
	0.2532	29.52	43.64	15.11	380.52	414.87	16.57	-17.77	-32.89	-3.29
	0.2977	36.68	51.70	-29.11	643.56	766.04	32.22	-90.25	-61.14	-6.11

	Depth	F_1	F_2	ΣSF	W	$F_1-F_2-\Sigma SF+W$	$\rho\beta_2Q_2U_2$	$\rho\beta_1Q_1U_1$	$\rho\beta_1Q_2U_2-\rho\beta_1Q_1U_1$	Error	Error per metre
	m	*N*	*N*	*N*	*N*	*N*	*N*	*N*	*N*	*N*	*N/m*
Overall	0.176	296.71	296.71	39.69	39.66	-0.03	206.65	186.86	19.79	19.82	1.98
	0.1981	391.05	391.05	52.29	52.29	0.00	295.04	286.80	8.24	8.24	0.82
	0.2532	748.01	748.01	84.19	84.21	0.02	632.72	685.05	-52.33	-52.35	-5.24
	0.2977	1166.67	1166.67	110.39	110.43	0.04	1232.95	1416.78	-183.83	-183.87	-18.39

Table 7.22a-Force-momentum balance for FCF skew data series A14, s=1, $\theta=5.1^{o}$ ignoring all hydrostatic forces in the zonal analysis. Adjusted velocities and inclusion of β

	Depth	ΣSF	W	-ΣSF+W	$\rho Q_{2L}U_{2L}$	$\rho Q_{1L}U_{1L}$	$\rho q_{cfL}U_{cfL}\cos\theta$	$\rho Q_{2L}U_{2L}-\rho Q_{1L}U_{1L}-\rho q_{cfL}U_{cfL}\cos\theta$	ASF_{cfL}	ASF_{cfL} per metre
	m	*N*	*N*	*N*	*N*	*N*	*N*	*N*	*N*	*N/m*
Left floodplain	0.176	8.70	5.88	-2.82	8.20	15.40	-1.50	-5.70	-2.88	-0.29
	0.1981	18.32	11.07	-7.25	40.30	26.80	16.00	-2.50	4.75	0.48
	0.2532	31.23	22.39	-8.84	185.70	125.70	69.40	-9.40	-0.56	-0.06
	0.2977	43.31	33.96	-9.35	398.10	240.80	154.00	3.30	12.65	1.27

	Depth	ΣSF	W	-ΣSF+W	$\rho Q_{2R}U_{2R}$	$\rho Q_{1R}U_{1R}$	$\rho q_{cfR}U_{cfR}\cos\theta$	$\rho Q_{2R}U_{2R}-\rho Q_{1R}U_{1R}-\rho q_{cfR}U_{cfR}\cos\theta$	ASF_{cfR}	ASF_{cfR} per metre
	m	*N*	*N*	*N*	*N*	*N*	*N*	*N*	*N*	*N/m*
Right floodplain	0.176	5.24	4.41	-0.83	2.90	5.90	-2.70	-0.30	0.53	0.05
	0.1981	10.63	8.32	-2.31	13.90	23.70	-9.60	-0.20	2.11	0.21
	0.2532	17.54	16.90	-0.64	67.60	132.90	-60.30	-5.00	-4.36	-0.44
	0.2977	31.30	25.73	-5.57	153.00	300.30	-135.70	-11.60	-6.03	-0.60

Table 7.22b-Force-momentum balance for FCF skew data series A14, s=1:1, θ=5.1° Elliott & Sellin's (1990) results

	Depth	ΣSF	W	-ΣSF+W	$\rho\beta_{2L}Q_{2L}U_{2L}$	$\rho\beta_{1L}Q_{1L}U_{1L}$	$\rho q_{cfL}U_{cfL}\cos\theta$	$\rho\beta_{2R}Q_{2L}U_{2L}-\rho\beta_{1L}Q_{1L}U_{1L}-\rho q_{cfL}U_{cfL}\cos\theta$	ASF_{cfL}	ASF_{cfL} per metre
	m	*N*	*N*	*NN*	*N*	*N*	*N*	*N*	*N*	*N/m*
Left floodplain	0.1756	11.30	3.94	-7.36	10.98	5.55	9.88	-4.45	2.92	0.29
	0.1978	16.61	7.41	-9.20	45.21	15.98	35.90	-6.67	2.52	0.25
	0.2534	26.02	16.32	-9.71	192.90	59.95	143.69	-10.75	-1.04	-0.10
	0.299	32.47	23.85	-8.62	407.41	123.38	266.49	17.54	26.16	2.62

	Depth	ΣSF	W	-ΣSF+W	$\rho\beta_{2R}Q_{2R}U_{2R}$	$\rho\beta_{1R}Q_{1R}U_{1R}$	$\rho q_{cfR}U_{cfR}\cos\theta$	$\rho\beta_{2R}Q_{2R}U_{2R}-\rho\beta_{1R}Q_{1R}U_{1R}-\rho q_{cfR}U_{cfR}\cos\theta$	ASF_{cfR}	ASF_{cfR} per metre
	m	*N*	*N*		*N*	*N*	*N*	*N*	*N*	*N/m*
Right floodplain	0.1756	7.65	5.92	-1.72	2.92	7.80	-4.12	-0.76	0.97	0.10
	0.1978	14.00	11.12	-2.88	11.94	33.14	-17.31	-3.89	-1.01	-0.10
	0.2534	29.05	24.33	-4.71	66.47	189.42	-100.24	-22.72	-18.01	-1.80
	0.299	41.85	35.41	-6.44	168.94	481.64	-227.43	-85.27	-78.84	-7.88

	Depth	ΣSF	W	$-\Sigma SF+W-ASF_L-ASF_R$	$\rho\beta_{2MC}Q_{2MC}U_{2MC}$	$\rho\beta_{1MC}Q_{1MC}U_{1MC}$	$\rho q_{cfL}U_{cfL}\cos\theta+\rho q_{cfR}U_{cfR}\cos\theta$	$\rho\beta_{2MC}Q_{2MC}U_{2MC}-\rho\beta_{1MC}Q_{1MC}U_{1MC}+\rho q_{cfL}U_{cfL}\cos\theta+\rho q_{cfR}U_{cfR}\cos\theta$	Error	Error per metre
	m	*N*	*N*	*N*	*N*	*N*	*N*	*N*	*N*	*N/m*
Main channel	0.1756	20.53	29.57	7.09	184.43	180.33	5.77	9.87	2.78	0.28
	0.1978	21.52	33.59	8.54	210.13	217.61	18.60	11.12	2.58	0.26
	0.2534	29.27	43.67	-2.56	365.47	397.08	43.45	11.84	14.41	1.44
	0.299	36.90	51.94	-89.96	659.35	670.45	39.06	27.96	117.92	11.79

	Depth	F_1	F_2	ΣSF	W	$F_1-F_2-\Sigma SF+W$	$\rho\beta_2Q_2U_2$	$\rho\beta_1Q_1U_1$	$\rho\beta_1Q_2U_2-\rho\beta_1Q_1U_1$	Error	Error per metre
	m	*N*	*N*	*N*	*N*		*N*	*N*	*N*	*N*	*N/m*
Overall	0.1756	295.25	295.25	39.43	39.43	0.00	198.67	193.72	4.95	4.95	0.49
	0.1978	389.59	389.59	52.10	52.12	0.02	270.77	266.91	3.85	3.84	0.38
	0.2534	749.63	749.63	84.30	84.32	0.02	642.49	644.95	-2.47	-2.49	-0.25
	0.299	1180.70	1180.70	111.17	111.20	0.03	1294.25	1279.75	14.50	14.47	1.45

Table 7.23a-Force-momentum balance for FCF skew data series A15, s=1, $\theta=9.2^{o}$ ignoring all hydrostatic forces in the zonal analysis. Adjusted velocities and inclusion of β

	Depth	ΣSF	W	-ΣSF+W	$\rho Q_{2L}U_{2L}$	$\rho Q_{1L}U_{1L}$	$\rho q_{cfL}U_{cfL}\cos\theta$	$\rho Q_{2L}U_{2L}-\rho Q_{1L}U_{1L}-\rho q_{cfL}U_{cfL}\cos\theta$	ASF_{cfL}	ASF_{cfL} per metre
	m	*N*	*N*	*N*	*N*	*N*	*N*	*N*	*N*	*N/m*
Left floodplain	0.1756	10.00	3.70	-6.30	10.30	5.30	9.90	-4.90	1.40	0.14
	0.1978	16.82	6.98	-9.84	43.70	16.00	36.40	-8.70	1.14	0.11
	0.2534	22.63	14.19	-8.44	180.50	62.40	131.60	-13.50	-5.06	-0.51
	0.299	29.51	21.63	-7.88	348.10	122.90	244.00	-18.80	-10.92	-1.09

	Depth	ΣSF	W	-ΣSF+W	$\rho Q_{2R}U_{2R}$	$\rho Q_{1R}U_{1R}$	$\rho q_{cfR}U_{cfR}\cos\theta$	$\rho Q_{2R}U_{2R}-\rho Q_{1R}U_{1R}-\rho q_{cfR}U_{cfR}\cos\theta$	ASF_{cfR}	ASF_{cfR} per metre
	m	*N*	*N*	*N*	*N*	*N*	*N*	*N*	*N*	*N/m*
Right floodplain	0.1756	6.82	5.56	-1.26	3.30	7.70	-4.00	-0.40	0.86	0.09
	0.1978	14.28	10.47	-3.81	15.20	31.80	-15.90	-0.70	3.11	0.31
	0.2534	25.34	21.17	-4.17	87.80	179.20	-91.90	0.50	4.67	0.47
	0.299	38.02	32.10	-5.92	210.40	419.00	-207.60	-1.00	4.92	0.49

Table 7.23b-Force-momentum balance for FCF skew data series A15, s=1:1, θ=9.2° Elliott & Sellin's (1990) results

	Depth	ΣSF	W	-ΣSF+W	$\rho\beta_{2L}Q_{2L}U_{2L}$	$\rho\beta_{1L}Q_{1L}U_{1L}$	$\rho q_{cfL}U_{cfL}\cos\theta$	$\rho\beta_{2R}Q_{2L}U_{2L}-\rho\beta_{1L}Q_{1L}U_{1L}-\rho q_{cfL}U_{cfL}\cos\theta$	ASF_{cfL}	ASF_{cfL} per metre
	m	*N*	*N*	*N*	*N*	*N*	*N*	*N*	*N*	*N/m*
Left floodplain	0.1755	11.39	6.00	-5.39	8.70	6.96	3.88	-2.14	3.26	0.33
	0.1984	21.42	11.44	-9.98	43.42	29.78	17.65	-4.01	5.97	0.60
	0.2528	34.77	24.58	-10.19	200.64	132.26	72.24	-3.86	6.33	0.63
	0.2968	46.29	35.42	-10.87	465.97	306.02	159.77	0.19	11.05	1.11

	Depth	ΣSF	W	-ΣSF+W	$\rho\beta_{2R}Q_{2R}U_{2R}$	$\rho\beta_{1R}Q_{1R}U_{1R}$	$\rho q_{cfR}U_{cfR}\cos\theta$	$\rho\beta_{2R}Q_{2R}U_{2R}-\rho\beta_{1R}Q_{1R}U_{1R}-\rho q_{cfR}U_{cfR}\cos\theta$	ASF_{cfR}	ASF_{cfR} per metre
	m	*N*	*N*	*N*	*N*	*N*	*N*	*N*	*N*	*N/m*
Right floodplain	0.1755	7.58	4.60	-2.98	2.95	6.31	-2.82	-0.54	2.43	0.24
	0.1984	12.68	8.78	-3.90	13.75	26.56	-11.02	-1.80	2.10	0.21
	0.2528	23.79	18.94	-4.85	74.66	139.28	-59.38	-5.24	-0.39	-0.04
	0.2968	34.27	27.37	-6.90	201.55	384.56	-138.07	-44.94	-38.04	-3.80

	Depth	ΣSF	W	$-\Sigma SF+W-ASF_L-ASF_R$	$\rho\beta_{2MC}Q_{2MC}U_{2MC}$	$\rho\beta_{1MC}Q_{1MC}U_{1MC}$	$\rho q_{cfL}U_{cfL}\cos\theta+\rho q_{cfR}U_{cfR}\cos\theta$	$\rho\beta_{2MC}Q_{2MC}U_{2MC}-\rho\beta_{1MC}Q_{1MC}U_{1MC}+\rho q_{cfL}U_{cfL}\cos\theta+\rho q_{cfR}U_{cfR}\cos\theta$	Error	Error per metre
	m	*N*	*N*	*N*	*N*	*N*	*N*	*N*	*N*	*N/m*
Main channel	0.1755	18.18	26.51	7.52	154.61	153.06	1.07	2.62	-4.90	-0.49
	0.1984	19.61	29.97	6.50	187.13	184.87	6.63	8.89	2.39	0.24
	0.2528	23.17	38.19	8.30	302.37	301.05	12.86	14.18	5.88	0.59
	0.2968	27.11	44.84	-31.36	552.32	596.99	21.70	-22.97	8.40	0.84

	Depth	F_1	F_2	ΣSF	W	$F_1-F_2-\Sigma SF+W$	$\rho\beta_2Q_2U_2$	$\rho\beta_1Q_1U_1$	$\rho\beta_1Q_2U_2-\rho\beta_1Q_1U_1$	Error	Error per metre
	m	*N*	*N*	*N*	*N*	*N*	*N*	*N*	*N*	*N*	*N/m*
Overall	0.1755	239.72	239.72	37.11	37.11	0.00	151.07	153.24	-2.17	-2.17	-0.22
	0.1984	337.36	337.36	50.17	50.20	0.03	232.51	230.66	1.85	1.82	0.18
	0.2528	689.62	689.62	81.69	81.71	0.02	561.61	557.49	4.12	4.11	0.41
	0.2968	1101.86	1101.86	107.62	107.63	0.01	1177.74	1223.65	-45.91	-45.92	-4.59

Table 7.24-Force-momentum balance for FCF skew data series A16, s=0, $\theta=5.1^{o}$ ignoring all hydrostatic forces in the zonal analysis. Adjusted velocities and inclusion of β

	Depth	ΣSF	W	-ΣSF+W	$\rho\beta_{2L}Q_{2L}U_{2L}$	$\rho\beta_{1L}Q_{1L}U_{1L}$	$\rho q_{cfL}U_{cfL}\cos\theta$	$\rho\beta_{2R}Q_{2L}U_{2L}-\rho\beta_{1L}Q_{1L}U_{1L}-\rho q_{cfL}U_{cfL}\cos\theta$	ASF_{cfL}	ASF_{cfL} per metre
	m	*N*	*N*	*N*	*N*	*N*	*N*	*N*	*N*	*N/m*
Left floodplain	0.1755	9.79	5.61	-4.18	7.49	7.58	2.25	-2.33	1.85	0.18
	0.198	17.34	10.62	-6.72	39.19	27.83	17.74	-6.38	0.34	0.03
	0.2513	31.56	22.68	-8.88	178.94	111.69	77.08	-9.83	-0.95	-0.09
	0.292	40.31	32.09	-8.23	355.49	215.71	141.11	-1.33	6.90	0.69

	Depth	ΣSF	W	-ΣSF+W	$\rho\beta_{2R}Q_{2R}U_{2R}$	$\rho\beta_{1R}Q_{1R}U_{1R}$	$\rho q_{cfR}U_{cfR}\cos\theta$	$\rho\beta_{2R}Q_{2R}U_{2R}-\rho\beta_{1R}Q_{1R}U_{1R}-\rho q_{cfR}U_{cfR}\cos\theta$	ASF_{cfR}	ASF_{cfR} per metre
	m	*N*	*N*	*N*	*N*	*N*	*N*	*N*	*N*	*N/m*
Right floodplain	0.1755	5.86	4.21	-1.65	2.79	6.47	-2.64	-1.03	0.61	0.06
	0.198	9.97	7.98	-1.99	11.14	25.66	-12.39	-2.13	-0.14	-0.01
	0.2513	19.89	17.12	-2.77	58.23	124.23	-62.07	-3.93	-1.16	-0.12
	0.292	28.08	24.29	-3.79	133.64	266.89	-131.72	-1.54	2.26	0.23

	Depth	ΣSF	W	$-\Sigma SF+W-ASF_L-ASF_R$	$\rho\beta_{2MC}Q_{2MC}U_{2MC}$	$\rho\beta_{1MC}Q_{1MC}U_{1MC}$	$\rho q_{cfL}U_{cfL}\cos\theta+\rho q_{cfR}U_{cfR}\cos\theta$	$\rho\beta_{2MC}Q_{2MC}U_{2MC}-\rho\beta_{1MC}Q_{1MC}U_{1MC}+\rho q_{cfL}U_{cfL}\cos\theta+\rho q_{cfR}U_{cfR}\cos\theta$	Error	Error per metre
	m	*N*	*N*	*N*	*N*	*N*	*N*	*N*	*N*	*N/m*
Main channel	0.1755	26.00	30.68	3.45	259.27	254.43	-0.39	4.45	1.00	0.10
	0.198	27.17	34.76	7.11	286.40	298.13	5.35	-6.39	-13.50	-1.35
	0.2513	33.94	44.43	10.27	458.14	460.34	15.01	12.81	2.54	0.25
	0.292	40.95	51.80	6.21	691.48	669.83	9.39	31.04	24.83	2.48

	Depth	F_1	F_2	ΣSF	W	$F_1-F_2-\Sigma SF+W$	$\rho\beta_2Q_2U_2$	$\rho\beta_1Q_1U_1$	$\rho\beta_1Q_2U_2-\rho\beta_1Q_1U_1$	Error	Error per metre
	m	*N*	*N*	*N*	*N*	*N*	*N*	*N*	*N*	*N*	*N/m*
Overall	0.1755	322.47	322.47	41.64	40.51	-1.13	261.30	260.27	1.03	2.16	0.22
	0.198	418.15	418.15	54.49	53.37	-1.13	334.36	338.35	-4.00	-2.87	-0.29
	0.2513	760.34	760.34	85.35	84.23	-1.12	692.15	696.18	-4.03	-2.91	-0.29
	0.292	1133.99	1133.99	109.30	108.18	-1.12	1179.91	1152.88	27.03	28.15	2.82

Table 7.25-Force-momentum balance for FCF skew data series A18, s=2, $\theta=5.1^o$ ignoring all hydrostatic forces in the zonal analysis. Adjusted velocities and inclusion of β

						Momentum			Momentum flux in each zone	Total momentum residual for section
Series A No.	**s**	**θ**	**Depth, H**	**Discharge, Q**		**Upstream**	**Downstream**	**Lateral**		
		°	*m*	m^3/s						
A14-1	1	5.1	0.1760	0.261	***Left floodplain***	21.24	9.54	-1.47	10.22	-19.55
					Main channel	167.47	201.63		-30.01	
					Right floodplain	6.09	3.18	2.67	0.24	
A14-2	1	5.1	0.1981	0.361	***Left floodplain***	30.40	47.09	15.55	-1.14	-11.13
					Main channel	238.79	244.76		-12.21	
					Right floodplain	26.57	15.04	9.31	2.22	
A14-3	1	5.1	0.2532	0.710	***Left floodplain***	154.51	197.49	70.0	27.02	77.33
					Main channel	424.38	387.16		28.31	
					Right floodplain	155.81	72.71	61.1	22.00	
A14-4	1	5.1	0.2977	1.109	***Left floodplain***	340.89	455.41	153.2	38.68	222.95
					Main channel	771.39	653.21		99.38	
					Right floodplain	399.55	180.27	134.4	84.89	

Table 7.26a -Momentum balance FCF skewed data using Elliot's data and applying β values

						Momentum			Momentum flux in each zone	Total momentum residual for section
Series A No.	**s**	**θ**	**Depth, H**	**Discharge, Q**		**Upstream**	**Downstream**	**Lateral**		
		o	***m***	***m^3/s***						
A15-1	1	9.2	0.1756	0.257	***Left floodplain***	5.88	12.02	9.59	3.45	-7.30
					Main channel	186.11	191.80		-11.46	
					Right floodplain	8.21	3.67	3.83	0.70	
A15-2	1	9.2	0.1978	0.356	***Left floodplain***	16.91	47.99	35.39	4.31	-7.48
					Main channel	223.95	217.74		-13.76	
					Right floodplain	33.82	16.43	15.42	1.97	
A15-3	1	9.2	0.2534	0.700	***Left floodplain***	74.16	203.26	133.11	4.01	2.56
					Main channel	402.63	372.02		-5.34	
					Right floodplain	201.84	100.78	97.17	3.90	
A15-4	1	9.2	0.2990	1.100	***Left floodplain***	156.28	432.58	243.70	-32.60	-19.99
					Main channel	677.46	668.15		-26.79	
					Right floodplain	516.27	269.28	207.59	39.41	

Table 7.26b-Momentum balance FCF skewed data using Elliot's data and applying β values

						Momentum			Momentum flux in each zone	Total momentum residual for section
Series A No.	**s**	**θ**	**Depth, H**	**Discharge, Q**		**Upstream**	**Downstream**	**Lateral**		
		o	***m***	***m^3/s***						
A16-1	0	5.1	0.1755	0.232	***Left floodplain***	7.39	9.32	3.53	1.60	-0.96
					Main channel	157.42	159.78		-3.29	
					Right floodplain	6.60	3.27	2.61	0.72	
A16-2	0	5.1	0.1984	0.331	***Left floodplain***	31.69	45.91	16.59	2.37	-5.08
					Main channel	189.09	192.45		-9.52	
					Right floodplain	27.78	15.28	10.43	2.07	
A16-3	0	5.1	0.2528	0.668	***Left floodplain***	141.28	208.05	67.77	1.01	-5.54
					Main channel	305.42	307.21		-13.72	
					Right floodplain	147.64	84.63	55.84	7.17	
A16-4	0	5.1	0.2968	1.065	***Left floodplain***	351.25	485.44	135.10	0.92	89.79
					Main channel	604.13	559.75		32.88	
					Right floodplain	411.52	231.93	123.60	55.99	

Table 7.26c-Momentum balance FCF skewed data using Elliot's data and applying β values

						Momentum			Momentum flux in each zone	Total momentum residual for section
Series A No.	**s**	**θ**	**Depth, H**	**Discharge, Q**		**Upstream**	**Downstream**	**Lateral**		
		o	***m***	***m^3/s***						
A17-1	0	2.1	0.1746	0.233	***Left floodplain***	6.89			6.89	
					Main channel	166.37			166.37	-
					Right floodplain	4.24			4.24	
A17-2	0	2.1	0.1981	0.332	***Left floodplain***	29.31			29.31	
					Main channel	203.25			203.25	-
					Right floodplain	18.51			18.51	
A17-3	0	2.1	0.2540	0.668	***Left floodplain***	151.51			151.51	
					Main channel	323.83			323.83	-
					Right floodplain	104.49			104.49	

Table 7.26d-Momentum balance FCF skewed data using Elliot's data and applying β values

						Momentum			Momentum flux in each zone	Total momentum residual for section
Series A No.	**s**	**θ**	**Depth, H**	**Discharge, Q**		**Upstream**	**Downstream**	**Lateral**		
		o	*m*	m^3/s						
A18-1	2	5.1	0.1755	0.298	***Left floodplain***	8.16	8.35	2.49	2.30	-2.41
					Main channel	262.46	268.62		-5.91	
					Right floodplain	6.81	2.87	2.74	1.20	
A18-2	2	5.1	0.1980	0.400	***Left floodplain***	29.92	41.09	17.30	6.13	13.00
					Main channel	305.64	295.78		4.57	
					Right floodplain	27.04	12.74	12.00	2.30	
A18-3	2	5.1	0.2513	0.740	***Left floodplain***	120.72	186.70	72.50	6.52	-1.05
					Main channel	466.78	466.31		-13.64	
					Right floodplain	132.59	68.12	58.39	6.08	
A18-4	2	5.1	0.2920	1.089	***Left floodplain***	234.66	371.71	131.70	-5.35	-35.62
					Main channel	676.84	703.93		-32.18	
					Right floodplain	287.76	159.24	126.60	1.92	

Table 7.26e-Momentum balance FCF skewed data using Elliot's data and applying β values

Figure 7.1-Photograph of FCF skewed channel geometry for skew angle, θ=5.1^{o}

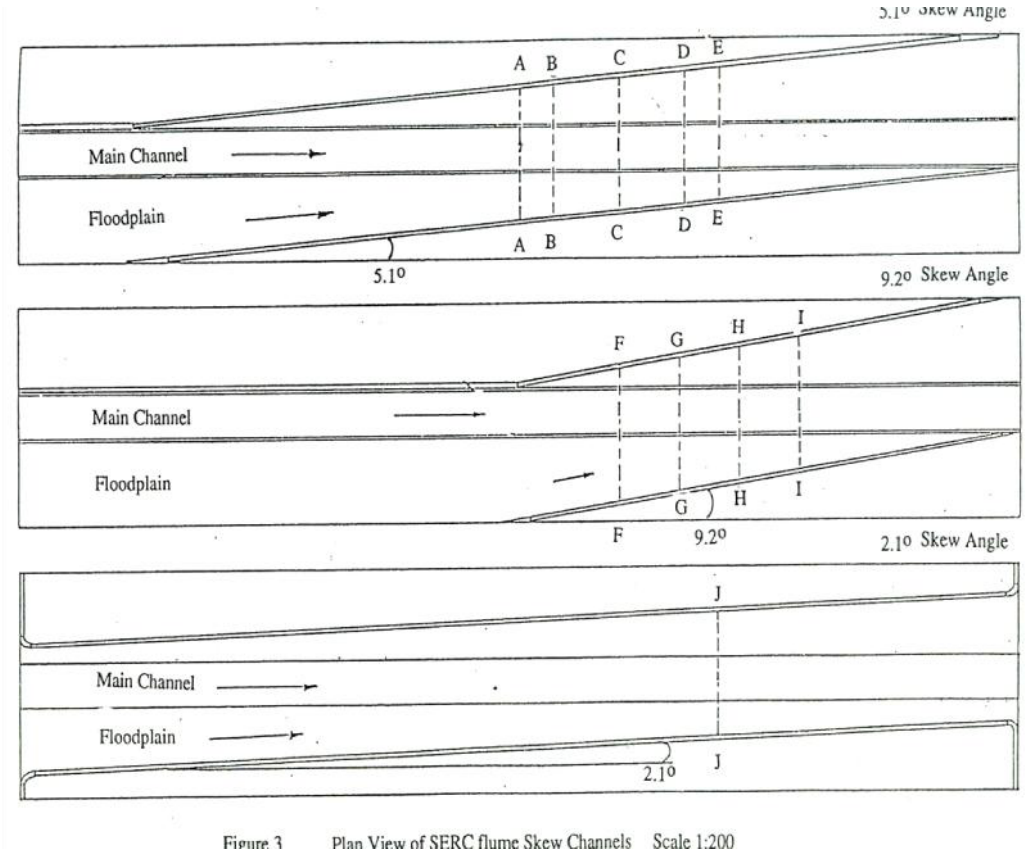

Figure 3 Plan View of SERC flume Skew Channels Scale 1:200

Figure 7.2-Plan view of SERC (FCF) flume skew channel (Elliott, 1990) Scale 1:200 (See Table 7.1)

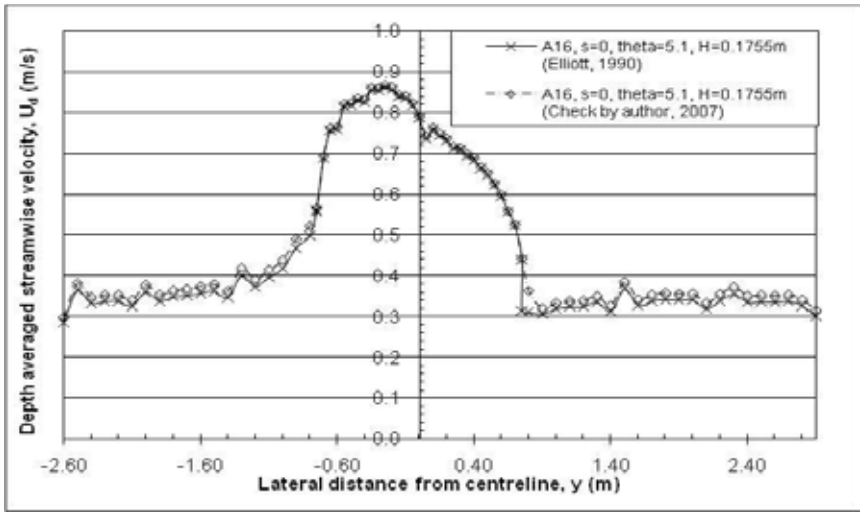

Figure 7.3-Comparison between Elliott's (1990) original depth averaging and re-analysis in 2007

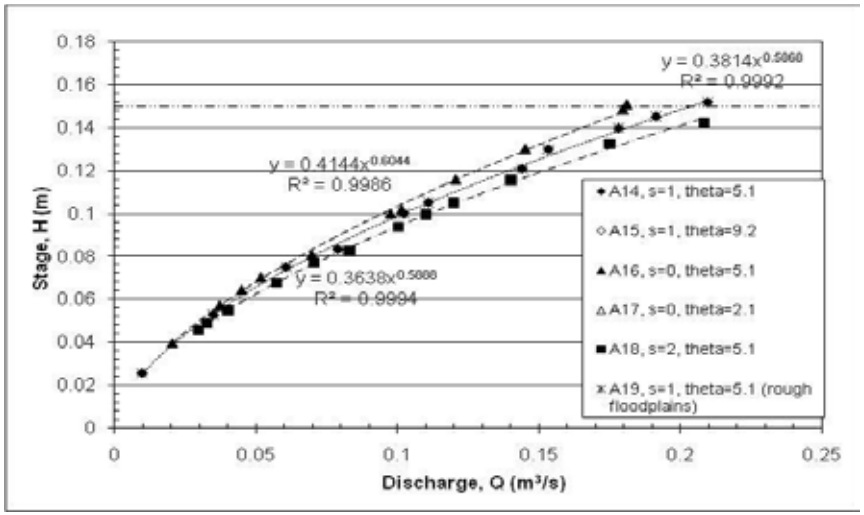

Figure 7.4-Inbank-stage discharge relationships for FCF skew channel from Elliott (1990)

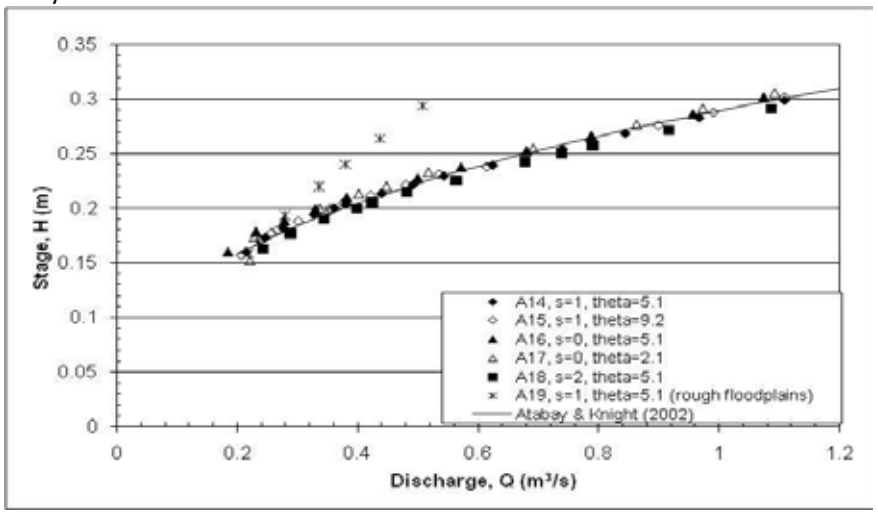

Figure 7.5-Overbank stage-discharge relationships for FCF skew channels from Elliott (1990)

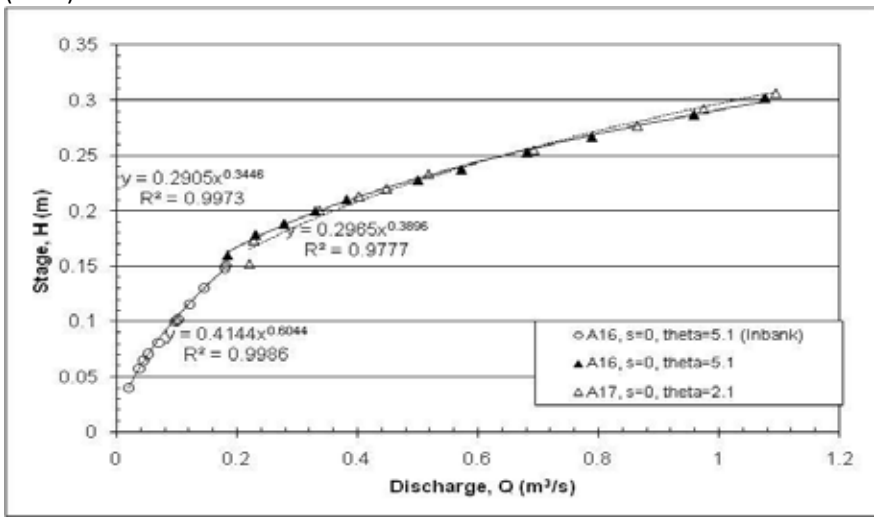

Figure 7.6-Overbank stage-discharge relationships for FCF skew channels, s=0, Elliot (1990)

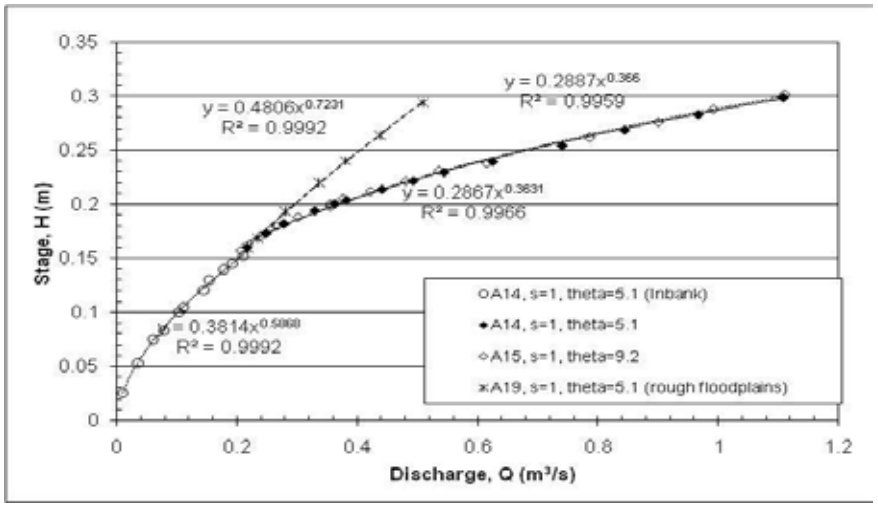

Figure 7.7-Overbank stage-discharge relationships for FCF skew channels, s=1, Elliot (1990)

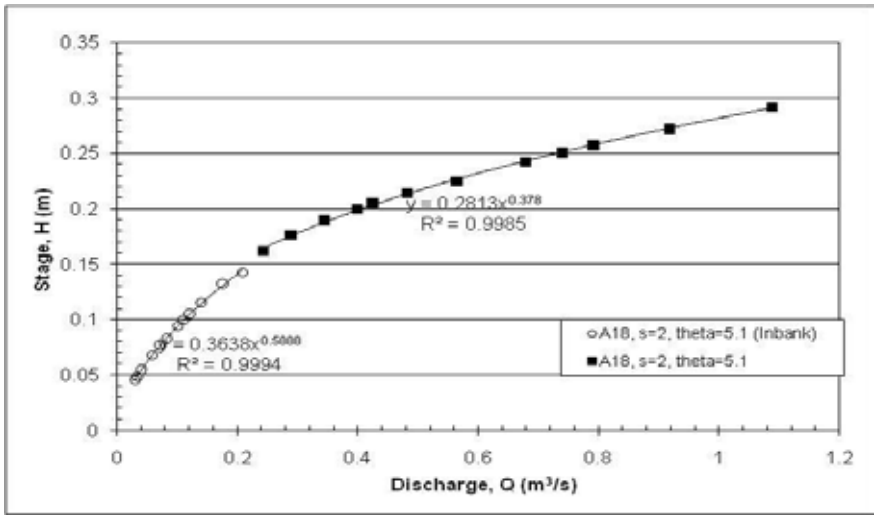

Figure 7.8-Overbank stage-discharge relationships for FCF skew channels, s=2, Elliot (1990)

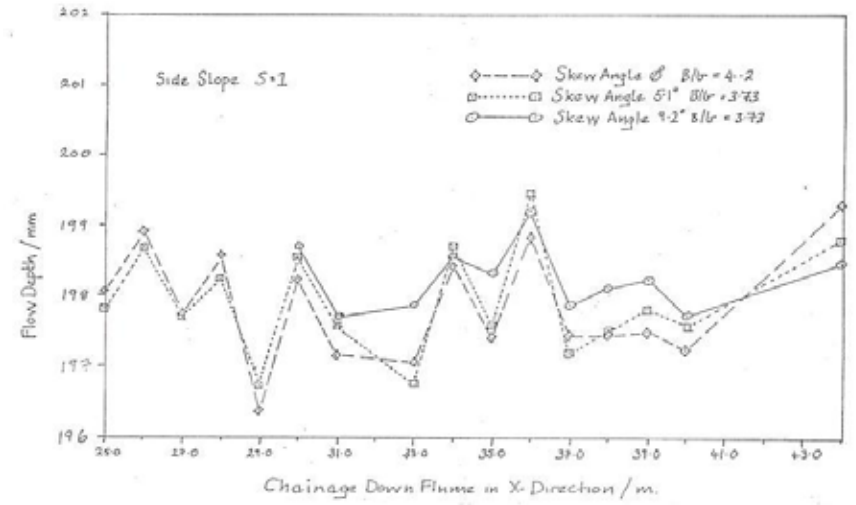

Figure 7.9-Local depth fluctuations for FCF skewed flume, side slope 1:1, Dr=0.25

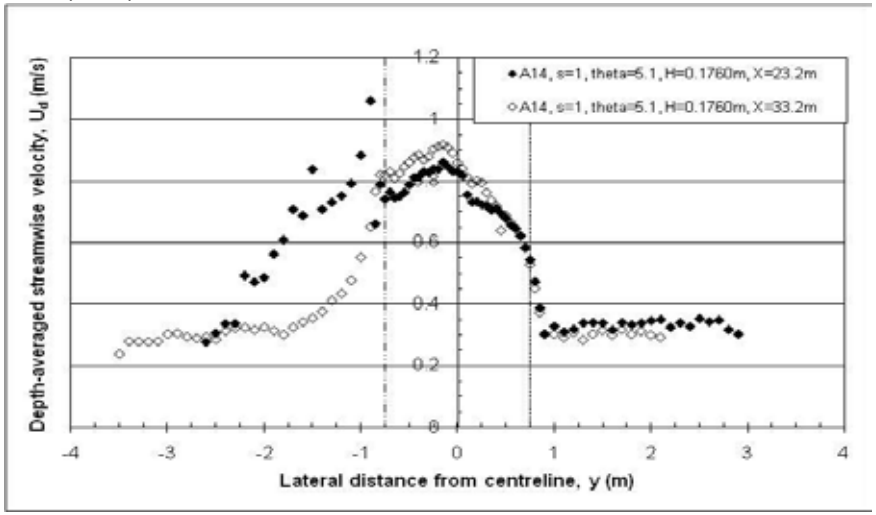

Figure 7.10a-A14, s=1, θ=5.1°, H=0.1760m, depth-averaged velocity between upstream (x=23.2m)

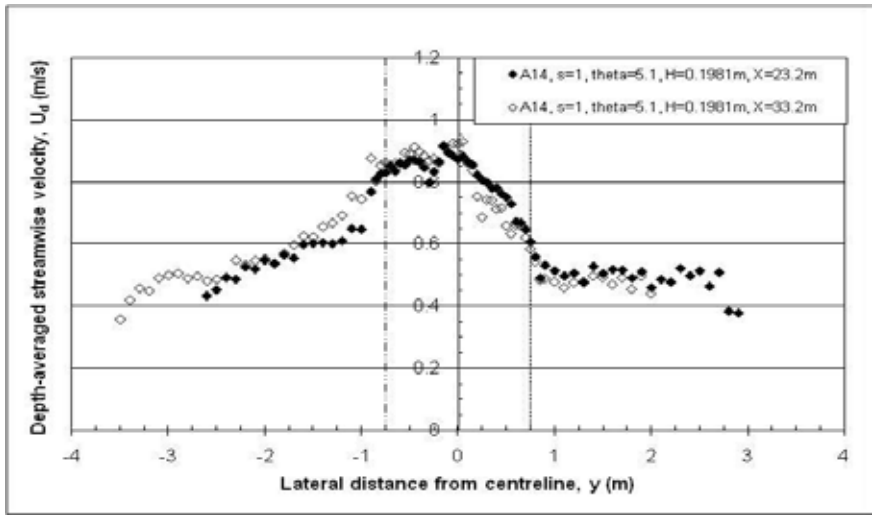

Figure 7.10b-A14, s=1, θ=5.1°, H=0.1981m, depth-averaged velocity between upstream (x=23.2m) and downstream sections (x=33.2m)

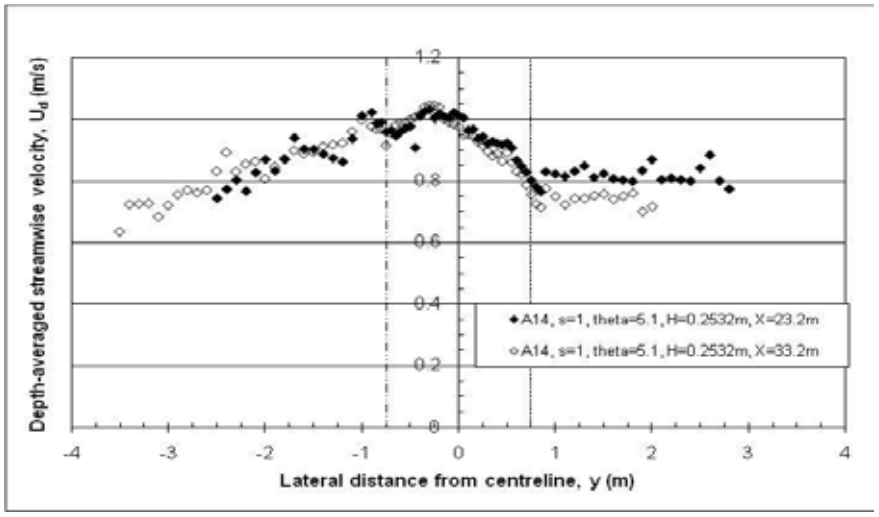

Figure 7.10c-A14, s=1, θ=5.1°, H=0.2532m, depth-averaged velocity between upstream (x=23.2m) and downstream sections (x=33.2m)

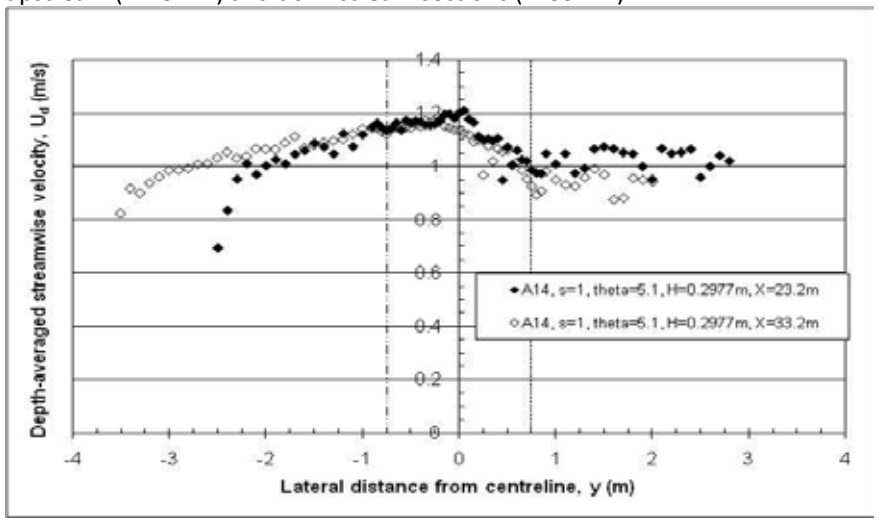

Figure 7.10d-A14, s=1, θ=5.1°, H=0.2977m, depth-averaged velocity between upstream (x=23.2m) and downstream sections (x=33.2m)

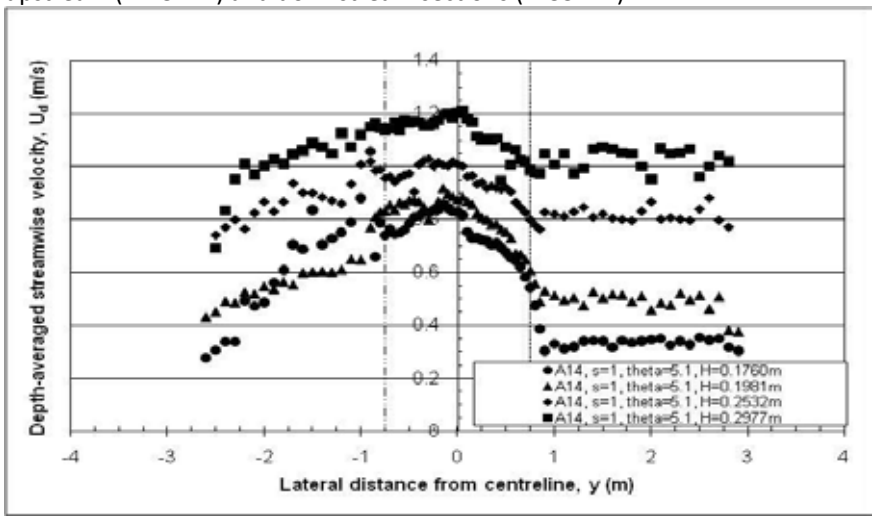

Figure 7.11a-A14, s=1, θ=5.1°, depth-averaged velocity at upstream (x=23.2m) section

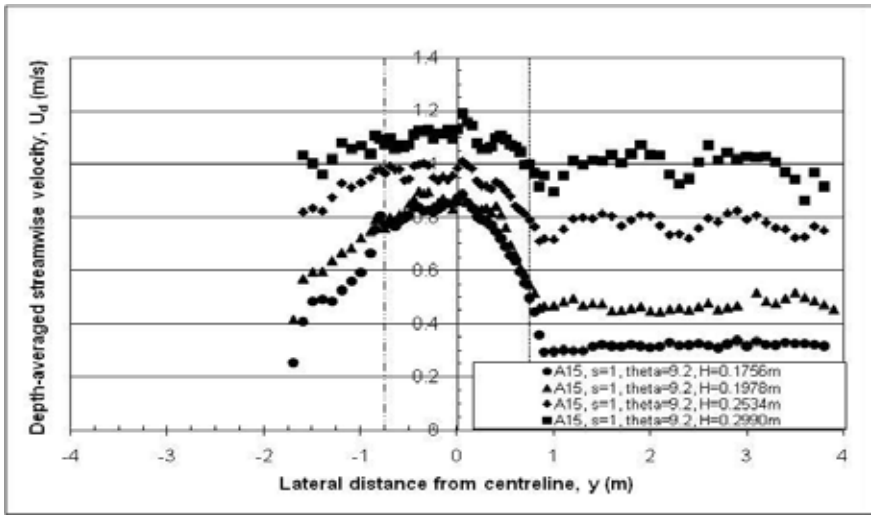

Figure 7.11b-A15, s=1, θ=9.2^{o}, depth-averaged velocity at upstream (x=28.2m) section

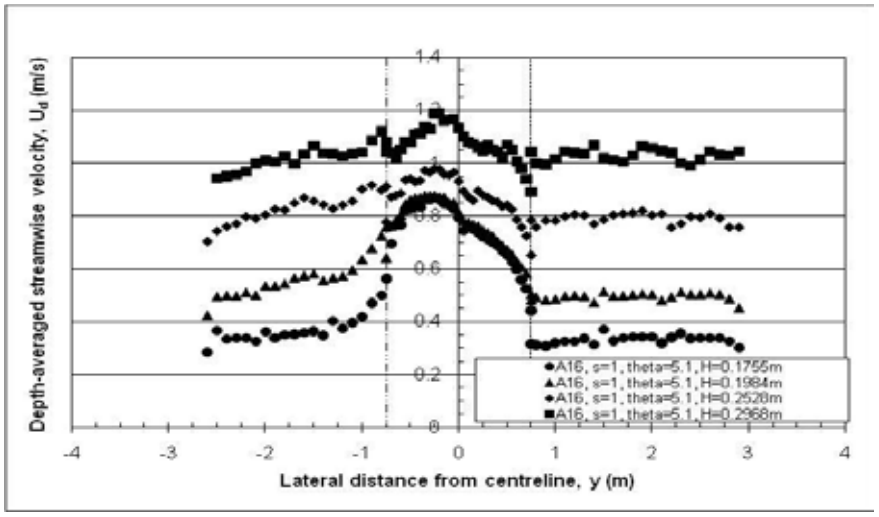

Figure 7.11c-A16, s=0, θ=5.1^{o}, depth-averaged velocity at upstream (x=23.2m) section

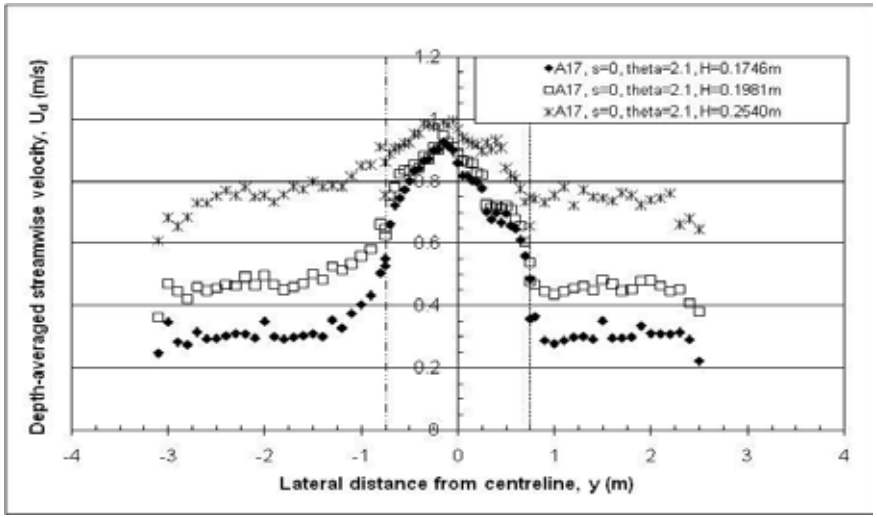

Figure 7.11d-A17, s=0, θ=2.1^{o}, depth-averaged velocity at upstream (x=32.4m) section

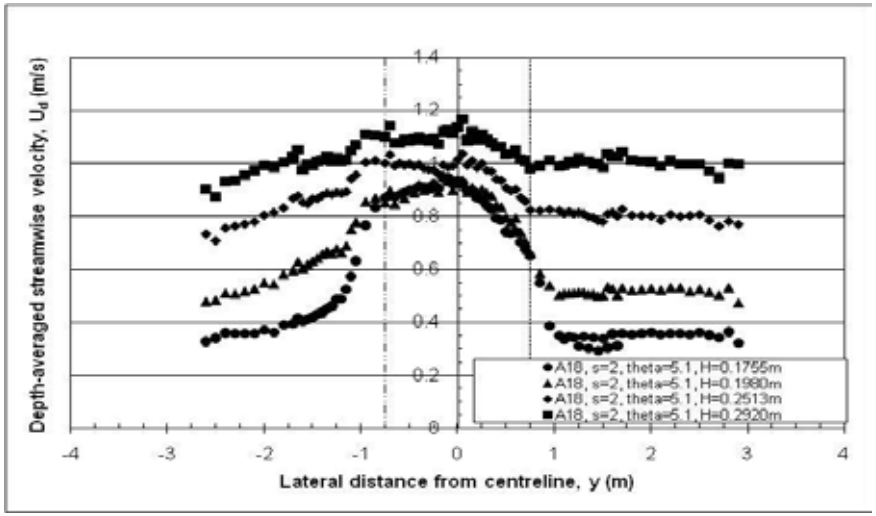

Figure 7.11e-A18, s=2, θ=5.1^{o}, depth-averaged velocity at upstream (x=23.2m) section

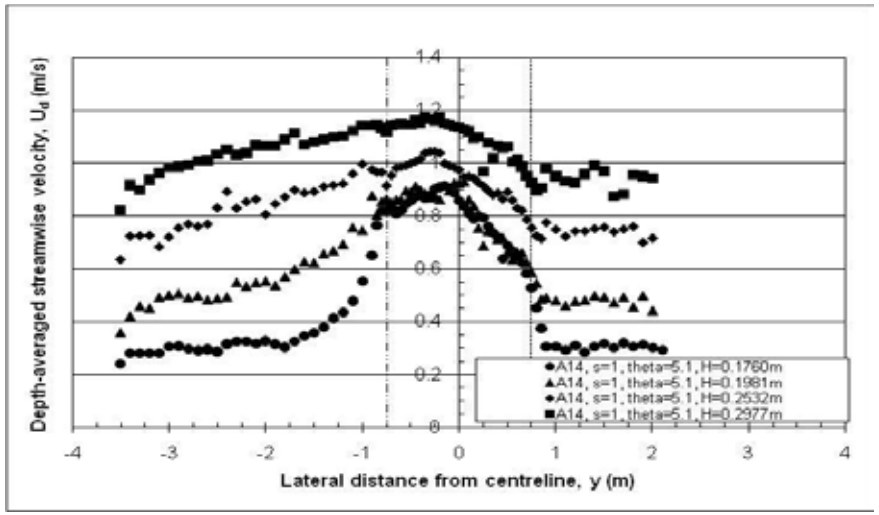

Figure 7.12a-A14, s=1, θ=5.1^{o}, depth-averaged velocity at downstream (x=33.2m) section

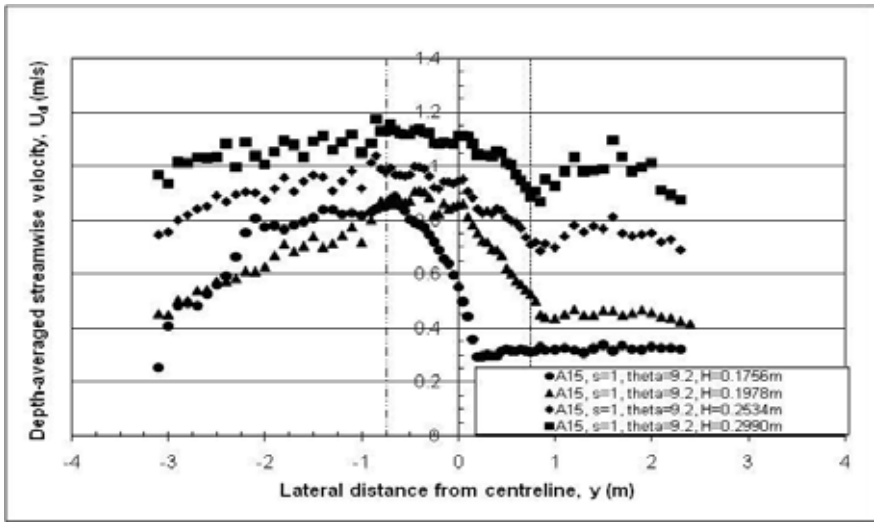

Figure 7.12b-A15, s=1, θ=9.2^{o}, depth-averaged velocity at downstream (x=38.2m) section

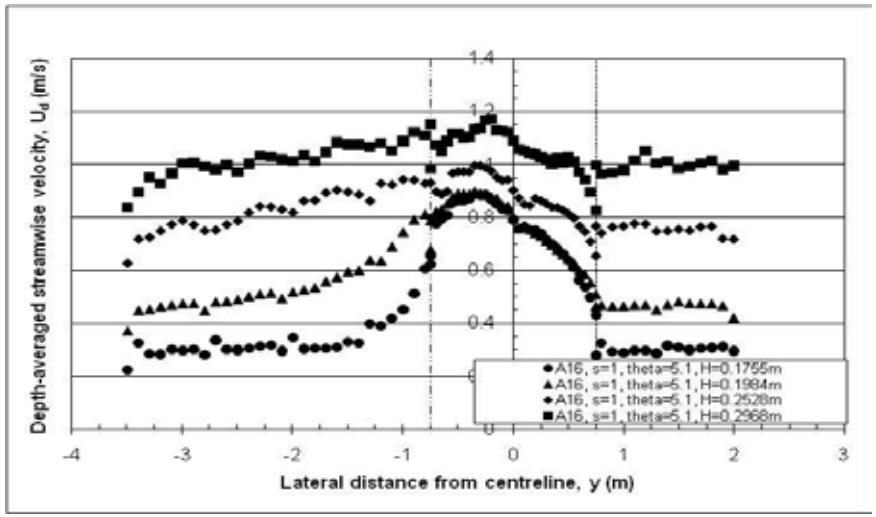

Figure 7.12c-A16, s=0, θ=5.1^{o}, depth-averaged velocity at downstream (x=33.2m) section

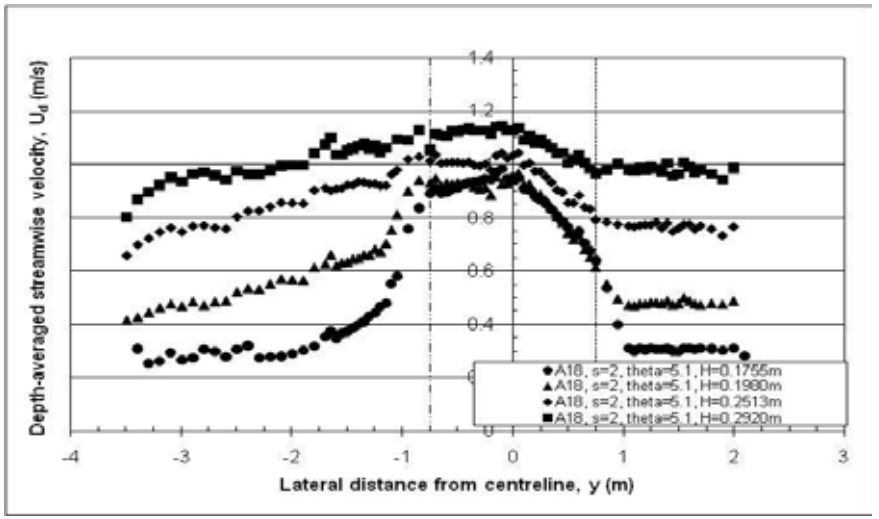

Figure 7.12d-A18, s=2, θ=5.1^{o}, depth-averaged velocity at downstream (x=33.2m) section

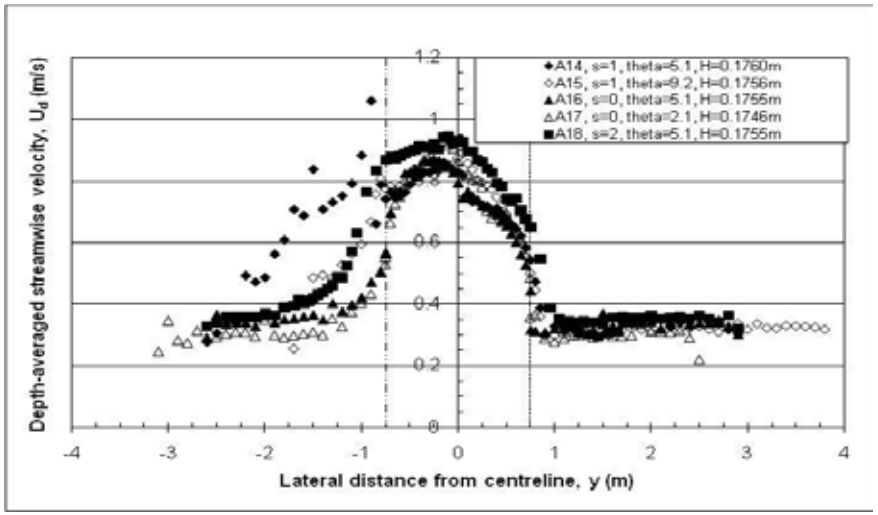

Figure 7.13a-Depth-averaged velocity at upstream sections, Dr=0.15 (A14, A16, A18 x=23.2m; A15 x=28.2m, A17 x=32.4m)

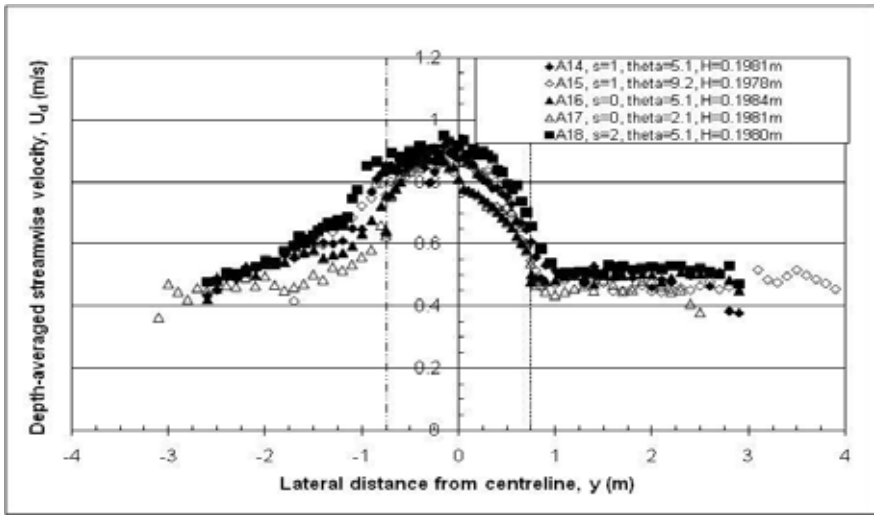

Figure 7.13b-Depth-averaged velocity at upstream sections, Dr=0.25 (A14, A16, A18 x=23.2m; A15 x=28.2m, A17 x=32.4m)

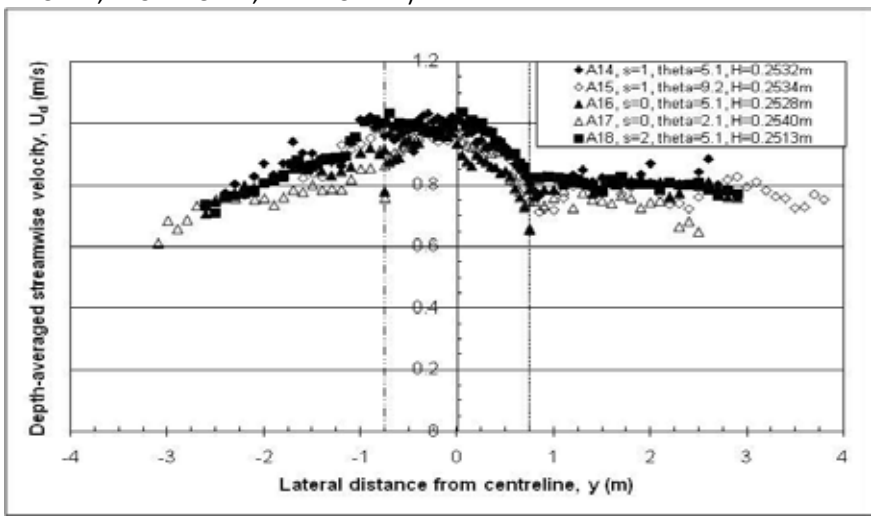

Figure 7.13c-Depth-averaged velocity at upstream sections, Dr=0.4 (A14, A16, A18 x=23.2m; A15 x=28.2m, A17 x=32.4m)

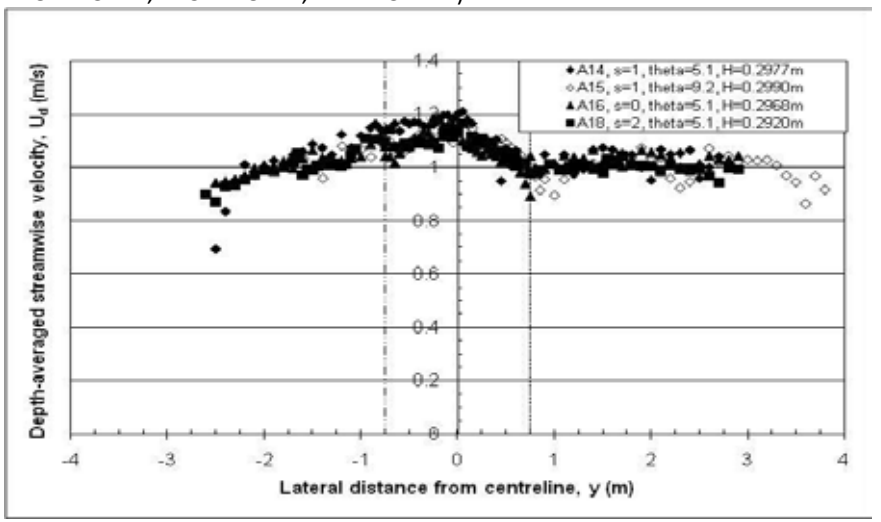

Figure 7.13d-Depth-averaged velocity at upstream sections, Dr=0.5 (A14, A16, A18 x=23.2m; A15 x=28.2m, A17 x=32.4m)

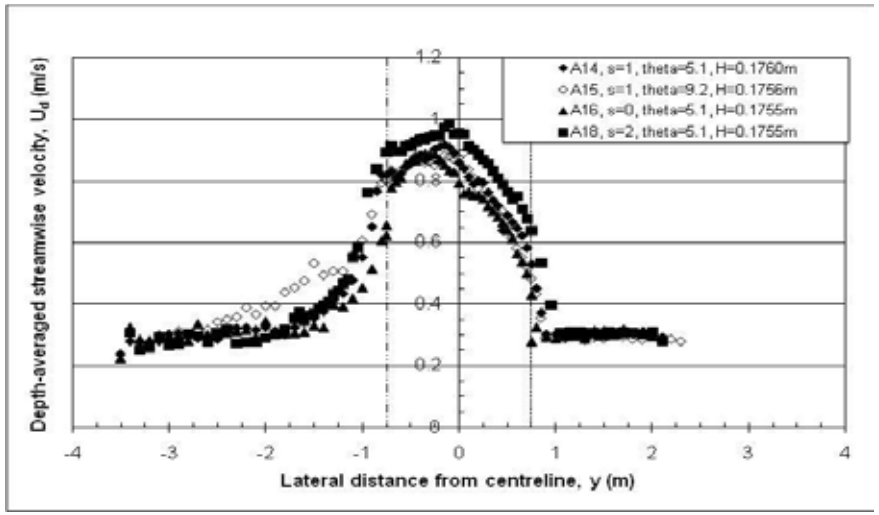

Figure 7.14a-Depth-averaged velocity at downstream sections, Dr=0.15 (A14, A16, A18 x=33.2m; A15 x=38.2m)

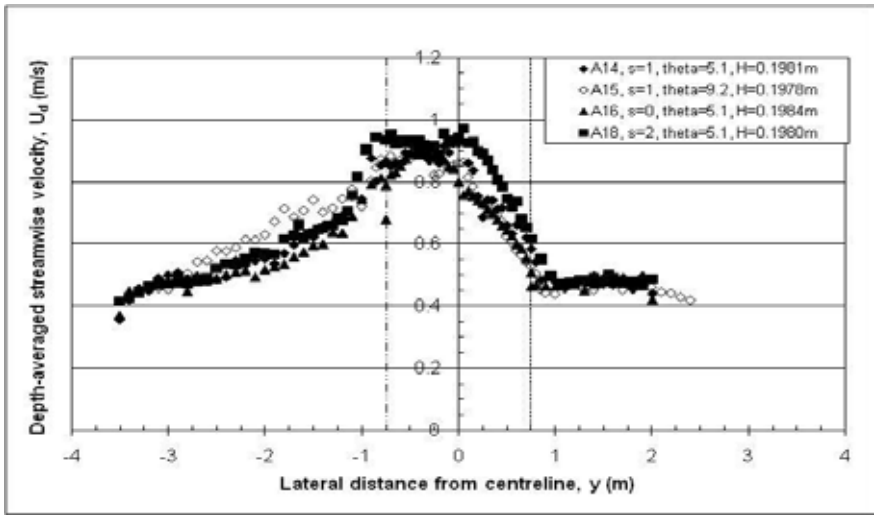

Figure 7.14b-Depth-averaged velocity at downstream sections, Dr=0.25 (A14, A16, A18 x=33.2m; A15 x=38.2m)

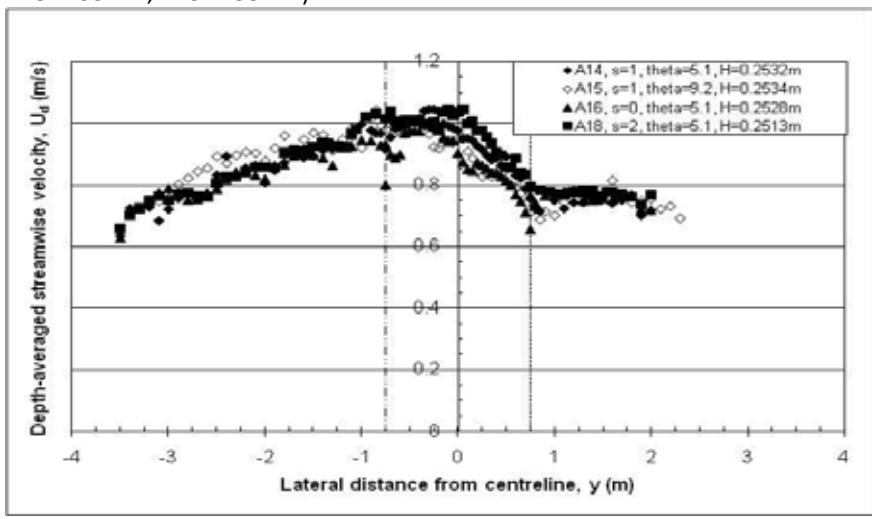

Figure 7.14c-Depth-averaged velocity at downstream sections, Dr=0.4 (A14, A16, A18 x=33.2m; A15 x=38.2m)

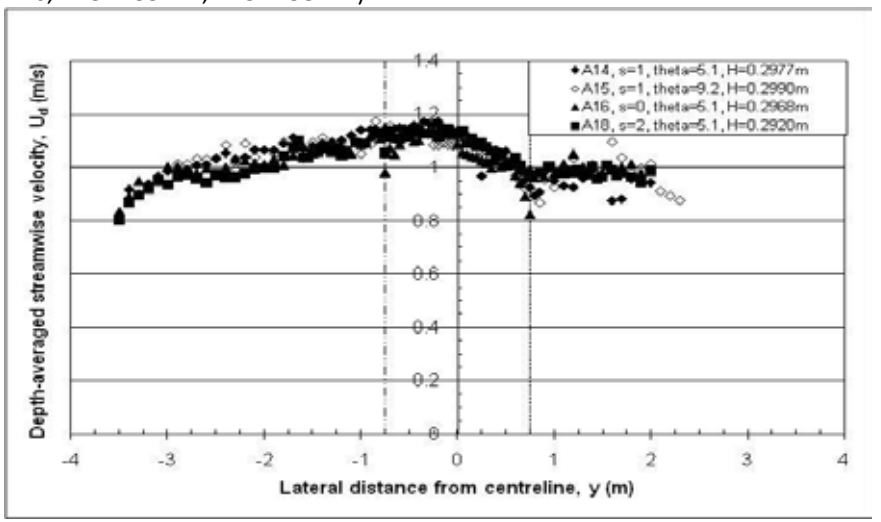

Figure 7.14d-Depth-averaged velocity at downstream sections, Dr=0.5 (A14, A16, A18 x=33.2m; A15 x=38.2m)

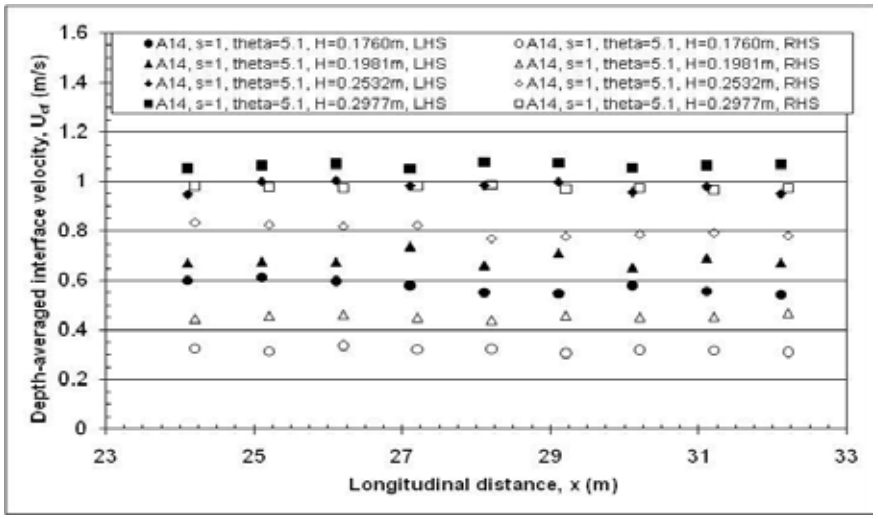

Figure 7.15a-Depth-averaged interface velocity for FCF Series A14, s=1, θ=5.1^o

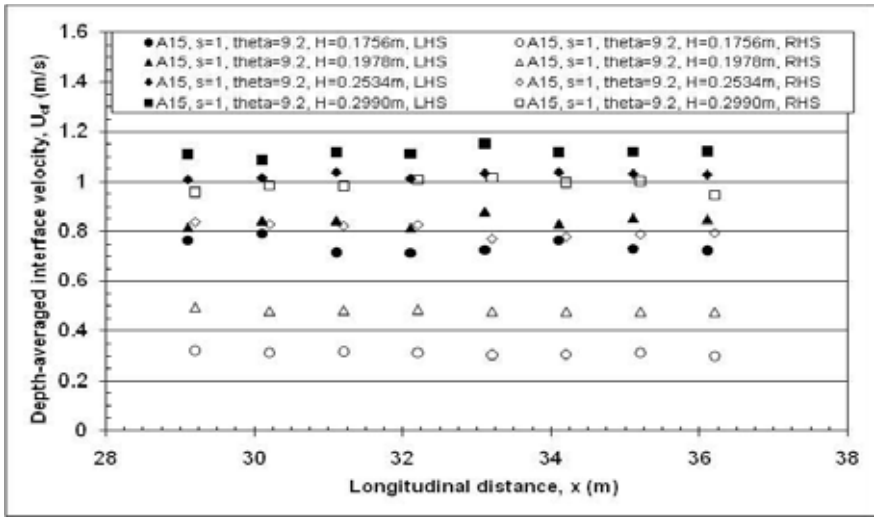

Figure 7.15b-Depth-averaged interface velocity for FCF Series A15, s=1, θ=9.2^o

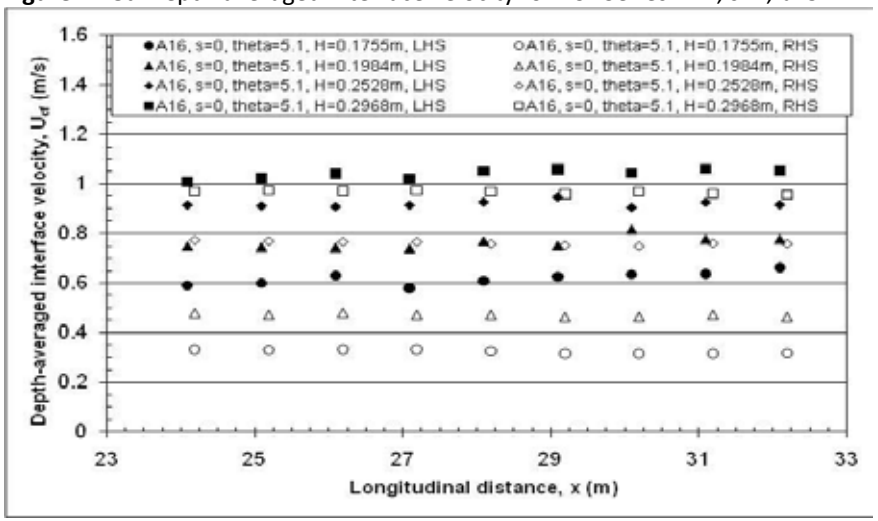

Figure 7.15c-Depth-averaged interface velocity for FCF Series A16, s=0, θ=5.1^o

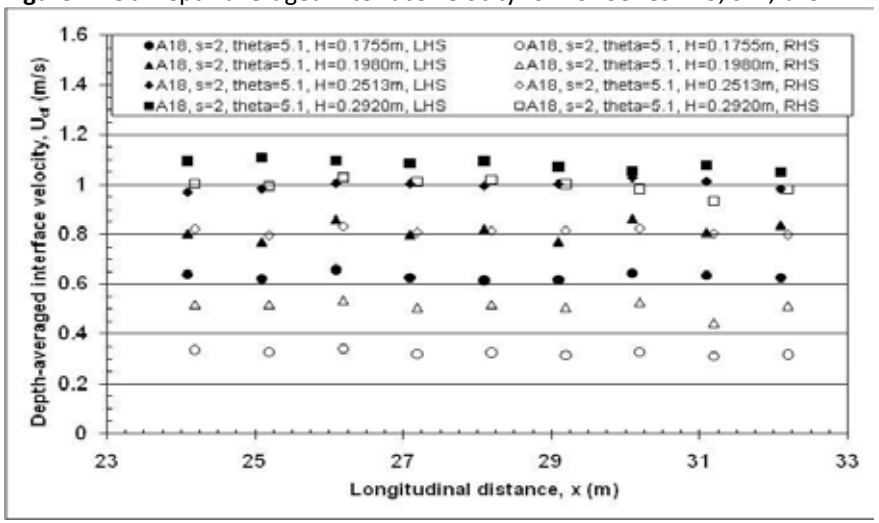

Figure 7.15d-Depth-averaged interface velocity for FCF Series A18, s=2, θ=5.1^o

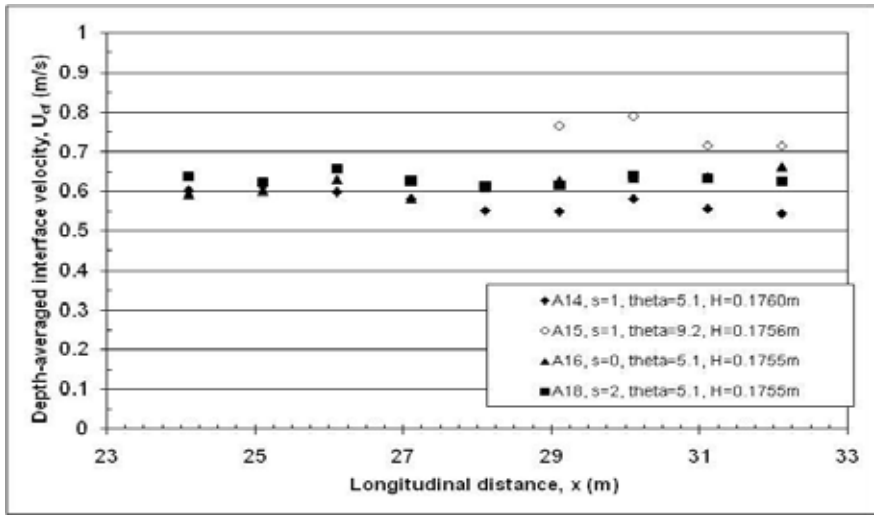

Figure 7.16a-Depth-averaged interface velocity for left interface Dr=0.15

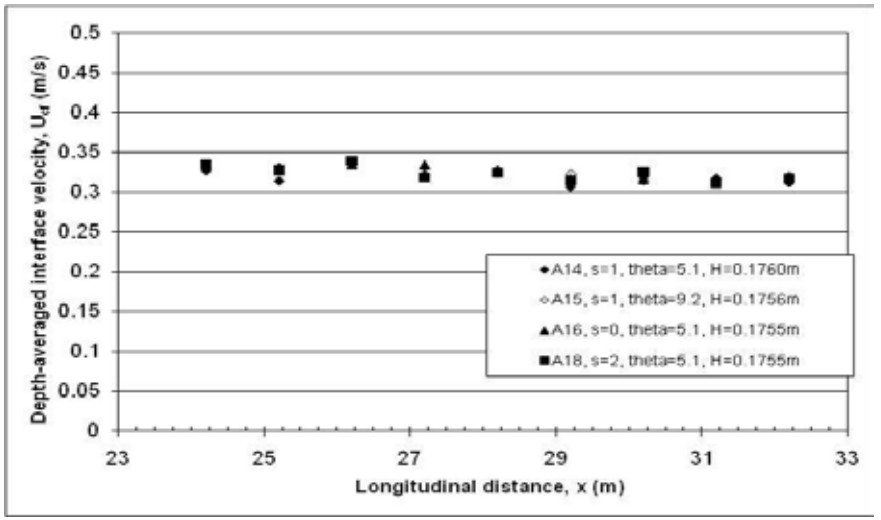

Figure 7.16b-Depth-averaged interface velocity for right interface Dr=0.15

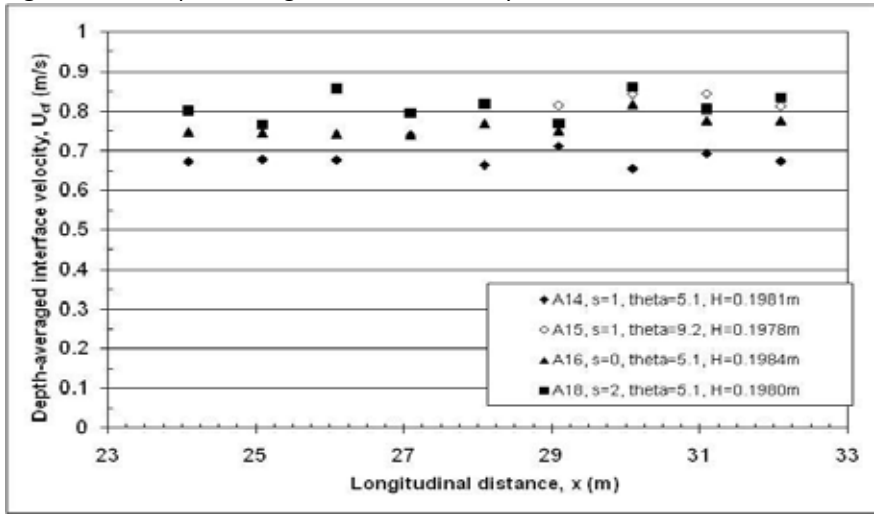

Figure 7.16c-Depth-averaged interface velocity for left interface Dr=0.25

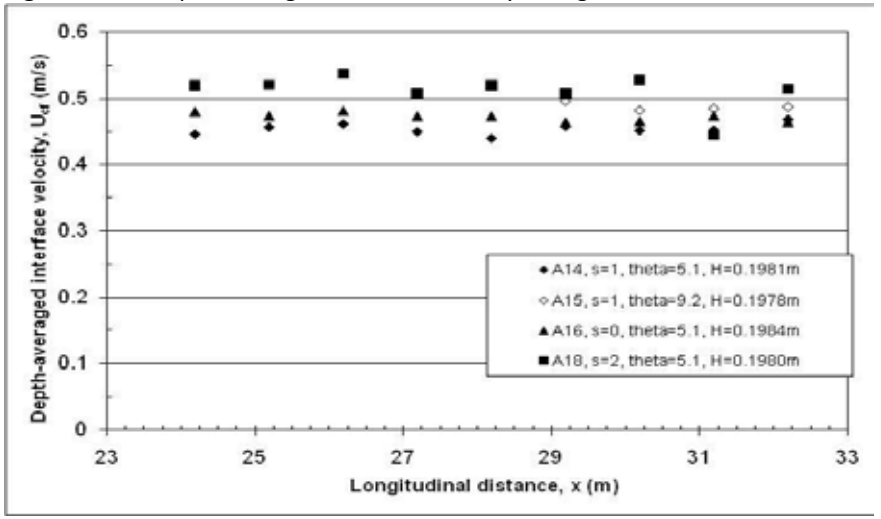

Figure 7.16d-Depth-averaged interface velocity for right interface Dr=0.25

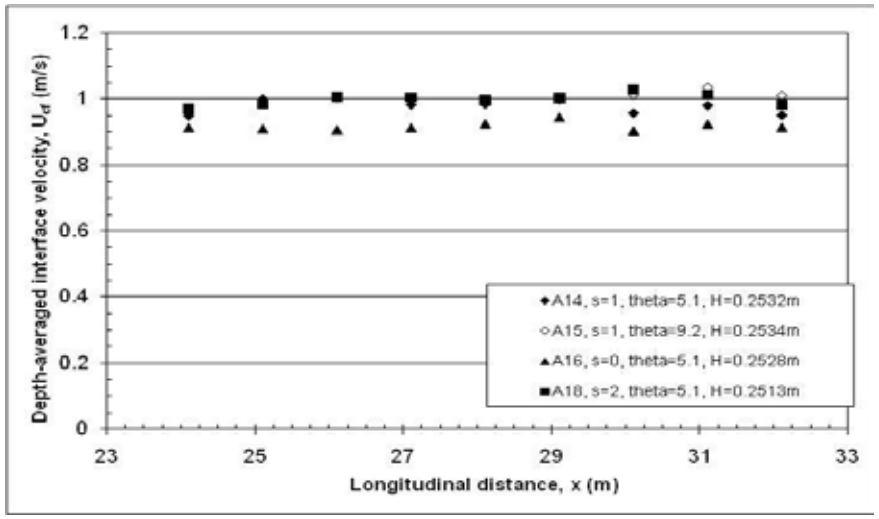

Figure 7.16e-Depth-averaged interface velocity for left interface Dr=0.4

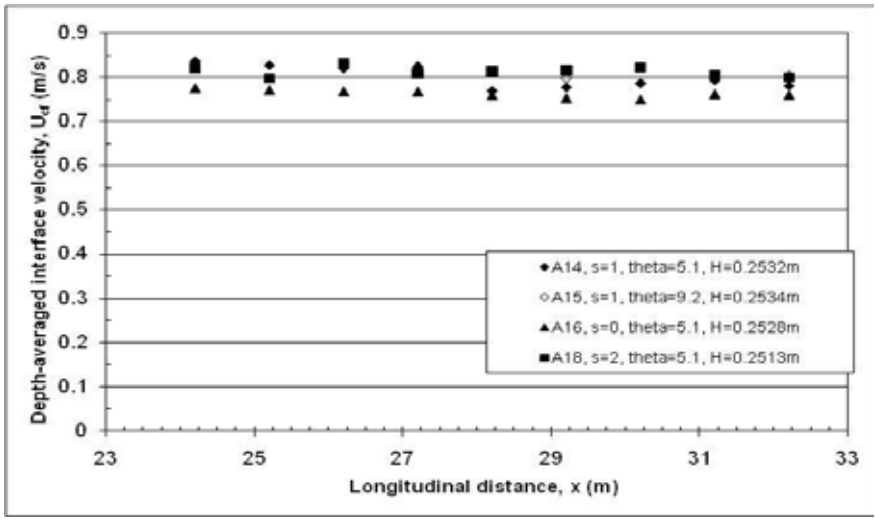

Figure 7.16f-Depth-averaged interface velocity for right interface Dr=0.4

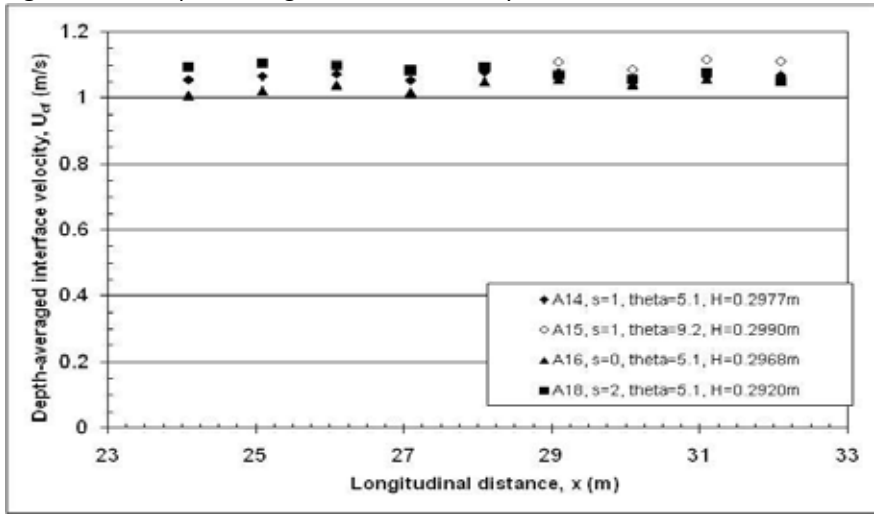

Figure 7.16g-Depth-averaged interface velocity for left interface Dr=0.5

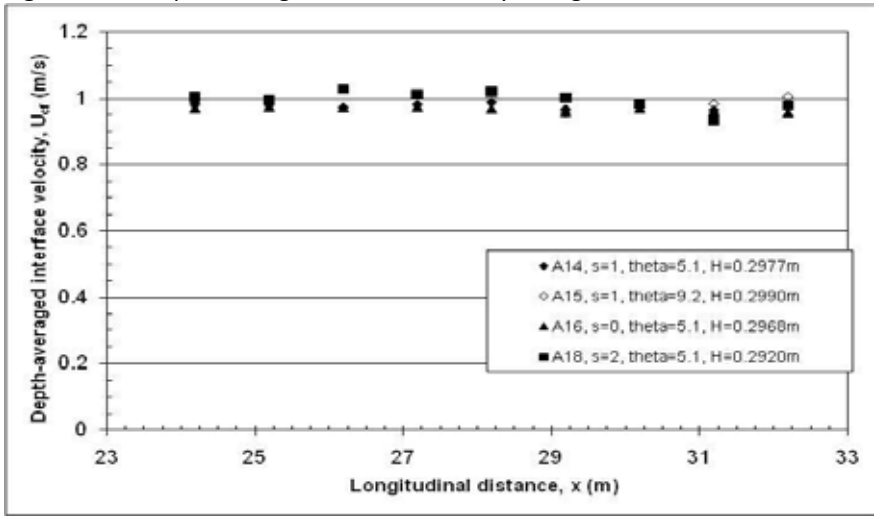

Figure 7.16h-Depth-averaged interface velocity for right interface Dr=0.5

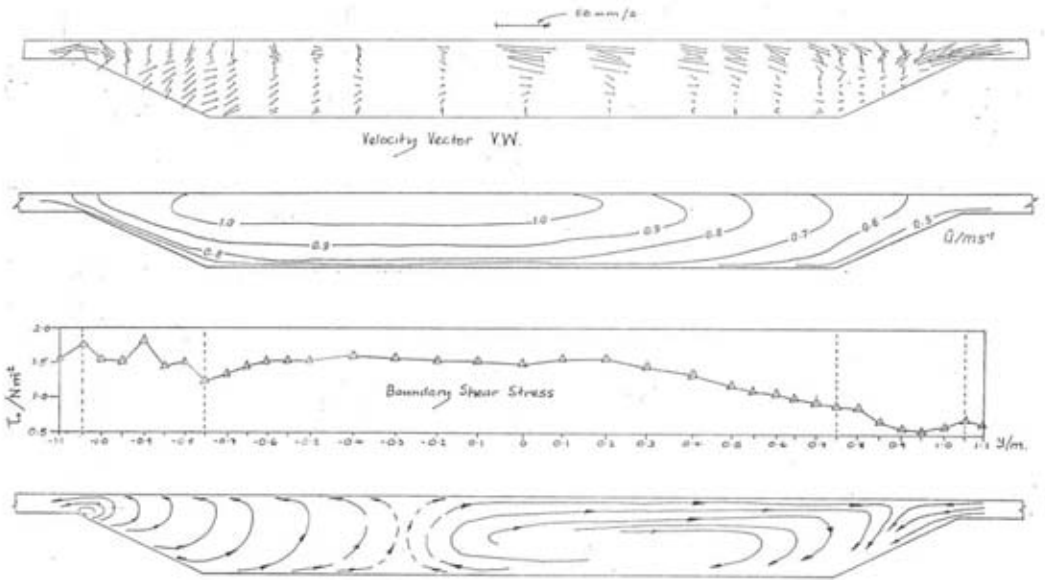

Figure 7.17a-Secondary current patterns, skew angle 5.1°, depth ratio 0.25, s=2 (Elliott, 1990)

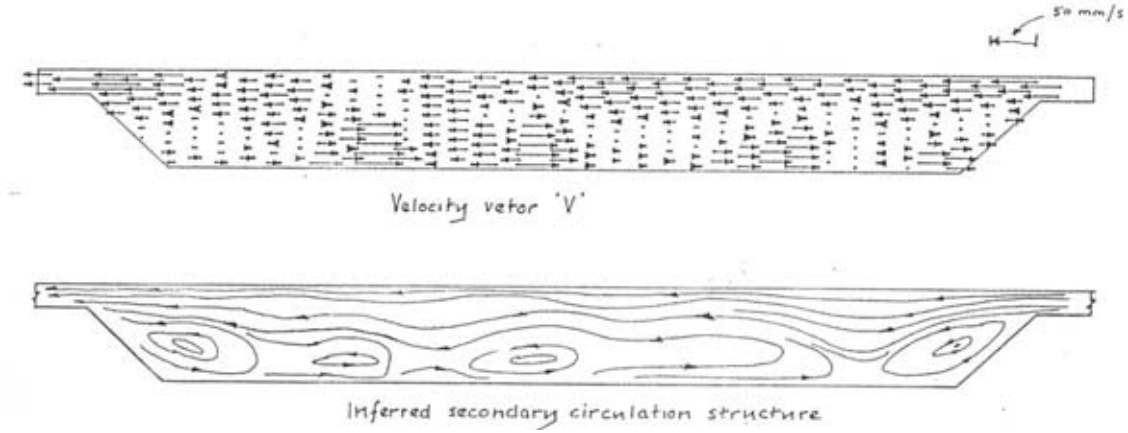

Figure 7.17b-Secondary current patterns, skew angle 5.1°, skew ratio 0.68, depth ratio 0.25, s=1 (Elliott, 1990)

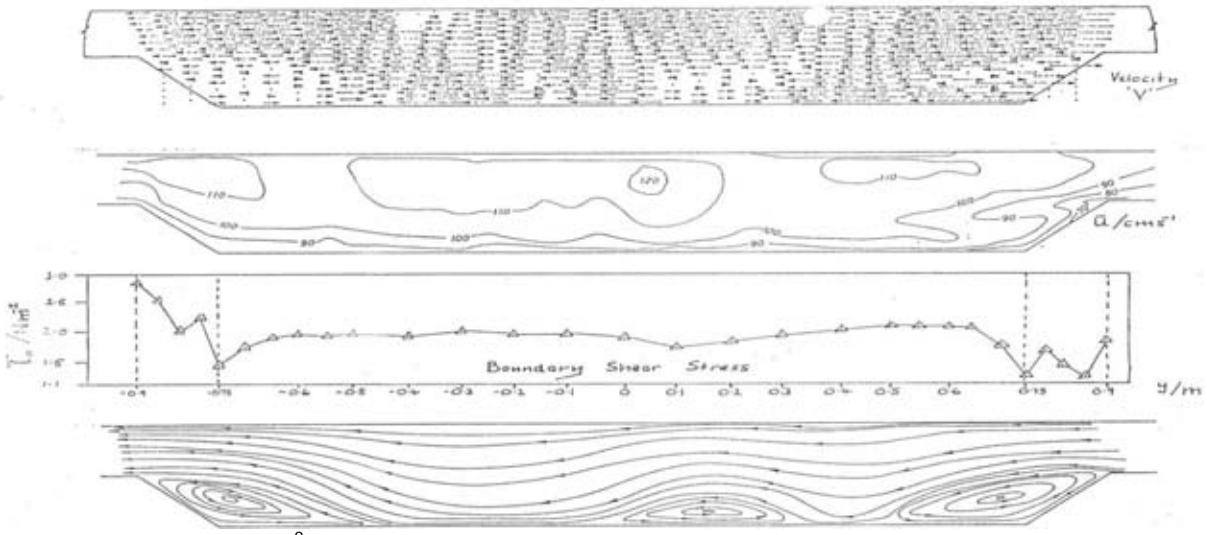

Figure 7.17c-Secondary current patterns, skew angle 9.2°, depth ratio 0.5, upstream section (Elliott, 1990)

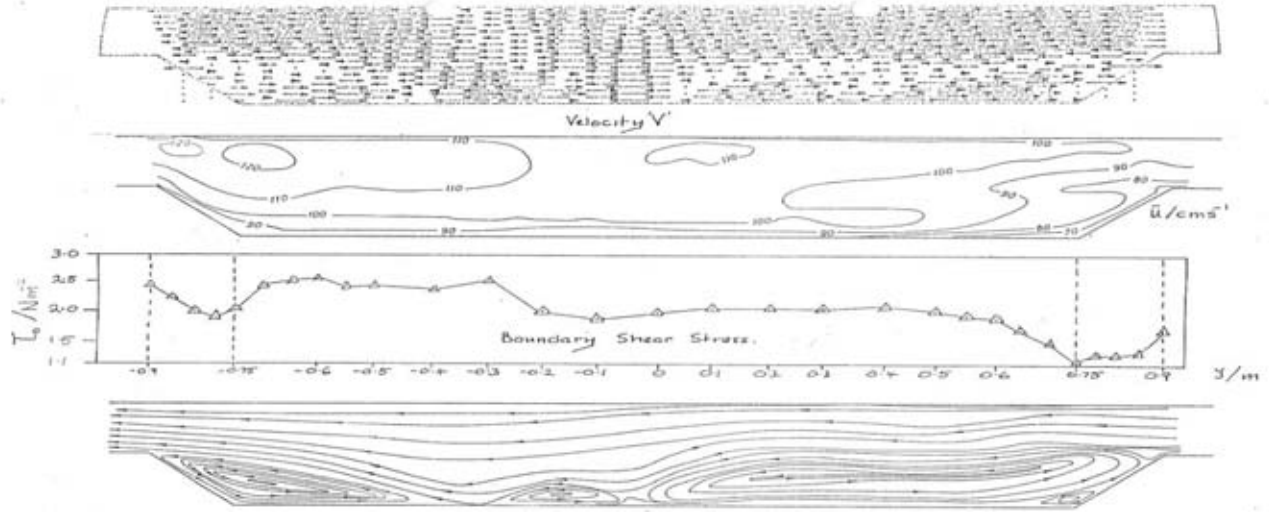

Figure 7.17d-Secondary current patterns, skew angle 9.2°, depth ratio 0.5, downstream section (Elliott, 1990)

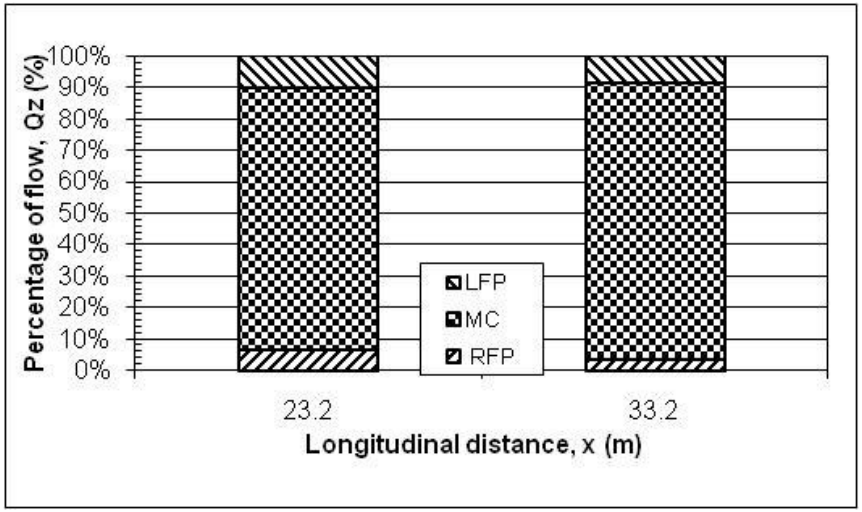

Figure 7.18a-Proportion of flow for FCF skewed series A14, H=0.1760m s=1, θ=5.1^{o}

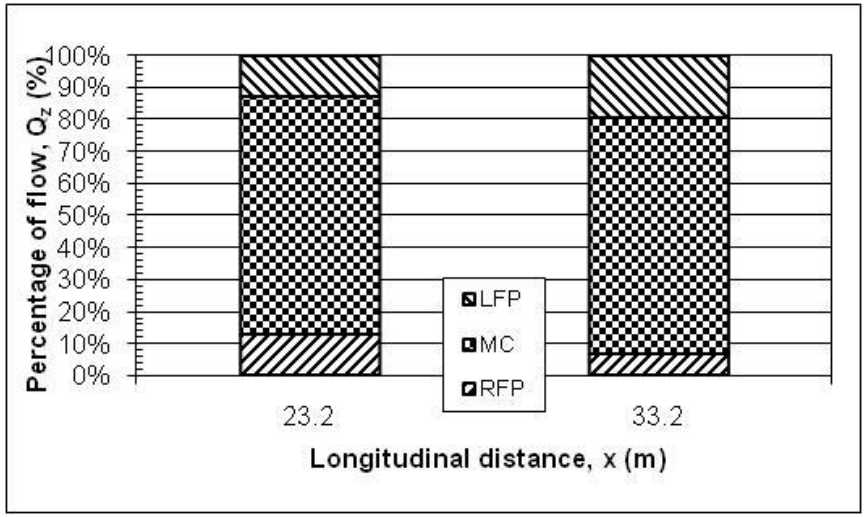

Figure 7.18b-Proportion of flow for FCF skewed series A14 H=0.1981m s=1, θ=5.1^{o}

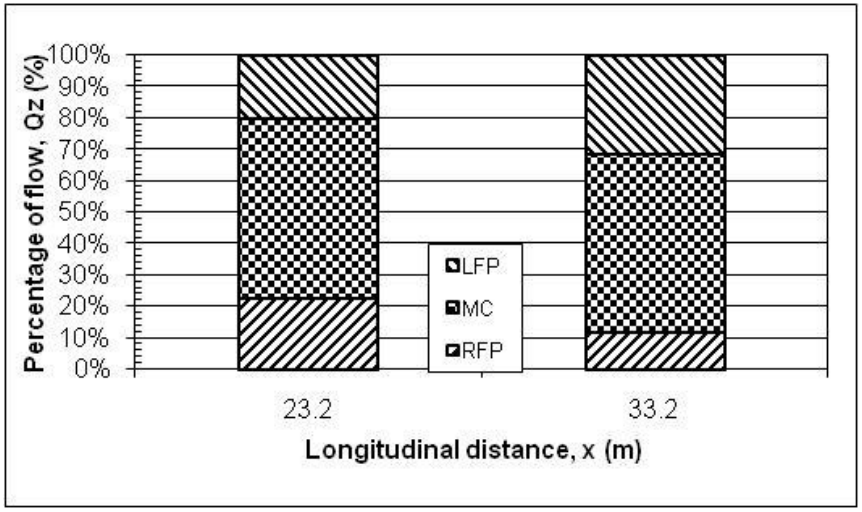

Figure 7.18c-Proportion of flow for FCF skewed series A14 H=0.2532m s=1, θ=5.1^{o}

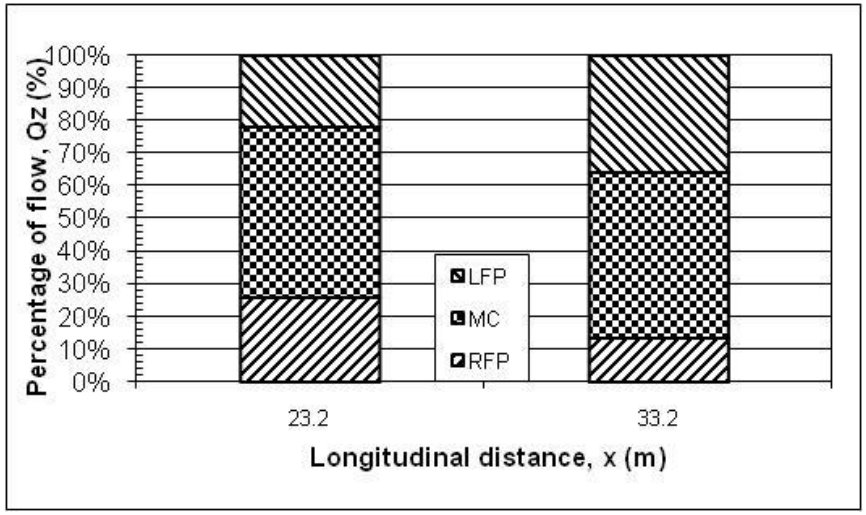

Figure 7.18d-Proportion of flow for FCF skewed series A14 H=0.2977m s=1, θ=5.1^{o}

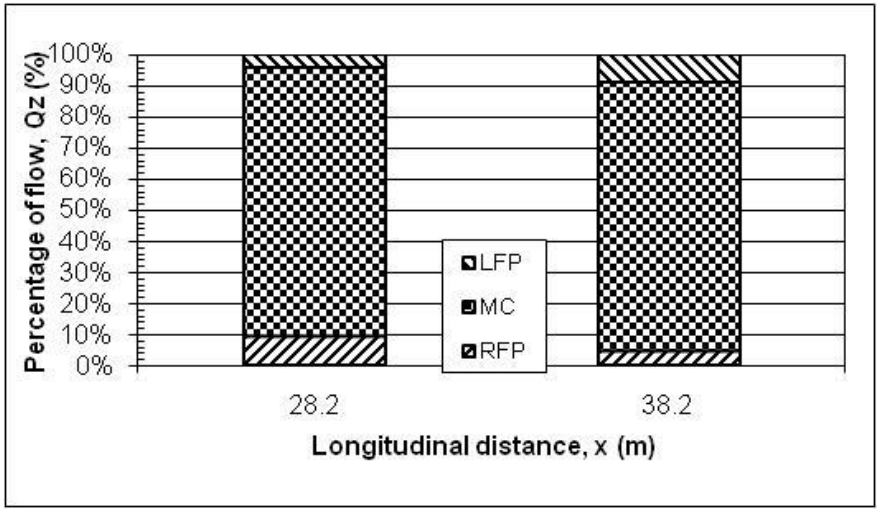

Figure 7.19a-Proportion of flow for FCF skewed series A15, H=0.1756m s=1, θ=9.2^{o}

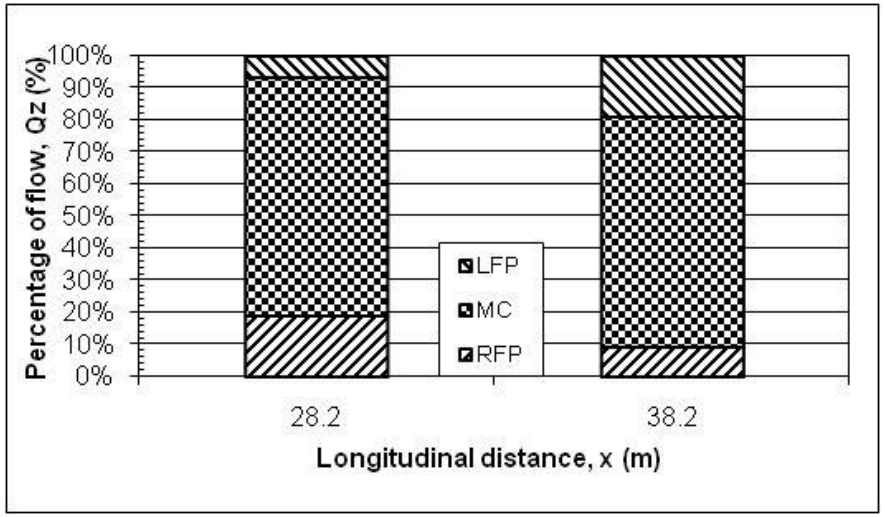

Figure 7.19b-Proportion of flow for FCF skewed series A15, H=0.1978m s=1, θ=9.2^{o}

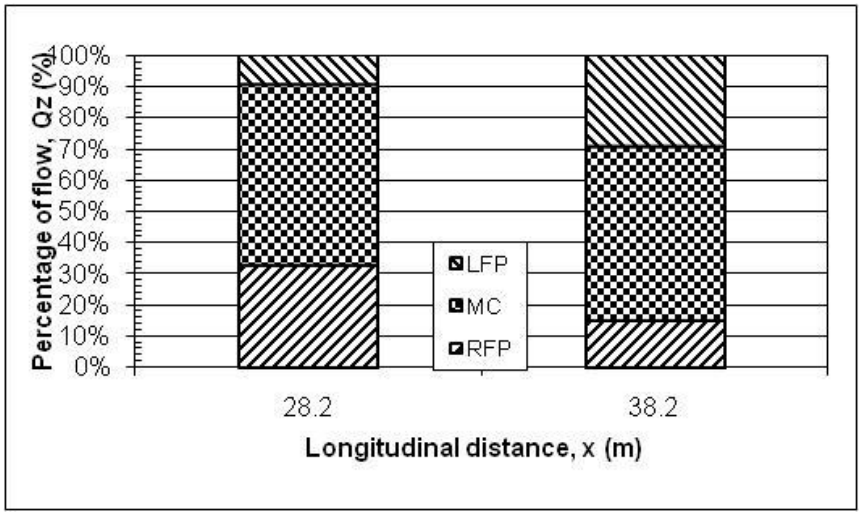

Figure 7.19c-Proportion of flow for FCF skewed series A15, H=0.2534m s=1, θ=9.2^{o}

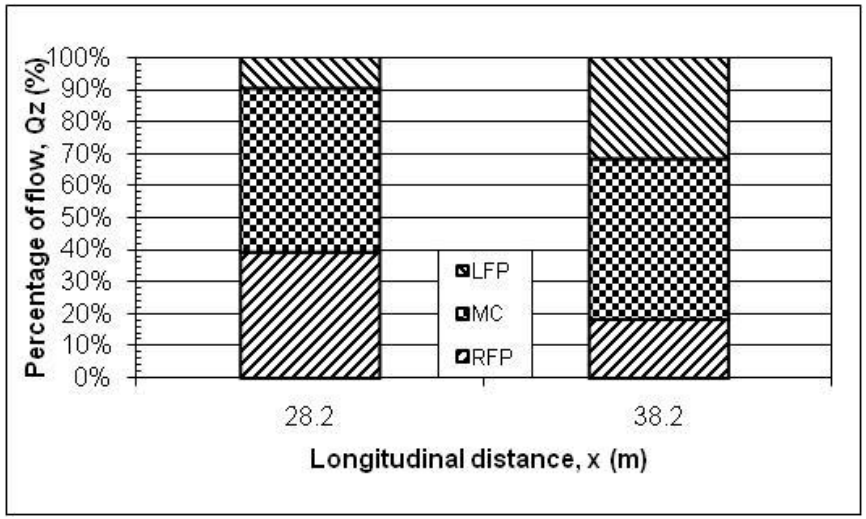

Figure 7.19d-Proportion of flow for FCF skewed series A15, H=0.2990m s=1, θ=9.2^{o}

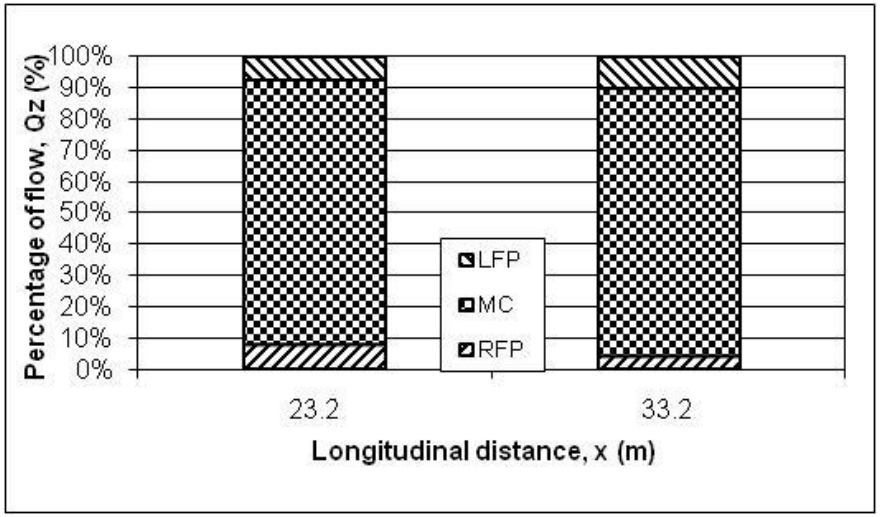

Figure 7.20a-Proportion of flow for FCF skewed series A16 H=0.1755m s=0, θ=5.1^{o}

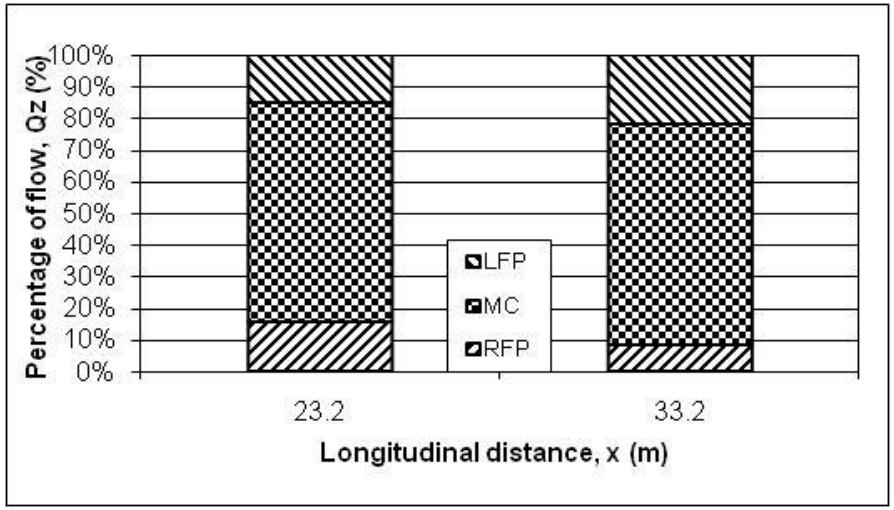

Figure 7.20b-Proportion of flow for FCF skewed series A16 H=0.1984m s=0, θ=5.1^{o}

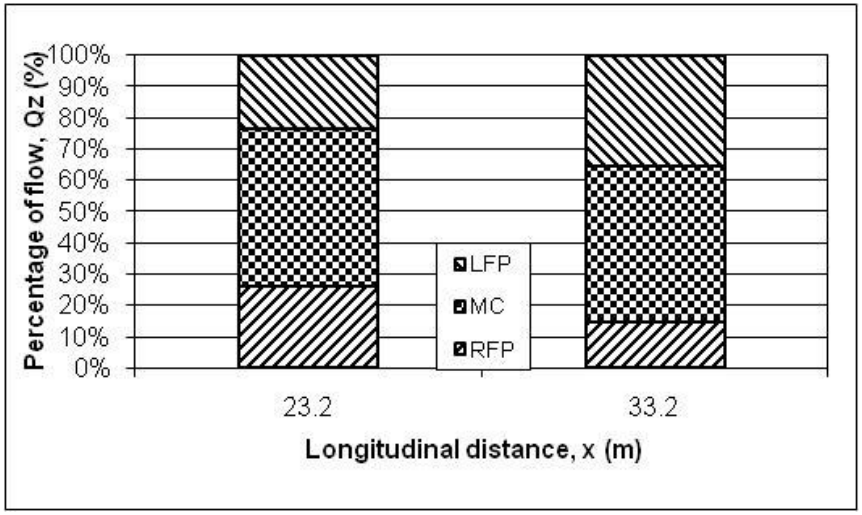

Figure 7.20c-Proportion of flow for FCF skewed series A16 H=0.2528m s=0, θ=5.1^{o}

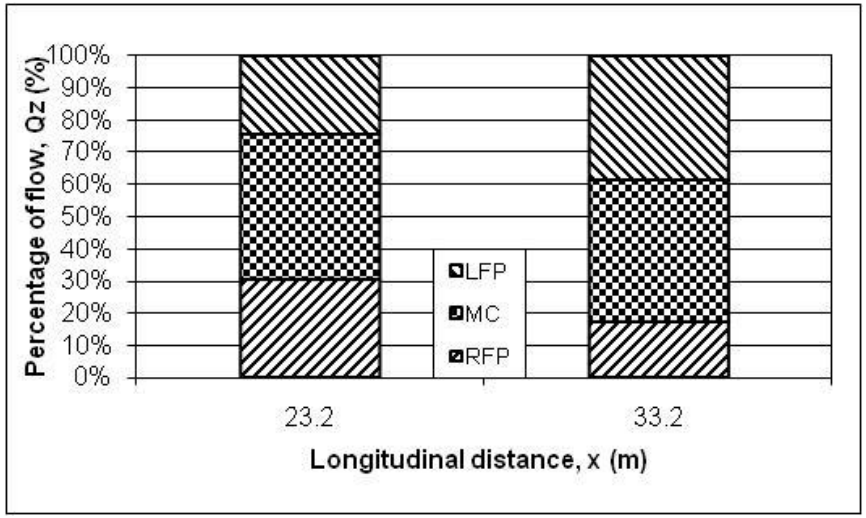

Figure 7.20d-Proportion of flow for FCF skewed series A16 H=0.2968m s=0, θ=5.1^{o}

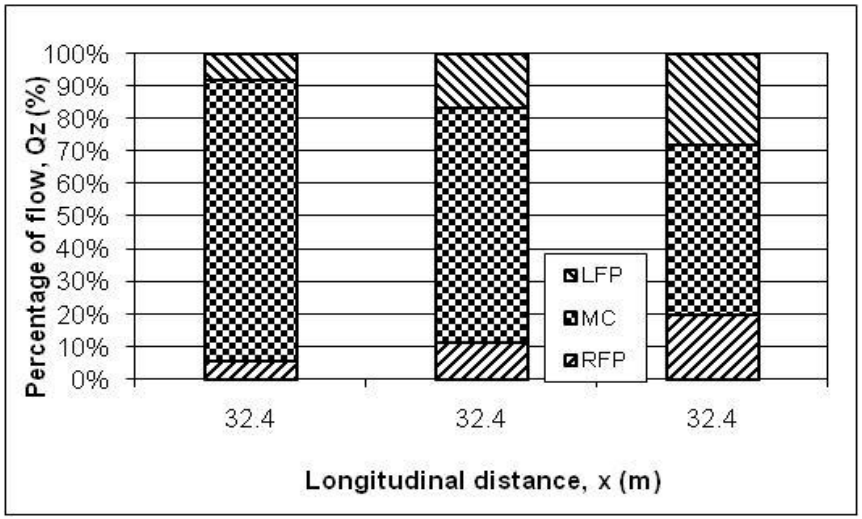

Figure 7.21-Proportion of flow for FCF skewed series A17 all depths s=0, θ=2.1°

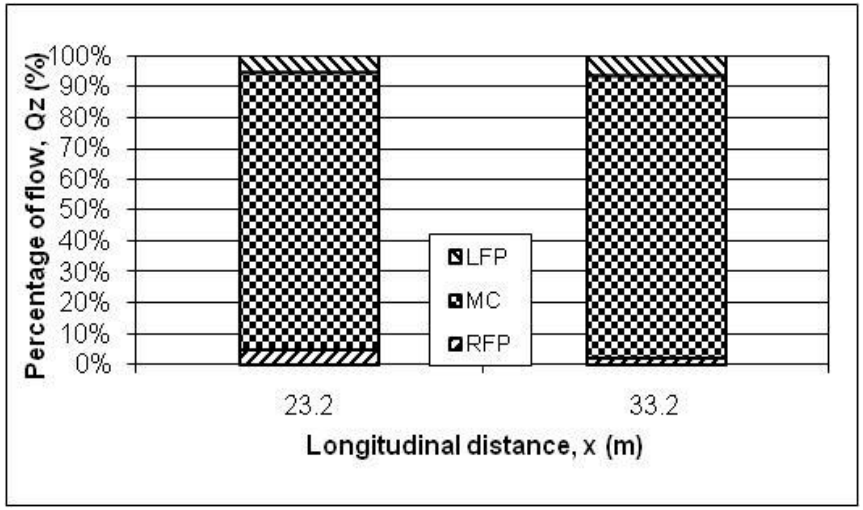

Figure 7.22a-Proportion of flow for FCF skewed series A18 H=0.1755m s=2, θ=5.1°

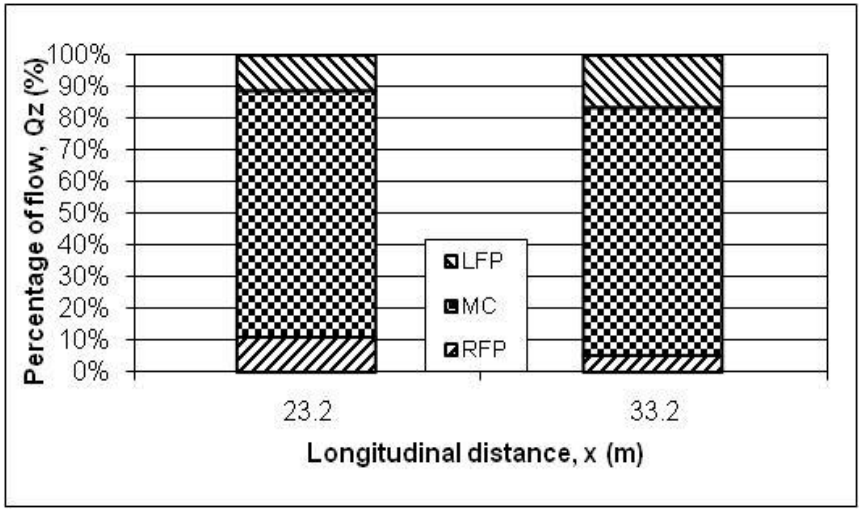

Figure 7.22b-Proportion of flow for FCF skewed series A18 H=0.1980m s=2, θ=5.1°

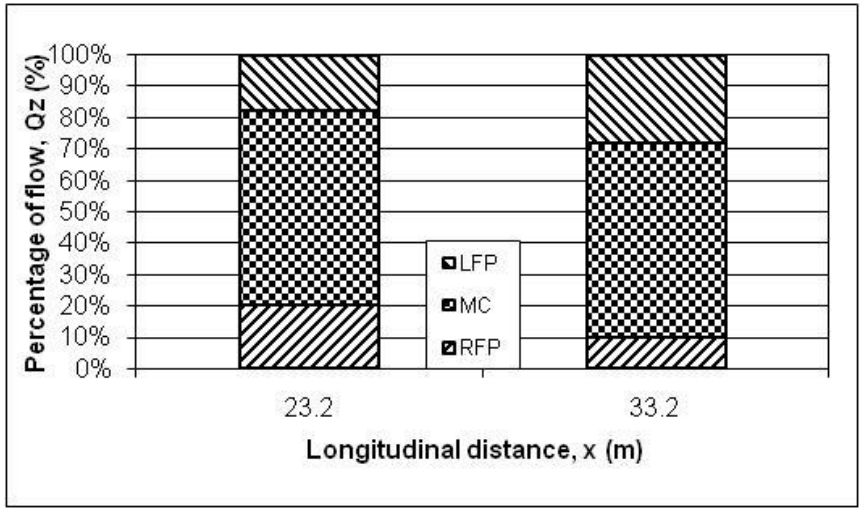

Figure 7.22c-Proportion of flow for FCF skewed series A18 H=0.2513m s=2, θ=5.1°

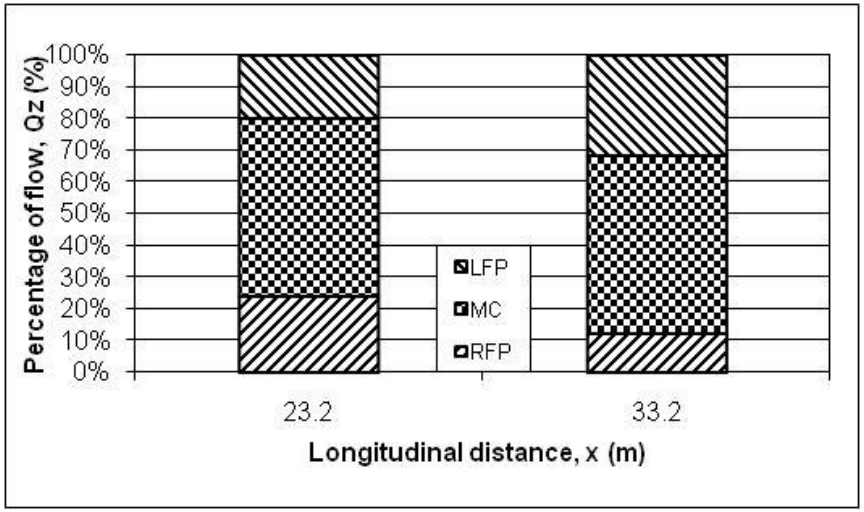

Figure 7.22d-Proportion of flow for FCF skewed series A18 H=0.2920m s=2, θ=5.1°

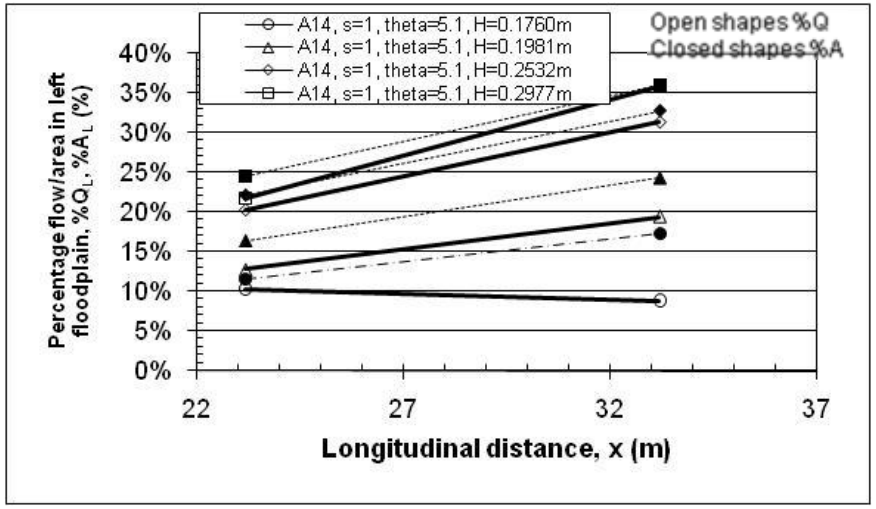

Figure 7.23a-Proportion of total flow on left floodplain for Series A14, s=1, θ=5.1°

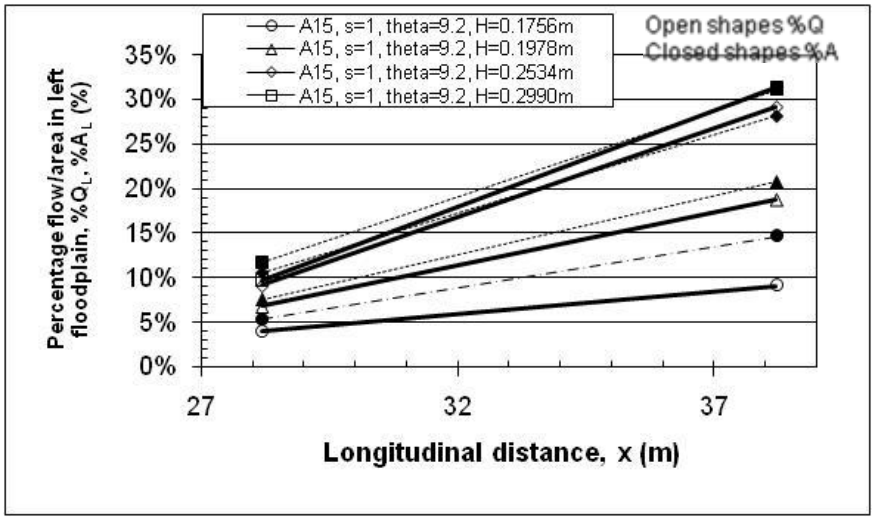

Figure 7.23b-Proportion of total flow on left floodplain for Series A15, s=1, θ=9.2°

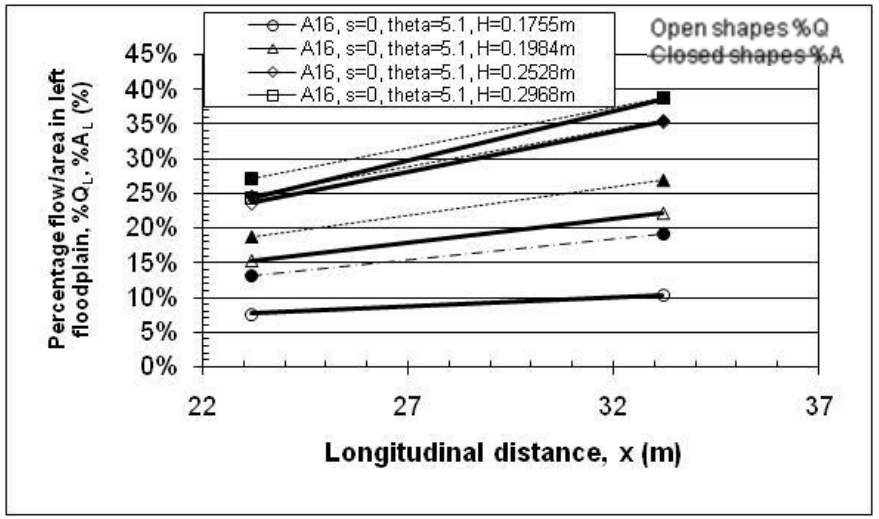

Figure 7.23c-Proportion of total flow on left floodplain for Series A16, s=0, θ=5.1°

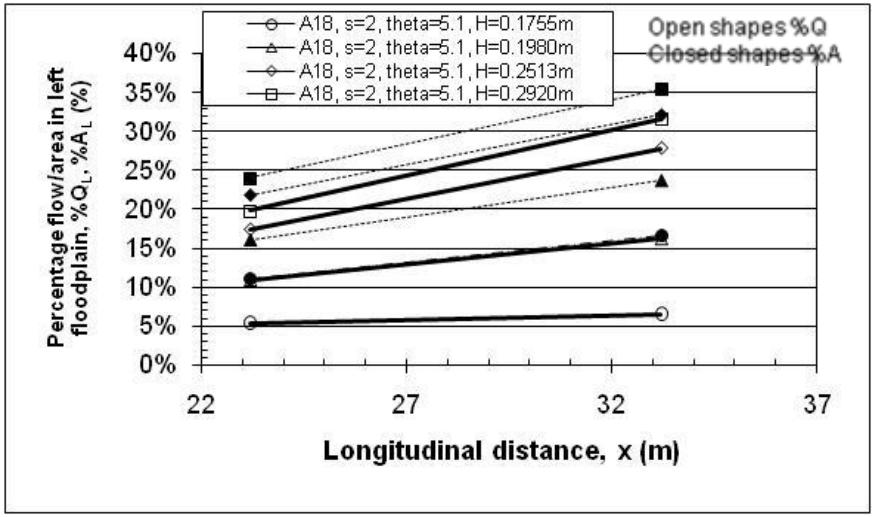

Figure 7.23d-Proportion of total flow on left floodplain for Series A18, s=2, θ=5.1^o

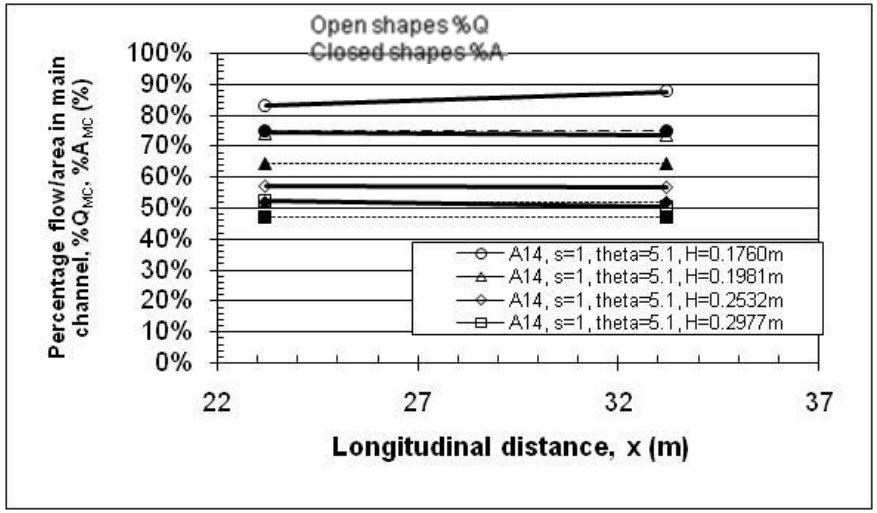

Figure 7.24a-Proportion of total flow on main channel for Series A14, s=1, θ=5.1^o

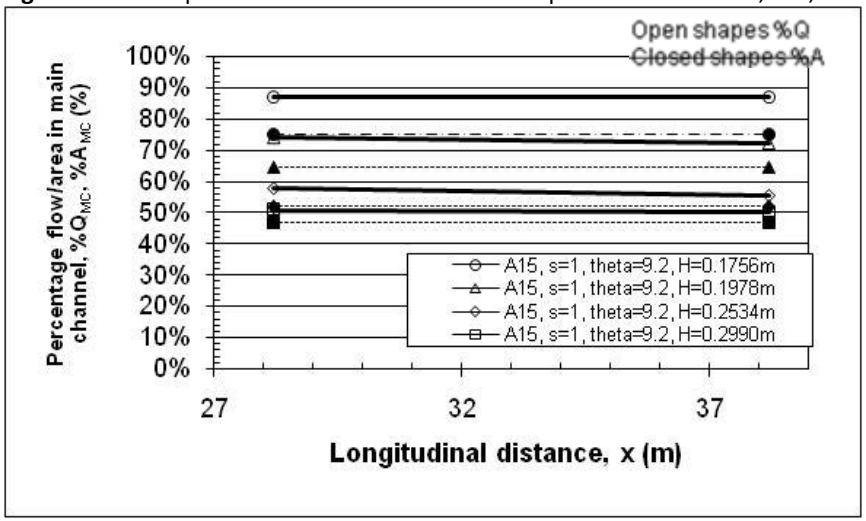

Figure 7.24b-Proportion of total flow on main channel for Series A15, s=1, θ=9.2^o

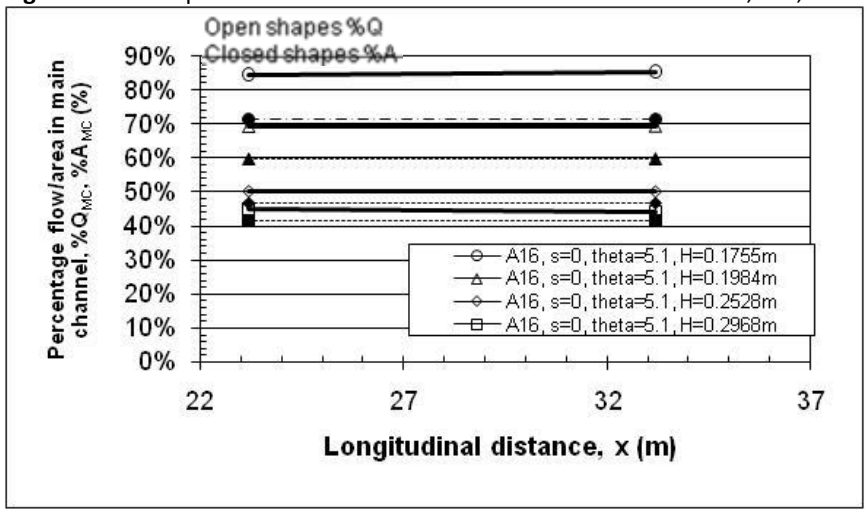

Figure 7.24c-Proportion of total flow on main channel for Series A16, s=0, θ=5.1^o

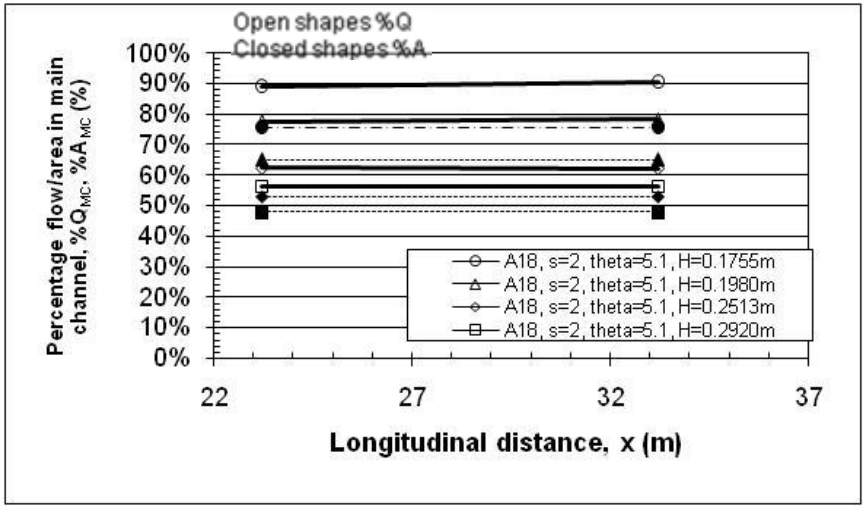

Figure 7.24d-Proportion of total flow on main channel for Series A18, s=2, θ=5.1^{o}

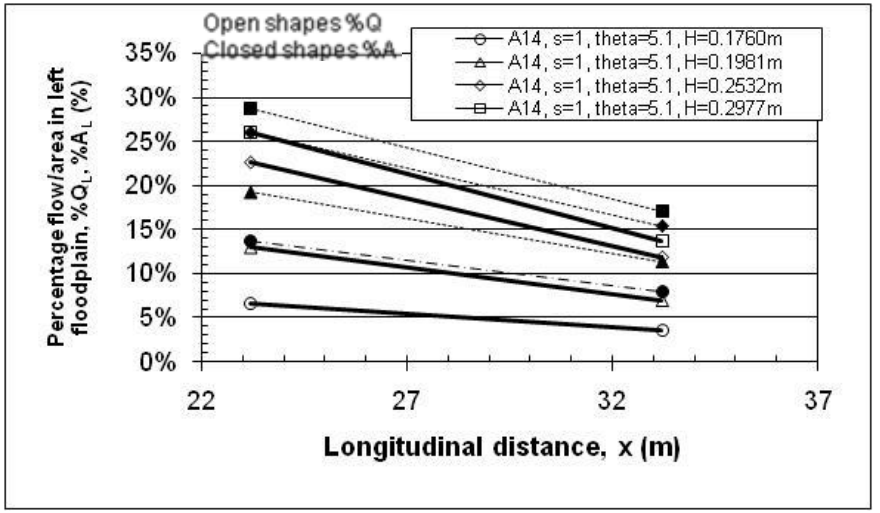

Figure 7.25a-Proportion of total flow on right floodplain for Series A14, s=1, θ=5.1^{o}

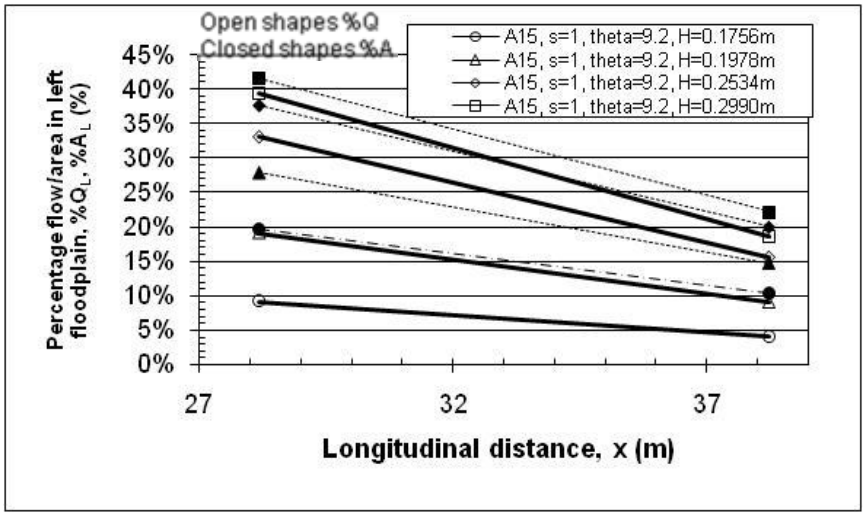

Figure 7.25b-Proportion of total flow on right floodplain for Series A15, s=1, θ=9.2^{o}

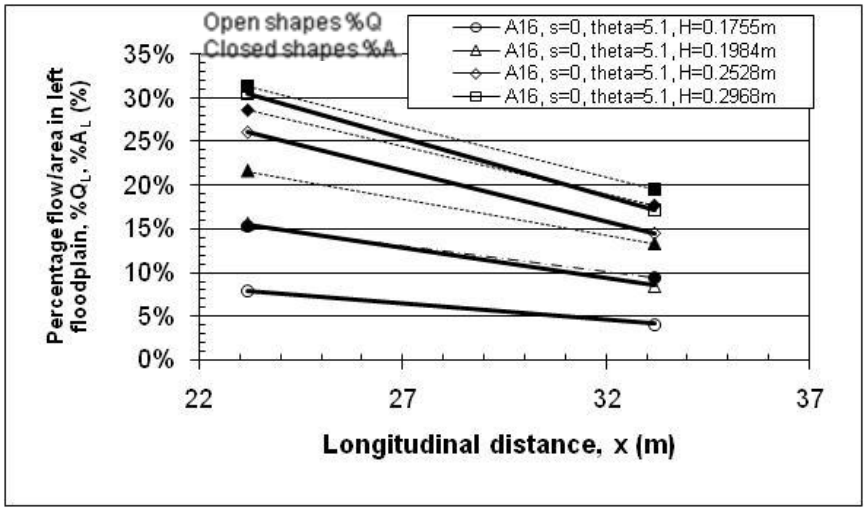

Figure 7.25c-Proportion of total flow on right floodplain for Series A16, s=0, θ=5.1^{o}

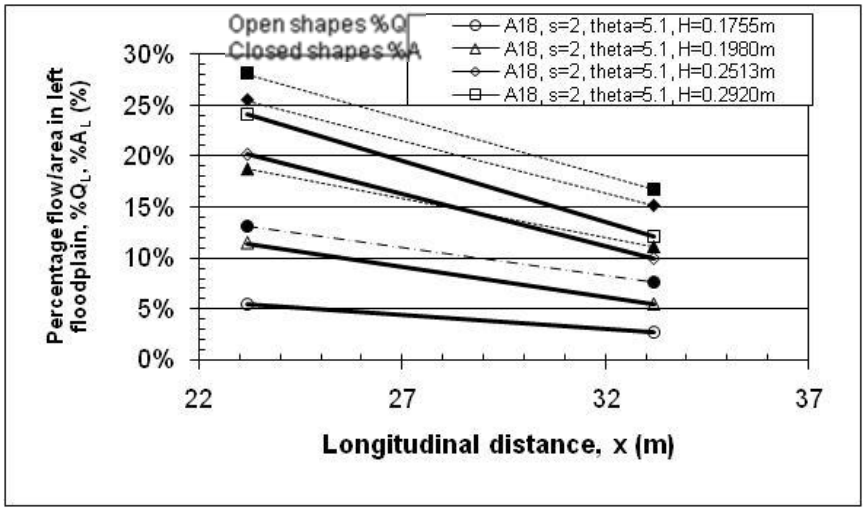

Figure 7.25d-Proportion of total flow on right floodplain for Series A18, s=2, θ=5.1°

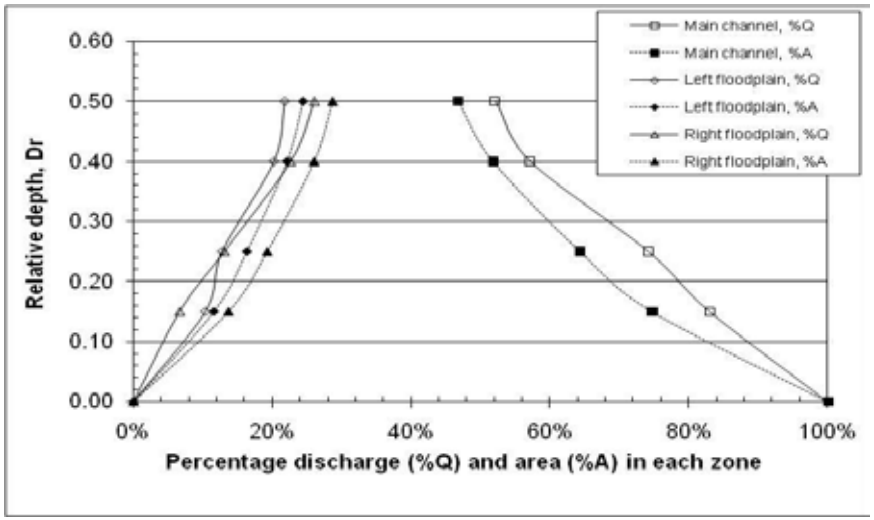

Figure 7.26a-Percentage discharge and area in each zone for Series A14, θ=5.1°, s=1 Upstream values

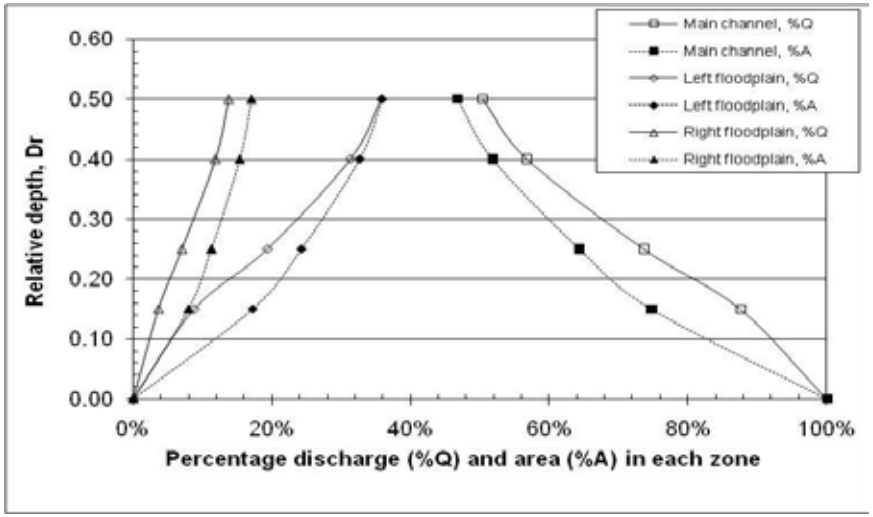

Figure 7.26b-Percentage discharge and area in each zone for Series A14, θ=5.1°, s=1 Downstream values

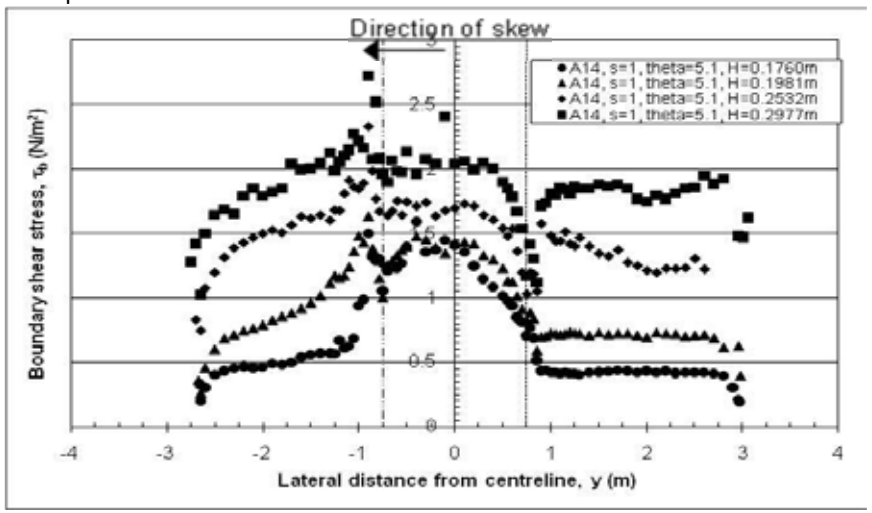

Figure 7.27a-A14, s=1, θ=5.1°, boundary shear stress at upstream (x=23.2m) section

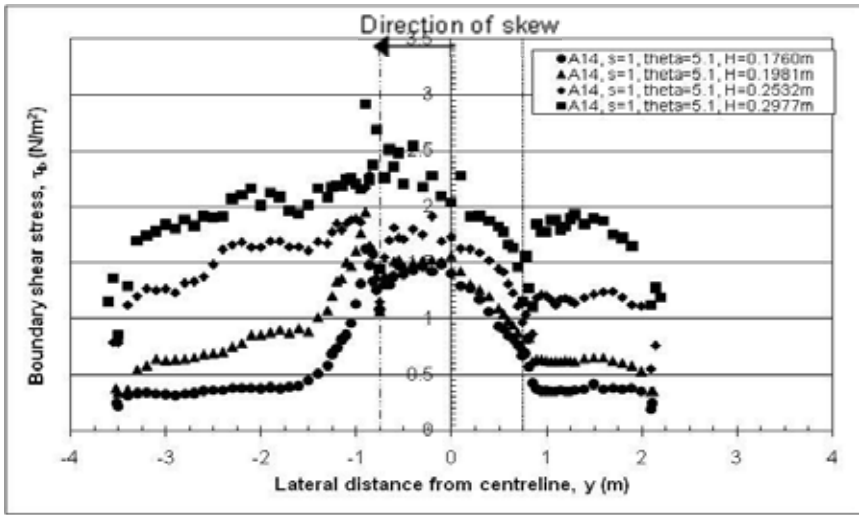

Figure 7.27b-A14, s=1, θ=5.1°, boundary shear stress at downstream (x=23.2m) section

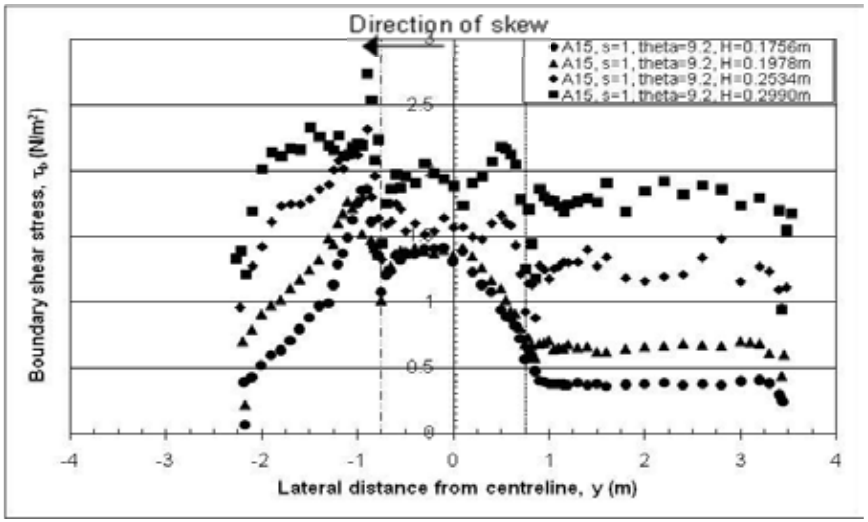

Figure 7.27c-A15, s=1, θ=9.2°, boundary shear stress at upstream (x=23.2m) section

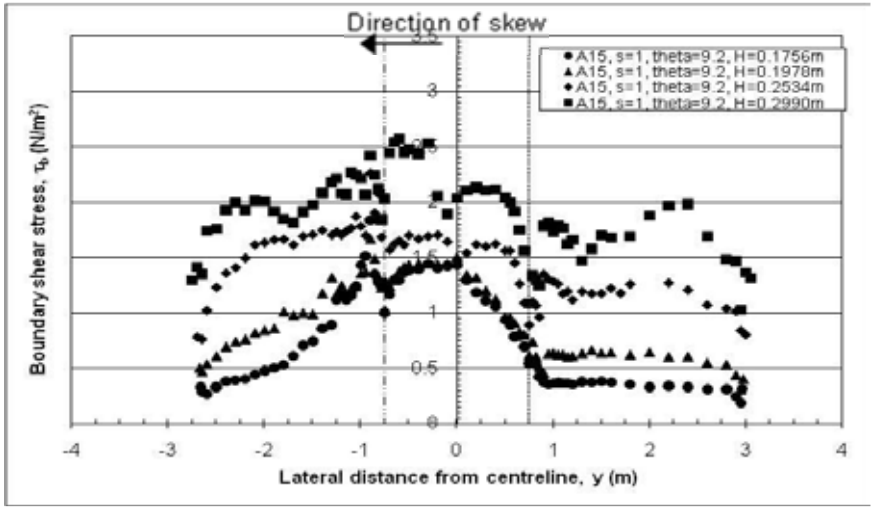

Figure 7.27d-A15, s=1, θ=9.2°, boundary shear stress at downstream (x=23.2m) section

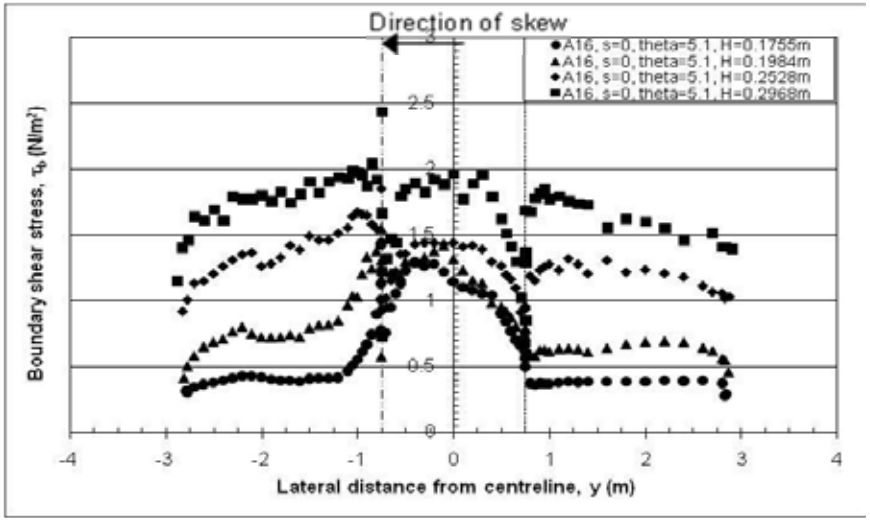

Figure 7.27e-A16, s=0, θ=5.1°, boundary shear stress at upstream (x=23.2m) section

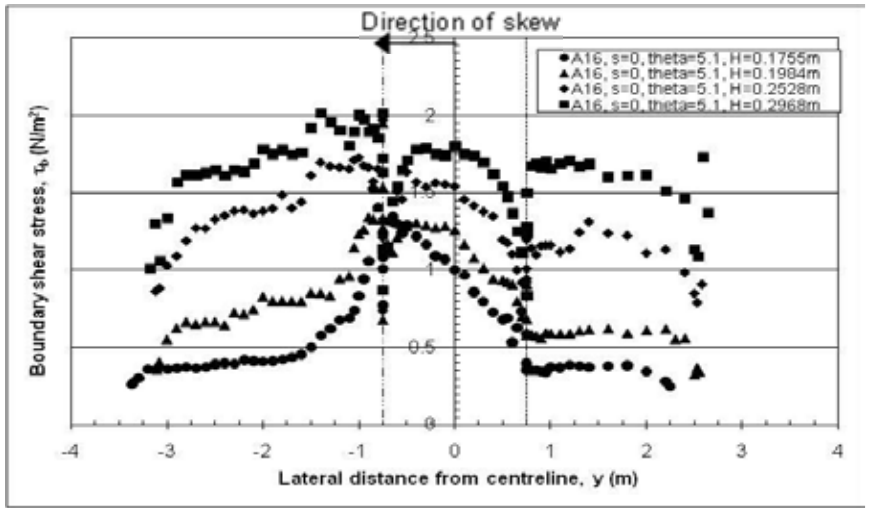

Figure 7.27f-A16, s=0, θ=5.1°, boundary shear stress at intermediate (x=23.2m) section

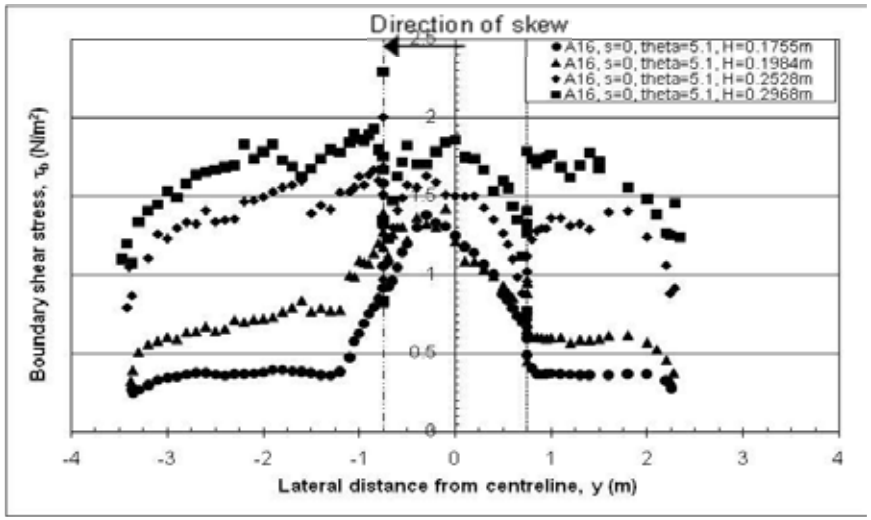

Figure 7.27g-A16, s=0, θ=5.1°, boundary shear stress at downstream (x=23.2m) section

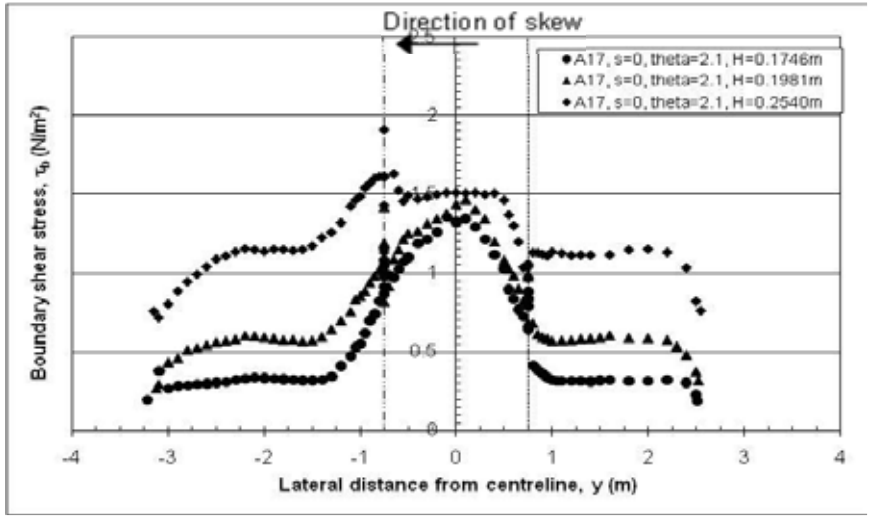

Figure 7.27h-A16, s=0, θ=2.1°, boundary shear stress at upstream (x=23.2m) section

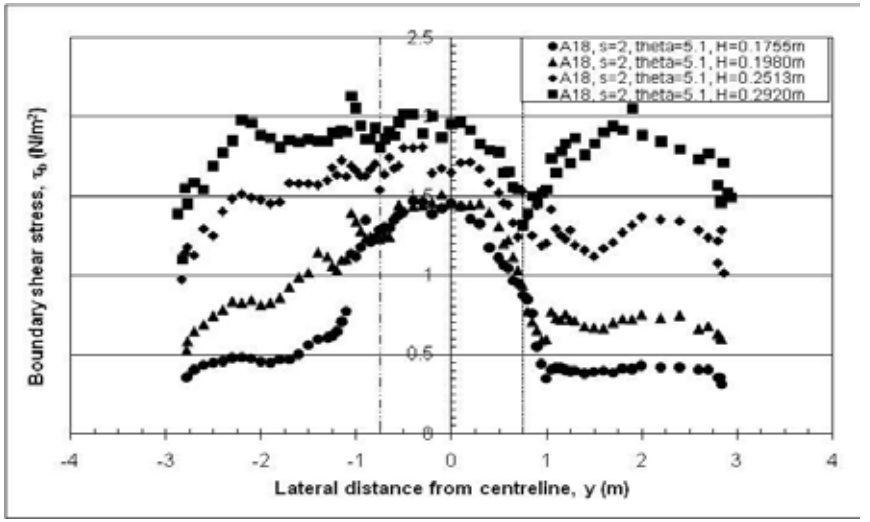

Figure 7.27i-A18, s=2, θ=5.1°, boundary shear stress at upstream (x=23.2m) section

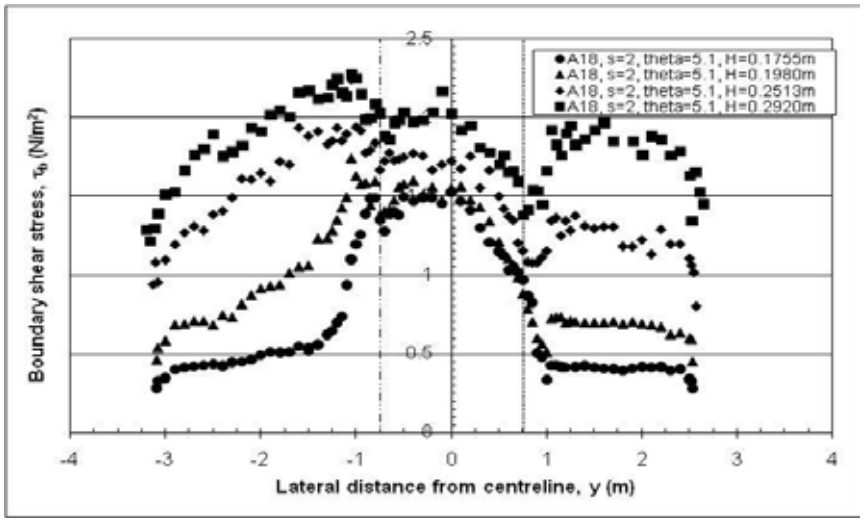

Figure 7.27j-A18, s=2, θ=5.1°, boundary shear stress at intermediate (x=23.2m) section

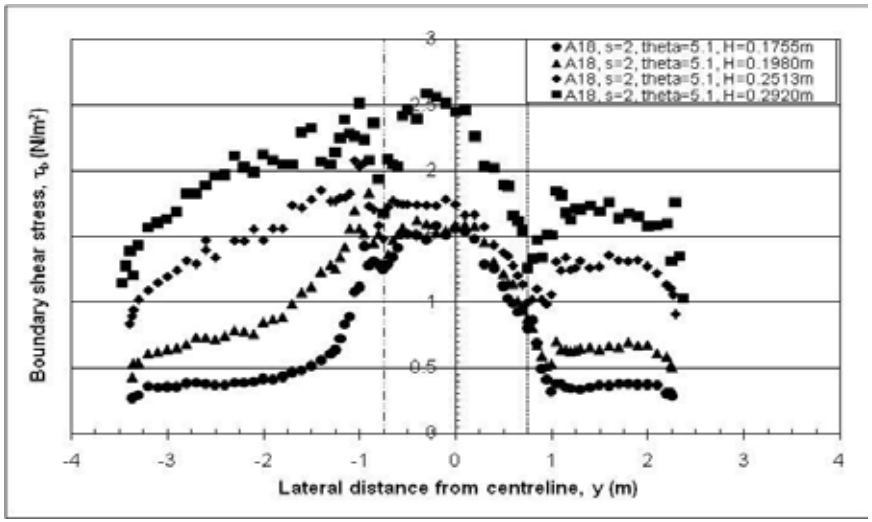

Figure 7.27k-A18, s=2, θ=5.1°, boundary shear stress at downstream (x=23.2m) section

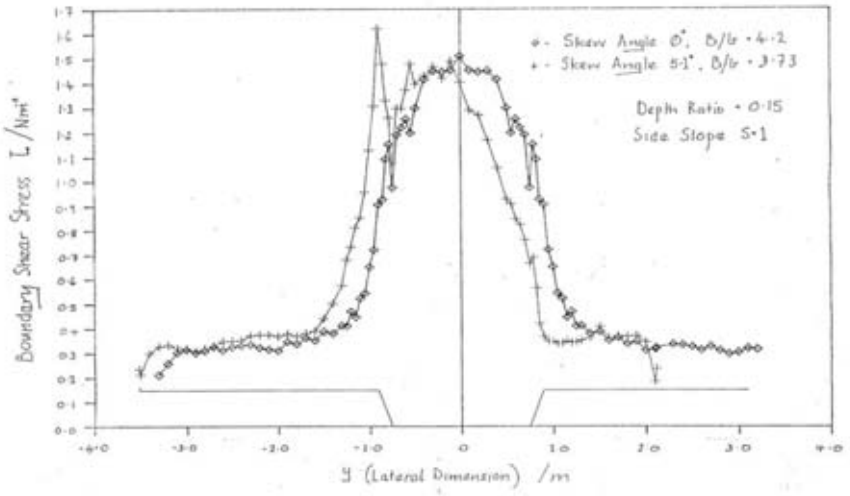

Figure 7.28a-Boundary shear distribution, comparison of straight and skewed channels (Elliott, 1990)

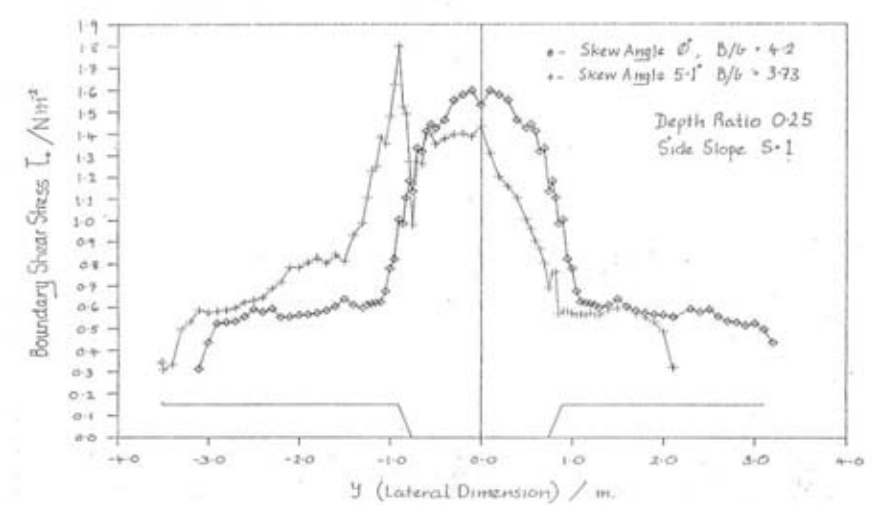

Figure 7.28b-Boundary shear distribution, comparison of straight and skewed channels (Elliott, 1990)

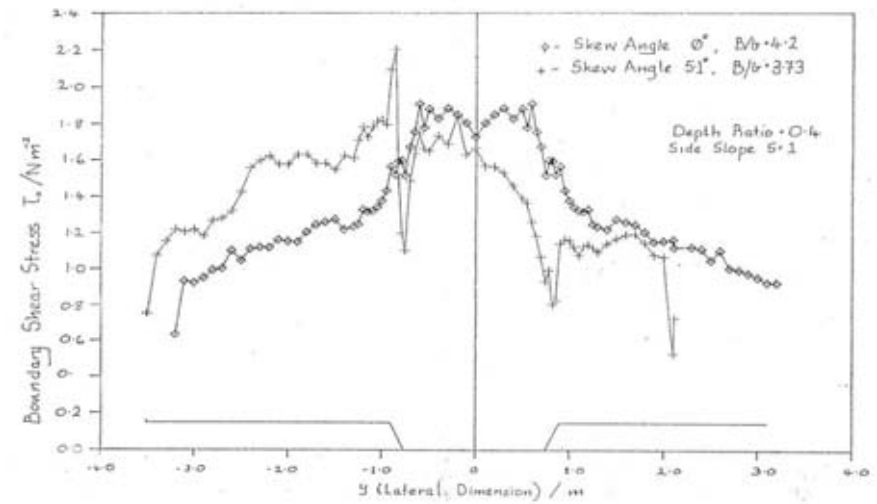

Figure 7.28c-Boundary shear distribution, comparison of straight and skewed channels (Elliott, 1990)

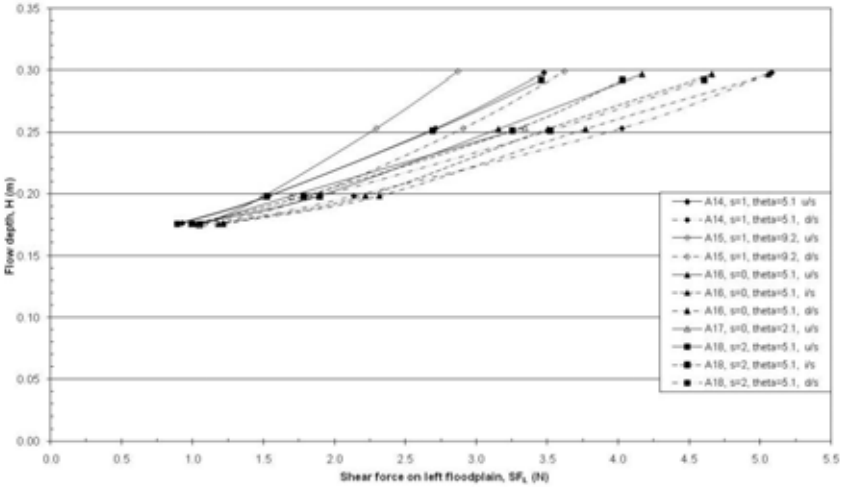

Figure 7.29a-Average shear force acting on the left hand floodplain after Elliott (1990)

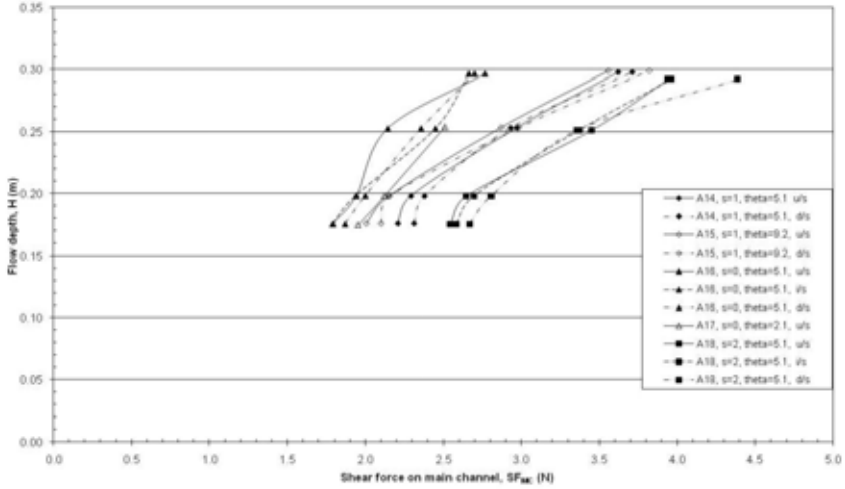

Figure 7.29b-Average shear force acting on the main channel after Elliott (1990)

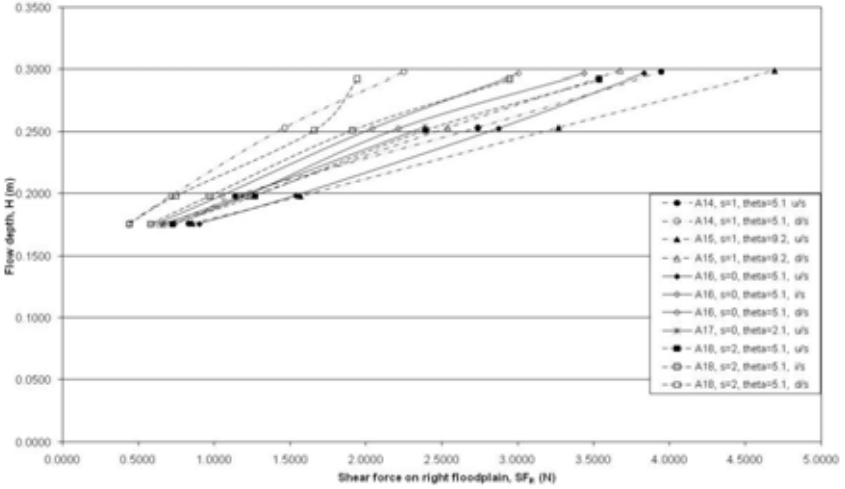

Figure 7.29c-Average shear force acting on the right hand floodplain after Elliott (1990)

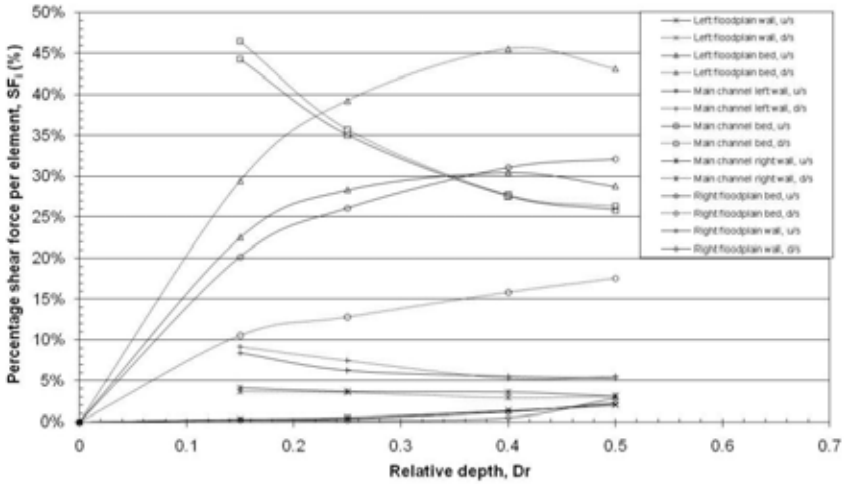

Figure 7.30a-Percentage of shear force on any element, Series A14, s=1, θ=5.1^{o}

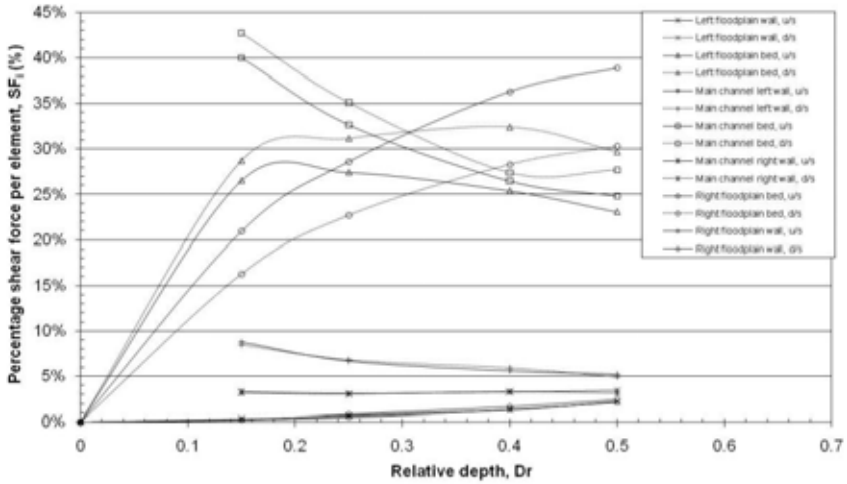

Figure 7.30b-Percentage of shear force on any element, Series A15, s=1, θ=9.2^{o}

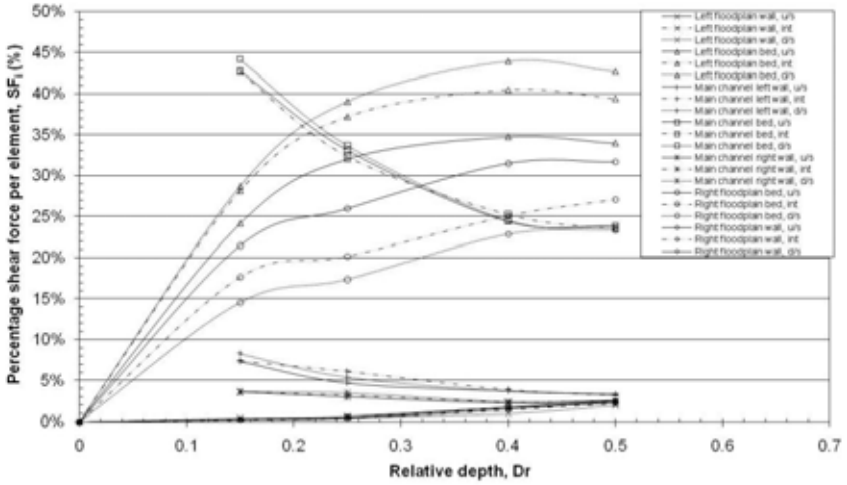

Figure 7.30c-Percentage of shear force on any element, Series A16, s=0, θ=5.1^{o}

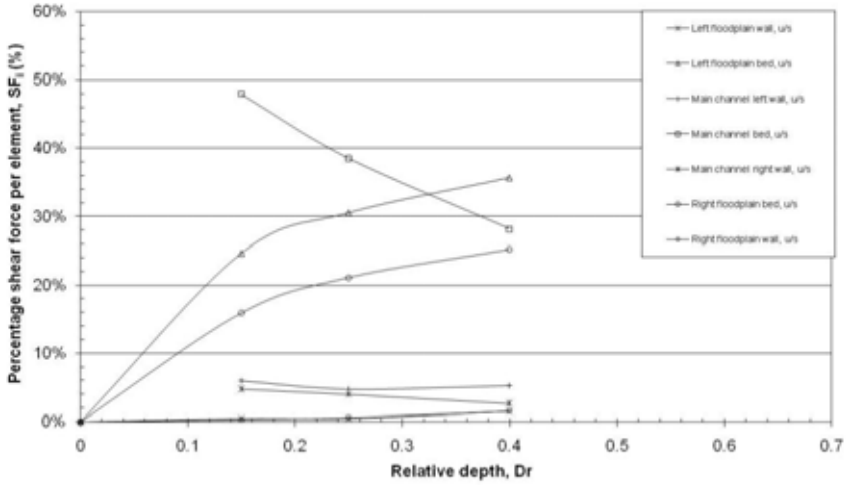

Figure 7.30d-Percentage of shear force on any element, Series A17, s=0, θ=2.1^{o}

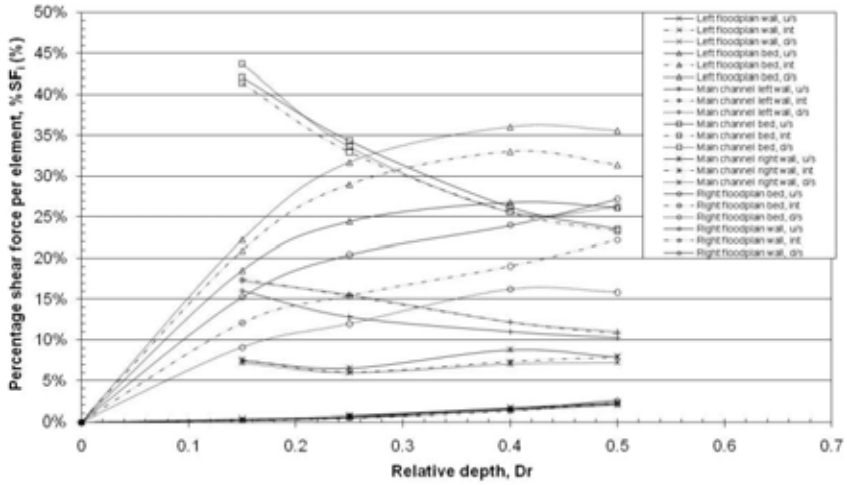

Figure 7.30e-Percentage of shear force on any element, Series A18, s=2, θ=5.1^{o}

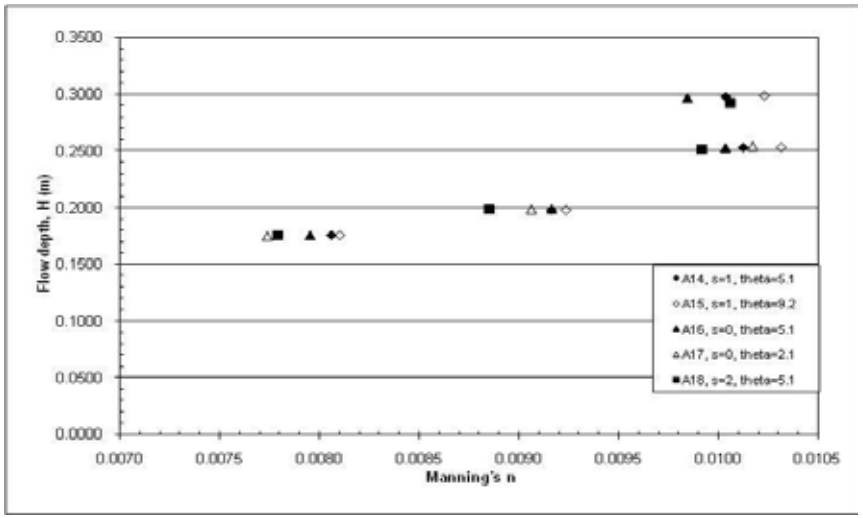

Figure 7.31-Manning's global roughness coefficient, *n*, against depth for the FCF skewed data

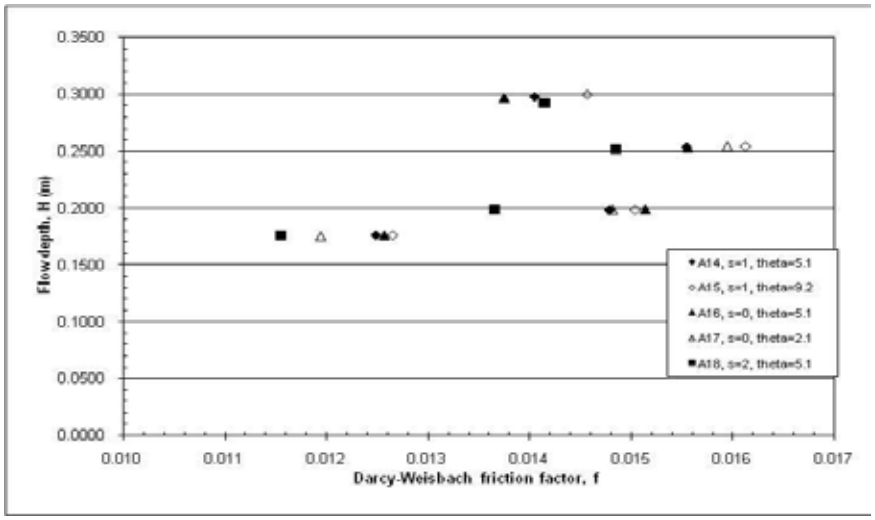

Figure 7.32-Darcy-Weisbach global friction factor, *f*, against depth for the FCF skewed data

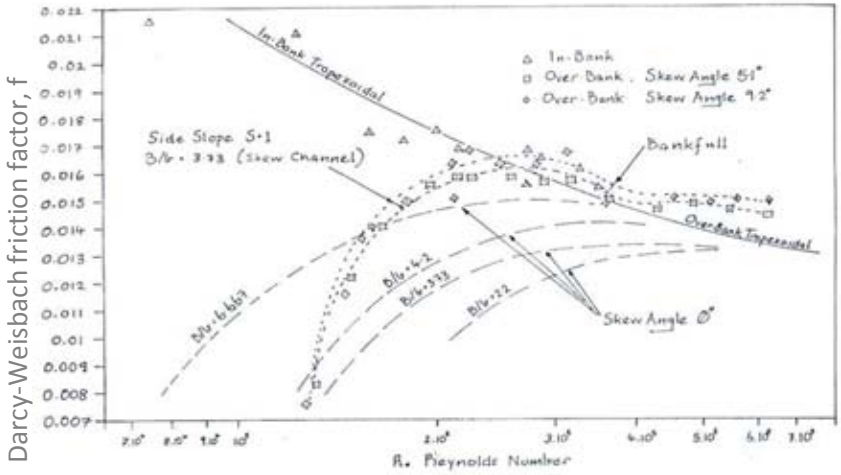

Figure 7.33-Skew channel Moody type diagram including straight channel data after Elliott (1990)

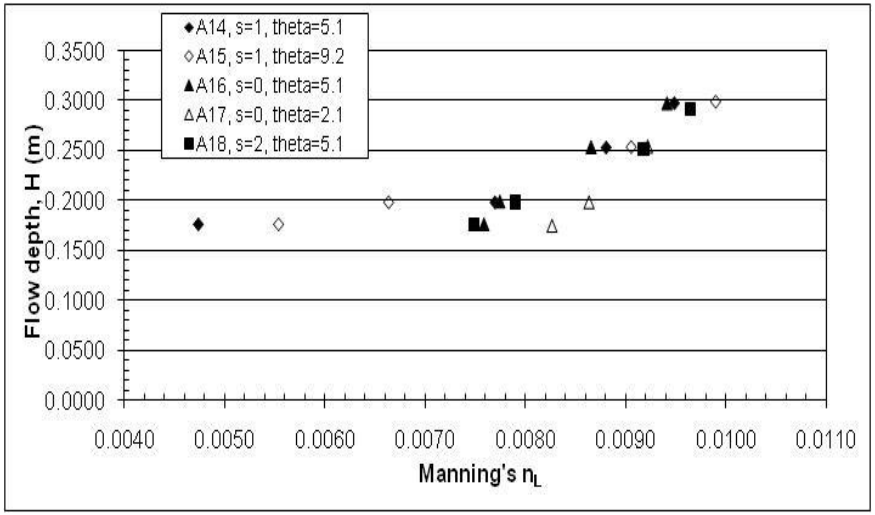

Figure 7.34a-Manning's zonal roughness coefficient, *n*, against depth for upstream left floodplain

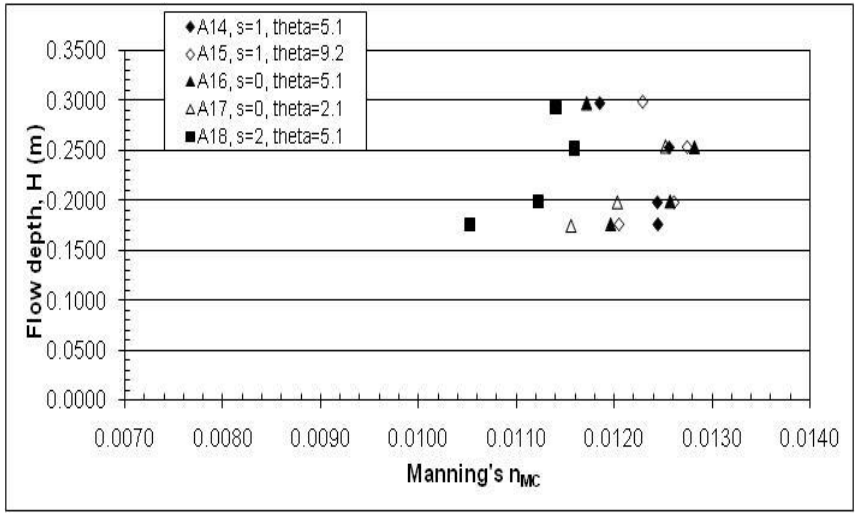

Figure 7.34b-Manning's zonal roughness coefficient, *n*, against depth for upstream main channel

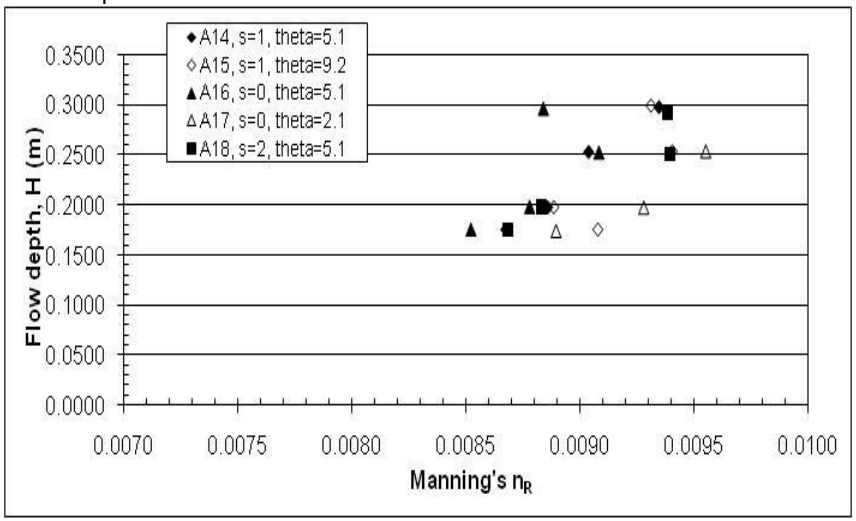

Figure 7.34c-Manning's zonal roughness coefficient, *n*, against depth for upstream right floodplain

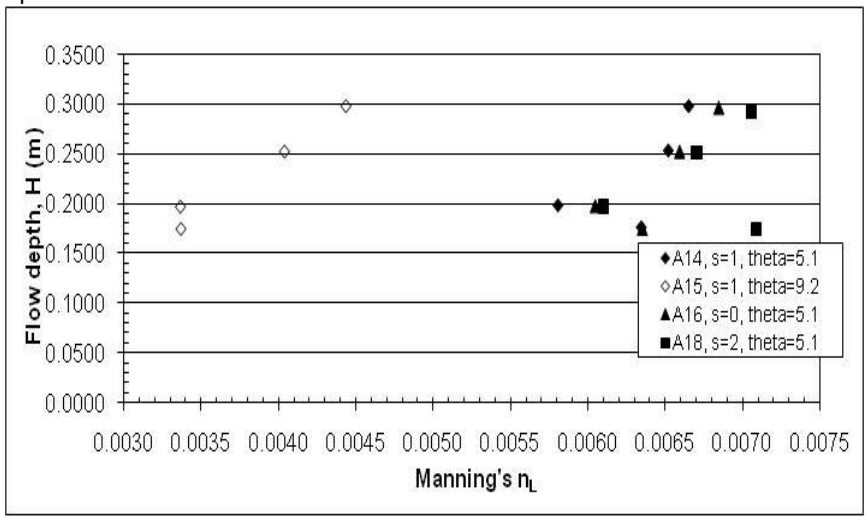

Figure 7.35a-Manning's zonal roughness coefficient, *n*, against depth for downstream left floodplain

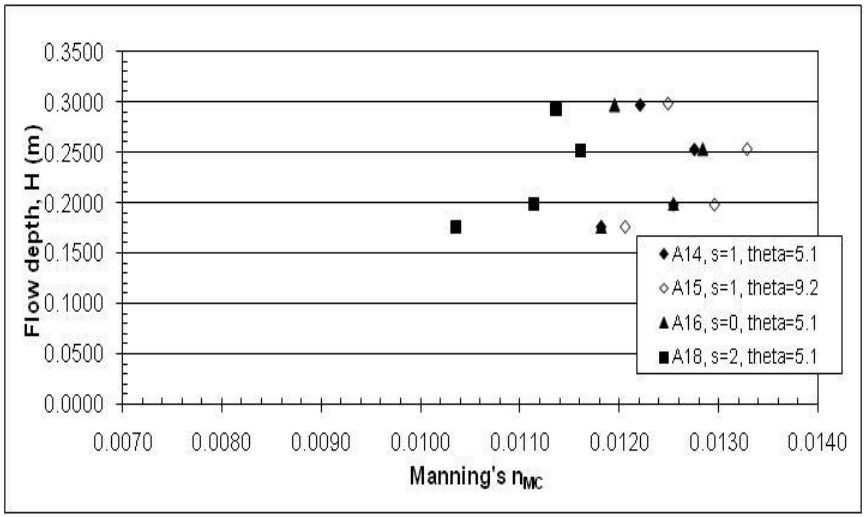

Figure 7.35b-Manning's zonal roughness coefficient, *n*, against depth for downstream main channel

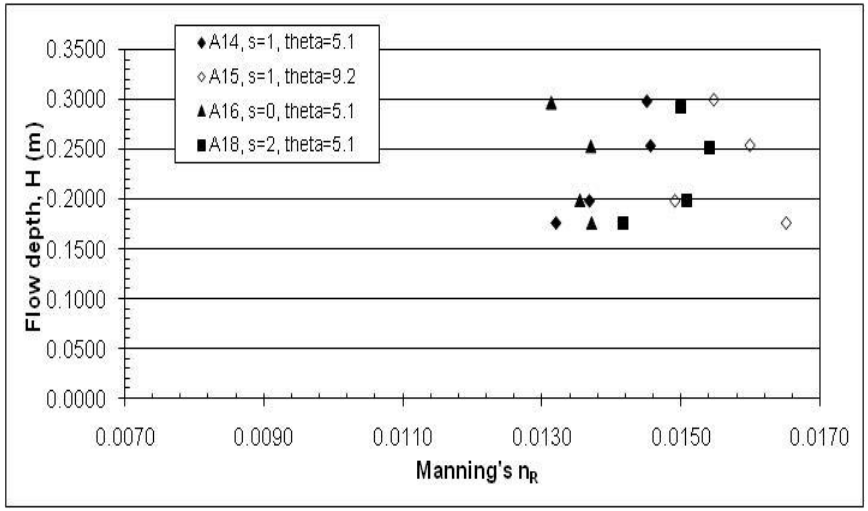

Figure 7.35c-Manning's zonal roughness coefficient, *n*, against depth for downstream right floodplain

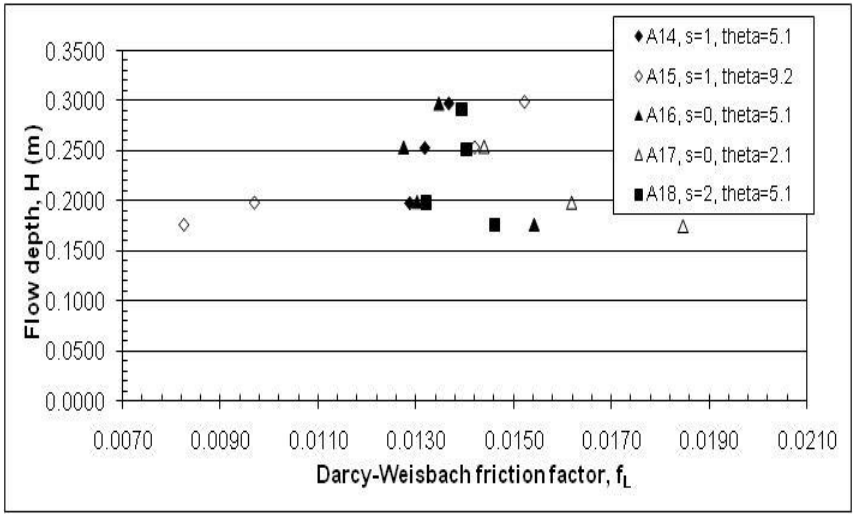

Figure 7.36a-Darcy-Weisbach zonal roughness coefficient, *f*, against depth for upstream left floodplain

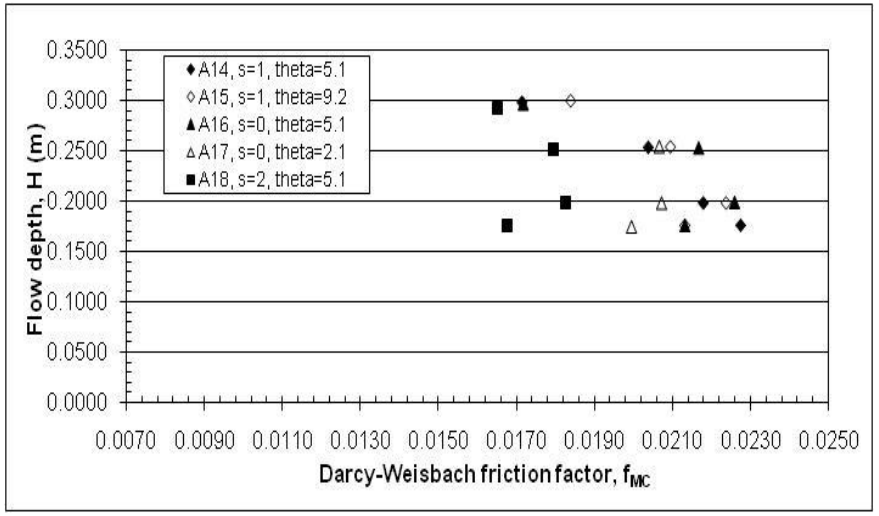

Figure 7.36b-Darcy-Weisbach zonal roughness coefficient, *f*, against depth for upstream left floodplain

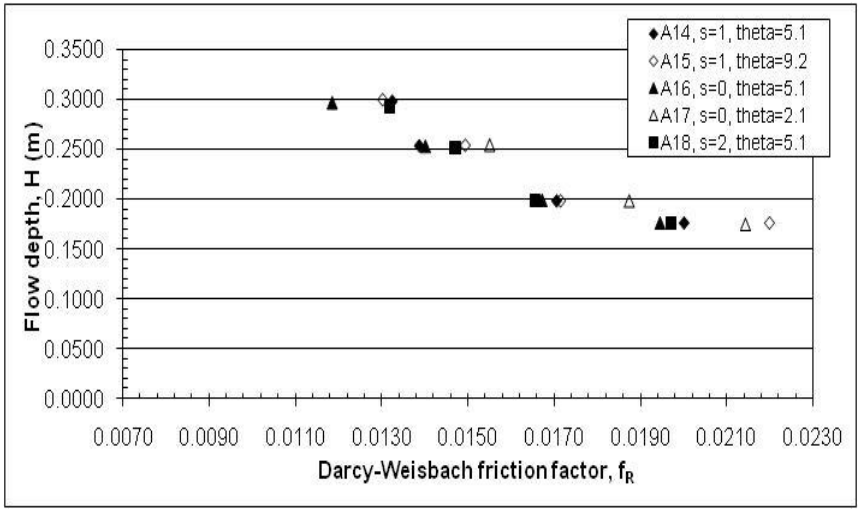

Figure 7.36c-Darcy-Weisbach zonal roughness coefficient, *f*, against depth for upstream left floodplain

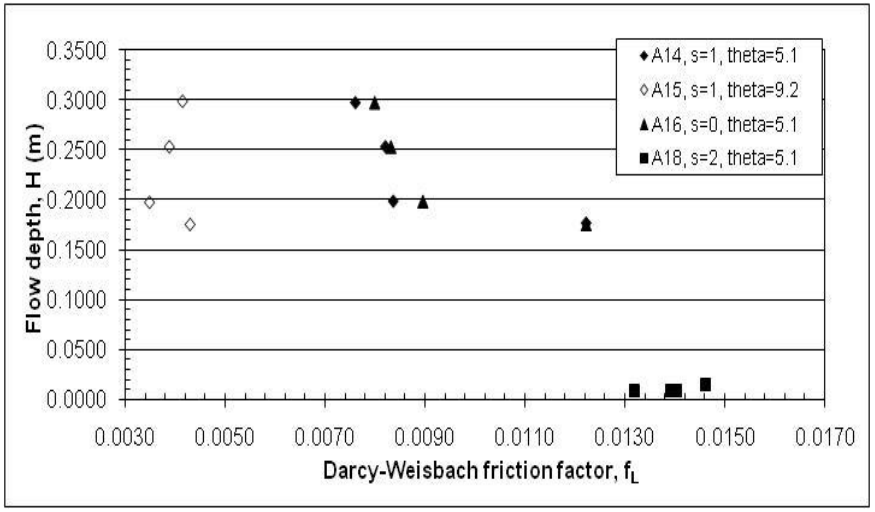

Figure 7.37a-Darcy-Weisbach zonal roughness coefficient, *f*, against depth for downstream left floodplain

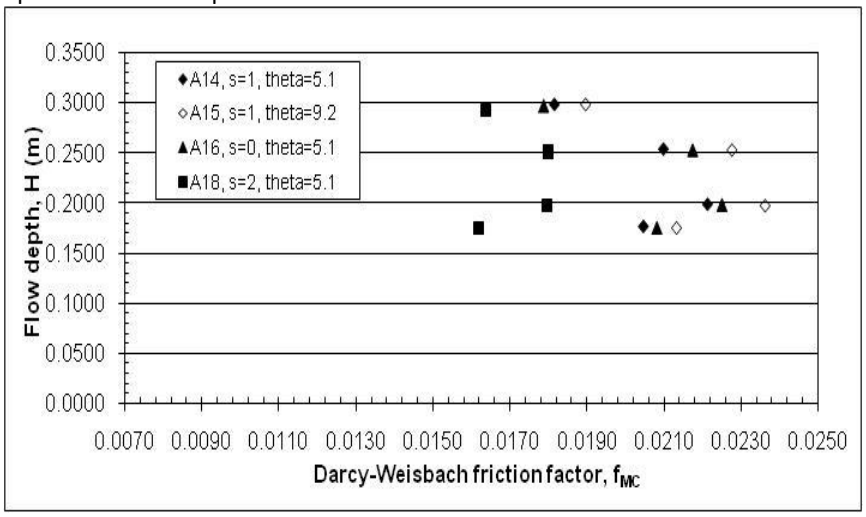

Figure 7.37b-Darcy-Weisbach zonal roughness coefficient, *f*, against depth for downstream left floodplain

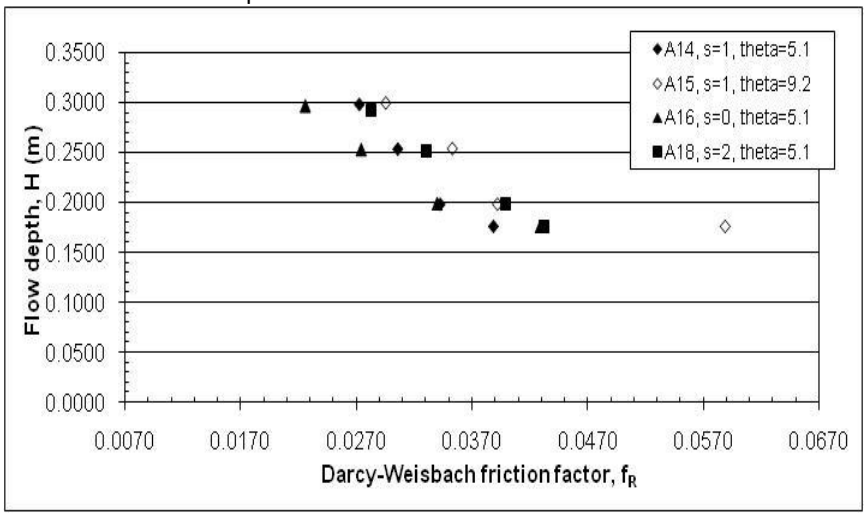

Figure 7.37c-Darcy-Weisbach zonal roughness coefficient, *f*, against depth for downstream left floodplain

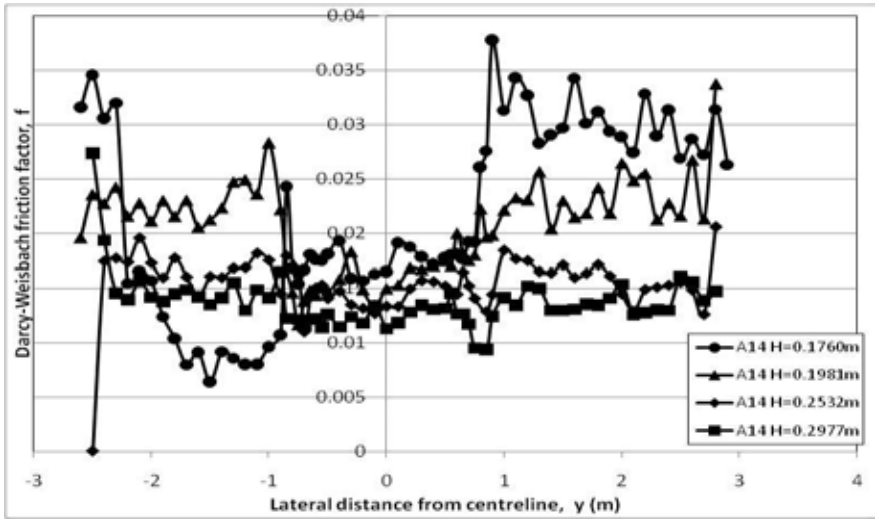

Figure 7.38a-Lateral distributions of local Darcy-Weisbach friction factor, *f*, for A14 upstream, s=1, θ=5.1^{o}

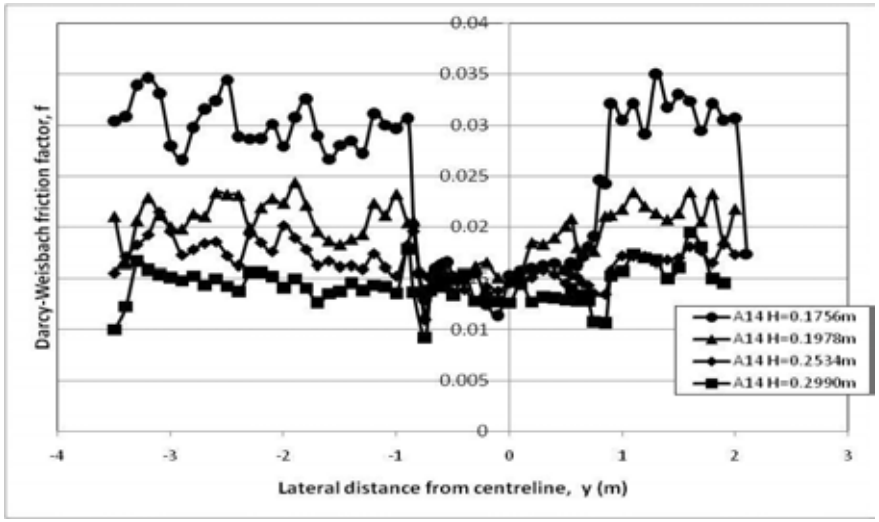

Figure 7.38b-Lateral distributions of local Darcy-Weisbach friction factor, *f*, for A14 downstream, s=1, θ=5.1^{o}

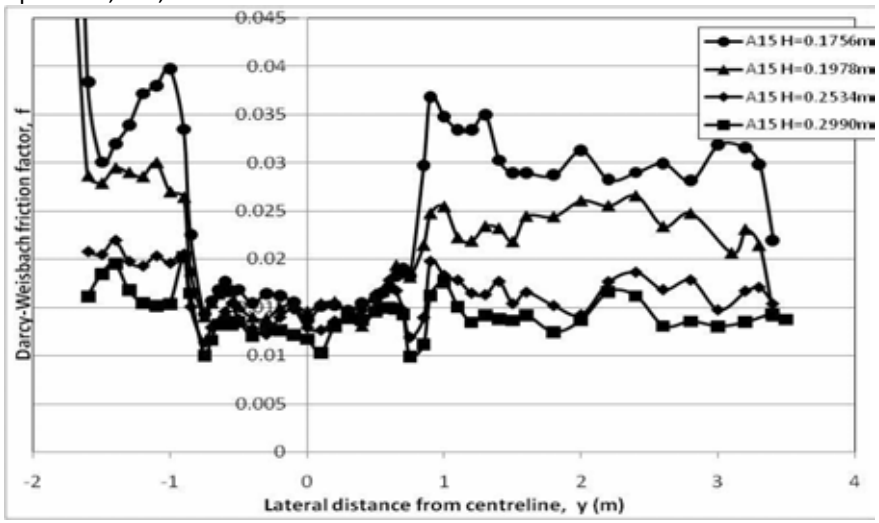

Figure 7.38c-Lateral distributions of local Darcy-Weisbach friction factor, *f*, for A15 upstream, s=1, θ=9.2^{o}

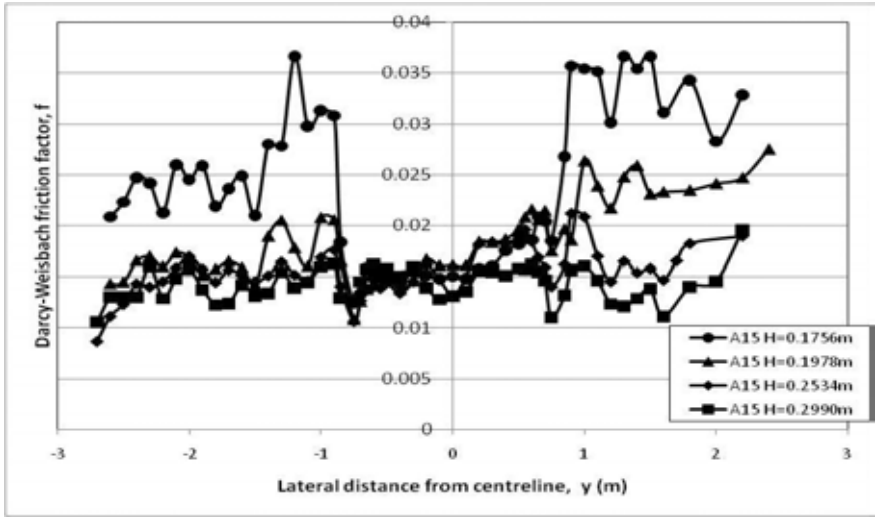

Figure 7.38d-Lateral distributions of local Darcy-Weisbach friction factor, *f*, for A15 downstream, s=1, θ=9.2^{o}

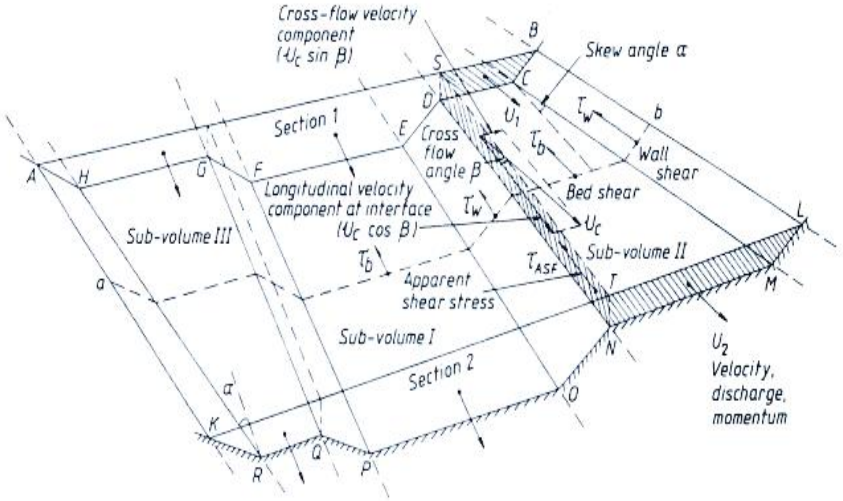

Figure 7.39-Perspective view of FCF skewed channel showing control volume used in force momentum balance (after Elliott & Sellin, 1990)

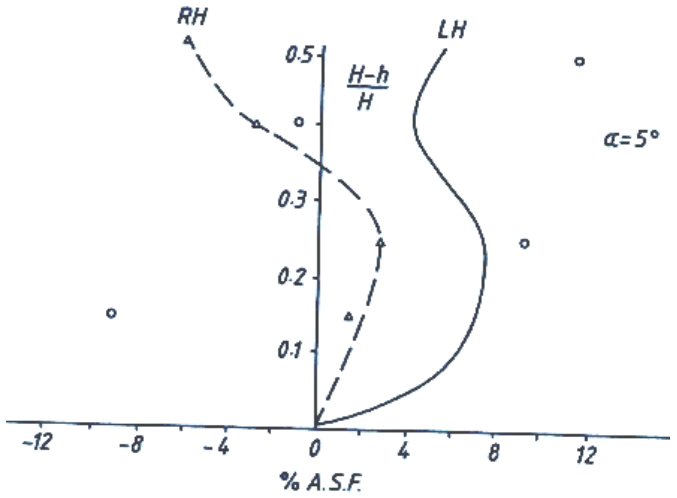

Figure 7.40-Percentage apparent shear force, after Elliott & Sellin (1990)

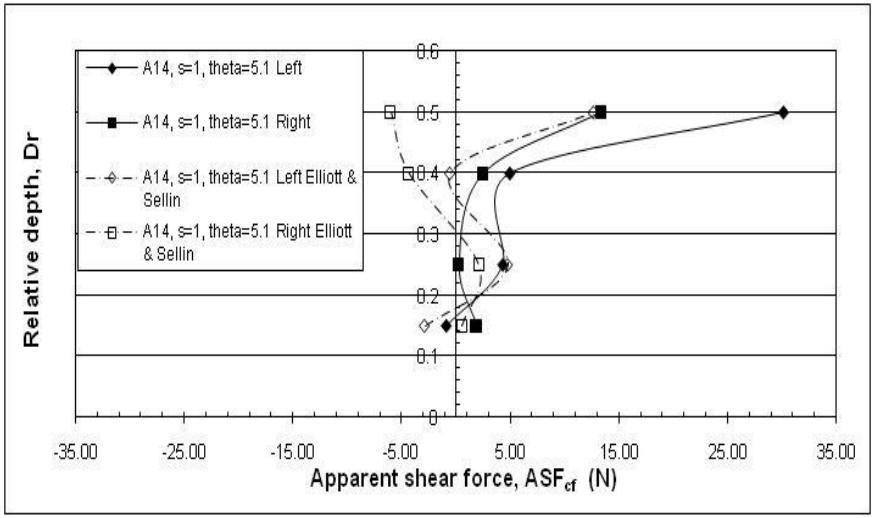

Figure 7.41a-Comparison of Elliot & Sellin (1990) with re-analysis, Series A14, s=1, θ=5.1° unadjusted velocities, β=1

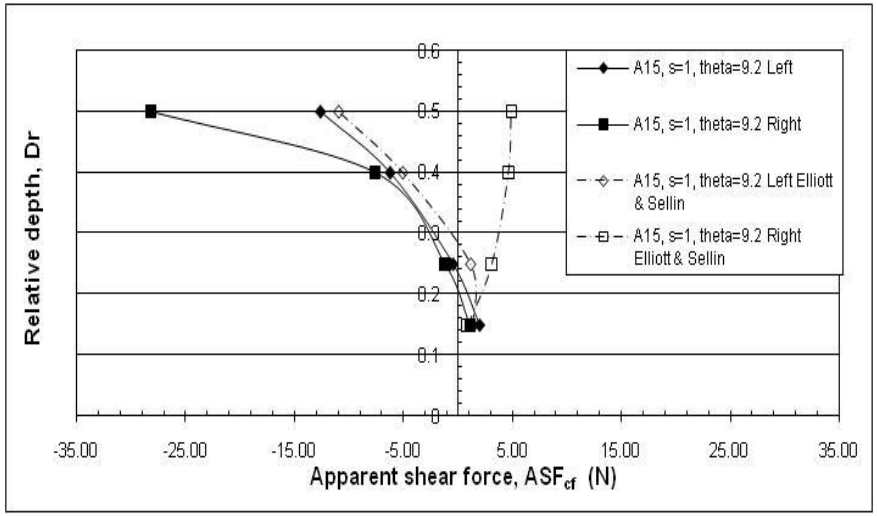

Figure 7.41b-Comparison of Elliot & Sellin (1990) with re-analysis, Series A15, s=1, θ=9.2° unadjusted velocities, β=1

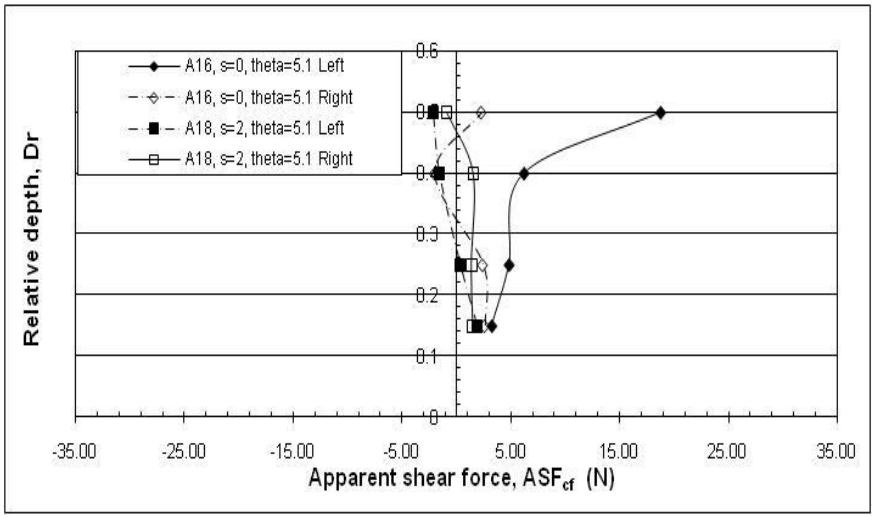

Figure 7.41c-Vertical apparent shear forces for Series A16, s=0, θ=5.1^{o} and A18, s=2, θ=5.1^{o} unadjusted velocities, β=1

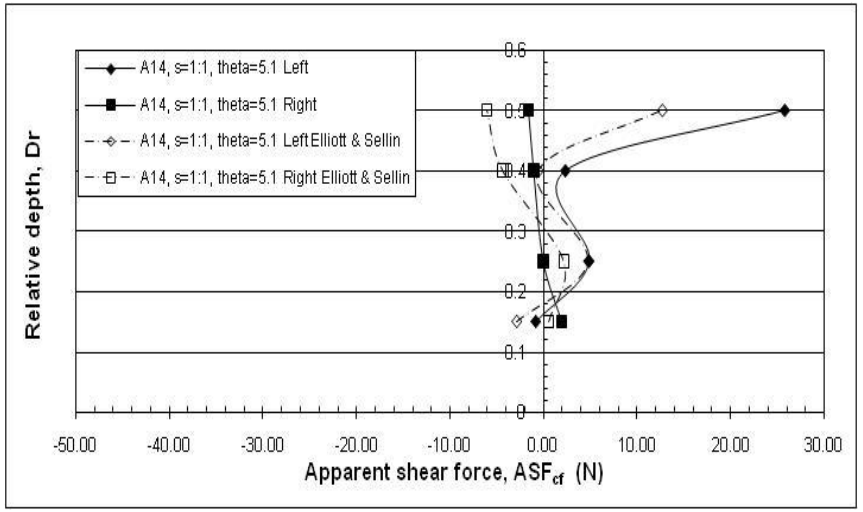

Figure 7.42a-Comparison of Elliot & Sellin (1990) with re-analysis, Series A14, s=1, θ=5.1^{o} adjusted velocities, β=1

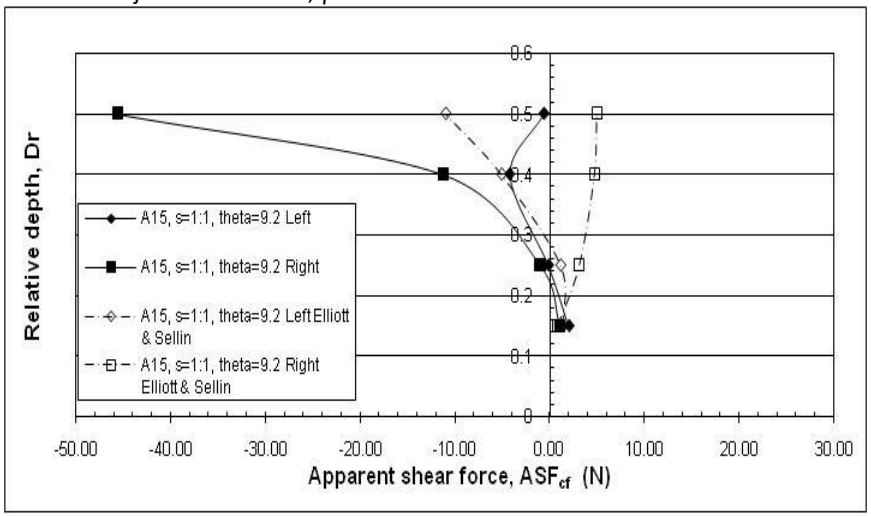

Figure 7.42b-Comparison of Elliot & Sellin (1990) with re-analysis, Series A15, s=1, θ=9.2^{o} adjusted velocities, β=1

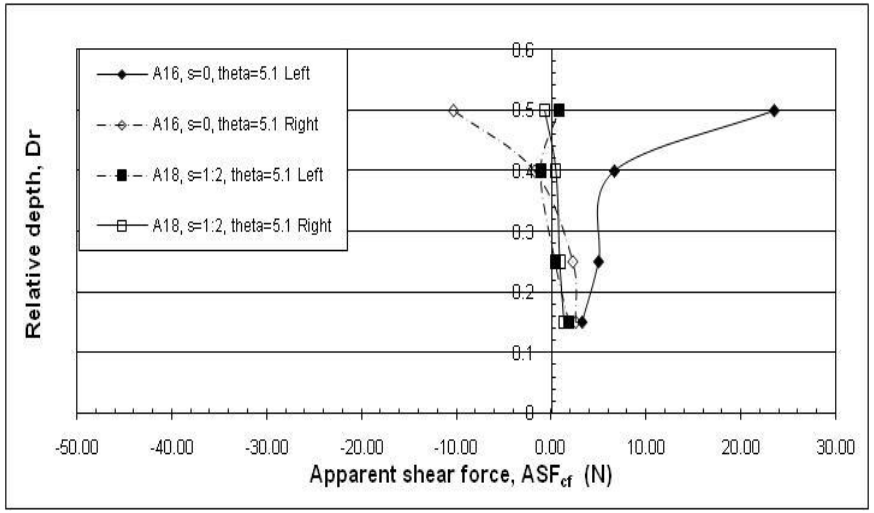

Figure 7.42c-Vertical apparent shear forces for Series A16, s=0, θ=5.1^{o} and A18, s=2, θ=5.1^{o} adjusted velocities, β=1

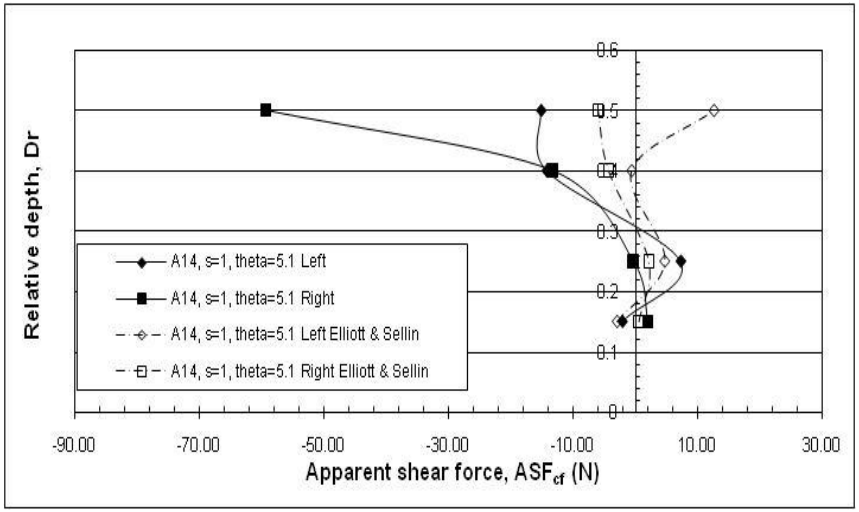

Figure 7.43a-Comparison of Elliot & Sellin (1990) with re-analysis, Series A14, s=1, θ=5.1^{o} adjusted velocities and including β

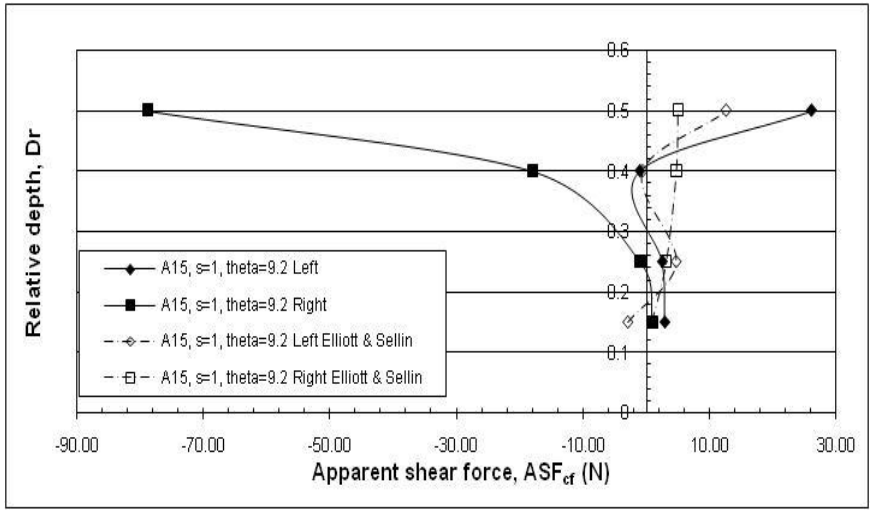

Figure 7.43b-Comparison of Elliot & Sellin (1990) with re-analysis, Series A15, s=1, θ=9.2^{o} adjusted velocities and including β

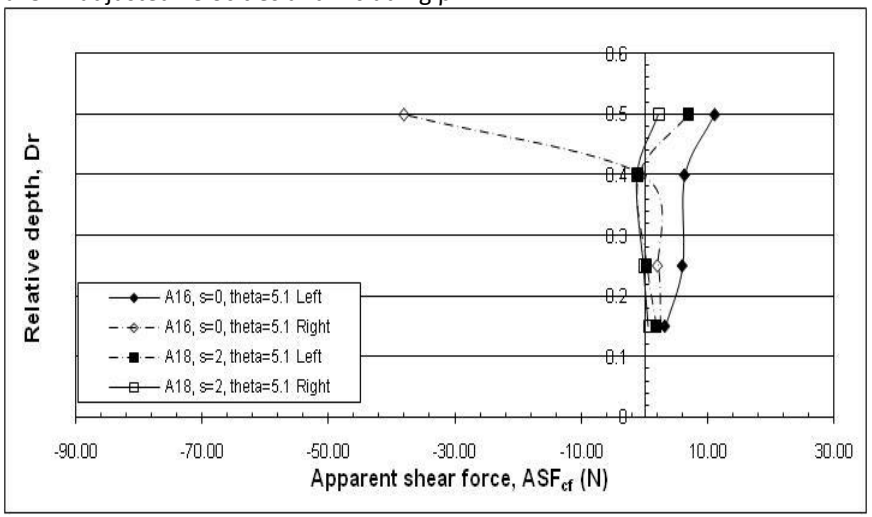

Figure 7.43c-Vertical apparent shear forces for Series A16, s=0, θ=5.1^{o} and A18, s=2, θ=5.1^{o} adjusted velocities and including β

CHAPTER 8-EXPERIMENTAL RESULTS AND ANALYSIS FOR COMPOUND SKEWED CHANNEL

There are three principal means of acquiring knowledge: observation of nature, reflection, and experimentation. Observation collects facts; reflection combines them; experimentation verifies the result of that combination. Denis Diderot

8.1 Introduction

As mentioned in Section 7.15, there are very few data on skewed channels. This is surprising, given their occurrence in fluvial systems and their importance in generating flow mechanisms that are intermediate between those occurring in straight prismatic and meandering geometries. This chapter details experimental work carried out in a compound channel which contained a transitional section where the floodplain changed from the right hand side to the left as shown in **Figures 8.1-8.3**. For the first 9m the channel (from x=10 to 19m) was asymmetrical, with the floodplain on the right, thus ensuring that the flow approaching the skew transition was fully developed. For the next 6m, the floodplains skewed at an angle of 3.81° and after the end of the transition the channel was again asymmetrical with the floodplain on the left for the remaining 2m (**Figure 8.1**). Additional views have already been presented as **Figures 6.1-6.4**. **Tables 8.1a-d** give details of the as-built cross-sections through the transition and indicates the location of the 6 measuring sections. All chainages are given from the flume entrance, labelled as x=10m. These were chosen to be at the start of the transition, at section x=19m, one at the end of the transition (x=25m), three equally spaced through the transition (x=20.5m, x=22m and x=23.5m) and one final section 1m downstream of the transition at x=26m. Due to

time constraints, only one skew angle was assessed. This was chosen to allow the data to be compared with Rezeai (2006) who carried out experiments in the same flume but with various converging geometries.

In order to smooth an otherwise abrupt inlet contraction at the entrance of the flume, as well as the cross-waves, a transition section was constructed in both vertical and horizontal directions using a PVC material. Chapter 6 gives full details on the construction of the flume and the measuring apparatus.

The main objectives of these experiments were to investigate the hydraulic characteristics of skewed channels and to add new data to the very limited data sets currently available (e.g. the Flood Channel Facility data described in Chapter 7), to examine stage-discharge and resistance relationships for skewed channels, the velocity and boundary shear stress distributions within the skewed transition, the shear forces acting in the channel, and finally to compare these results with data from the equivalent straight asymmetric and converging cases studied previously in the same flume (Atabay, 2001, Rezeai, 2006 and Ayymbzadah, 1997). The results were also used to investigate the momentum and energy balances in the skewed channel and in individual zones, such as the main channel and the floodplains.

Four flows were investigated namely 16.2ℓ/s, 21.4ℓ/s, 29.6ℓ/s and 43.4ℓ/s that correspond to relative depths, Dr $\left[=(H-h)/H\right]$, of 0.205, 0.313, 0.415 and 0.514. These corresponded to total flow depths, H, of between 62.9mm to 102.8mm Preliminary experiments were carried out in order to determine the tailgate level for

each depth which would give normal depth at the upstream end of the transition. By setting the normal depth upstream of the transition allowed the flow to develop along the whole approach length up to the transition. Details on the choice of flows and details on the setting of the tailgates are found in Sections 6.2.3 and 6.2.4 respectively. After the tailgate setting was determined, velocity and boundary shear stress distributions were taken for all flows at 6 locations along the flume; see **Figure 8.1-8.3**. The general details of the flume's geometry (**Figures 6.1-6.3**), construction and the measuring apparatus can be found in Chapter 6.

8.2 Stage-discharge results

The stage-discharge relationship is one of the most important relationships for river engineers. It is fundamental in river modelling at the calibration stage, vital in the design of hydraulic structures and very important when determining flood risk and in flood mapping.

As already indicated, before any measurements could be made, normal depth had to be set upstream of the transition. This was done through the adjustment of three downstream tailgates (**Figure 6.8**). The three tailgates were all set together at a particular level and depth measurements taken along the centreline of the channel at 1.0m intervals. The tailgate levels were then altered several times and water level readings repeated to give a number of *M1* and *M2* profiles. By plotting the water surface slope and the depth at the start of the transition (x=19m) against tailgate setting, allowed the tailgate setting for the required slope of, 2.003×10^{-3}, to be interpolated (i.e. water surface slope equal to that of the bed slope). These plots are

given in **Figures 6.15-6.18**. The depth associated with this tailgate reading was then taken as the normal depth at the selected upstream position (x=19m). This was repeated for each discharge in order to obtain the stage discharge curve for this configuration, as shown in **Figure 8.4**.

Using these stage-discharge data, a line of best fit was obtained mathematically in the form of a simple power function, given by Equation 8.1.

$$H = 0.5587Q^{0.5325} \quad \textbf{8.1}$$

where H is the flow depth in metres, m, (where H≥0.05m) and Q is the discharge in m^3/s.

Atabay (2001) carried out experiments in the same flume, but with a prismatic, asymmetric geometry, i.e. the left hand floodplain was isolated over the entire length of the 22m long channel. From the stage-discharge data, Atabay (2001) developed two equations to describe the stage-discharge relationship, one for inbank and one for overbank flows, Equations 8.2 and 8.3 respectively.

Inbank flow relationship:

$$H = 0.8475Q^{0.6357} \quad \textbf{8.2}$$

Overbank flow relationship:

$$H = 0.4476Q^{0.4777} \quad \textbf{8.3}$$

These are shown in **Figure 8.5**, along with the skewed stage-discharge curve. As can be seen, the skewed data lies slightly above the prismatic asymmetric curve. This is due to two factors; (1) the floodplains have been narrowed slightly from 407.3mm in the original experiments in 2001 to 400mm and (2) the slope of the channel decreased from 2.024×10^{-3} to 2.003×10^{-3}. This results in a small reduction in conveyance capacity and hence a slightly larger depth of flow. The reduction in capacity is approximately 0.5% which leads to increased flow depths of approximately 2-3mm.

8.3 Water surface profiles

In channels where there are non-prismatic flow conditions, the water surface profile is one of the most significant parameters required when estimating the relative contribution of the mass and corresponding momentum transfer to energy and force balances (Rezaei, 2006).

In order to gain an insight into the overall behaviour of the skewed transition, water surface readings were taken on a number of separate occasions throughout the experiments. These were carried out using a pointer gauge, which was fixed onto the instrument carriage and could be read to 0.1mm. Sets of water level readings were taken before the experiments, in order to check that the interpolated reading of the tailgate depth gave the desired normal depth upstream of the transition (x=19m). On the day of each experiment the local depth was also taken just at the measuring location and water level data was taken twice more in order to double check the levels giving a total of 4 readings for each experiment. **Figures 8.6a-d** show the water surface and bed elevations for each experiment along the flume and **Figures 8.18a-d**

(discussed later in more detail) show the water surface profiles through the transition. The water level results on the 26th January 2006 show an anomaly at x=24m. At this location, air infiltrated under the bed which caused one of the PVC bed panels to rise locally, the consequence of which being that the water level dropped dramatically. This can more clearly be seen in **Figure 8.18a-d**, where the water levels are plotted to a larger scale for use in the force-momentum calculations.

It can be seen that in general the water surface profile follows the bed slope until the skewed transition begins, at x=19m. At this point the water depth rises over the length of the 6m skew transition before coming back towards normal depth downstream. The rising water level has a marked effect on the velocity data which is discussed in the following section. The water surface data is re-examined and discussed further in Section 8.6, in light of its importance in the force-momentum calculations.

8.4 Velocity measurements

Velocity measurements were taken in order to assess the proportion of flow in the main channel and on the right and left floodplains at different locations along the flume (**Tables 8.2a-d**). The velocity distributions were subsequently used in order to examine the force and energy balances in a skewed channel.

8.4.1 Lateral, streamwise depth-averaged velocities

The depth-averaged streamwise velocity was taken at all 6 measuring sections (x=19m, x=20.5m, x=22m, x=23.5m, x=25m and x=26m) for each relative depth.

They were taken in the spanwise direction at only one vertical location, 0.4H on the main channel and 0.4(H-h) on the floodplains, where *h* is the bankfull height and *H* the total depth of flow. Theoretically the mini-propeller should only be used on depths above 16.25mm to allow for sufficient coverage, however, in the few cases where the depth was just below this level, the propeller was still used, as reasonable readings were apparently possible. **Figures 8.7a-d** show the adjusted results of these measurements. **Section 6.2.6.1** describes the methodology of this method.

From these Figures a number of observations can be made:

1. The maximum velocity moves from the centreline (where the velocity reaches a maximum in prismatic channels) to a location left of the centreline in the direction of skew. **Figures 8.7d** and **8.8** clearly show the progression of the maximum velocity from the centreline towards the left floodplain. **Figure 8.8** (Dr=0.514, Q=43.4*l*/s) shows that the point of maximum velocity moves from y=0.0mm (i.e. the main channel centreline) when x=19m (start of transition) to y=-75mm at x=25m (end of transition).
2. The velocities in the left hand floodplain (the receiving floodplain) are always greater than those on the right hand floodplain (the giving floodplain). From **Table 8.2**, at x=20.5m (Dr=0.313, Q=21.4*l*/s), the velocity on the left floodplain is up to 0.17m/s greater than the right, however, as the water depth increases the difference between the right and left floodplains lessen and at Dr=0.514 the difference between the two is only 0.03m/s.

3. The velocity peaks slightly on the receiving floodplain at the interface between the main channel and floodplain, at this location the peak is approximately 50% larger than mean velocity on the left floodplain and similarly dips at the interface of the giving floodplain and main channel, as seen in **Figures 8.7a-d**.

4. From **Table 8.2**, it is clear that the average velocity in the channel decreases through the transition due to the increasing water levels caused by the increasing lateral mixing. The section average velocity decreases by approximately 0.04m/s between x=19m and x=26m regardless of experiment.

In order to determine the discharge at a particular section, Q_i, the depth-averaged velocities were integrated numerically over the cross-sectional area using Equation 8.4. This value was then compared with the actual discharge, Q_m, as measured through the Electromagnetic Flow Meter (EFM), Venturi meter and Dall tube. The percentage errors between the experimental and measured data were also determined, using Equation 8.5.

$$Q_i = \sum_{i=1}^{n} u_i a_i \qquad \textbf{8.4}$$

Where u_i is the local velocity reading, a_i is the surrounding sub-area and n is the number of points.

$$\% \ error = \frac{Q_i - Q_m}{Q_m} \times 100\% \qquad \textbf{8.5}$$

The average errors were 0.13%, -0.53%, 0.95% and –1.07% for Dr=0.205, Dr=0.313, Dr=0.415 and Dr=0.514 respectively, well within the ±3% tolerance allowed for in this study. For details of each experiment see **Tables 8.3a-d**. These errors were distributed throughout each velocity reading to normalise them to the measured as described in Section 6.2.6.1 and using Equation 6.12.

8.4.2 Full lateral, streamwise velocity distributions

Four sections were examined more closely with detailed velocity measurements taken within the cross-sections. This was done in order to obtain the energy and momentum coefficients and also served as a check against the depth-averaged velocity profiles above. Velocities were measured at points every 25mm laterally and every 10mm vertically. These measurements were taken at x=19m, x=22m, x=25m and x=26m, i.e. at the start, middle and end of the skew transition and one 1m downstream. These point velocity measurements were then adjusted and integrated over the depth (Equation 8.6).

$$U_d = \frac{\sum_{1}^{N} u_i h_i}{H} \qquad \textbf{8.6}$$

The point values of velocity were numerically integrated using Equation 8.6 and the errors associated with the measured discharge also determined using Equation 8.5.

The average errors in this case for each depth were –3.15%, -2.09%, -0.96% and –2.35% for Dr=0.205, Dr=0.313, Dr=0.415 and Dr=0.514 respectively. Details of these discharge data for each experiment can be found in **Tables 8.3a-d** and section/zonal mean velocities in **Tables 8.2a-d**. The average errors using the more detailed point velocities are only slightly greater than the depth-averaged results (-0.96% to –3.15% compared to 0.13% to –1.07% for the depth-averaged velocity measurements). Nevertheless, the errors are still within an acceptable range and the data are considered sufficiently accurate for further analysis. These errors were distributed throughout the point velocities to normalise the readings to the measured discharge (Equation 6.12).

The results for the more detailed velocity measurements are presented in **Figures 8.9a-d**. These plots are similar to the lateral depth-averaged distributions shown in **Figures 8.7a-d**; the velocities are comparable in magnitude and show similar trends. The velocity peak moves from the centreline towards the left floodplain as it travels downstream, for example, in Figure 8.9b (Dr=0.313, Q=21.4l/s) the peak velocity moves from y=-25mm to y=-75mm. The velocity profile becomes flatter as the depth increases (Dr≥0.313).

Figures 8.10a-d show the velocity isovels for sections x=19m, x=22m, x=25m and x=26m where full velocity measurements were taken. From these the progression of the maximum velocity from the centre of the main channel towards the left floodplain can easily be seen.

The results from the depth-averaged and point velocity results are used to assess the proportion of flow in each zone and also for calculation of the velocity and momentum coefficients α and β.

8.5 Distribution of discharge

The proportion of flow in each zone of the channel was determined as this information can be used to assess the apparent shear stresses and forces used in modelling the channel by the Shiono & Knight Method (SKM). Wherever possible, the distributions were based on point velocity readings, but where this was not possible (at sections x=20.5m and x=23.5m) the depth-averaged values were used instead.

Using the adjusted measured velocity data (**Tables 8.2a-d**), the proportion of flow on the main channel and floodplains could be assessed, as shown in **Figures 8.11a-d** and **Table 8.4**. It was found (unsurprisingly) that the proportion of flow in the right hand floodplain decreases along the channel while the left hand floodplain carried more flow. The flow in the main channel also decreases along the length by approximately 5%, regardless of the discharge or depth tested.

Second order mathematical relationships were established between relative depth and the percentage of flow in the main channel and left and right hand floodplains, the basic form of which is shown in Equation 8.7.

$$\%Q_z = aDr^2 + bDr + c \qquad \textbf{8.7}$$

where Q_z is the proportion of flow in a given area, Dr the relative depth and a, b and c are all constants.

Figures 8.12a-c show the relationships established for the main channel and left and right hand floodplains respectively. A holistic approach for the relationship between relative depth and proportion of total flow in the main channel was taken for all data sets as there was not a great deal of scatter (±3% from the mean). The equation describing the best fit is given by Equation 8.8 and has an accuracy (R^2 value) of 0.9863.

$$\%Q_{mc} = -0.6924Dr^2 - 0.2866Dr + 1 \qquad \textbf{8.8}$$

where Q_{mc} is the proportion of discharge in the main channel.

For the floodplains, each floodplain required its own relationship with regards to distance along the channel and relative depth.

Left hand flood plain:

x=19m No relationship as this floodplain is isolated

x=20.5m $\%Q_{LFP} = -0.1004Dr^2 + 0.2036Dr$ **8.9**

x=22m $\%Q_{LFP} = 0.0216Dr^2 + 0.3218Dr$ **8.10**

x=23.5m $\%Q_{LFP} = -0.0158Dr^2 + 0.4754Dr$ **8.11**

x=25m $\%Q_{LFP} = 0.2182Dr^2 + 0.5184Dr$ **8.12**

x=26m $\%Q_{LFP} = 0.3532Dr + 0.4443Dr$ **8.13**

where Q_{LFP} is the proportion of discharge in the left floodplain.

Right hand floodplain:

x=19m $\%Q_{RFP} = 0.5138Dr^2 + 0.3048Dr$ **8.14**

x=20.5m $\%Q_{RFP} = 0.3048Dr^2 + 0.2705Dr$ **8.15**

x=22m $\%Q_{RFP} = 0.3652Dr^2 + 0.1007Dr$ **8.16**

x=23.5m $\%Q_{RFP} = 0.1644Dr^2 + 0.0402Dr$ **8.17**

x=25m No relationship as this floodplain is isolated

x=26m No relationship as this floodplain is isolated

where Q_{RFP} is the proportion of discharge in the right floodplain.

Mass transfer can be estimated from the distribution of discharge along the channel, as shown in **Figures 8.13a-c**. From this is can be seen that at low relative depths the mass transfer between zones is low. The proportion of flow in the main channel decreases slightly through the transition and is generally linear with x. The proportion of flow on the receiving floodplain is greater than that on the giving floodplain at a comparable floodplain width. At the final measuring section (x=26m) the flow on the left floodplain began to plateau and in all but the highest flow, began to fall. It is believed that if there were further measuring sections downstream it would show the flow mirroring the entry conditions.

A simple mathematical correlation between the percentage discharge, as seen in **Figures 8.14a-c**, in each region of the channel and relative position (x) along the skewed transition length (section x=19m to x=25m) were determined using a simple linear relationship (Equation 8.18) through the data each relative depth.

$$\%Q_z = ax + b \qquad \textbf{8.18}$$

Left hand floodplain

Dr=0.205 $\%Q_{LFP} = 0.0206x - 0.3921$ Valid for 19<x<25 **8.19**

Dr=0.313 $\%Q_{LFP} = 0.0351x - 0.6643$ Valid for 19<x<25 **8.20**

Dr=0.415 $\%Q_{LFP} = 0.0475x - 0.9053$ Valid for 19<x<25 **8.21**

Dr=0.514 $\%Q_{LFP} = 0.0526x - 0.9977$ Valid for 19<x<25 **8.22**

where Q_{LFP} is the proportion of discharge in the left floodplain, Q_m the total measured discharge and x the longitudinal distance. In all cases the R^2 value was greater than 0.991.

Main channel

Dr=0.205 $\%Q_{MC} = -0.0077x + 1.0693$ Valid for 19<x<25 **8.23**

Dr=0.313 $\%Q_{MC} = -0.0111x + 1.0668$ Valid for 19<x<25 **8.24**

Dr=0.415 $\%Q_{MC} = -0.012x + 1.017$ Valid for 19<x<25 **8.25**

Dr=0.514 $\%Q_{MC} = -0.0046x + 0.8009$ Valid for 19<x<25 **8.26**

where Q_{MC} is the proportion of discharge in the main channel. In all cases the R^2 value was greater than 0.930 with the exception of Dr=0.514 where the R^2 value was 0.775.

Right hand floodplain

Dr=0.205 $\%Q_{RFP} = -0.0129x + 0.3218$ Valid for 19<x<25 **8.27**

Dr=0.313 $\%Q_{RFP} = -0.024x + 0.5975$ Valid for 19<x<25 **8.28**

Dr=0.415 $\%Q_{RFP} = -0.0356x + 0.8883$ Valid for 19<x<25 **8.29**

Dr=0.514 $\%Q_{RFP} = -0.048x + 1.1968$ Valid for 19<x<25 **8.30**

where Q_{RFP} is the proportion of discharge in the right floodplain. In all cases the R^2 value was greater than 0.998.

Figures 8.14d-f show the percentage of area in addition to the percentage of discharge in each zone of the channel along the length of the skewed section, whereas **Figures 8.15a-f** show the comparison of percentage area to discharge against relative depths for each measuring section. From these it can be seen that generally, the percentage of area in the main channel tends to be lower than the corresponding discharge, conversely, in the floodplains, the percentage of area tends to be greater than the percentage discharge. As the depth increased (Dr>0.313), the agreement between the percentage area and discharge increases.

8.6 Boundary shear stress distributions

Boundary shear stresses in channels are often neglected in the analysis of river systems. However, the distributions of boundary shear stress is important as it is often required in the calibration of more sophisticated models, for studying force balances and in sediment transportation calculations. It can give an indication of the location of secondary flow cells and also areas of deposition and erosion in natural channels.

The wetted perimeter was divided into a number of boundary elements (see **Figures 8.16a-c**), for the purpose of determining the shear force acting on each boundary element in different regions of the channel.

The boundary shear stress was measured with a Preston tube of outer diameter 4.77mm every 25mm horizontally on the main channel and floodplain(s) bed and every 10mm vertically on the vertical side walls. The boundary shear stress measurements were carried out at each measuring section in order to determine the boundary shear stress distribution around the wetted perimeter and also to determine the forces acting on each element and in the whole section. The methodology and procedure are explained in detail in Sections 2.2.6 and 6.2.7.

The measured, and hence unadjusted, boundary shear stress distributions are shown in **Figures 8.17a-d**. From these results, there is clearly a peak at the interface of the main channel and left hand floodplain. The peak at this interface can be as great as twice that of the section average boundary shear stress when Dr=0.205 (**Figure 8.17a**), but at the highest flow depth (Dr=0.514, **Figure 8.17d**) the peak approximately equals the section mean. This might be expected as it is here that the floodplain is receiving cross-over flows and is a particularly turbulent region. The peak in boundary shear stress at the interface of the left floodplain and the main channel could be up to double of that of the section mean. Elliott (1990) found similar trends in the skewed channel work carried out at the FCF. Elliott found that the peak shear stress was up to 2.5 times that of the section average boundary shear stress.

These boundary shear stress results were subsequently numerically integrated over the contributing area to give the shear force acting on each element and then divided by the whole perimeter giving the average boundary shear stress, τ_b. This was then compared with the theoretical value for uniform flow, which is based on the hydraulic radius and the friction slope, i.e. $\tau_0 = \rho g R S_f$. In the case of uniform flow one can normally assume that $S_o=S_f=S_e$, but as can be seen from **Figures 8.6a-d** that the flow is non-uniform throughout the transition section. **Figures 8.18a-d** show the depth of flow as it travels through the transition, in general, the depth generally decreases slightly through the first quarter of the skew, then rises steeply through the middle portion before levelling out again in the last quarter. This makes the analysis of the boundary shear stress results in the usual manner a more difficult task.

In order to carry out a traditional shear stress analysis approach, the overall boundary shear stress results were compared to $\tau_0 = \rho g R S_o$. The overall error is calculated using Equation 8.31.

$$\%\tau_{error} = \left(\frac{\tau_{\exp} - \tau_o}{\tau_o} \right) \times 100\% \qquad \textbf{8.31}$$

This gave "errors" of –26.81%, -22.52%, -19.23% and –18.31% for Dr=0.205, Dr=0.313, Dr=0.415 and Dr=0.514, which indicate the point made previously about the non-uniform flow and the inadvisability of using the $\tau_0 = \rho g R S_o$ approach.

The next approach was to take into account the rising water levels over the 6m transition by using $\tau_o = \rho g R\left(S_o - \frac{\Delta H}{\Delta x}\right)$. Because of the non-uniformity in the water level data a number of different approaches were tried as follows:

1. Linear increase of flow depth
2. Linear transition between section x=19m and x=20.5 and a second linear transition between section x=20.5m and x=25m (2 leg approach)
3. Three linear transition between sections x=19m to x=20.5m, x=20.5m to x=23.5m and from x=23.5m to x=25m (three leg approach). The divisions are based on similar water slopes, x=19m to x=20.5m and x=23.5m to x=25m had quite shallow slopes, whereas x=20.5m to x=23.5m has a steeply rising water surface slope.

Figures 8.19a-d give a representation of the division of the water surface through the skewed transition for each approach outlined above for each of the flows examined. As there were 4 sets of water level data taken, an average of all the sets were used when determining the change in water flow depth. The results of the averaging process can be found in **Tables 8.5a-d**. The average errors for each approach for Dr=0.205, Dr=0.313, Dr=0.415 and Dr=0.514 respectively were:

1. 12.86%, 26.80%, 7.04% and 25.98%
2. 4.60%, 16.05%, 5.90% and 14.40%
3. –13.75%, -6.68%, -8.61% and –4.31%

From this it can be seen that the average errors for the three chosen approaches cover a wide range and are quite dispersed. This can also be seen in **Tables 8.6a-d** where full boundary shear stress data and associated errors are given. Overall, it was considered that approach 3, where the channel is broken down into three representative areas, gave the most acceptable average errors. However, no single method gave an accurate enough approach to adjust the boundary shear stress distributions. They were therefore left unadjusted in subsequent calculations.

The boundary shear forces on each element (see **Figures 8.16a-c** for numbering) are given in **Tables 8.7a-d** and are based on the unadjusted values of boundary shear stress. The percentage shear force carried by each element ($\%SF_i$) are also shown in **Tables 8.7a-d**. The percentage shear force per element has been plotted against the channel length (**Figures 8.20a-g**). From these plots the bed elements (for both the right and left floodplain beds) have an almost linear appearance. The percentage shear force on left floodplain bed increases along the length of the channel increasing from 0% to between 33% and 50%. The right floodplain decreases from between 40%-15% to 0% over the transition, but the distribution is less linear. The percentage shear force on the main channel bed decreases by between 5%-15% over the 6m transition. These trends are similar to those observed in the distributions of discharge. The left main channel wall tends to peak at the start of the transition and similarly, the right main channel wall peaks at the end of the transition, this is due to there being no left or right floodplains respectively, at these locations. Therefore at the start of the transition, x=19m, the left main channel wall is equal to the total depth of flow, but as the left floodplain expands the main channel wall becomes the actual inbank depth of

0.05m, hence the reduction in contribution. Similarly the percentage shear force rises steeply for the left floodplain wall between x=19m and x=20.5m, this is due to there being no floodplain and hence no floodplain wall at x=19m. Polynomial equations have been fitted through the distributions taking the basic form:

$$\%\, SF_i = ax^3 + bx^2 + cx + d \qquad \textbf{8.32}$$

where $\%SF_i$ is the percentage shear force on any element, x is the longitudinal distance and a, b, c and d are all constants. The coefficients a, b, c and d can be found in **Table 8.8**.

8.7 Energy balance and head loss analysis

In hydraulics there are a number of possible slopes which are used for different purposes; the bed slope, S_o, the water slope, S_w the energy slope S_e sometimes termed the friction slope, S_f. The energy slope can be estimated from the streamwise variation energy head, H_e, summarised in Equations 8.33 and 8.34.

$$H_e = H + z_b + \alpha \frac{U^2}{2g} \qquad \textbf{8.33}$$

where H is the water depth, z_b the bed elevation, $\alpha \frac{U^2}{2g}$ the kinetic energy head and α the energy correction coefficient (Section 7.12, Equation 7.38).

$$S_e = \frac{\Delta H_e}{\Delta x} \quad \textbf{8.34}$$

and,

$$S_f = S_o - \frac{\partial h}{\partial x} - \frac{u}{g}\frac{\partial u}{\partial x} = \frac{n^2 Q^2}{R^{4/3} A^2} \quad \textbf{8.35}$$

The energy slope was estimated section to section and also over the whole skewed reach. The energy correction coefficient has been determined for all experiments and detailed in **Tables 8.2a-d**. Where possible the full velocity distributions were used to calculate α, otherwise the depth-averaged velocities were used. The head loss results of which can be found in **Table 8.9**. On average the head losses were approximately 0.01m and did not appear to be influenced by relative depth, since as the depth increases the head loss decreases (**Figure 8.21**). In Rezaei's converging experiments the head losses ranged between 0.0062m to 0.0098m, with the highest head loss being found in the lowest depth.

In addition the head loss coefficients, *K*, were determined using Equations 8.36 to 8.38.

$$h_e = K_1 \frac{U_1^2}{2g} \quad \textbf{8.36}$$

$$h_e = K_2 \frac{U_2^2}{2g} \quad \textbf{8.37}$$

$$h_e = K_{12}\frac{\left|U_2^2 - U_1^2\right|}{2g} \qquad \textbf{8.38}$$

where h_e are the head losses. In the case of Equation 8.38, the magnitude of the difference of the velocities has been taken since in all cases the velocity upstream is greater than that downstream due to rising water levels. These results can also be found in **Table 8.9** and in **Figure 8.22**. It was found that both K_1 and K_2 decreased as relative depth increased. For K_1, the skewed channel experiments had values in the range of 0.771 (Dr=0.205) to 0.306 (Dr=0.514), similarly K_2 also decrease with relative depth from 0.878 (Dr=0.205) to 0.320 (Dr=0.514). Rezeai also found similar trends in the converging experiments but found that as the converging angle increases the head loss coefficients increase as the relative depth increases.

8.8 Resistance

The resistance of a channel is another important factor to the engineer when analysing most flow problems. The main factors used are the Manning's coefficient n and the Darcy-Weisbach friction factor f.

8.8.1 Global resistance factors

In order to compute the global values of Manning's n (n_g) and friction factor, f (f_g), for the channel, the stage-discharge results were used and the bed slope as the overall water slope (from section x=10m to x=27m) was approximately equal to the bed slope (S_o=2.003 x 10^{-3}), although in the skewed channel section it was clearly different These friction factors were computed using Equations 8.39 and 8.40.

$$n_g = \frac{R^{2/3}\sqrt{S_o}}{U} \quad \textbf{8.39}$$

$$f_g = \frac{8\,g\,R\,S_o}{U^2} \quad \textbf{8.40}$$

On average the Manning's coefficient was approximately 0.0098 for the whole channel and the Darcy-Weisbach friction factor of 0.0209. The results for each experiment can be found in **Table 8.2**. **Figures 8.23-8.28** show the relationship between friction and depth and friction and discharge. From **Figures 8.23-8.26**, the resistance within the channel increases with flow depth. **Figure 8.24** shows that as the discharge increases, the values of Manning's n_g also increase slightly, by about 0.002, between the lowest and highest discharge. A Moody diagram plot is also given in **Figures 8.29** and **8.30**.

8.8.2 Zonal resistance factors

The Darcy-Weisbach friction factor, f_z, and Manning's n_z have been calculated for each zone; left floodplain, main channel and right floodplain, for each experiment. These were also calculated using Equations 8.39 and 8.40 but the interface between the main channel and floodplains has been excluded from the wetted perimeter i.e. only solid boundaries are included. The results are presented in **Table 8.2**. Plots of the zonal friction data are shown in **Figures 8.31a-c** and **8.32a-c**. From these it can be seen that in all cases the friction (both Manning's *n* and Darcy-Weisbach, *f*) rise along the length of the skewed portion of the channel and continue to do so until the final measuring section. This is due to the rising water levels and decreasing velocities and the skewing effect which causes the flow to mix more. It is also

apparent that the roughness decreases as the flow increases, an indication that the skewing (and hence increased mixing of flow) is having less effect on the flow.

8.8.3 Local resistance factors

In addition to the global and zonal friction factors, the local friction factor, f_l, was determined using Equation 8.41. The unadjusted boundary shear stresses were used in conjunction with the normalised velocities. Where possible the full velocity distribution results were used.

$$f = \frac{8\tau_b}{\rho u^2} \qquad \textbf{8.41}$$

Figures 8.33a-d show the transverse distributions of the local Darcy-Weisbach friction factor for each experiment. Generally the friction factor in the main channel varies only by approximately 0.005. In the right floodplain, the friction factor increases through the length of the transition, whereas in the left floodplain the friction factor decreases locally. This is due to the flow experiencing more mixing at the start of the transition on the left floodplain.

8.9 Force-momentum analysis and apparent shear forces

The momentum fluxes and forces on the channel through the transition were determined using the experimental data. Furthermore, a force-momentum balance was carried out for each zone of the channel (i.e. floodplain(s) and main channel) to determine the apparent shear forces acting at the vertical interfaces of the floodplain(s) and main channel.

Initially the whole skewed section of the channel (section x=19m to x=25m) was selected as the control volume (Δx=6m) and the force-momentum equation applied. The same equation was then applied for each control volume between the four individual sections (Δx=1.5m) within the transition, and finally the channel was broken down into floodplain(s) and main channel zones and another force-momentum balance carried out for each section (Δx=1.5m). A perspective view of the channel and its sections can be found in **Figure 8.3**.

If a steady state approach is taken then for conservation of momentum, the net rate of momentum flux in a control volume is equal to the sum of the body force (gravity) and surface forces acting on the control volume (friction and pressure). This can be written more formally as Equation 8.42 with the expanded version given in Equation 8.43. It should be noted in the analysis for the whole channel, Q1=Q2, therefore q_{cf}=0 and the last term in Equation 8.42 becomes zero.

$$F_1 - F_2 - \sum SF + W = \rho Q(\beta_2 U_2 - \beta_1 U_1) + \rho q_{cf} U_{cf} L \qquad \textbf{8.42}$$

$$\rho g A_1 z_1 - \rho g A_2 z_2 - \sum SF + \rho g V S_o = \rho Q(\beta_2 U_2 - \beta_1 U_1) + \rho \left(\frac{Q_2 - Q_1}{L} \right) U_{cf} L \qquad \textbf{8.43}$$

where F_1 and F_2 are the hydrostatic pressure forces, z is the distance to the centroid below the free surface, V is the control volume, U_1 and U_2 are the section mean velocities, U_{cf} is the mean velocity along the interface of the main channel and floodplain(s), Q is the discharge, q_{cf} is the cross-flow which is the discharge between

the main channel and the floodplain(s), L is the longitudinal distance and β is the momentum correction coefficient (**Tables 8.2a-d**).

Due to the amount of water surface data, water levels and cross-sectional areas are based on the average water depths, **Table 8.10**. This will allow for smoothing of the data. In addition to the smoothed water surface data, smoothed data will also be used for discharge, velocity and shear force. The proportional discharge relationships (Equation 8.19 to 8.30) will be used and the mean section velocity is assumed to be $U = \frac{Q}{A}$. It is further assumed that the bed level of each floodplain at a given cross-section is at the same elevation for the left and right floodplains i.e. left floodplain elevation equals the right floodplain elevation.

8.9.1 Force-momentum balance of whole skew transition (x=19m to x=25m)

In this case the whole skewed transition was taken as the control volume using the assumptions discussed above in Section 8.9. In this case, the shear force was taken as the mean of the boundary shear forces at each section. **Table 8.11a** gives details of the average flow depths for both the main channel and floodplains in addition to the location of centroid, cross-sectional area and perimeter based on these average depths. The measured boundary shear stress and forces are also shown here. Using Equation 8.42, **Table 8.11b** gives the results from the force-momentum balance for the whole channel with an example calculation give below for Dr=0.313, Q=21.4*l*/s.

Calculation	Table cross-reference
$F_1 = \rho g A_1 z_1 = 1000 \times 9.807 \times 0.037 \times 0.03 = 10.73\text{N}$	**Table 8.11a**
$F_2 = \rho g A_2 z_2 = 1000 \times 9.807 \times 0.040 \times 0.032 = 12.52\text{N}$	**Table 8.11a**
$\Sigma SF = \Sigma \overline{SF_b} \times L = \left[(0.688 + 0.568 + 0.550 + 0.660 + 0.566) / 5 \right] \times 6$ $\Sigma\text{SF}=3.64\text{N}$	**Table 8.11a**
$W = \rho g S_o L \overline{A} = 1000 \times 9.807 \times 2.003 \times 10^{-3} \times 6 \times \frac{(0.037 + 0.040)}{2}$ $\text{W}=4.54\text{N}$	**Table 8.11a**
$\rho Q(\beta_2 U_2 - \beta_1 U_1) + \rho q_{cf} U_{cf} L \qquad but\ q_{cf} = 0\ as\ Q_2 = Q_1$ $\rho Q(\beta_2 U_2 - \beta_1 U_1) =$ $1000 \times 0.0214 \times \left[\left(1.0582 \times \frac{0.0214}{0.040} \right) - \left(1.1881 \times \frac{0.0214}{0.037} \right) \right]$ $\rho Q(\beta_2 U_2 - \beta_1 U_1) = -1.14N$	**β values Table 8.3** **Other data Table 8.11a**

This method resulted in an average out of balance force of 0.80N, or 2.43%. The percentage error is taken as the out of balance force divided by the sum of the magnitudes of each term in Equation 8.42. Generally the errors were within 1.75%, but the lowest flow had a much higher error of 6.59%. In comparison to the other terms in the equation, the out of balance forces are small. This is due to the rising water surface causing a decrease in velocity. In addition, no correction has been applied to the shear force data resulting in a significant difference between shear force and weight, with shear force being approximately 1.0N less than the weight component. In order to take into account differences between the section, a force-momentum balance was applied to the channel for each section.

8.9.2 Force-momentum balance for each section in skew transition

Measurements were taken at 5 locations throughout the skewed transition, one at the beginning and end with a further three, equally spaced, in the middle. A force-momentum balance was applied to each section using Equation 8.42. Again, the shear force acting in the channel was taken as the section average. The results from the force-momentum balance are given in **Tables 8.12a-d** with a sample calculation for Dr=0.313 section x=20.5m to x=22m given below.

Calculation	Table cross-reference
$F_1 = \rho\, g\, A_1 z_1 = 1000 \times 9.807 \times 0.037 \times 0.03 = 10.68\text{N}$	**Table 8.11a**
$F_2 = \rho\, g\, A_2 z_2 = 1000 \times 9.807 \times 0.039 \times 0.031 = 11.78\text{N}$	**Table 8.11a**
$\Sigma SF = \Sigma \overline{SF_b} \times L = \left[\left(0.568 + 0.550\right) \Big/ 2 \right] \times 1.5 = 0.84\text{N}$	**Table 8.11a**
$W = \rho\, g\, S_o\, L\, \overline{A} = 1000 \times 9.807 \times 2.003 \times 10^{-3} \times 1.5 \times \dfrac{(0.037 + 0.039)}{2}$ W=1.12N	**Table 8.11a**
$\rho Q(\beta_2 U_2 - \beta_1 U_1) + \rho q_{cf} U_{cf} L \qquad but\ q_{cf} = 0\ as\ Q_2 = Q_1$ $\rho Q(\beta_2 U_2 - \beta_1 U_1) =$ $1000 \times 0.0214 \times \left[\left(1.0605 \times \dfrac{0.0214}{0.039} \right) - \left(1.0467 \times \dfrac{0.0214}{0.037} \right) \right]$ $\rho Q(\beta_2 U_2 - \beta_1 U_1) = -0.63N$	**β values Table 8.2** **Other data Table 8.11a**

In **Tables 8.12a-d**, the section force-momentum balance has been summed to give the force-balance for the whole channel. It may be seen from **Tables 8.12a-d** and **8.11b**,

that the results are quite similar. The differences are due to the shear forces and momentum correction factors being applied to each sub-volume, resulting in small differences when summed over the whole transition. The residual, or out of balance momenta, are generally less than 1.0N with the exception of Dr=0.205 where it is slightly larger at 1.667N. Again, the percentage error was calculated (residual/magnitude of terms), this gave a average error of 0.80%, with the lowest relative depth giving the highest error. Overall these are very small errors in comparison to the overall magnitude of the other terms in the equation.

In order to determine the apparent shear forces on the left and right hand floodplains the force-momentum balance will be applied to the main channel and floodplains independently.

8.9.3 Force-momentum balance for each zone per section

The apparent shear forces acting along the interface of the main channel and floodplain(s) has been determined using the force-momentum equation (8.42) and applying it to the floodplain and the main channel independently.

For the left hand floodplain

$$F_{1L} - F_{2L} - \Sigma SF_L + W_L + R_{FL} + ASF_{VL} = \rho\left(Q_{2L}U_{2L}\beta_{2L} - Q_{1L}U_{1L}\beta_{1L} - Lq_{cfL}U_{cfL}\right) \quad \textbf{8.44}$$

And for the right floodplain

$$F_{1R} - F_{2R} - \Sigma SF_R + W_R + R_{FR} + ASF_{vR} = \rho\left(Q_{2R}U_{2R}\beta_{2R} - Q_{1R}U_{1R}\beta_{1R} - Lq_{cfR}U_{cfR}\right) \quad \textbf{8.45}$$

For the main channel

$$F_{1MC} - F_{2MC} - \Sigma SF_{MC} + W_{MC} - ASF_{VR} - ASF_{cVL} - R_{FR} - R_{FL} = \rho\left(Q_2U_2\beta_2 - Q_1U_1\beta_1 + Lq_{cfL}U_{cfL} + Lq_{cfR}U_{cfR}\right) \quad \textbf{8.46}$$

$$And, \qquad q_{cf(L\,or\,R)} = \frac{Q_{2(L\,or\,R)} - Q_{1(L\,or\,R)}}{L} \quad \textbf{8.47}$$

where R_F is the hydrostatic wall reaction, ASF_V is the vertical apparent shear forces on the interface of the main channel and floodplain(s), q_{cf} is the lateral (cross-flow) discharge, similarly, U_{cf} is the interface velocities between the main channel and floodplain(s) and subscripts *MC*, *L* and *R* refer to the main channel, left and right floodplains respectively. All other symbols take on the meanings of Section 8.9.

Results from the force-momentum balance are given in **Tables 8.13-8.16**. A sample calculation is given for Dr=0.313 section x=20.5m to x=22m for the left floodplain.

Calculation	Table cross-reference
$F_{1L} = \rho\, g\, A_{1L} z_{1L} = 1000 \times 9.807 \times 0.022 \times 0.0111 = 0.24\text{N}$	**Table 8.14**
$F_{2L} = \rho\, g\, A_{2L} z_{2L} = 1000 \times 9.807 \times 0.0051 \times 0.0126 = 0.63\text{N}$	**Table 8.14**
$R_{FL} = \rho\, g\, \overline{A}\overline{z}$ $= 1000 \times 9.807 \times \left[\left(\frac{0.022+0.025}{2}\right) \times 1.5\right] \times \left(\frac{0.0111+0.0126}{2}\right)$ $R_{FL} = 4.14N$	**Table 8.14**
$\Sigma SF = \Sigma\overline{SF_b} \times L = (0.01 \times 1.5) + (0.12 \times 1.5) = 0.20N$	**Figure 8.20**
$W = \rho\, g\, S_o\, L\overline{A}$ $= 1000 \times 9.807 \times 2.003 \times 10^{-3} \times 1.5 \times \frac{(0.0022+0.0051)}{2} = 0.11N$	**Table 8.11a**
$\rho(Q_{2L}\beta_{2L}U_{2L} - Q_{L1}\beta_{1L}U_{L1}) = \rho\left(Q_{2L}^2\beta_2 / A_{2L} - Q_{1L}^2\beta_1 / A_{1L}\right)$ $= 1000\left[\left(1.0216\frac{(0.1079 \times 0.0214)^2}{0.0051}\right) - \left(1.0079\frac{(0.05525 \times 0.0214)^2}{0.0022}\right)\right]$ $\rho(Q_{2L}\beta_{2L}U_{2L} - Q_{L1}\beta_{1L}U_{L1}) = 0.45N$	**β values Table 8.3** **Discharge Figure 8.14 and Table 8.1a-d** **Other data Table 8.14**
$\rho(q_{cfL}U_{cfL}L) =$ $= 1000\left(\frac{(0.1079 \times 0.0214) - (0.05525 \times 0.0214)}{1.5}\right) \times \left(\frac{0.595+0.581}{2}\right) \times 1.5$ $\rho(q_{cfL}U_{cfL}L) = 0.66N$	**Discharge Figure 8.14 and Table 8.1a-d** **Other data Table 8.14**

Figure 8.34 plots the apparent shear force on the vertical interface (ASF_V) between the main channel and the left and right floodplain for each measurement depth and **Figure 8.35** shows the variation of apparent shear force along each vertical interface (left floodplain and right floodplain). **Figures 8.34** and **8.35** clearly show that the

vertical apparent shear forces acting on the main channel/floodplain vertical interfaces are approximately equal and opposite, as would be expected, unlike those calculated for the FCF flume in Section 7.13. It is also clear that for each discharge the apparent shear force also increases along the length of the transition as the depth increases.

From these Figures and **Tables 8.13-8.16**, the vertical apparent shear force on the left floodplain/main channel interface is seen to increase along the length of the channel. This is especially apparent at the left floodplain interface where the ASF_V increases by about 0.5N for Dr=0.514 between the first and last sections. This indicates that as the depth along the channel increases, with increasing lateral mixing, so does the ASF_V in this region. The ASF_V on the right floodplain/main channel interface generally reduces along the transition length by about 0.5N for Dr=0.514.

In the section by section analysis, the apparent shear on the horizontal interface (ASF_H) between the lower main channel (inbank portion) and upper main channel has been determined using Equation 8.48 with results given in **Tables 8.12a-d to Table 8.16** and **Figure 8.36**. This equation assumes that there is a flow balance in and out of the main channel (inbank), this is a valid assumption in this case as the velocity in the main channel (inbank) is relatively consistent between measuring sections.

$$ASF_H = \left(\rho\, g\, A_{MCIB}\, S_o\, L\right) - \left(\Sigma SF_{MC} L\right) \qquad \textbf{8.48}$$

From these Figures and Tables, it is clear that as the flow depth increases, the ASF_H becomes increasingly negative indicating that the flow in the upper channel

accelerates that in the lower main channel. This effect of the upper flow accelerating that of the flow in the lower main channel can also be seen in the isovel plots shown in **Figures 8.10 a-d**. Knight & Demetriou (1983) found similar patterns of results in their experiments in compound rectangular channels.

8.10 Comparison with prismatic asymmetric channel and non-prismatic converging channel

Previous work has been carried out at The University of Birmingham on prismatic asymmetric channels (Atabay, 2001) and non-prismatic converging channels (Rezaei, 2006) in the same 18m flume. Atabay (2001) conducted, amongst others, experiments whereby the left hand floodplain was in isolation along the flume and took measurements at 4 different flow depths. Rezaei (2006) on the other hand carried out a number of experiments using both prismatic and non-prismatic channels. The ones of interest to this study are the non-prismatic converging compound channel experiments. Although the configuration of the channels differ somewhat, comparisons can still be drawn. At sections x=19m, x=25m and x=26m the results can be likened to Atabay (2001), and likewise, at section x=22m (the centre of the skew) the results can be related to Rezaei (2006) where each floodplain was 200mm wide. Comparisons can be made with regards to friction within the channel, velocity and boundary shear stresses and also the shear forces acting on particular elements of the channel.

8.10.1 Comparison of velocity measurements

Comparisons will be drawn with Atabay's (2001) asymmetrical channel data for sections x=19m, x=25m and x=26m; where one floodplain is in isolation. Atabay's channel had the left hand floodplain in isolation along the length of the channel, therefore, in order to compare it to having a right hand floodplain in isolation, Atabay's results were simply reversed. Atabay's discharges were similar to those used herein, the 16.2ℓ/s experiment will be compared to Atabay's 15ℓ/s and 18ℓ/s experiments, the 21.4 ℓ/s, 29.6 ℓ/s and 43.4 ℓ/s tests will be compared to Atabay's 21 ℓ/s, 30 ℓ/s and 43.8 ℓ/s results. The results of the comparison can be seen in **Figures 8.37a-d**. + × Δ represent the skewed channel data at sections x=19m, x=25m and x=26m respectively. In **Figures 8.37a-d** ■ represents Atabay's measured velocity and ▲ represents the reversed data.

For the upstream section, x=19m, the results agree closely with Atabay's, in so far as most of the main channel velocities were similar to those found by Atabay, but the floodplain velocities in the skewed channel (both left and right) were slightly higher. However, at the higher discharges of 29.6 ℓ/s and 43.4 ℓ/s, the results from Atabay are closer to those of the skewed channel. It is believed any increase in velocity on the floodplains is due to the slightly narrower floodplain at this location. Atabay's floodplain was 407.3mm, whereas the floodplain in the skewed channel at this location was 390mm. At the highest discharge of 43.4 ℓ/s, this is an approximate reduction in area of 4% and 3% in velocity.

Comparing the two downstream measuring sections, x=25m and x=26m, with Atabay's there is once again good correlation, especially at the larger flow depth (Dr=0.514). At the lower discharges (Q≤29.6ℓ/s), the velocity on the floodplain in the skewed channel is greater than that of the asymmetrical channel, but at section x=26m the velocity in the floodplain is decreasing back towards the asymmetrical case. From **Tables 8.17a** and **8.17b** it is clear that the proportion of flow in the main channel and floodplain for section x=19m is remarkably similar to that of the asymmetric channel, as are the velocities.

Rezaei (2006) carried out a number of experiments assessing the effects of converging floodplains. The floodplains examined were 400mm-0mm over a 2m length, 400mm-0mm over a 6m length and 400mm-200mm over a 6m length. The results which are of particular interest to this study are the 6m transition lengths. Some of the skewed data results will be compared to the 400mm-0mm floodplain and some to the 400mm-200mm floodplain as they give the closest comparison to the skewed discharges. The comparisons can be seen in **Figures 8.38a-e**.

For the depth-averaged velocity, the comparisons for the 400mm to 0mm converging case were made to the skewed 16.2 ℓ/s and 21.4 ℓ/s results. All of the skewed data were compared to the 400mm to 200mm converging results at section x=22m. In most cases the discharges between the skewed and converging floodplains experiments varied, therefore, the closest discharges were used as the comparisons. In general, as the discharge increased the results from the skewed and converging floodplains had fewer discrepancies, as shown in **Figures 8.38d** and **8.38e**. For lower

flows, there were marked differences between the left hand floodplains, as shown in **Figure 8.38a-c**. This was to be expected as in the skewed results, flow is being forced onto the left hand floodplain whereas in the converging floodplain experiments flow is being removed. In all cases, the skewed floodplains showed slightly elevated left hand floodplain flows and slightly lower right hand floodplain flows for similar discharges. Comparisons to discharge have not been made to Rezaei's data due to the dissimilar discharges involved.

8.10.2 Boundary shear stress and shear forces

In a similar manner, the skewed data were compared to Atabay (2001) at locations x=19m, x=25m and x=26m (**Figures 8.39a-d**). From these it is clear that the values of boundary shear stress in the skewed channel are significantly less than in the prismatic asymmetrical channel for similar discharges, especially within the main channel. The floodplain values are somewhat similar. If the shear force is examined for sections x=19m, x=25m and x=26m and compared to Atabay (2001), **Figures 8.40 a-e** and **Tables 8.18a-d**, it can be seen that the shear force on each element follows the same trend, with the exception of the main channel bed shear force at low discharges where Atabay's results are slightly larger than those of the skewed channel. When comparing the percentage shear force on each element, again there is good agreement. Atabay derived formulae for computing the percentage shear force on any element in an asymmetric channel based on the relative depth, as given by Equations 8.49 to 8.54.

$$\%SF_1 = 0.3524Dr \quad (if\ D < 0.15) \tag{8.49}$$

$$\%SF_1 = 12.778Dr^2 + 0.2185Dr - 0.3618 \quad (else) \tag{8.50}$$

$$\%SF_2 = -119.64Dr^2 + 134.23Dr + 0.8263 \tag{8.51}$$

$$\%SF_3 = 4.0808Dr^2 - 5.0925Dr + 6.7169 \tag{8.52}$$

$$\%SF_4 = 97.977Dr^2 - 131.01Dr + 85.352 \tag{8.53}$$

$$\%SF_5 = 2.4531Dr^2 + 3.493Dr + 7.1349 \tag{8.54}$$

where SF_1 is the floodplain wall, SF_2 is the floodplain bed, SF_3 is the main channel (right) wall, SF_4 is the main channel bed and SF_5 is the main channel (left) wall.

Boundary shear stresses are compared to Rezaei's data at the centre (x=22m) of the skewed transition where both floodplains are approximately 200mm wide. In **Figures 8.41a-d**, which show the distributions of boundary shear stress, the skewed results are significantly higher than those of the converging results, when compared to the 400mm-0mm floodplains over a 6m length. This is especially so on the left hand floodplain, which is not unsurprising given that in Rezaei's experiments the velocity is approximately equal to the right floodplain, whereas with the skewed experiments it is increasing. There are less discrepancies between the results when analysing the higher flows and comparing them to Rezaei's 400mm-200mm convergence data over 6m. This is due to less mixing, as the angle of convergence is much less.

When comparing the shear force on each element, the skewed channel data (**Figures 8.42a-g**) compares well with the converging data. The main exception to this was the

left main channel wall and the left floodplain bed where the skewed channel had significantly more shear force acting (at low discharge, 16ℓ/s, the shear force acting on the left floodplain bed of the skewed channel was approximately double that of the converging channel) . This is due to the effects of the left floodplain, where flow in the skewed channel is being forced onto it, increasing the shear forces in this region.

8.10.3 Resistance

From **Figures 8.43a-d** and **8.44**, it can be seen that some of the friction data is in keeping with the prismatic data with varying floodplain widths (Rezaei, 2006). However, as the flow passes through the skewed channel the resistance increases, for both the Darcy-Weisbach friction factor and Manning's resistance coefficient.

When comparing the skewed channel resistance to the converging data by Rezaei (2006), it was noted that the resistance in the skewed channel was slightly higher. In the converging data, the Manning's coefficient varied between 0.0096-0.011 in the main channel, whereas, the skewed data was in the range of 0.011-0.012. Similar differences were noted in the friction factor, *f*. In the converging data the friction factor was between 0.019 and 0.02. In the skewed data the friction factor was up to 0.023. More significant differences were noted in the resistance on the floodplains, especially the right floodplain of the skewed channel data. In the skewed channel, the friction factor on the right floodplain was up to 0.04 and 0.019 on the left floodplain, both substantially more than the floodplains of the converging channel which were in the region of 0.01. These differences are due to the complex mixing occurring on the floodplains in the skewed channel. On the left floodplain, which is expanding, there

is increased friction due to the flow from the right floodplain passing over the main channel and being forced onto the left floodplain. On the right floodplain, which is converging, the roughness parameters are far higher than those on the left. This may be due to planform vortices acting similarly to those found in meandering channels.

8.11 Comparison of FCF skewed data with Birmingham skewed channel data

Although the skewed data was carried out on a much larger scale in the Flood Channel Facility than at the University of Birmingham, comparisons can still be drawn between the two.

The lateral velocity distributions of streamwise velocity (**Figures 8.7-8.9** for the Birmingham data and **Figures 7.10-7.14** for the FCF data) clearly show similar trends, both exhibit a peak in velocity at the interface between the main channel and the left hand floodplain at lower flows and a flattening of velocity at higher flows. Although the discharge in the FCF work was in excess of $1m^3/s$, in comparison to only $0.0434m^3/s$ at Birmingham, this phenomena was apparent in both flumes with similar percentage peak values. In addition the maximum velocity usually occurs just off the centreline of the main channel in the direction of the skew. The Birmingham data has a peak of up to 50% greater than the average velocity on the floodplain which is similar to the FCF data which peaks up to a value of 60% greater than the section mean velocity.

The boundary shear stress exhibits similar patterns to the velocity in that there is a clear peak at the interface of the main channel and receiving floodplain. This is

evident in virtually all flow depths, in both the Birmingham (**Figures 8.17a-d**) and FCF flume (**Figures 7.27a-k**). This peak is between 2-2.5 times that of the section mean boundary shear stress for both channels, with the greatest peaks being seen at low depth ratios (Dr≤0.3). The right hand floodplain generally demonstrates a relatively flat boundary shear stress profile, with the exception of a few high flows.

It is more difficult to compare the percentage of shear force (%SF) on each element (i.e. walls and bed values) due to the differences in the two channel configurations. In the FCF work (**Figures 7.29** and **7.30**), the percentage shear force on each element remained relatively constant regardless of location along the channel on almost all elements. Only the floodplain beds had significant changes between sections due to the left floodplain increasing in width and therefore carrying a higher percentage of shear force. Therefore, the left hand floodplain carried much more shear force downstream than upstream, and conversely the right hand floodplain carried less shear force at the downstream location. The Birmingham data, shown in **Figures 8.20a-g,** shows that the skewing of flow had a significant effect on the left main channel wall where the peak in shear stress was located, as seen in **Figure 8.20c**. As more discharge was passing onto the floodplain, there was an increase in the percentage of total shear force carried by the left main channel wall. In the Birmingham channel, the percentage of total shear force carried by an element was affected by location at all measuring sections. In general, all values decreased along the length of the channel with the exception of the receiving floodplain, which increased, and the left main channel wall. The differences between trends in the FCF and Birmingham flume may be due to the Birmingham flume having more measuring sections and

small changes being noticed along the length, but it should also be borne in mind that the FCF flume had achieved near-uniform flow, resulting in smaller changes.

A force-momentum balance was carried out for both the Birmingham and FCF flumes. **Tables 8.11-8.16** and **Figures 8.34-8.36** show the results from the Birmingham flume and the FCF results shown in **Tables 7.14-7.26**. From these, the Birmingham flume had a residual force of approximately 1.0N and the FCF up to 183.0N depending on the method employed (inclusion or exclusion of β values). This maybe due to the FCF being on a much larger scale, however in a few cases the FCF flume had significant out of balance momentum terms of up to 60N, in these cases this was purely down to the momentum correction factors and the differences between the upstream and downstream locations. Out of balance forces in the Birmingham flume were due to an increasing water level through the flume, resulting in errors in estimating the hydrostatic forces and with boundary shear force being uncorrected. Whereas, in the FCF flume any discrepancy was entirely due to changes in momentum. From the force momentum balances the apparent shear force was calculated for both the FCF (**Figures 7.40-7.43**) and Birmingham data (**Figures 8.34-8.36**). From these, the Birmingham data gave much more consistent values of ASF on the right and left floodplain/main channel interfaces. The FCF data resulted in very large values of ASF which is due to the inclusion of the momentum correction coefficients which were not included in the original study.

To conclude, the FCF and Birmingham flumes are both quite different in terms of geometry, discharge and measurement positions. However, some common trends

exist between the two data sets; primarily the velocity and boundary shear stress distributions.

8.12 Concluding remarks

Skewed channel experimental results have been presented and discussed with particular attention paid to the velocity distributions, boundary shear stress and shear forces acting on the channel. Furthermore these results have been compared to two similar configurations; the prismatic asymmetric channel (Atabay, 2001) and the converging channel (Razaei, 2006). The conclusions drawn are summarised below:

- The water surface profiles for the different flows investigated (shown in **Figures 8.6a-d**) became more significant than first thought. In the upstream, prismatic, asymmetric portion of the flume, the profile of the water surface follows that of the bed (uniform flow). Once the flow passes into the skewed transition it takes on an M1 profile. Initially over the first quarter of the channel the water surface rises slightly, over the middle portion it rises rapidly and in the last quarter becomes flat again. Downstream of the transition the flow comes back to a uniform flow profile.
- All sections had the lateral streamwise depth-averaged velocities measured and 4 sections had full lateral streamwise velocity data gathered. **Figures 8.7a-d** show these depth-integrated velocity profiles. It is clear that the velocity in the right hand floodplain decreases though the transition, whilst the left hand floodplain velocity increases. The velocity in the main channel decreases through the transition. The peak velocity (up to 50% greater than

the mean left floodplain velocity) is biased in the direction of the skew. In addition, as the relative depth increases (Dr≥0.415) the left hand floodplain peak velocity becomes closer to the main channel peak velocity.

- Using the full transverse velocities or the depth-averaged velocities where no full velocity profiles were taken, the velocity and momentum correction coefficients, α and β, have been calculated (see **Tables 8.2a-d**).
- Proportional flow results have been presented in **Figures 8.11-8.14** and **Table 8.4**. From these, the discharge on the right floodplain decreases as the discharge on the left floodplain increases by a similar amount. The proportion of discharge in the main channel is approximately constant for each relative depth. This indicates that the discharge being forced off the right floodplain enters the main channel and immediately transfers onto the left floodplain.
- The boundary shear stress was measured at all sections and the results given in **Figures 8.17a-d**, these show a peak, in cases double that of the section mean, in shear stress at the interface between the main channel and left hand floodplain, the receiving floodplain. This is similar to the FCF work (**Figures 7.27a-k**) which exhibit peak shear stresses of up to 2.5 times the section mean at the main channel/left floodplain interface.
- The shear force on each element in the channel were calculated and are presented in **Table 8.7** and **Figures 8.20a-g**. The percentage shear force has also been determined. From these it was found that the shear force on the left floodplains increases more than the values on the right floodplain decreases by. There is also an increase in the left main channel wall caused by the fluid being forced onto the left floodplain.

- A number of approaches of calculating the theoretical boundary shear stress have been presented in **Tables 8.6a-d**. From these, no one method was suitable to use to correct the boundary shear stress results, therefore unadjusted boundary shear stress was used in the subsequent force-momentum balances.
- Based on the calculated shear forces, a number of force-momentum balances have been carried out; a full 6m analysis (**Table 8.11b**), a section by section analysis of the whole channel (**Tables 8.12a-d**), and a separate analysis of the main channel and floodplain(s) (**Tables 8.13-8.16**). This also allowed for calculation of the apparent shear force at the vertical interface of the main channel and floodplain(s). From these, in all cases there is a small out of balance moment of approximately 1N. It is believed this is due to using smoothed data, but as the boundary shear stresses could not be corrected, using smoothed data will remove some rogue results. The apparent shear force on a vertical interface is approximately equal and opposite for the left and right floodplains. Along the length of the channel, the left floodplain increases in magnitude whereas the right floodplain decreases in magnitude.
- An energy balance was examined through the 6m transition which showed that head losses were not related to relative depth and were approximately 0.01m. This is similar to those found by Rezaei in his converging channel experiments.
- Comparisons have been made in terms of velocity, discharge, shear stress and force and the resistance of the channel to Atabay, 2001 and Rezaei, 2006. As shown in **Figures 8.37a-d,** the upstream and downstream lateral velocity

distributions compare well to Atabay's (2001) asymmetric channel results. The mid-section, shown in **Figure 8.38a-e** (x=22m) compare well to Rezaei's converging channel experiments. There are however some differences between the converging and skewed data. Generally, the left hand velocity on the skewed channel is greater than the converging channel which is due to the fluid being forced onto the left floodplain and hence accelerating.

This data, in conjunction with the FCF data is judged to give a clear insight into the hydrodynamic behaviour of skewed channels. Both data sets are distinct in many ways, the FCF had a uniform flow allowing for correction of the boundary shear stress whereas in Birmingham it was evident that uniform flow was unachievable, and hence no boundary shear stress adjustment possible. The Birmingham flume also had many more measuring sections while the FCF data had only a couple but more configurations were considered. Notwithstanding these difficulties, the data is of sufficient accuracy and clarity to be used to develop the Shiono and Knight Method in such a way that skewed channels can be accurately modelled for lateral depth-averaged velocity and boundary shear stress distributions.

Experiment	Section	Discharge	TG	Depth	Dr	S_o	Main Channel Width	Floodplain width		Perimeter	Area	Hydraulic Radius	Velocity	ν	Re	Fr
								Left	Right							
	m	*m^3/s*	*mm*	*m*			*m*	*m*	*m*	*m*	*m^2*	*m*	*m/s*			
Q=16.2 ℓ/s	19	0.0162	45.7	0.0634	0.211	2.003E-03	0.398	0.000	0.390	0.915	0.031	0.033	0.530	9.88E-07	7.16E+04	0.860
Q=16.2 ℓ/s	20.5	0.0162	45.7	0.0615	0.187	2.003E-03	0.398	0.100	0.291	0.915	0.030	0.032	0.547	9.88E-07	7.16E+04	0.903
Q=16.2 ℓ/s	22	0.0162	45.7	0.0629	0.205	2.003E-03	0.398	0.200	0.192	0.920	0.031	0.034	0.524	9.45E-07	7.44E+04	0.847
Q=16.2 ℓ/s	23.5	0.0162	45.7	0.066	0.242	2.003E-03	0.398	0.298	0.097	0.926	0.033	0.035	0.493	9.76E-07	7.16E+04	0.774
Q=16.2 ℓ/s	25	0.0162	45.7	0.0662	0.245	2.003E-03	0.398	0.392	0.000	0.922	0.033	0.035	0.496	9.45E-07	7.42E+04	0.780
Q=16.2 ℓ/s	26	0.0162	45.7	0.0672	0.256	2.003E-03	0.398	0.400	0.000	0.932	0.033	0.036	0.483	9.45E-07	7.34E+04	0.753

Table 8.1a-As built dimensions and basic channel data for 16.2ℓ/s

Experiment	Section	Discharge	TG	Depth	Dr	S_o	Main Channel Width	Floodplain width		Perimeter	Area	Hydraulic Radius	Velocity	ν	Re	Fr
								Left	Right							
	m	*m^3/s*	*mm*	*m*			*m*	*m*	*m*	*m*	*m^2*	*m*	*m/s*			
Q=21.4 ℓ/s	19	0.0214	47.1	0.0717	0.303	2.003E-03	0.398	0.000	0.390	0.931	0.037	0.040	0.579	9.57E-07	9.61E+04	0.855
Q=21.4 ℓ/s	20.5	0.0214	47.1	0.0702	0.288	2.003E-03	0.398	0.100	0.291	0.933	0.036	0.039	0.588	9.09E-07	1.01E+05	0.873
Q=21.4 ℓ/s	22	0.0214	47.1	0.0741	0.325	2.003E-03	0.398	0.200	0.192	0.940	0.039	0.042	0.545	9.42E-07	9.68E+04	0.781
Q=21.4 ℓ/s	23.5	0.0214	47.1	0.0758	0.340	2.003E-03	0.398	0.298	0.097	0.946	0.041	0.043	0.527	9.09E-07	9.96E+04	0.744
Q=21.4 ℓ/s	25	0.0214	47.1	0.0756	0.339	2.003E-03	0.398	0.392	0.000	0.941	0.040	0.043	0.532	9.23E-07	9.84E+04	0.753
Q=21.4 ℓ/s	26	0.0214	47.1	0.0764	0.346	2.003E-03	0.398	0.400	0.000	0.951	0.041	0.043	0.522	8.99E-07	1.00E+05	0.735

Table 8.1b-As built dimensions and basic channel data for 21.4ℓ/s

Experiment	Section	Discharge	TG	Depth	Dr	S_o	Main Channel Width	Floodplain width		Perimeter	Area	Hydraulic Radius	Velocity	ν	Re	Fr
								Left	Right							
	m	*m^3/s*	*mm*	*m*			*m*	*m*	*m*	*m*	*m^2*	*m*	*m/s*			
Q=29.6 ℓ/s	19	0.0296	47.2	0.0835	0.401	2.003E-03	0.398	0.000	0.390	0.955	0.046	0.048	0.640	1.03E-06	1.21E+05	0.843
Q=29.6 ℓ/s	20.5	0.0296	47.2	0.0826	0.395	2.003E-03	0.398	0.100	0.291	0.957	0.046	0.048	0.640	1.01E-06	1.22E+05	0.844
Q=29.6 ℓ/s	22	0.0298	47.2	0.0874	0.428	2.003E-03	0.398	0.200	0.192	0.966	0.050	0.051	0.599	1.01E-06	1.22E+05	0.762
Q=29.6 ℓ/s	23.5	0.0296	47.2	0.0881	0.432	2.003E-03	0.398	0.298	0.097	0.971	0.050	0.052	0.587	1.01E-06	1.20E+05	0.743
Q=29.6 ℓ/s	25	0.0296	47.2	0.0865	0.422	2.003E-03	0.398	0.392	0.000	0.964	0.049	0.051	0.603	1.02E-06	1.20E+05	0.772
Q=29.6 ℓ/s	26	0.0295	47.2	0.0875	0.429	2.003E-03	0.398	0.400	0.000	0.973	0.050	0.051	0.594	1.03E-06	1.18E+05	0.761

Table 8.1c-As built dimensions and basic channel data for 29.6 ℓ/s

Experiment	Section	Discharge	TG	Depth	Dr	S_o	Main Channel Width	Floodplain width		Perimeter	Area	Hydraulic Radius	Velocity	ν	Re	Fr
								Left	Right							
	m	*m^3/s*	*mm*	*m*			*m*	*m*	*m*	*m*	*m^2*	*m*	*m/s*			
Q=43.4 ℓ/s	19	0.0434	51.4	0.1025	0.512	2.003E-03	0.398	0.000	0.390	0.993	0.061	0.062	0.709	9.88E-07	1.77E+05	0.812
Q=43.4 ℓ/s	20.5	0.0434	51.4	0.1012	0.506	2.003E-03	0.398	0.100	0.291	0.994	0.061	0.061	0.714	9.88E-07	1.77E+05	0.822
Q=43.4 ℓ/s	22	0.0434	51.4	0.1002	0.501	2.003E-03	0.398	0.200	0.192	0.995	0.060	0.061	0.718	9.45E-07	1.85E+05	0.829
Q=43.4 ℓ/s	23.5	0.0434	51.4	0.1056	0.527	2.003E-03	0.398	0.298	0.097	1.006	0.064	0.064	0.675	9.76E-07	1.77E+05	0.757
Q=43.4 ℓ/s	25	0.0434	51.4	0.1039	0.519	2.003E-03	0.398	0.392	0.000	0.998	0.063	0.063	0.693	9.45E-07	1.84E+05	0.786
Q=43.4 ℓ/s	26	0.0434	51.4	0.1069	0.532	2.003E-03	0.398	0.400	0.000	1.011	0.065	0.064	0.667	9.45E-07	1.82E+05	0.746

Table 8.1d-As built dimensions and basic channel data for 43.4 ℓ/s

				Velocity				Energy correction coefficient				Momentum correction coefficient				Global				Zonal friction					
Experiment	Section	Depth	Area	U_{ave}	U_{LFP}	U_{MC}	U_{RFP}	α_{LFP}	α_{MC}	α_{RFP}	α	β_{LFP}	β_{MC}	β_{RFP}	β	f_g	n_g	f_L	n_L	n_{LFP}	n_{MC}	n_{RFP}	f_{LFP}	f_{MC}	f_{RFP}
	m	*m*	m^2	*m/s*	*m/s*	*m/s*	*m/s*																		
Q=16.2 l/s	19	0.0634	0.031	0.5299	0.0000	0.5911	0.2383	-	1.0598	1.0495	1.3487	-	1.0206	1.0047	1.1881	0.0187	0.0088	0.0069	0.0053	-	0.0102	0.0105	-	0.0222	0.0364
Q=16.2 l/s	20.5	0.0615	0.030	0.5474	0.3908	0.6038	0.2363	1.0201	1.0313	1.0306	1.1730	1.0070	1.0109	1.0103	1.0651	0.0169	0.0083	0.0077	0.0056	0.0058	0.0099	0.0102	0.0118	0.0212	0.0350
Q=16.2 l/s	22	0.0629	0.031	0.5243	0.3406	0.5801	0.2243	1.2841	1.0590	1.1436	1.2176	1.1338	1.0119	1.0899	1.0741	0.0192	0.0089	0.0084	0.0059	0.0076	0.0105	0.0114	0.0187	0.0235	0.0429
Q=16.2 l/s	23.5	0.066	0.033	0.4929	0.3105	0.5463	0.1817	1.2123	1.0510	1.0553	1.1935	1.0689	1.0179	1.0184	1.0714	0.0229	0.0098	0.0078	0.0057	0.0090	0.0115	0.0144	0.0256	0.0278	0.0674
Q=16.2 l/s	25	0.0662	0.033	0.4963	0.3186	0.5383	0.0000	1.3360	1.0584	-	1.1729	1.1277	1.0138	-	1.0582	0.0225	0.0097	0.0080	0.0058	0.0086	0.0115	-	0.0236	0.0278	-
Q=16.2 l/s	26	0.0672	0.033	0.4831	0.2964	0.5301	0.0000	1.1092	1.0811	-	1.1925	1.0052	1.0277	-	1.0646	0.0242	0.0101	0.0073	0.0055	0.0096	0.0117	-	0.0288	0.0290	-

Tables 8.2a-Velocity and velocity and momentum correction coefficients for Q=16.2*l*/s

				Velocity				Energy correction coefficient				Momentum correction coefficient				Global				Zonal friction					
Experiment	Section	Depth	Area	U_{ave}	U_{LFP}	U_{MC}	U_{RFP}	α_{LFP}	α_{MC}	α_{RFP}	α	β_{LFP}	β_{MC}	β_{RFP}	β	f_g	n_g	f_L	n_L	n_{LFP}	n_{MC}	n_{RFP}	f_{LFP}	f_{MC}	f_{RFP}
	m	*m*	m^2	*m/s*	*m/s*	*m/s*	*m/s*																		
Q=21.4 l/s	19	0.0717	0.037	0.5794	0.0000	0.6415	0.3682	-	1.0546	1.0829	1.1692	-	1.0187	1.0283	1.0593	0.0186	0.0090	0.0102	0.0067	-	0.0101	0.0091	-	0.0210	0.0236
Q=21.4 l/s	20.5	0.0702	0.036	0.5876	0.5209	0.6458	0.3540	1.0234	1.0312	1.8457	1.1308	1.0079	1.0108	1.3531	1.0467	0.0178	0.0088	0.0083	0.0060	0.0059	0.0102	0.0094	0.0104	0.0211	0.0254
Q=21.4 l/s	22	0.0741	0.039	0.5454	0.4847	0.5948	0.3040	1.0630	1.0852	1.0281	1.1738	1.0216	1.0295	1.0098	1.0605	0.0221	0.0099	0.0086	0.0062	0.0073	0.0114	0.0116	0.0148	0.0263	0.0375
Q=21.4 l/s	23.5	0.0758	0.041	0.5273	0.4672	0.5638	0.2829	1.0724	1.1183	1.0242	1.1920	1.0247	1.0410	1.0084	1.1073	0.0243	0.0104	0.0106	0.0069	0.0080	0.0122	0.0120	0.0175	0.0299	0.0409
Q=21.4 l/s	25	0.0756	0.040	0.5320	0.4310	0.5660	0.0000	1.1732	1.1057	-	1.1532	1.0660	1.0366	-	1.0540	0.0237	0.0103	0.0091	0.0064	0.0087	0.0118	-	0.0205	0.0282	-
Q=21.4 l/s	26	0.0764	0.041	0.5218	0.4123	0.5594	0.0000	1.1434	1.1009	-	1.1535	1.0569	1.0348	-	1.0538	0.0249	0.0105	0.0084	0.0061	0.0093	0.0120	-	0.0231	0.0291	-

Tables 8.2b-Velocity and velocity and momentum correction coefficients for Q=21.4*l*/s

				Velocity				Energy correction coefficient				Momentum correction coefficient				Global				Zonal friction					
Experiment	Section	Depth	Area	U_{ave}	U_{LFP}	U_{MC}	U_{RFP}	α_{LFP}	α_{MC}	α_{RFP}	α	β_{LFP}	β_{MC}	β_{RFP}	β	f_g	n_g	f_L	n_L	n_{LFP}	n_{MC}	n_{RFP}	f_{LFP}	f_{MC}	f_{RFP}
	m	*m*	m^2	*m/s*	*m/s*	*m/s*	*m/s*																		
Q=29.6 l/s	19	0.0835	0.046	0.6399	0.0000	0.7028	0.4796	-	1.0505	1.1194	1.1322	-	1.0172	1.0482	1.0471	0.0186	0.0093	0.0098	0.0068	-	0.0100	0.0092	-	0.0199	0.0210
Q=29.6 l/s	20.5	0.0826	0.046	0.6399	0.5649	0.6970	0.4765	1.0210	1.0352	1.0284	1.0948	1.0072	1.0121	1.0098	1.0325	0.0185	0.0093	0.0108	0.0071	0.0069	0.0105	0.0092	0.0125	0.0214	0.0211
Q=29.6 l/s	22	0.0874	0.050	0.5990	0.5458	0.6429	0.4458	1.0370	1.0712	0.9516	1.1045	1.0128	1.0242	0.9813	1.0322	0.0226	0.0103	0.0098	0.0068	0.0083	0.0118	0.0101	0.0169	0.0266	0.0252
Q=29.6 l/s	23.5	0.0881	0.050	0.5868	0.5533	0.6199	0.3808	1.0116	1.0190	1.0123	1.1123	1.0116	1.0190	1.0123	1.0775	0.0237	0.0106	0.0104	0.0070	0.0085	0.0123	0.0108	0.0176	0.0288	0.0300
Q=29.6 l/s	25	0.0865	0.049	0.6026	0.5657	0.6184	0.0000	1.1319	1.0917	-	1.1069	1.0523	1.0313	-	1.0385	0.0221	0.0102	0.0112	0.0073	0.0083	0.0116	-	0.0168	0.0265	-
Q=29.6 l/s	26	0.0875	0.050	0.5944	0.5243	0.6242	0.0000	1.1367	1.0877	-	1.1167	1.0527	1.0300	-	1.0414	0.0227	0.0104	0.0108	0.0071	0.0090	0.0116	-	0.0194	0.0262	-

Tables 8.2c-Velocity and velocity and momentum correction coefficients for Q=29.6*l*/s

				Velocity				Energy correction coefficient				Momentum correction coefficient				Global				Zonal friction					
Experiment	Section	Depth	Area	U_{ave}	U_{LFP}	U_{MC}	U_{RFP}	α_{LFP}	α_{MC}	α_{RFP}	α	β_{LFP}	β_{MC}	β_{RFP}	β	f_g	n_g	f_L	n_L	n_{LFP}	n_{MC}	n_{RFP}	f_{LFP}	f_{MC}	f_{RFP}
	m	*m*	m^2	*m/s*	*m/s*	*m/s*	*m/s*																		
Q=43.4 l/s	19	0.1025	0.061	0.7090	0.0000	0.7587	0.6097	-	1.0469	1.1473	1.0983	0.0000	1.0161	1.0572	1.0362	0.0193	0.0099	0.0113	0.0075	-	0.0104	0.0095	-	0.0202	0.0195
Q=43.4 l/s	20.5	0.1012	0.061	0.7142	0.6338	0.7673	0.6018	1.0222	1.0255	1.0166	1.0569	1.0077	1.0087	1.0058	1.0192	0.0188	0.0097	0.0122	0.0078	0.0075	0.0109	0.0093	0.0135	0.0216	0.0193
Q=43.4 l/s	22	0.1002	0.060	0.7183	0.6876	0.7520	0.6168	1.0244	1.0311	0.9598	1.0379	1.0083	1.0106	0.9601	1.0092	0.0185	0.0096	0.0117	0.0077	0.0078	0.0111	0.0087	0.0138	0.0223	0.0170
Q=43.4 l/s	23.5	0.1056	0.064	0.6752	0.6094	0.7208	0.5267	1.0210	1.0435	1.0412	1.0928	1.0073	1.0151	1.0141	1.0610	0.0220	0.0106	0.0110	0.0075	0.0096	0.0119	0.0092	0.0200	0.0255	0.0202
Q=43.4 l/s	25	0.1039	0.063	0.6932	0.6428	0.7191	0.0000	1.1347	1.0648	-	1.0923	1.0529	1.0221	-	1.0339	0.0205	0.0102	0.0116	0.0077	0.0091	0.0111	-	0.0181	0.0228	-
Q=43.4 l/s	26	0.1069	0.065	0.6672	0.6363	0.6836	0.0000	1.1441	1.0816	-	1.1040	1.0576	1.0282	-	1.0386	0.0227	0.0108	0.0111	0.0075	0.0095	0.0118	-	0.0192	0.0258	-

Tables 8.2d-Velocity and velocity and momentum correction coefficients for Q=43.4*l*/s

	Section	Q_M	$Q_{i\ (0.4H)}$	$\%Q_e$	$Q_{i\ (full)}$	$\%Q_e$
		m^3/s	m^3/s		m^3/s	
Dr=0.205	**19**	0.01618	0.01670	3.20%	0.01611	-0.41%
	20.5	0.01618	0.01604	-0.89%	N/A	
	22	0.01617	0.01612	-0.27%	0.01547	-4.30%
	23.5	0.01618	0.01615	-0.18%	N/A	
	25	0.01617	0.01619	0.14%	0.01541	-4.70%
	26	0.01617	0.01597	-1.20%	0.01565	-3.18%
			Average error	**0.13%**		**-3.15%**

	Section	Q_M	$Q_{i\ (0.4H)}$	$\%Q_e$	$Q_{i\ (full)}$	$\%Q_e$
		m^3/s	m^3/s		m^3/s	
Dr=0.313	**19**	0.02139	0.02090	-2.30%	0.02086	-2.50%
	20.5	0.02143	0.02156	0.64%	N/A	
	22	0.02141	0.02208	3.13%	0.02163	1.05%
	23.5	0.02143	0.02085	-2.68%	N/A	
	25	0.02139	0.02100	-1.84%	0.02075	-3.01%
	26	0.02140	0.02137	-0.10%	0.02056	-3.90%
			Average error	**-0.53%**		**-2.09%**

	Section	Q_M	$Q_{i\ (0.4H)}$	$\%Q_e$	$Q_{i\ (full)}$	$\%Q_e$
		m^3/s	m^3/s		m^3/s	
Dr=0.415	**19**	0.02960	0.02919	-1.40%	0.02865	-3.23%
	20.5	0.02957	0.02991	1.16%	N/A	
	22	0.02980	0.03037	1.89%	0.03023	1.43%
	23.5	0.02957	0.02999	1.43%	N/A	
	25	0.02960	0.03041	2.73%	0.02989	0.97%
	26	0.02952	0.02948	-0.14%	0.02863	-3.02%
			Average error	**0.95%**		**-0.96%**

	Section	Q_M	$Q_{i\ (0.4H)}$	$\%Q_e$	$Q_{i\ (full)}$	$\%Q_e$
		m^3/s	m^3/s		m^3/s	
Dr=0.514	**19**	0.04341	0.04412	1.63%	0.04288	-1.21%
	20.5	0.04343	0.04245	-2.26%	N/A	
	22	0.04343	0.04207	-3.13%	0.04223	-2.74%
	23.5	0.04340	0.04253	-1.99%	N/A	
	25	0.04340	0.04297	-0.99%	0.04196	-3.30%
	26	0.04344	0.04358	0.33%	0.04250	-2.16%
			Average error	**-1.07%**		**-2.35%**

Table 8.3a-d-Measured and integrated discharges and associated errors

		Discharge				Percentage Discharge		
Relative depth	**Section**	**Qm**	**Q, LFP**	**Q, MC**	**Q, RFP**	**%Q, LFP**	**%Q, MC**	**%Q, RFP**
	m	***l/s***	***l/s***	***l/s***	***l/s***	***l/s***	***l/s***	***l/s***
0.205	19	16.1806	0.0000	14.9165	1.2642	0.00%	92.19%	7.81%
0.205	20.5	16.1806	0.5081	14.7786	0.8939	3.14%	91.34%	5.52%
0.205	22	16.1685	1.0082	14.5230	0.6372	6.24%	89.82%	3.94%
0.205	23.5	16.1784	1.5359	14.3499	0.2926	9.49%	88.70%	1.81%
0.205	25	16.1685	1.9860	14.1825	0.0000	12.28%	87.72%	0.00%
0.205	26	16.1685	1.9916	14.1769	0.0000	12.32%	87.68%	0.00%
0.313	19	21.3942	0.0000	18.3064	3.0878	0.00%	85.57%	14.43%
0.313	20.5	21.4258	1.1355	18.0444	2.2460	5.30%	84.22%	10.48%
0.313	22	21.4095	2.4139	17.5422	1.4535	11.27%	81.94%	6.79%
0.313	23.5	21.4258	3.6894	17.0092	0.7272	17.22%	79.39%	3.39%
0.313	25	21.3891	4.3590	17.0302	0.0000	20.38%	79.62%	0.00%
0.313	26	21.3955	4.3864	17.0091	0.0000	20.50%	79.50%	0.00%
0.415	19	29.6015	0.0000	23.3547	6.2468	0.00%	78.90%	21.10%
0.415	20.5	29.5679	1.9264	22.9132	4.7283	6.52%	77.49%	15.99%
0.415	22	29.8042	4.1700	22.3646	3.2696	13.99%	75.04%	10.97%
0.415	23.5	29.5679	6.3976	21.7370	1.4333	21.64%	73.52%	4.85%
0.415	25	29.6036	8.3153	21.2883	0.0000	28.09%	71.91%	0.00%
0.415	26	29.5185	7.7801	21.7384	0.0000	26.36%	73.64%	0.00%
0.514	19	43.4107	0.0000	30.9512	12.4595	0.00%	71.30%	28.70%
0.514	20.5	43.4258	3.3273	30.9053	9.1933	7.66%	71.17%	21.17%
0.514	22	43.4258	7.2198	29.9887	6.2173	16.63%	69.06%	14.32%
0.514	23.5	43.3952	10.2244	30.2945	2.8763	23.56%	69.81%	6.63%
0.514	25	43.3952	13.6569	29.7383	0.0000	31.47%	68.53%	0.00%
0.514	26	43.4401	14.3548	29.0852	0.0000	33.05%	66.95%	0.00%

Table 8.4-Proportional flow results

Q	Date	H_{19}	$H_{20.5}$	$H_{23.5}$	H_{25}
l/s		*mm*	*mm*	*mm*	*mm*
16.2	09/10/2006	64.1	63.75	66	65.9
	26/01/2007	63.3	63.2	67.9	68.8
	30/01/2007	61.7	61.4	65.8	68.5
	Meas Point	63.4	61.5	66	66.2
	Average, m	0.0631	0.0625	0.0664	0.0674

Q	Date	H_{19}	$H_{20.5}$	$H_{23.5}$	H_{25}
l/s		*mm*	*mm*	*mm*	*mm*
21.4	19/09/2006	69.3	69.35	72.8	74.2
	26/01/2007	71.6	71.8	76.3	77.3
	30/01/2007	71.8	69.9	74.7	76
	Meas Point	71.7	70.2	75.8	75.6
	Average, m	0.0711	0.0703	0.0749	0.0758

Q	Date	H_{19}	$H_{20.5}$	$H_{23.5}$	H_{25}
l/s		*mm*	*mm*	*mm*	*mm*
29.6	02/10/2006	85	82.6	86.05	87
	26/01/2007	84.3	84.2	87.6	87.4
	30/01/2007	83.9	81.7	87	87.6
	Meas Point	83.5	83.2	88.1	86.5
	Average, m	0.0842	0.0829	0.0872	0.0871

Q	Date	H_{19}	$H_{20.5}$	$H_{23.5}$	H_{25}
l/s		*mm*	*mm*	*mm*	*mm*
43.4	02/10/2006	102.8	99.25	104.3	106.4
	26/01/2007	100.5	103.7	106	107.2
	30/01/2007	100.4	100.2	104.5	105.6
	Meas Point	102.5	101.2	105.6	103.9
	Average, m	0.1016	0.1011	0.1051	0.1058

Table 8.5a-d-Average flow depths used in calculated (theoretical) boundary shear stress

							6m Transition			2-leg approach			3-leg approach		
Experiment	**Section**	**Discharge**	**S_o**	**τ_b**	**$\rho g R S_o$**	**%error**	**$(S_o-(\Delta H/\Delta x))$**	**$\rho g R(S_o-(\Delta H/\Delta x))$**	**%error**	**$(S_o-(\Delta H/\Delta x))$**	**$\rho g R(S_o-(\Delta H/\Delta x))$**	**%error**	**$(S_o-(\Delta H/\Delta x))$**	**$\rho g R(S_o-(\Delta H/\Delta x))$**	**%error**
	m	***m^3/s***		***N/m^2***				***N/m^2***			***N/m^2***			***N/m^2***	
Q=16.2 l/s	19	0.0162	2.003E-03	0.4567	0.6556	-30.33%	0.001	0.4251	7.44%	0.002	0.6917	-33.97%	0.002	0.6917	-33.97%
Q=16.2 l/s	20.5	0.0162	2.003E-03	0.5255	0.6346	-17.19%	0.001	0.4115	27.70%	0.002	0.6696	-21.52%	0.002	0.6696	-21.52%
Q=16.2 l/s	22	0.0162	2.003E-03	0.5508	0.6587	-16.38%	0.001	0.4271	28.96%	0.001	0.3908	40.94%	0.001	0.4415	24.76%
Q=16.2 l/s	23.5	0.0162	2.003E-03	0.4818	0.6962	-30.80%	0.001	0.4514	6.72%	0.001	0.4131	16.64%	0.001	0.4666	3.24%
Q=16.2 l/s	25	0.0162	2.003E-03	0.4939	0.6941	-28.83%	0.001	0.4501	9.75%	0.001	0.4118	19.95%	0.002	0.6406	-22.90%
Q=16.2 l/s	26	0.0162	2.003E-03	0.4418	0.7053	-37.36%	0.001	0.4574	-3.40%	0.001	0.4185	5.58%	0.002	0.6511	-32.13%
			Average	*0.4918*	*0.6741*	*-26.81%*	*0.0013*	*0.4371*	*12.86%*	*0.0015*	*0.4992*	*4.60%*	*0.0018*	*0.5935*	*-13.75%*

Tables 8.6a-Boundary shear stress results compared to theoretical values for Q=16.2*l*/s

							6m Transition			2-leg approach			3-leg approach		
Experiment	**Section**	**Discharge**	**S_o**	**τ_b**	**$\rho g R S_o$**	**%error**	**$(S_o-(\Delta H/\Delta x))$**	**$\rho g R(S_o-(\Delta H/\Delta x))$**	**%error**	**$(S_o-(\Delta H/\Delta x))$**	**$\rho g R(S_o-(\Delta H/\Delta x))$**	**%error**	**$(S_o-(\Delta H/\Delta x))$**	**$\rho g R(S_o-(\Delta H/\Delta x))$**	**%error**
	m	***m^3/s***		***N/m^2***				***N/m^2***			***N/m^2***			***N/m^2***	
Q=21.4 l/s	19	0.0214	2.003E-03	0.7392	0.7789	-5.10%	0.001	0.4759	55.32%	0.002	0.8299	-10.93%	0.002	0.8299	-10.93%
Q=21.4 l/s	20.5	0.0214	2.003E-03	0.6093	0.7680	-20.67%	0.001	0.4693	29.84%	0.002	0.8184	-25.55%	0.002	0.8184	-25.55%
Q=21.4 l/s	22	0.0214	2.003E-03	0.5849	0.8204	-28.71%	0.001	0.5013	16.67%	0.001	0.4475	30.69%	0.001	0.5073	15.30%
Q=21.4 l/s	23.5	0.0214	2.003E-03	0.6974	0.8438	-17.35%	0.001	0.5156	35.26%	0.001	0.4603	51.51%	0.001	0.5217	33.67%
Q=21.4 l/s	25	0.0214	2.003E-03	0.6021	0.8389	-28.22%	0.001	0.5126	17.47%	0.001	0.4576	31.58%	0.002	0.7778	-22.59%
Q=21.4 l/s	26	0.0214	2.003E-03	0.5499	0.8471	-35.09%	0.001	0.5176	6.23%	0.001	0.4621	19.00%	0.002	0.7854	-29.99%
			Average	*0.6304*	*0.8162*	*-22.52%*	*0.0012*	*0.4987*	*26.80%*	*0.0014*	*0.5793*	*16.05%*	*0.0017*	*0.7067*	*-6.68%*

Tables 8.6b-Boundary shear stress results compared to theoretical values for Q=21.4*l*/s

							6m Transition			2-leg approach			3-leg approach		
Experiment	**Section**	**Discharge**	**S_o**	**τ_b**	**$\rho g R S_o$**	**%error**	**$(S_o-(\Delta H/\Delta x))$**	**$\rho g R(S_o-(\Delta H/\Delta x))$**	**%error**	**$(S_o-(\Delta H/\Delta x))$**	**$\rho g R(S_o-(\Delta H/\Delta x))$**	**%error**	**$(S_o-(\Delta H/\Delta x))$**	**$\rho g R(S_o-(\Delta H/\Delta x))$**	**%error**
	m	***m^3/s***		***N/m^2***				***N/m^2***			***N/m^2***			***N/m^2***	
Q=29.6 l/s	19	0.0296	2.003E-03	0.7873	0.9516	-17.27%	0.002	0.7180	9.64%	0.002	1.0506	-25.06%	0.002	1.0506	-25.06%
Q=29.6 l/s	20.5	0.0296	2.003E-03	0.8601	0.9483	-9.30%	0.002	0.7155	20.20%	0.002	1.0469	-17.85%	0.002	1.0469	-17.85%
Q=29.6 l/s	22	0.0298	2.003E-03	0.7320	1.0114	-27.63%	0.002	0.7632	-4.09%	0.001	0.6580	11.25%	0.001	0.6527	12.14%
Q=29.6 l/s	23.5	0.0296	2.003E-03	0.7640	1.0198	-25.09%	0.002	0.7695	-0.72%	0.001	0.6634	15.16%	0.001	0.6581	16.09%
Q=29.6 l/s	25	0.0296	2.003E-03	0.8431	1.0011	-15.78%	0.002	0.7553	11.62%	0.001	0.6512	29.46%	0.002	1.0063	-16.22%
Q=29.6 l/s	26	0.0295	2.003E-03	0.7991	1.0031	-20.34%	0.002	0.7569	5.58%	0.001	0.6525	22.46%	0.002	1.0083	-20.75%
			Average	*0.7976*	*0.9892*	*-19.23%*	*0.0015*	*0.7464*	*7.04%*	*0.0016*	*0.7871*	*5.90%*	*0.0018*	*0.9038*	*-8.61%*

Tables 8.6c-Boundary shear stress results compared to theoretical values for Q=29.6ℓ/s

							6m Transition			2-leg approach			3-leg approach		
Experiment	**Section**	**Discharge**	**S_o**	**τ_b**	**$\rho g R S_o$**	**%error**	**$(S_o-(\Delta H/\Delta x))$**	**$\rho g R(S_o-(\Delta H/\Delta x))$**	**%error**	**$(S_o-(\Delta H/\Delta x))$**	**$\rho g R(S_o-(\Delta H/\Delta x))$**	**%error**	**$(S_o-(\Delta H/\Delta x))$**	**$\rho g R(S_o-(\Delta H/\Delta x))$**	**%error**
	m	***m^3/s***		***N/m^2***				***N/m^2***			***N/m^2***			***N/m^2***	
Q=43.4 l/s	19	0.0434	2.003E-03	1.0001	1.2114	-17.44%	0.001	0.7855	27.32%	0.002	1.2580	-20.50%	0.002	1.2580	-20.50%
Q=43.4 l/s	20.5	0.0434	2.003E-03	1.0890	1.2016	-9.38%	0.001	0.7792	39.75%	0.002	1.2479	-12.74%	0.002	1.2479	-12.74%
Q=43.4 l/s	22	0.0434	2.003E-03	1.0548	1.1936	-11.63%	0.001	0.7740	36.28%	0.001	0.7280	44.88%	0.001	0.7951	32.67%
Q=43.4 l/s	23.5	0.0434	2.003E-03	0.9252	1.2554	-26.30%	0.001	0.8141	13.65%	0.001	0.7657	20.82%	0.001	0.8363	10.64%
Q=43.4 l/s	25	0.0434	2.003E-03	1.0089	1.2320	-18.11%	0.001	0.7989	26.29%	0.001	0.7515	34.25%	0.002	1.1628	-13.24%
Q=43.4 l/s	26	0.0434	2.003E-03	0.9231	1.2646	-27.01%	0.001	0.8200	12.57%	0.001	0.7714	19.67%	0.002	1.1936	-22.66%
			Average	*1.0002*	*1.2264*	*-18.31%*	*0.0013*	*0.7953*	*25.98%*	*0.0015*	*0.9204*	*14.40%*	*0.0018*	*1.0823*	*-4.31%*

Tables 8.6d-Boundary shear stress results compared to theoretical values for Q=43.4ℓ/s

				Experimental shear force on each element							Total	Percentage experimental shear force on each element						
Experiment	**Section**	**Discharge**	**Dr**	**SF_1**	**SF_2**	**SF_3**	**SF_4**	**SF_5**	**SF_6**	**SF_7**	**SF_T**	**SF_1**	**SF_2**	**SF_3**	**SF_4**	**SF_5**	**SF_6**	**SF_7**
	m	***m^3/s***		***N***	***N***	***N***	***N***	***N***	***N***	***N***	***N***							
Q=16.2ℓ/s	19	0.0162	0.211	0.0000	0.0000	0.0411	0.2881	0.0247	0.0628	0.0012	0.4179	0.00%	0.00%	9.84%	68.93%	5.91%	15.02%	0.29%
Q=16.2ℓ/s	20.5	0.0162	0.187	0.0031	0.0600	0.0348	0.2990	0.0266	0.0554	0.0020	0.4808	0.65%	12.47%	7.25%	62.18%	5.53%	11.51%	0.41%
Q=16.2ℓ/s	22	0.0162	0.205	0.0031	0.1148	0.0365	0.2890	0.0246	0.0366	0.0021	0.5065	0.61%	22.67%	7.20%	57.05%	4.85%	7.22%	0.41%
Q=16.2ℓ/s	23.5	0.0162	0.242	0.0015	0.1236	0.0357	0.2633	0.0175	0.0042	0.0004	0.4462	0.33%	27.70%	8.00%	59.01%	3.92%	0.94%	0.10%
Q=16.2ℓ/s	25	0.0162	0.245	0.0011	0.1502	0.0361	0.2454	0.0216	0.0000	0.0000	0.4545	0.24%	33.05%	7.95%	54.00%	4.75%	0.00%	0.00%
Q=16.2ℓ/s	26	0.0162	0.256	0.0008	0.1269	0.0315	0.2344	0.0182	0.0000	0.0000	0.4118	0.20%	30.81%	7.65%	56.93%	4.42%	0.00%	0.00%

Tables 8.7a-Shear force on each element and percentage shear forces for Q=16.2ℓ/s

				Experimental shear force on each element							Total	Percentage experimental shear force on each element						
Experiment	**Section**	**Discharge**	**Dr**	**SF_1**	**SF_2**	**SF_3**	**SF_4**	**SF_5**	**SF_6**	**SF_7**	**SF_T**	**SF_1**	**SF_2**	**SF_3**	**SF_4**	**SF_5**	**SF_6**	**SF_7**
	m	***m^3/s***		***N***	***N***	***N***	***N***	***N***	***N***	***N***	***N***							
Q=21.4ℓ/s	19	0.0214	0.303	0.0000	0.0000	0.0649	0.3535	0.0336	0.2295	0.0069	0.6883	0.00%	0.00%	9.42%	51.35%	4.88%	33.34%	1.01%
Q=21.4ℓ/s	20.5	0.0214	0.288	0.0107	0.0858	0.0331	0.3136	0.0266	0.0923	0.0063	0.5682	1.89%	12.46%	4.80%	45.56%	3.86%	13.40%	0.91%
Q=21.4ℓ/s	22	0.0214	0.325	0.0061	0.1400	0.0380	0.2952	0.0234	0.0428	0.0042	0.5497	1.11%	20.33%	5.52%	42.89%	3.41%	6.22%	0.61%
Q=21.4ℓ/s	23.5	0.0214	0.340	0.0110	0.2321	0.0457	0.3177	0.0243	0.0235	0.0054	0.6597	1.67%	33.72%	6.64%	46.16%	3.53%	3.41%	0.79%
Q=21.4ℓ/s	25	0.0214	0.339	0.0044	0.2455	0.0386	0.2557	0.0214	0.0000	0.0000	0.5656	0.77%	35.67%	5.61%	37.15%	3.11%	0.00%	0.00%
Q=21.4ℓ/s	26	0.0214	0.346	0.0043	0.2260	0.0325	0.2391	0.0210	0.0000	0.0000	0.5229	0.82%	32.83%	4.72%	34.74%	3.05%	0.00%	0.00%

Tables 8.7b-Shear force on each element and percentage shear forces for Q=21.4ℓ/s

				Experimental shear force on each element							Total	Percentage experimental shear force on each element						
Experiment	**Section**	**Discharge**	**Dr**	**SF_1**	**SF_2**	**SF_3**	**SF_4**	**SF_5**	**SF_6**	**SF_7**	**SF_T**	**SF_1**	**SF_2**	**SF_3**	**SF_4**	**SF_5**	**SF_6**	**SF_7**
	m	***m^3/s***		***N***	***N***	***N***	***N***	***N***	***N***	***N***	***N***							
Q=29.6ℓ/s	19	0.0296	0.401	0.0000	0.0000	0.0680	0.3767	0.0403	0.2552	0.0135	0.7537	0.00%	0.00%	9.02%	49.99%	5.34%	33.86%	1.79%
Q=29.6ℓ/s	20.5	0.0296	0.395	0.0239	0.0913	0.0455	0.4113	0.0422	0.1930	0.0160	0.8233	2.90%	12.11%	6.03%	54.57%	5.60%	25.61%	2.12%
Q=29.6ℓ/s	22	0.0298	0.428	0.0186	0.1755	0.0378	0.3548	0.0287	0.0835	0.0084	0.7074	2.63%	23.28%	5.02%	47.08%	3.81%	11.08%	1.11%
Q=29.6ℓ/s	23.5	0.0296	0.432	0.0184	0.2651	0.0469	0.3304	0.0235	0.0458	0.0114	0.7415	2.49%	35.17%	6.22%	43.83%	3.12%	6.08%	1.52%
Q=29.6ℓ/s	25	0.0296	0.422	0.0139	0.3784	0.0494	0.3341	0.0353	0.0000	0.0000	0.8111	1.72%	50.20%	6.56%	44.32%	4.68%	0.00%	0.00%
Q=29.6ℓ/s	26	0.0295	0.429	0.0122	0.3142	0.0490	0.3596	0.0422	0.0000	0.0000	0.7772	1.57%	41.69%	6.50%	47.71%	5.60%	0.00%	0.00%

Tables 8.7c-Shear force on each element and percentage shear forces for Q=29.6ℓ/s

				Experimental shear force on each element							Total	Percentage experimental shear force on each element						
Experiment	**Section**	**Discharge**	**Dr**	**SF_1**	**SF_2**	**SF_3**	**SF_4**	**SF_5**	**SF_6**	**SF_7**	**SF_T**	**SF_1**	**SF_2**	**SF_3**	**SF_4**	**SF_5**	**SF_6**	**SF_7**
	m	***m^3/s***		***N***	***N***	***N***	***N***	***N***	***N***	***N***	***N***							
Q=43.4ℓ/s	19	0.0434	0.512	0.0000	0.0000	0.0883	0.4359	0.0520	0.3828	0.0341	0.9930	0.00%	0.00%	8.89%	43.90%	5.23%	38.55%	3.44%
Q=43.4ℓ/s	20.5	0.0434	0.506	0.0467	0.1045	0.0458	0.4973	0.0534	0.2923	0.0424	1.0824	4.70%	10.53%	4.61%	50.08%	5.38%	29.44%	4.27%
Q=43.4ℓ/s	22	0.0434	0.501	0.0529	0.2214	0.0492	0.4679	0.0460	0.1733	0.0389	1.0495	5.33%	22.30%	4.95%	47.11%	4.63%	17.45%	3.92%
Q=43.4ℓ/s	23.5	0.0434	0.527	0.0401	0.3147	0.0498	0.4008	0.0378	0.0605	0.0266	0.9304	4.04%	31.69%	5.02%	40.36%	3.81%	6.09%	2.68%
Q=43.4ℓ/s	25	0.0434	0.519	0.0333	0.4431	0.0590	0.4005	0.0690	0.0000	0.0000	1.0049	3.35%	44.62%	5.95%	40.33%	6.95%	0.00%	0.00%
Q=43.4ℓ/s	26	0.0434	0.532	0.0314	0.4290	0.0515	0.3678	0.0538	0.0000	0.0000	0.9335	3.16%	43.20%	5.19%	37.04%	5.42%	0.00%	0.00%

Tables 8.7d-Shear force on each element and percentage shear forces for Q=43.4ℓ/s

SF_1 Shear force on left floodplain wall

SF_2 Shear force on left floodplain bed

SF_3 Shear force on main channel left wall

SF_4 Shear force on main channel bed

SF_5 Shear force on main channel right wall

SF_6 Shear force on right floodplain bed

SF_7 Shear force on right floodplain wall

		Left floodplain wall, SF_1				
Experiment	**Dr**	**a**	**b**	**c**	**d**	**R^2**
Q=16.2 l/s	0.205	0.00022	-0.01497	0.33976	-2.55034	0.9999
Q=21.4 l/s	0.313	0.00030	-0.02089	0.48780	-3.75745	0.7081
Q=29.6 l/s	0.415	0.00063	-0.04389	1.01315	-7.72802	0.957
Q=43.4 l/s	0.514	0.00115	-0.08023	1.84891	-14.08481	0.9999

		Left floodplain bed SF_2				
Experiment	**Dr**	**a**	**b**	**c**	**d**	**R^2**
Q=16.2 l/s	0.205	0.00064	-0.04847	1.25128	-10.67389	0.9985
Q=21.4 l/s	0.313	-0.00169	0.10678	-2.16604	14.22112	0.9882
Q=29.6 l/s	0.415	0.00101	-0.06438	1.44512	-11.12378	1
Q=43.4 l/s	0.514	0.00057	-0.03664	0.85846	-6.97213	0.9989

		Main channel left wall, SF_3				
Experiment	**Dr**	**a**	**b**	**c**	**d**	**R^2**
Q=16.2 l/s	0.205	-0.00084	0.05709	-1.29322	9.79600	1
Q=21.4 l/s	0.313	-0.00185	0.12429	-2.77716	20.65742	0.9939
Q=29.6 l/s	0.415	-0.00070	0.04895	-1.13665	8.81007	0.9832
Q=43.4 l/s	0.514	-0.00093	0.06454	-1.48717	11.41875	0.9574

		Main channel bed, SF_4				
Experiment	**Dr**	**a**	**b**	**c**	**d**	**R^2**
Q=16.2 l/s	0.205	-0.00212	0.14350	-3.23665	24.94927	0.9582
Q=21.4 l/s	0.313	-0.00380	0.25070	-5.50141	40.61124	0.9413
Q=29.6 l/s	0.415	0.00391	-0.25903	5.68152	-40.72693	0.9487
Q=43.4 l/s	0.514	0.00392	-0.26369	5.87329	-42.83052	0.9948

Table 8.8-Constants for percentage shear force on any channel element (Equation 8.32)

		Right main channel wall, SF_5				
Experiment	**Dr**	**a**	**b**	**c**	**d**	**R^2**
Q=16.2 l/s	0.205	0.00051	-0.03282	0.70037	-4.88225	0.9777
Q=21.4 l/s	0.313	-0.00028	0.01874	-0.42515	3.25068	0.9898
Q=29.6 l/s	0.415	0.00106	-0.06898	1.48088	-10.47343	0.9866
Q=43.4 l/s	0.514	0.00120	-0.07726	1.65048	-11.64040	0.9725

		Right floodplain bed SF_6				
Experiment	**Dr**	**a**	**b**	**c**	**d**	**R^2**
Q=16.2 l/s	0.205	0.00151	-0.09880	2.11297	-14.70161	0.9939
Q=21.4 l/s	0.313	-0.00329	0.22933	-5.33254	41.46142	0.9998
Q=29.6 l/s	0.415	0.00128	-0.08034	1.60261	-9.91141	0.9874
Q=43.4 l/s	0.514	0.00201	-0.13050	2.74215	-18.38731	1

		Right floodplain wall, SF_7				
Experiment	**Dr**	**a**	**b**	**c**	**d**	**R^2**
Q=16.2 l/s	0.205	8.0E-05	-5.5E-03	1.3E-01	-9.4E-01	0.9452
Q=21.4 l/s	0.313	-1.9E-04	1.2E-02	-2.6E-01	1.9E+00	0.8972
Q=29.6 l/s	0.415	-1.4E-04	8.7E-03	-1.8E-01	1.2E+00	0.8025
Q=43.4 l/s	0.514	-6.0E-05	1.5E-03	1.7E-02	-4.1E-01	0.9991

Table 8.8 (Cont.)-Constants for percentage shear force on any channel element (Equation 8.32)

Dr	Chainage, m	z_e, m	H, m	α	U, m/s	H_e, m	h_e, m	S_e
0.234	19	0.072	0.063	1.349	0.530	0.154		
0.234	20.5	0.070	0.062	1.173	0.547	0.150	0.004	2.72E-03
0.234	22	0.067	0.064	1.218	0.524	0.148	0.002	1.31E-03
0.234	23.5	0.064	0.067	1.194	0.493	0.146	0.003	1.87E-03
0.234	25	0.061	0.067	1.173	0.496	0.143	0.002	1.46E-03
						Total	**0.011**	

K_1	K_2	K_{12}
0.771	0.878	6.274429

S_e	0.001838

Dr	Chainage, m	z_e, m	H, m	α	U, m/s	H_e, m	h_e, m	S_e
0.314	19	0.072	0.071	1.169	0.579	0.163		
0.314	20.5	0.070	0.071	1.131	0.588	0.161	0.002	1.45E-03
0.314	22	0.067	0.074	1.174	0.545	0.158	0.003	1.76E-03
0.314	23.5	0.064	0.076	1.192	0.527	0.157	0.002	1.04E-03
0.314	25	0.061	0.076	1.153	0.532	0.154	0.003	2.00E-03
						Total	**0.009**	

K_1	K_2	K_{12}
0.548	0.649	3.488584

S_e	0.001562

Dr	Chainage, m	z_e, m	H, m	α	U, m/s	H_e, m	h_e, m	S_e
0.414	19	0.072	0.084	1.132	0.640	0.180		
0.414	20.5	0.070	0.083	1.095	0.640	0.176	0.004	2.48E-03
0.414	22	0.067	0.086	1.105	0.599	0.173	0.003	2.03E-03
0.414	23.5	0.064	0.088	1.112	0.587	0.171	0.002	1.14E-03
0.414	25	0.061	0.087	1.107	0.603	0.169	0.002	1.60E-03
						Total	**0.011**	

K_1	K_2	K_{12}
0.521	0.587	4.599627

S_e	0.001812

Dr	Chainage, m	z_e, m	H, m	α	U, m/s	H_e, m	h_e, m	S_e
0.518	19	0.072	0.102	1.098	0.709	0.202		
0.518	20.5	0.070	0.102	1.057	0.714	0.200	0.002	1.40E-03
0.518	22	0.067	0.104	1.038	0.718	0.198	0.001	8.28E-04
0.518	23.5	0.064	0.105	1.093	0.675	0.195	0.003	2.22E-03
0.518	25	0.061	0.106	1.092	0.693	0.194	0.001	7.67E-04
						Total	**0.008**	

K_1	K_2	K_{12}
0.306	0.320	6.962922

S_e	0.001306

Table 8.9-Energy balance, calculation of head losses, energy slope and head loss correction coefficients

			Average flow depth from all water surface data							
	Elevation		Main channel	Floodplain	Main channel	Floodplain	Main channel	Floodplain	Main channel	Floodplain
Chainage	Main Channel	Floodplains	*Dr=0.234*	*Dr=0.234*	*Dr=0.314*	*Dr=0.314*	*Dr=0.414*	*Dr=0.414*	*Dr=0.518*	*Dr=0.518*
m	*mm*	*mm*	*mm*	*mm*	*mm*	*mm*	*mm*	*mm*	*mm*	*mm*
19	72.048	121.967	63.133	13.214	71.108	21.189	84.183	34.264	101.558	51.639
19.5	71.500		63.050		71.800		82.100		99.850	
20	71.011		62.956		70.522		83.389		100.522	
20.5	70.461	118.879	62.033	13.615	70.633	22.215	82.833	34.415	101.700	53.282
21	69.756		63.378		70.911		83.178		99.844	
21.5	68.600		63.450		72.750		85.000		104.500	
22	67.005	115.298	64.375	16.082	73.550	25.257	85.900	37.607	104.100	55.807
22.5	66.350		64.850		74.350		86.400		105.550	
23	64.633		66.800		75.367		87.600		106.533	
23.5	64.300	113.286	66.567	17.581	75.600	26.614	87.567	38.581	105.367	56.381
24	65.389		64.744		72.111		83.378		102.878	
24.5	64.650		64.800		73.200		83.450		104.100	
25	61.371	111.000	67.358	17.730	75.783	26.155	87.133	37.505	105.783	56.155

Table 8.10-Average flow depths as used in force-momentum balance

Dr=0.205	Average Depth, m			Boundary			
	Main channel	Floodplain	Centroid, m	τ_b, N/m^2	SF, N	A, m^2	P, m
Section 1	0.063	0.013	0.027	0.457	0.418	0.030	0.914
Section 2	0.062	0.014	0.027	0.526	0.481	0.030	0.916
Section 3	0.064	0.016	0.027	0.551	0.507	0.032	0.922
Section 4	0.067	0.018	0.028	0.482	0.446	0.033	0.928
Section 5	0.067	0.018	0.029	0.494	0.454	0.034	0.925

Dr=0.313	Average Depth, m			Boundary			
	Main channel	Floodplain	Centroid, m	τ_b, N/m^2	SF, N	A, m^2	P, m
Section 1	0.071	0.021	0.030	0.739	0.688	0.037	0.930
Section 2	0.071	0.022	0.030	0.609	0.568	0.037	0.933
Section 3	0.074	0.025	0.031	0.585	0.550	0.039	0.941
Section 4	0.076	0.027	0.031	0.697	0.660	0.041	0.946
Section 5	0.076	0.026	0.032	0.602	0.566	0.040	0.942

Dr=0.415	Average Depth, m			Boundary			
	Main channel	Floodplain	Centroid, m	τ_b, N/m^2	SF, N	A, m^2	P, m
Section 1	0.084	0.034	0.035	0.787	0.754	0.047	0.956
Section 2	0.083	0.034	0.034	0.860	0.823	0.046	0.958
Section 3	0.086	0.038	0.036	0.732	0.707	0.049	0.965
Section 4	0.088	0.039	0.036	0.764	0.742	0.050	0.970
Section 5	0.087	0.038	0.036	0.843	0.811	0.049	0.965

Dr=0.514	Average Depth, m			Boundary			
	Main channel	Floodplain	Centroid, m	τ_b, N/m^2	SF, N	A, m^2	P, m
Section 1	0.102	0.052	0.042	1.000	0.993	0.061	0.991
Section 2	0.102	0.053	0.043	1.089	1.082	0.061	0.996
Section 3	0.104	0.056	0.044	1.055	1.050	0.063	1.002
Section 4	0.105	0.056	0.044	0.925	0.930	0.064	1.006
Section 5	0.106	0.056	0.044	1.009	1.005	0.064	1.002

Table 8.11a-Data for force-momentum balance for whole channel using smoothed data where applicable

Force-Momentum Balance, where $U = Q/A$

Average Measured Discharge	Relative depth	F_1	F_2	F_1-F_2	$\rho g(\Delta H)A$	ΣSF	W	F_1-F_2-ΣSF+W	$\rho Q(\beta_2 U_2-\beta_1 U_1)-\rho Q_{cf} U_i L$	Residual	Magnitude of terms	%Error
m^3/s		*N*	*N*	*N*	*N*	*N*	*N*	*N*	*N*	*N*	*N*	*%*
0.0162	0.205	8.1126	9.4589	-1.3463	-1.3267	2.7672	3.7739	-0.3396	-2.0645	1.7249	26.1770	6.59%
0.0214	0.313	10.7267	12.5231	-1.7965	-1.7647	3.6378	4.5364	-0.8979	-1.3246	0.4268	32.7486	1.30%
0.0296	0.415	16.0758	17.5207	-1.4448	-1.3923	4.6043	5.6720	-0.3772	-1.1522	0.7750	45.0249	1.72%
0.0434	0.514	25.2285	27.8998	-2.6714	-2.5829	6.0724	7.3471	-1.3967	-1.8562	0.4595	68.4040	0.67%
									Average	0.8465		

Table 8.11b-Force-momentum balance for whole channel (x=19m-x=25m)

Dr=0.205

Average Measured Discharge	Section, m	F_1	F_2	F_1-F_2	ρg(ΔH)A	ΣSF	W	F_1-F_2-ΣSF+W	$\rho Q(\beta_2 U_2-\beta_1 U_1)-\rho Q_{cf} U_i L$	Residual	Magnitude of terms	%Error
m^3/s		N	N	N	N	N	N	N	N	N	N	%
0.0162	19-20.5	8.1126	7.8654	0.2472	0.3252	0.6741	0.8883	0.4614	-0.9811	1.4425	18.5215	7.79%
0.0162	20.5-22	7.8654	8.5848	-0.7194	-0.7112	0.7405	0.9125	-0.5474	-0.4822	-0.0652	18.5854	-0.35%
0.0162	22-23.5	8.5848	9.2464	-0.6616	-0.7024	0.7146	0.9630	-0.4132	-0.4194	0.0062	19.9281	0.03%
0.0162	23.5-25	9.2464	9.4589	-0.2125	-0.2609	0.6755	0.9900	0.1020	-0.1818	0.2838	20.5526	1.38%
Total for x=19m-25m		***33.809***	***35.155***	***-1.346***	***-1.349***	***2.805***	***3.754***	***-0.397***	***-2.064***	***1.667***	***77.588***	***2.15%***

Table 8.12a-Force-momentum balance for whole channel for each measuring section for Q=16.2ℓ/s

Dr=0.313

Average Measured Discharge	Section, m	F_1	F_2	F_1-F_2	ρg(ΔH)A	ΣSF	W	F_1-F_2-ΣSF+W	$\rho Q(\beta_2 U_2-\beta_1 U_1)-\rho Q_{cf} U_i L$	Residual	Magnitude of terms	%Error
m^3/s		N	N	N	N	N	N	N	N	N	N	%
0.0214	19-20.5	10.7267	10.6828	0.0438	0.1709	0.9424	1.0808	0.1823	-0.2411	0.4233	23.6738	1.79%
0.0214	20.5-22	10.6828	11.7835	-1.1007	-1.0865	0.8384	1.1193	-0.8198	-0.6299	-0.1900	25.0539	-0.76%
0.0214	22-23.5	11.7835	12.5260	-0.7425	-0.8019	0.9070	1.1753	-0.4742	0.0921	-0.5663	26.4839	-2.14%
0.0214	23.5-25	12.5260	12.5231	0.0029	-0.0728	0.9190	1.1936	0.2774	-0.5457	0.8232	27.7074	2.97%
Total for x=19m-25m		***45.719***	***47.515***	***-1.796***	***-1.790***	***3.607***	***4.569***	***-0.834***	***-1.325***	***0.490***	***102.919***	***0.48%***

Table 8.12b-Force-momentum balance for whole channel for each measuring section for Q=21.6ℓ/s

Dr=0.415

Average Measured Discharge	Section, m	F_1	F_2	F_1-F_2	ρg(ΔH)A	ΣSF	W	F_1-F_2-ΣSF+W	ρQ(β_2U_2-β_1U_1)-ρ$Q_{cf}U_jL$	Residual	Magnitude of terms	%Error
m^3/s		*N*	*N*	*N*	*N*	*N*	*N*	*N*	*N*	*N*	*N*	*%*
0.0296	19-20.5	16.0758	15.6614	0.4144	0.6176	1.1827	1.3744	0.6061	-0.0892	0.6953	34.3836	2.02%
0.0296	20.5-22	15.6614	17.1189	-1.4575	-1.4339	1.1480	1.4048	-1.2007	-1.0055	-0.1951	36.3387	-0.54%
0.0296	22-23.5	17.1189	17.8477	-0.7288	-0.8092	1.0867	1.4588	-0.3566	0.3643	-0.7209	37.8764	-1.90%
0.0296	23.5-25	17.8477	17.5207	0.3270	0.2114	1.1644	1.4655	0.6281	-0.4217	1.0497	38.4199	2.73%
Total for x=19m-25m		***66.704***	***68.149***	***-1.445***	***-1.414***	***4.582***	***5.704***	***-0.323***	***-1.152***	***0.829***	***147.019***	***0.56%***

Table 8.12c-Force-momentum balance for whole channel for each measuring section for Q=29.6ℓ/s

Dr=0.514

Average Measured Discharge	Section, m	F_1	F_2	F_1-F_2	ρg(ΔH)A	ΣSF	W	F_1-F_2-ΣSF+W	ρQ(β_2U_2-β_1U_1)-ρ$Q_{cf}U_jL$	Residual	Magnitude of terms	%Error
m^3/s		*N*	*N*	*N*	*N*	*N*	*N*	*N*	*N*	*N*	*N*	*%*
0.0434	19-20.5	25.2285	25.6282	-0.3997	-0.0847	1.5566	1.7954	-0.1609	-0.9160	0.7552	55.1247	1.37%
0.0434	20.5-22	25.6282	27.1355	-1.5073	-1.4666	1.5990	1.8359	-1.2703	-1.2878	0.0174	57.4863	0.03%
0.0434	22-23.5	27.1355	27.8238	-0.6883	-0.7920	1.4849	1.8786	-0.2947	1.0996	-1.3943	59.4225	-2.35%
0.0434	23.5-25	27.8238	27.8998	-0.0760	-0.2622	1.4515	1.8905	0.3630	-0.7521	1.1150	59.8177	1.86%
Total for x=19m-25m		***105.816***	***108.487***	***-2.671***	***-2.605***	***6.092***	***7.400***	***-1.363***	***-1.856***	***0.493***	***231.851***	***0.21%***

Table 8.12d-Force-momentum balance for whole channel for each measuring section for Q=43.4ℓ/s

Dr=0.205		Bed widths, m			Average Depth, m		Centroid, m		
		Left floodplain	Main channel	Right floodplain	Main channel	Floodplain	Left floodplain	Main channel	Right floodplain
Section 1	1	0	0.398	0.39	0.063	0.013	0.0000	0.0316	0.0066
Section 2	2	0.1	0.398	0.291	0.062	0.014	0.0068	0.0310	0.0068
Section 3	3	0.2	0.398	0.192	0.064	0.016	0.0080	0.0322	0.0080
Section 4	4	0.298	0.398	0.097	0.067	0.018	0.0088	0.0333	0.0088
Section 5	5	0.392	0.398	0	0.067	0.018	0.0089	0.0337	0.0000

		Perimeter, m			Area, m^2			Interface velocity, m/s	
		Left floodplain	Main channel	Right floodplain	Left floodplain	Main channel	Right floodplain	Left	Right
Section 1	1	0.000	0.511	0.403	0.0000	0.0251	0.0052	0.000	0.291
Section 2	2	0.114	0.498	0.305	0.0014	0.0247	0.0040	0.428	0.289
Section 3	3	0.216	0.498	0.208	0.0032	0.0256	0.0031	0.475	0.248
Section 4	4	0.316	0.498	0.115	0.0052	0.0265	0.0017	0.477	0.224
Section 5	5	0.410	0.466	0.000	0.0070	0.0268	0.0000	0.489	0.000

Left floodplain

Average Measured Discharge	Section, m	F_{1L}	F_{2L}	$F_{1L}-F_{2L}$	$\rho g(\Delta H)A$	R_{FL}	ΣSF_L	W_L	$F_{1L}-F_{2L}-\Sigma SF_L+W_L$	$\rho(Q_{2L}\beta_{2L}U_{2L}-Q_{1L}\beta_{1L}U_{1L})$	$\rho Q_{cfL}U_{iL}L$	$\rho(Q_{2L}\beta_{2L}U_{2L}-Q_{1L}\beta_{1L}U_{1L})-\rho Q_{cfL}U_{iL}L$	ASF_{iL}	Magnitude of terms	$\%ASF_{iL}$
m^3/s		N	N	N	N	N	N	N	N	N	N	N	N	N	%
0.0162	19-20.5	0.0000	0.0909	-0.0909	0.3252	1.3236	0.0480	0.0201	-0.1188	0.1872	0.1076	0.0796	-0.3060	1.5622	
0.0162	20.5-22	0.0909	0.2536	-0.1627	-0.7112	1.6217	0.1245	0.0674	-0.2198	0.1674	0.2255	-0.0581	-0.3872	2.2163	
0.0162	22-23.5	0.2536	0.4516	-0.1980	-0.7024	2.0837	0.1665	0.1246	-0.2399	0.1160	0.2378	-0.1218	-0.3559	3.2019	
0.0162	23.5-25	0.4516	0.6042	-0.1526	-0.2609	2.2927	0.2115	0.1796	-0.1845	0.1116	0.2413	-0.1298	-0.2961	3.8694	
Total for x=19m-25m		***0.796***	***1.400***	***-0.604***	***-1.349***	***7.322***	***0.551***	***0.392***	***-0.763***	***0.582***	***0.812***	***-0.230***	***-1.345***	***10.850***	

Right floodplain

Average Measured Discharge	Section, m	F_{1R}	F_{2R}	$F_{1R}-F_{2R}$	$\rho g(\Delta H)A$	R_{FL}	ΣSF_R	W_R	$F_{1R}-F_{2R}-\Sigma SF_R+W_R$	$\rho(Q_{2R}\beta_{2R}U_{2R}-Q_{1R}\beta_{1R}U_{1R})$	$\rho Q_{cfR}U_{iR}L$	$\rho(Q_{2R}\beta_{2R}U_{2R}-Q_{1R}\beta_{1R}U_{1R})-\rho Q_{cfR}U_{iR}L$	ASF_{iR}	Magnitude of terms	$\%ASF_{iR}$
m^3/s		N	N	N	N	N	N	N	N	N	N	N	N	N	%
0.0162	19-20.5	0.3339	0.2645	0.0694	-0.0179	1.3236	0.1005	0.1343	0.1032	-0.0805	-0.0909	0.0104	0.1837	2.1672	
0.0162	20.5-22	0.2645	0.2435	0.0210	-0.0853	1.6217	0.0630	0.1039	0.0619	-0.0861	-0.0841	-0.0020	0.1480	2.2985	
0.0162	22-23.5	0.2435	0.1470	0.0965	-0.0352	2.0837	0.0315	0.0706	0.1356	-0.0790	-0.0739	-0.0051	0.2146	2.5814	
0.0162	23.5-25	0.1470	0.0000	0.1470	-0.0012	2.2927	0.0000	0.0251	0.1721	-0.9192	-0.0338	-0.8854	1.0913	3.3502	
Total for x=19m-25m		***0.989***	***0.655***	***0.334***	***-0.140***	***7.322***	***0.195***	***0.334***	***0.473***	***-1.165***	***-0.283***	***-0.882***	***1.638***	***10.397***	

Main channel

Average Measured Discharge	Section, m	F_{1MC}	F_{2MC}	$F_{1MC}-F_{2MC}$	$\rho g(\Delta H)A$	R_{FMC}	ΣSF_{MC}	W_{MC}	$F_{1MC}-F_{2MC}-\Sigma SF_{MC}+W_{MC}$	$\rho(Q_{2MC}\beta_{2MC}U_{2MC}-Q_{1MC}\beta_{1MC}U_{1MC})$	$\rho(Q_{2MC}\beta_{2MC}U_{2MC}-Q_{1MC}\beta_{1MC}U_{1MC})+\rho Q_{cfL}U_{iL}L+\rho Q_{cfR}U_{iR}L$	Residual	Magnitude of terms	%Error	ASF_H
m^3/s		N	N	N	N	N	N	N	N	N	N	N	N	%	N
0.0162	19-20.5	7.7787	7.5100	0.2687	0.2687	0.0000	0.5460	0.7339	0.4566	-0.1374	-0.1207	0.5773	16.6893	3.46%	0.0404
0.0162	20.5-22	7.5100	8.0877	-0.5777	-0.5777	0.0000	0.5235	0.7412	-0.3600	-0.5407	-0.3994	0.0394	17.2617	0.23%	0.0629
0.0162	22-23.5	8.0877	8.6477	-0.5601	-0.5601	0.0000	0.4875	0.7678	-0.2798	-0.6056	-0.4417	0.1619	18.4324	0.88%	0.0989
0.0162	23.5-25	8.6477	8.8547	-0.2069	-0.2069	0.0000	0.4440	0.7853	0.1344	-0.5390	-0.3315	0.4659	19.0632	2.44%	0.1424
Total for x=19m-25m		***32.024***	***33.100***	***-1.076***	***-1.076***	***0.000***	***2.001***	***3.028***	***-0.049***	***-1.823***	***-1.293***	***1.244***	***71.447***	***1.74%***	

Table 8.13-Force-momentum balance for each zone of the transition (floodplains and main channel) for Dr=0.205, Q=16.2//s

Dr=0.313		Bed widths, m			Average Depth, m		Centroid, m		
		Left floodplain	Main channel	Right floodplain	Main channel	Floodplain	Left floodplain	Main channel	Right floodplain
Section 1	1	0	0.398	0.39	0.071	0.021	0.0000	0.0356	0.0106
Section 2	2	0.1	0.398	0.291	0.071	0.022	0.0111	0.0353	0.0111
Section 3	3	0.2	0.398	0.192	0.074	0.025	0.0126	0.0368	0.0126
Section 4	4	0.298	0.398	0.097	0.076	0.027	0.0133	0.0378	0.0133
Section 5	5	0.392	0.398	0	0.076	0.026	0.0131	0.0379	0.0000

		Perimeter, m			Area, m^2			Interface velocity, m/s	
		Left floodplain	Main channel	Right floodplain	Left floodplain	Main channel	Right floodplain	Left	Right
Section 1	1	0.000	0.519	0.411	0.0000	0.0283	0.0083	0.000	0.434
Section 2	2	0.122	0.498	0.313	0.0022	0.0281	0.0065	0.595	0.388
Section 3	3	0.225	0.498	0.217	0.0051	0.0293	0.0048	0.581	0.325
Section 4	4	0.325	0.498	0.124	0.0079	0.0301	0.0026	0.600	0.316
Section 5	5	0.418	0.474	0.000	0.0103	0.0302	0.0000	0.562	0.000

Left floodplain

Average Measured Discharge	Section, m	F_{1L}	F_{2L}	F_{1L}-F_{2L}	$\rho g(\Delta H)A$	R_{FL}	ΣSF_L	W_L	F_{1L}-F_{2L}-ΣSF_L+W_L	$\rho(Q_{2L}\beta_{2L}U_{2L}$-$Q_{1L}\beta_{1L}U_{1L})$	$\rho Q_{cfL}U_{iL}L$	$\rho(Q_{2L}\beta_{2L}U_{2L}$-$Q_{1L}\beta_{1L}U_{1L})$-$\rho Q_{cfL}U_{iL}L$	ASF_{iL}	Magnitude of terms	$\%ASF_{iL}$
m^3/s		N	N	N	N	N	N	N	N	N	N	N	N	N	%
0.0214	19-20.5	0.0000	0.2420	-0.2420	0.3252	3.4642	0.0675	0.0327	-0.2768	0.6347	0.3520	0.2827	-0.9115	4.0892	
0.0214	20.5-22	0.2420	0.6256	-0.3836	-0.7112	4.1440	0.1950	0.1071	-0.4715	0.4445	0.6631	-0.2186	-0.9160	5.5323	
0.0214	22-23.5	0.6256	1.0350	-0.4094	-0.7024	4.9475	0.2910	0.1913	-0.5092	0.4472	0.6657	-0.2185	-0.9564	7.3089	
0.0214	23.5-25	1.0350	1.3149	-0.2799	-0.2609	5.1203	0.3690	0.2679	-0.3810	0.6396	0.6548	-0.0152	-1.0206	8.1223	
Total for x=19m-25m		***1.903***	***3.218***	***-1.315***	***-1.349***	***17.676***	***0.923***	***0.599***	***-1.638***	***2.166***	***2.336***	***-0.170***	***-3.804***	***25.053***	

Right floodplain

Average Measured Discharge	Section, m	F_{1R}	F_{2R}	F_{1R}-F_{2R}	$\rho g(\Delta H)A$	R_{FL}	ΣSF_R	W_R	F_{1R}-F_{2R}-ΣSF_R+W_R	$\rho(Q_{2R}\beta_{2R}U_{2R}$-$Q_{1R}\beta_{1R}U_{1R})$	$\rho Q_{cfR}U_{iR}L$	$\rho(Q_{2R}\beta_{2R}U_{2R}$-$Q_{1R}\beta_{1R}U_{1R})$-$\rho Q_{cfR}U_{iR}L$	ASF_{iR}	Magnitude of terms	$\%ASF_{iR}$
m^3/s		N	N	N	N	N	N	N	N	N	N	N	N	N	%
0.0214	19-20.5	0.8586	0.7042	0.1544	-0.0741	3.4642	0.2190	0.2170	0.1524	-0.0742	-0.1704	0.0962	0.2266	5.5593	
0.0214	20.5-22	0.7042	0.6006	0.1036	-0.1687	4.1440	0.0975	0.1667	0.1728	-0.6067	-0.1477	-0.4591	0.7796	6.1720	
0.0214	22-23.5	0.6006	0.3369	0.2637	-0.0495	4.9475	0.0533	0.1095	0.3199	-0.2601	-0.1328	-0.1273	0.5800	6.1750	
0.0214	23.5-25	0.3369	0.0000	0.3369	0.0058	5.1203	0.0345	0.0380	0.3404	-0.2009	-0.0631	-0.1378	0.5413	5.6675	
Total for x=19m-25m		***2.500***	***1.642***	***0.859***	***-0.286***	***17.676***	***0.404***	***0.531***	***0.986***	***-1.142***	***-0.514***	***-0.628***	***2.127***	***23.574***	

Main channel

Average Measured Discharge	Section, m	F_{1MC}	F_{2MC}	F_{1MC}-F_{2MC}	$\rho g(\Delta H)A$	R_{FMC}	ΣSF_{MC}	W_{MC}	F_{1MC}-F_{2MC}-ΣSF_{MC}+W_{MC}	$\rho(Q_{2MC}\beta_{2MC}U_{2MC}$-$Q_{1MC}\beta_{1MC}U_{1MC})$	$\rho(Q_{2MC}\beta_{2MC}U_{2MC}$-$Q_{1MC}\beta_{1MC}U_{1MC})$+$\rho Q_{cfL}U_{iL}L$+$\rho Q_{cfR}U_{iR}L$	Residual	Magnitude of terms	%Error	ASF_H
m^3/s		N	N	N	N	N	N	N	N	N	N	N	N	%	N
0.0214	19-20.5	9.8680	9.7366	0.1314	0.1314	0.0000	0.5865	0.8311	0.3760	-0.4783	-0.2966	0.6727	21.3189	3.16%	-0.0001
0.0214	20.5-22	9.7366	10.5573	-0.8207	-0.8207	0.0000	0.5340	0.8454	-0.5093	-0.7001	-0.1847	-0.3246	21.8581	-1.49%	0.0524
0.0214	22-23.5	10.5573	11.1541	-0.5967	-0.5967	0.0000	0.5640	0.8746	-0.2862	-0.6068	-0.0738	-0.2123	23.2238	-0.91%	0.0224
0.0214	23.5-25	11.1541	11.2082	-0.0542	-0.0542	0.0000	0.5370	0.8876	0.2965	-0.4865	0.1052	0.1913	23.8921	0.80%	0.0494
Total for x=19m-25m		***41.316***	***42.656***	***-1.340***	***-1.340***	***0.000***	***2.222***	***3.439***	***-0.123***	***-2.272***	***-0.450***	***0.327***	***90.293***	***0.36%***	

Table 8.14-Force-momentum balance for each zone of the transition (floodplains and main channel) for Dr=0.313, Q=21.4ℓ/s

Dr=0.415		Bed widths, m			Average Depth, m		Centroid, m		
		Left floodplain	Main channel	Right floodplain	Main channel	Floodplain	Left floodplain	Main channel	Right floodplain
Section 1	1	0	0.398	0.39	0.084	0.034	0.0000	0.0421	0.0171
Section 2	2	0.1	0.398	0.291	0.083	0.034	0.0172	0.0414	0.0172
Section 3	3	0.2	0.398	0.192	0.086	0.038	0.0188	0.0430	0.0188
Section 4	4	0.298	0.398	0.097	0.088	0.039	0.0193	0.0438	0.0193
Section 5	5	0.392	0.398	0	0.087	0.038	0.0188	0.0436	0.0000

		Perimeter, m			Area, m^2			Interface velocity, m/s	
		Left floodplain	Main channel	Right floodplain	Left floodplain	Main channel	Right floodplain	Left	Right
Section 1	1	0.000	0.532	0.424	0.0000	0.0335	0.0134	0.000	0.550
Section 2	2	0.134	0.498	0.325	0.0034	0.0330	0.0100	0.628	0.531
Section 3	3	0.238	0.498	0.230	0.0075	0.0342	0.0072	0.616	0.465
Section 4	4	0.337	0.498	0.136	0.0115	0.0349	0.0037	0.642	0.416
Section 5	5	0.430	0.486	0.000	0.0147	0.0347	0.0000	0.685	0.000

Left floodplain

Average Measured Discharge	Section, m	F_{1L}	F_{2L}	F_{1L}-F_{2L}	$\rho g(\Delta H)A$	R_{FL}	ΣSF_L	W_L	F_{1L}-F_{2L}-ΣSF_L+W_L	$\rho(Q_{2L}\beta_{2L}U_{2L}$-$Q_{1L}\beta_{1L}U_{1L})$	$\rho Q_{cfL}U_{iL}L$	$\rho(Q_{2L}\beta_{2L}U_{2L}$-$Q_{1L}\beta_{1L}U_{1L})$-$\rho Q_{cfL}U_{iL}L$	ASF_{iL}	Magnitude of terms	$\%ASF_{iL}$
m^3/s		N	N	N	N	N	N	N	N	N	N	N	N	N	%
0.0296	19-20.5	0.0000	0.5808	-0.5808	0.3252	8.6735	0.0855	0.0507	-0.6156	1.2038	0.6367	0.5670	-1.8193	9.9575	
0.0296	20.5-22	0.5808	1.3870	-0.8062	-0.7112	9.5383	0.2295	0.1615	-0.8742	1.1034	1.3133	-0.2099	-1.9776	12.1070	
0.0296	22-23.5	1.3870	2.1750	-0.7881	-0.7024	10.6735	0.3450	0.2802	-0.8529	1.1301	1.3285	-0.1984	-1.9830	15.0591	
0.0296	23.5-25	2.1750	2.7037	-0.5287	-0.2609	10.6449	0.5010	0.3860	-0.6437	1.5666	1.4011	0.1654	-2.2103	16.5761	
Total for x=19m-25m		***4.143***	***6.847***	***-2.704***	***-1.349***	***39.530***	***1.161***	***0.878***	***-2.986***	***5.004***	***4.680***	***0.324***	***-7.990***	***53.700***	

Right floodplain

Average Measured Discharge	Section, m	F_{1R}	F_{2R}	F_{1R}-F_{2R}	$\rho g(\Delta H)A$	R_{FL}	ΣSF_R	W_R	F_{1R}-F_{2R}-ΣSF_R+W_R	$\rho(Q_{2R}\beta_{2R}U_{2R}$-$Q_{1R}\beta_{1R}U_{1R})$	$\rho Q_{cfR}U_{iR}L$	$\rho(Q_{2R}\beta_{2R}U_{2R}$-$Q_{1R}\beta_{1R}U_{1R})$-$\rho Q_{cfR}U_{iR}L$	ASF_{iR}	Magnitude of terms	$\%ASF_{iR}$
m^3/s		N	N	N	N	N	N	N	N	N	N	N	N	N	%
0.0296	19-20.5	2.2452	1.6901	0.5551	-0.0173	8.6735	0.3510	0.3444	0.5486	-0.8682	-0.8553	-0.0129	1.4167	13.3170	
0.0296	20.5-22	1.6901	1.3315	0.3586	-0.2697	9.5383	0.2220	0.2539	0.3905	-0.9059	-0.7880	-0.1179	1.2964	13.1537	
0.0296	22-23.5	1.3315	0.7080	0.6235	-0.0524	10.6735	0.1215	0.1615	0.6635	-0.6832	-0.6972	0.0140	1.3468	13.0100	
0.0296	23.5-25	0.7080	0.0000	0.7080	0.0197	10.6449	0.0390	0.0551	0.7241	-0.6347	-0.3186	-0.3161	1.3588	11.7631	
Total for x=19m-25m		***5.975***	***3.730***	***2.245***	***-0.320***	***39.530***	***0.734***	***0.815***	***2.327***	***-3.092***	***-2.659***	***-0.433***	***5.419***	***51.244***	

Main channel

Average Measured Discharge	Section, m	F_{1MC}	F_{2MC}	F_{1MC}-F_{2MC}	$\rho g(\Delta H)A$	R_{FMC}	ΣSF_{MC}	W_{MC}	F_{1MC}-F_{2MC}-ΣSF_{MC}+W_{MC}	$\rho(Q_{2MC}\beta_{2MC}U_{2MC}$-$Q_{1MC}\beta_{1MC}U_{1MC})$	$\rho(Q_{2MC}\beta_{2MC}U_{2MC}$-$Q_{1MC}\beta_{1MC}U_{1MC})$ +$\rho Q_{cfL}U_{iL}L$+$\rho Q_{cfR}U_{iR}L$	Residual	Magnitude of terms	%Error	ASF_H
m^3/s		N	N	N	N	N	N	N	N	N	N	N	N	%	N
0.0296	19-20.5	13.8306	13.3906	0.4400	0.4400	0.0000	0.7440	0.9793	0.6753	-0.5705	-0.7891	1.4644	29.7336	4.93%	-0.1576
0.0296	20.5-22	13.3906	14.4004	-1.0098	-1.0098	0.0000	0.6990	0.9894	-0.7195	-1.1219	-0.5966	-0.1229	30.0760	-0.41%	-0.1126
0.0296	22-23.5	14.4004	14.9647	-0.5642	-0.5642	0.0000	0.6120	1.0171	-0.1591	-1.0449	-0.4136	0.2545	31.4078	0.81%	-0.0256
0.0296	23.5-25	14.9647	14.8169	0.1477	0.1477	0.0000	0.5940	1.0244	0.5781	-0.4456	0.6369	-0.0588	32.0369	-0.18%	-0.0076
Total for x=19m-25m		***56.586***	***57.573***	***-0.986***	***-0.986***	***0.000***	***2.649***	***4.010***	***0.375***	***-3.183***	***-1.162***	***1.537***	***123.254***	***1.25%***	

Table 8.15-Force-momentum balance for each zone of the transition (floodplains and main channel) for Dr=0.415, Q=29.6ℓ/s

Dr=0.514		Bed widths, m			Average Depth, m		Centroid, m		
		Left floodplain	Main channel	Right floodplain	Main channel	Floodplain	Left floodplain	Main channel	Right floodplain
Section 1	1	0	0.398	0.39	0.102	0.052	0.0000	0.0508	0.0258
Section 2	2	0.1	0.398	0.291	0.102	0.053	0.0266	0.0509	0.0266
Section 3	3	0.2	0.398	0.192	0.104	0.056	0.0279	0.0521	0.0279
Section 4	4	0.298	0.398	0.097	0.105	0.056	0.0282	0.0527	0.0282
Section 5	5	0.392	0.398	0	0.106	0.056	0.0281	0.0529	0.0000

		Perimeter, m			Area, m^2			Interface velocity, m/s	
		Left floodplain	Main channel	Right floodplain	Left floodplain	Main channel	Right floodplain	Left	Right
Section 1	1	0.000	0.550	0.442	0.0000	0.0404	0.0201	0.000	0.714
Section 2	2	0.153	0.498	0.344	0.0053	0.0405	0.0155	0.696	0.628
Section 3	3	0.256	0.498	0.248	0.0112	0.0414	0.0107	0.732	0.640
Section 4	4	0.354	0.498	0.153	0.0168	0.0419	0.0055	0.685	0.602
Section 5	5	0.448	0.504	0.000	0.0220	0.0421	0.0000	0.771	0.000

Left floodplain

Average Measured Discharge	Section, m	F_{1L}	F_{2L}	F_{1L}-F_{2L}	$\rho g(\Delta H)A$	R_{FL}	ΣSF_L	W_L	F_{1L}-F_{2L}-ΣSF_L+W_L	$\rho(Q_{2L}\beta_{2L}U_{2L}$-$Q_{1L}\beta_{1L}U_{1L})$	$\rho Q_{cfL}U_{iL}L$	$\rho(Q_{2L}\beta_{2L}U_{2L}$-$Q_{1L}\beta_{1L}U_{1L})$-$\rho Q_{cfL}U_{iL}L$	ASF_{iL}	Magnitude of terms	$\%ASF_{iL}$
m^3/s		*N*	*N*	*N*	*N*	*N*	*N*	*N*	*N*	*N*	*N*	*N*	*N*	*N*	*%*
0.0434	19-20.5	0.0000	1.3921	-1.3921	0.3252	20.2425	0.1350	0.0785	-1.4486	1.6699	1.0335	0.6364	-3.1185	22.4845	
0.0434	20.5-22	1.3921	3.0543	-1.6622	-0.7112	21.8825	0.3210	0.2429	-1.7403	1.6526	2.2082	-0.5555	-3.3929	27.4484	
0.0434	22-23.5	3.0543	4.6450	-1.5907	-0.7024	23.1434	0.4695	0.4120	-1.6482	1.7051	2.1924	-0.4873	-3.3533	32.2115	
0.0434	23.5-25	4.6450	6.0613	-1.4163	-0.2609	23.2872	0.6075	0.5718	-1.4520	2.1503	2.2516	-0.1013	-3.6023	35.2741	
Total for x=19m-25m		***9.091***	***15.153***	***-6.061***	***-1.349***	***88.556***	***1.533***	***1.305***	***-6.289***	***7.178***	***7.686***	***-0.508***	***-13.467***	***117.419***	

Right floodplain

Average Measured Discharge	Section, m	F_{1R}	F_{2R}	F_{1R}-F_{2R}	$\rho g(\Delta H)A$	R_{FL}	ΣSF_R	W_R	F_{1R}-F_{2R}-ΣSF_R+W_R	$\rho(Q_{2R}\beta_{2R}U_{2R}$-$Q_{1R}\beta_{1R}U_{1R})$	$\rho Q_{cfR}U_{iR}L$	$\rho(Q_{2R}\beta_{2R}U_{2R}$-$Q_{1R}\beta_{1R}U_{1R})$-$\rho Q_{cfR}U_{iR}L$	ASF_{iR}	Magnitude of terms	$\%ASF_{iR}$
m^3/s		*N*	*N*	*N*	*N*	*N*	*N*	*N*	*N*	*N*	*N*	*N*	*N*	*N*	*%*
0.0434	19-20.5	5.0995	4.0510	1.0486	-0.2871	20.2425	0.5685	0.5251	1.0052	-2.4882	-2.0974	-0.3908	3.4934	30.8774	
0.0434	20.5-22	4.0510	2.9321	1.1188	-0.3246	21.8825	0.4080	0.3863	1.0971	-2.1885	-1.9812	-0.2073	3.2856	29.8672	
0.0434	22-23.5	2.9321	1.5120	1.4202	-0.0456	23.1434	0.2175	0.2384	1.4411	-1.6933	-1.9412	0.2479	3.1344	28.2913	
0.0434	23.5-25	1.5120	0.0000	1.5120	0.0061	23.2872	0.0690	0.0806	1.5235	-1.6541	-0.8997	-0.7544	3.1776	25.7031	
Total for x=19m-25m		***13.595***	***8.495***	***5.100***	***-0.651***	***88.556***	***1.263***	***1.230***	***5.067***	***-8.024***	***-6.920***	***-1.105***	***13.091***	***114.739***	

Main channel

Average Measured Discharge	Section, m	F_{1MC}	F_{2MC}	F_{1MC}-F_{2MC}	$\rho g(\Delta H)A$	R_{FMC}	ΣSF_{MC}	W_{MC}	F_{1MC}-F_{2MC}-ΣSF_{MC}+W_{MC}	$\rho(Q_{2MC}\beta_{2MC}U_{2MC}$-$Q_{1MC}\beta_{1MC}U_{1MC})$	$\rho(Q_{2MC}\beta_{2MC}U_{2MC}$-$Q_{1MC}\beta_{1MC}U_{1MC})$+$\rho Q_{cfL}U_{iL}L$+$\rho Q_{cfR}U_{iR}L$	Residual	Magnitude of terms	%Error	ASF_H
m^3/s		*N*	*N*	*N*	*N*	*N*	*N*	*N*	*N*	*N*	*N*	*N*	*N*	*%*	*N*
0.0434	19-20.5	20.1289	20.1851	-0.0562	-0.0562	0.0000	0.8955	1.1918	0.2401	-0.6671	-1.7310	1.9712	44.1324	4.47%	-0.3091
0.0434	20.5-22	20.1851	21.1490	-0.9639	-0.9639	0.0000	0.8610	1.2067	-0.6182	-0.9439	-0.7170	0.0987	44.1188	0.22%	-0.2746
0.0434	22-23.5	21.1490	21.6668	-0.5178	-0.5178	0.0000	0.7755	1.2282	-0.0651	-0.6112	-0.3600	0.2949	45.1796	0.65%	-0.1891
0.0434	23.5-25	21.6668	21.8385	-0.1717	-0.1717	0.0000	0.7470	1.2381	0.3194	-0.3697	0.9823	-0.6629	46.4728	-1.43%	-0.1606
Total for x=19m-25m		***83.130***	***84.840***	***-1.710***	***-1.710***	***0.000***	***3.279***	***4.865***	***-0.124***	***-2.592***	***-1.826***	***1.702***	***179.904***	***0.95%***	

Table 8.16-Force-momentum balance for each zone of the transition (floodplains and main channel) for Dr=0.514, Q=43.4//s

Experiments	Q	H	Dr	Q_{mc}	Q_{fp}	$\%Q_{mc}$	$\%Q_{fp}$	U_{mc}	U_{fp}
	m^3/s	m		m^3/s	m^3/s			m/s	m/s
ROA315	0.0150	0.0593	0.157	0.0140	0.0010	93.51%	6.49%	0.5946	0.2572
ROA318	0.0180	0.0662	0.245	0.0161	0.0019	89.36%	10.64%	0.6118	0.2909
ROA321	0.0210	0.0725	0.310	0.0181	0.0029	86.05%	13.95%	0.6273	0.3201
ROA330	0.0302	0.0827	0.395	0.0236	0.0066	78.14%	21.86%	0.7164	0.4951
ROA344	0.0438	0.0991	0.495	0.0306	0.0132	69.89%	30.11%	0.7758	0.6592

Table 8.17a-Atabay's (2001) stage-discharge and velocity results for certain asymmetric channel experiments

Experiments	Q	H_{ave}	Dr	Q_{mc}	Q_{fp}	$\%Q_{mc}$	$\%Q_{fp}$	U_{mc}	U_{fp}
	m^3/s	m		m^3/s	m^3/s			m/s	m/s
Skewed	0.0162	0.0634	0.211	0.0149	0.0013	92.19%	7.81%	0.5911	0.2383
Skewed	0.0214	0.0717	0.303	0.0183	0.0031	85.57%	14.43%	0.6415	0.3682
Skewed	0.0296	0.0835	0.401	0.0234	0.0062	78.90%	21.10%	0.7028	0.4796
Skewed	0.0434	0.1025	0.512	0.0310	0.0125	71.30%	28.70%	0.7587	0.6097

Table 8.17b-Skewed stage-discharge and velocity results for x=19m

Experiment	Discharge	Depth	Dr	Experimental Shear Forces (N)					Total SF
	l/s	*m*		SF_1	SF_2	SF_3	SF_4	SF_5	*(N)*
ROA415r	0.0150	0.0609	0.179	0.0004	0.1414	0.0354	0.3799	0.0478	0.6049
ROA418r	0.0182	0.0666	0.249	0.0036	0.1947	0.0408	0.4037	0.0574	0.7003
ROA421r	0.0209	0.0711	0.296	0.0064	0.2115	0.0402	0.4172	0.0655	0.7408
ROA430	0.0301	0.0834	0.400	0.0142	0.2949	0.0398	0.4081	0.0761	0.8332
ROA444	0.0460	0.1010	0.505	0.0363	0.4808	0.0685	0.5343	0.1189	1.2389

Table 8.18a-Atabay's (2001) shear force results for certain asymmetrical channel experiments

	Dr	Percentage Shear Forces (%SF_i/SF_{total})					Vertical Apparent Shear Forces	
		SF_1%	SF_2%	SF_3%	SF_4%	SF_5%	ASF_v	ASF_v%
ROA415r	0.179	0.06%	23.37%	5.85%	62.81%	7.91%	0.0225	3.91%
ROA418r	0.249	0.52%	27.81%	5.83%	57.65%	8.19%	0.0224	3.40%
ROA421r	0.296	0.86%	28.55%	5.43%	56.32%	8.84%	0.0312	4.33%
ROA430	0.400	1.71%	35.40%	4.78%	48.99%	9.13%	0.1303	14.13%
ROA444	0.505	2.93%	38.81%	5.53%	43.13%	9.60%	0.0950	7.67%

Table 8.18b-Atabay's (2001) percentage shear force and vertical apparent shear force results for certain asymmetrical channel experiments

	Dr	Percentage Shear Forces (%SF_i/SF_{total})				
		SF_1%	SF_2%	SF_3%	SF_4%	SF_5%
Skewed	0.211	0.26%	23.85%	5.82%	62.04%	7.98%
Skewed	0.303	0.87%	30.49%	5.55%	54.68%	8.42%
Skewed	0.401	1.78%	35.42%	5.33%	48.56%	8.93%
Skewed	0.512	3.10%	38.19%	5.18%	43.95%	9.57%

Table 8.18c-Atabay's (2001) percentage shear force equation applied to skewed data at x=19m

	Dr	Percentage Shear Forces (%SF_i/SF_{total})				
		SF_1%	SF_2%	SF_3%	SF_4%	SF_5%
Skewed	0.211	0.29%	15.02%	5.91%	68.93%	9.84%
Skewed	0.303	1.01%	33.34%	4.88%	51.35%	9.42%
Skewed	0.401	1.79%	33.86%	5.34%	49.99%	9.02%
Skewed	0.512	3.44%	38.55%	5.23%	43.90%	8.89%

Table 8.18d-Skewed channel percentage shear force on each element at section x=19m

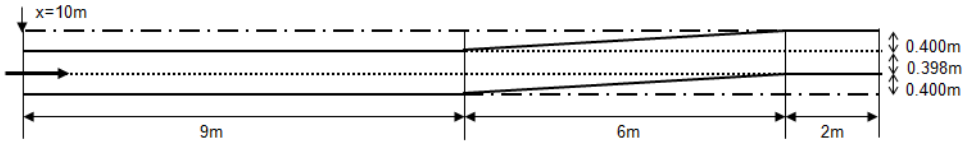

Figure 8.1-Skewed channel schematic

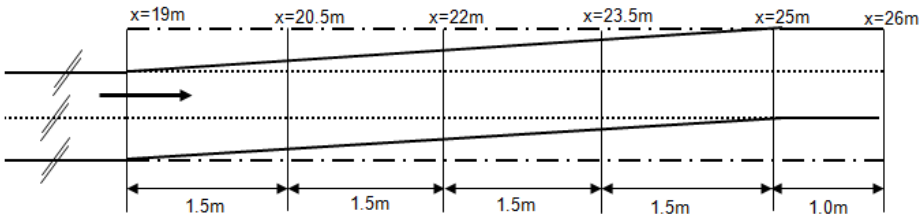

Figure 8.2-Schematic of transition section and measurement sections

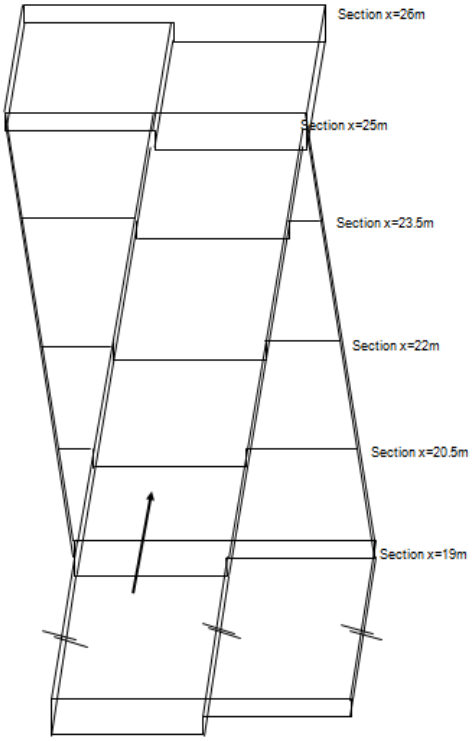

Figure 8.3-Perspective view of skewed channel

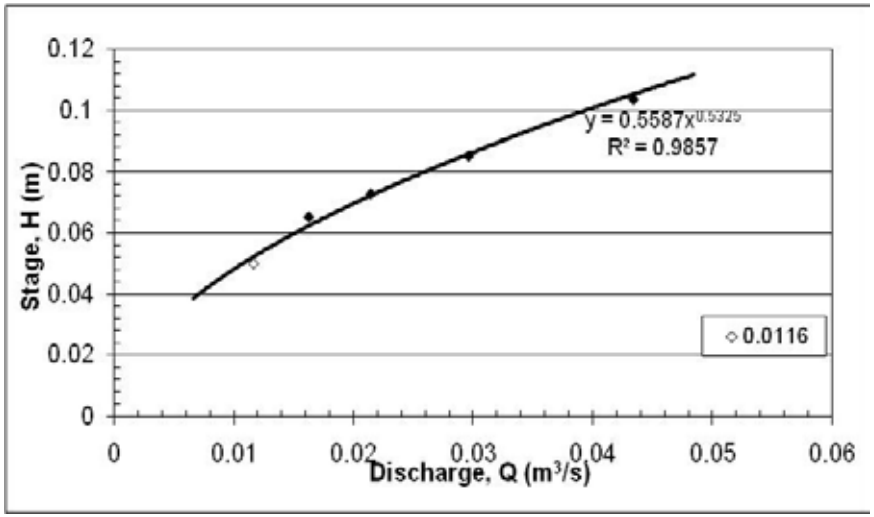

Figure 8.4-Stage~discharge relationship for skewed channel

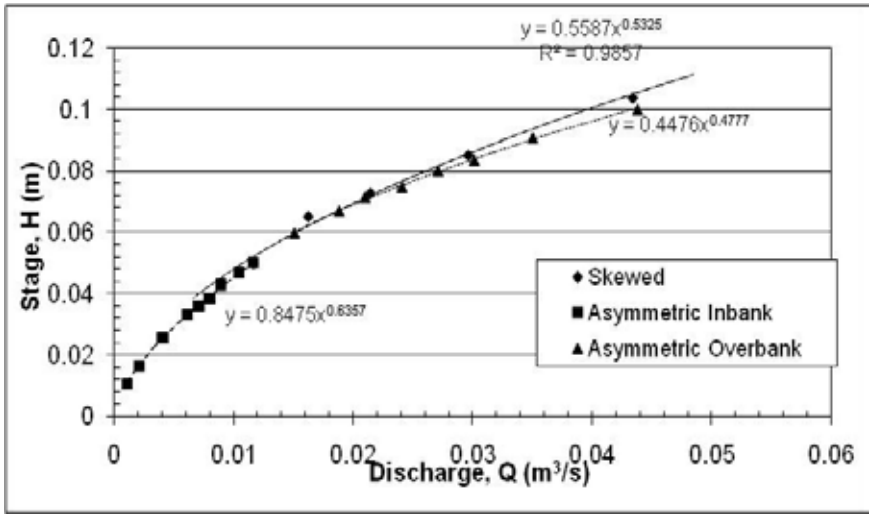

Figure 8.5-Stage~discharge relationship for skewed, asymmetric inbank and asymmetric overbank channels

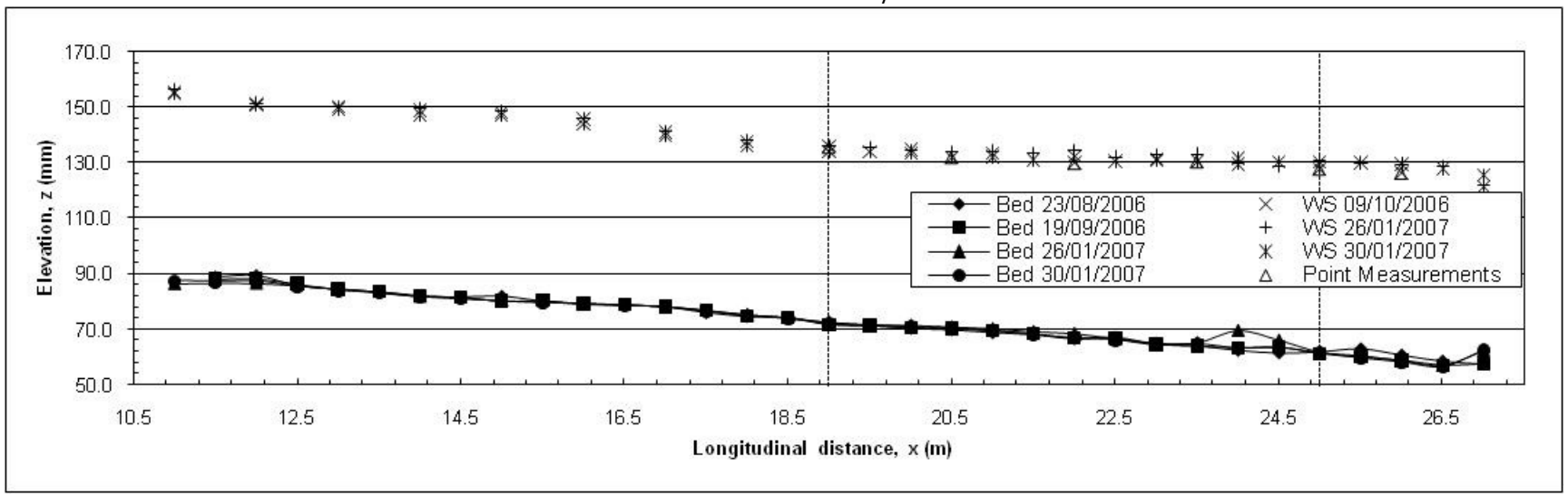

Figure 8.6a-Water surface and bed elevations for skewed channel with Dr=0.205, Q=16.2ℓ/s

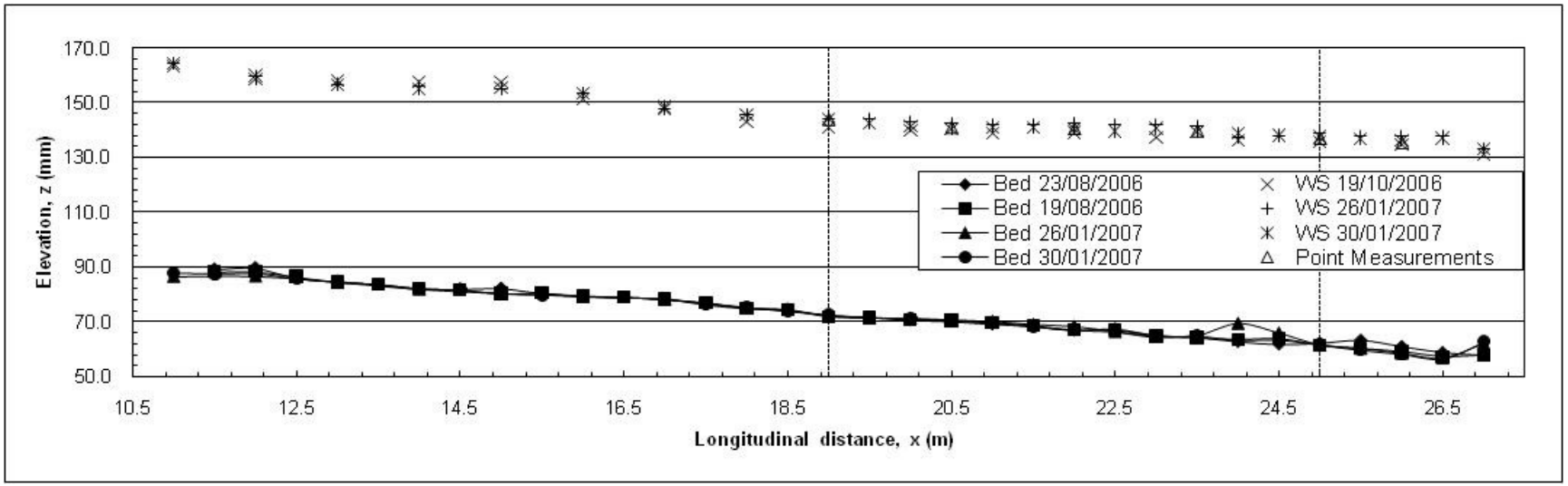

Figure 8.6b-Water surface and bed elevations for skewed channel with Dr=0.313, Q=21.4ℓ/s

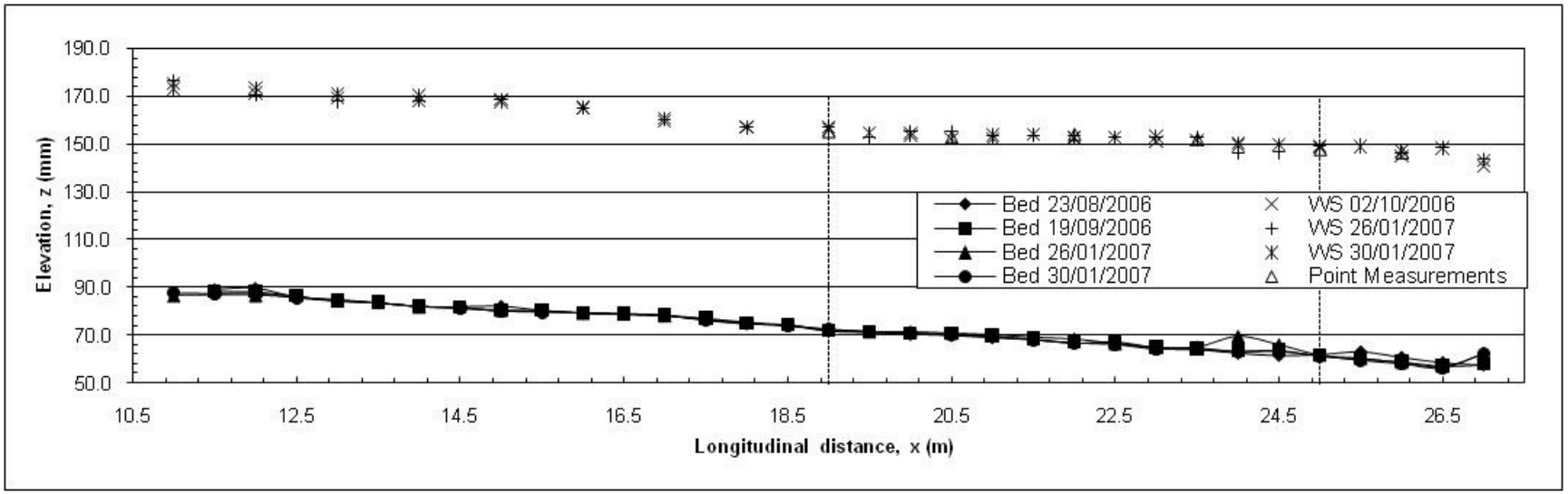

Figure 8.6c-Water surface and bed elevations for skewed channel with Dr=0.415, Q=29.6ℓ/s

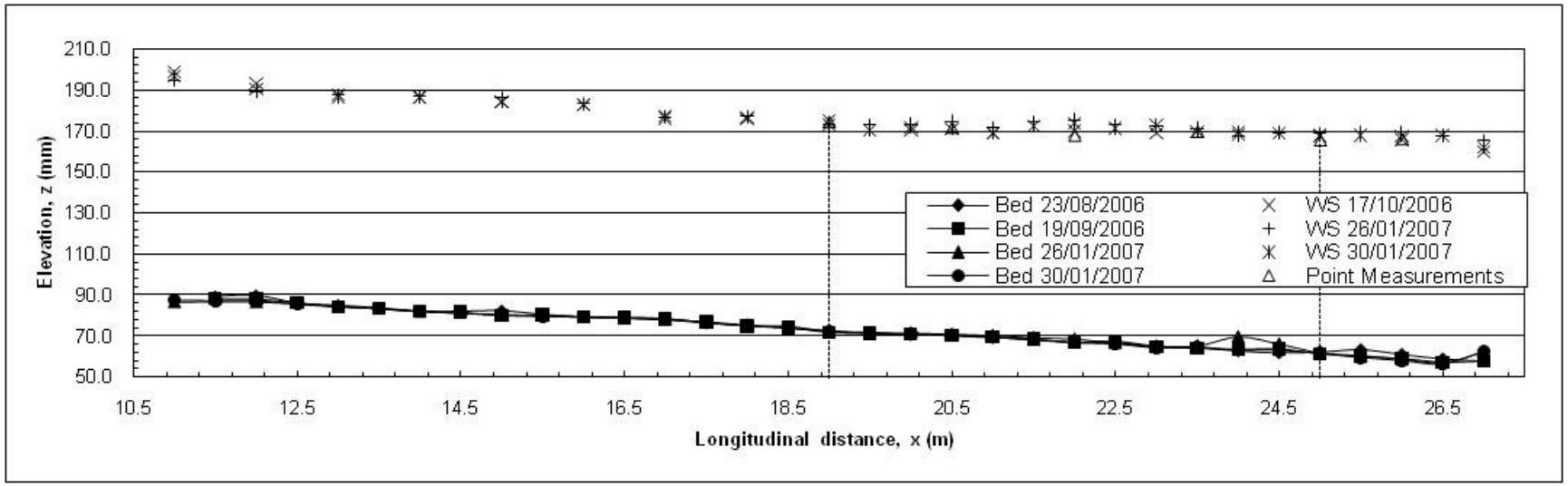

Figure 8.6d-Water surface and bed elevations for skewed channel with Dr=0.514, Q=43.4ℓ/s

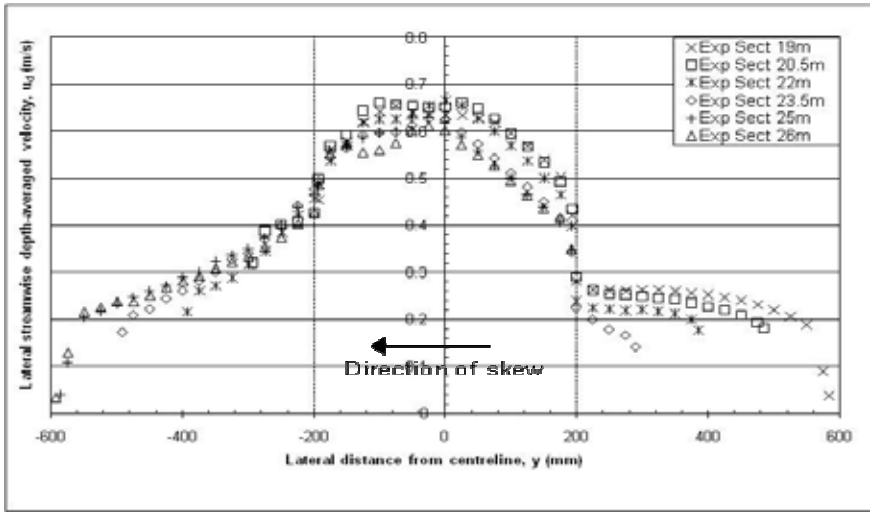

Figure 8.7a-Lateral distributions of streamwise depth-averaged velocity for Dr=0.205, Q=16.2ℓ/s

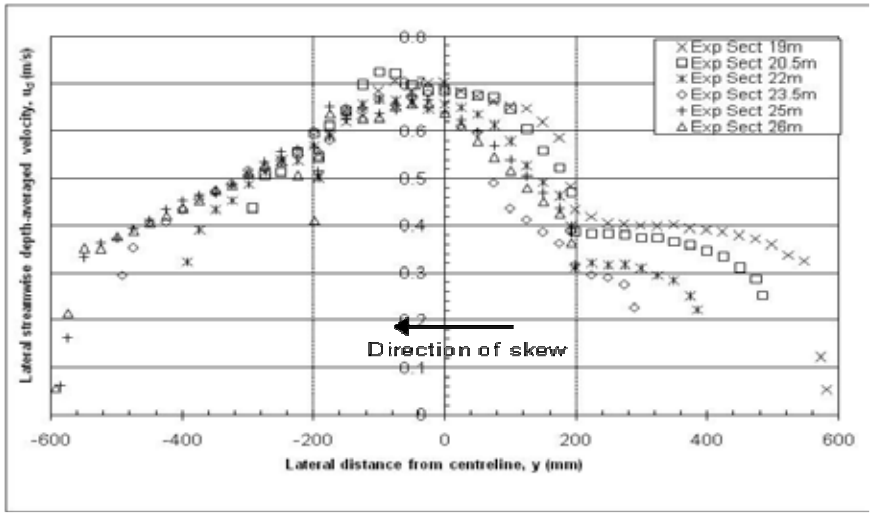

Figure 8.7b-Lateral distributions of streamwise depth-averaged velocity for Dr=0.313, Q=21.4ℓ/s

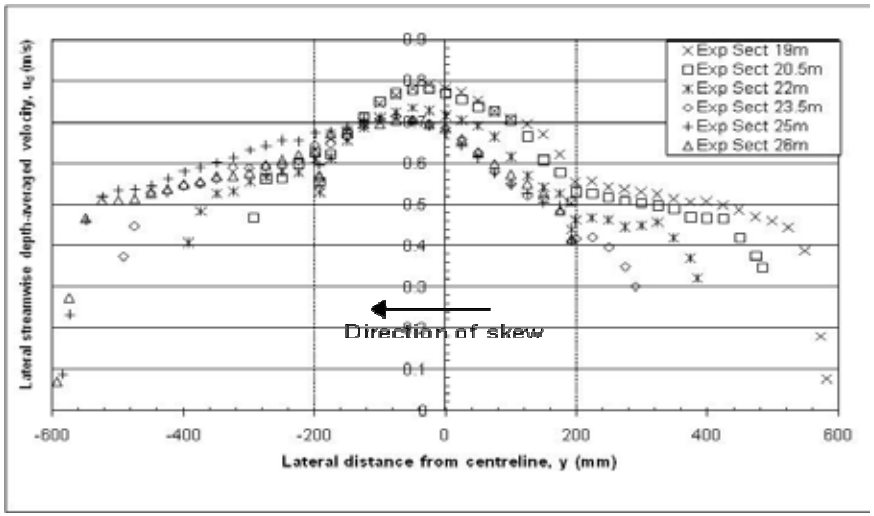

Figure 8.7c-Lateral distributions of streamwise depth-averaged velocity for Dr=0.415, Q=29.6ℓ/s

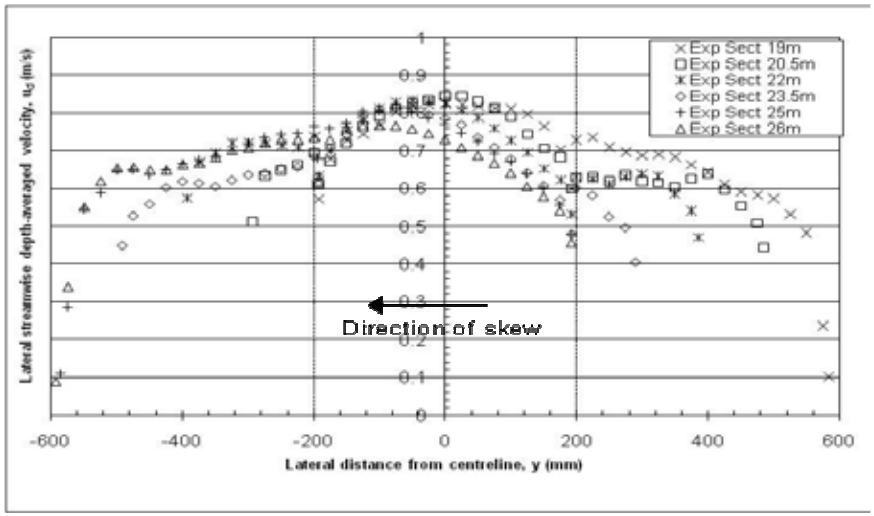

Figure 8.7d-Lateral distributions of streamwise depth-averaged velocity for Dr=0.514, Q=43.4ℓ/s

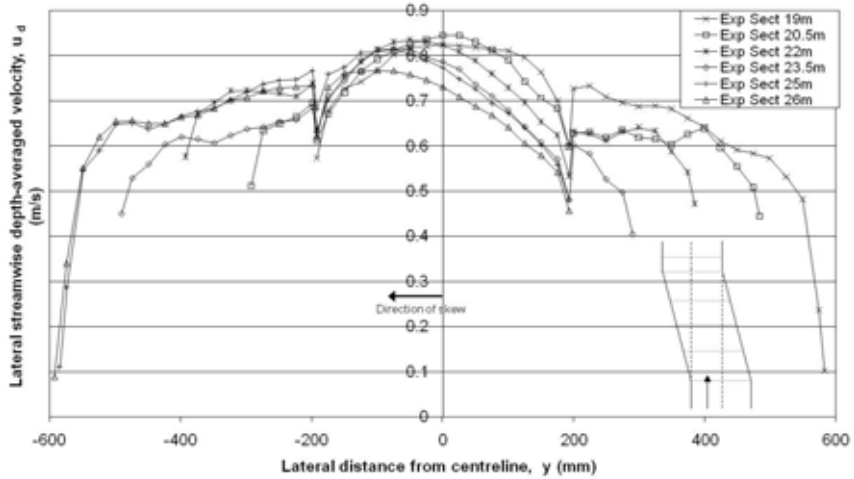

Figure 8.7d (enlarged)-Lateral distributions of streamwise depth-averaged velocity for Dr=0.514, Q=43.4ℓ/s

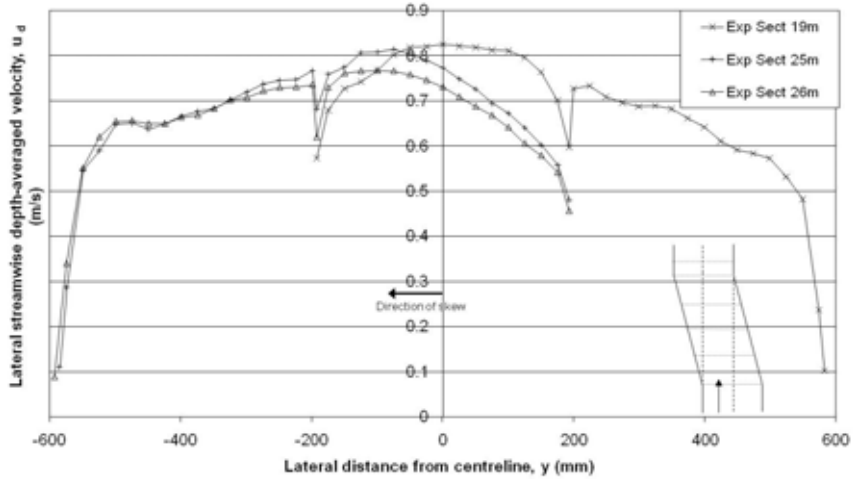

Figure 8.8-Lateral distributions of streamwise depth-averaged velocity for Dr=0.514, Q=43.4ℓ/s showing the decreasing velocity in the main channel

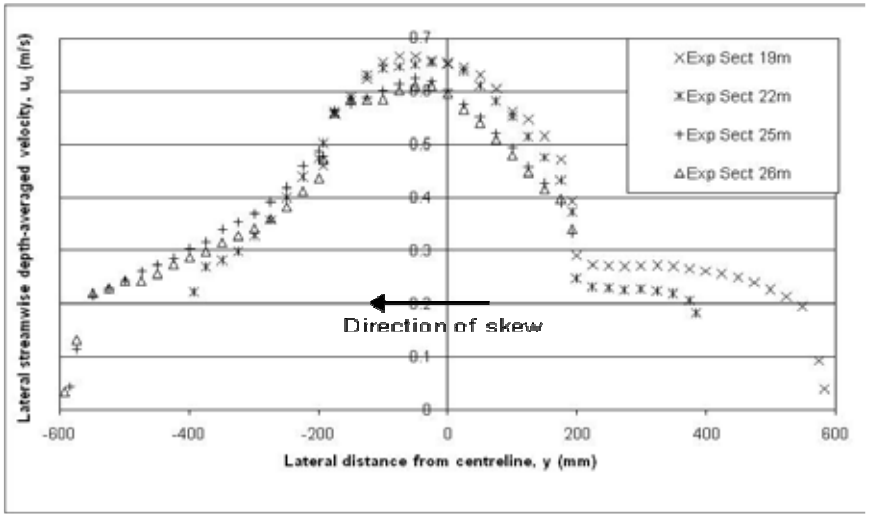

Figure 8.9a-Lateral distributions of streamwise depth-integrated velocity for Dr=0.205, Q=16.2ℓ/s

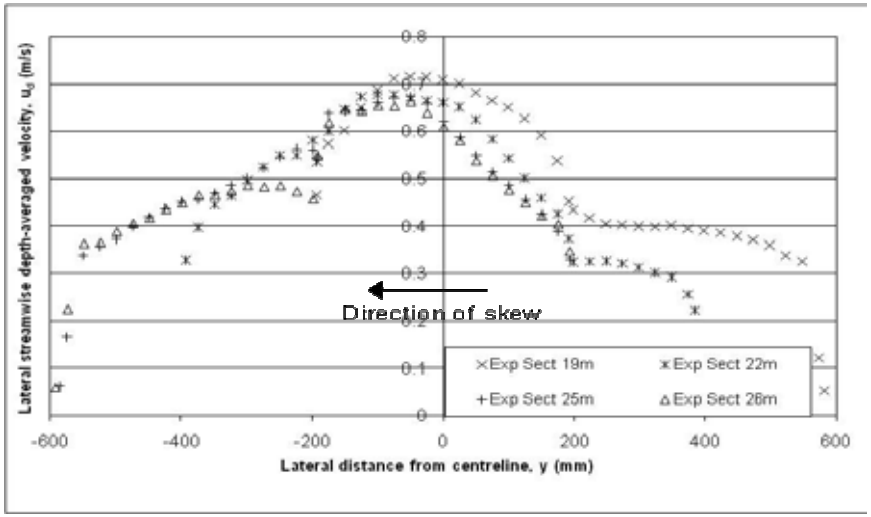

Figure 8.9b-Lateral distributions of streamwise depth-integrated velocity for Dr=0.313, Q=21.4ℓ/s

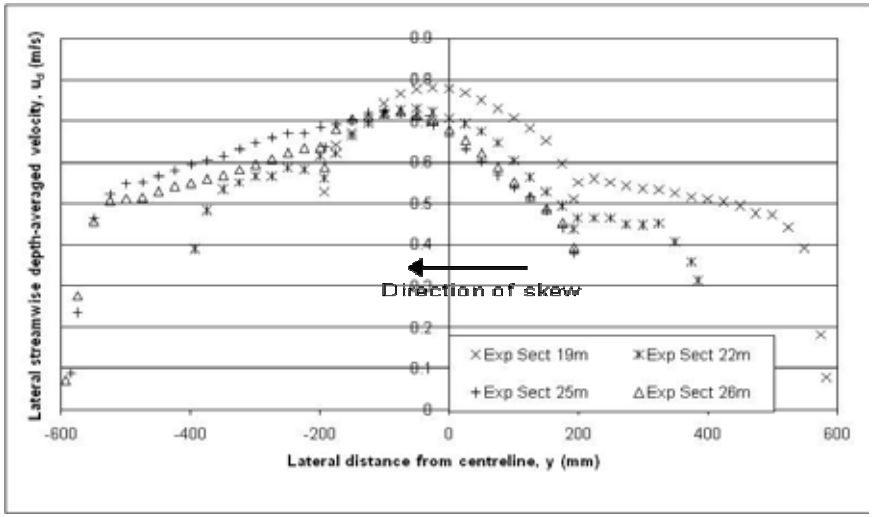

Figure 8.9c-Lateral distributions of streamwise depth-integrated velocity for Dr=0.415, Q=29.6ℓ/s

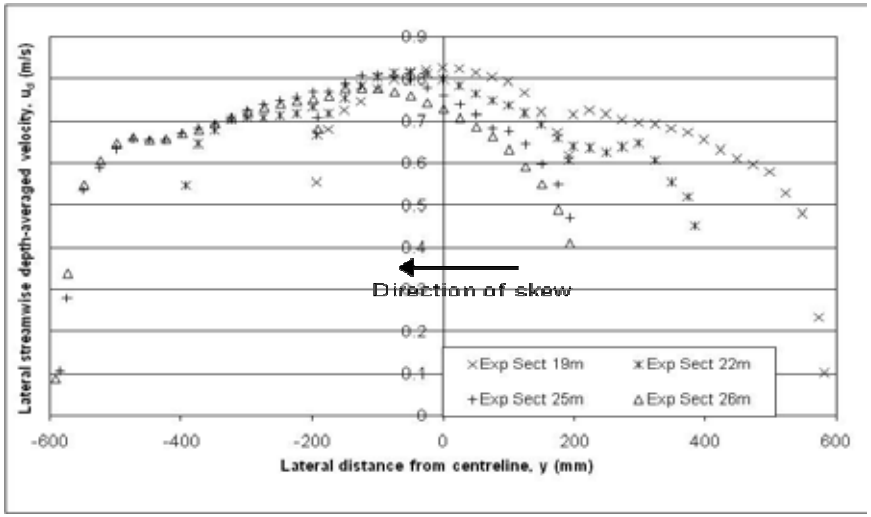

Figure 8.9d-Lateral distributions of streamwise depth-integrated velocity for Dr=0.514, Q=43.4ℓ/s

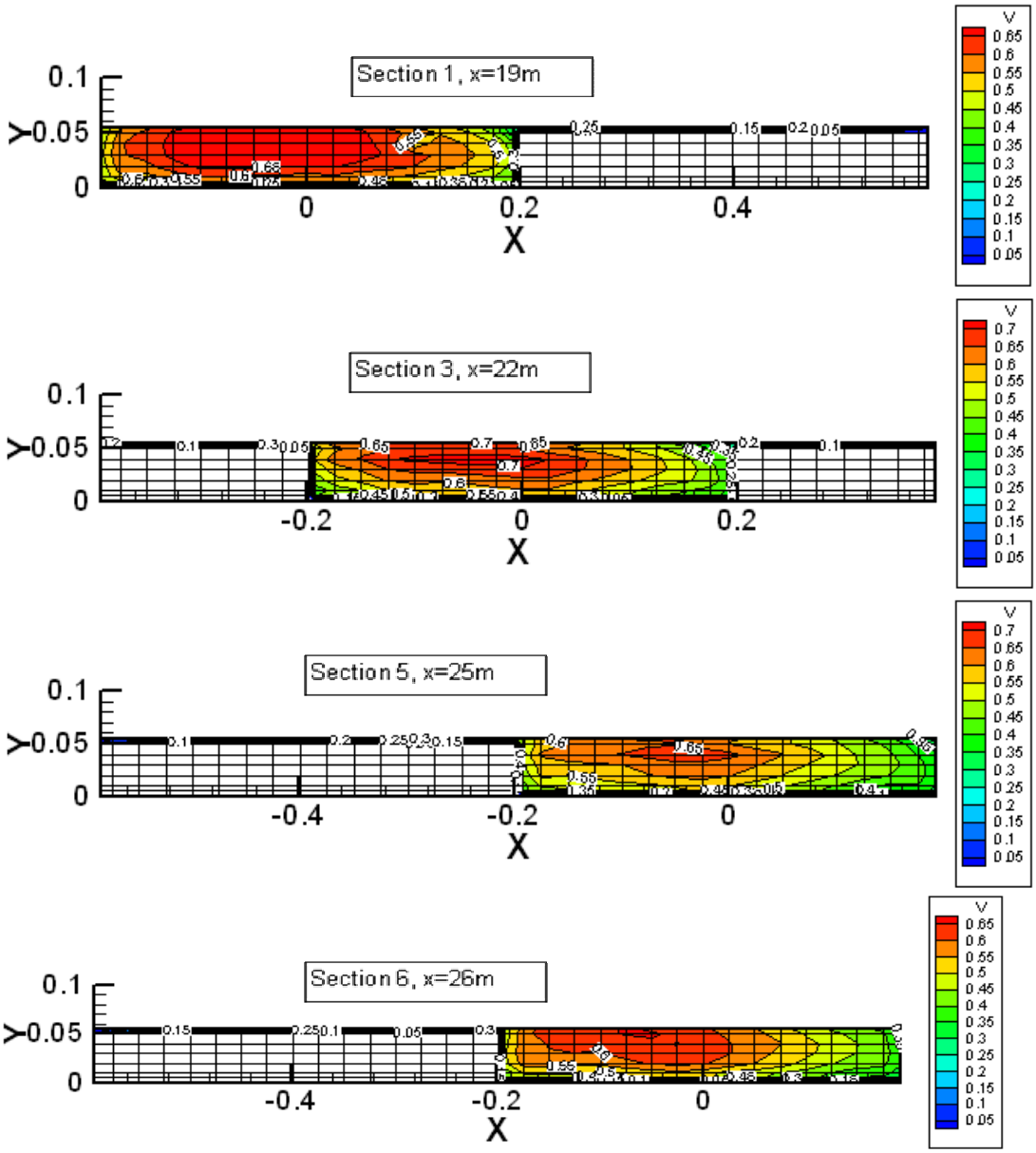

Figure 8.10a-Velocity distribution (m/s) in skewed channel where Dr=0.205, Q=16.2ℓ/s

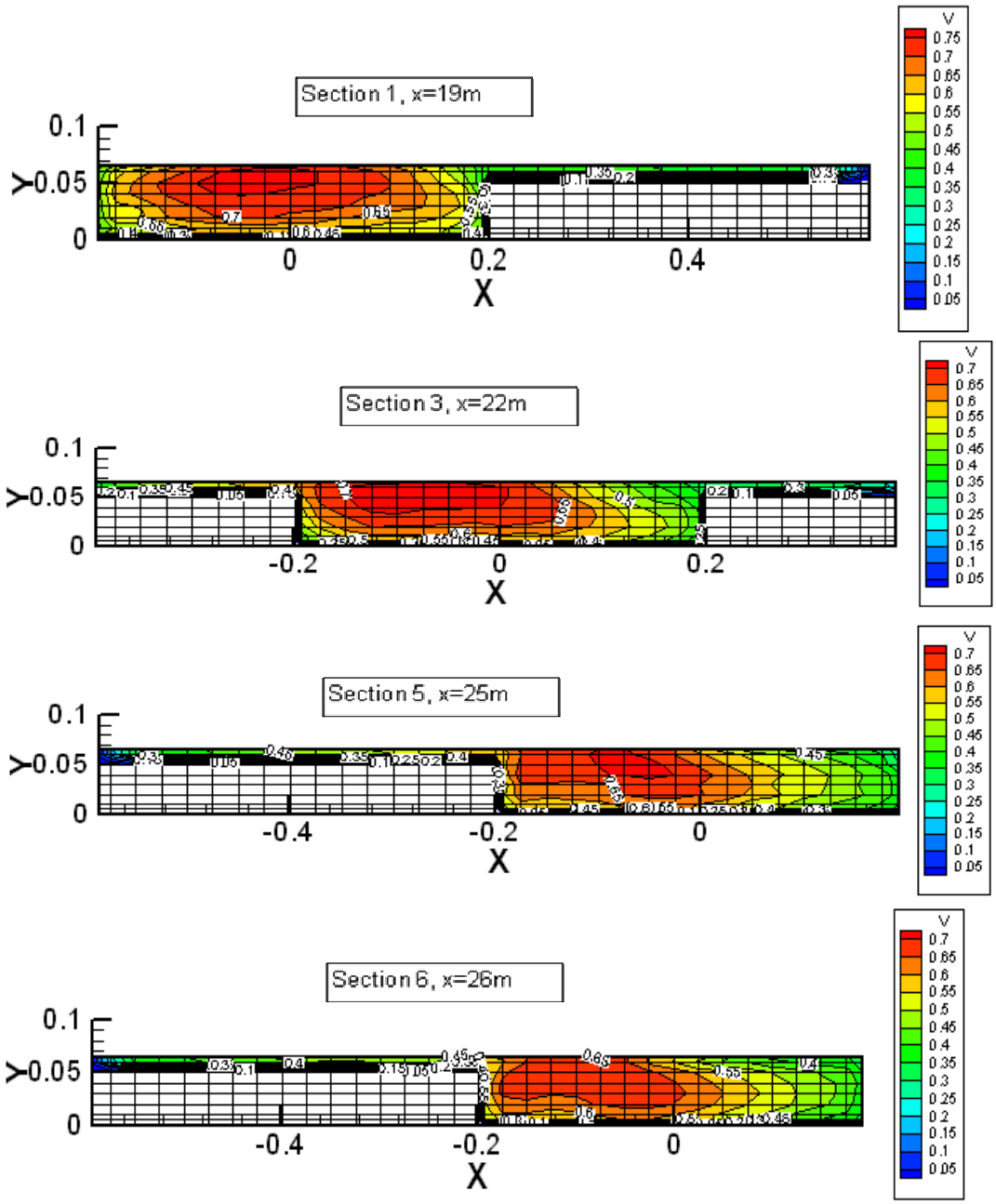

Figure 8.10b-Velocity distribution (m/s) in skewed channel where Dr=0.313, Q=21.4ℓ/s

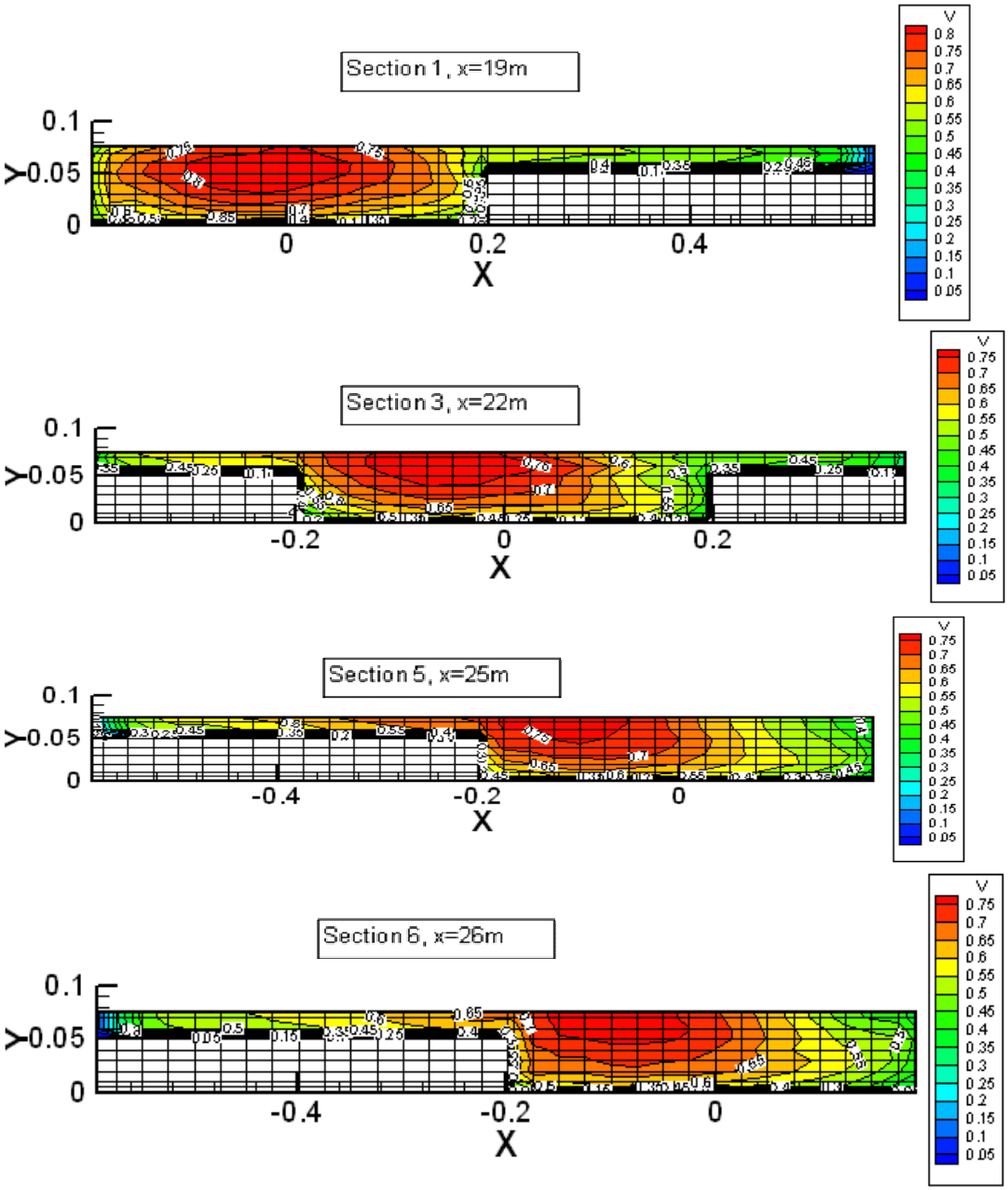

Figure 8.10c-Velocity distribution (m/s) in skewed channel where Dr=0.415, Q=29.6ℓ/s

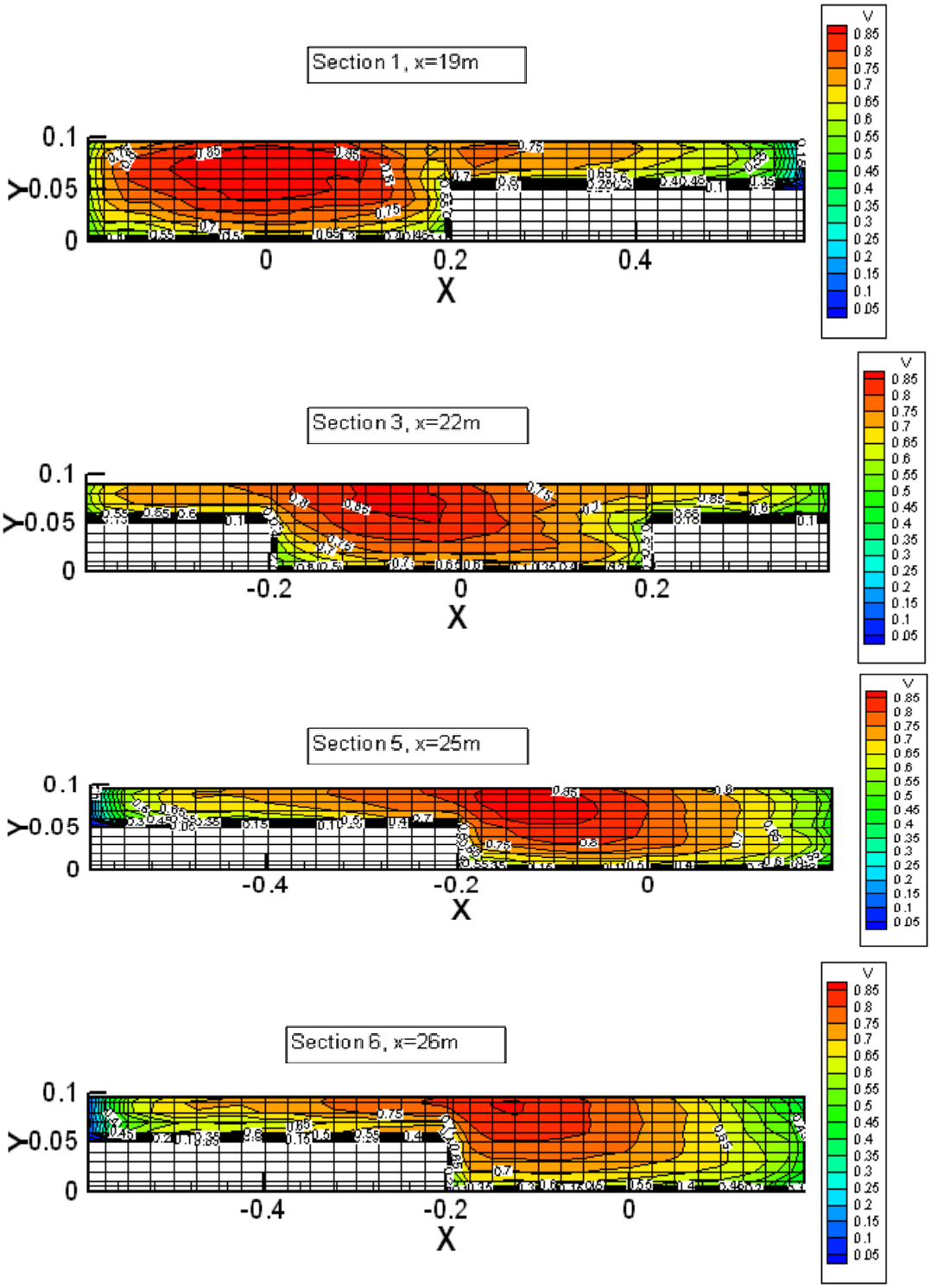

Figure 8.10d-Velocity distribution (m/s) in skewed channel where Dr=0.514, Q=43.4ℓ/s

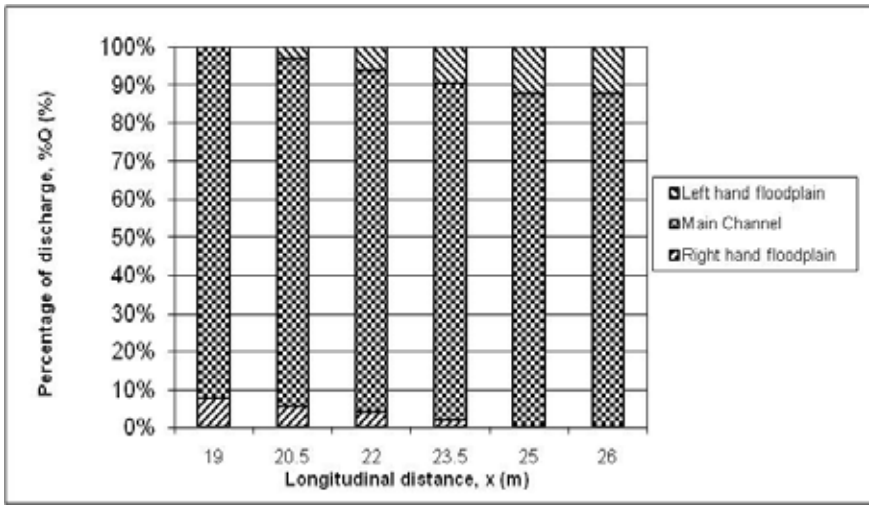

Figure 8.11a-Percentage of discharge along the experimental section for Dr=0.205, Q=16.2ℓ/s

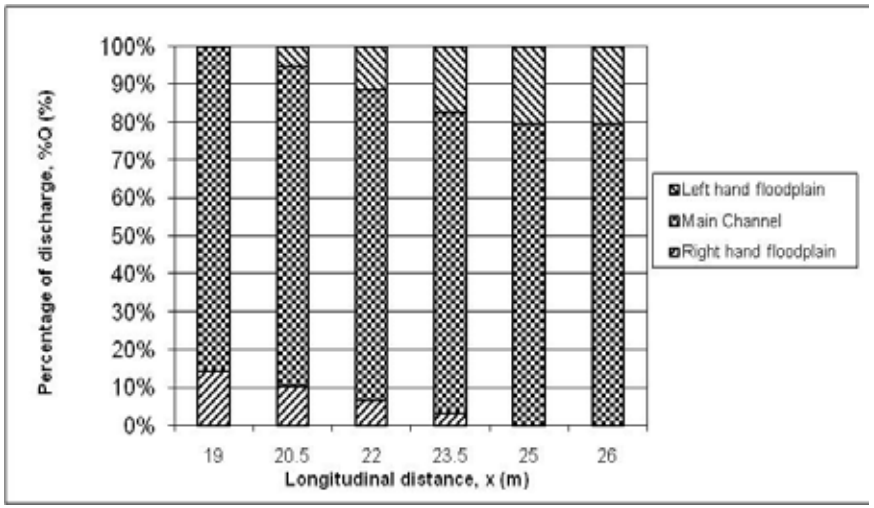

Figure 8.11b-Percentage of discharge along the experimental section for Dr=0.313, Q=21.4ℓ/s

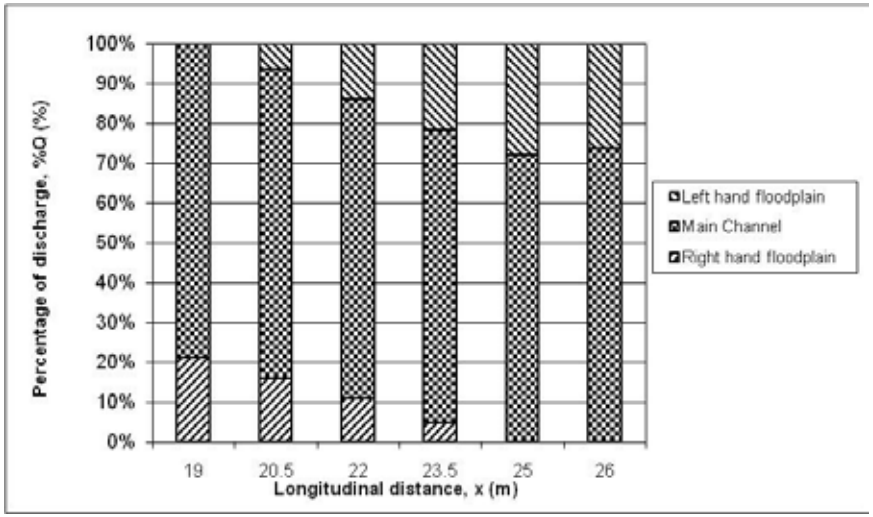

Figure 8.11c-Percentage of discharge along the experimental section for Dr=0.415, Q=29.6ℓ/s

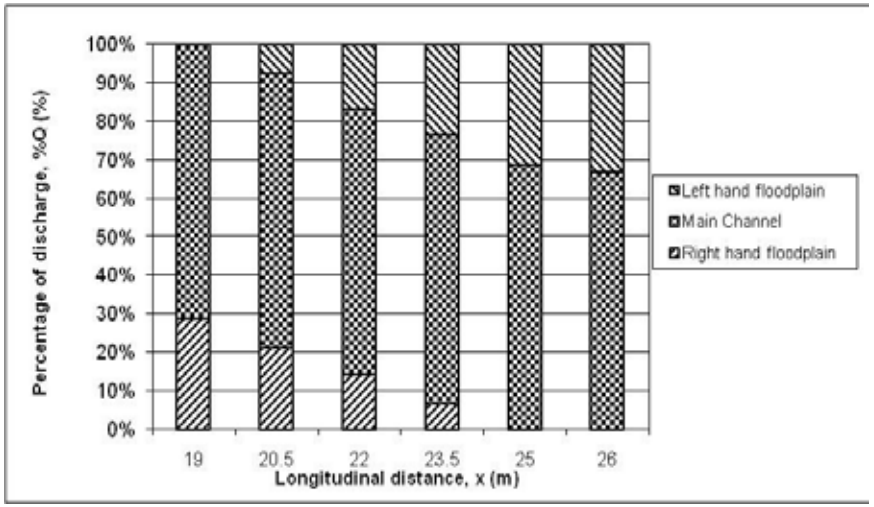

Figure 8.11d-Percentage of discharge along the experimental section for Dr=0.514, Q=43.4ℓ/s

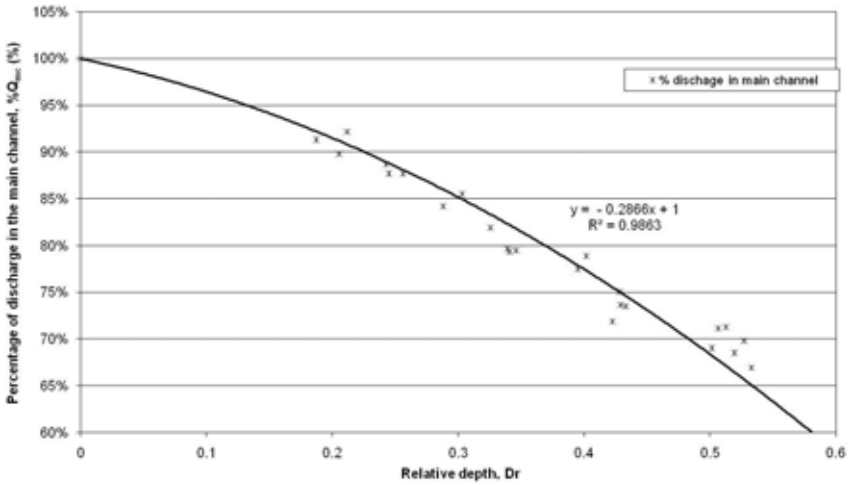

Figure 8.12a-Relationship between relative depth and percentage of the total flow in the main channel

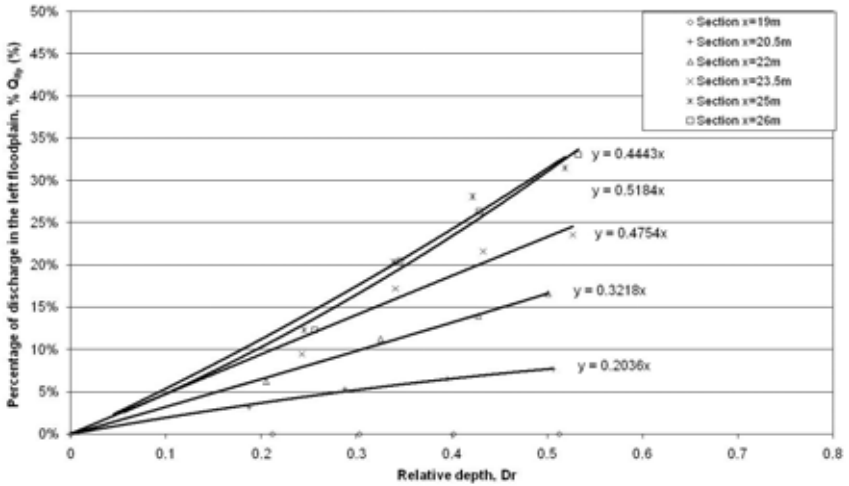

Figure 8.12b-Relationship between relative depth and percentage of the total flow in the left hand floodplain

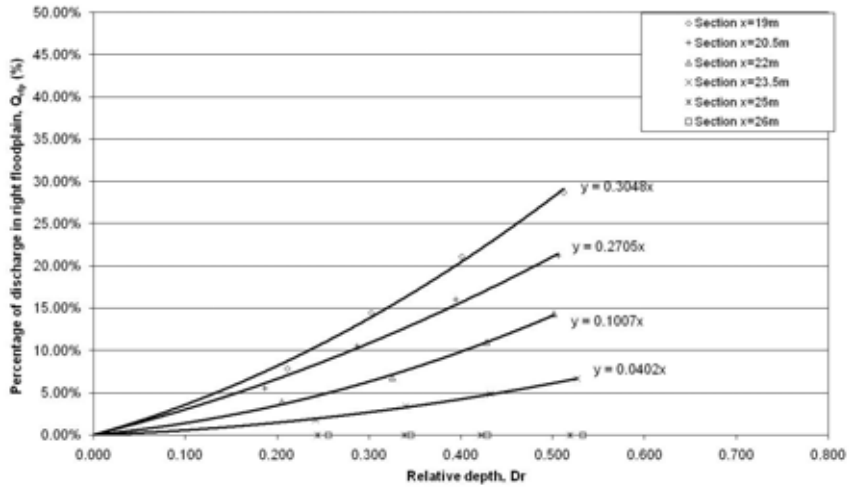

Figure 8.12c-Relationship between relative depth and percentage of the total flow in the right hand floodplain

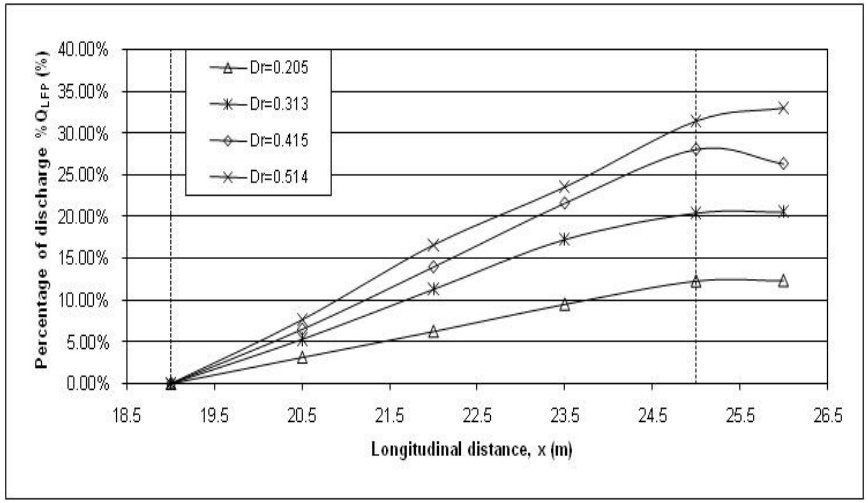

Figure 8.13a-Percentage of discharge along the channel length for left hand floodplain

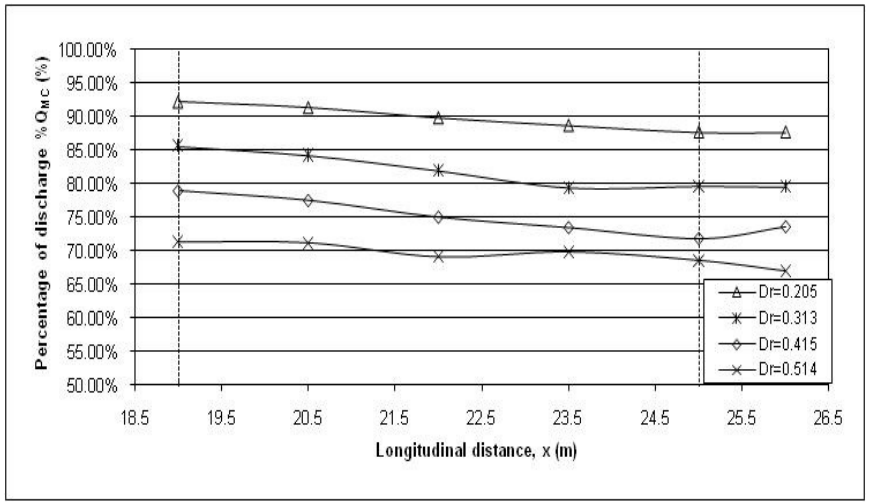

Figure 8.13b-Percentage of discharge along the channel length for main channel

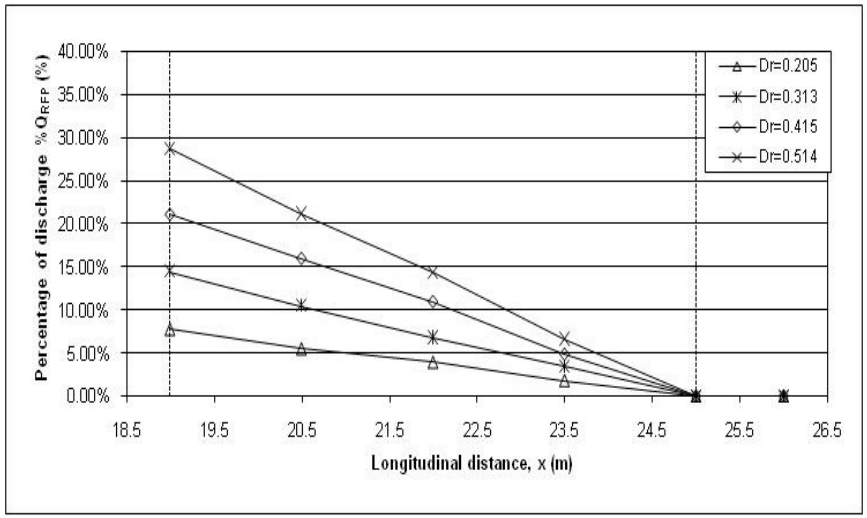

Figure 8.13c-Percentage of discharge along the channel length for right hand floodplain

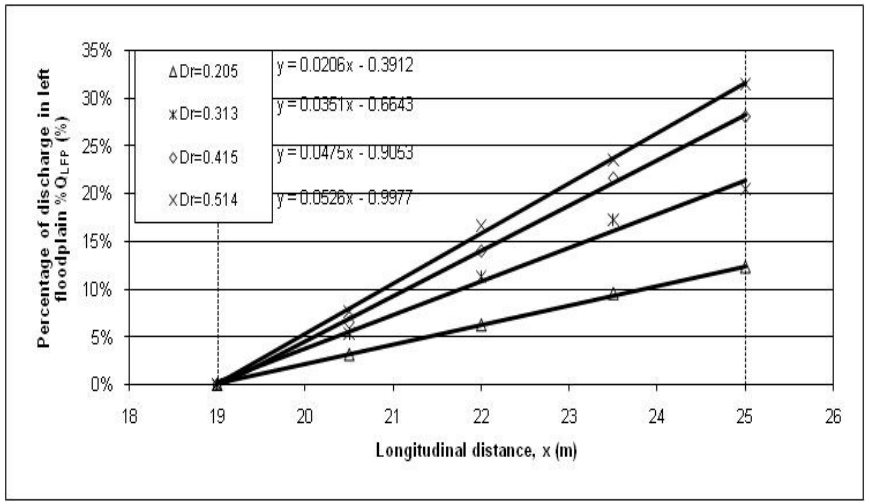

Figure 8.14a-Percentage of discharge along the channel length for left hand floodplain

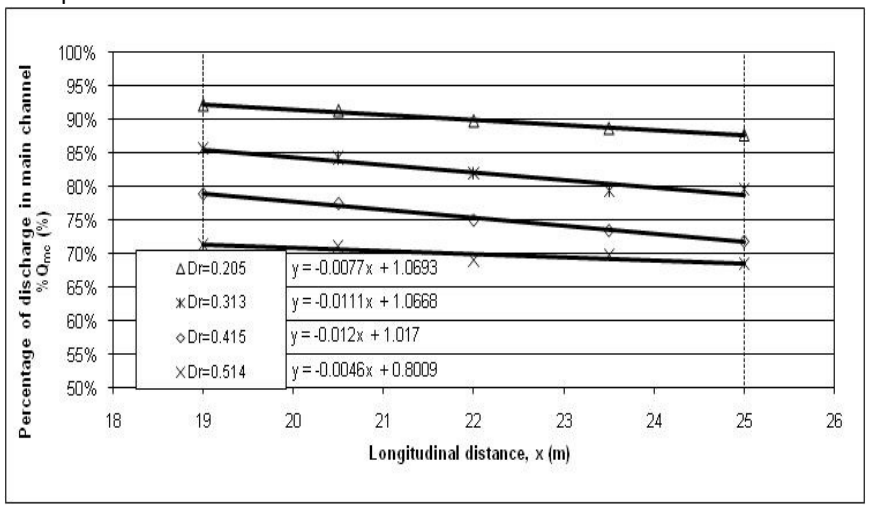

Figure 8.14b-Percentage of discharge along the channel length for main channel

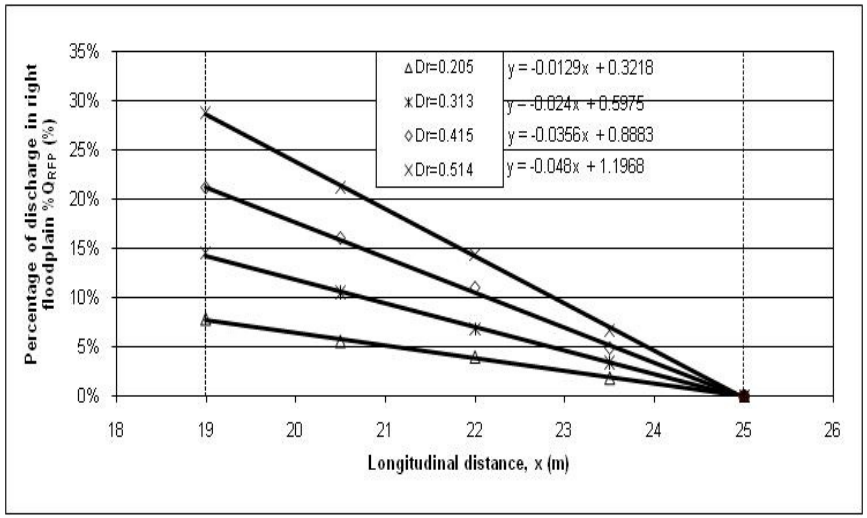

Figure 8.14c-Percentage of discharge along the channel length for right hand floodplain

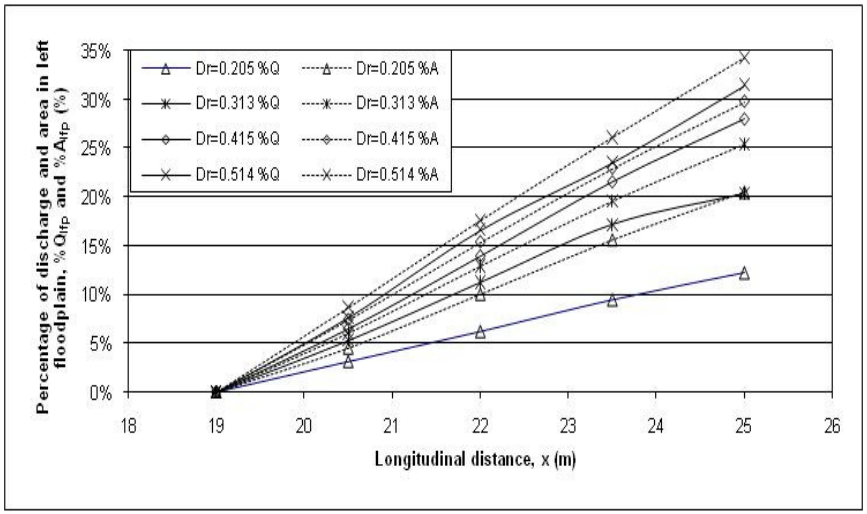

Figure 8.14d-Percentage of discharge and area along the channel length for left hand floodplain

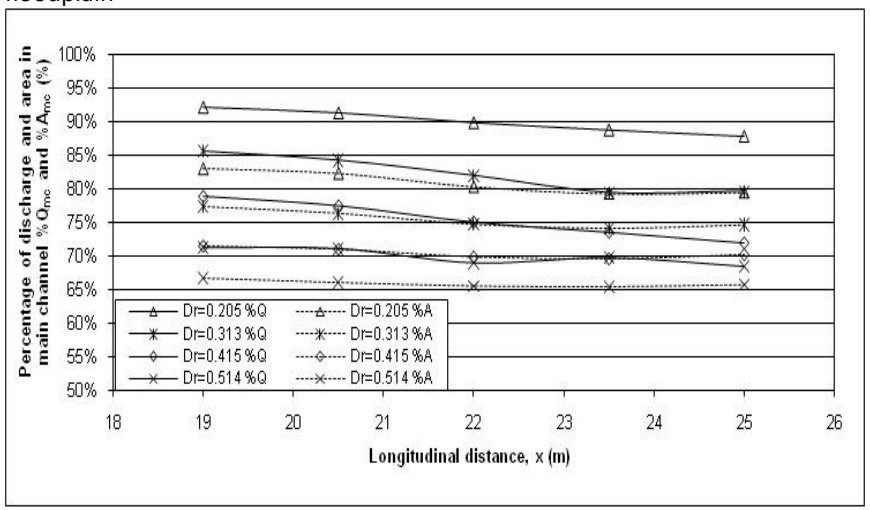

Figure 8.14e-Percentage of discharge and area along the channel length for main channel

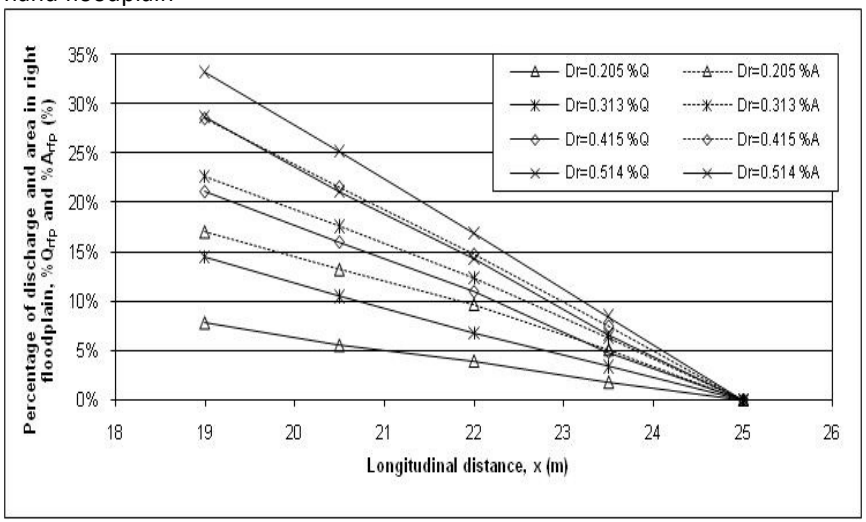

Figure 8.14f-Percentage of discharge and area along the channel length for right hand floodplain

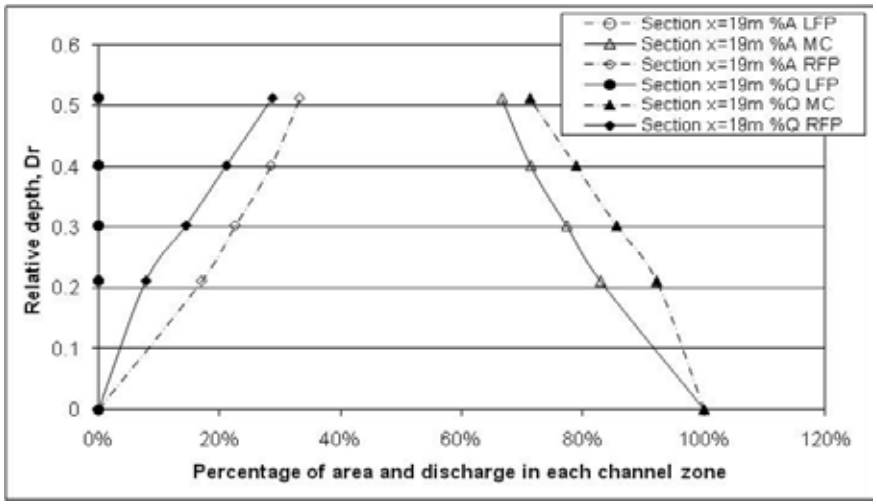

Figure 8.15a-Percentage of area and discharge at section x=19m for each flow depth

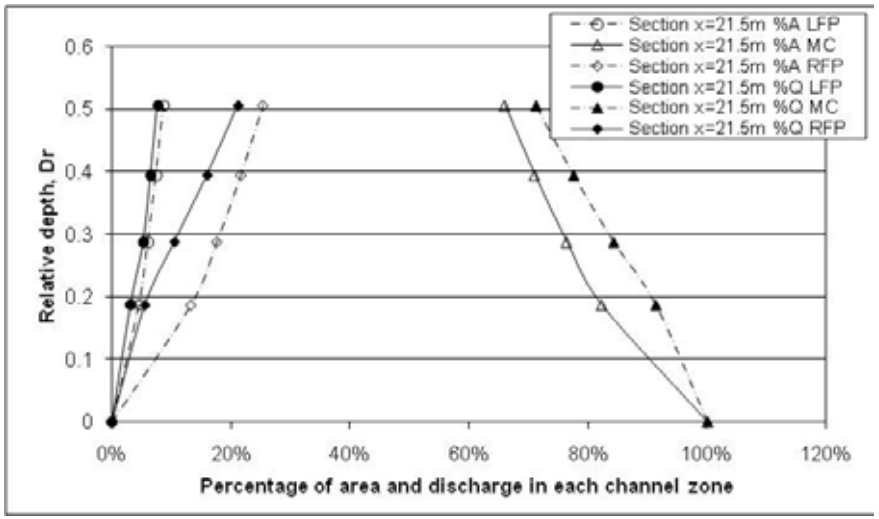

Figure 8.15b-Percentage of area and discharge at section x=21.5m for each flow depth

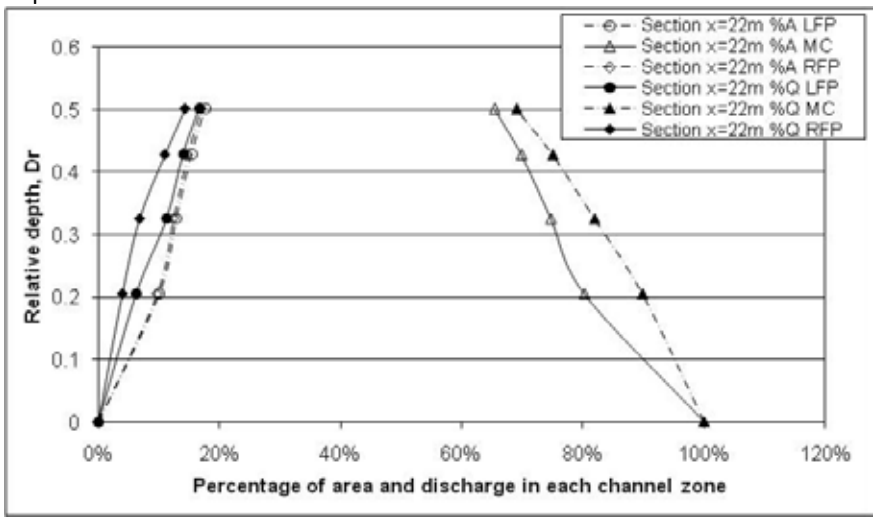

Figure 8.15c-Percentage of area and discharge at section x=22m for each flow depth

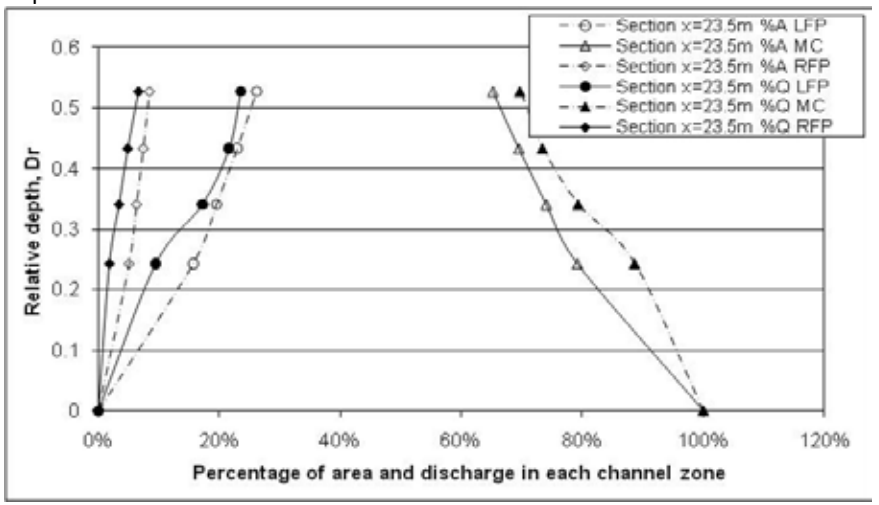

Figure 8.15d-Percentage of area and discharge at section x=23.5m for each flow depth

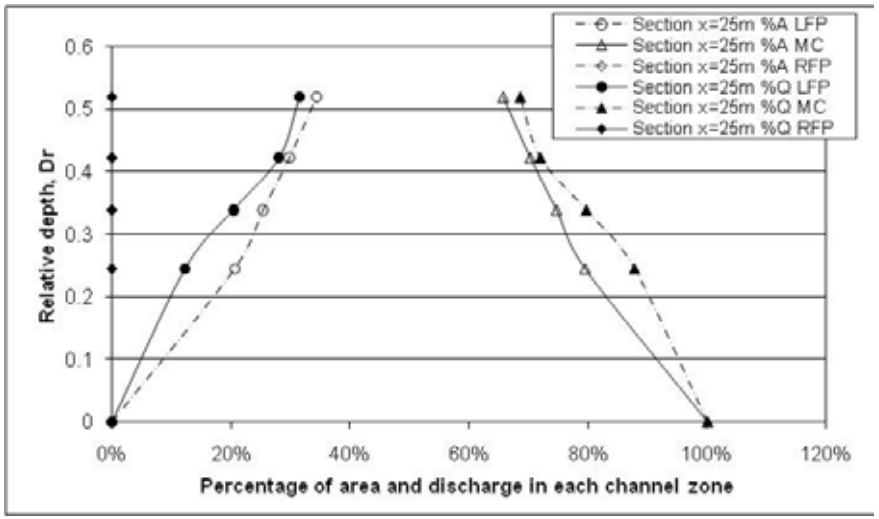

Figure 8.15e-Percentage of area and discharge at section x=26m for each flow depth

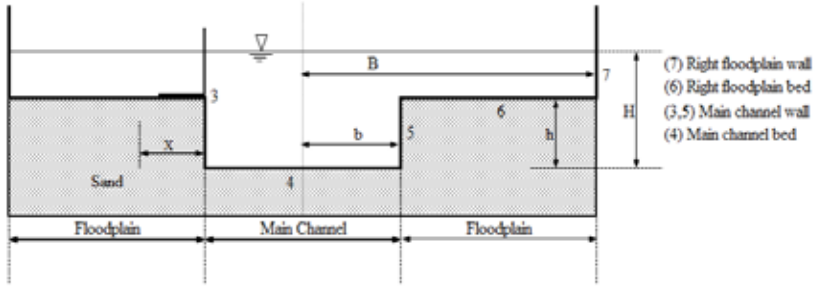

Figure 8.16a-Typical cross-section of skewed channel with isolated left hand floodplain (adapted from Rezaei, 2006)

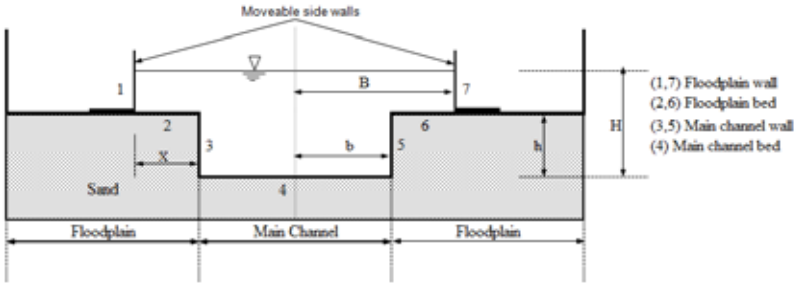

Figure 8.16b -Typical cross-section of skewed channel with isolated left hand floodplain (from Rezaei, 2006)

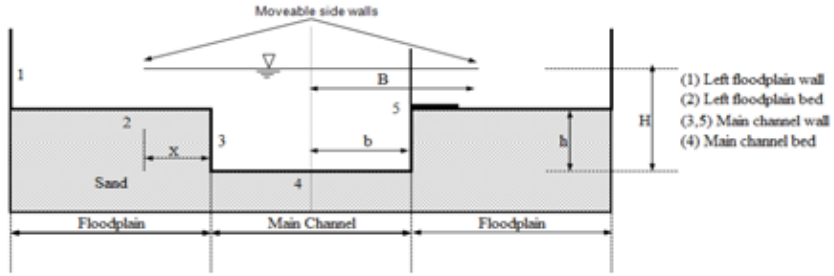

Figure 8.16c -Typical cross-section of skewed channel with isolated right hand floodplain (from Rezaei, 2006)

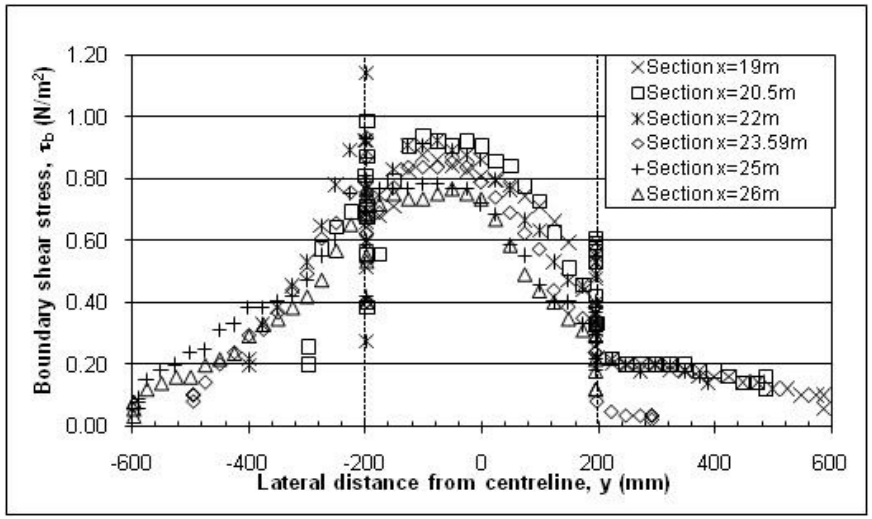

Figure 8.17a-Boundary shear stress distribution for Dr=0.205, Q=16.2ℓ/s

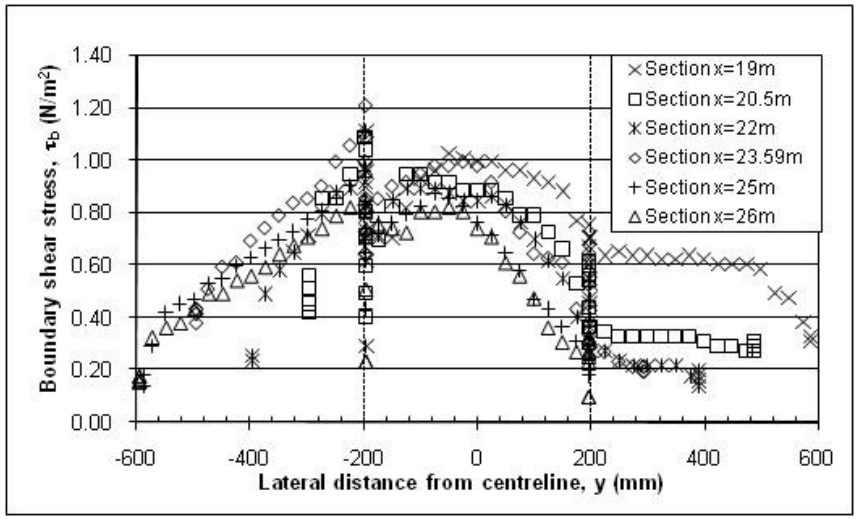

Figure 8.17b-Boundary shear stress distribution for Dr=0.313, Q=21.4ℓ/s

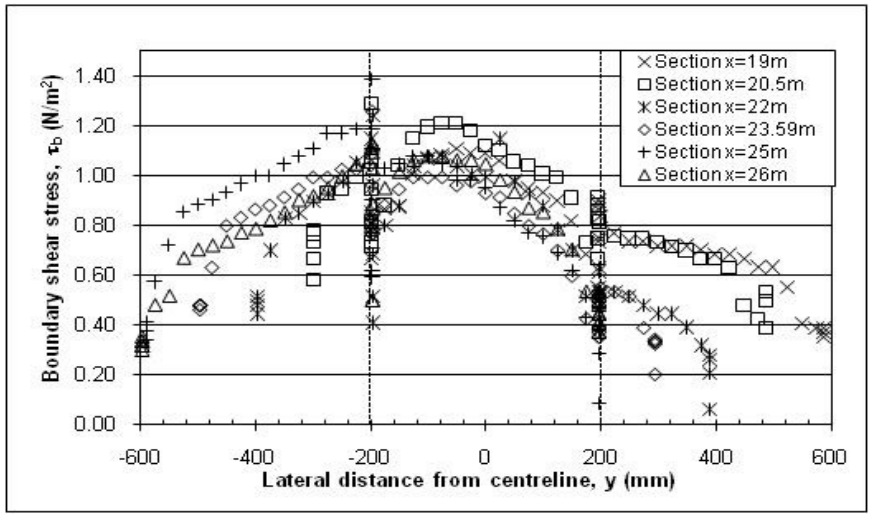

Figure 8.17c-Boundary shear stress distribution for Dr=0.415, Q=29.6ℓ/s

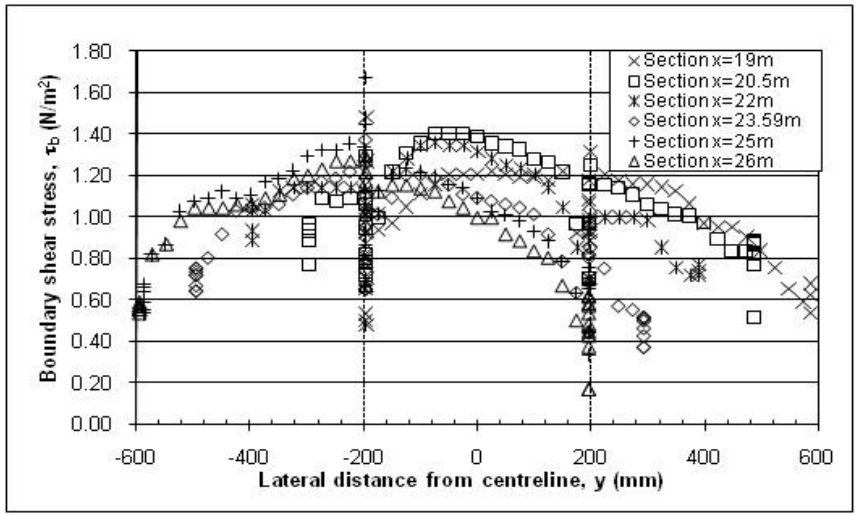

Figure 8.17d-Boundary shear stress distribution for Dr=0.514, Q=43.4ℓ/s

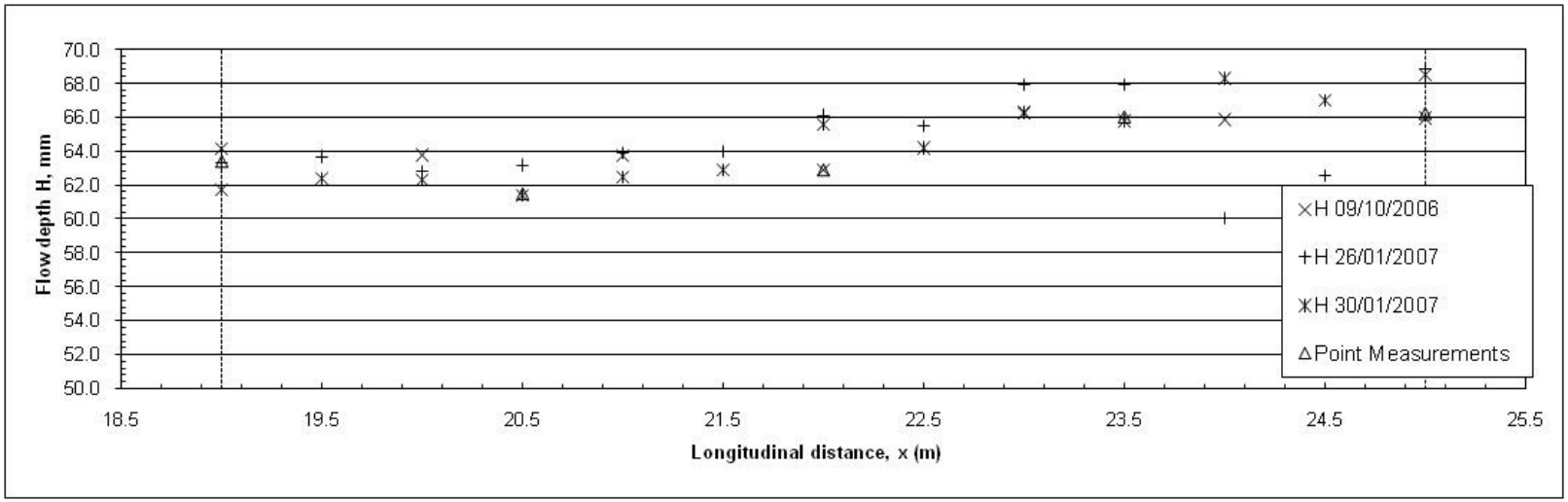

Figure 8.18a-Flow depth for skewed channel with Dr=0.205, Q=16.2ℓ/s

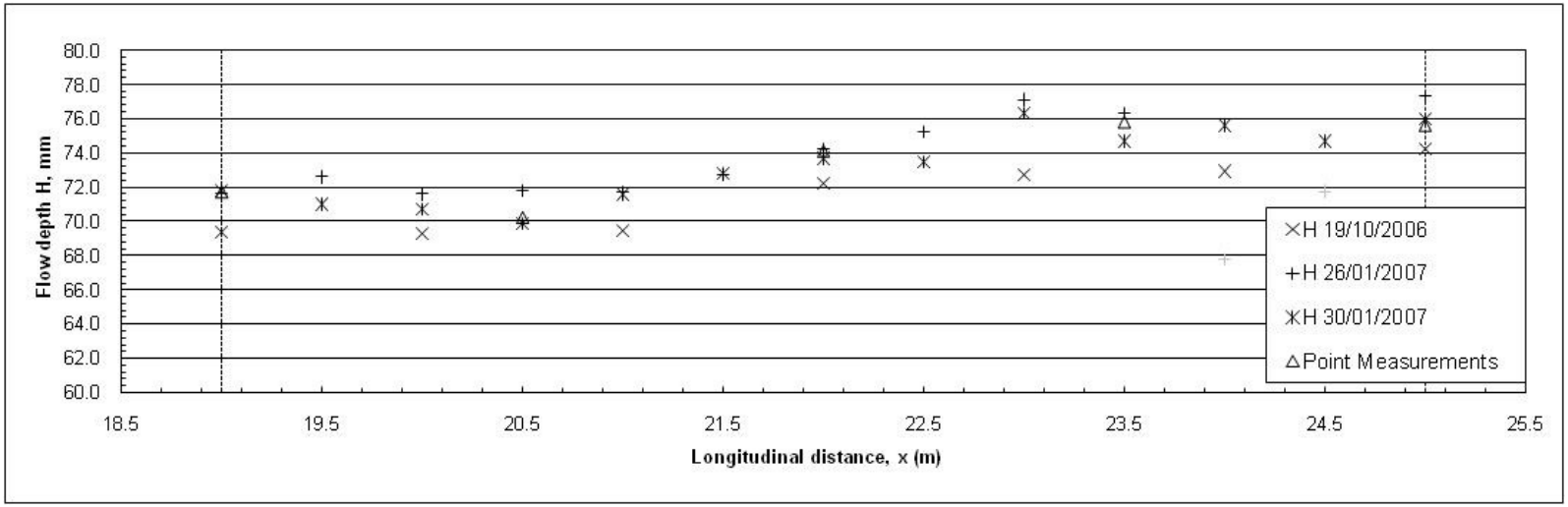

Figure 8.18b-Flow depth for skewed channel with Dr=0.313, Q=21.4ℓ/s

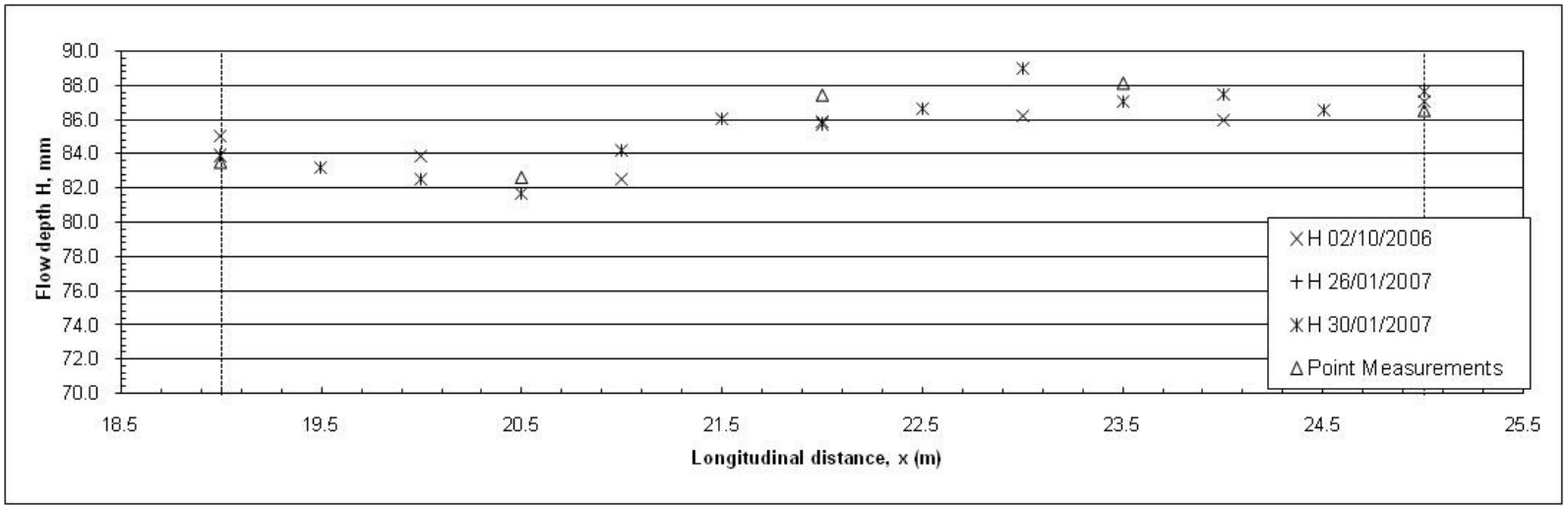

Figure 8.18c-Flow depth for skewed channel with Dr=0.415, Q=29.6ℓ/s

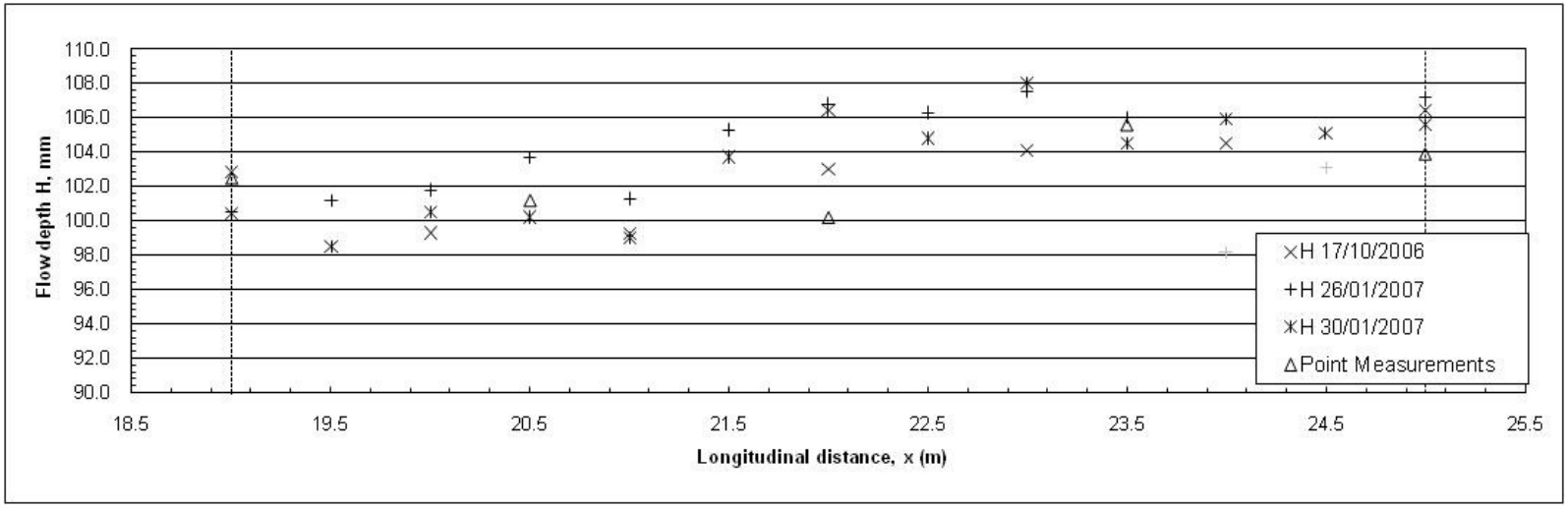

Figure 8.18d-Flow depth for skewed channel with Dr=0.514, Q=43.4ℓ/s

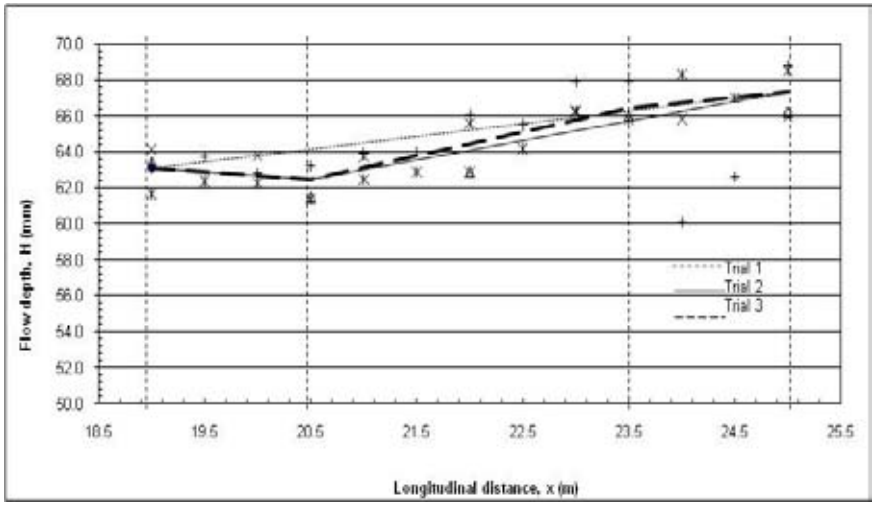

Figure 8.19a-Representation of water surface slope using three methods of estimation Dr=0.205, Q=16.2ℓ/s

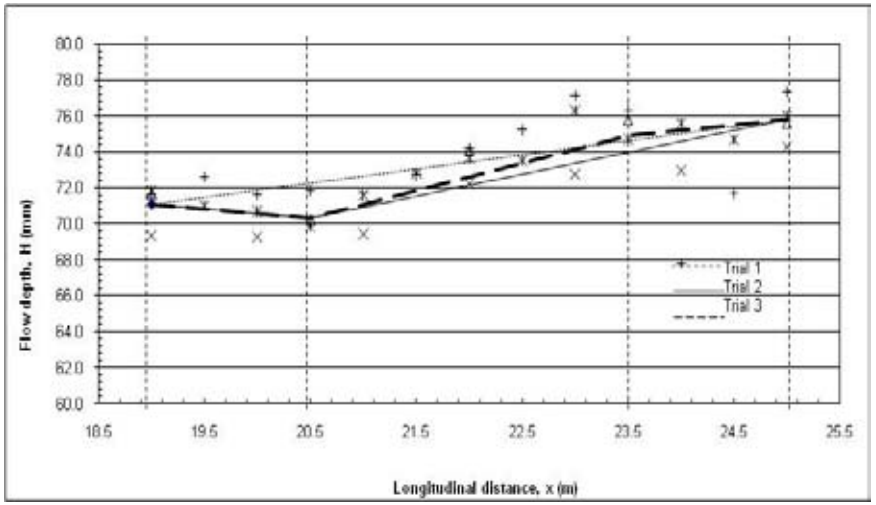

Figure 8.19b-Representation of water surface slope using three methods of estimation Dr=0.313, Q=21.4ℓ/s

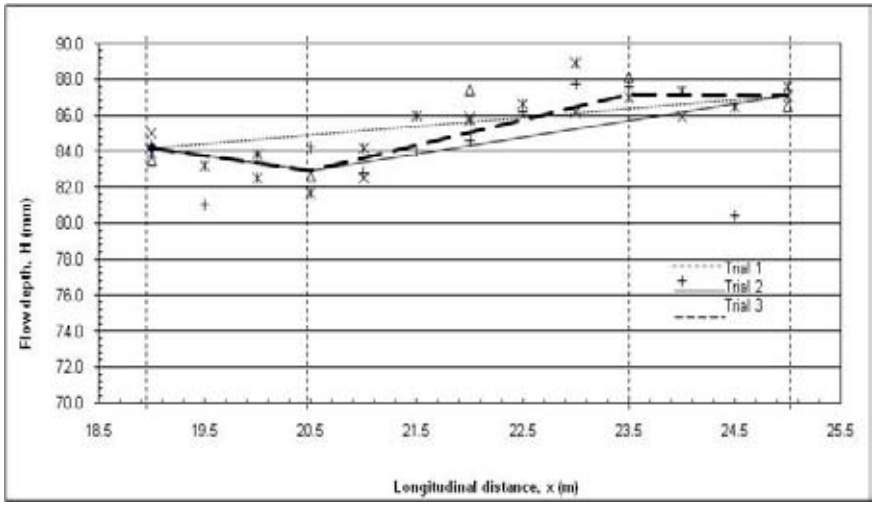

Figure 8.19c-Representation of water surface slope using three methods of estimation Dr=0.415, Q=29.6ℓ/s

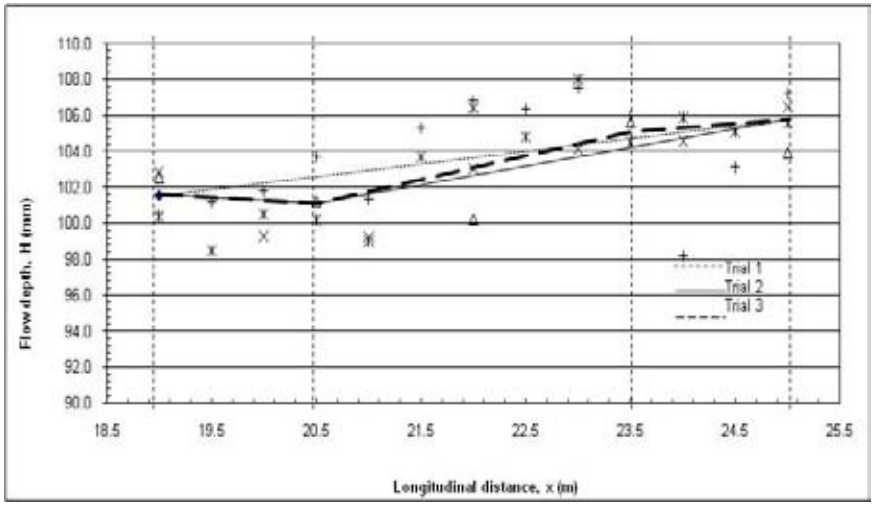

Figure 8.19d-Representation of water surface slope using three methods of estimation Dr=0.515, Q=43.4ℓ/s

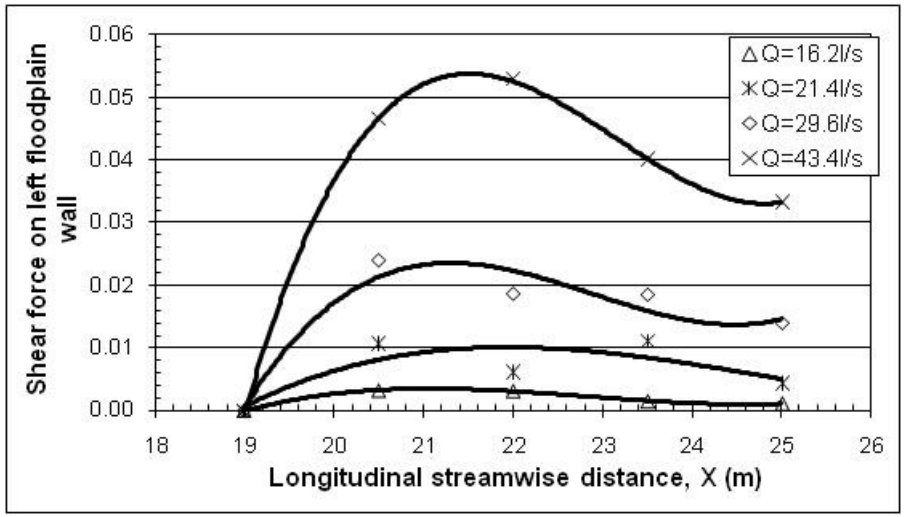

Figure 8.20a-Shear force on left floodplain wall

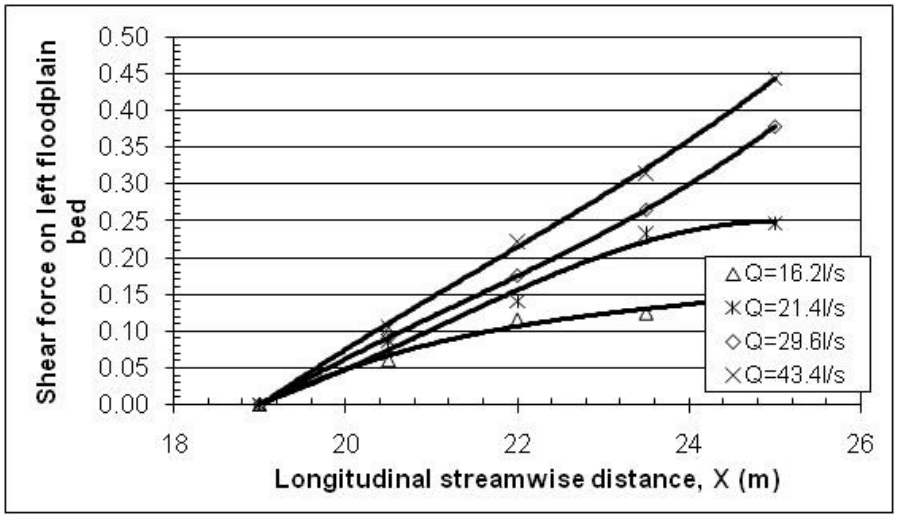

Figure 8.20b-Shear force on left floodplain bed

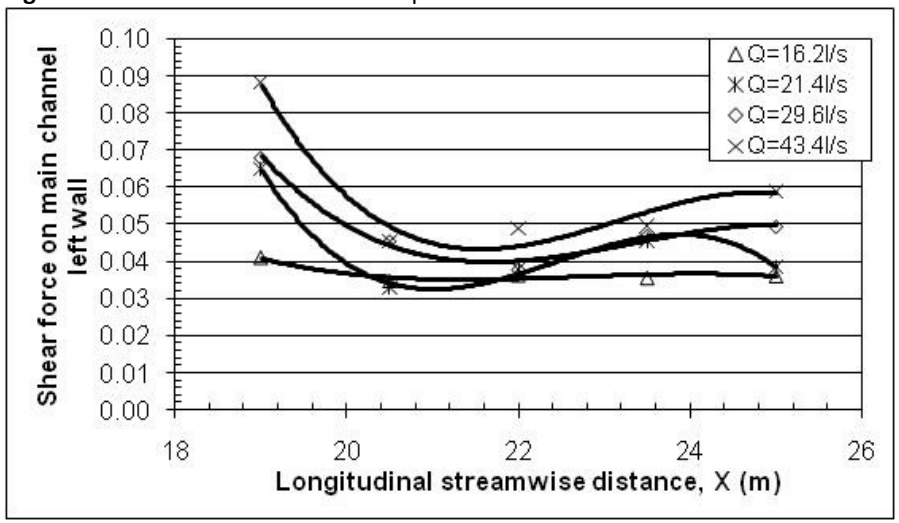

Figure 8.20c-Shear force on main channel left wall

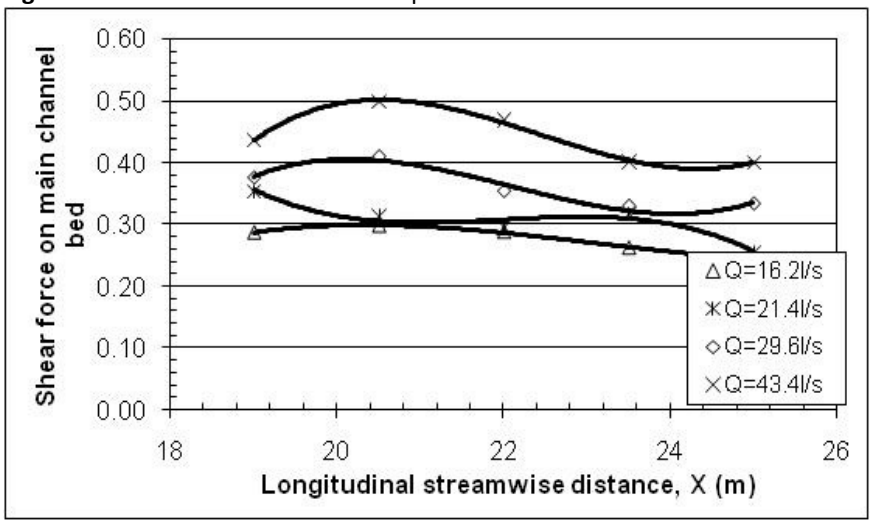

Figure 8.20d-Shear force on main channel bed

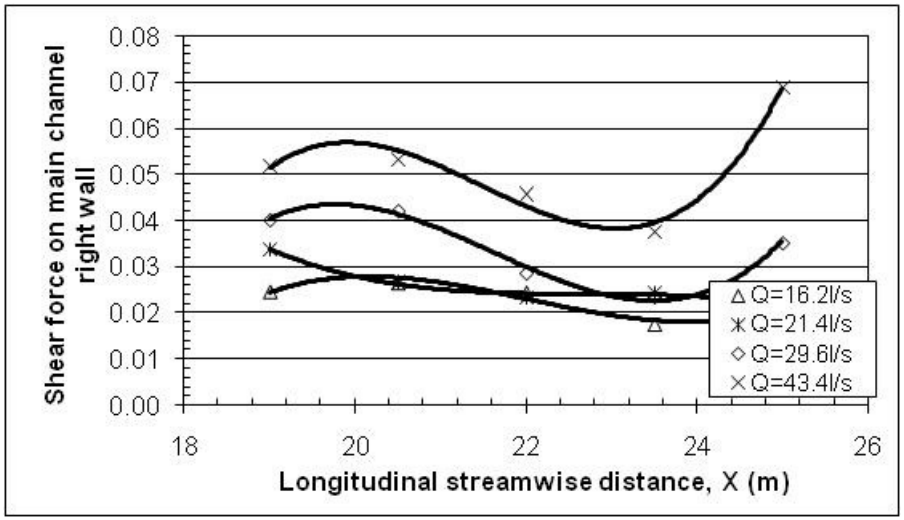

Figure 8.20e-Shear force on main channel right wall

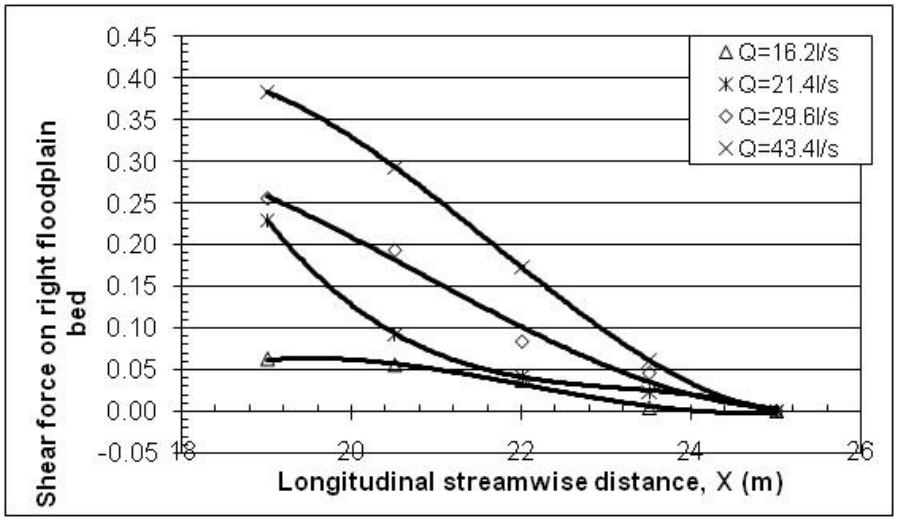

Figure 8.20f-Shear force on right floodplain bed

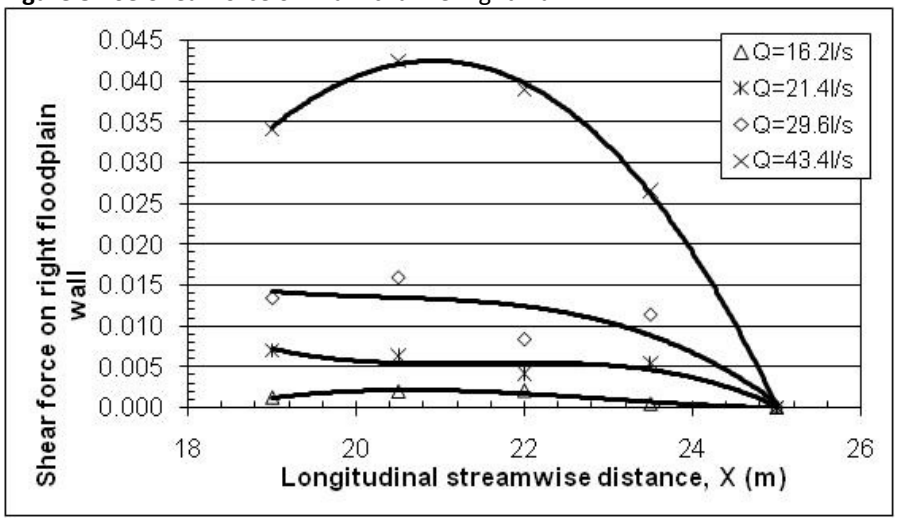

Figure 8.20g-Shear force on right floodplain wall

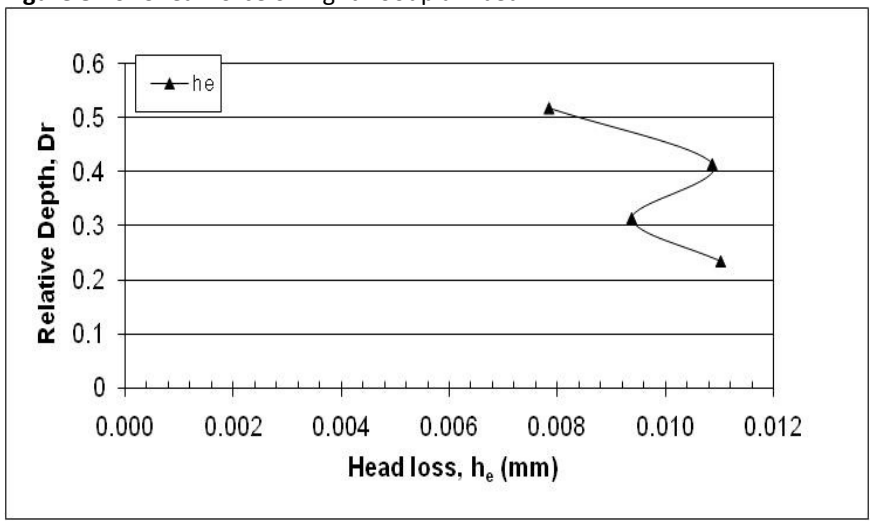

Figure 8.21-Head losses against relative depth

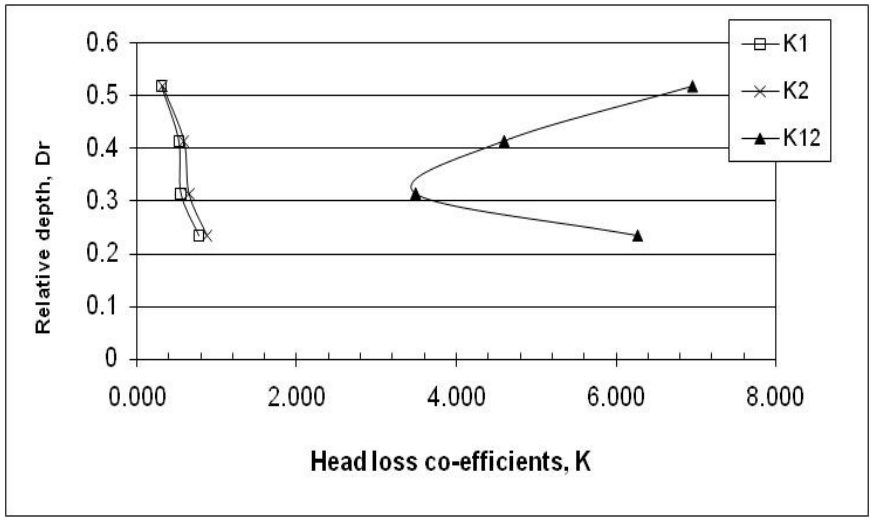

Figure 8.22-Head loss coefficients against relative depth

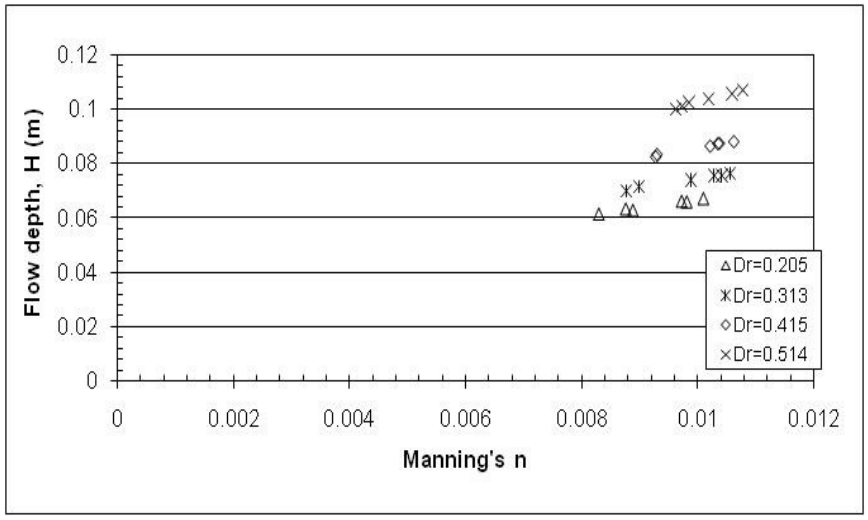

Figure 8.23-Global Manning's *n*~flow depth relationship for skew floodplain of different depths

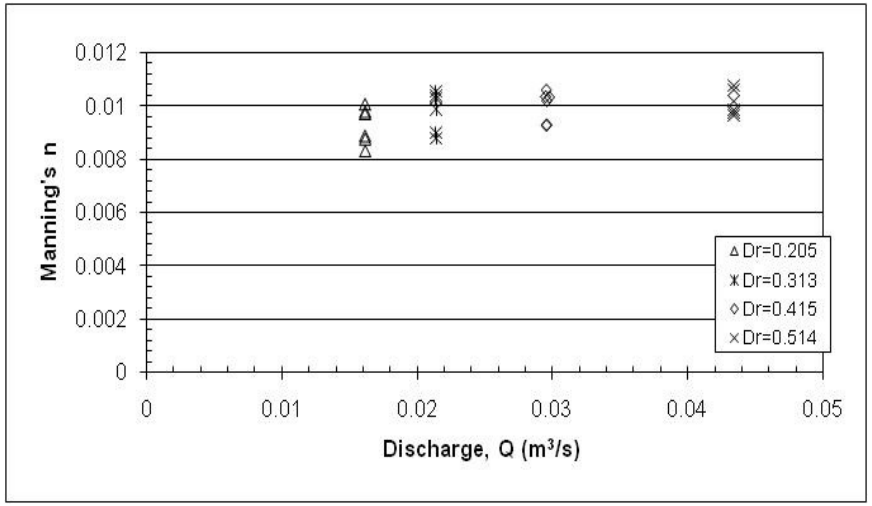

Figure 8.24-Global Manning's *n*~discharge relationship for skew floodplain of different depths

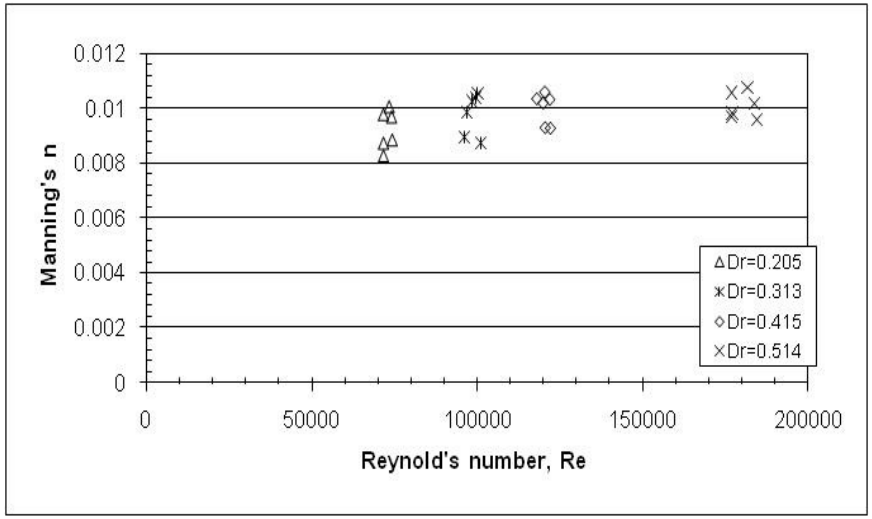

Figure 8.25-Global Manning's *n*~Reynold's number relationship for skew floodplain of different depths

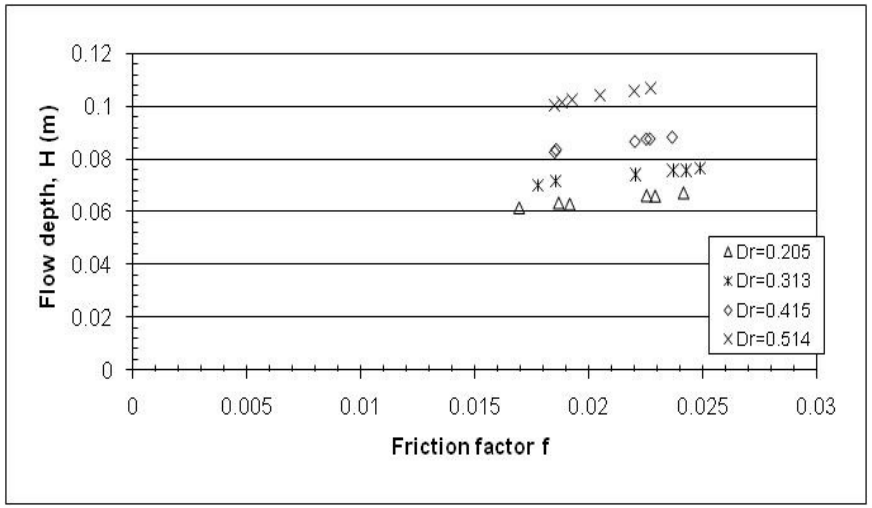

Figure 8.26-Global friction factor *f*~flow depth relationship for skew floodplain of different depths

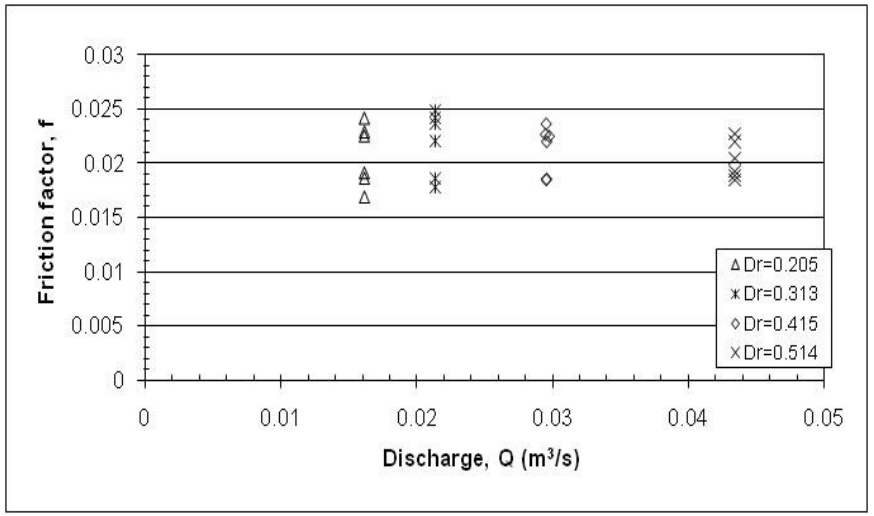

Figure 8.27-Global friction factor *f*~discharge relationship for skew floodplain of different depths

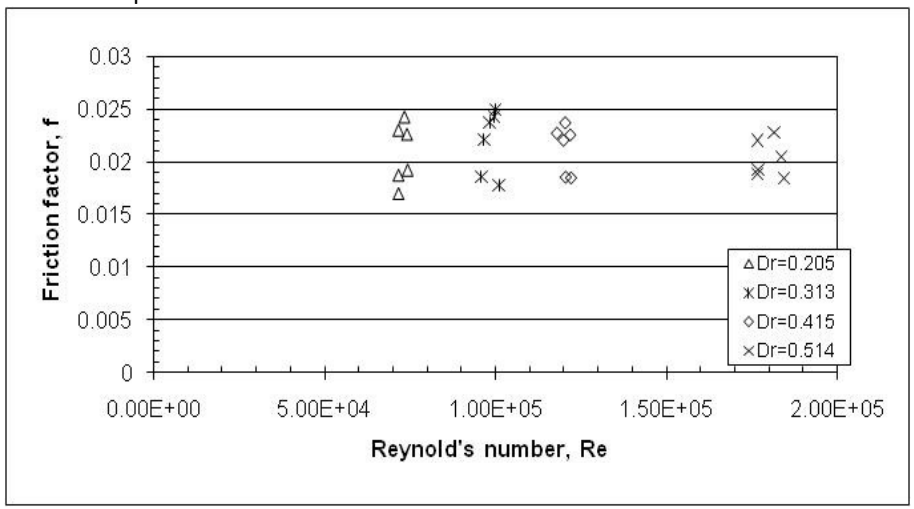

Figure 8.28-Global friction factor *f*~Reynold's number relationship for skew floodplain of different depths

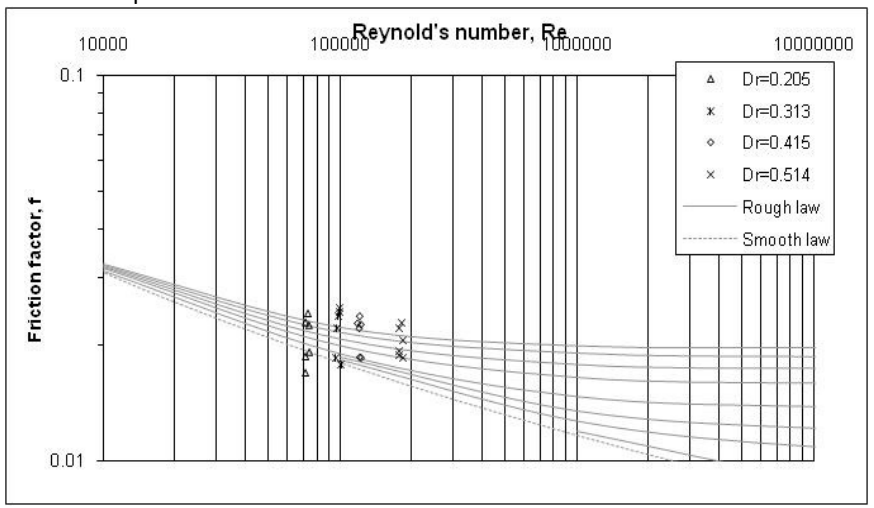

Figure 8.29-Global friction factor *f*~Reynolds number (Moody Diagram) for skew channel rough law

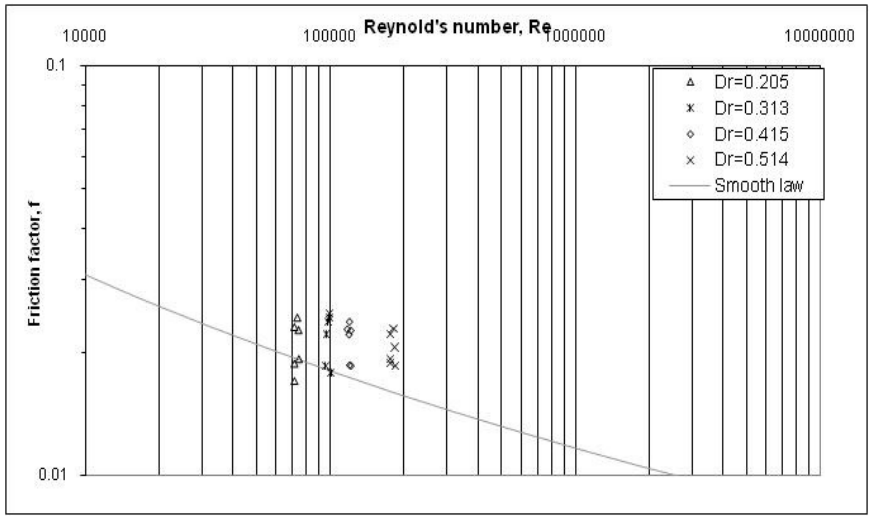

Figure 8.30-Global friction factor *f*~Reynolds number (Moody Diagram) for skew channel smooth law

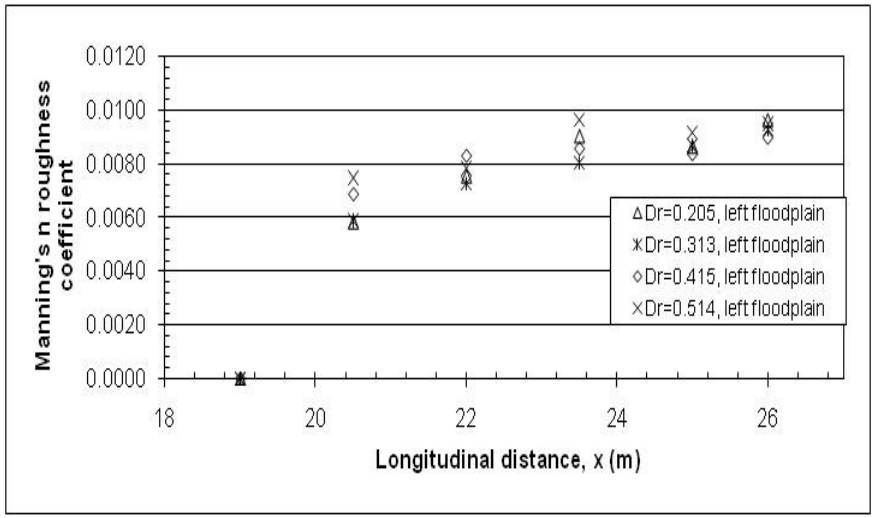

Figure 8.31a-Zonal Manning's *n* roughness for left floodplain along length of channel

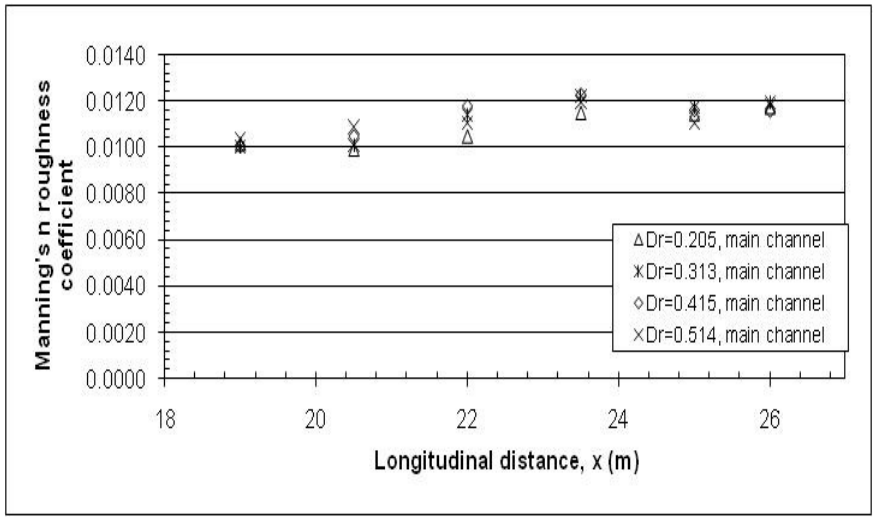

Figure 8.31b-Zonal Manning's *n* roughness for main channel along length of channel

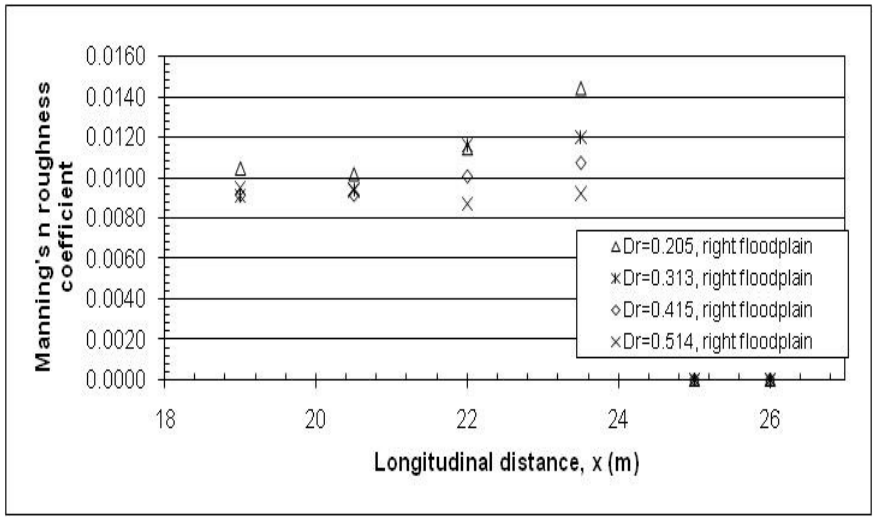

Figure 8.31c-Zonal Manning's *n* roughness for right floodplain along length of channel

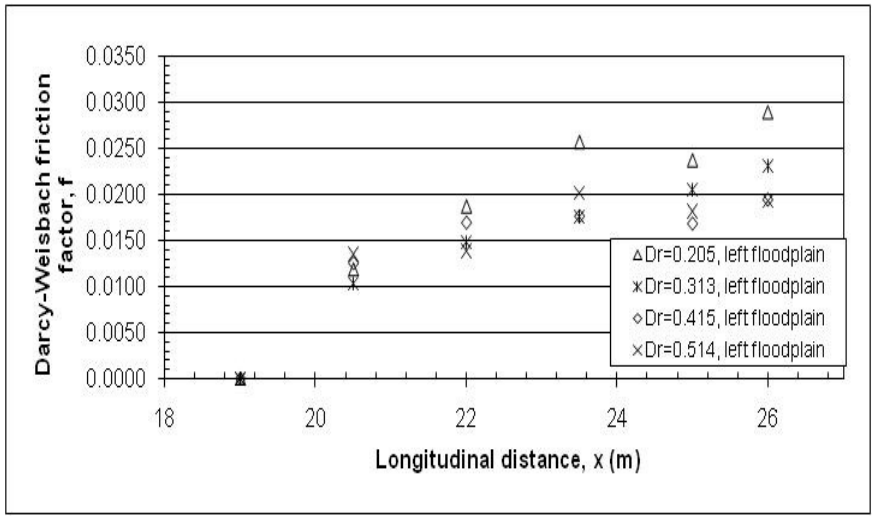

Figure 8.32a-Zonal Darcy-Weisbach friction factor, *f*, for left floodplain along length of channel

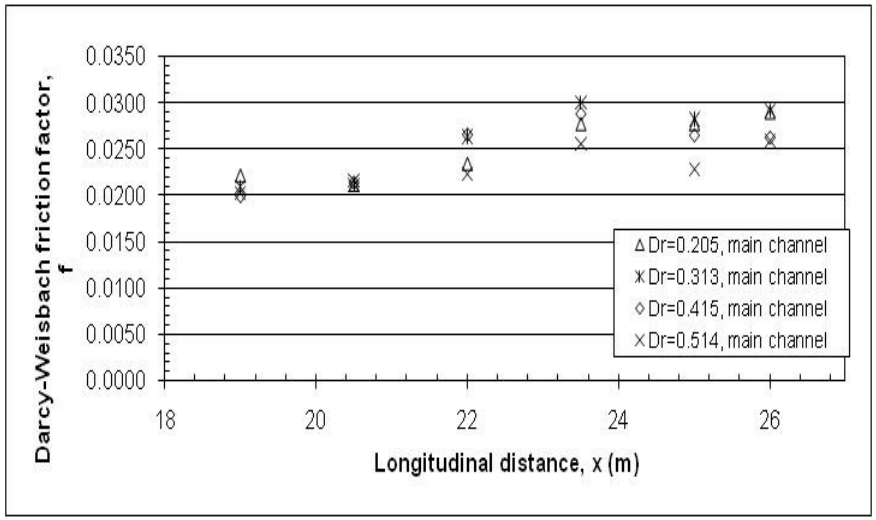

Figure 8.32b-Zonal Darcy-Weisbach friction factor, *f*, for main channel along length of channel

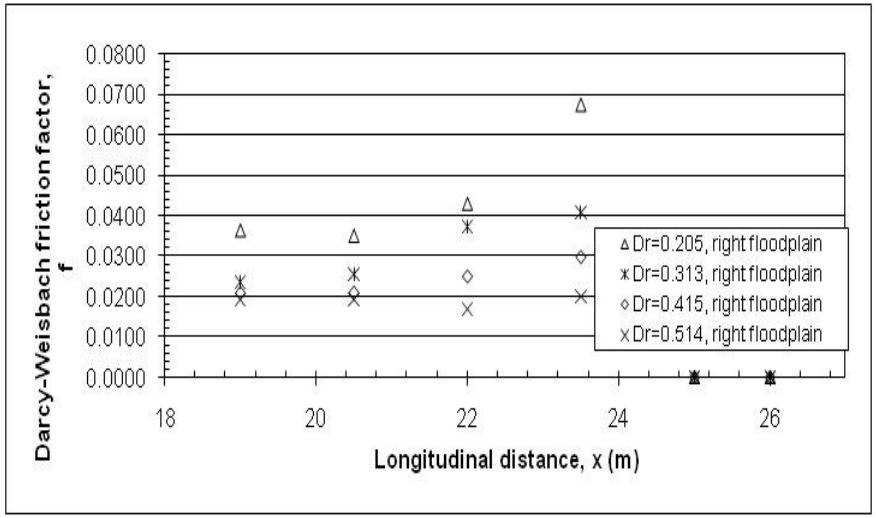

Figure 8.32c-Zonal Darcy-Weisbach friction factor, *f*, for right floodplain along length of channel

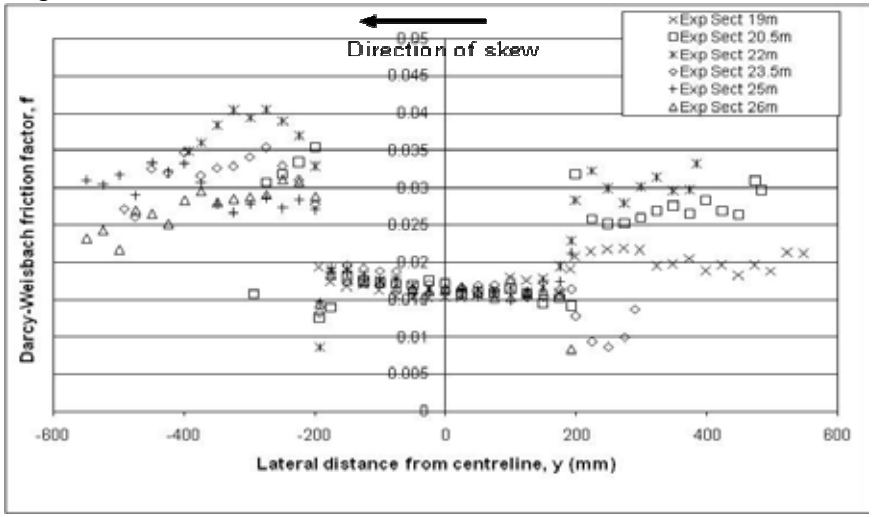

Figure 8.33a-Lateral distributions of local Darcy-Weisbach friction factor, *f*, for Q=16.2ℓ/s, Dr=0.205

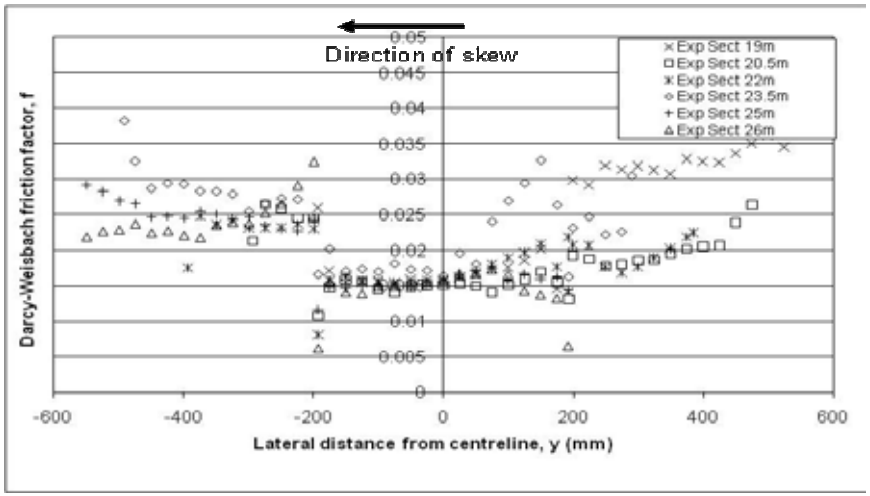

Figure 8.33b-Lateral distributions of local Darcy-Weisbach friction factor, *f*, for Q=21.4ℓ/s, Dr=0.313

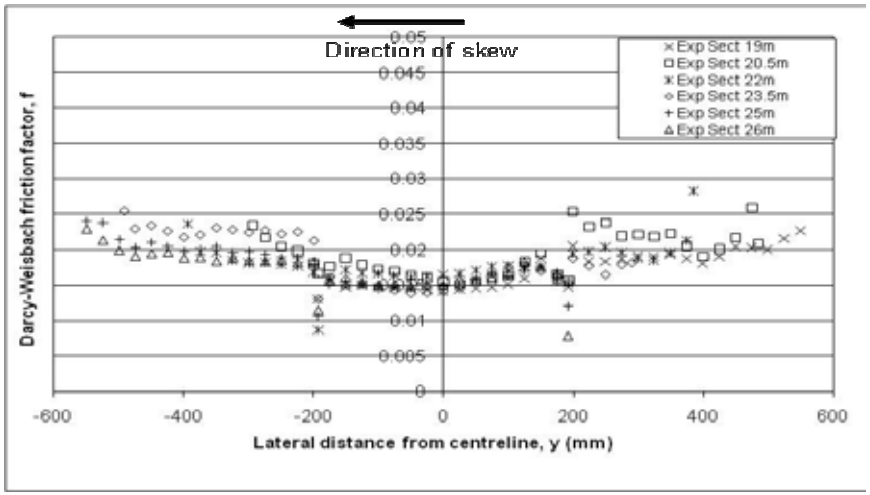

Figure 8.33d-Lateral distributions of local Darcy-Weisbach friction factor, *f*, for Q=43.4ℓ/s, Dr=0.514

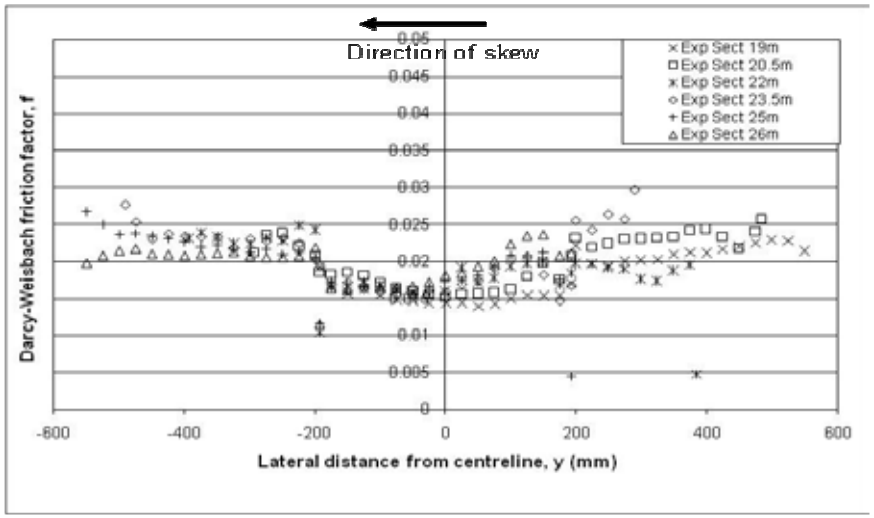

Figure 8.33c-Lateral distributions of local Darcy-Weisbach friction factor, *f*, for Q=29.6ℓ/s, Dr=0.415

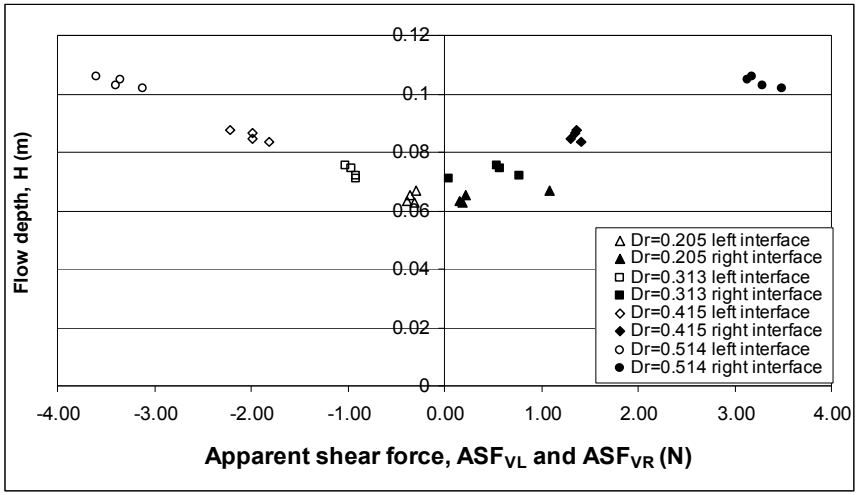

Figure 8.34-Vertical apparent shear force on left and right floodplain/main channel interface against depth

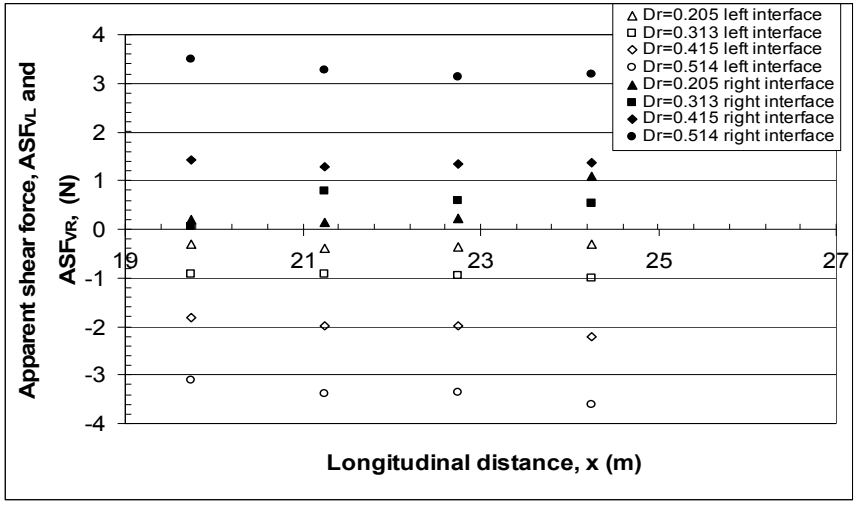

Figure 8.35-Vertical apparent shear force on left and right floodplain/main channel interface along length of the channel

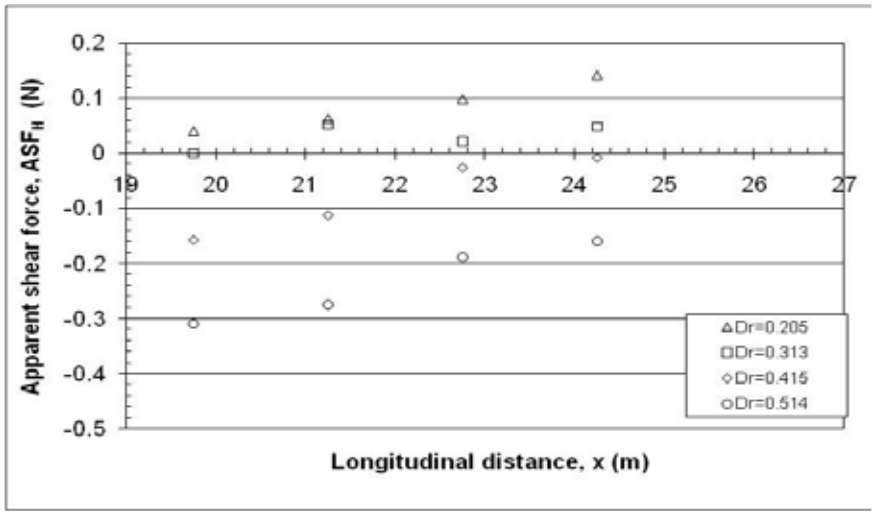

Figure 8.36-Horizontal apparent shear force on interface of the upper and lower main channel

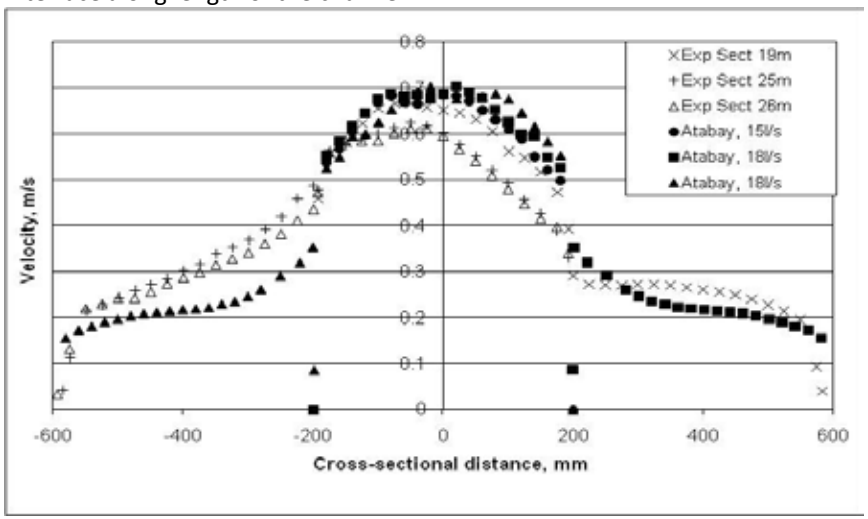

Figure 8.37a-Lateral distributions of streamwise depth-averaged velocity compared to Atabay, 2001 comparison of skewed data (16.2ℓ/s) to asymmetric data (15ℓ/s and 18.8ℓ/s)

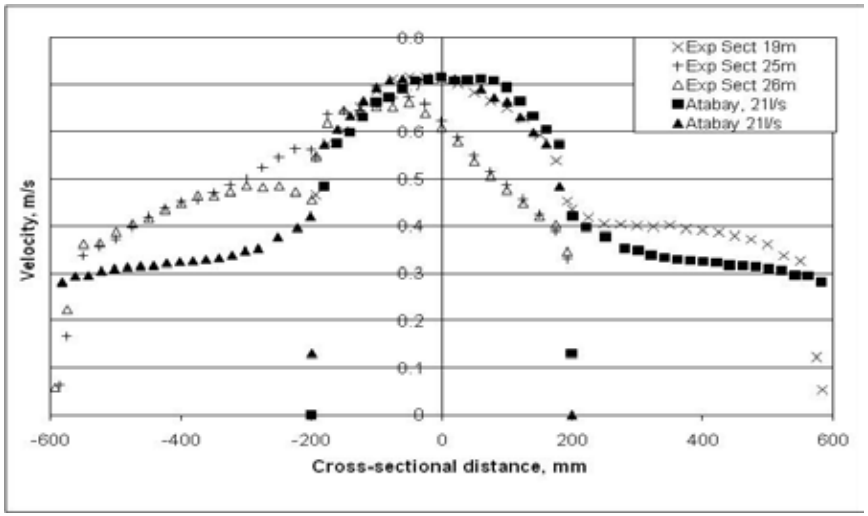

Figure 8.37b-Lateral distributions of streamwise depth-averaged velocity compared to Atabay, 2001 comparison of skewed data (21.4ℓ/s) to asymmetric data (21ℓ/s)

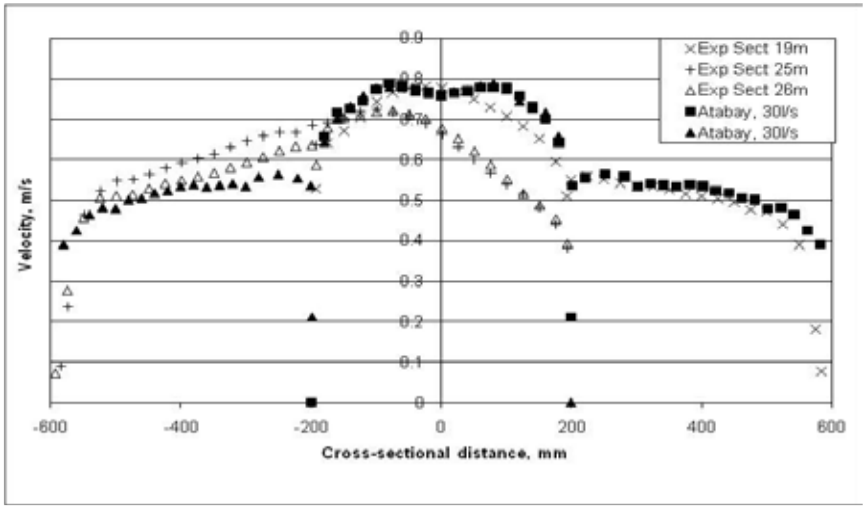

Figure 8.37c-Lateral distributions of streamwise depth-averaged velocity compared to Atabay, 2001 comparison of skewed data (29.6ℓ/s) to asymmetric data (30.1ℓ/s)

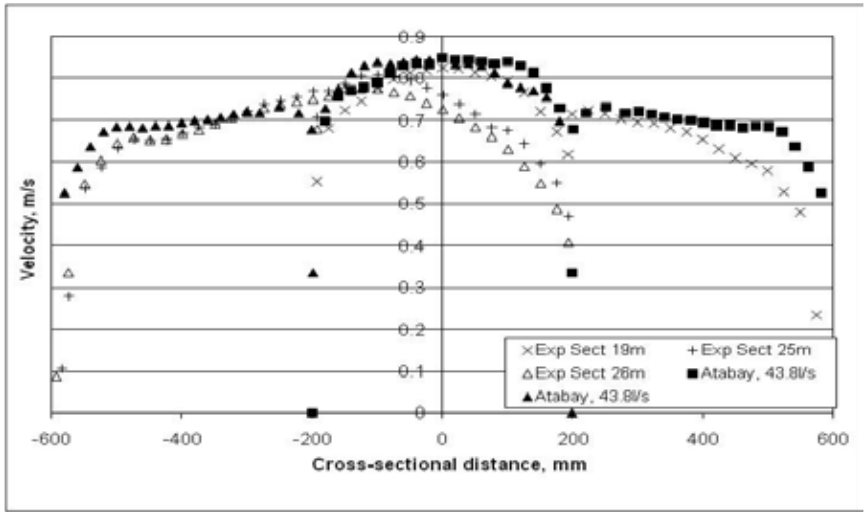

Figure 8.37d-Lateral distributions of streamwise depth-averaged velocity compared to Atabay, 2001 comparison of skewed data (43.4ℓ/s) to asymmetric data (43.8ℓ/s)

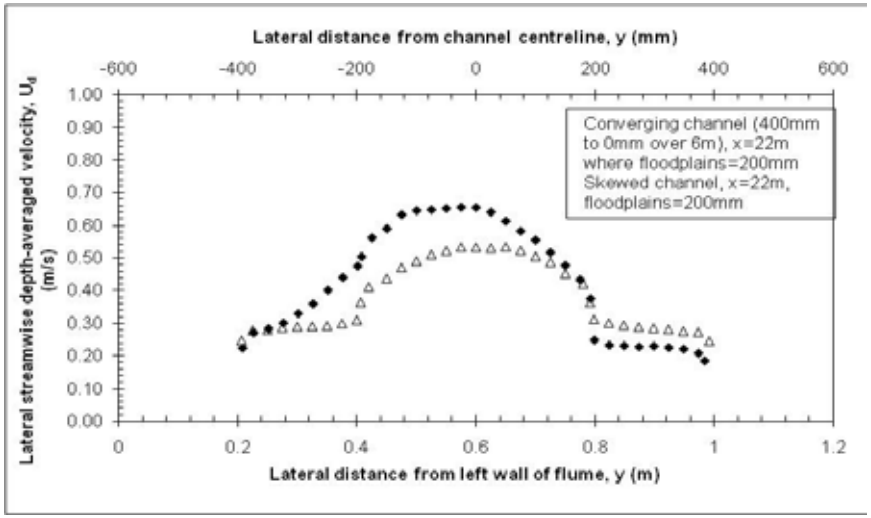

Figure 8.38a-Lateral distributions of streamwise depth-averaged velocity compared to Rezaei, 2006 comparison of skewed data (16.2ℓ/s) to converging data (16.4ℓ/s)

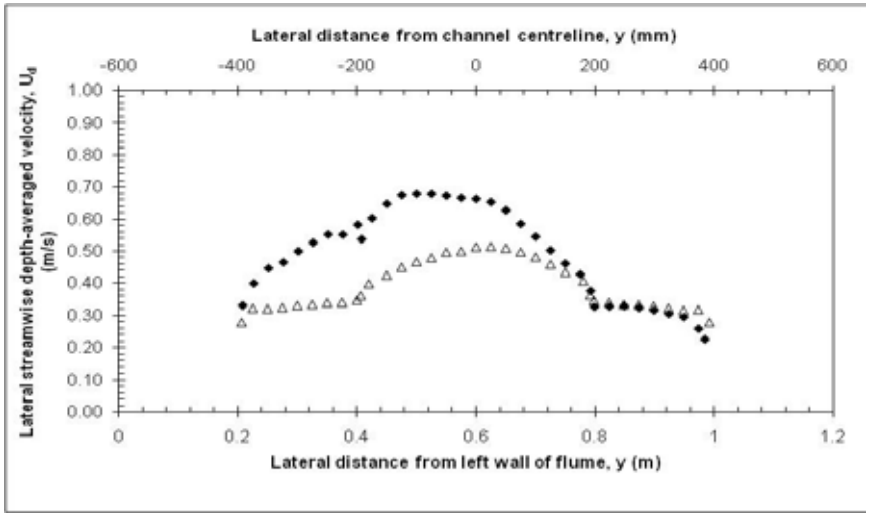

Figure 8.38b-Lateral distributions of streamwise depth-averaged velocity compared to Rezaei, 2006 comparison of skewed data (21.4ℓ/s) to converging data (19.8ℓ/s)

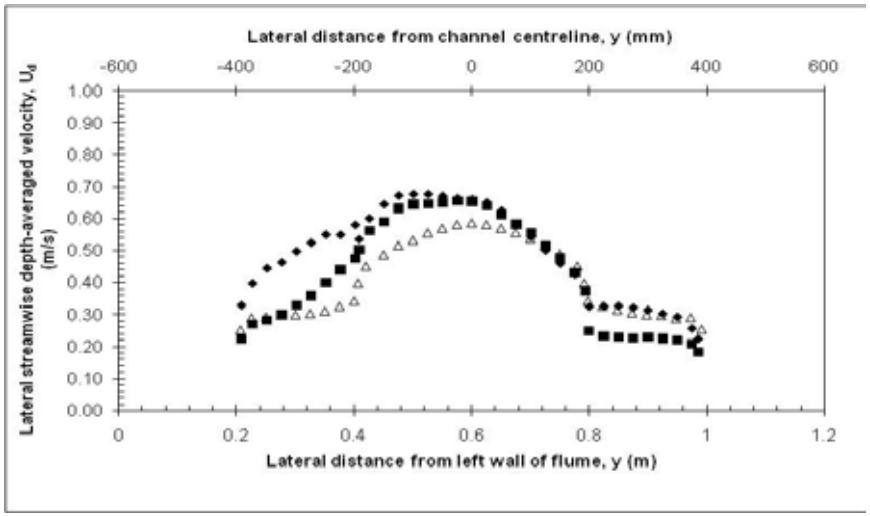

Figure 8.38c-Lateral distributions of streamwise depth-averaged velocity compared to Rezaei, 2006 Comparison of skewed data (16.2ℓ/s and 21.4ℓ/s) to converging data (18ℓ/s)

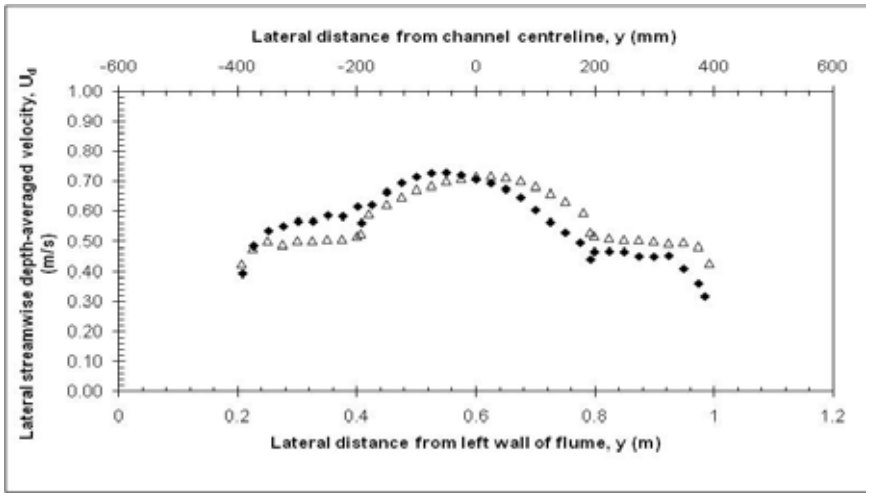

Figure 8.38d-Lateral distributions of streamwise depth-averaged velocity compared to Rezaei, 2006 Comparison of skewed data (29.6ℓ/s) to converging data (27ℓ/s)

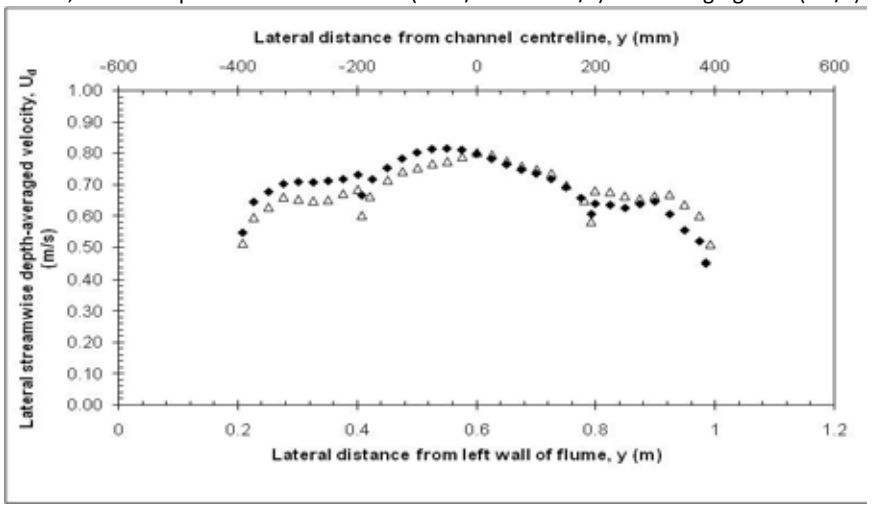

Figure 8.38e-Lateral distributions of streamwise depth-averaged velocity compared to Rezaei, 2006 Comparison of skewed data (43.4ℓ/s) to converging data (40ℓ/s)

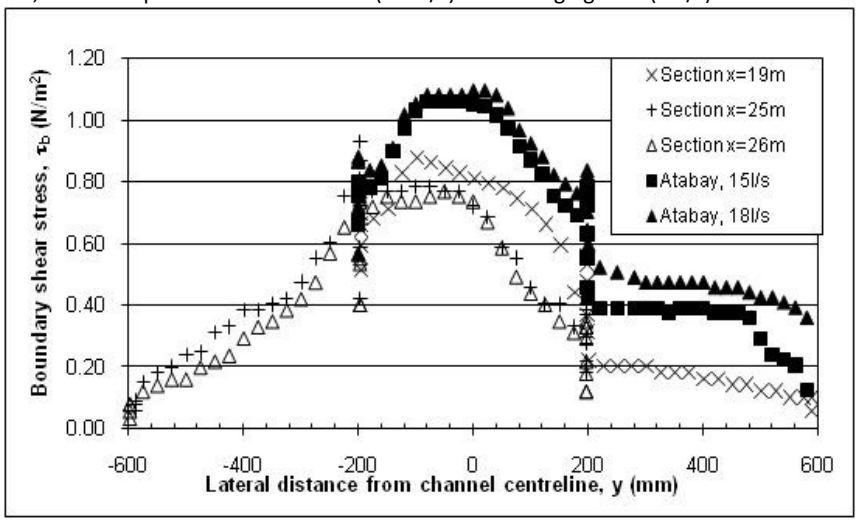

Figure 8.39a-Boundary shear stress distribution for Dr=0.205, Q=16.2ℓ/s Compared to Atabay (2001) asymmetric channel

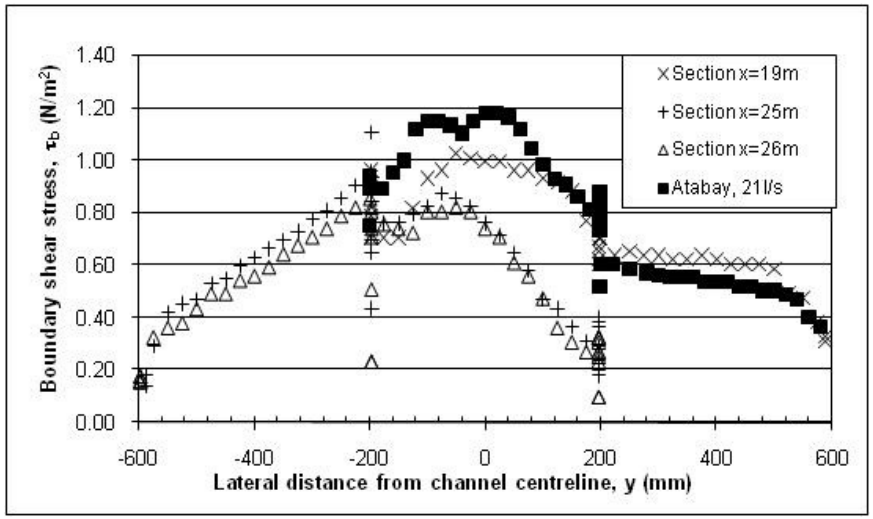

Figure 8.39b-Boundary shear stress distribution for Dr=0.313, Q=21.4ℓ/s Compared to Atabay (2001) asymmetric channel

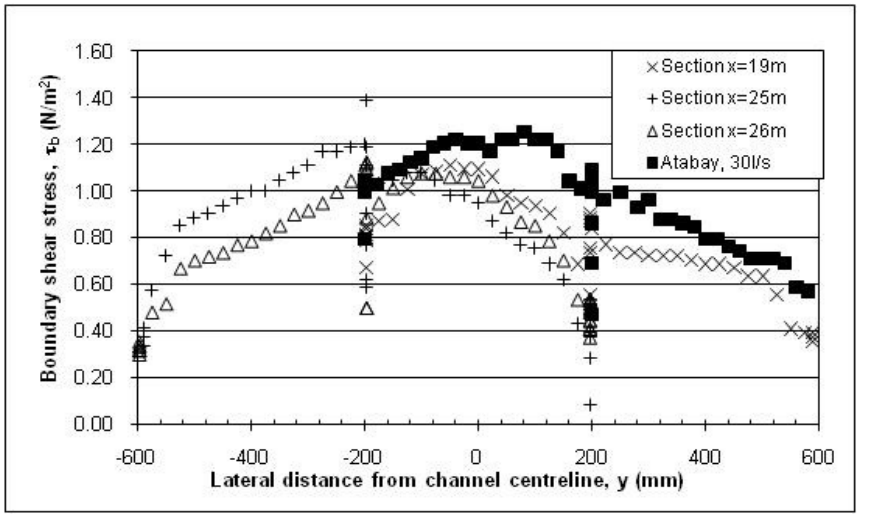

Figure 8.39c-Boundary shear stress distribution for Dr=0.415, Q=29.6ℓ/s Compared to Atabay (2001) asymmetric channel

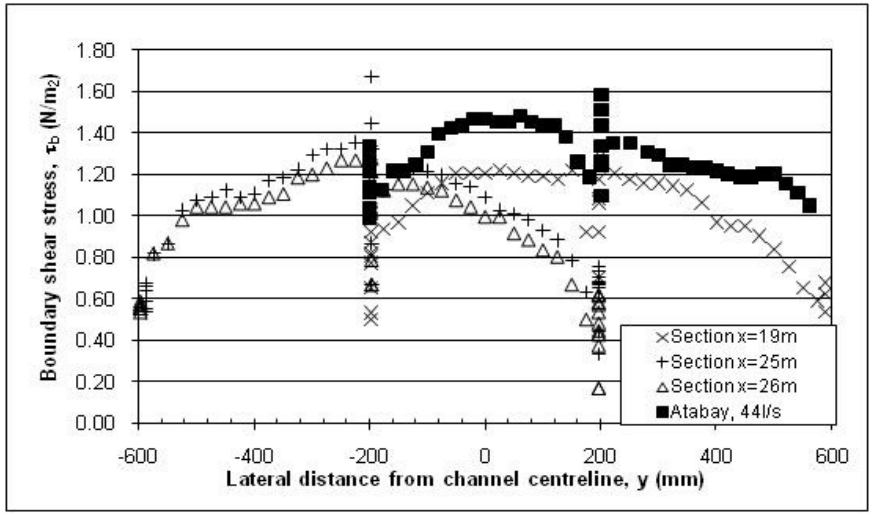

Figure 8.39d-Boundary shear stress distribution for Dr=0.514, Q=43.4ℓ/s Compared to Atabay (2001) asymmetric channel

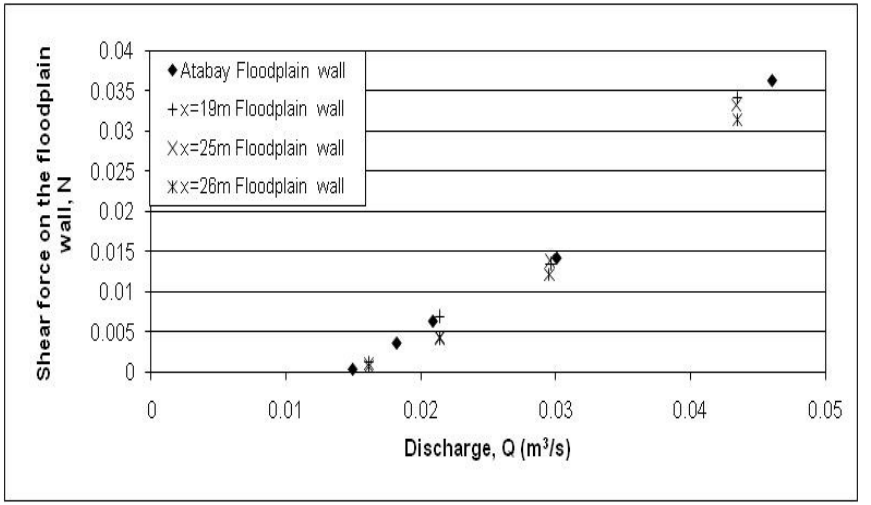

Figure 8.40a-Shear force on the floodplain wall compared to Atabay, 2001

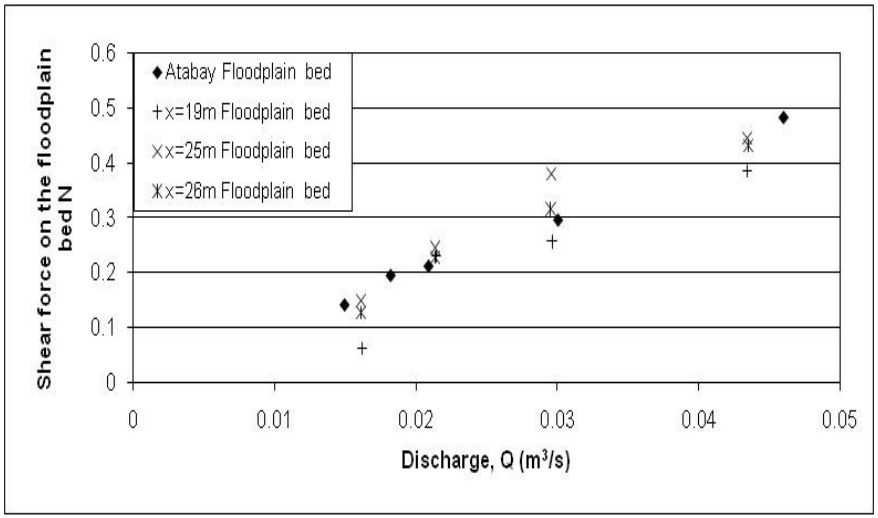

Figure 8.40b-Shear force on the floodplain bed compared to Atabay, 2001

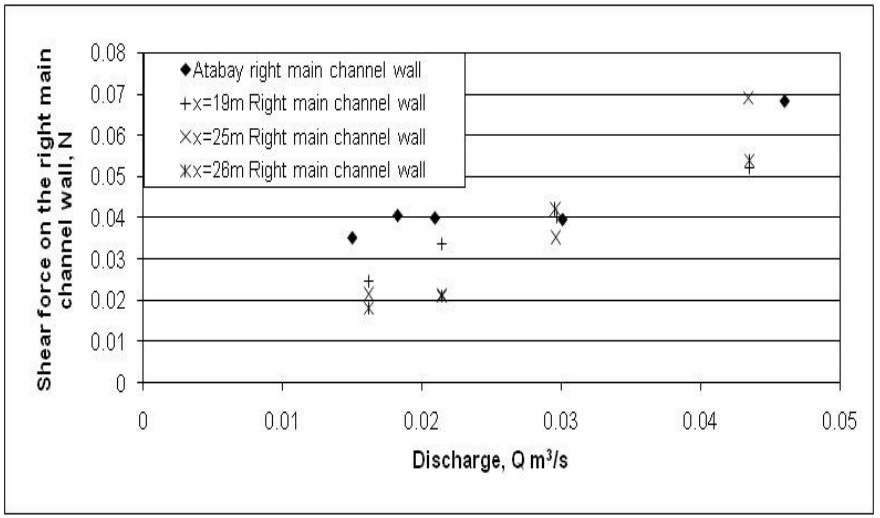

Figure 8.40c-Shear force on the main channel right wall compared to Atabay, 2001

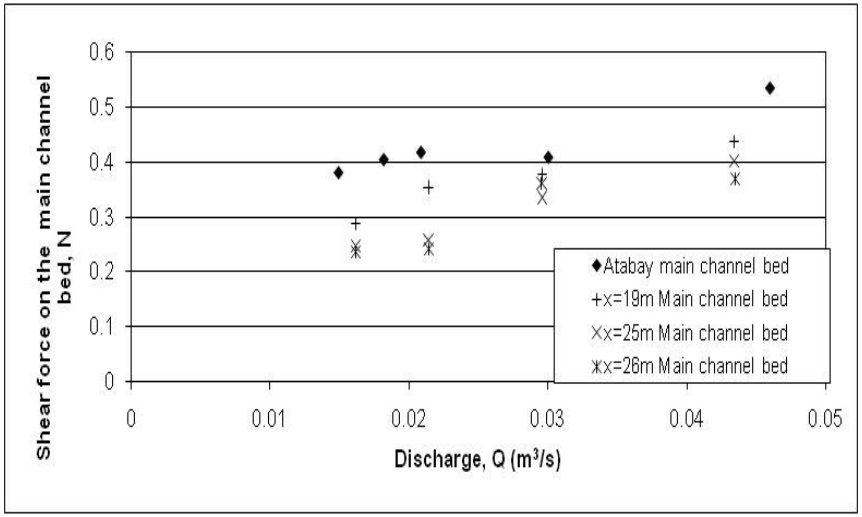

Figure 8.40d-Shear force on the main channel bed compared to Atabay, 2001

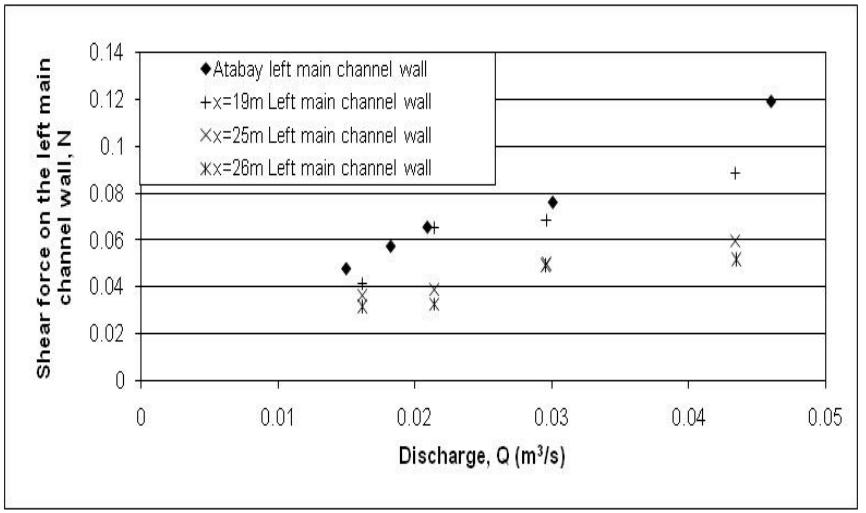

Figure 8.40e-Shear force on the main channel left wall compared to Atabay, 2001

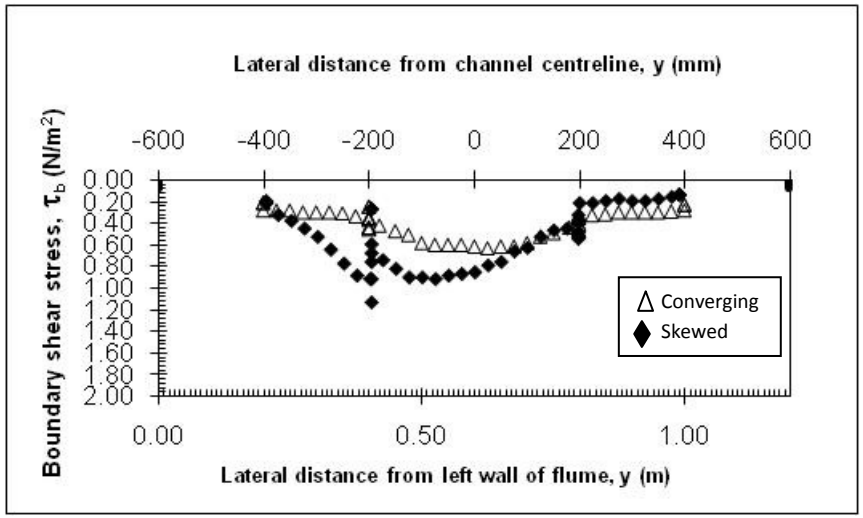

Figure 8.41a-Shear stress distribution for Dr=0.205, Q=16.2ℓ/s Compared to Rezaei (2006) converging channel with 400mm-0mm floodplains, 16.4ℓ/s

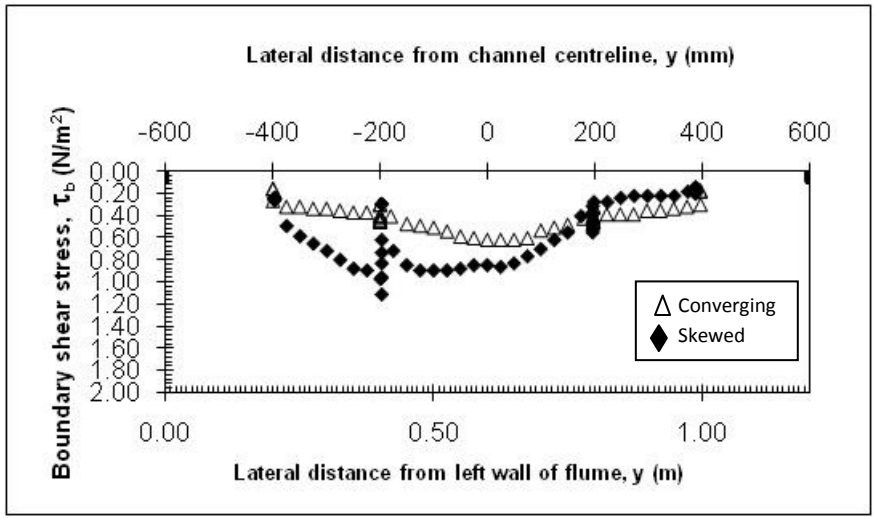

Figure 8.41b-Shear stress distribution for Dr=0.313, Q=21.4ℓ/s Compared to Rezaei (2006) converging channel with 400mm-0mm floodplains, 19.7ℓ/s

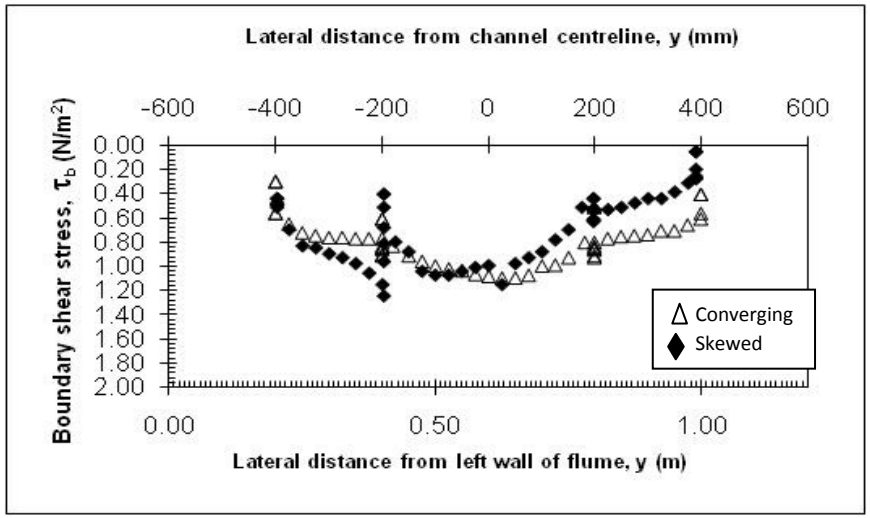

Figure 8.41c-Shear stress distribution for Dr=0.415, Q=29.6ℓ/s Compared to Rezaei (2006) converging channel with 400mm-200mm floodplains, 27ℓ/s

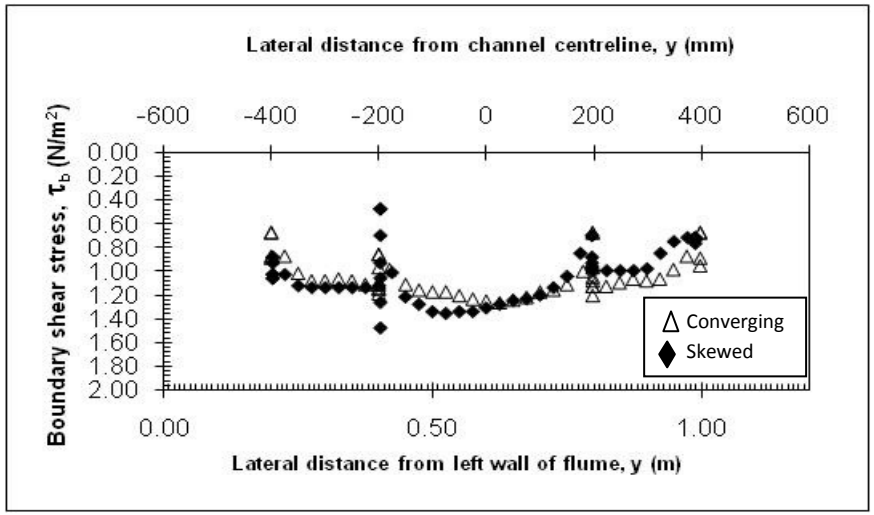

Figure 8.41d-Shear stress distribution for Dr=0.514, Q=43.4ℓ/s Compared to Rezaei (2006) converging channel with 400mm-200mm floodplains, 40ℓ/s

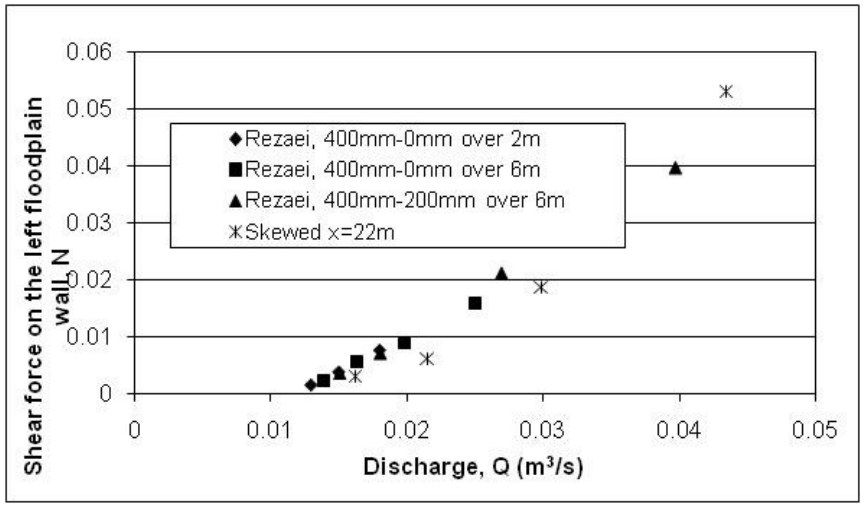

Figure 8.42a-Shear force on the left floodplain wall compared to Rezaei, 2006

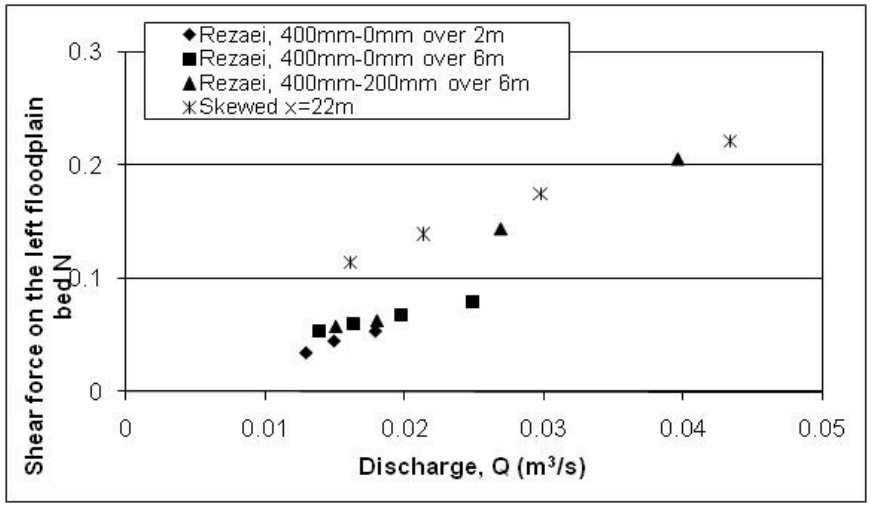

Figure 8.42b-Shear force on the left floodplain bed compared to Rezaei, 2006

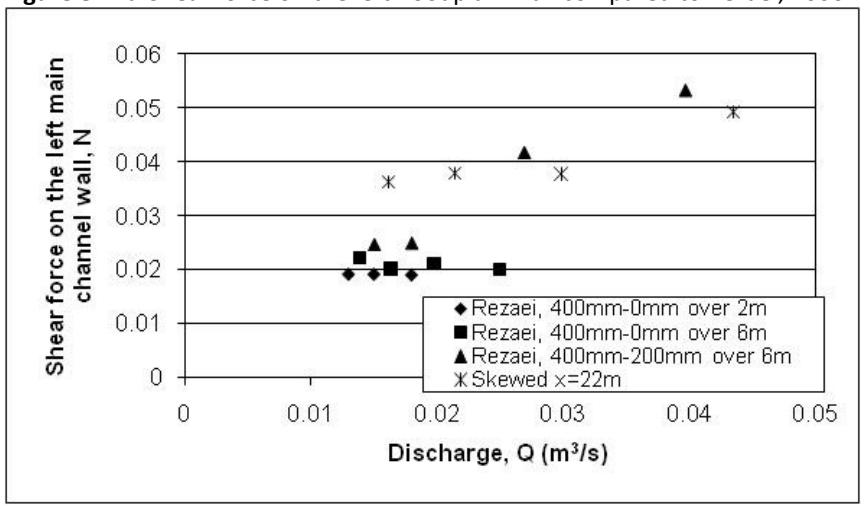

Figure 8.42c-Shear force on the left main channel wall compared to Rezaei, 2006

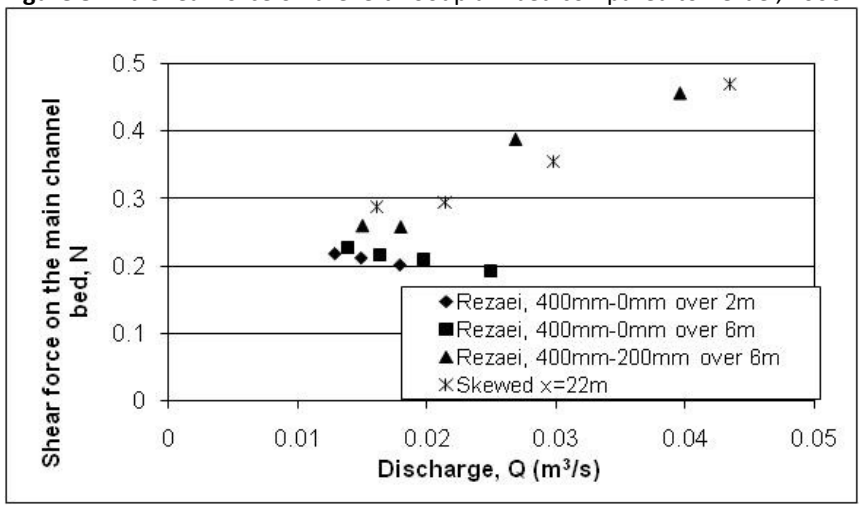

Figure 8.42d-Shear force on the main channel bed compared to Rezaei, 2006

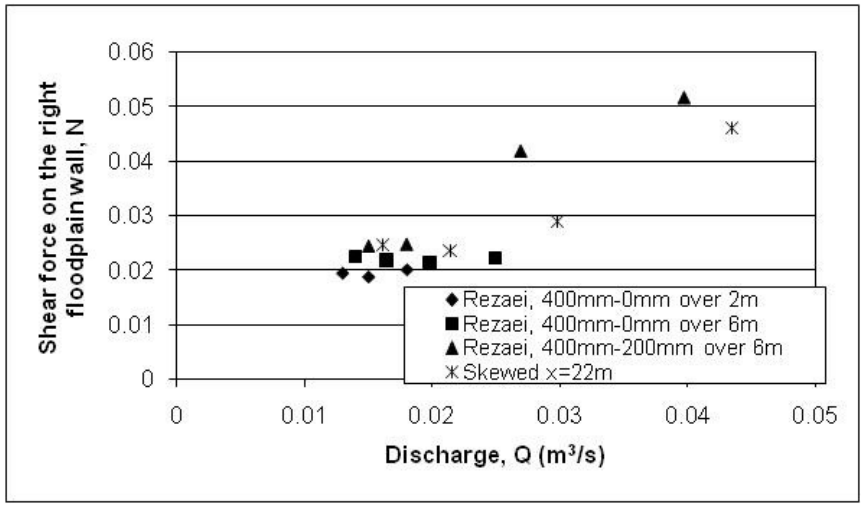

Figure 8.42e-Shear force on the right main channel wall compared to Rezaei, 2006

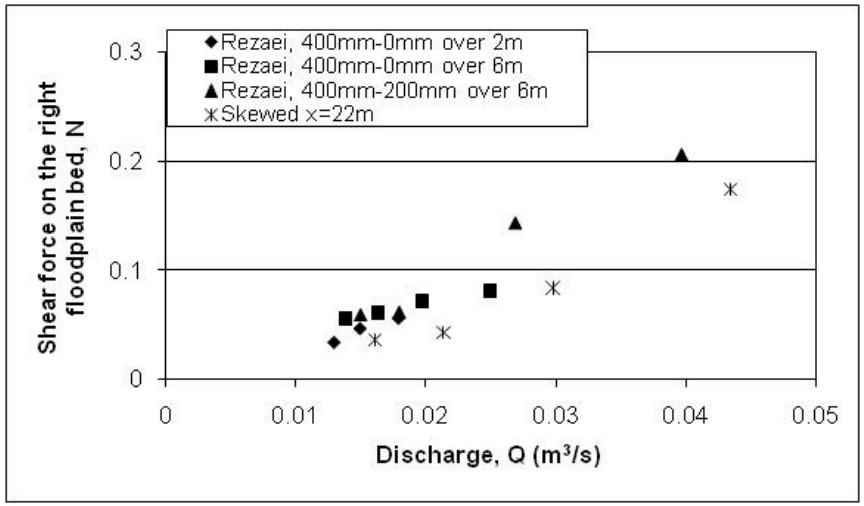

Figure 8.42f-Shear force on the right floodplain bed compared to Rezaei, 2006

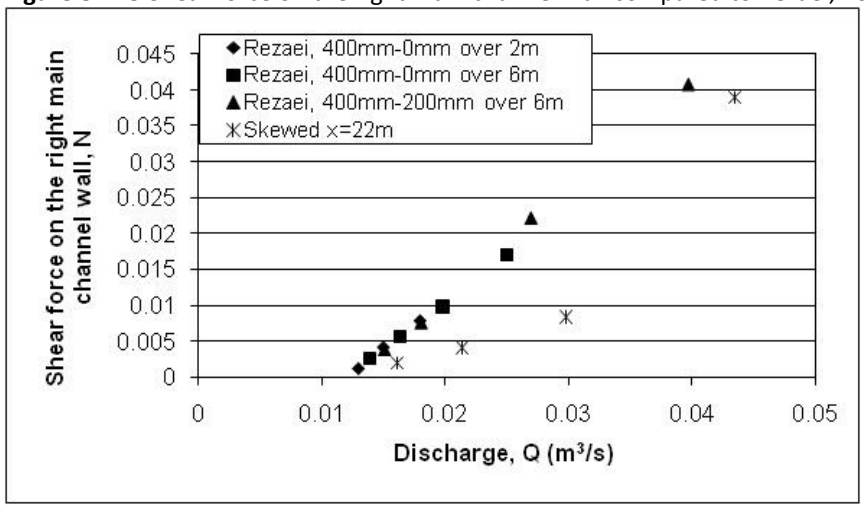

Figure 8.42g-Shear force on the right floodplain wall compared to Rezaei, 2006

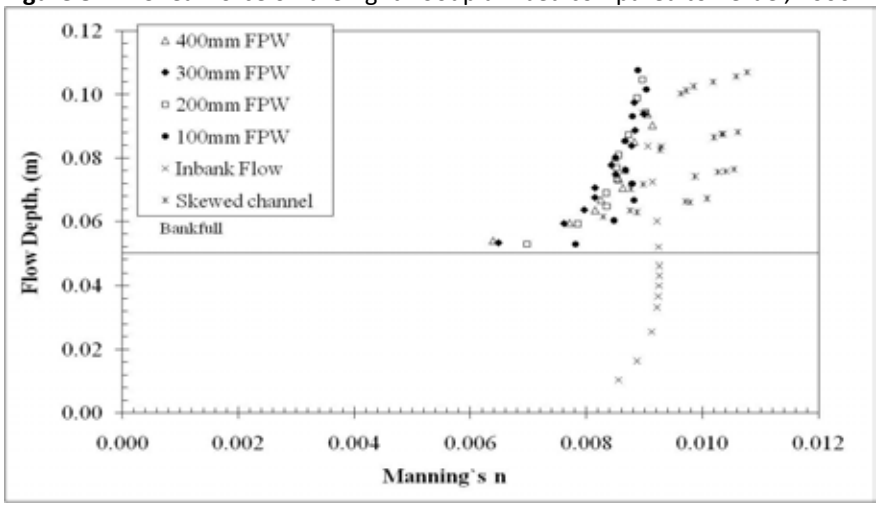

Figure 8.43a-Manning's *n*~flow depth for prismatic channel with different floodplain widths and skewed channel

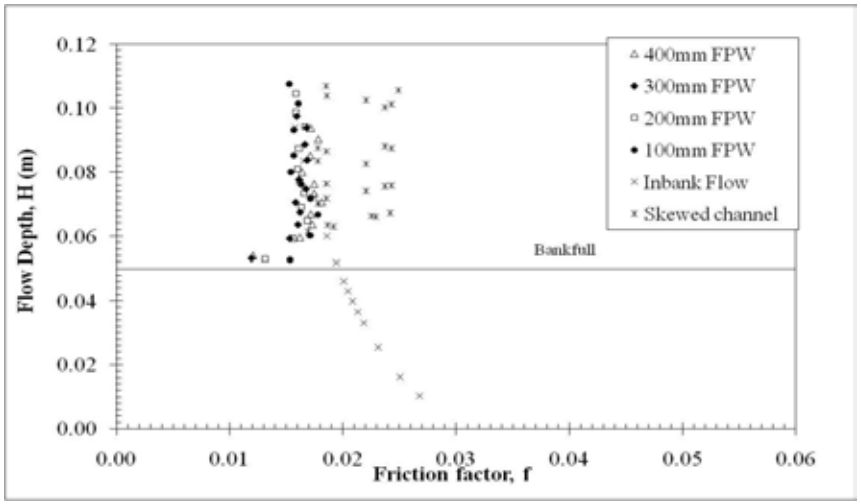

Figure 8.43b-Friction factor *f*~flow depth for prismatic channel with different floodplain widths and skewed channel

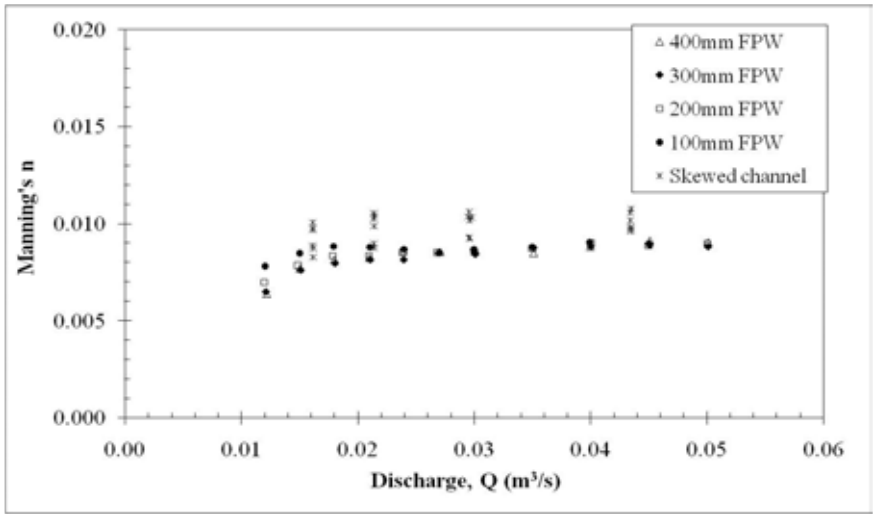

Figure 8.43c-Manning's *n*~discharge for prismatic channel with different floodplain widths and skewed channel

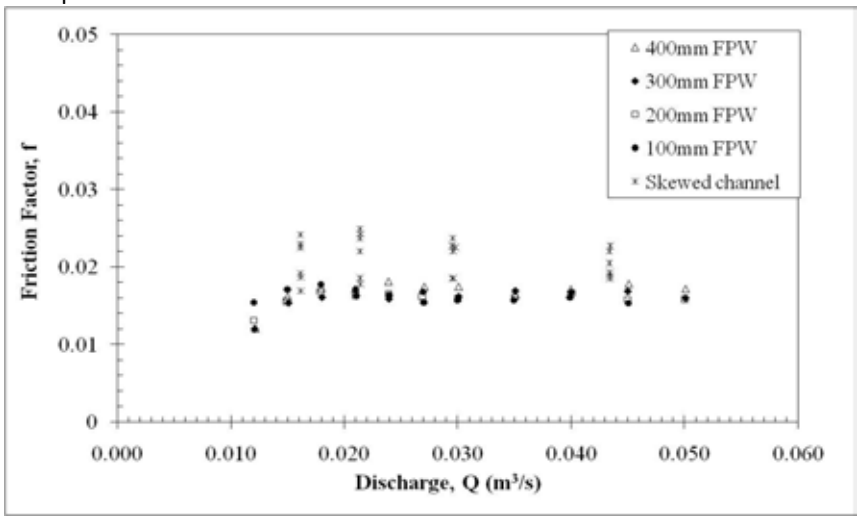

Figure 8.43d-Friction factor *f*~discharge for prismatic channel with different floodplain widths and skewed channel

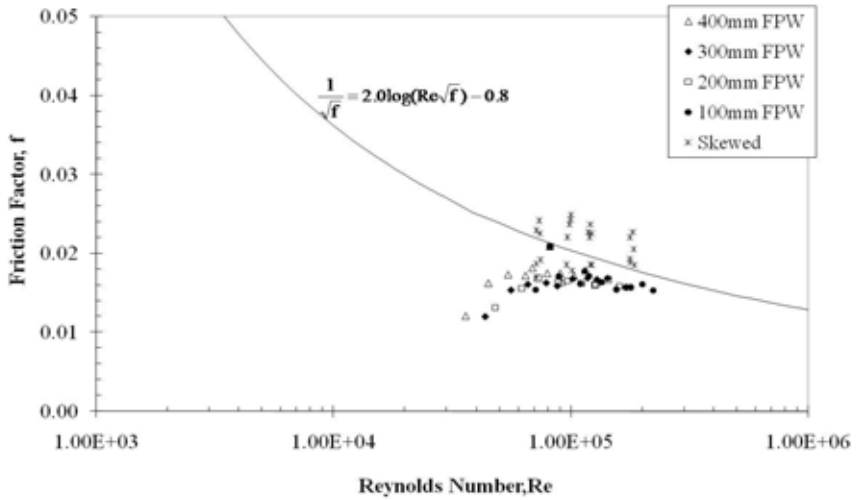

Figure 8.44-Friction factor *f*~Reynolds number, Re for skewed data and prismatic channel of varying floodplain widths

CHAPTER 9-DISCUSSION

In science the credit goes to the man who convinces the world, not the man to whom the idea first occurs. Sir Francis Darwin (1848 - 1925)

9.1 Introduction

It has been shown in Chapter 1 that it is important to be able to accurately model, both numerically and physically, flows in simple and compound channels. This thesis has examined both types of modelling, as well as both types of channel. As an aid to understanding, the thesis was divided into two parts dealing with each problem separately. It was however acknowledged that the two are not mutually exclusive and therefore in this Chapter, the two issues will be examined as one, highlighting the key findings and practical applications of the outcomes.

9.2 Discussion

It is important to be able to accurately model inbank flow as for the majority of the time, the flow is contained inbank. Although the SKM has been shown to be able to accurately model the lateral distributions of depth-averaged velocity and boundary shear stress for overbank flow in compound channels, there had been little work on the application to inbank flow in trapezoidal and rectangular channels. From these distributions, the overall discharge and percentage shear force on the walls ($\%SF_w$) can be determined, but to date, there had been no research carried out on the model's application to the problem of sidewall correction procedures, for which $\%SF_w$ is fundamental. The primary goal behind the modelling work undertaken was to simplify the method with a view to obtaining the "best" solution for the least number

of panels. For a simple smooth rectangular channel, it was found that a one panel (per half channel, assuming symmetry along the centreline), could give good overall values of discharge and $\%SF_w$ (less than 5% error), although the distributions of depth-averaged velocity and boundary shear stress were not acceptable (**Figures 3.3** and **3.4**). This however allows for direct, analytical, calculation of $\%SF_w$, and is comparable with other sidewall correction procedures (such as Vanoni & Brooks (1957) and Brownlie (1981)). These procedures cannot compute the distribution of boundary shear stress, and unlike this approach, cannot calculate the discharge within the channel. For the one panel solution, equations have been presented for the calculation of f, λ and Γ (Equations 3.17-3.19).

This method was extended to a four panel (per half channel) solution for flow in rectangular channels. Initially the panels were kept at constant spacing (spacing=0.25b, where b is the half-width). This yielded good results of discharge and $\%SF_w$, and improved distributions of depth-averaged velocity and boundary shear stress, as shown in **Figures 3.19** and **3.20**, for variable f across the channel, constant λ (=0.07) in panels 1-3, but varying it in panel 4 and varying Γ in panels 1 and 4. However, this resulted in the model under predicting the depth-averaged velocity and boundary shear stress near to the wall. To rectify this, the four panels were retained, but the width of the panel nearest to the wall was decreased to 0.1b and the middle panels increased to 0.325b. This gave good distributions of boundary shear stress and depth-averaged velocity (**Figures 3.21** and **3.22**) in addition to overall discharge and $\%SF_w$ (**Figure 3.23**). Γ should be varied in panels 1 and 4, with panels 2 and 3 being kept constant and close to zero. It was found that Γ was most significant in panel 4,

but Γ in panel 1 is still influential, particularly on boundary shear stress. Γ_4 becomes increasingly negative with decreasing aspect ratio, while Γ_1 becomes increasingly positive. In most cases for smooth experimental flume data, λ=0.07 should be adopted, at least in panels 1 and 2. Depending on the aspect ratio of the channel, λ_3 should be reduced from 0.07 and in all cases λ_4 is smaller than $\lambda_{1\text{-}3}$.

Although it is important to study flow in rectangular channels, they are in many ways harder to model than other channel configurations due to the arrangement of secondary current cells within the corner region. It has been demonstrated herein that the SKM can be applied to rectangular channels and can offer an alternative to conventional sidewall correction procedures to calculate the $\%SF_w$.

Trapezoidal channels are especially important since many natural river cross-sections are in fact idealised by a trapezoidal shape. Therefore, the study of flows in trapezoidal channels has significant practical application. In this study, the discharge, distribution of depth-averaged velocity, distribution of boundary shear stress and the $\%SF_w$ have been modelled using the SKM for smooth, heterogeneously roughened and homogeneously roughened channels. These channels were also modelled using 4 panels, 2 of which were equally spaced on the flat bed, and 2 equally spaced on the sloping bed. It was found that this configuration gave good estimates of $\%SF_w$ and discharge, with errors in the region of ±2%. It is possible to model the channel with only 2 panels; one on the flat bed and one on the sloping region, this gives good results for overall discharge and $\%SF_w$, but compromises on the accuracy of the distributions. Although 6 panels may improve the solution in terms of distributions of

depth-averaged velocity and boundary shear stress, as the secondary current cells are more accurately represented (Omran, 2005), the additional computational effort does not significantly improve the overall solution as shown by **Figures 3.37-3.38**. It has also been shown that it is possible to model homogeneously roughened channels using the same calibration coefficients (λ and Γ) as the smooth channel equivalent, and obtain acceptable errors (approximately ±5%).

The calibration coefficients used within the model are paramount to the successful generation of lateral distributions of depth-averaged velocity and boundary shear stress, and hence, discharge and $\%SF_w$. Therefore, it is important that these are initially represented accurately. The friction factor, f, is particularly important in the model, especially in the cases of differential roughness. Wherever possible, it is advisable to obtain this value from experimental data and application of the Darcy-Weisbach equation. Where this is not possible, for example in field measurements where direct measurement of boundary shear stress is problematic, suitable values should be selected and reviewed using sources such as Chow (1959) or the Roughness Advisor available within the Conveyance and Afflux Estimation System, CAES (www.river-conveyance.net). The value of f needs to be linearly varied across the channel to avoid spikes in the distribution of boundary shear stress, and should also increase towards the edge of the channel, which is consistent with the physics.

The value of λ can be assumed for many studies, with commonly used values, such as: 0.07, 0.13 and 0.24. However, there needs to be flexibility in the value of λ especially near to the wall where it has been found to decrease as Γ and f increase.

Where there is heterogeneous roughness, the value of λ increases, particularly on the flat bed region of trapezoidal channels.

It was observed that Γ should increase towards the wall, and in the case of the rectangular channel, the Γ values in panels 2 and 3 are close to zero. In trapezoidal channels, Γ_2 and Γ_3 are more important and where there is a steep bed slope ($S_0 \geq 8.7 \times 10^{-3}$) Γ is more constant across the channel.

In addition to the numerical modelling undertaken on flows in simple channels, another topical area is the study of flows in two-stage channels where a form has been imposed on the floodplain, by, for example, by distant floodplain banks. With increasing development on floodplains, it is important to understand the behaviour of flows in these channels as the flow patterns are quite different from the prismatic equivalents. However, there has been relatively little research undertaken in this field. In this study, the floodplain was skewed at an angle of 3.81° to the main channel over a length of 6m (total channel length 18m). A series of four experiments with differing depths were undertaken and measurements taken at 6 intervals throughout the transition. Further details are given in Chapter 6. In addition to these experiments, a re-assessment of the experiments undertaken in the Flood Channel Facility by Elliot & Sellin, (1990) was carried out. This allowed for a comparison to be drawn with the new experimental data and an examination of the force-momentum balance to be embarked on.

In the FCF experiments, the upstream and downstream water levels were constant, unlike those in the Birmingham experiments. This could be due to the Birmingham experiments having 6 measuring sections, as opposed to the FCF data which had a limited number, between 1 and 3. Both sets of data showed a clear peak in boundary shear stress (2.5 times the section mean) and depth-averaged velocity (up to 150% of the main channel velocity) at the interface of the main channel and the expanding floodplain. The distributions of lateral streamwise depth-averaged velocity are shown in **Figures 7.10-7.14** and **Figures 8.7a-d.** From these, it is clear that the velocity in the right hand floodplain (reducing in width) decreases through the transition, and in contrast, the left hand floodplain (increasing in width) increases. In the Birmingham flume, the peak velocity is biased in the direction of the skew i.e. the peak velocity is not in the centre of the channel as it is for flow in prismatic channels. The boundary shear stress results for the FCF data are presented in **Figures 7.27a-7.27k** and **Figures 7.28a-c** with the Birmingham data given in **Figures 8.17a-d**.

The proportional discharges have been calculated for the FCF (**Figures 7.18-7.22**) and for the Birmingham data (**Figures 8.11-8.14** and **Table 8.4**). From these, the discharge on the right floodplain decreases as the discharge on the left floodplain increases by a similar amount. The proportion of discharge in the main channel is approximately constant for each relative depth. This indicates that the discharge being forced off the right floodplain enters the main channel and immediately transfers onto the left floodplain. Simple relationships have been determined for the floodplains and main channel for each experiment (with the exception of A17), **Figures 7.23-7.25**. Although only 2 locations were measured and linear expressions

fitted, the author's skewed data show similar trends (Section 8.5). **Figures 7.23-7.25** also show a comparison been made between the percentage of discharge and area in any zone, with **Figures 7.26a-b** showing it on a larger scale. From these it is clear that the percentage discharge is usually greater than the percentage area, and that as the depth increases the difference lessens.

The shear force on each boundary element in the FCF flume and the percentage of the total shear force acting on each element have been determined and given in **Tables 7.10** and **7.11** respectively, **Figures 7.29-7.30**. The shear force data on each element in the channel for the Birmingham flume were calculated and are presented in **Table 8.7** and **Figures 8.20a-g**. From these it was found that the shear force on the left floodplains increases more than the values on the right floodplain decreases by. There is also an increase for the left main channel wall caused by the fluid being forced onto the left floodplain.

Force-momentum balances were carried out for both flumes, see **Tables 7.22-7.24** for the FCF flume data. For the Birmingham flume data, a number of force-momentum balances have been carried out; a full 6m analysis (**Table 8.11b**), a section by section analysis of the whole channel (**Tables 8.12a-d**), and a separate analysis of the main channel and floodplain(s) (**Tables 8.13-8.16**). This also allowed for calculation of the apparent shear force at the vertical interface of the main channel and floodplain(s). From these, in all cases there is a small out of balance momentum of approximately 1N. It is believed this is due to using smoothed data, but as the boundary shear stresses could not be corrected, using smoothed data will remove some rogue results.

The apparent shear force on a vertical interface is approximately equal and opposite for the left and right floodplains. Along the length of the channel, the left floodplain increases in magnitude whereas the right floodplain decreases in magnitude. For the FCF data, β factors were included, which resulted in significant differences between the values presented herein and those presented by Elliott & Sellin (1990). Using the data with β factors included, the vertical apparent shear forces acting at the interface of the main channel and floodplains has also been determined and compared to Elliott & Sellin's results for all three variations as listed above. The results from **Tables 7.22-7.24** are thought to give the best indication of the apparent shear forces. From these Tables and **Figures 7.43a-c**, as the skew angle increases the apparent shear force also increases in magnitude from approximately 1.0N to –80N in the case of Series A15, s=1, θ=9.2°.

With the Birmingham data, direct comparisons could be made with the asymmetric prismatic channel studies of Atabay (2001) and with the converging non-prismatic data of Rezaei (2006). **Figures 8.37a-d** show that the upstream and downstream lateral velocity distributions compare well to Atabay's (2001) asymmetric channel results. The mid-section, shown in **Figure 8.38a-e** (x=22m) compares well to Rezaei's converging channel experiments. There are however some differences between the converging and skewed data. Generally, the left hand velocity on the skewed channel is greater than the converging channel which is due to the fluid being forced onto the left floodplain and hence accelerating.

To summarise, a number of numerical and physical modelling studies have been undertaken. Both are of significant practical importance as they address the key issues of inbank flow, particularly when there is differential roughness, and flow on floodplains which have an imposed form. From the work contained herein, it is believed that some of the knowledge gaps have been filled. It is however noted that there is still research which could be undertaken to help further the understanding of these two key problems. The section below highlights these issues with the hope that they will be addressed in the future.

CHAPTER 10-CONCLUSIONS AND RECOMMENDATIONS

History will be kind to me for I intend to write it. Sir Winston Churchill (1874 - 1965)

10.1 Conclusions

This thesis examined two key practical and topical problems:

- accurate numerical modelling of inbank flow with smooth, differentially rough and homogeneously roughened boundaries using the Shiono & Knight Method (SKM) for flow in both rectangular and trapezoidal channels, and
- a reassessment of skewed floodplain data from the Flood Channel Facility carried out in conjunction with a series of new experiments investigating two-stage skewed channel flows which were undertaken at The University of Birmingham.

The main conclusions can be summarised below.

10.1.1 Simple channels with homogeneous and heterogeneous roughness

- The SKM method was shown to be able to accurately predict the lateral distributions of depth-averaged velocity and boundary shear stress, in addition to the overall discharge and $\%SF_w$ (within 2%).
- The method was able to accurately model the flow characteristics using only 4 panels, keeping the model simple and easy to apply, errors were generally less than 2%. In natural channels, the number of panels may need to be increased to take into account irregularly changing side slopes.

- The method has shown to be a suitable alternative to conventional sidewall correction procedures as this method was able to accurately compute the $\%SF_w$ in addition to generating the distributions of boundary shear stress and depth-averaged velocity. This method also more accurately represents the physics of the flow characteristics.
- Guidance has been given to the values of the three calibration coefficients, f, λ and Γ in each panel which will enable to user to understand how the parameters interact and can also give starting values of f, λ and Γ.

10.1.2 Compound channels with skewed floodplains

- A thorough re-examination of the Flood Channel Facility data has been undertaken to examine the characteristics of the flow, including the distribution of discharge in each zone (main channel and floodplain(s)), the depth-averaged velocity and the velocity profile in each zone, the characteristics of boundary shear stress, particularly at the interface of the main channel and floodplain.
- It was found from the FCF data and the Birmingham data that the point of maximum depth-averaged velocity and boundary shear stress is biased in the direction of skew, and the values of the peak being up to 200% greater than the section mean values.
- A force-momentum balance has been carried out to assess the apparent shear force acting horizontally and vertically for both the FCF and Birmingham data. It has been shown that the values of vertical apparent shear force are approximately equal and opposite on the two floodplains, the value on the

receiving floodplain also increases along the length of the transition, whilst on the reducing floodplain it is decreasing.

10.2 Recommendations

The work here has shown that it is possible to accurately model the lateral distribution of depth-averaged velocity and boundary shear stress in inbank channel flow for a number of roughness values and geometries. From the work undertaken herein, the following recommendations for further work are given:

10.2.1 Recommendations for modelling simple channels with homogeneous and heterogeneous roughness

- Further exploration of the coefficients f, λ, and Γ should be undertaken to investigate the physical implications of f, λ and Γ. The author notes that there have been attempts to formalise an expression for Γ (Abril & Knight, 2004), however, these do not take account of the changing sign of Γ across the channel when there is inbank flow.
- With advancements in measurement techniques (such as Acoustic Doppler Velocimeters) which can obtain the velocity in three-directions, it is hoped that this can allow for further study of natural river flows, and further laboratory experiments into the secondary current cells which form, particularly in heterogeneously roughened channels. This would aid the understanding as to the value of this term in different areas within the channel and the overall weighting within the solution.

- Additional examination of λ would also be advantageous, as this has only been achieved using existing data. It would be recommended that further study of heterogonous roughened channels would aid the understanding of this term within the solution.
- The work herein has investigated the effects of varying each of the SKM coefficients in turn. It would be useful to investigate the combined effects of altering all three simultaneously. Work undertaken by Sharifi et al. (2008) has shown that this is possible although there is still much to be done in this regard.
- Application of the method to natural rivers is key to showing the practical applications of the approach. Much has been carried out by Defra/EA for the Conveyance and Afflux Estimation System, but this was with an emphasis on two-stage channels. Therefore, it would be a useful addition to further study inbank flow but in natural channels to better understand the flow characteristics and hence modelling methods.
- Extension of the method to analyse erosion, deposition and sediment transport due to the accurate modelling of boundary shear stress and $\%SF_w$.

10.2.2 Recommendations for further work on compound channels with skewed floodplains

- Additional investigation into the mixing processes in skewed channels to provide further insight into the forces acting within the channel and therefore provide an improved force-momentum balance.
- The experiments undertaken at The University of Birmingham on skewed channel flow have filled a significant knowledge gap, and the reassessment of

the FCF data has validated many findings. However, it is acknowledged that it would be helpful for practicing engineers to have a numerical model to examine the effects of their flood management/mitigation measures. Rezaei (2006) applied the SKM to the converging channel data with some success. It was found that with the use of the energy slope, as opposed to the bed slope generally used, the solution improved. It is hoped that the SKM can be applied to skewed channel flow using the experimental data examined herein. It is well documented to be successful for the calculation of flow in prismatic channel flow, and through the addition of empirical k-factors (Ervine et al., 2000) can be applied to meandering channels. These experiments will offer insight into the flow behaviour of skewed channels and through this an analytical solution to the SKM for skewed and meandering channel flow may be determined.

- It would also be advantageous to physically model skewed channel flow with roughened floodplains or with artificial vegetation as often the floodplains are rougher than the main channel. This is more representative of reality and would give further insight into the behaviour of skewed channel flow.

CHAPTER 11-REFERENCES

Abril, J.B. and Knight, D.W., 2004, Stage-discharge prediction for rivers in flood applying a depth-averaged model, **Journal of Hydraulic Research**, IAHR, Vol. 42, No. 6, pp 616-629

Alhamid, 1991, **Boundary shear stress and velocity distribution in differentially roughened trapezoidal open channels**, PhD Thesis, The University of Birmingham

Atabay, S., 2001, **Stage-discharge, resistance and sediment transport relationships for flow in straight compound channels**, PhD Thesis, The University of Birmingham, April

Atabay, S. and Knight, D.W., 2002, The influence of floodplain width on the stage-discharge relationship for compound channels, **1st International Symposium on Fluvial Hydraulics**, River Flow 2002, Editors Bousmar & Zech, Balkema, Belgium.

Ayyoubzadeh, S.A., 1997, **Hydraulic aspects of straight-compound channel flow & bed load sediment transport**, PhD Thesis, University of Birmingham, April

Berz, G., 2000, Flood disasters: lessons from the past-worries for the future, Proceedings of the Institution of Civil Engineers, **Journal of Water, Maritime and Energy**, Vol. 142, pp 3-8, March, 12212

Blasius, H., 1913, Das Ähnlichkeitsgesetz bei Reibungsvorgängen in Flüssigkeiten, **Forschungs-Arbeit des Ingenieur-Wesens**, Vol. 131 (in German)

Bousmar, D. and Zech, Y., 1999, Momentum transfer for practical flow computation in compound channels, **Journal of Hydraulic Engineering**, ASCE, Vol. 125, No. 7, July, pp 696-706, Paper No. 18224

Bousmar, D. 2002, **Flow modelling in compound channels – Momentum transfer between main channel and prismatic or non-prismatic floodplains**, PhD Thesis, Universite Catholique de Louvain.

Boussinesq, J., 1877, Théorie de l'Écoulement Tourbillant, **Mem. Présentés par Divers Savants Acad. Sci. Inst. Fr.**, Vol. 23, pp. 46-50.

Bradshaw, P. and Gregory, M.A., 1961, The determination of local turbulent skin friction from observations in the viscous sub-layer, **Aeronautical research council reports and memoranda**, R&M No. 3202

Brownlie, W.R. 1981, Re-examination of Nikuradse roughness data, **Journal of the Hydraulics Division**, ASCE, Vol. 107, HY1, January, pp. 115-119

Chang, H.H., 1988, **Fluvial processes in river engineering**, John Wiley & Sons

Chen, C.L., 1991, Unified theory on power laws for flow resistance, **Journal of Hydraulic Engineering**, ASCE, Vol.117, No. 3, pp. 371-389.

Cheng, N-S and Chua, L.H.C., 2005, Comparisons of sidewall correction of bed shear stress in open channel flows, **Journal of Hydraulic Engineering**, ASCE, Vol. 131, No. 7, July, pp 605-609

Chiu, C.L. and Chiou, J.D., 1986, Structure of 3-D flow in rectangular open channels, **Journal of Hydraulic Engineering**, ASCE, Vol. 112, No. 11, November, pp.1050-1068

Chlebek, J. and Knight, D.W., 2006, A new perspective on sidewall correction procedures, based on SKM modelling, **3rd International Symposium on Fluvial Hydraulics**, River Flow 2006, Vol. 1, Editors Ferreira, Alves, Leal & Cardoso, Portugal

Chow, V.T., 1959, **Open channel hydraulics**, International Edition, McGraw Hill, New York

Colebrook, C.F., 1939, Turbulent flow in pipes, with particular reference to the transition region between smooth and rough pipe laws, Journal of the Institute of Civil Engineers, London

Cunge, J. A., Holly, F.M. and Verwey, A., 1980, **Practical aspects of computational river hydraulics**, The Pitman Press, Bath, UK

Darcy, H., 1857, **Recherches experimentales relatives au mouvement de l'eau dans les tuyaux**, 2 volumes, Mallet-Bachelier, Paris, pp 1-268 and atlas ("Experimental Research Relating to the Movement of Water in Pipes").

DEFRA/EA, 2004, **Reducing uncertainty in river flood conveyance**, Conveyance Manual, Project W5A-057, HR Wallingford, UK.

Einstein, H.A., 1934, Der hydraulische oder profil-radius, **Schweizerische Bauzeitung**, Zurich, Vol. 103, No. 8, pp 89-91

Einstein, H.A., 1942, Formulas for the transportation of bedload, **Transactions of ASCE**, Vol. 107, pp 561-577

Einstein, H.A. and Li, H., 1958, Secondary currents in straight channels, **Transactions of the American Geophysical Union**, Vol. 39, No.6, pp 1085-1088

Elliott, S. C.A., 1990, **An investigation into skew channel flow**, PhD Thesis, The University of Bristol, January

Elliott, S.C.A. and Sellin, R.H.J., 1990, SERC flood channel facility: skewed flow experiments, **Journal of Hydraulic Research**, IAHR, Vol. 28, No. 2, pp 197-214

Ervine, D.A., Babaeyan-Koopaei, K. and Sellin, R.H.J., 2000, Two-dimensional solution for straight and meandering overbank flows, **Journal of Hydraulic Engineering**, ASCE, Vol. 126, No. 9, September, pp 653-669, Paper No. 22144

Ervine, D.A. and Jasem, H.K., 1995, Observations on flows in skewed compound channels, **Journal of Water, Maritime and Energy**, ICE, Vol. 112, pp 249-259, September, 10687

Evans, E.P., Pender, G., Samuels, P.G. and Escarameia, M., 2001, Reducing uncertainty in river flood conveyance: scoping study, R&D Technical Report to **DEFRA/Environment Agency**, Project W5A-057, HR Wallingford, UK.

Fleming, G., Frost, L., Huntingdon, S., Knight, D.W., Law, F.M. and Rickard, C., 2001, **Learning to live with rivers**, Final report of the Institution of Civil Engineers' Presidential Commission to review the technical aspects of flood risk management in England and Wales, November, 1-83

Fleming, G., Frost, L., Huntingdon, S., Knight, D.W., Law, F. and Rickard, C., 2002, **Flood risk management**, Thomas Telford, London

Gessner, F.B., 1973, The origin of secondary flow in turbulent flow along a corner, **Journal of Fluid Mechanics**, Vol. 58, Part 1, pp 1-25

Gessner, F.B. and Jones, J.B., 1965, On some aspects of fully-developed turbulent flow in rectangular channels, **Journal of Fluid Mechanics**, Vol. 23, Part 4, pp 689-713

Guo, J. and Julien, Y., 2005, Shear stress in smooth rectangular open-channel flows, **Journal of Hydraulic Engineering**, ASCE, Vol. 131, No. 1, January, pp 30-37

Horton, R.E, 1933, Separate roughness coefficients for change bottoms and sides, **Engineering News Record**, Vol. 111, No. 22, pp652-653

Head, M. R., and Rechenberg, I., 1962, The Preston tube as a means of measuring skin friction, **Journal of Fluid Mechanics**, Vol. 14, pp. 1-17

Ikeda, S., 1981, Self-formed straight channels in sandy beds, **Journal of the Hydraulics Division**, ASCE, Vol. 107, HY4, April, pp. 389-406.

Ikeda, S., 1999, **Role of lateral eddies in sediment transport and channel formation**, River Sedimentation, Jayawardena, Lee and Wang, eds., Balkema Rotterdam, 195-203

Ikeda, S., Kawamura, K., Toda, Y. and Kasuya, I., 2002, Quasi-three dimensional computation and laboratory tests on flow in curved open channels, **1st International Symposium on Fluvial Hydraulics**, River Flow 2002, Vol. 1, pp 233-245, Editors Bousmar & Zech, Balkema, Belgium

Ikeda, S. and Kuga, T., 1997, Laboratory study on large horizontal vortices in compound open channel flow, **Journal of Hydraulic, Coastal and Environmental Engineering**, JSCE, Vol. 45, pp 493- 498

Ikeda, S., Sano, T., Fukumoto, M. And Kawamura, K., 2001, Organised horizontal vortices and lateral sediment transport in compound channel flows, Journal of JSCE, (accepted)

James, M. & Brown, B.J., 1977, **Geometric parameters that influence floodplain flow**, Waterways Experiment Section, Hydraulics Laboratory, Deptartment of Defense, US Army Corps of Engineers

Jasem, H., 1990, **Flow in Skew compound channels**, PhD Thesis, The University of Glasgow

Johansson, A.V. and Alfredsson, P.H., 1986, **Structure of turbulent channel flows**, Chapter 25, Encyclopedia of Fluid Mechanics, Volume 1-Flow phenomena and measurement, Editor Cheremisinoff, N.P., Gulf Publishing House

Jones, W.P. and Launder, B.E., 1973, Prediction of low-Reynolds-number phenomena with a 2-equation model of turbulence, **International Journal of Heat & Mass Transfer**, Vol. 16, p. 1119.

Kiely, G.K., and McKeogh, E.J., 1993, Secondary current rotations during flood flow in meandering channels, **Advances in Hydro-Science and Engineering**, Vol. 1, pp. 1215-1225.

Klein, A., 1981, Turbulent developing pipe flow, **Journal of Fluids Engineering**, ASME, Vol. 103, pp. 243–249.

Kline, S.J., Reynolds, W.C., Schraub, F.A. & Runstadler, P.W., 1967, The structure of turbulence in boundary layers, **Journal of Fluid Mechanics**, Cambridge University Press, Vol. 30, pp 741-773.

Khodashenas, S.A. and Paquier, A., 1999, A geometric method for computing the distribution of boundary shear stress across irregular straight open channels, **Journal of Hydraulic Research**, IAHR, Vol. 37, No. 3, pp. 381–388

Knight, D.W., 2001, **Flow and sediment transport in two-stage channels**, Keynote Lecture, Proc. 2nd IAHR Symposium on River, Coastal and Estuarine Morphodynamics, September, Obihiro, Japan, 1-20.

Knight, D.W., 2006, **River flood hydraulics: theoretical issues and stage-discharge relationships**, Chapter 17, River Basin Modelling for Flood Risk Mitigation, pp 301-334, Editors DW Knight & A Y Shamseldin, Taylor & Francis

Knight, D.W. and Abril C., J.B., 1996, Refined calibration of a depth-averaged model for turbulent flow in a compound channel, Proceedings of the Institution of Civil Engineers, **Journal of Water, Maritime and Energy**, Vol. 118, pp 151-159, September, 11017

Knight, D. W., Brown, F., Valentine, E., Nalluri, C., Bathurst, J., Benson, I., Myers, R., Lyness, J. and Cassells, J., 1999, The response of straight mobile bed channels to inbank and overbank flows, **Journal of Water, Maritime and Energy**, ICE, Vol. 136, pp. 211-224, December, 11810

Knight, D.W. and Demetriou, J.D., 1983, Flood plain and main channel flow interaction, Journal of Hydraulic Engineering, ASCE, Vol. 109, No. 8, August, Paper No. 18168, pp 1073-1092

Knight, D.W., Demetriou, J.D. and Hamed, M.E., 1984, Boundary shear in smooth rectangular channels, **Journal of Hydraulic Engineering**, ASCE, Vol. 110, No. 4, April, 405-422

Knight, D.W. and Macdonald, J.A., 1979a, Hydraulic resistance of artificial strip roughness, **Journal of the Hydraulics Division**, ASCE, Vol. 105, No HY6, June

Knight, D.W. and Macdonald, A., 1979b, Open channel flow with varying bed roughness, Journal **of the Hydraulics Division**, ASCE, Vol. 105, No. HY9, September

Knight, D.W. and Mohammed, E., 1984, Boundary shear in symmetrical compound channels, **Journal of Hydraulic Engineering**, ASCE, Vol. 109, pp.1073-1092

Knight, D.W., Omran, M. and Abril, J.B., 2004, Boundary conditions between panels in depth-averaged flow models revisited, **2nd International Symposium on Fluvial Hydraulics**, River Flow 2004, Editors Greco, Carravetta & Della Morte, Taylor & Francis Group, Italy

Knight, D.W., Omran, M. and Tang, X., 2007, Modelling depth-averaged velocity and boundary shear in trapezoidal channels with secondary flows, **Journal of Hydraulic Engineering**, ASCE, Vol. 133, No. 1, January, pp. 39-47

Knight, D.W. and Patel, H.S., 1985, Boundary shear in smooth rectangular ducts, **Journal of Hydraulic Engineering**, ASCE, Vol. 111, No. 1, January, pp. 29-47

Knight, D.W. and Samuels, P., 2007, Examples of recent floods in Europe, **Journal of Disaster Research**, Vol. 2, No. 3, pp. 190-199

Knight, D.W. and Sellin, R. H.J., 1987, The SERC flood channel facility, **Journal of the Institution of Water and Environmental Managers, Water and Environmental Management**, Vol. 1, No. 2, October

Knight, D.W. and Shiono, K., 1990, Turbulence measurements in a shear layer region of a compound channel, Journal of Hydraulic Research, IAHR, Vol. 28, No. 2, pp 175-196

Knight, D.W. and Shiono, K., 1996, **River channel and floodplain hydraulics**, Chapter 5, Floodplain Processes, Editors Anderson, M.G., Walling, D.E. and Bates, P.D., John Wiley & Sons Ltd, Chichester,

Knight, D.W., Yuen, K.W.H. and Al-Hamid, A.A.I., 1994, **Boundary shear stress distributions in open channel flow**, Mixing and Transport in the Environment, Chapter 4, Editors Beven, Chatwin and Millbank, John Wiley & Sons Ltd., pp. 51-87

Lai, C.J., 1986, **Flow Resistance, Discharge Capacity And Momentum Transfer In Smooth Compound Closed Ducts**, PhD Thesis, The University of Birmingham

Lambert, M.F. and Myers, W.R., 1998, Estimating the discharge capacity in straight compound channels, Proceedings of the Institution of Civil Engineers, **Journal of Water, Maritime and Energy**, Vol. 130, pp 84-94, June, 11530

Liao, H. and Knight, D.W., 2007, Analytical stage-discharge formulas for flow in straight prismatic channels, **Journal of Hydraulic Engineering**, ASCE, Vol. 131, No. 4, April, pp. 1111-1122

Lotter, G.K., 1933, Considerations on hydraulic design of channels with different roughness of walls, **Translations of the All-Union Scientific Research Institute of Hydraulic Engineering**, Leningrad, Vol. 9, pp 238-241.

Manning, R., 1889, On the flow of water in open channels and pipes, **Translations of the ICE of Ireland**, Vol. 20, pp 161-207

McGahey, C., 2006, A **practical approach to estimating the flow capacity of rivers**, PhD Thesis, The Open University, May

McGahey, C. and Samuels, P.G., 2003, Methodology for conveyance estimation in two-stage straight, skewed and meandering channels, **IAHR International Association of Hydraulic Engineering and Research XXX Congress "Water Engineering and Research in a Learning Society"**, Greece

McKee, P.M., Elsawy E.M., and McKeogh, E.J., 1985, A study of the hydraulic characteristics of open channels with floodplains, **Proceedings of the 21th International Congress**, IAHR, Melbourne, August

Munson, B.R., Young, D.F. and Okiishi, T.H., 2002, **Fundamentals of fluid mechanics**, John Wiley & Sons, 4th Edition

Myers, W.R.C., 1978, Momentum transfer in a compound channel, **Journal of Hydraulic Research**, IAHR, Vol 16, No 2 p.139-150.

Myers, W.R.C. and Brennan, E.K., 1990, Flow resistance in compound channels, **Journal of Hydraulic Research**, IAHR, Vol. 28, No. 2, pp 141-155.

Myers, W.R.C. & Elsawy, E.M., 1975, Boundary shear in channel with flood plain, **Journal of the Hydraulics Division**, ASCE, Vol. 101, No. 7, pp 933-946

Nalluri, C. and Featherstone, R.E., 2001, **Civil Engineering Hydraulics**, Blackwell Publishing, Fourth Edition, pp 177-193

Nezu, I. and Nakagawa, H., 1984, Cellular secondary currents in straight conduit, **Journal of Hydraulic Engineering**, ASCE, Vo. 110, No. 2, February, pp. 173-193, Paper No. 18581

Nezu, I. & Nakagawa, H., 1993, **Turbulence in open channel flow**, IAHR Monograph, A. A. Balkema, Rotterdam.

Omran, M.N., 2005, **Modelling stage-discharge curves, velocity and boundary shear stress distributions in natural and artificial channels using a depth-averaged model**, PhD Thesis, The University of Birmingham

Patel, V.C., 1965, Calibration of the Preston tube and limitations on its use in pressure gradients, **Journal of Fluid Mechanics**, Cambridge University Press, Vol. 23, Part 1, pp 185-208

Patel, H.S, 1984, **Boundary shear in rectangular and compound ducts**, PhD Thesis, The University of Birmingham

Pavlovskii, N., 1931, On a design for uniform movement in channels with non-homogeneous walls, **All-Union Scientific Research Institute of Hydraulic Engineering**, Leningrad, Vol. 3, pp 157-164

Pitt, M., 2007, **The Pitt Review, Learning the lessons from the 2007 floods**, An independent review by Sir Michael Pitt, Interim Report, Cabinet Office, Crown Copyright, December.

Pitt, M., 2008, **The Pitt Review, Learning the lessons from the 2007 floods**, An independent review by Sir Michael Pitt, Cabinet Office, Crown Copyright, June.

Prandtl, L., 1925, Bericht uber untersuchungen zur ausgebildete Turbulenz, **Z. angew. Math. Mech.,** Vol. 5, pp.136–139

Prandtl, L., 1926, Uber die ausgebildete turbulenz, **Verh. 2nd Intl Kong. Fur Tech. Mech.,** Zurich [English translation, NACA Tech. Memo. 435]

Preston, J. H., 1954. The Determination of Turbulent Skin Friction by means of Pitot Tubes, **Journal of Royal Aeronautical Society**, London, England, Vol. 58, 109–121.

Purseglove, J., 1989, **Taming the flood: A history and natural history of rivers and wetlands**, Oxford University Press

Rajaratnam, N., and Ahmadi, R.M., 1981, Hydraulics of channels with floodplains, **Journal of Hydraulic Research**, IAHL, Vol. 19, No. 1, pp43-60.

Ramwshwaran, P. and Willetts, B.B., 1999, Conveyance prediction for meandering two-stage channel flows, Proceedings of the Institution of Civil Engineers, **Journal of Water, Maritime and Energy**, Vol. 136, pp. 153-166, September, 11765

Reynolds, O., 1883, An experimental investigation whether the motion of water shall be direct or sinuous, and of the laws of resistance in parallel channels, **Philosophical Transactions of the Royal Society of London**, Vol. 174, pp 935–982.

Rezaei, B., 2006, **Overbank flow in compound channels with prismatic and non-prismatic floodplains**, PhD thesis, The University of Birmingham.

Richardson, L.F., 1922, **Weather prediction by numerical process**, Cambridge University Press

Rhodes, D.G. and Knight, D.W., 1994, Distribution of shear force on boundary of smooth rectangular duct, **Journal of Hydraulic Engineering**, ASCE, Vol. 120, No. 7, July, pp. 787-807, Paper No. 6195

Rhodes, D.G., and Knight, D.W., 1995, Lateral shear in a wide compound duct. **Journal of Hydraulic Engineering**, ASCE, Vol. 121, No.11, Technical Note, 829-832

Rouse, H., 1959, **Advanced mechanics of fluids**, New York, Wiley & Sons

Rouse, H., 1965, Critical analysis of open-channel resistance, **Journal of the Hydraulics Division**, ASCE, Vol. 91, No. 4387, HY4, pp 1-25.

Rutherford, J.C., 1994, **River mixing**, John Wiley and Sons

Saint-Venant de, B., 1843, Note a joindre au Memoire sur la dynamique des fluides, **Comptes-rendus hebdomadaires des Seances de l'Acadamie des Sciences**, Vol. 17

Samuels, P.G., 1985, **Modelling of river and flood plain flow using the finite element method**, PhD Thesis, University of Reading, November.

Schlichting, H. and Gersten, K, 2000, **Boundary-layer theory**, Springer, p13

Sellin, R.H.J, 1993a, SERC Flood Channel Facility, **Experimental data-Series A, Straight two-stage channels**, Skewed floodplain boundaries, Volume 1, The University of Bristol, June

Sellin, R.H.J, 1993b, SERC Flood Channel Facility, **Experimental data-Series A, Straight two-stage channels**, Skewed floodplain boundaries, Volume 2, The University of Bristol, June

Sharifi, S., Knight, D.W. and Sterling, M., 2008, Modelling flow using SKM and multi-objective evolutionary algorithm, **4th International Symposium on Fluvial Hydraulics, River Flow 2008**, Vol. 3, pp. 2149-2158, Editors Altinakar, Kokpinar, Darama, Yegen & Harmancioglu, Turkey

Shiono, K. and Knight, D.W., 1989, Transverse and vertical Reynolds stress measurements in a shear layer region of a compound channel, **7th International Symposium on Turbulent Shear Flows**, Stanford University, USA, August, Paper 28-1

Shiono, K. and Knight, D.W., 1988, Two dimensional analytical solution for a compound channel, **Proceedings of the 3rd International Symposium on Refined Flow Modelling and Turbulence Measurements**, Tokyo, Japan, July, Iwasa, Tamai & Wada (eds.), IAHR, Universal Academy Press Inc., pp. 503-510

Shiono, K. and Knight, D.W., 1990, Mathematical models of flow in two or multi stage straight channels, **International Conference on River Flood Hydraulics**, September, Paper G1, pp. 229-238

Shiono, K. and Knight, D.W., 1991, Turbulent open-channel flows with variable depth across the channel, **Journal of Fluid Mechanics**, Vol. 222, pp. 617-646

Shiono, K. & Muto, Y., 1998, Complex flow mechanisms in compound meandering channels with overbank flow, **Journal of Fluid Mechanics**, Cambridge University Press, Vol. 376: 221-261.

Spooner, J. and Shiono, K., 2002, Modelling of meandering channels for overbank flow, **Water and Maritime Engineering**, ICE, Vol. 156, Issue WM3, pp 225-233, paper 13067

Tang, X., 1999, **Derivation of The Wave Speed-Discharge Relationship from Cross Section Survey For Use In Approximate Flood Routing Methods**, PhD Thesis, The University of Birmingham

Tang, X. and Knight, D.W, 2008a, Lateral Depth-Averaged Velocity Distributions and Bed Shear in Rectangular Compound Channels, **Journal of Hydraulic Engineering**, ASCE, Vol. 134, No. 9, September, pp. 1337-1342

Tang, X. and Knight, D.W, 2008b, A general model of lateral depth-averaged velocity distributions for open channel flows, **Advances in Water Resources**, Elsevier, Vol. 31, pp. 846-857

Tibbetts, G, 2007, **Summer floods cost Britain £3bn, say insurers**, The Telegraph.co.uk, http://www.telegraph.co.uk/news/uknews/1571448/Summer-floods-cost-Britain-andpound3bn,-say-insurers.html, accessed 13th July 2008.

Tominaga, A., Nezu, I., Ezaki, K. and Nakagawa, H., 1989, Three-dimensional turbulent structure in straight open channel flows, **Journal of Hydraulic Research**, IAHR, Vol. 27, No. 1, pp. 149-173

Tominaga, A. and Nezu, I., 1991, Turbulent structure in compound open-channel flows, **Journal of Hydraulic Engineering**, ASCE, Vol. 117, No. 1, January, pp. 21-41, Paper no. 25422

Vanoni, V.A. and Brooks, N.H., 1957, Laboratory studies of the roughness and suspended load of alluvial streams, **Sedimentation Laboratory Report No. E68**, California Institute of Technology, Pasadena, USA.

Vreugdenhil, C.B. and Wijbenga, J.H.A., 1982, Computation of flow patterns in rivers, **Journal of the Hydraulic Division**, ASCE, Vol. 108, no. HY11, pp 1296-1309

Wark, J. B., Samuels, P.G., and Ervine, D.A., 1990, A Practical method of estimating velocity and discharge in compound channels, **Proceedings of the International Conference on River Flood Hydraulics**, Wiley and Sons, UK, 163-172.

Wark, J.B., Slade, J.E. and Ramsbottom, D.M., 1991, **Flood discharge assessment by the lateral distribution method**, Hydraulics Research Limited

Weisbach, J., 1845, **Lehrbuch der Ingenieur-und Maschinen-Mechanik**, Braunschwieg

Wormleaton, P.R., 1988, Determination of discharge in compound channels using the dynamic equation of lateral velocity distribution. **Proceedings of the International Conference on Fluvial Hydraulics**, IAHR, Budapest, Hungary.

Wormleaton, P.R., 1996, **Floodplain secondary circulation as a mechanism for flow and shear stress redistribution in straight compound channels**., Chapter 28, Coherent Flow Structures in Open Channels, Editors Ashworth, Bennett, Best & McLelland, J Wiley, pp. 581-608.

Wright, N.G., 2001, Scoping study for reducing uncertainty in river flood conveyance, Conveyance implications for 2-D and 3-D modelling, Prepared for **HR Wallingford and the Environment Agency**, March

Yang, S.-Q. and McCorquodale, J.A, 2004, Determination of Boundary Shear Stress and Reynolds Shear Stress in Smooth Rectangular Channel Flows, **Journal of Hydraulic Engineering**, ASCE, Vol. 130, No. 5, May, pp. 458-462

Yang, S.-Q. and Lim, S.-Y., 2005, Boundary shear stress distributions in trapezoidal channels, **Journal of Hydraulic Research**, IAHR, Vol. 43, No. 1, pp. 98-102

Yen, C.L. and Overton, D.E., 1973, Shape effects on resistance in floodplain channels, **Journal of the Hydraulics Division**, ASCE, Vol. 99, No. 1, pp 219-238

Yuen, K.W.H, 1989, **A Study Of Boundary Shear Stress, Flow Resistance And Momentum Transfer In Open Channels With Simple And Compound Trapezoidal Cross Sections**, PhD Thesis, The University of Birmingham

APPENDIX A-AUTHOR'S PUBLICATIONS

River Flow 2006 – Ferreira, Alves, Leal & Cardoso (eds)

A new perspective on sidewall correction procedures, based on SKM modelling

J. Chlebek & D.W. Knight
The University of Birmingham, Department of Civil Engineering, Birmingham, UK

ABSTRACT: This paper explores whether a simple depth-averaged flow model, based on the RANS equations, can provide the engineer with a relatively simple tool that can be used to estimate the shear force taken by the sidewalls of rectangular channels for a given aspect ratio. The Shiono & Knight Method (SKM) is used in conjunction with an extensive experimental data set of boundary shear stress measurements to investigate the issue over a wide range of aspect ratios ($0.3 < Asp < 20$). Particular consideration is given to the calibration of the three governing parameters, f, λ and Γ within SKM, bearing in mind the two requirements of simulating both the correct channel discharge and the percentage of the total shear force that is taken by the channel sidewalls. This exploratory attempt, using only one panel to simulate the flow in one half of the rectangular channel, appears to be promising and some equations are presented for the three calibration parameters based on this preliminary analysis. Further work is required to elucidate the physical basis of these equations, to undertake more detailed modelling using multi-panels and to study heterogeneous roughness effects.

River flow 2008-Altinakar, Kokpinar, Aydin, Cokgor & Kirkgoz (eds)
 ISBN 978-605-60136-1-4

Observations on flow in channels with skewed floodplains

J. Chlebek
Arup Campus, Solihull, UK.

D.W. Knight
Department of Civil Engineering, The University of Birmingham, UK.

ABSTRACT
Although non-prismatic floodplains occur frequently in rivers, either due to natural causes or to soft engineering solutions to flooding and the re-naturalisation of rivers, there has been little research carried out into overbank flows in such channels. This paper gives an overview of the results of some experiments carried out on a compound channel with one floodplain that changed gradually from one side of the main channel to another in the streamwise direction. The upper flow was thus skewed to the flow in the lower main channel. Measurements of boundary shear stress and depth-averaged velocity within the skewed region are presented, as well as an analysis of the resistance characteristics and the apparent shear forces acting on the vertical interfaces between the main channel and the two floodplains.

Keywords: Boundary shear, floods, overbank flow, skewed floodplains, velocity